PLASMA FUSION CENTER

PFC/RR-95-1

Thermal Hydraulics of High Heat Flux Components

Anthony Edward Hechanova

January 1995

MASSACHUSETTS INSTITUTE OF TECHNOLOGY

Cambridge, Massachusetts 02139

This work was supported by the U. S. Department of Energy Contract No. DOE-FC02-93-ER-54186.

Thermal Hydraulics of High Heat Flux Components

by

Anthony Edward Hechanova

Submitted to the Department of Nuclear Engineering
in partial fulfillment of the requirements for the degree of

Doctor of Philosophy in Nuclear Engineering

at the

MASSACHUSETTS INSTITUTE OF TECHNOLOGY

January 1995

Author .....
Department of Nuclear Engineering
January 13, 1995

Certified by .....
Mujid S. Kazimi
Professor
Thesis Supervisor

Certified by .....
John E. Meyer
Professor
Thesis Supervisor

Accepted by .....
Allan F. Henry
Chairman, Departmental Committee on Graduate Students

Thermal Hydraulics of High Heat Flux Components

by

Anthony Edward Hechanova

Submitted to the Department of Nuclear Engineering
on January 13, 1995, in partial fulfillment of the
requirements for the degree of
Doctor of Philosophy in Nuclear Engineering

Abstract

The thermal hydraulic phenomena, particularly the critical heat flux (CHF) limits, for highly-subcooled water in unobstructed pipe flow are investigated using experiments and computational models. These phenomena are important in the design of plasma facing components in fusion tokamak reactors. The experiments employ filtered and de-ionized water flowing through a 9.5 mm bore in a 19 mm x 19 mm x 130 mm copper monoblock. Single-sided heating of the block is achieved by direct electric heating of a 51 mm long plasma sprayed thin layer (0.4 mm) of tungsten overlaying a thin film (0.1 mm) of plasma sprayed ceramic on an outer wall. In the analysis, the heat transfer coefficient on the coolant-side wall relies on extrapolation of the existing Chen and Shah nucleate boiling correlations but is validated using outer wall temperature measurements and a heat conduction model.

A total of 33 test runs were conducted, of which 17 qualify as bench mark CHF data points. Fifteen of the bench mark runs are in a region where it is argued that bubble detachment cannot occur. The hydraulic boundary conditions for the 15 bench mark data points are: pressure between 2.2 and 3.0 MPa, coolant mass flux between 2.6 and 15 Mg/m^2s, and equilibrium exit quality between -0.44 and -0.49. The critical heat flux ranges between 13 and 28 MW/m^2. A correlation is formulated in which the data is fit as a relation between Stanton and Peclet numbers.

Our results are combined with a CHF data base of 275 points from several sources to enhance the generality of the following proposed CHF correlation:

$St_{CHF} = 50\frac{\rho_l}{\rho_v}(\frac{1}{Ja} + 0.00216p_r^{1.8}Re^{0.5})(1 + \frac{10}{20+L_h/D_h})Pr^{0.6}Pe^{-0.9}$

The CHF data base parameter ranges are as follows: Pe [7 x 10^4 to 3.2 x 10^6], heated length/heated diameter ratio [5 to 78], pressure [1 to 7 MPa], coolant channel diameter [5 to 25 mm], and equilibrium exit quality [-0.49 to -.07]. The proposed correlation bounds the CHF data base as a lower limit and, thus, is an appropriate conservative limit for design applications.

Thesis Supervisor: Mujid S. Kazimi, Professor of Nuclear Engineering

Thesis Supervisor: John E. Meyer, Professor of Nuclear Engineering

Acknowledgments

This thesis is the culmination of 6.3 years as a graduate student at MIT. I could not begin to recount my fond memories nor mention all the people who have made this experience so full. However, the most influential person during my tenure at MIT has been Professor Mujid S. Kazimi whose incessant support and encouragement has brought my academic career to such fruition. I am speechless in my ability to convey my gratitude for his involvement in this endeavor as a professor and supervisor. I am also indebted to Professor John E. Meyer for his enthusiasm and help during the research and writing of this thesis. There have been too many students involved with this project to name them all but I would like to thank those who took interest in my research and I hope it was an experience of invaluable learning.

My intellectual and personal growth over these past years have clearly resulted from the open-minded atmosphere amongst my peers and the bonds of friendship which I have shared with countless people. To mention names at this point would be an injustice to the memories of all the experiences I have shared with so many wondrous people.

Contents

List of Figures

List of Tables

Chapter 1

Introduction and Literature Review

1.1 Motivation

One only needs to consider the economic and environmental consequences of energy use to appreciate the potential importance of fusion energy technology to future generations. Fusion programs around the world are steadily making advances in understanding plasma phenomena; and, fusion systems technology now require in-depth engineering studies to become reality. The most common fusion reactor concept (the tokamak) uses toroidal magnetic field lines to confine a plasma. However, the highly energetic ions in the plasma eventually diffuse out of their toroidal confinement and impact upon a material structure. In order to minimize the damage of such particles and vent them out of the reactor chamber, the particles are diverted along a well characterized magnetic surface onto a component known as a divertor plate. The present thermal hydraulic investigation is focused on the cooling requirements of the divertor plate because it is the plasma facing component that must endure the harshest physical environment under normal operation. Techniques of high heat flux removal must be reliable to ensure component performance. A failure in the divertor plate could result in an irreparable or destructive accident resulting from coolant leaking into the vacuum chamber. Thus, divertor reliability is indispensable

to tokamak reactor technology. Unfortunately, very few heat transfer laboratories are producing experimental data relevant to fusion divertors, i.e., at very high heat fluxes that are sharply peaked and circumferentially non-uniform.

In a prelimimary accident analysis for the International Thermonuclear Experimental Reactor (ITER), designers identified significant events and surmised that the highest anticipated risk (leading to safety concerns) to be a "major rupture of divertor or first wall cooling pipes inside the vacuum vessel."[1]. The next event on this list was a major failure of vacuum vessel elements, vacuum ducts and pumps, and heating and fueling devices (Loss Of Vacuum Accident type). In order to have appropriate design goals with adequate safety margins to prevent component failure, the various modes of failure (such as Critical Heat Flux (CHF) and consequent tube burnout) and the associated phenomena at the relevant fusion system conditions must be understood and characterized.

1.2 Background Information

Experiments in the large tokamak research reactors such as the Joint European Torus (JET) in England, the Tokamak Facility Test Reactor (TFTR) in Princeton, as well as in smaller ones such as Alcator C-MOD at MIT, are not specifically designed to study the physical structure surrounding the plasma. Thus far, the thermal and mechanical design of plasma facing components have relied heavily on extrapolation or theoretical modeling with little *in situ* validation. By the end of this chapter, it should be clear that the present status of reliable thermal-hydraulic experiments relevant to divertor design is sparse. Indeed, the lack of a suitable material property database can alone attribute large uncertainties to component performance.

This situation is not unreasonable since definitive validation only comes from actual testing in a reactor. Unfortunately, large uncertainties exist in the reactor conditions that define the task as well as the calculated performance of the component under those conditions. In order to have a well-defined engineering task for the present study, the plasma parameters given by the conceptual design team for ITER [2] were

assumed to be representative of second generation experimental tokamaks.

The International Thermonuclear Experimental Reactor is a joint design, research and development effort involving the European Community, Japan, the former Soviet Union, the United States and other countries. Scientists and engineers began to meet under the auspices of the International Atomic Energy Agency on April 21, 1988, at the Max Planck Institute for Plasma Physics in Garching, West Germany. The overall objective of the ITER project is to "demonstrate the scientific and technological feasibility of fusion power"[1]. The ITER team has finished the conceptual design and is presently working on the engineering design of ITER.

1.3 ITER Divertor Plates

The divertor plates in a tokamak machine are the focus of the present study because they must endure the harshest physical environment under normal operating conditions. Operation will inevitably include plasma disruptions during experimental phases of operation. Currently, the mechanical design of the divertors push present technology to the extent that no optimum material or geometry can yet be identified.

The ITER divertor operating specifications are shown in Table 1.1 [3][4]. These conditions will define the physical environment that the divertor must withstand. The layout of the divertor plates for which these conditions are relevant is shown in Figures 1-1 and 1-2.

Divertor design is a demanding task because of the large uncertainties that exist both on the plasma side and the coolant side of the channel. Divertor performance depends to a large extent on the ability to calculate the heat transfer conditions for the coolant. As will be shown in the next chapter, the critical heat flux (CHF) alone will not suffice as the limiting thermal hydraulic criterion in determining acceptable parameter space for fusion divertor operation. Assuming that the operating conditions of ITER are representative of near-term divertor parameters, the heat flux incident on a divertor is expected to be very high and highly peaked as illustrated in Figure 1-3. The heat flux is not only highly nonuniform in the axial direction of the divertor

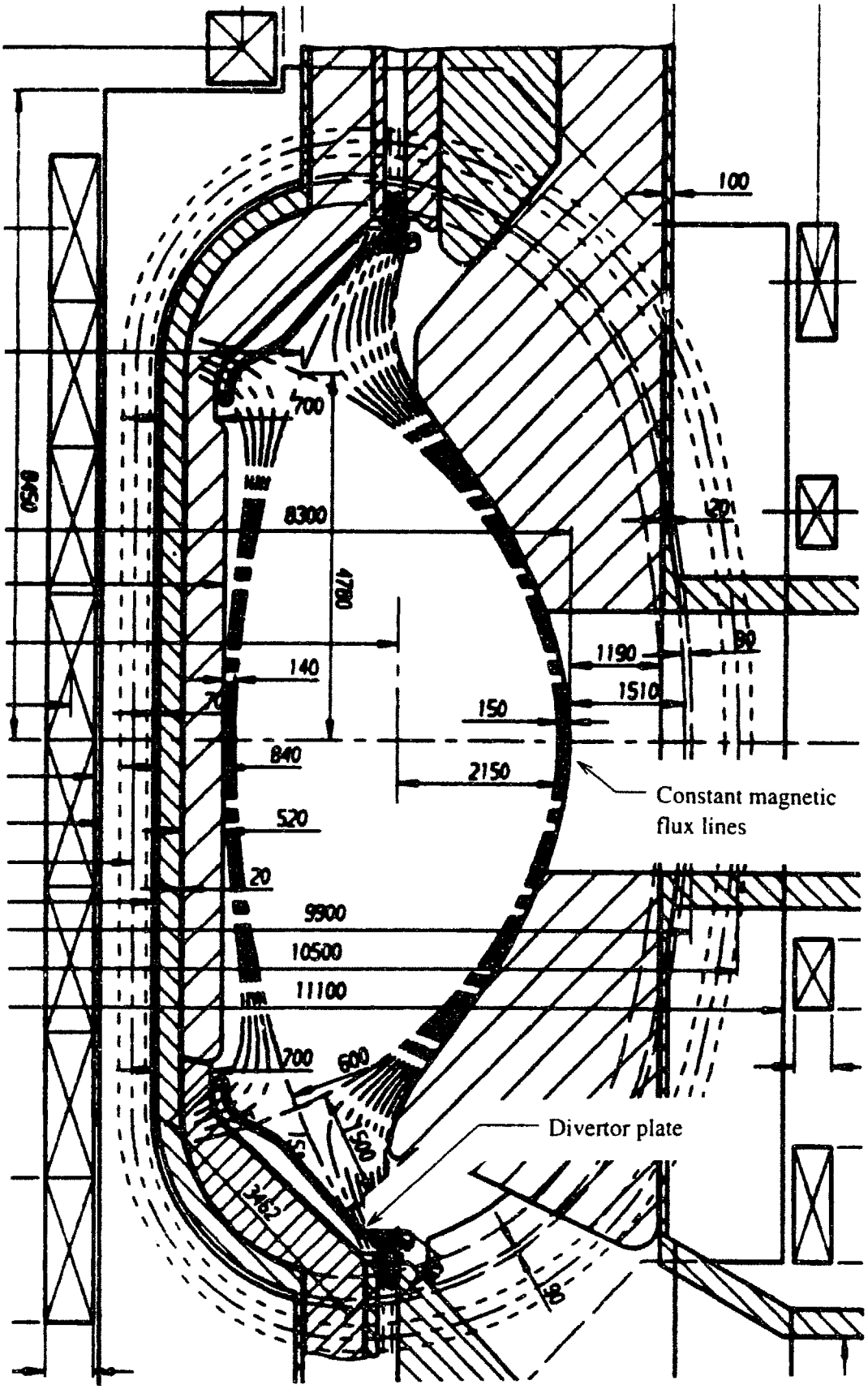

Figure 1-1: Cross-section of ITER vacuum vessel, dimensions in mm [3]

Table 1.1: Main Operating Requirements for ITER Divertors [2]

	Physics Phase	Technology Phase
Nominal Operation		
Fusion Power (MW)	1000	850
Divertor Power (MW)	160	210
Divertor Neutron Load (MW/m^2)	0.7	0.5
Neutron Fluence (MWa/m^2)	0.03	1.0
Pulse Length (s)	200	1200
Number of Pulses	7000	50,000
Nominal Peak Heat Flux (MW/m^2)	15	11
Disruptions		
Thermal Quench:		
Total Number	1000	10-100
Duration (ms)	0.1-3.0	0.1-3.0
Peak Energy Deposition (MJ/m^2)	10-20	10-20
Current Quench:		
Total Number	2000	10-100
Duration (ms)	5-50	5-50
Peak Energy Deposition (MJ/m^2)	2	2

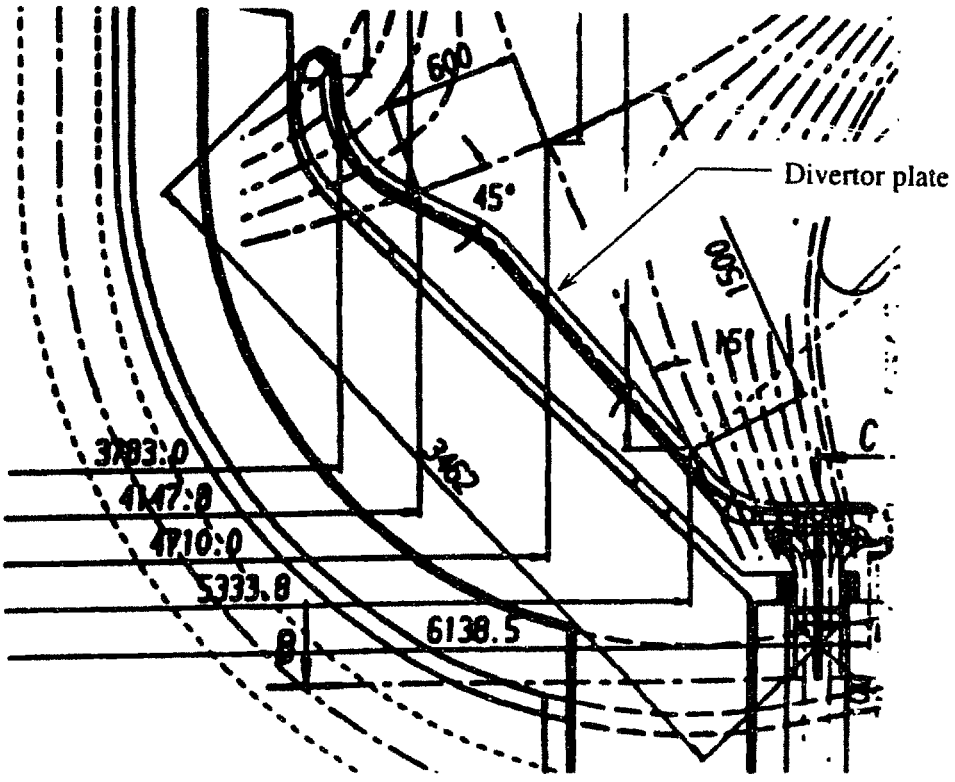

Figure 1-2: Detail of divertor configuration from Figure 1-1, dimensions in mm [3]

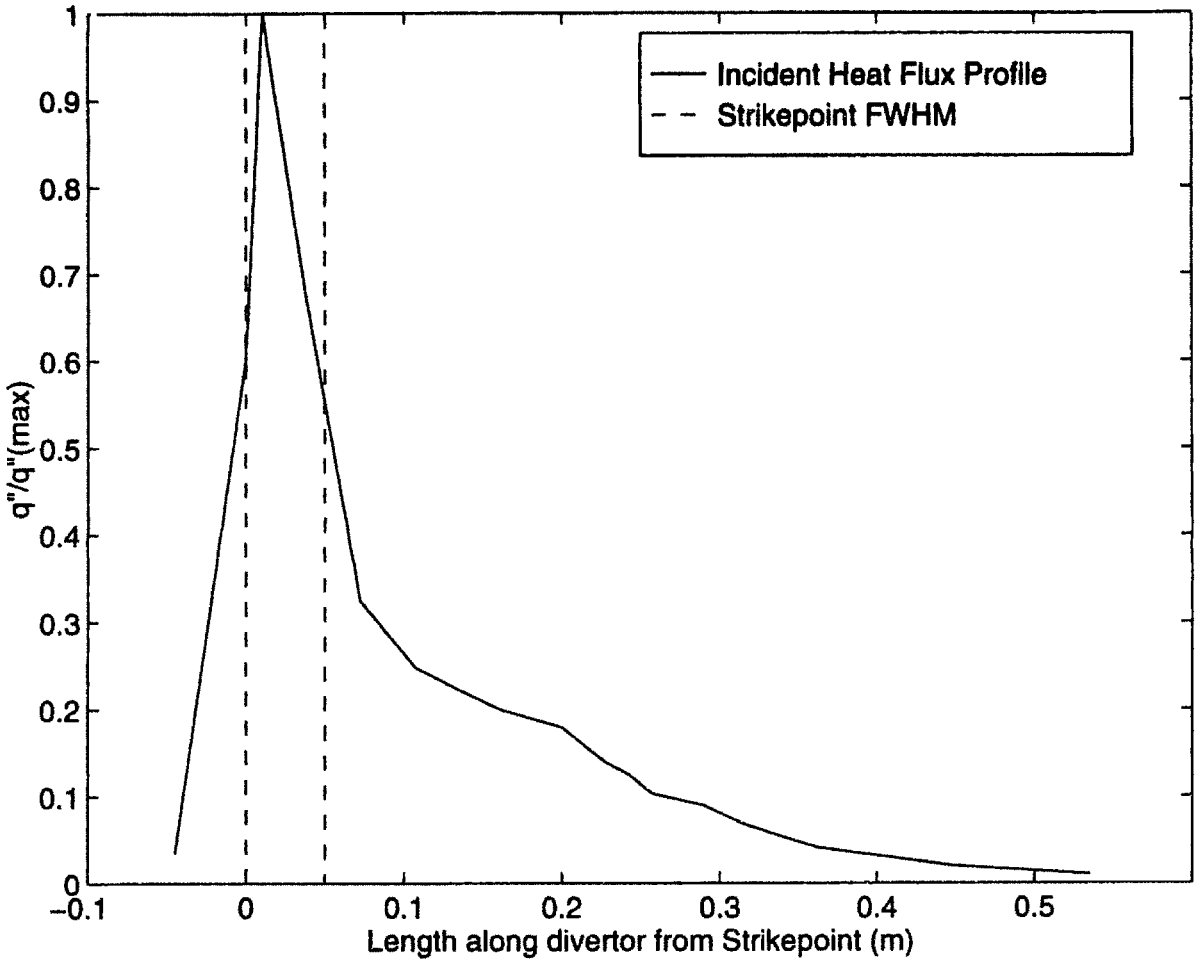

Figure 1-3: Incident Axial Heat Flux Profile [3]

plate, but also nonuniform in the circumferential direction since it applies to only one side of the coolant channel. This nonuniformity has not been well characterized in the literature and, currently, designs rely on extrapolating correlations which are based on data taken under different thermal and hydraulic conditions.

The goal of the present experimental study is to characterize thermal-hydraulic phenomena and validate predictions to be used in design. In order to permit comparisons of analyses, the ITER designers [3] proposed the thermal hydraulic parameters given in Table 1.2 as an initial design point for the first option divertor. This ITER conceptual design consists of a copper coolant tube and graphite protective tiles

Table 1.2: Proposed ITER Thermal Hydraulic Parameters [3]

Inlet temperature	50°C
Inlet pressure	3.5 MPa
Inlet velocity	10 m/s
Tube inner diameter	15 mm
Tube outer diameter	18 mm
Tube cross-section	circular
Flow enhancement	twisted tape (Twist ratio, $Y = 2$, only at strikepoint)
Desired burnout safety margin ($q''_{burnout}/q''_{design}$)	4
Minimum expected carbon tile peak temperature	1100°C

brazed together via a soft interlayer as shown in Figure 1-4 [3]. A flat surface facing the plasma is preferable to a curved surface to produce a more uniform temperature profile (among other less obvious reasons). However, brazing the tiles leads to very large stresses at the interface of the different materials. One concern with all braze approaches, according to Koski [5], is that several hundred thousand reliable joints must be made. If only one percent of braze joints fail, as was experienced on the braze inner bumper limiter for Tore Supra, then several thousand tiles would be lost from the divertor surface. These missing tiles have several bad effects including redistributing the incident heat flux and increasing the risk of tube burnout [5].

1.4 Problem Definition

The impetus of the present study was to avoid brazing by using a monoblock design and assuming a plasma-spray deposited armor, such as beryllium, on the surface. In an initial investigation by the author [6], a coolant-side analysis of an ITER divertor indicated that boiling may occur under pipe flow but could be avoided using heat transfer enhancement such as twisted tape inserts. However, a flow obstruction such as a twisted tape will produce a large pressure loss which may lower the saturation temperature of the coolant or, at least, require more pumping power. Thus, it would be desirable to forgo such obstructions. Subcooled boiling is one of the most effective

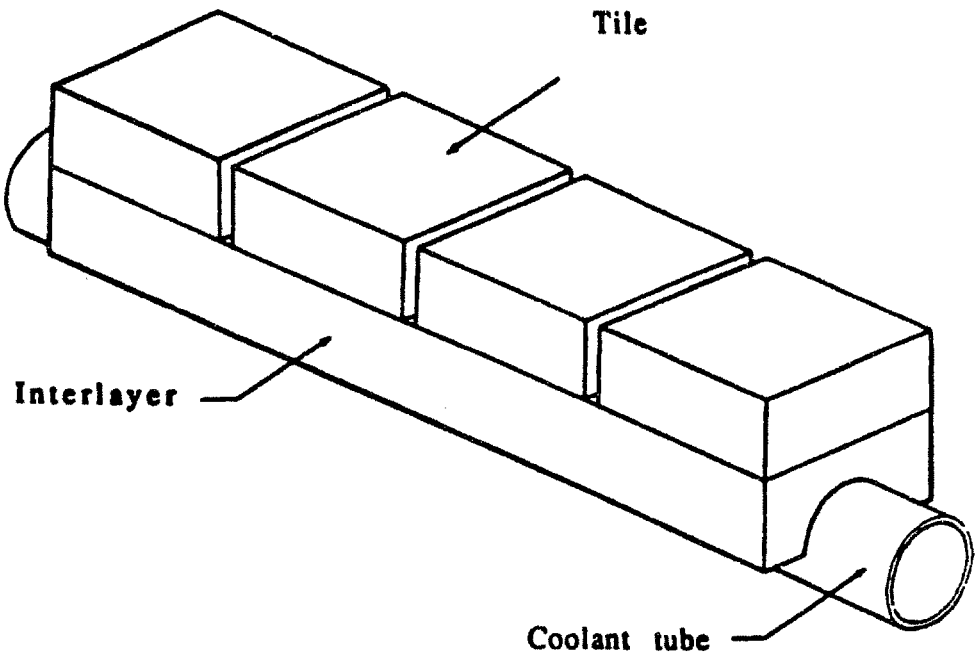

Figure 1-4: Conceptual design of ITER divertor [3]

ways to remove large amounts of heat. A design objective could be to have some boiling, say at the sharp heat flux peak, but remain well below CHF everywhere. This is not a new idea, however there is a scarcity of published research at ITER conditions. This will be discussed further in the next section.

The choice of water as a coolant in the ITER conceptual design and the present study is appropriate considering the vast amount of experience gained from the power industry and the sizable experimental data. A preliminary study in Watson et al. [3] comparing different coolants and modes of cooling found that water performed roughly the same way with respect to maximum heat flux as other approaches as shown in Table 1.3. However, the engineering advantages of using water, such as ease of pumping, continue to make it a primary candidate. In addition, subcooled boiling is an attractive mechanism for cooling a high heat flux component due to the large amount of energy associated with the phase change.

Table 1.3: Theoretical Heat Flux Limits of Alternate Power Handling Approaches

Concept	Peak Heat Flux Capability (MW/m^2)
Thermal Capacitor	50
Lithium Heat Pipe	50
Helium Microchannel	53
Water Cooled	55

1.5 Literature Review

The literature contains many CHF data and correlations, and several theories exist for the physical mechanisms [7]. However, except for a few investigations, the data are usually outside the operating parameter space of divertors both in flow conditions and heat flux profile. Nevertheless, many studies have shown that very high heat fluxes can be accommodated by using highly subcooled water at very high velocities in small diameter channels. Table 1.4 and 1.5 identify a few of these studies measuring extremely high CHF value. Vandervort et al. [8] [9] have demonstrated that heat fluxes as high as 100 MW/m^2 can be extracted with highly subcooled boiling. However, this high value is associated with small diameter channels (about 0.5 to 3 mm) with very high coolant velocities (about 40 m/s). These conditions would be too costly in terms of pumping requirements since a divertor system would contain tens of thousands of such tubes. For example, if a simple microchannel divertor were used in the ITER divertor of Figure 1-1, the flow work alone to push water through 3 mm tubes at 40 m/s from inlet to exit plenum would require 68 MW of power. Assuming ITER could produce 300 MW_e (about 30 percent of the Fusion power), then the divertor flow work would amount to 23 percent of the generated power from the power plant. Possibly even more limiting than the power requirement are the flow instability issues inherent in a microchannel over three meters long. Nonetheless, these studies indicate that the attainable heat flux values using subcooled water are very large and well within those required for fusion applications.

The author has compiled an extensive database from high heat flux, subcooled bulk, critical heat flux experiments for diameters larger than 5 mm. The database

Table 1.4: Published Experimental Investigations of Very High Heat Fluxes With Diameters Less Than 5 mm

Investigator	ΔT^a K	p MPa	Mass flux Mg/m^2s	D mm	L_h/D^b	q"max MW/m^2
Celata et al. (1991) [10]	210	2.6	40	2.5	40	60.6
Falter et al. (1991) [11]	140	0.53	10.5	3 x 3[f]	58	26[c]
Vandervort et al. (1990) [8]	135[e]	1.2	40	0.3	2	100
Boyd (1989) [12]	180	1.66	32.0	3	96.6	36.2
Boyd (1988) [13]	150	0.77	40.6	3	96.6	41.6
Zeigarnik et al. (1981) [14]	126	1.99	20	4 x 4	62.5	45.7[c]
Drizius et al. (1978) [15]	58	0.8	19.3	1.6	231	81[d]
Ornatskii and	160	2.1	90	0.5	28	230
Vinyarski (1965) [16]	175	3.1	90	0.4	28	320[c]

[a] $\Delta T = T_{sat} - T_{bulk(inlet)}$
[b] L_h/D = Axially Heated length (Full Width at Half Maximum flux)/Diameter
[c] NU = nonuniform circumferential heating
[d] SW = swirl flow
[e] $\Delta T = T_{sat} - T_{bulk(exit)}$
[f] 4 mm fin "Hypervapotron"

includes 972 points, 469 of which are for annular flow or internally finned channels. These parameters are not considered in the present study; however, for completeness all the points are listed in Appendix B. Of the remaining 503 points, 466 are from published papers in journals or conference proceedings and 37 points are unpublished. The latter points will be of interest in comparison to the experimental data reported herein in subsequent chapters. However, the published data provide a reliable database consisting of 466 points from 12 different groups of researchers and will be used to introduce experimental knowledge of the thermal hydraulic phenomena found in high heat flux applications such as on the ITER divertor plate. Table 1.5 lists the 12 groups and some of the major parameters of their experiments. Figure 1-5 is a comprehensive plot of these data over the mass flux range and the large scatter illustrates that the data must be further categorized in order to make meaningful deductions and comparisons. The first division considers that the inclusion of swirl tapes produce heat transfer enhancement and introduces further confounding phenomena such as increased turbulence and non-axial velocity vectors. Removal of

Table 1.5: Critical Heat Flux Investigations of High Heat Flux Experiments With Diameter Larger Than 5 mm

Investigator	ΔT^a K	p MPa	Mass flux Mg/m^2s	D mm	L_h^b m	q"max MW/m^2
Achilli et al. (1992) [17]	88	5.52	14.9	15.0	0.15	35.6
Araki et al. (1992) [18]	220	0.9	10.0	7.0	0.035	38.5[cd]
Cardella (1992) [19]	180	3.5	15.0	10.0	0.15	53[d]
Celata et al. (1992) [20]	79	2.18	11.2	5.0	0.10	25.2
Celata et al. (1992) [21]	111	5.12	10.0	8.0	0.10	29.5
Nariai et al. (1992) [22]	76	1.50	7.0	6.0	0.10	29.1[cd]
Schlosser (1992) [23]	100	3.40	9.1	14.0	0.09	49.2[cd]
Araki et al. (1989) [24]	67	0.96	13.5	7.0	0.50	41.8[cd]
Koski (1987) [25]	77	1.14	10.2	8.0	0.04	40.0[cd]
Burck and Hufschmidt (1965) [26]	86	3.09	3.27	10.	0.35	12.2
Mayersak et al. (1964) [27]	99	2.89	44.4	11.7	0.58	42.8
Babcock (1962) [28]	71	7.85	11.4	25.4	0.61	11.8
Gambill et al. (1961) [29]	67	0.51	22.4	7.7	0.05	41.6[d]
Mirshak et al. (1959) [30]	55	0.59	9.8	6.4	0.49	10.0
Gambill and Greene (1958) [31]	46	0.1	7.8	0.61	0.05	33.1[d]

[a] $\Delta T = T_{sat} - T_{bulk(exit)}$
[b] L_h = Axially Heated length (FWHM) (m)
[c] Nonuniform circumferential heating
[d] Swirl flow

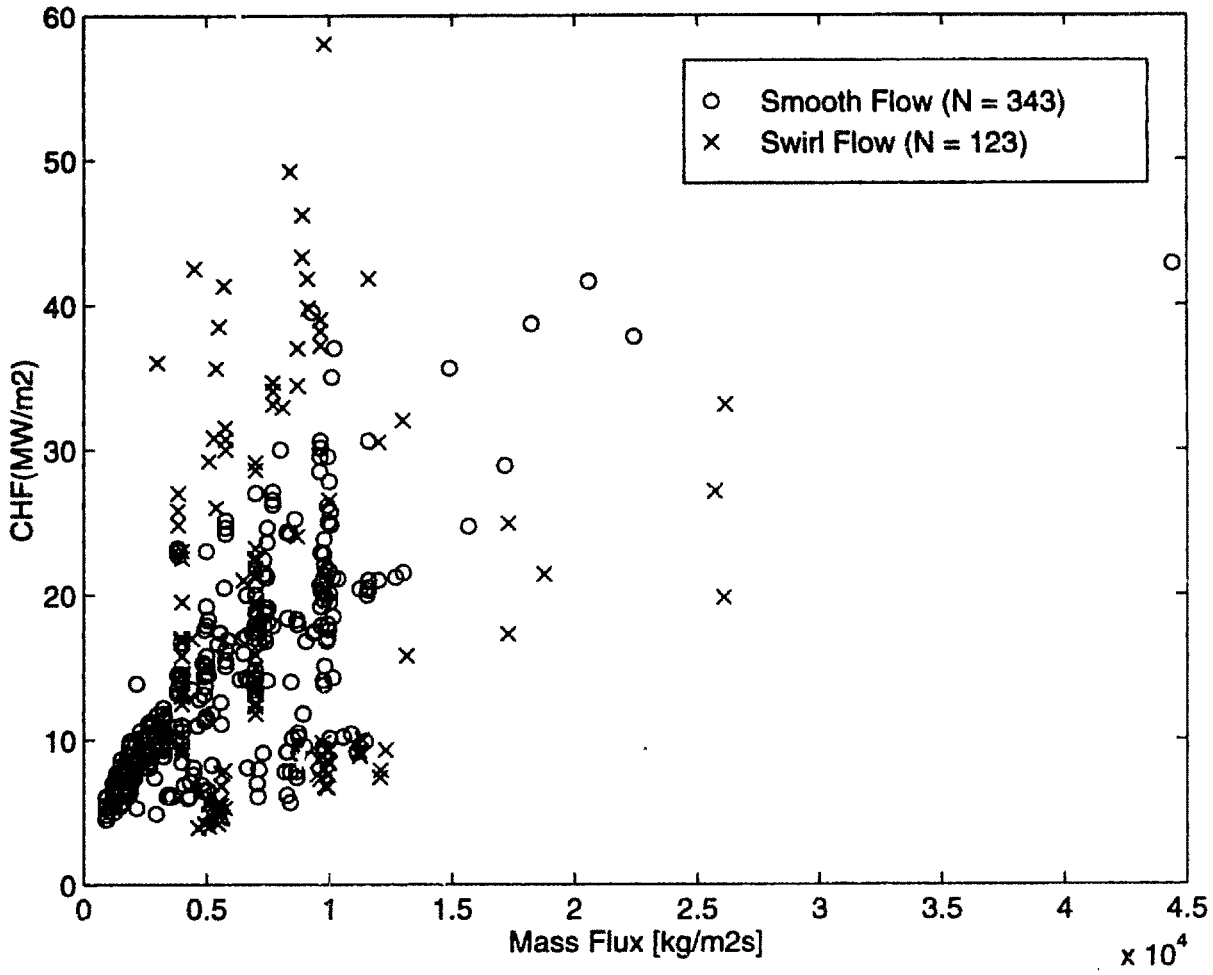

Figure 1-5: Database of Published Critical Heat Flux Experiments

the 123 swirl flow data leaves the data shown in Figure 1-6.

The heated length along the divertor plate (Full Width at Half Maximum flux) is on the order of only 0.05 m. Thus, the effects of the thermal boundary's history may confound comparison of the data. As illustrated in Figure 1-6, this distinction appears reasonably founded as much of the data that had a heated length longer than 0.25 m are concentrated around the lower values of critical heat flux. Those data with the higher value of heated length shown in the high critical heat flux region (between 30 and 40 MW/m^2) had external fins and their critical heat flux values were not reported locally; they should be considered to have a high uncertainty in the local value of

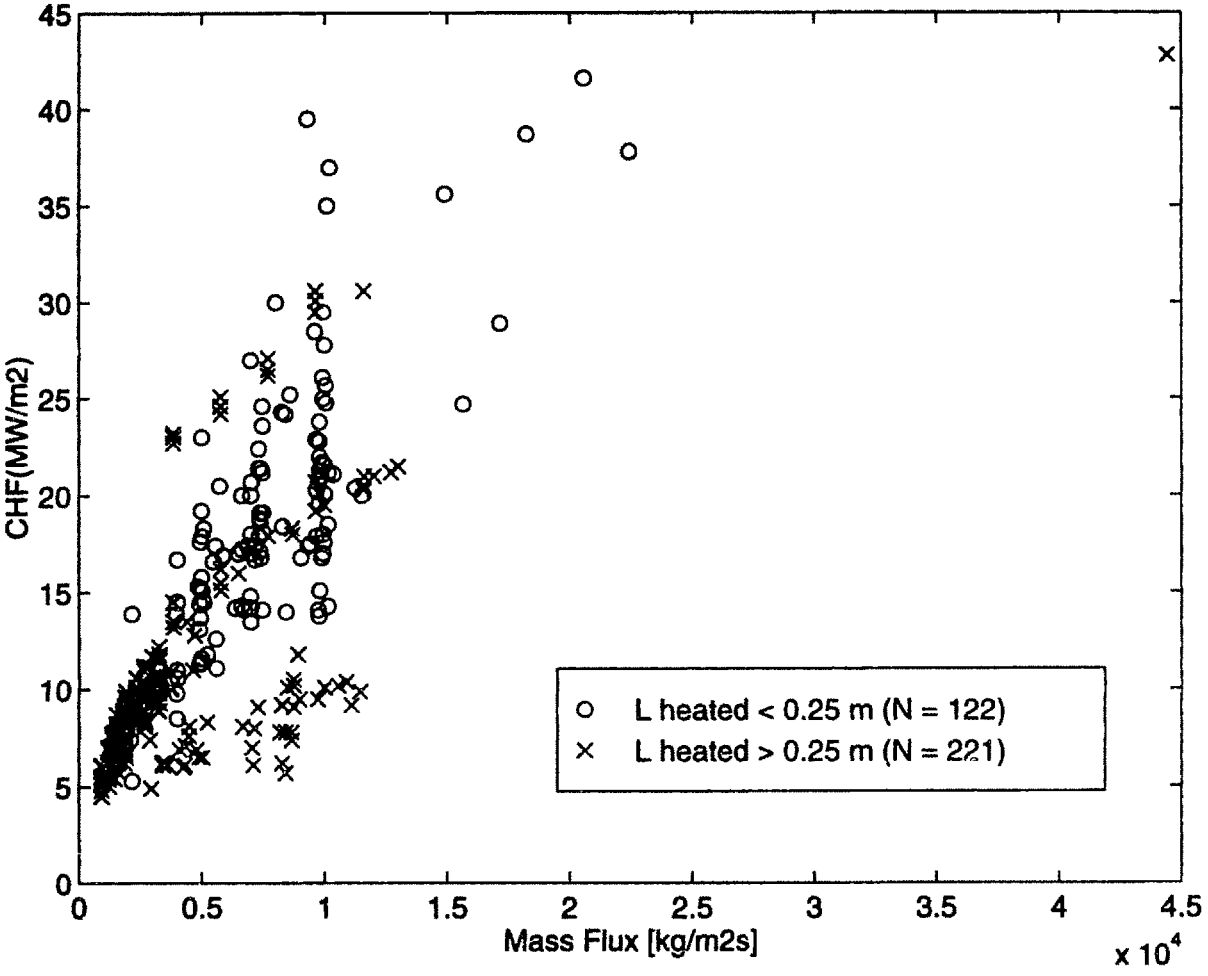

Figure 1-6: Database of Published, Smooth Flow, Critical Heat Flux Experiments

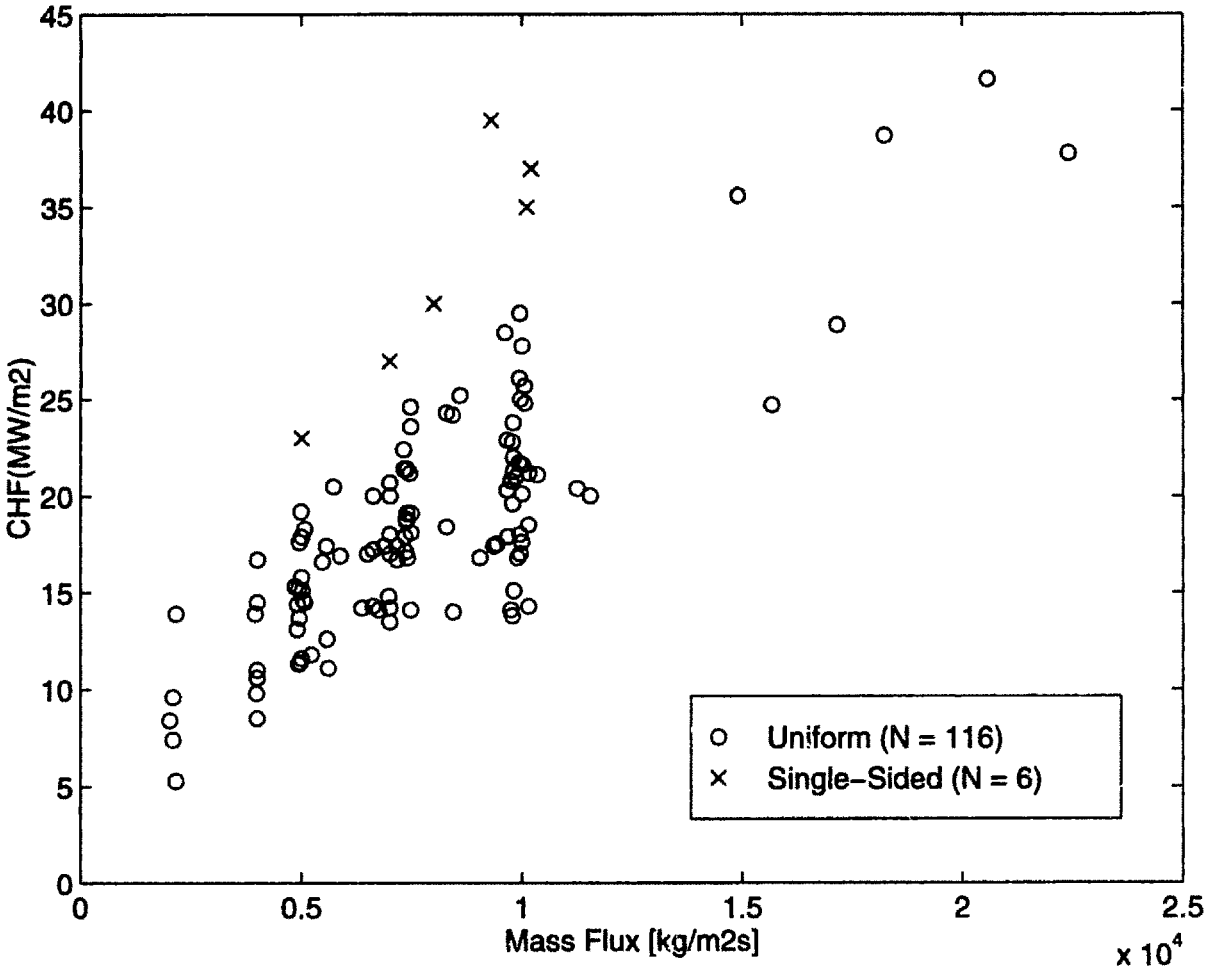

Figure 1-7: Database of Published, Smooth Flow, Heated Length less than 0.25 m, Critical Heat Flux Experiments With Respect to Mass Flux

critical heat flux. The remaining data are now shown in Figure 1-7 with a distinction made between a uniform circumferential heat flux and a nonuniform, typically single-sided, heat flux which emulates the divertor plate boundary conditions.

The rapidly shrinking database is beginning to show signs of correlation. In addition to the mass flux and circumferential heat flux profile used to present the data in Figures 1-5 to 1-7, the major parameters that can be used to determine the thermal hydraulic boundary conditions are the coolant pressure, the bulk subcooling (represented by the exit equilibrium quality), the coolant channel diameter and the axial heated length. The data in Figure 1-7 are illustrated in these other parameter spaces

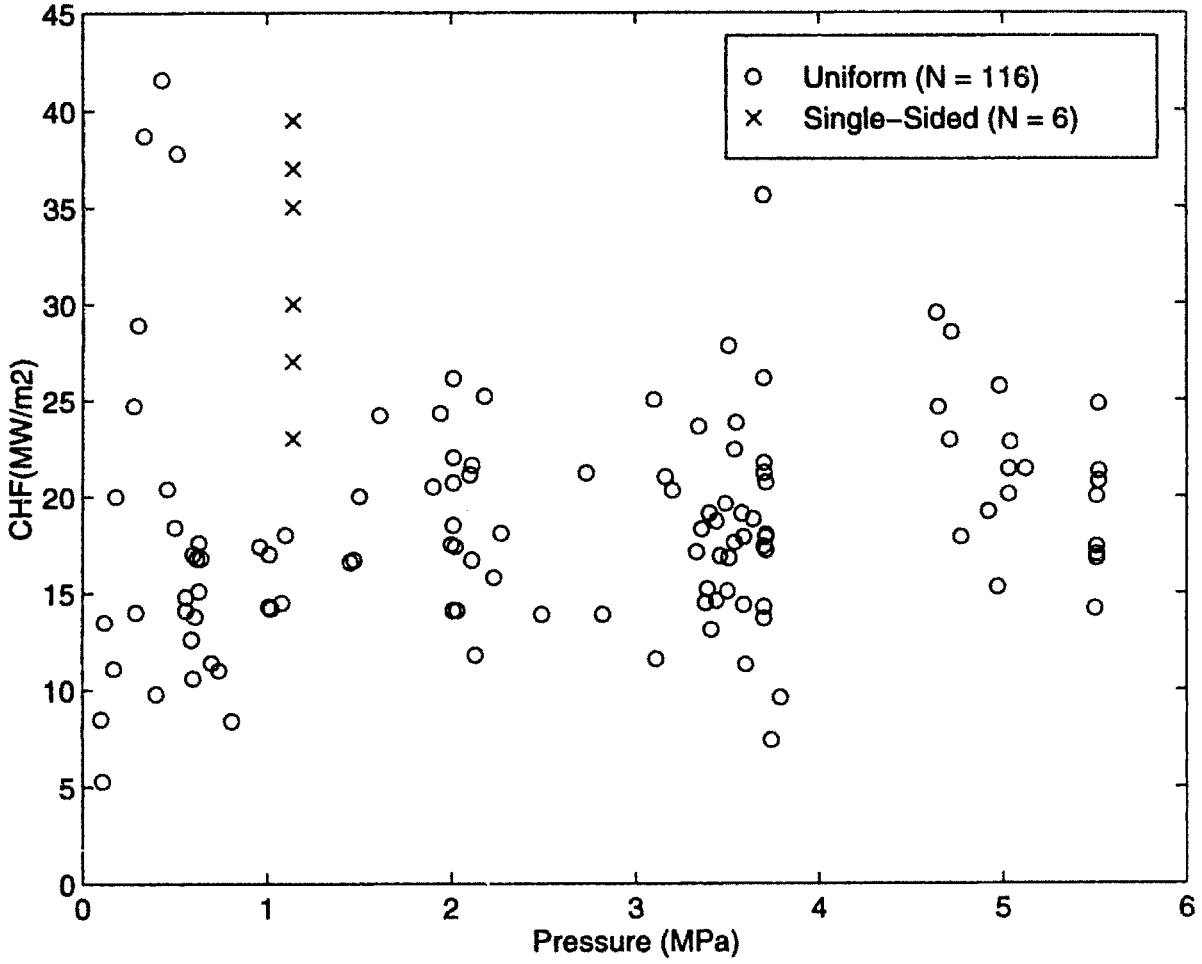

Figure 1-8: Database of Published, Smooth Flow, Heated Length less than 0.25 m, Critical Heat Flux Experiments With Respect to Coolant Pressure

in Figures 1-8 to 1-11. From Figures 1-8 and 1-9, it is apparently necessary to categorize the data further in terms of pressure and subcooling. This becomes obvious if the variation in water properties is to be taken into account. The rather narrow range of diameters (5 - 10 mm) and heated lengths (5 - 20 cm), on the other hand, do not so obviously affect the results and may unnecessarily prevent a meaningful comparison of data should the database be even further reduced.

The pressure is divided into five regions between 0.1 and 6.0 MPa and the bulk subcooling is divided into two divisions based on the exit equilibrium quality as shown in Table 1.6. The bulk subcooling is evaluated at the end of the heated length and is

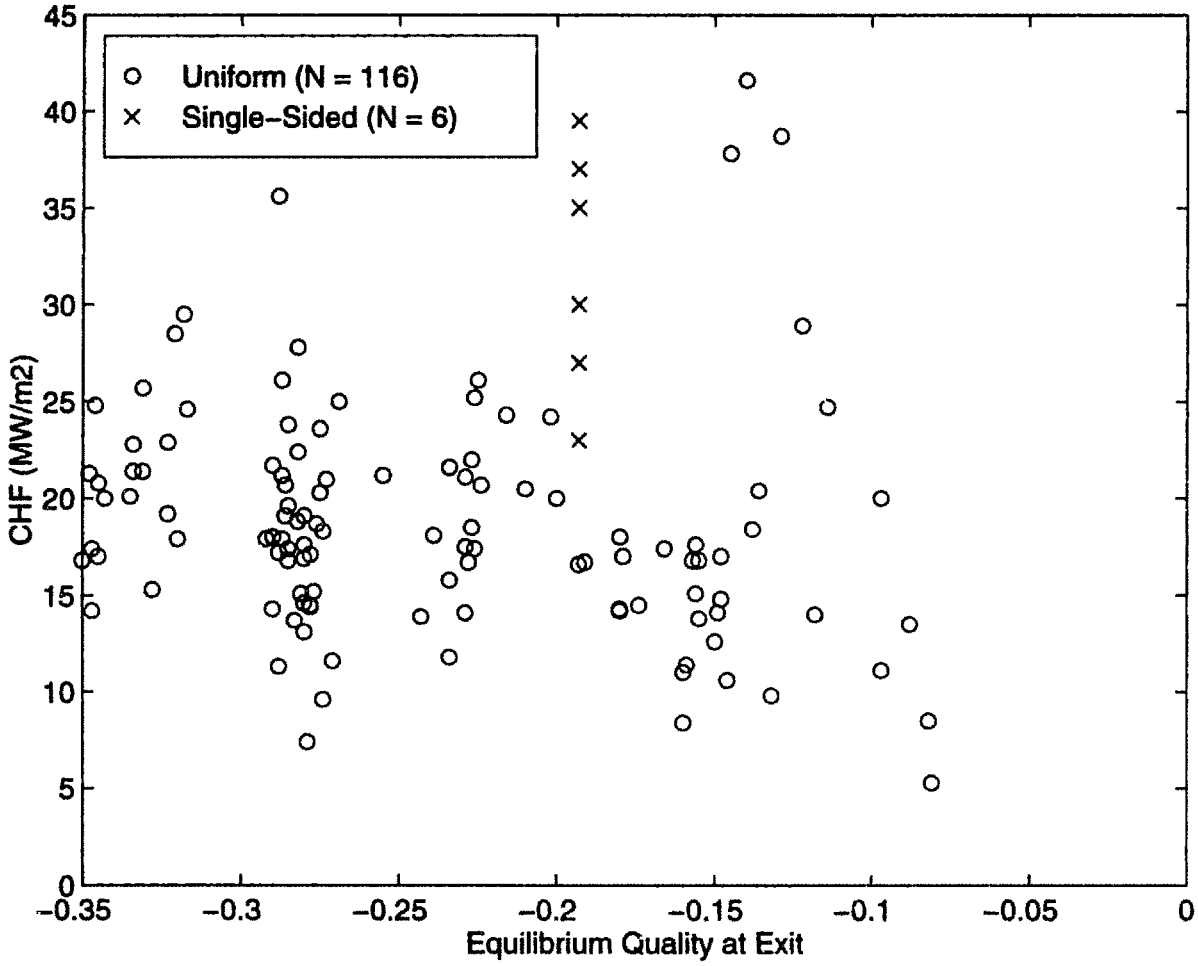

Figure 1-9: Database of Published, Smooth Flow, Heated Length less than 0.25 m, Critical Heat Flux Experiments With Respect to Exit Equilibrium Quality

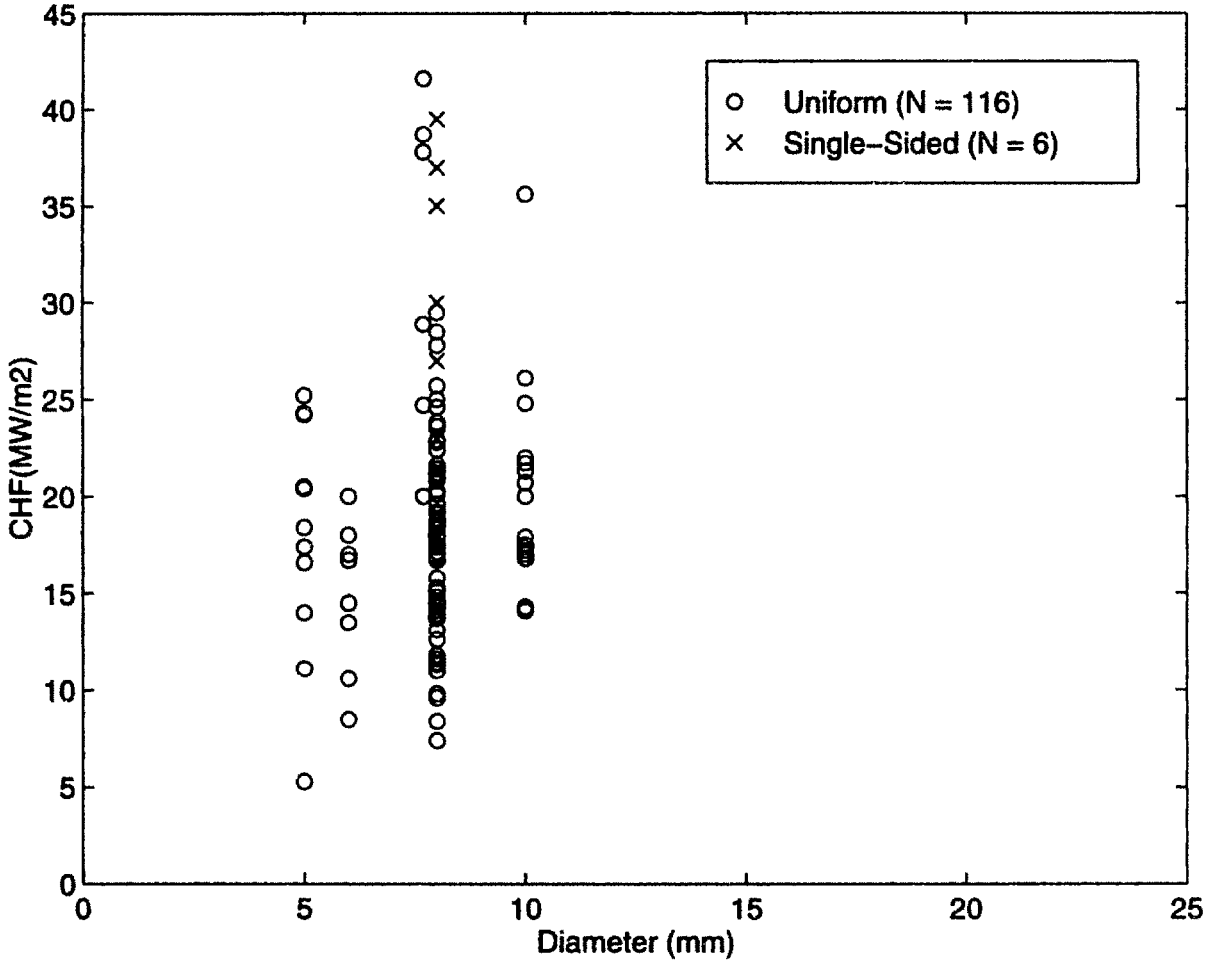

Figure 1-10: Database of Published, Smooth Flow, Heated Length less than 0.25 m, Critical Heat Flux Experiments With Respect to Coolant Channel Diameter

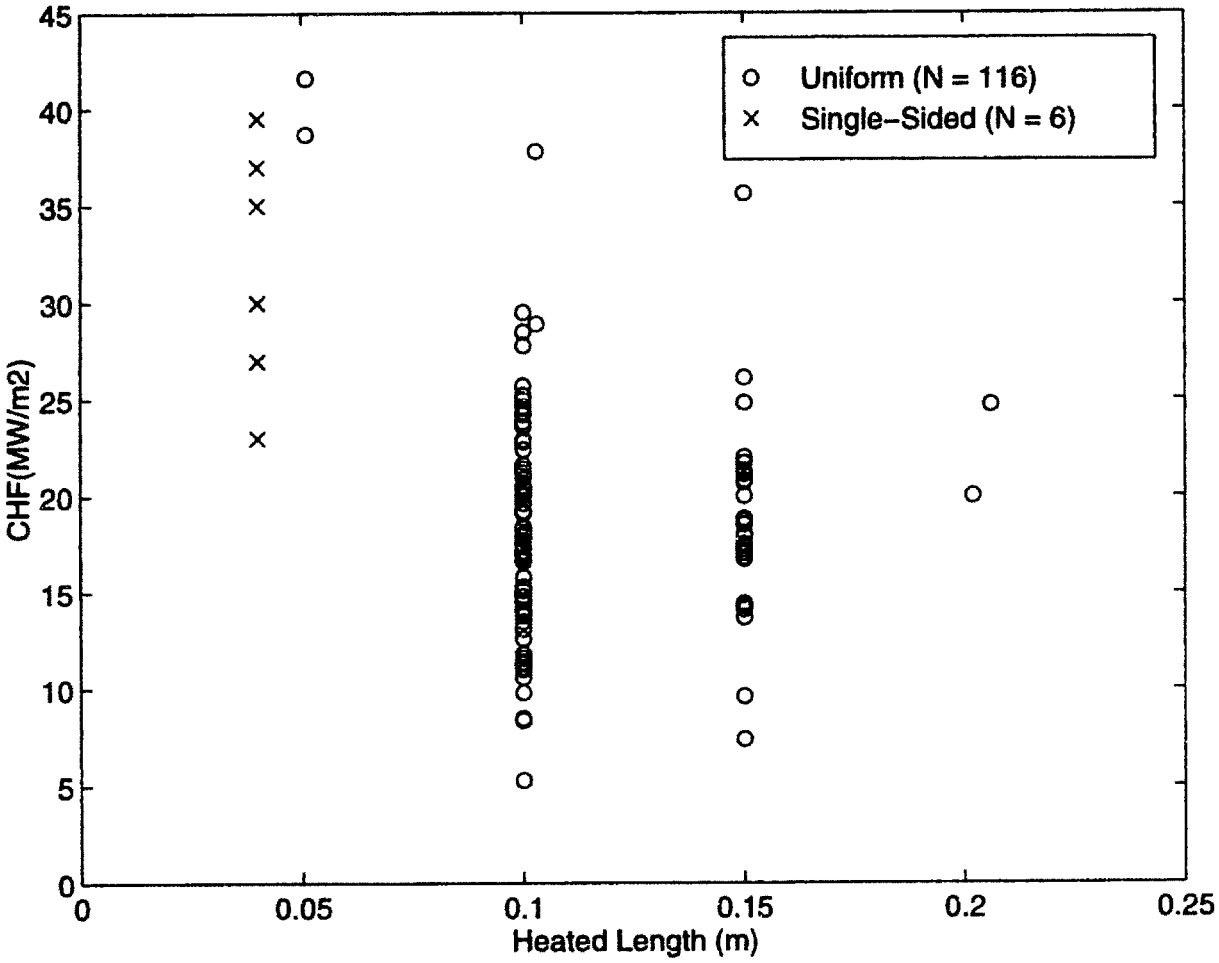

Figure 1-11: Database of Published, Smooth Flow, Heated Length less than 0.25 m, Critical Heat Flux Experiments With Respect to Axial Heated Length

Table 1.6: Number of Points in Published Database versus Coolant Exit Quality and Pressure

Pressure (MPa)	0.1 - 0.3	0.3 - 1.0	1.0 - 3.0	3.0 - 4.5	4.5 - 6.0
Equilibrium Quality at Exit					
-0.2 to 0.0	10	21	14	0	0
-0.35 to -0.2	0	0	21	39	20

quantified using the equilibrium quality. Much of the published literature report inlet bulk subcooling in absolute temperature differences, as illustrated in Tables 1.4 and 1.5. However, the affect of subcooling should also be influenced by the pressure and coolant properties. Therefore, the equilibrium quality is used in the present study as a measure of the degree of subcooling.

The above partitioning into windows of significant thermal hydraulic parameters results in small data sets as shown in Table 1.6. These data are plotted in Figures 1-12 to 1-17. Although still scattered, there now appear discernible patterns such as a marked difference between the single-sided circumferential heating and uniform heating in Figure 1-13 and a weak tendency for higher critical heat flux at higher bulk subcoolings (Note that the scales on Figures 1-12 to 1-17 are the same to facilitate comparison). On the other hand, the large scatter of data between mass fluxes of 5 to 10 Mg/m^2s in most of the figures (especially Figure 1-14) is evidence either of the difficulty of accurate measurements or a thermal hydraulic phenomenon not yet delineated.

Experiments at Sandia National Laboratory [7][25] have started to address critical heat flux questions for fusion applications. These experiments used an electron beam focused onto a coolant tube to emulate divertor thermal boundary conditions. Using water at 30 °C and pressurized to 1.14 MPa (i.e. 156 K inlet subcooling), critical heat flux values of 40 MW/m^2 were achieved in unobstructed flow as shown by the six x's in Figure 1-18. The addition of twisted tapes to enhance heat transfer led to a critical heat flux of 60 MW/m^2. Koski et al. [7] found good agreement between their nine experimental data points [25] and the 1975 Tong critical heat flux correlation [32]. This correlation was based on data points at very different conditions having much

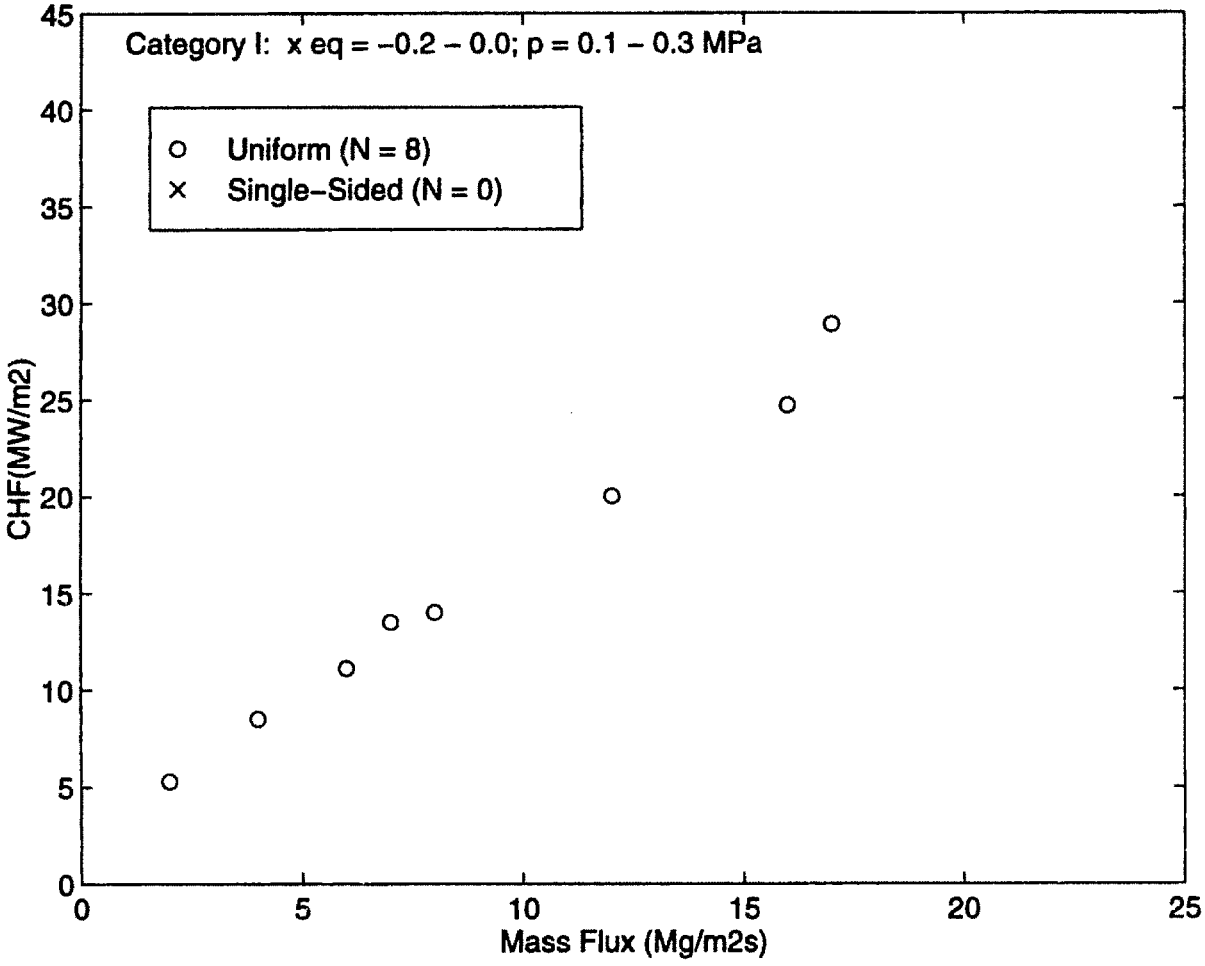

Figure 1-12: Database of Published, Smooth Flow, Heated Length less than 0.25 m, Critical Heat Flux Experiments in Category I

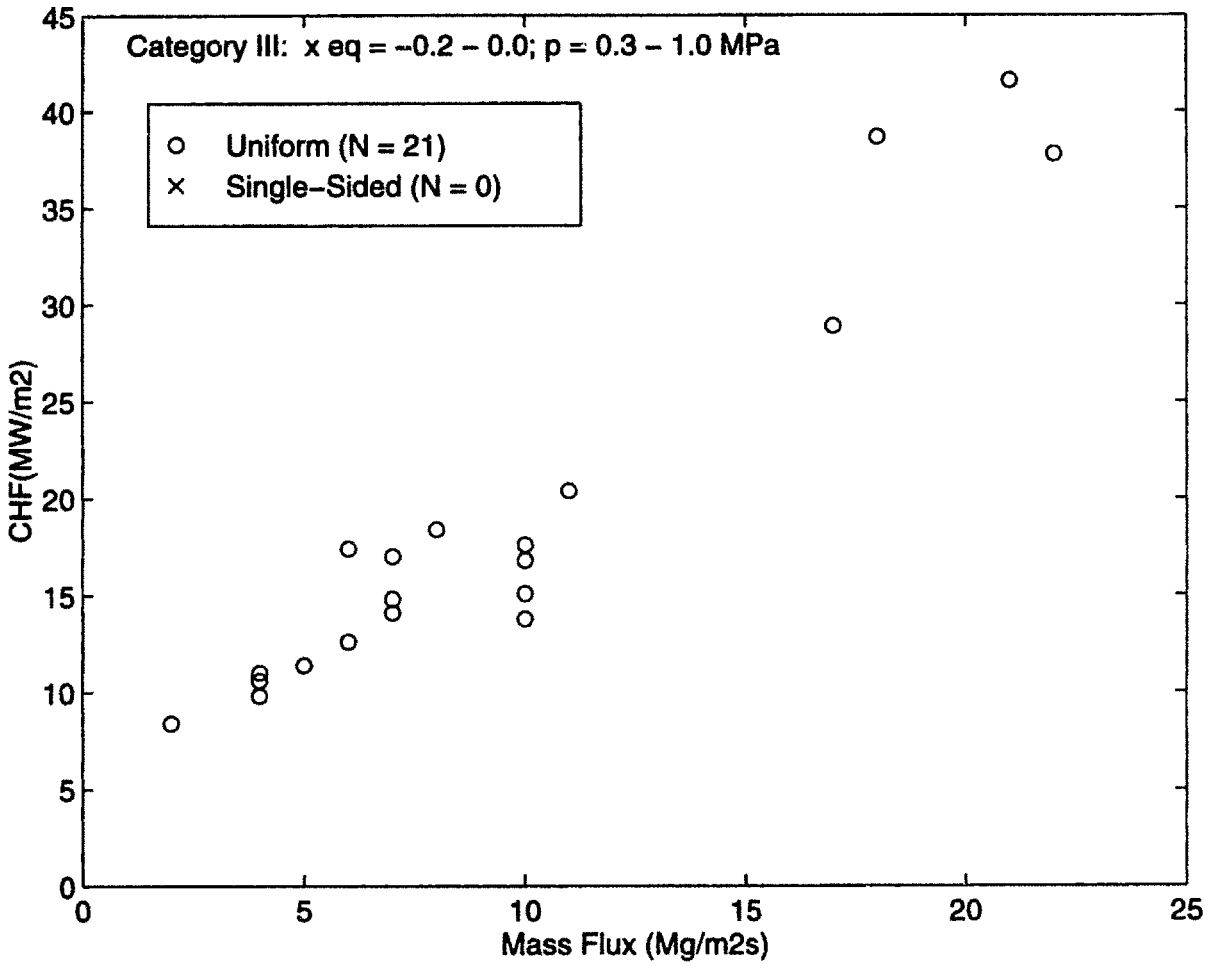

Figure 1-13: Database of Published, Smooth Flow, Heated Length less than 0.25 m, Critical Heat Flux Experiments in Category III

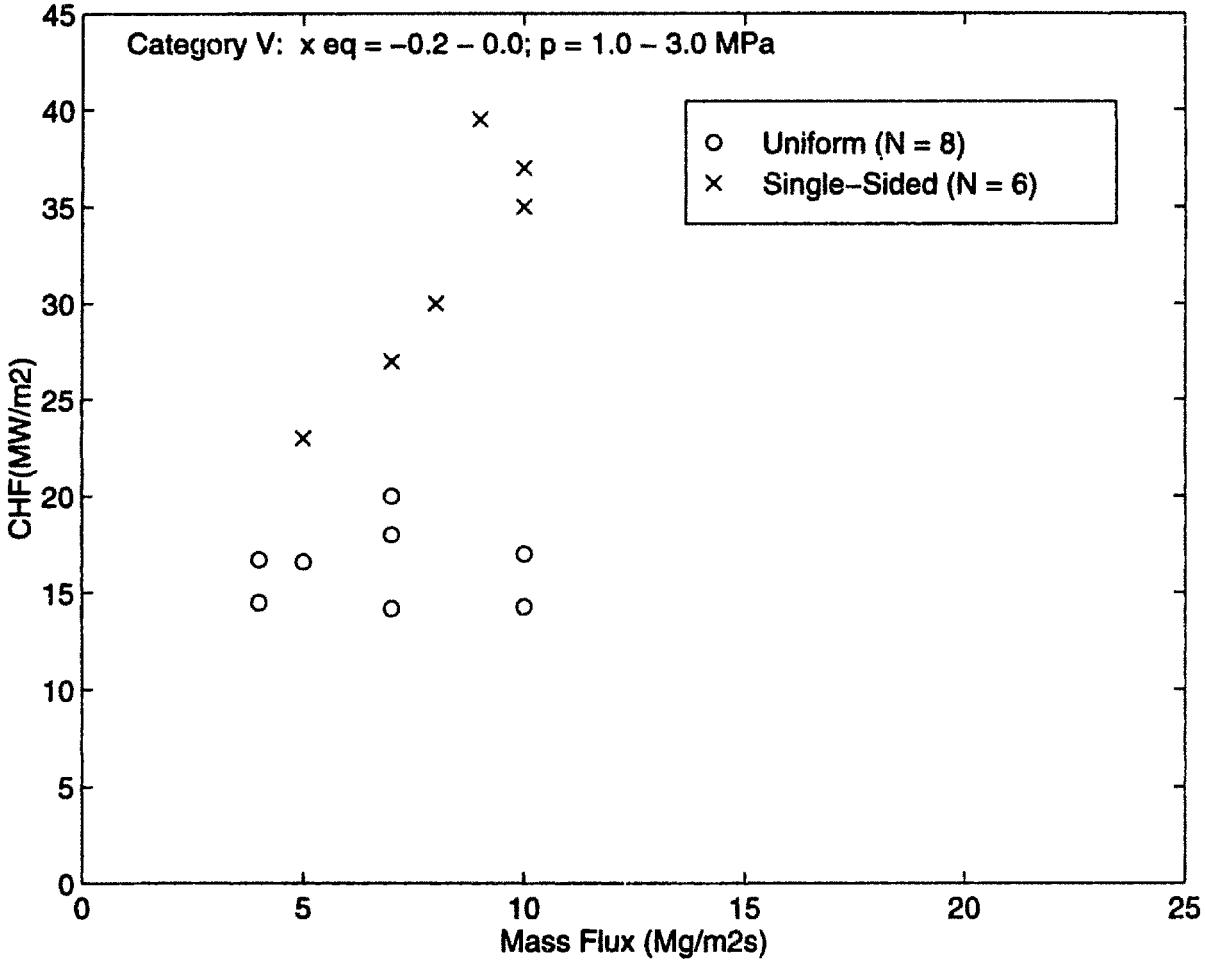

Figure 1-14: Database of Published, Smooth Flow, Heated Length less than 0.25 m, Critical Heat Flux Experiments in Category V

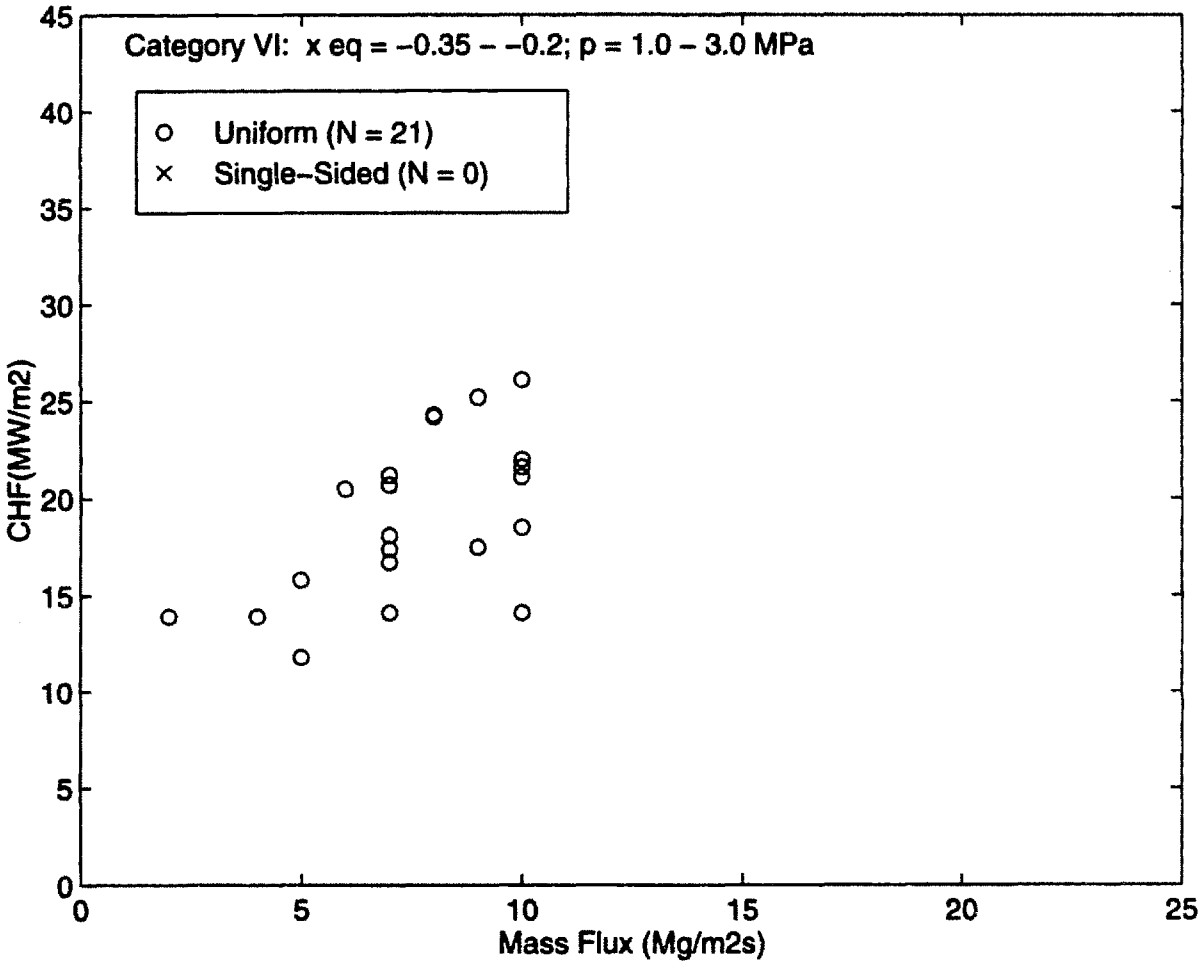

Figure 1-15: Database of Published, Smooth Flow, Heated Length less than 0.25 m, Critical Heat Flux Experiments in Category VI

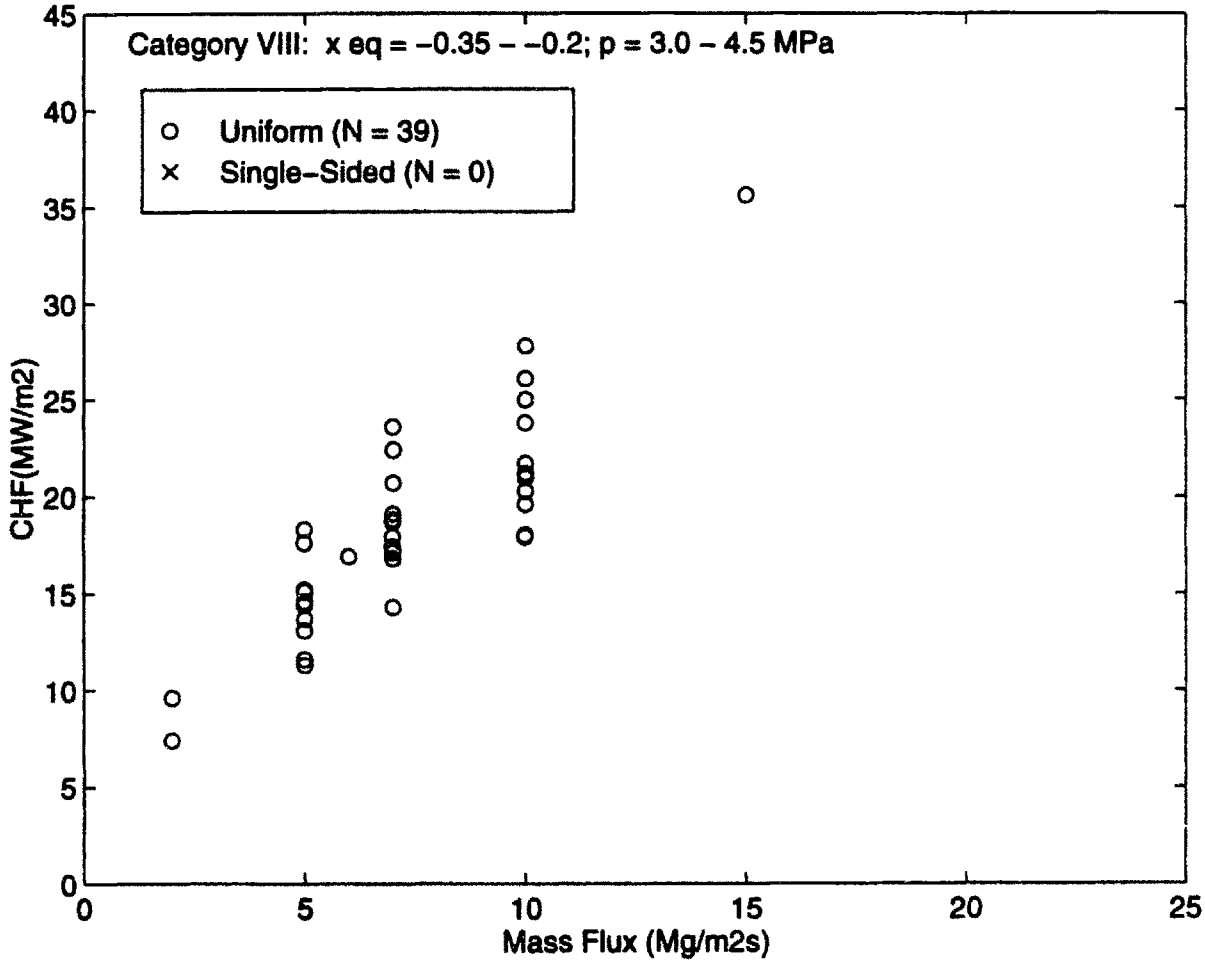

Figure 1-16: Database of Published, Smooth Flow, Heated Length less than 0.25 m, Critical Heat Flux Experiments in Category VIII

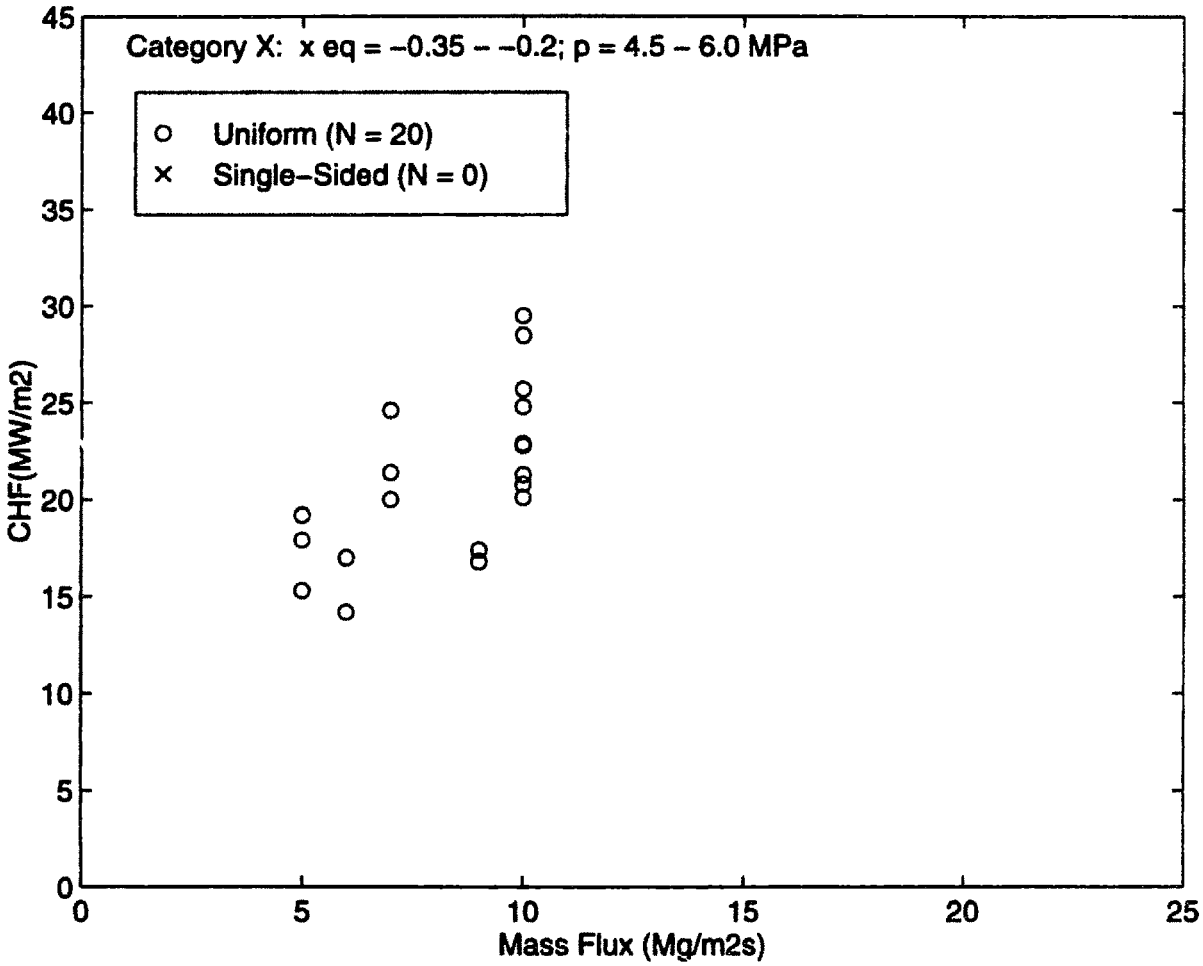

Figure 1-17: Database of Published, Smooth Flow, Heated Length less than 0.25 m, Critical Heat Flux Experiments in Category X

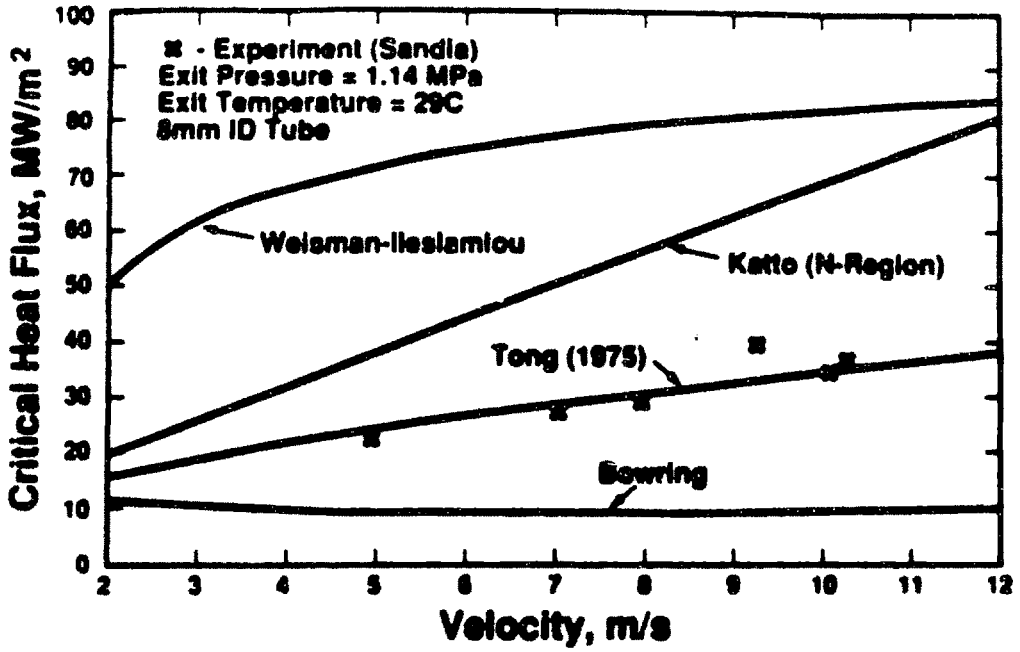

Figure 1-18: Comparison of Critical Heat Flux Correlations Extrapolated to Fit Sandia Results [7]

lower subcooling and higher pressure (relevant mostly to fission reactors). Therefore, Koski et al. [7] indicate that the choice of the Tong (1975) correlation is somewhat arbitrary and that the close comparison to their data as shown in Figure 1-18 may be fortuitous. The figure also shows poor comparison to other extrapolated correlations (Weisman-Ileslamlou [7], Katto [7], and Bowring [7]). Nevertheless, these studies provide important attempts to characterize fusion divertor relevant thermal-hydraulics.

Analysis of the extensive data base for large diameter (greater than 5 mm) coolant channels has indicated that very little data exists to validate characterization of the thermal hydraulic phenomena expected in a divertor. This characterization is integral to design procedure and the main motivation of the present experimental study.

Chapter 2 will expand on the current phenomenological understanding of limiting heat fluxes and detail the Tong (1975) correlation as well as several other correlations that will be used in subsequent chapters to aid in deciphering experimental data.

Chapter 2

Possible Heat Flux Limits

This section explores some limits associated with providing an acceptable thermal design in which highly subcooled nucleate boiling is used to remove the high heat flux at the strikepoint location on a divertor. Four major thermal limits musts be considered in judging design acceptability: the critical heat flux, flow excursion instability, the limiting plasma facing surface temperature, and the homogeneous nucleation limit. Each limitation will be discussed and illustrated in the following subsections.

Acceptable design margins must be adopted for each of the four limits and may lead to different safety factors depending on uncertainties of data, on uncertainties of calculations, and on the consequences of exceeding the limits.

Divertor design depends, to a large extent, on the ability to predict the heat transfer phenomena of the component. For the case of water as a coolant, the focus of this study, subcooled boiling is an attractive mechanism for cooling due to the large amount of energy associated with the phase change. However, operation in the subcooled boiling region may be precarious if an adequate safety margin from the critical heat flux is not available or if flow instabilities are not properly guarded against such that premature burnout may occur. At divertor thermal-hydraulic conditions (i.e., high heat flux and high subcooling), homogeneous nucleation may occur before nucleate boiling can develop on the wall. This may lead to unexpected burnout since the low bulk temperature and high velocity coolant can cause nucleate boiling to be suppressed which will invalidate the extrapolation of CHF correlations based on

bubble characteristics to very high heat fluxes.

2.1 Critical Heat Flux

The flow regimes in forced convection boiling are well characterized for uniform heat flux and moderate subcooling. Critical heat flux occurs when vapor generation at the hot wall prevents effective heat removal from the surface and the temperature of the surface material increases. This temperature increase can occur rapidly in cases with very high heat fluxes and the wall material strength is degraded or melted. The flow regime desirable in divertor applications is highly subcooled and high velocity flow. The bulk temperature of the coolant always remains well below saturation and, thus, bulk boiling never occurs. However, for very high heat fluxes, critical heat flux can be a limiting factor.

As illustrated in the previous chapter, the literature reports much about critical heat flux but only a few studies are within the parameter space of divertors (some of which are mentioned in Table 1.4). Experiments using the Sandia National Laboratory Electron Beam have started to address critical heat flux questions for fusion applications. These experiments use an electron beam focused onto a coolant tube to emulate divertor thermal boundary conditions. Using water at an inlet temperature of 30 °C and pressurized to 1.14 MPa (i.e., -0.3 equilibrium quality), critical heat flux values of 40 MW/m^2 were achieved in unobstructed flow. The addition of twisted tapes to enhance heat transfer lead to a critical heat flux of 60 MW/m^2. Koski et al. [25] found good agreement between their nine experimental data points (six are shown in Figure 1-18) and the 1975 Tong critical heat flux correlation (Tong-75 correlation) [32]:

$$q''_{CHF} = 8C_oC_1GH_{fg}(1 + 0.00216p_r^{1.8}Re_m^{0.5}Ja)(\frac{GD_h}{\mu_l})^{-0.6}(\frac{D_h}{D_o})^{0.32} \qquad (2.1)$$

where:

q''_{CHF} = Critical heat flux (W/m^2)

$C_oC_1 = 0.23$

Table 2.1: Range of Data in Tong-75 Critical Heat Flux Correlation

Channel Geometry	Heat Flux Distribution	p MPa	Void Fraction	G Mg/m^2s	Data Points
Circular Tube	Uniform	7-14	≤ 0.35	0.5-4.4	469
Annulus	Uniform	10.5-14	≤ 0.30	1.0-3.0	317
Rod Bundle	Non-uniform	7-18	≤ 0.61	0.5-4.3	201

G = Mass flux (kg/m^2s)

H_{fg} = Heat of vaporization (J/kg)

p_r = Reduced pressure (absolute pressure/critical pressure)

Re_m = Reynolds number ($G\frac{D_e}{\mu(1-\alpha)}$)

Ja = Jakob number $\frac{\rho_l C_{lp} \Delta T_{sub}}{H_{fg}\rho_v}$

D_h = Heated perimeter (m)

D_o = 0.0127 m (reference diameter)

This correlation was based on data at very different conditions having much lower subcooling and higher pressure (relevant mostly to fission reactors). The original data used by Tong [32] for the above correlation are shown in Table 2.1. The use of this correlation in the present study goes beyond the range listed in Table 2.1 and is extrapolated in pressure (from 7 to circa 3 MPa) and highly subcooled equilibrium qualities (circa -0.45). Therefore, Koski et al. [25] indicate that the choice of the Tong-75 correlation is somewhat arbitrary and that the close comparison to their data may be fortuitous. However, for the sake of illustration, the Tong-75 correlation [32] will be used to calculate critical heat flux. This prediction is shown in Figure 2-1 for the proposed ITER thermal hydraulic parameters given in Table 1.2 except without swirl flow for ease of comparison later in this chapter. Indeed, if critical heat flux were the only limit of concern, then the Tong-75 correlation indicates satisfactory performance if the design point heat flux is 15 MW/m^2 with a 10 m/s coolant velocity as suggested in the ITER Conceptual Design [33].

A contemporary correlation suggested by Inasaka and Nariai (1993) [34] intended to extrapolate the Tong (1968) critical heat flux correlation (Tong-68 correlation) [35] from the recommended pressure range of 7-14 MPa to 0.1-7 MPa. The Tong-68

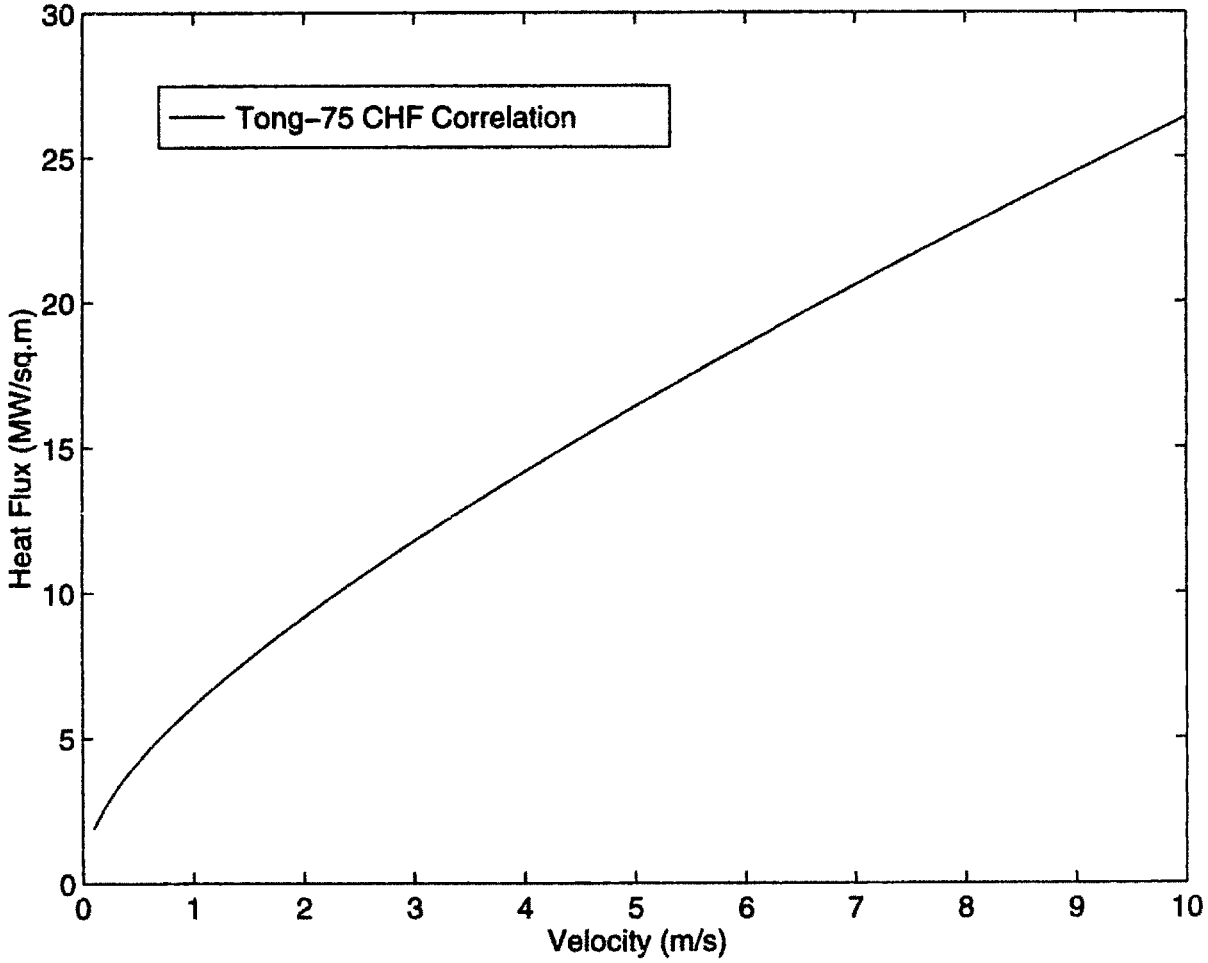

Figure 2-1: Predicted Critical Heat Flux using Tong-75 Correlation and ITER thermal hydraulic parameters (with unobstructed flow)

correlation is as follows:

$$q''_{CHF} = \frac{C_{Tong} H_{fg} G^{0.4} \mu^{0.6}}{D^{0.6}} \tag{2.2}$$

where:

q''_{CHF} = Critical heat flux (W/m^2)

C_{Tong} = 1.76 - 7.433 X_{ex} + 12.222 X_{ex}^2

H_{fg} = Heat of vaporization (J/kg)

G = Mass flux (kg/m^2s)

μ = Viscosity (kg/m s)

D = Diameter (m)

X_{ex} = Thermal equilibrium quality at tube exit = $\frac{C_{pl}(T_{sat} - T_{bulk}^{exit})}{H_{fg}}$

Inasaka and Nariai modified C_{Tong} for the pressure range 0.1-7 MPa as follows:

$$C_{Tong}(modified) = C_{Tong}(1 - 52.3 + 80X_{ex} - 50X_{ex}^2/60.5 + (p \times 10^{-5})^{1.4}) \tag{2.3}$$

where:

p = Pressure (Pa)

However, it should be noted that Inasaka and Nariai [34] have apparently used X_{ex} above -0.20 and an inner tube diameter of only 3 mm to determine the above fit. In subsequent chapters, these parameters will be shown to reduce the applicability of the modified Tong-68 correlation in predicting critical heat flux values especially in the range pertinent to large diameter and highly subcooled thermal hydraulic conditions.

Celata et al. (1994) [36] recently developed a mechanistic model to predict CHF based on dryout of a thin liquid layer beneath an intermittent vapor blanket formed by the coalescence of small bubbles. The model is described in [36] and tested on an extensive data base. Agreement with 1888 data points (from various sources) was typically within 30 percent, however, the minimum exit quality of their data base was above -0.35. The model will be discussed in Chapter 6 when applied to the experimental conditions of the present study. Further discussion of this model will

be postponed until Chapter 6.

2.2 Flow Instabilities

Forced convection instabilities, known as Ledinegg or excursion instabilities, may occur if the two-phase pressure drop in a coolant channel increases with decreasing flow rate. The statement "increases with decreasing flow rate" refers to the pressure drop obtained in steady state with constant heat input, constant inlet temperature, and varying flow rate. The instabilities refer to operating conditions in which the flow channel is forced to keep a constant pressure difference (inlet-to-outlet) with a change in the channel flow rate. This operating condition is expected when coolant tubes are arranged in parallel such as in a fusion divertor situation.

Some features related to the Ledinegg instability phenomenon are illustrated in Figure 2-2 [37]. A single demand curve, the dark S-shaped curve extending from the origin of the figure to the top right of the figure, gives pressure drop demand versus flow for the channel. The horizontal supply curve indicates three possible operating points, with the left and right points stable and the center point unstable. The center point can be demonstrated to be unstable by noting that a decrease in flow causes an increase in channel pressure drop demand but no increase in pressure drop supply; the flow tends to decrease even further giving a flow excursion. The flow excursion can terminate at the left point (low flow point) but often leads to adverse thermal conditions and to critical heat flux prior to reaching the left point.

The center point is useful for discussion purposes but cannot be reached in an actual operating channel. A more important point is the minimum on the demand curve (point A in Figure 2-2) which can potentially be reached during operation, e.g., due to a change in the supply curve. If the minimum point is reached and if the channel is then subjected to a slight change in operating conditions, a large flow excursion and subsequent critical heat flux could occur. What is important from a thermal margin standpoint is that the impending failure may be completely unexpected from evaluation of critical heat flux conditions at the minimum point.

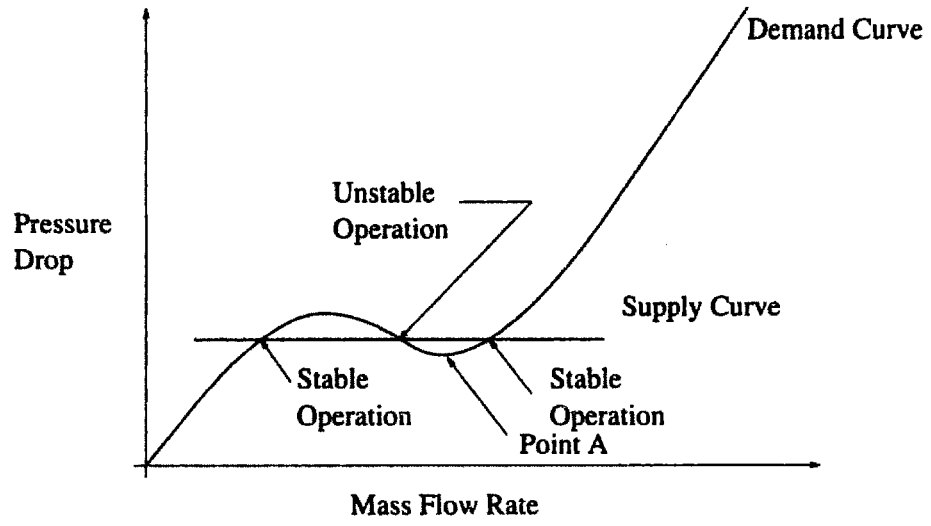

Figure 2-2: Illustration of excursive flow instabilities in a coolant channel

The onset of flow instability (OFI) can be defined as the point at which the demand pressure drop versus flow rate curve reaches a minimum. Dougherty et al. (1991) [38] remark that this point must be preceded by the onset of significant voids (OSV) which can, therefore, be used as a conservative estimate of OFI. Physically, OSV corresponds to conditions at which the vapor being produced in subcooled boiling begins to be located away from the boiling surface (bubble departure). Large increases in vapor friction occur beyond this point.

The well known Saha-Zuber correlation [39] for bubble departure considers two regions: hydrodynamically-controlled and thermally-controlled bubble departure. These regions are distinguished using the Peclet number. The bubble departure (BD) is determined using the Nusselt or Stanton numbers as follows:

$$Pe = \frac{GD_eC_{pl}}{k_l} \tag{2.4}$$

$$Nu = \frac{q''D_h}{k_l(T_{sat} - T_{bulk})} \tag{2.5}$$

$$St = \frac{q''}{GC_{pl}(T_{sat} - T_{bulk})} \tag{2.6}$$

where:

Nu = Nusselt number

St = Stanton number

G = Coolant mass flux (kg/m^{2}s)

D_e = Equivalent (or hydraulic) diameter (m)

D_h = Heated diameter (m)

C_{pl} = Liquid Specific heat (J/kg K)

k_l = Liquid conductivity (W/m K)

q'' = Local heat flux (W/m^2)

T_{sat} = Saturation temperature (^{o}C)

T_{bulk} = Exit bulk temperature (^{o}C)

For Pe $\leq$ 70,000, bubble departure is thermally-controlled and occurs when:

$Nu_{BD} \geq 455$

For Pe $\geq$ 70,000, bubble departure is hydrodynamically-controlled and occurs when:

$St_{BD} \geq 0.0065$

The data used by Saha and Zuber [39] for the above correlation are shown in Table 2.2. The use of this correlation in the present study goes beyond the range listed in Table 2.2 and is extrapolated in mass flux (from 2.76 to circa 10 Mg/m^{2}s) and heat flux (from 1.89 to circa 20 MW/m^2).

The Saha-Zuber correlation uses the local bulk temperature; however, Dougherty et al. [38] suggest using the exit bulk temperature as a conservative modification. For

Table 2.2: Range of Parameters Used by Saha and Zuber (1974) for Bubble Departure Correlation

	Pressure MPa	Mass Flux Mg/m^{2}s	Heat Flux MW/m^2
Water Only	0.1-13.8	0.095-2.76	0.28-1.89

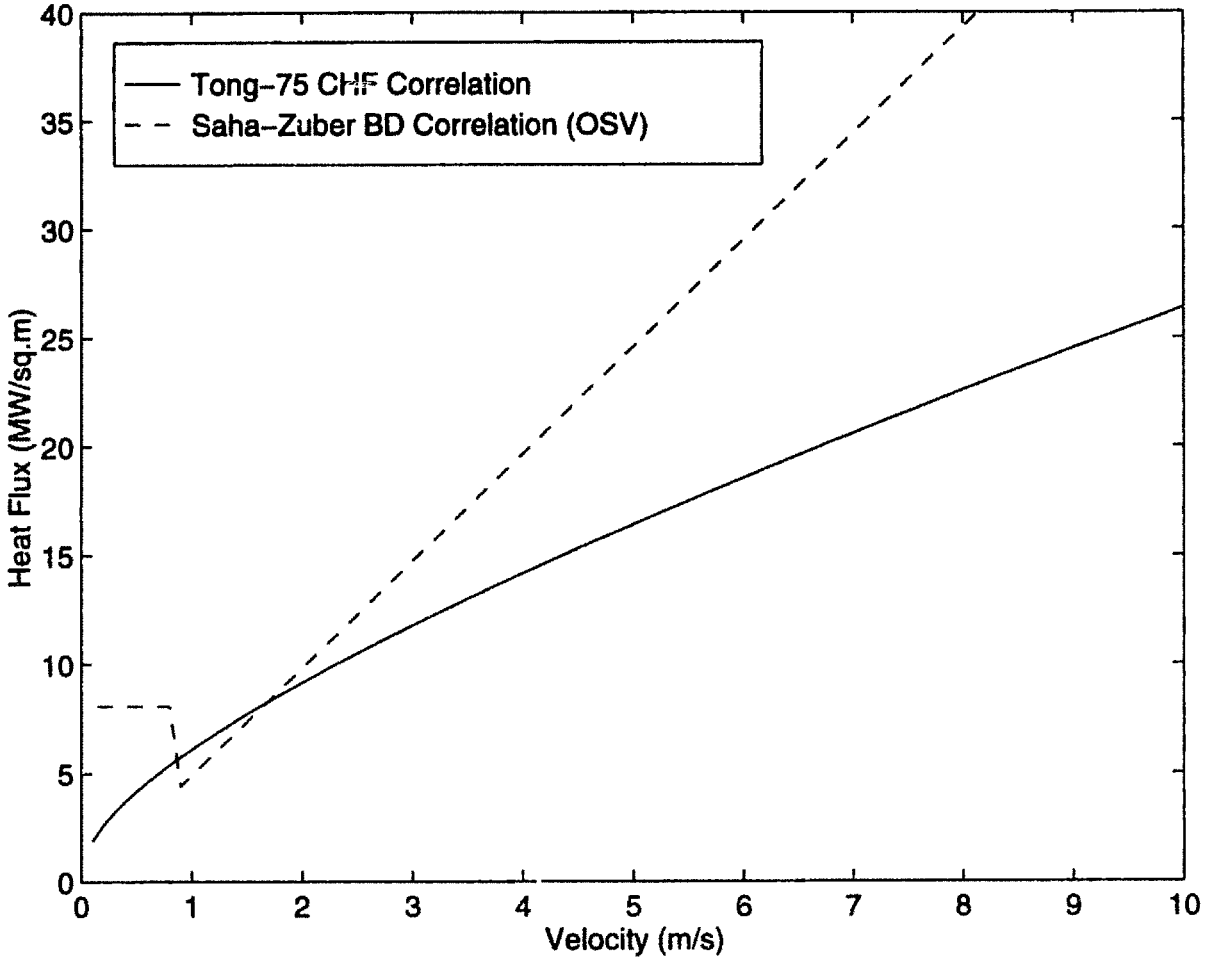

Figure 2-3: Predicted Flow Excursion and Critical Heat Flux Limits for ITER Operation

Peclet numbers greater than 70,000, the Stanton number criterion for OSV is 0.0065. Figure 2-3 illustrates this possible mode of failure for the ITER parameters given in Table 1.2 (except with unobstructed flow) and levels of flow velocity. As indicated for coolant velocities less than 2 m/s (such as a loss-of-flow accident), flow instabilities could produce burnout due to flow excursion before the expected critical heat flux limit is reached. In the present study, the local heat flux, q'', is used although the above correlation assumes a uniform azimuthal heat flux.

There are three considerations which could ameliorate the flow instability concern. First, at higher pressures (above 2 MPa) the bubbles produced are less voluminous

because they are of higher density. The violent bubble expansions which are observed at lower pressures are effectively suppressed and the slope of the demand curve flattens out. Second, use of larger diameter channels would lessen the effectiveness of bubble obstruction and also flatten out the demand curve slope. Finally, orificing the coolant channel inlets would produce large pressure drops which will lessen the relative effect of the pressure drop due to vapor generation (although at a cost of increased pumping power).

2.3 Temperature Limitations on Materials

Another important design consideration is the temperature limitations of the divertor materials. This limit can be shown as significant for defining the operational window for divertor channels. For example, it is straightforward to calculate the temperature difference for a divertor consisting of a circular tube coated evenly with an armor material assuming azimuthal symmetry. (Note: to illustrate the surface temperature limitation, uniform heating will be assumed. This assumption will be removed later in the present study when a three-dimensional conduction code, HEATING7.2, is introduced in Chapter 4.) The total temperature difference from the divertor surface to the bulk temperature of the coolant is the sum of the conduction solution and a convection correlation as follows:

$$\Delta T_{tot} = (T^{PF}_{surface} - T^{Coolant}_{wall}) + (T^{Coolant}_{wall} - T_{bulk}) \tag{2.7}$$

$$\Delta T_{tot} = \left[\frac{r_1 ln(\frac{r_2}{r_1})}{k_1} + \frac{r_1^2 ln(\frac{r_3}{r_2})}{r_2 k_2}\right] q_1'' + \frac{q_1''}{h} \tag{2.8}$$

where:

ΔT_{tot} = Total temperature drop between surface and coolant bulk (K)

$T^{PF}_{surface}$ = Temperature of plasma facing surface (^{o}C)

$T^{Coolant}_{wall}$ = Temperature of coolant-side wall (^{o}C)

T_{bulk} = Bulk coolant temperature (^{o}C)

r_1 = Inner wall radius (m)

r_2 = Radius to interface between coolant tube and armor (m)

r_3 = Outer radius of channel (m)

k_1 = Coolant tube thermal conductivity (W/m-K)

k_2 = Armor conductivity (W/m-K)

q_1'' = Peak heat flux on coolant-side wall (W/m^2)

h = Convective heat transfer coefficient (W/m^2K)

Equation 2.8 will estimate the peak divertor temperature if geometry and materials are defined and sufficient information is given to calculate the convective heat transfer coefficient. For illustration, the ITER thermal-hydraulic parameters mentioned in the previous chapter (Table 1.2) will be applied to a 15 mm diameter copper alloy tube of 1.5 mm thickness which is coated with 20 mm of graphite armor (representative of a candidate divertor [3]). The specifications call for a twisted tape (twist ratio, $Y = 2$, diameters per 180^o twist) insert to enhance convective heat transfer. Lopina and Bergles (1967) [40] studied pressure drop and axisymmetric heat transfer in tape generated swirl flow. They concluded that swirl flow heat transfer was due primarily to three mechanisms: turbulent forced convection, centrifugal convection, and the fin effect of the tape. The fin effect of the tape will be neglected since this effect is expected to be small and is dependent on the tape size and contact to the tube (parameters not defined herein). The total heat transfer coefficient for this swirl flow illustration is, therefore, the sum of the single-phase turbulent forced convection, h_{sp}, and the centrifugal convection, h_{cc} terms:

$$h_{swirl} = h_{sp} + h_{cc} \tag{2.9}$$

The following subsections will introduce various heat transfer correlations: a single-phase turbulent forced convection correlation; a centrifugal convection correlation; two subcooled nucleate boiling correlations; and a suppression of nucleate boiling correlation, respectively, before returning to the illustration at hand.

2.3.1 Single-Phase Turbulent Forced Convection Heat Transfer Correlation

The Petukhov single-phase liquid convection correlation described by Boyd and Meng (1992) [41] will be assumed as a reliable turbulent forced convection heat transfer correlation and is defined as follows:

$$h_{sp} = \frac{\frac{k}{D}(\frac{f}{8})Pe}{K_1(f) + K_2(Pr)(\frac{f}{8})^{1/2}(Pr^{2/3} - 1)} \tag{2.10}$$

where:

h_{sp} = Single-phase heat transfer coefficient (W/m^{2}K)

k = Thermal conductivity (W/m K)

D = Diameter (m)

f = (1.82 log Re - 1.64)$^{-2}$

Pe = Peclet number = $RePr$ = G D C_p/k

Pr = Prandlt number = μ C_{pl}/k_l

G = Mass flux (kg/m^{2}s)

C_p = Specific heat at constant pressure (J/kgK)

$K_1(f) = 1 + 3.4f$

$K_2(Pr) = 11.7 + 1.8Pr^{-1/3}$

$10^4 \leq$ Re $\leq$ 5.0 x 10^6

$0.5 \leq Pr \leq 200.0$

Note: all coolant properties are evaluated at the film temperature, T_f [41]:

$$T_f = \frac{T_{wall} + T_{bulk}}{2} \tag{2.11}$$

2.3.2 Centrifugal Convection Correlation

Lopina and Bergles (1967) [40] theorized that the centrifugal convection effect is due to low density warmer fluid at the tube wall being continuously forced into the cooler main flow as a result of a high centrifugal body force acting on the fluid

particles. They recommend using a modification of an equation given by Fishenden and Saunders that predicted the heat transfer coefficient for a horizontal hot plate facing up under normal gravity. In place of gravitational acceleration, Lopina and Bergles [40] base the Grashof number, Gr, on the centrifugal acceleration using the following formula:

$$Gr = \frac{4.94}{Y^2} Re_e^2 \frac{D_e}{D_i} \beta (T_w - T_{bulk}) \tag{2.12}$$

where:

Y = Twist ratio (diameters per 180^o twist)

Re_e = Reynolds number based on D_e

D_e = Equivalent (or hydraulic) diameter (m)

D_i = Inner diameter (m)

β = Fluid coefficient of thermal expansion (K^{-1})

T_w = Coolant-side wall temperature (^{o}C)

T_{bulk} = Coolant bulk temperature (^{o}C)

For flow with twisted tape inserts:

$$\frac{D_e}{D_i} = \frac{1 - \frac{4\delta f}{\pi D_i}}{1 + \frac{2}{\pi}(1 - \frac{\delta f}{D_i})} \tag{2.13}$$

where:

δf = thickness of twisted tape insert (m)

The centrifugal convection heat transfer coefficient is then given by:

$$h_{cc} = 0.114 (GrPr)^{1/3} \frac{k}{D_e} \tag{2.14}$$

where:

h_{cc} = Centrifugal convection contribution to Equation 2.9.

2.3.3 Subcooled Nucleate Boiling Correlation

Thus far, no vapor generation has been assumed in this section and the use of twisted tapes in the previous subsection effectively prevented entrance into the boiling region. However, subcooled boiling is itself a mode of enhanced heat transfer and the following subsections will introduce several correlations to analyze boiling heat transfer which will be used throughout the present study.

Yin et al. (1993) [42] developed a subcooled boiling heat transfer correlation based on the observation that for high heat fluxes ($\geq$ 10 MW/m^2), larger than previously predicted wall superheatings are measured.

In particular, the Bergles and Rohsenow (1964) method for the prediction of the onset of nucleate boiling [43] appeared to produce a marked underprediction of the wall superheat when extrapolated to high heat fluxes, according to the data of Yin et al. [44]. New correlations were developed by Yin et al. [42] [44] for high heat flux, subcooled boiling as described below.

For the Onset of Subcooled Nucleate Boiling (ONB) in smooth flow, Yin et al. [44] propose the following equation:

$$(\Delta T_{sat})_{ONB} = \left(\frac{1800 q''_{ONB} \sigma T_{sat}}{H_{fg} \rho_g k_f}\right)^{1/2} \tag{2.15}$$

where:

$(\Delta T_{sat})_{ONB} = T_w^{ONB} - T_{sat}$ (K)

T_w^{ONB} = Wall temperature at the Onset of Nucleate Boiling (K)

q''_{ONB} = Heat flux at the Onset of Nucleate Boiling location (W/m^2)

T_{sat} = Saturation temperature (K)

σ = Surface tension (N/m)

H_{fg} = Heat of vaporization (J/kg)

ρ_g = Vapor density (kg/m^3)

k_f = Liquid thermal conductivity (W/m K)

After ONB, Yin et al. [42] calculate the wall superheat in the subcooled nucleate boiling region using the following equation:

Table 2.3: Range of Parameters Used by Yin et al. (1993) for Subcooled Boiling Heat Transfer Correlation

Pressure MPa	Mass Flux Mg/m^2s	Inlet Subcooling K	Heat Flux MW/m^2	Heated Length m
2.0-10.3	5.0-15.0	92-212	up to 16.0	0.35

$$\Delta T_{sat} = 7.195 q'' \gamma(z)^{1.82} p^{-0.072} \tag{2.16}$$

where:

$\Delta T_{sat} = T_w - T_{sat}$ (K)

q'' = Heat flux at the coolant wall (MW/m^2)

$\gamma(z)$ = Fraction of total heated length. Allowed to vary from 0.7 to 1.0 (but set to 1.0 for the present study).

p = Pressure (MPa)

The data used by Yin et al. [42] for the above correlation are shown in Table 2.3. The use of this correlation in the present study extends beyond the range listed in Table 2.3 and is extrapolated in heat flux (from 16.0 to circa 20 MW/m^2). Also, Yin et al. [42] used a heated length of 0.35 m which is longer than the spiked heat flux criterion of the conditions in the present study which assumes a length of 0.05 m. This may have ramifications on the thermal boundary layer which is assumed to be under-developed at the divertor strikepoints. In addition, Yin et al. [42] used a 3.6 mm inner diameter tube which is classified as small diameter ($\leq$ 5 mm) pipe flow in the present study.

Equation 2.15 predicts very high wall superheats before the onset of nucleate boiling. For example, for a heat flux of 10 MW/m^2 and the proposed ITER thermal hydraulic conditions in Table 1.2, the superheat calculated by Equation 2.15 will be 133 K. This would put the coolant-side wall temperature at 50 K above the homogeneous nucleation temperature at (3.5 MPa) before the onset of vapor formation at the wall. The small to large diameter effects could explain such a large prediction of temperature for the 15 mm inner diameter tube specified in Table 1.2.

Table 2.4: Range of Parameters of All Fluids and Water in Shah (1977) Subcooled Nucleate Boiling Correlation

	D mm	p MPa	ΔT_{sub} K	q" MW/m^2	G Mg/m^{2}s
All Fluids	2.4-27.1	0.1-13.8	0-153	0.01-22.9	0.056-24
Water Only	2.4-27.1	0.1-13.8	0-153	0.02-18.4	0.056-8.14

On the other hand, if Equation 2.15 is not considered and Equation 2.16 were employed for nucleate boiling regardless of the prediction of the onset of nucleate boiling, a wall superheat of 66 K would be calculated. Although this example results in a high wall superheat, the superheat remains below a physical limit: the homogeneous nucleation temperature.

The following sections will introduce the Shah 1977 [45] subcooled nucleate boiling correlation and the Chen (1963) [46] suppressed nucleate boiling correlation. Neither the Shah (1977) nor Chen (1963) correlations require the prediction of the onset of nucleate boiling and are, therefore, more suitable for the calculations made in the present study. In other words, there is a smooth transition from the single-phase forced convection heat transfer coefficient to the nucleate boiling heat transfer coefficient.

Shah (1977) [45] endeavored to develop a general correlation to predict heat transfer coefficients during partial and fully developed subcooled boiling with an accuracy comparable to that of single phase correlations (about $\pm$ 30 percent). Shah used several fluids including water, freon, ammonia, and alcohols to develop a data base of about 500 data points. Thus, a wide range in parameters are covered in [45] as shown in Table 2.4. The use of this correlation in the present study extends somewhat beyond the range listed in Table 2.4 for water and is extrapolated in subcooling (from 153 to circa 200 K subcooling); heat flux (from 18.4 to circa 20 MW/m^2); and mass flux (from 8.14 to circa 10 Mg/m^{2}s).

The Shah (1977) [45] correlation was chosen for the present study because it specifically addressed subcooled nucleate boiling and categorized the subcooled region into a low and high subcooling region. These regions are demarked using a nondimensional

temperature parameter, ΔT^*, defined as follows:

$$\Delta T^*(\theta, z) = \frac{\Delta T_{sub}}{\Delta T_{sat}} = \frac{T_{sat} - T_{bulk}(z)}{T_{wall}(\theta, z) - T_{sat}} \tag{2.17}$$

where:

T_{sat} = Saturation temperature at the existing pressure (^{o}C)

$T_{bulk}(z)$ = Bulk coolant temperature (^{o}C)

$T_{wall}(\theta, z)$ = Wall temperature (^{o}C)

Shah's data base shows a clear demarcation of boiling phenomena at $\Delta T^* = 2$ in a nondimensional heat flux parameter $\psi(\theta, z)$. $\psi(\theta, z)$ is defined by Shah [45] as:

$$\psi(\theta, z) = \frac{q''(\theta, z)}{\Delta T_{sat} h_{lo}} \tag{2.18}$$

where:

$q''(\theta, z)$ = Local heat flux (W/m^2)

$\Delta T_{sat} = T_{wall}(\theta, z) - T_{sat}$

h_{lo} = Heat transfer coefficient for all mass flowing as liquid without any boiling (W/m^2K)

h_{lo} for the present study is calculated using the Petukhov correlation, Equation 2.10. Other important nondimensional parameters from Shah [45] are the Boiling number and $\psi_o(\theta, z)$, defined as follows:

$$Bo(\theta, z) = \frac{q''(\theta, z)}{G H_{fg}} \tag{2.19}$$

where:

$Bo(\theta, z)$ = Boiling number

$q''(\theta, z)$ = Local heat flux (W/m^2)

G = Mass flux (kg/m^{2}s)

H_{fg} = Heat of Vaporization (J/kg)

If $Bo(\theta, z) \leq 0.3 \times 10^{-4}$ then $\psi_o(\theta, z) = 1 + 46\ Bo(\theta, z)^{1/2}$

If $Bo(\theta, z) \geq 0.3 \times 10^{-4}$ then $\psi_o(\theta, z) = 230\ Bo(\theta, z)^{1/2}$

In the low subcooling region ($\Delta T^* \leq 2$), the heat transfer coefficient is calculated

using the following expression:

$$h(\theta,z) = h_{lo}\psi_o(\theta,z)\frac{T_{wall}(\theta,z) - T_{sat}}{T_{wall}(\theta,z) - T_{bulk}(z)} \tag{2.20}$$

Otherwise (for $\Delta T^* \geq 2$), the heat transfer coefficient is calculated using the following expression:

$$h(\theta,z) = \frac{h_{lo}(T_{wall}(\theta,z) - T_{bulk}(z)) + h_{lo}(\psi_o(\theta,z) - 1)(T_{wall}(\theta,z) - T_{sat})}{T_{wall}(\theta,z) - T_{bulk}(z)} \tag{2.21}$$

where the above variables are defined in the previous equations.

In the low subcooling region ($\Delta T^* \leq 2$), the $\psi_o(\theta,z)\frac{T_{wall}(\theta,z) - T_{sat}}{T_{wall}(\theta,z) - T_{bulk}(z)}$ term can fall below 1.0 for low Bo and relatively high subcooling. Thus, Equation 2.20 predicts extremely high wall temperatures which, for low mass fluxes, are unrealistic. The following subsection presents the Chen correlation for suppressed nucleate boiling which will be used in the low subcooling region.

2.3.4 Suppressed Nucleate Boiling Correlation

Chen (1963) [46] developed a saturated two-phase heat transfer correlation for nucleate boiling which involves two physically based parameters: the Reynolds number factor, F(z); and the suppression factor, S(z). These parameters affect the convective and the nucleate boiling heat transfer terms, respectively, as follows:

$$h(\theta,z) = F(z)h_c(\theta,z) + S(z)h_{nb}(\theta,z) \tag{2.22}$$

where:

$h(\theta,z)$ = Local heat transfer coefficient (W/m^2K)

$$\begin{aligned} \mathrm{F(z)} &= 1.0 && \text{if subcooled nucleate boiling} \\ &= 1.0 && \text{if } X_{tt}^{-1} \leq 0.10 \\ &= 2.35\,(X_{tt}^{-1} + 0.213)^{0.736} && \text{if } X_{tt}^{-1} \geq 0.10 \end{aligned} \tag{2.23}$$

$$X_{tt}^{-1} = (x/(1-x))^{0.9}(\rho_f/\rho_g)^{0.5}(\mu_g/\mu_f)^{0.1} \tag{2.24}$$

$h_c(\theta, z)$ = single-phase liquid convective heat transfer term (e.g. Petukhov correlation, Equation 2.10) (W/m^{2}K)

$$S(z) = \frac{1}{1 + 2.53 \times 10^{-6} Re_{2\phi}^{1.17}} \tag{2.25}$$

$$Re_{2\phi} = Re_l F(z)^{1.25} \tag{2.26}$$

$$Re_l = \frac{G(1-x)D}{\mu_f} \tag{2.27}$$

G = Mass flux (kg/m^{2}s)

x = Quality (assume $x = 0.0$ for subcooled nucleate boiling)

D = Flow diameter (m)

$h_{nb}(\theta, z)$ = Chen nucleate boiling heat transfer term (W/m^{2}K)

Chen correlates the nucleate boiling heat transfer term as follows:

$$h_{nb}(\theta, z) = 0.00122 \frac{k_f^{0.79} c_{pf}^{0.45} \rho_f^{0.49} (T_w(\theta, z) - T_{sat})(p(T_w(\theta, z)) - p(T_{sat}))^{0.75}}{\sigma^{0.5} \mu_f^{0.29} H_{fg}^{0.21} \rho_g^{0.24}} \tag{2.28}$$

where:

k_f = Fluid thermal conductivity (W/m K)

c_{pf} = Fluid specific heat at constant pressure (J/kgK)

ρ_f = Fluid density (kg/m^3)

$T_w(\theta, z)$ = Wall temperature (°C)

Table 2.5: Range of Parameters Used by Chen (1963) for Suppressed Nucleate Boiling Correlation

	Pressure MPa	Quality	Inlet Velocity m/s	Heat Flux MW/m^2
Water Only	0.17-3.5	0-0.7	0.06-4.5	up to 2.4

T_{sat} = Saturation temperature (°C)

$p(T_w(\theta, z))$ = Saturation pressure if T_{sat} were to equal $T_w(\theta, z)$ (MPa)

$p(T_{sat})$ = Saturation pressure corresponding to saturation temperature (MPa)

σ = Surface tension (N/m)

μ_f = Fluid dynamic viscosity (kg/ms)

H_{fg} = Heat of vaporization (J/kg)

ρ_g = Gas density (kg/m^3)

(Note: properties are evaluated at the saturation temperature in Equation 2.28 above.)

The original data used by Chen [46] for the above correlation are shown in Table 2.5. The use of this correlation in the present study goes beyond the range listed in Table 2.5 and is extrapolated in velocity (from 4.5 to circa 10 m/s) and heat flux (from 2.4 to circa 20 MW/m^2). Also, the Chen correlation was developed for saturated bulk boiling. Although the equilibrium quality in the present study is typically less than -0.45, at the lower mass fluxes, the equilibrium quality reaches -0.2. In these cases, when ΔT^* as defined by Shah (Equation 2.17) falls below 2, Equation 2.22 will be used to calculate the heat transfer coefficient.

In the present study, the Chen suppressed nucleate boiling correlation (developed for saturated bulk boiling) will be extrapolated to the subcooled region by extending the relationship of the local heat transfer coefficient, $h(\theta, z)$ in Equation 2.22, to the bulk temperature as follows:

$$q''(\theta, z) = (h_c(\theta, z) + S(z)h_{nb}(\theta, z))(T_w(\theta, z) - T_{bulk}(z)) \tag{2.29}$$

where the terms are defined as in Equation 2.22.

Table 2.6: Design Parameters used in PFC Surface Temperature Calculations

Analysis	Reference Group	Armor (Thickness, mm)	Flow Pattern (T_{bulk}^{inlet})	D_i mm	D_e mm	$T_{surface}^{PF}$ Limit °C
Design 1	ITER	Graphite (20)	Swirl (50 °C)	15	9.1	1100
Design 2	Present Study	Beryllium (3)	Smooth (20 °C)	9.5	9.5	900

Table 2.7: Results of Surface Temperature Limit Calculations for v = 10 m/s

Analysis	PF Armor (Thickness) mm	Flow Pattern	h_{tot} kW/m^{2}K	$T_{surface}^{PF}$ °C	q" MW/m^2
Design 1	Graphite (20)	Swirl	85	1100	6.5
Design 2	Beryllium (3)	Smooth	153	1000	18.6

2.3.5 Plasma Facing Surface Temperature Calculation Revisited

The result of applying the equations for swirl flow heat transfer, Equation 2.9 outlined above, to the ITER proposed thermal hydraulic parameters in Table 2.6 (also see Table 1.2) are given in the first row of Table 2.7. In addition, Table 2.7 gives the result of a second divertor concept (whose parameters are also shown in Table 2.6). The differences in the two designs are the armor material (hence, thickness), and the flow pattern (although assuming a coolant velocity of 10 m/s in both designs) as shown in Table 2.6. Design 2 uses a much thinner coating of Beryllium but forgoes the twisted tape inserts. The second design reflects the thermal hydraulic conditions used in the present experimental study. However, in all the cases of illustration in this chapter, the Chen correlation, Equation 2.22, is used to calculate the total convective heat transfer coefficient.

For Design 1, the limiting carbon surface temperature of 1100 °C [47] is reached at a heat flux of 6.5 MW/m^2 using the single-phase swirl flow analysis of Lopina and Bergles [40], Equation 2.9 above, and assuming a coolant velocity of 10 m/s. Figure 2-4 indicates that this design would not satisfy a design point heat flux of 15 MW/m^2 [33] and would be the restricting limit on the ITER heat flux window if the design point were relaxed to 5 MW/m^2.

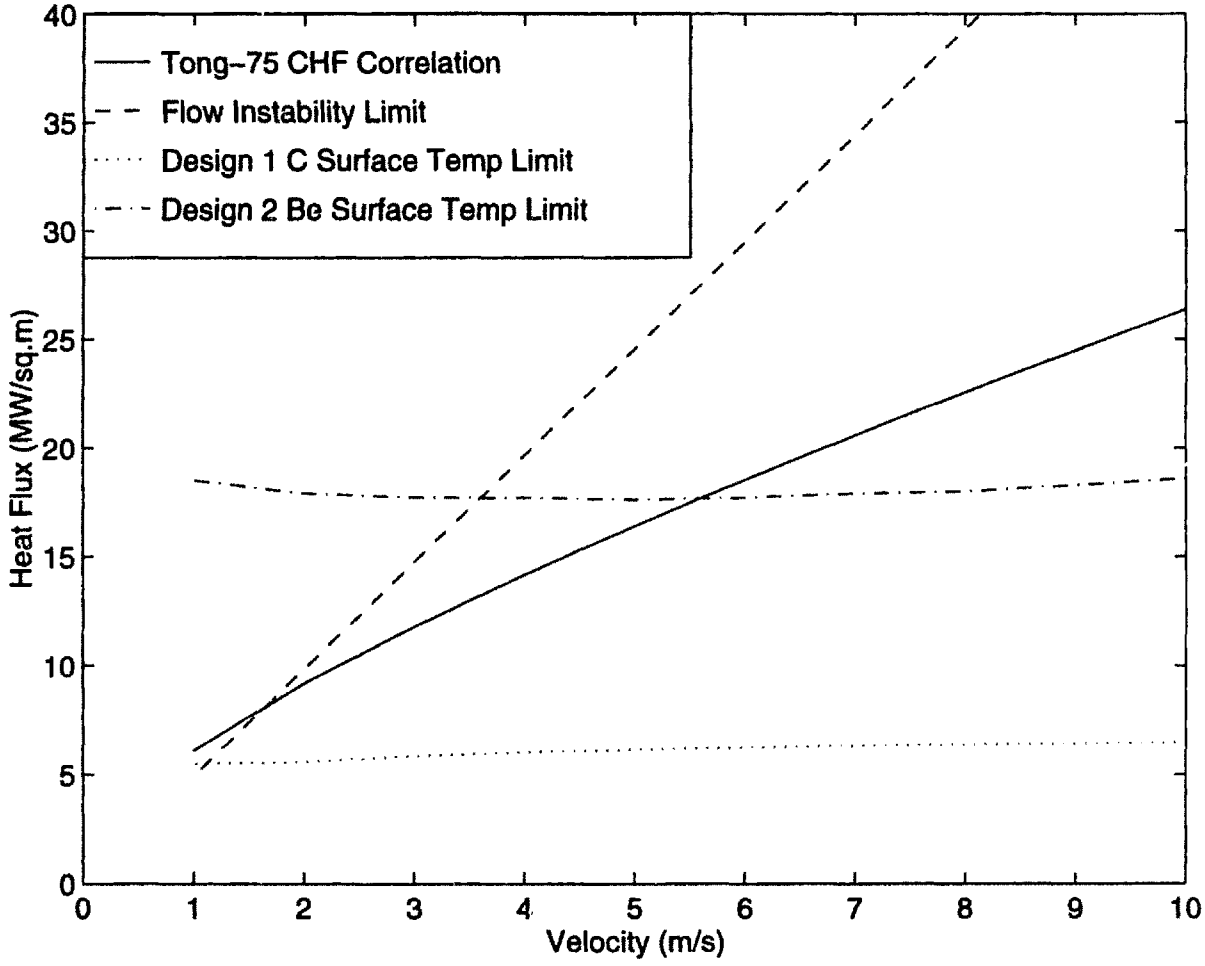

Figure 2-4: Predicted Heat Flux Limits on Divertor Operation (Note: Design 1 includes swirl flow, the other cases are for unobstructed flow)

On the other hand, for comparison, if a 9.5 mm inner diameter copper alloy tube is coated with 3 mm of Beryllium and subcooled nucleate boiling were allowed, then a maximum Beryllium temperature of 900 °C (to limit excessive evaporation [47]) would be reached at a heat flux of 17 MW/m^2 using the Chen suppressed nucleate boiling correlation, Equation 2.22 outlined above, and assuming a coolant velocity of 10 m/s. This limit is slightly above the design heat flux of 15 MW/m^2, but still more limiting than the critical heat flux limit for coolant velocity higher than 5.5 m/s as illustrated in Figure 2-4.

The above example illustrates that the flexibility in divertor design includes determining the flow regime (e.g., liquid-only convection, partially developed subcooled boiling or suppressed nucleate boiling conditions). In addition, although swirl flow is expected to enhance heat transfer, divertor designs using smooth flows can satisfy heat removal requirements. The ability of smooth flow heat removal will be further investigated relevant to divertor conditions. The following chapters will describe the heat transfer experiments used to characterize CHF limits under smooth flow conditions. However, in the above plasma facing surface temperature calculations, no attention was paid to the limiting coolant-side surface temperature. This will be done in the next section.

2.4 Homogeneous Nucleation Limit

The homogeneous nucleation limit is one limit that has not been widely discussed in the literature concerning fusion thermal hydraulics. However, the heat fluxes are so high that this nucleation mechanism may be present, especially in a region of suppressed nucleate boiling due to high subcooling and high velocity as discussed by Lekakh et al. (1994) [48] and especially of concern in enhanced turbulence flow patterns such as swirl flow. Thus, it is mentioned in this chapter for completeness. Collier [49] recommends a simple expression produced by Lienhard for the superheat required for homogeneous nucleation:

$$(T_{rg} - T_{rSAT}) = 0.905 - T_{rSAT} + 0.095T_{rSAT}^{8} \tag{2.30}$$

where

T_r = reduced temperature (absolute temperature (K)/the critical temperature (K))

T_{rg} = reduced superheated liquid temperature

T_{rSAT} = reduced saturation temperature

To determine T_{rg}, the wall superheat must be calculated using one of the above heat transfer correlations depending on the flow regime. The heat flux when the coolant-side wall reaches the homogeneous nucleation temperature using the ITER thermal hydraulic parameters (Table 1.2) with a 3 mm Be coating (as opposed to carbon as used in the previous example) and smooth flow (as opposed to swirl flow as used in the previous example) is shown in Figure 2-5. This possible limit is the most restrictive in the parameter space of ITER between 2.5 and 8 m/s, as illustrated. The fact that the homogeneous nucleation limit in this example lies slightly below the CHF correlation suggests that homogeneous nucleation may be the mechanism leading to CHF under the suppressed nucleation nature of highly subcooled swirl flow. However, more experimental work is required to verify this postulate since the calculated limiting heat flux for the homogeneous nucleation limit is very dependent on the accuracy of the heat transfer coefficient correlation selected.

For the above illustrations, recall, extrapolation of the Chen suppressed nucleate boiling correlation has been employed, although nothing has been said about the validity of such extrapolation. Figure 2-6 shows a comparison of the heat transfer coefficient at homogeneous nucleation (defined as q"/(T_{wall} - T_{bulk}) when T_{wall} equals the homogeneous nucleation temperature given by Equation 2.30) calculated using the Shah subcooled nucleate boiling correlation, Equation 2.21, and the Chen suppressed nucleate boiling correlation, Equation 2.22, and assuming the ITER thermal hydraulic conditions and smooth flow. For the case at hand, in which the correlations predict the homogeneous nucleation temperature, the heat transfer coefficient does not appear

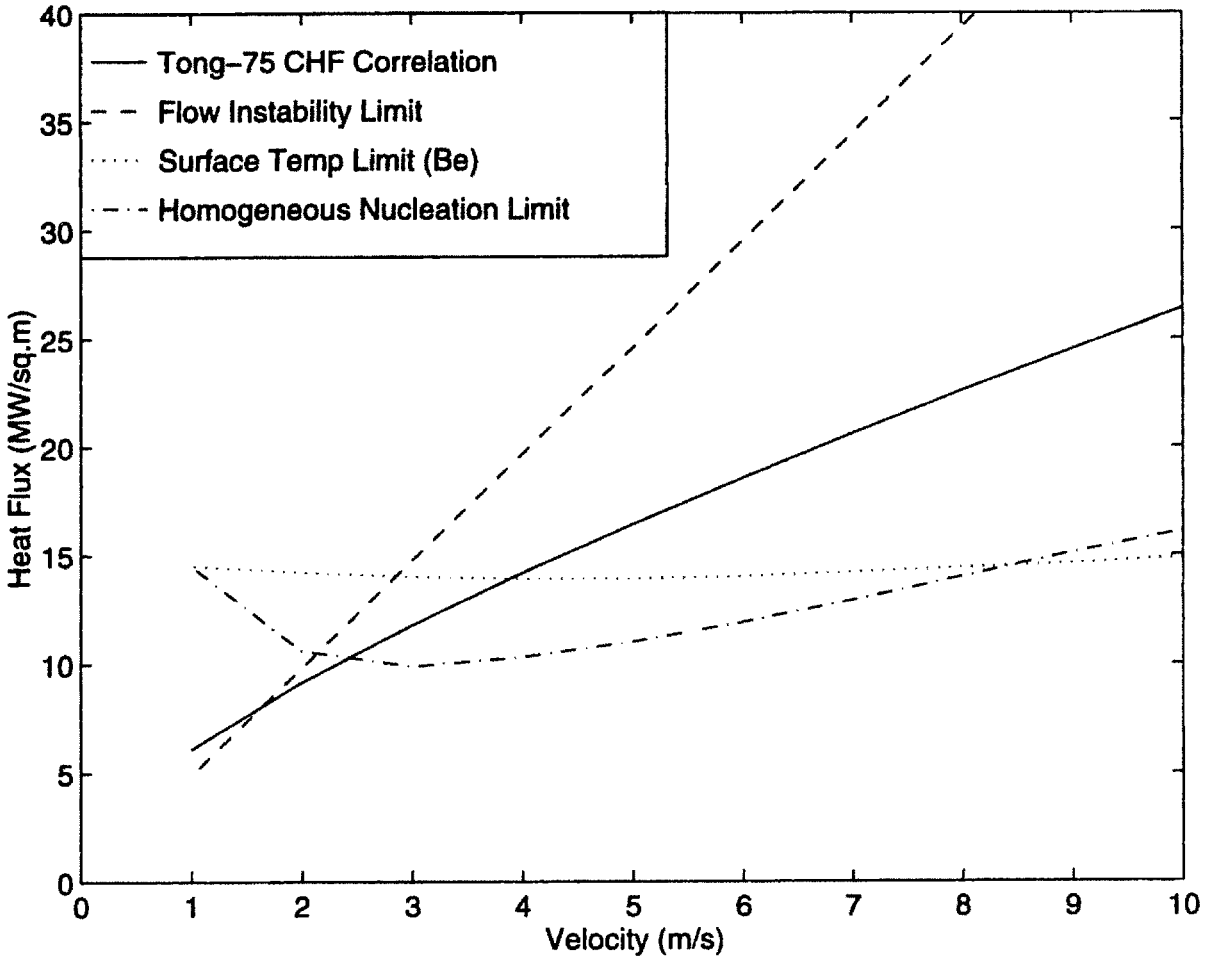

Figure 2-5: Comparison of Limiting Heat Fluxes including Homogeneous Nucleation for ITER Conditions with Unobstructed Flow

to vary significantly at velocities above 6.5 m/s (recall: the Shah correlation was shown to predict very low heat transfer coefficients at coolant velocities). However, Figure 2-7 shows that at heat fluxes below that predicting the homogeneous nucleation temperature, the Shah correlation actually gives a higher heat transfer coefficient once boiling starts (presumably at the first knee in the curves). The same calculations are shown in Figure 2-8 for those conditions of the present experimental study (essentially Design 2 in Table 2.6) to show that the oscillation in the Shah correlation is no longer observable and consistently greater than the Chen correlation.

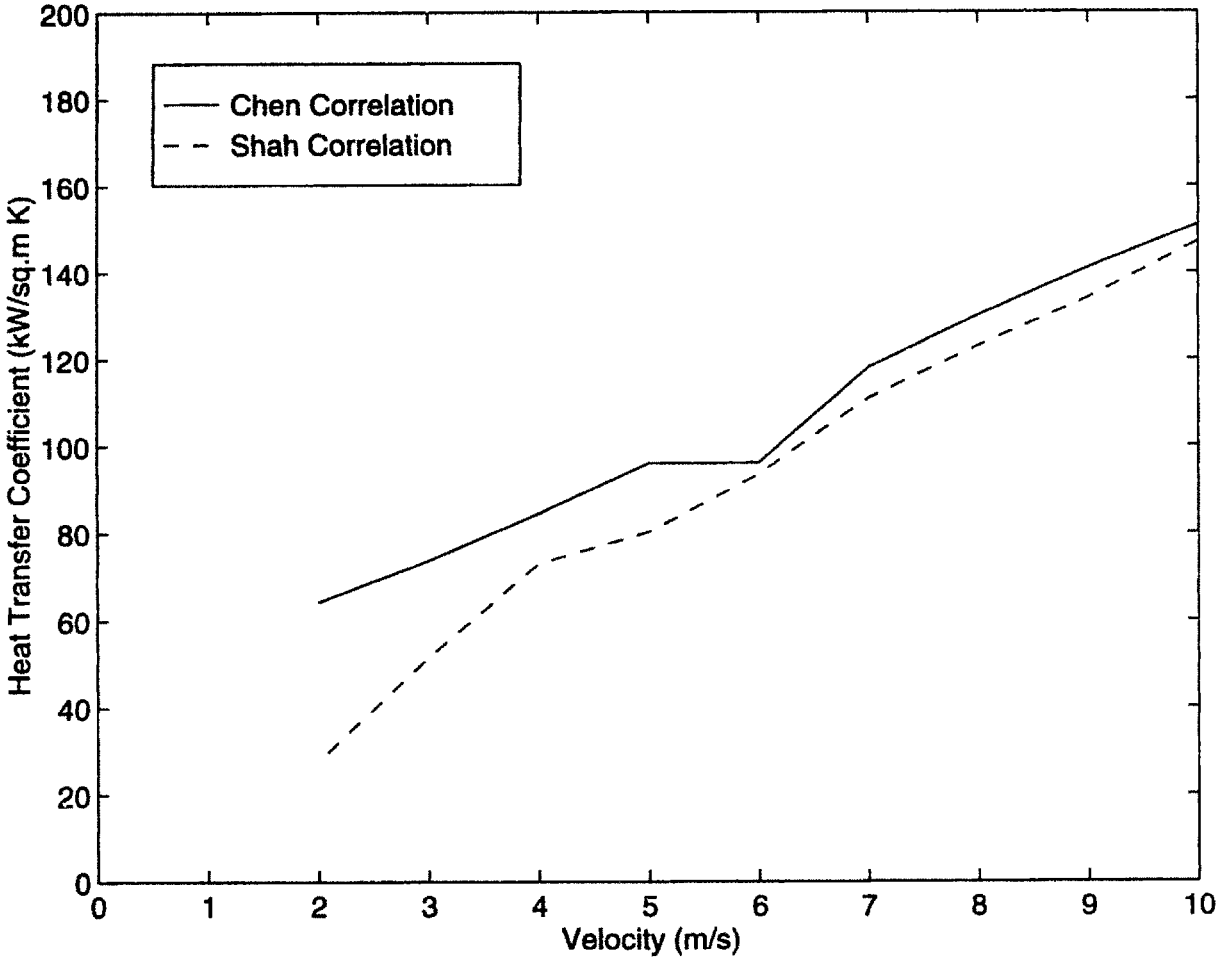

Figure 2-6: Comparison of Heat Transfer Coefficients at Homogeneous Nucleation using Two Nucleate Boiling Correlations with ITER proposed Thermal Hydraulic Parameters in Unobstructed Flow

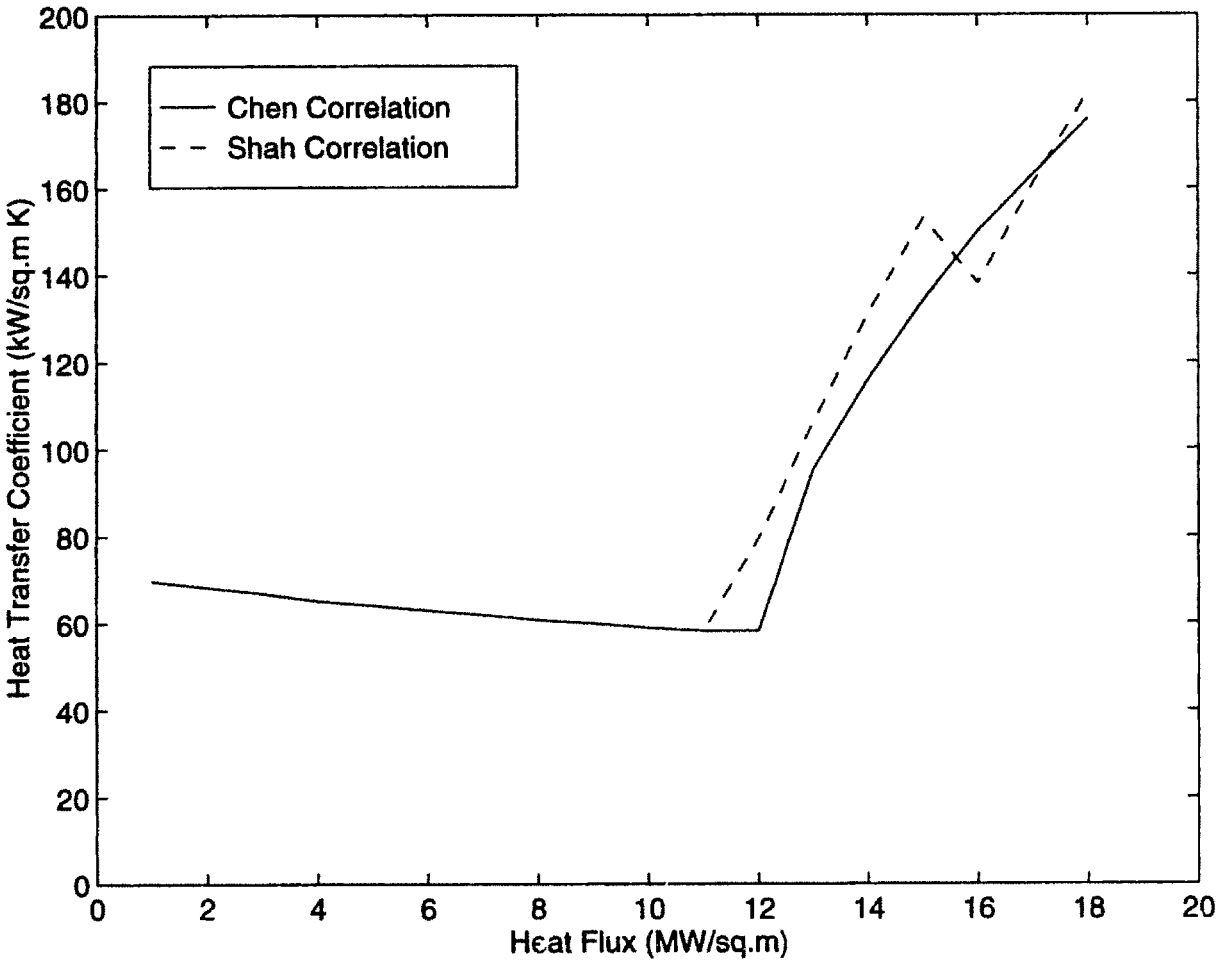

Figure 2-7: Comparison of Heat Transfer Coefficients Versus Heat Flux using Two Nucleate Boiling Correlations with ITER proposed Thermal Hydraulic Parameters (v = 10 m/s) in Unobstructed Flow

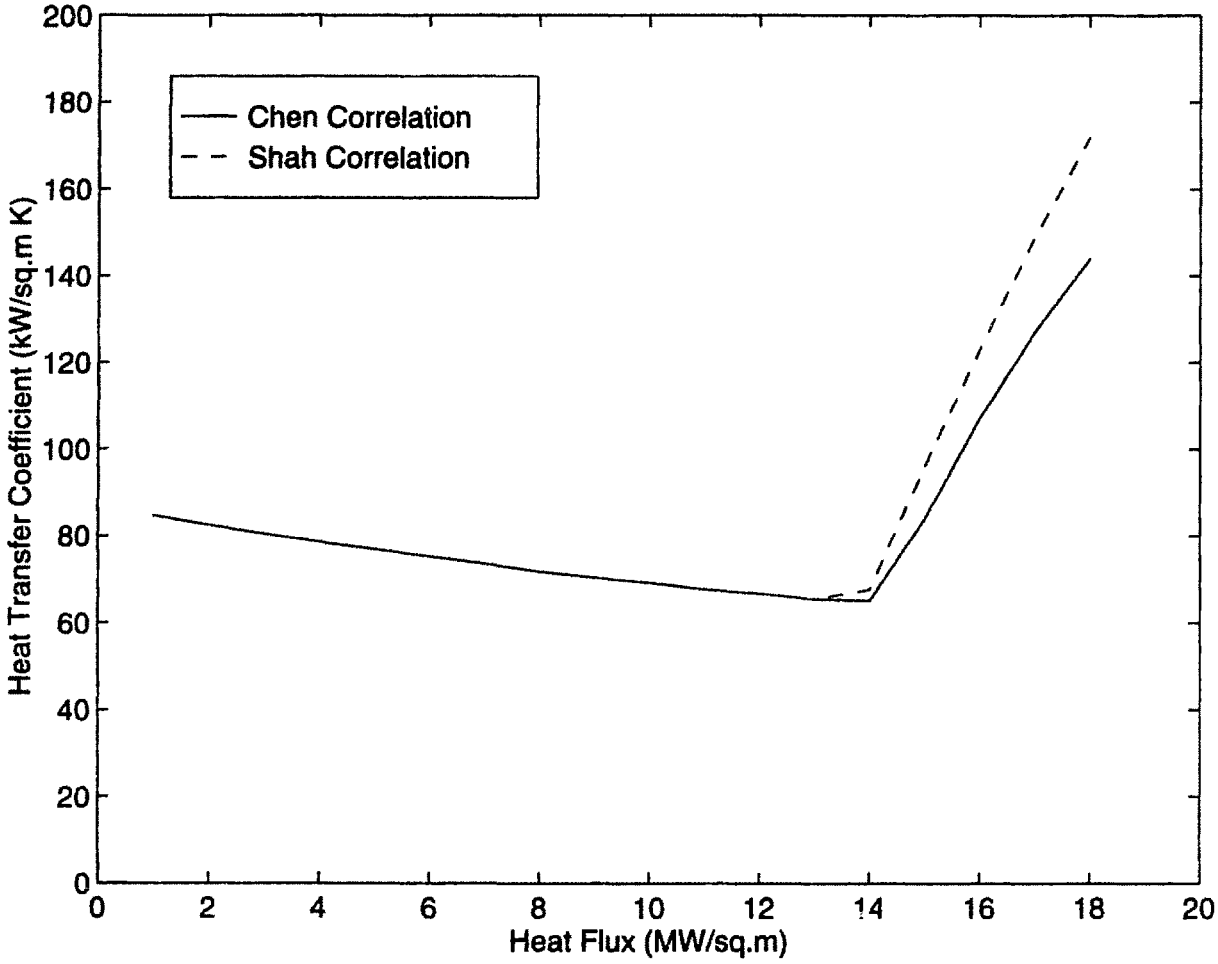

Figure 2-8: Comparison of Heat Transfer Coefficients Versus Heat Flux using Two Nucleate Boiling Correlations with Thermal Hydraulic Parameters (v = 10 m/s) similar to the Present Experimental Study

2.5 Comments

This chapter has indicated that there is still much to be determined about divertor-relevant thermal hydraulics. This is evident that the main correlations mentioned above must all be extrapolated outside their original regions of validity for use in the present study. In addition, published experimental data having axial and azimuthal non-uniformity in the thermal boundary conditions expected in a divertor is extremely sparse.

This chapter has also illustrated analytical tools to help identify and define the failure mechanisms. Figure 2-5 best illustrates the importance of considering a variety of failure mechanisms since at various flow rates, a different mechanism may be more limiting. Acceptable design margins must be adopted for each of the four limits and may lead to different safety factors depending on uncertainties of data, on uncertainties of calculations, and on the consequences of exceeding the limits.

The following two chapters outline the experimental apparatus and procedure used to investigate the above phenomena for smooth flow conditions. Subsequently, raw results and interpretation will be presented; and, a new phenomenological CHF correlation will be proposed for divertor applications.

Chapter 3

Experiments

3.1 Experimental Apparatus

The previous chapters mentioned the conditions of interest for the present study: highly subcooled smooth flow with single-sided heating. An experimental facility was designed and built from the ground up and operated within the test ranges given in Table 3.1. The reference parameters proposed by the ITER designers [3] (Table 1.2) are also given to indicate the similarity between the tested range and a reference design. This section describes the experimental apparatus used in the present study which consists of a hydraulic loop to supply pressurized coolant flow, an electrical heating circuit to provide the heat flux, and data acquisition components. Table 3.2 lists the actual equipment used in the experiments including the manufacturers and equipment numbers located on the instrument. The boldfaced terms in Table 3.2 correspond to the items in the schematics illustrated in Figures 3-1 to 3-2.

Virtually all CHF experiments were conducted using electrical heating of resistive elements. For uniform heat flux conditions, the coolant channel was typically used as the heater element. Single-sided heat flux experiments use either electrical heating or particle beams to provide the appropriate circumferential heat flux profiles. Electrical resistive heating was chosen for the present study, in part, to avoid the complexities of developing from scratch an electron beam facility. Very few (only nine) CHF data points came from the Sandia National Laboratory's Electron Beam Facility [25].

Table 3.1: Test Range of Present Study

Parameter	ITER Reference [2]	Tested Range	Units
Pressure	3.5	1.5-3.0	MPa
Inlet temperature	50	14-25	°C
Velocity	10	0.5-20	m/s
Tube inner diameter	15	9.5	mm
Tube equivalent diameter	9.1	9.5	mm
Heated Length	5	5	cm

The requirement of running experiments in a vacuum environment appeared to be a prodigious task compared to the straightforward heating of a resistive element. In addition, plasma spray technology is at the point of being both mature and economic, thus, allowing for reuse of test section stock by removing and re-spraying heater surfaces. The final heater specifications were a result of preliminary testing of various materials and thicknesses.

3.1.1 Hydraulic Loop

Figure 3-1 shows a schematic of the open loop in which water was pumped from Tank 1 to Tank 2 during an experimental run and then recirculated back to Tank 1 between runs using a bypass loop. The 500-gallon tanks were sized to accommodate space limitations and to allow for 30-minute continuous experiments at high velocities (e.g., 15 m/s). The pump is a 16-stage centrifugal pump with stainless steel wetted components to minimize corrosion products from entering the coolant. It is rated at 5.5 MPa with a flow rate of 50 gpm (3 L/s). The pump motor was equipped with a variable speed controller which allows the flow to be finely adjusted to a desired rate.

A stainless steel ball valve upstream and needle valve downstream were used to adjust the coolant pressure and velocity. The pressure was measured downstream of the test section but before the needle valve using a bourdon gauge.

A flow sensor rated between 3.0 and 60 Mg/m^2s (2.8 and 56 gpm) was located downstream of the needle valve with the manufacturer suggested entrance and exit pipe lengths, 10 and 5 diameters, respectively. The sensor's impeller transmits a fre-

Table 3.2: Equipment list

Description	Identifying #
Tanks Kerrco Vertical 500 Gallon Tanks (two)	CP# 51857
Pump GE Motor and Gould's Pump Inc.	MIT-0270245
Pump Controller 8803 Type P AC Drive	
Ball Valve Parker Stainless Steel B-Series Manual Ball Valve	
Needle Valve Parker Stainless Steel Rising Steam Plug Valve	
Pressure Gauge Ashcroft Test Gauge	Q-8602
Pressure Relief Valve Hoke	Model H 6548 L4Y
Flow Meter Data Industrial Flow Meter 4000 Series [50]	3681
Voltmeter Fluke 8010A Digital Multimeter	MIT-0050897
Power Supply 45 kW Newton Engineering Service Inc.	4971-1 NSF
Test Section Heater:	
Nichrome Rod, 1" Diameter (two)	
Tungsten and Alumina Coatings, Falmer Thermal Spray	
Copper Bus Bar Assembly - Made by Davila [51] and Folch [52]	
Data Acquisition:	
Universal Electronics Regulated Power Supply	850 16651
Priceton Applied Reseach Power - Reference Source	MIT-016959
Powerstat Variable Autotransformer - Triplett	Model: 320-M
Magnavox Professional Monitor	58844869
TechFusion Computer	MIT-0266095
Tegam Inc. Multipurpose Switchbox - Type K TC (three)	Model: 8012
Power Supply/Flow Meter Switchbox - Made by Minh [53]	
Analog Devices 16 Channel Backplane	9319
Analog Devices Isolated Wideband V input	9310 16/9417 17
Analog Devices Isolated Type K TC input Model 5B41-01 (five)	9321 11
Okidata Mircoline 193 Plus Personal Printer	603A1023787
Conductivity Meter Cole Palmer Model 1500-10	92061438

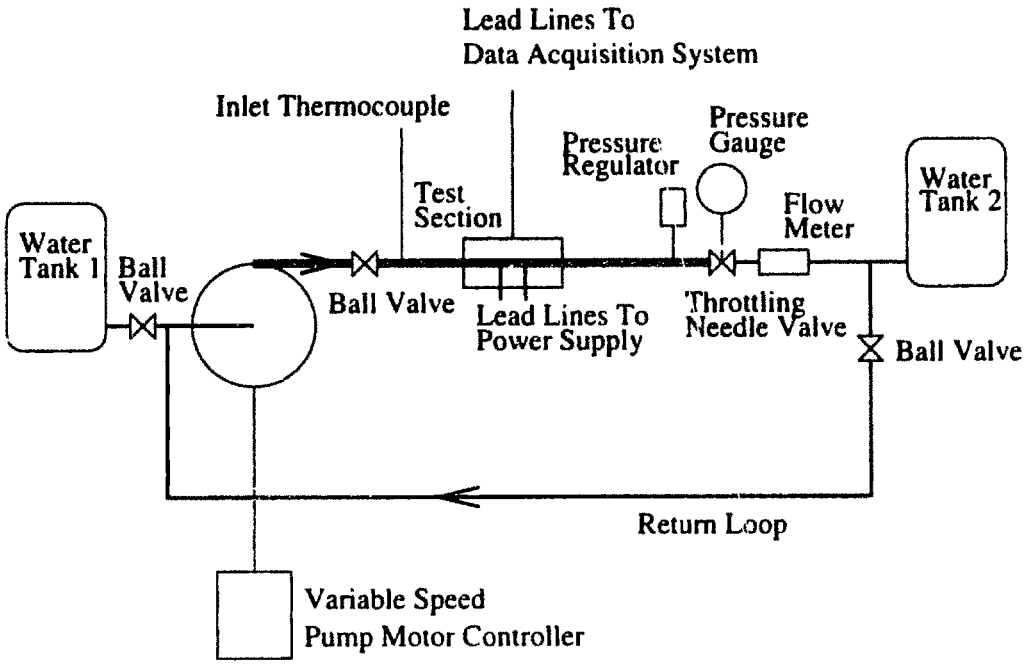

Figure 3-1: Schematic of Thermal Hydraulic Loop

quency proportional to the flow rate. The frequency was then converted into velocity (m/s) using a Fortran program (see Appendix C.1) in the data acquisition system. The flow meter's range was extended into the flow region below the manufacturer's rating and was therefore calibrated in this range as described later in this chapter.

3.1.2 Heater Loop

A current-controlled 45 kW Power Supply provides up to 2200 Amps to the test section heater. The power of the test section heater was measured by finding current and voltages across the heater. Redundant current and voltage measurements were made by manually noting the Power Supply ammeter and voltmeter readings concurrently with the voltage across the shunt resistor. All the while, the data acquisition system was scanning heater and shunt resistor voltages throughout the experimental run. The electrical resistances of the loop shown in Figure 3-3 were tested for currents from 100 to 2000 Amps and account for about one percent of power dissipation which

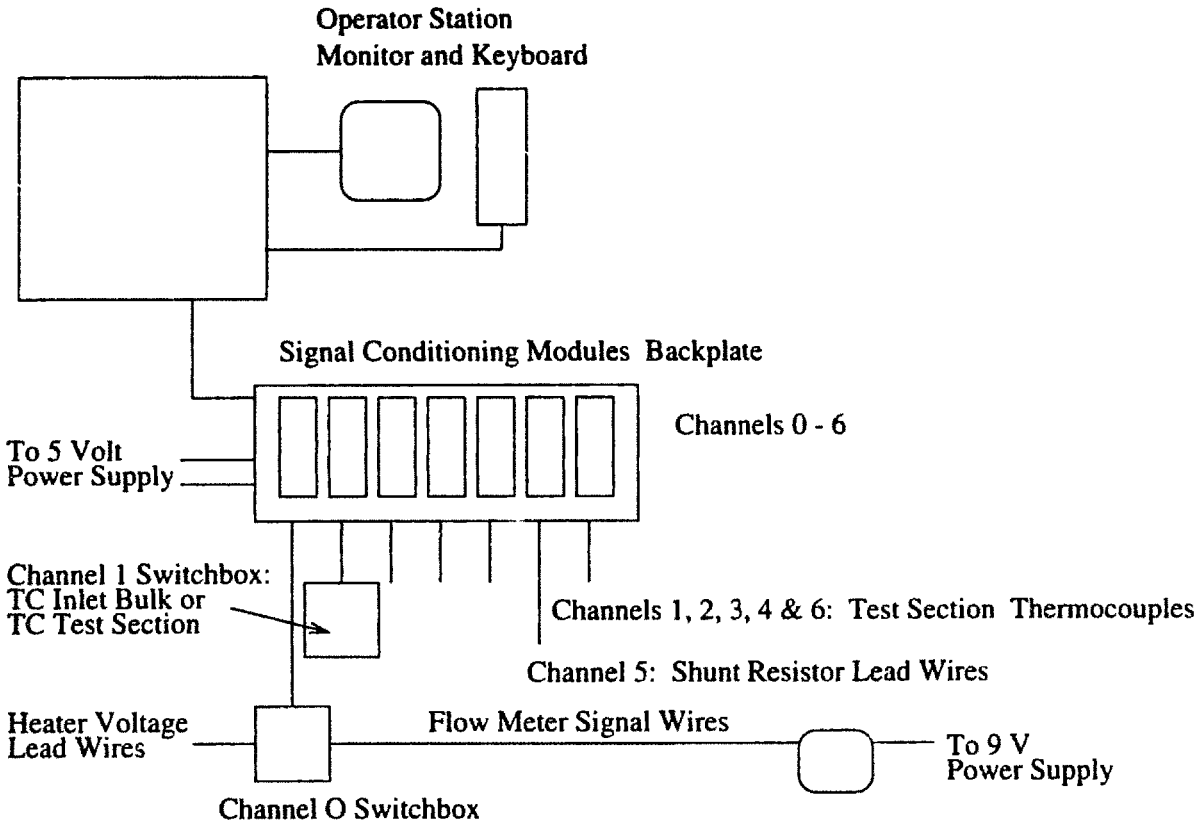

Figure 3-2: Schematic of Computerized Data Aquisition System

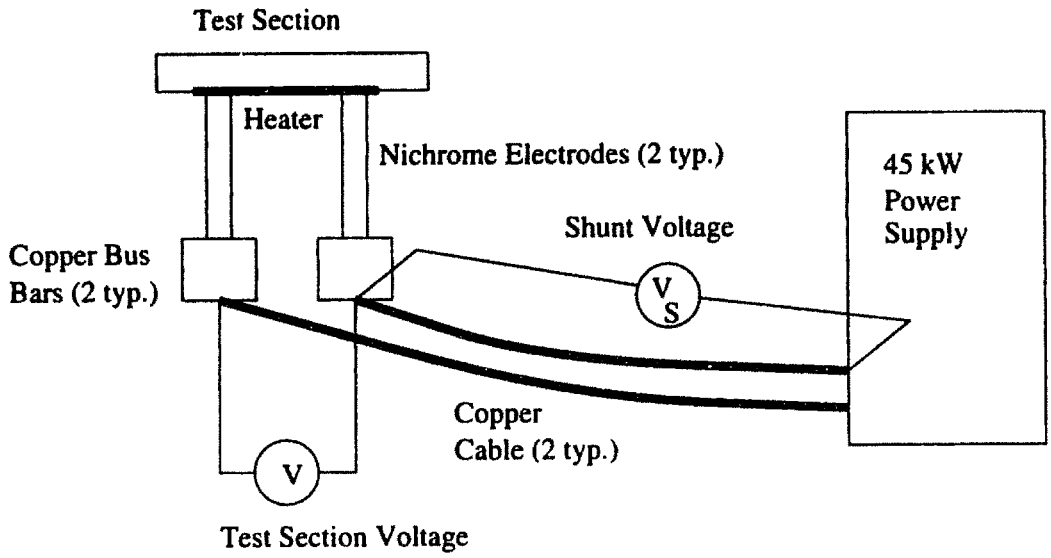

Figure 3-3: Electrical Loop of Test Section Heater

is predominantly in the cables leading to the test section. One side of these power transmission cables, from the Power Supply to the Test Section, was used as the shunt resistor.

The test section was resistively heated by passing current through a thin tungsten layer (about 0.25 mm) which was plasma sprayed over an alumina coating (about 0.1 mm) as specified in Figure 3-4. Table 3.3 gives the actual thicknesses as measured by a micrometer. Since the coatings were on opposite sides, an average value (per side) is given for each channel. The thicknesses of the tungsten and alumina layers were chosen as optimal among several used in preliminary testing. The alumina coating electrically isolates the copper coolant channel walls from the tungsten. The copper is too conductive to have any significant volumetric heating should current find a path through the alumina. If current does flow into the copper, however, the current limitation of the power supply causes a noticeable limitation on the test section power.

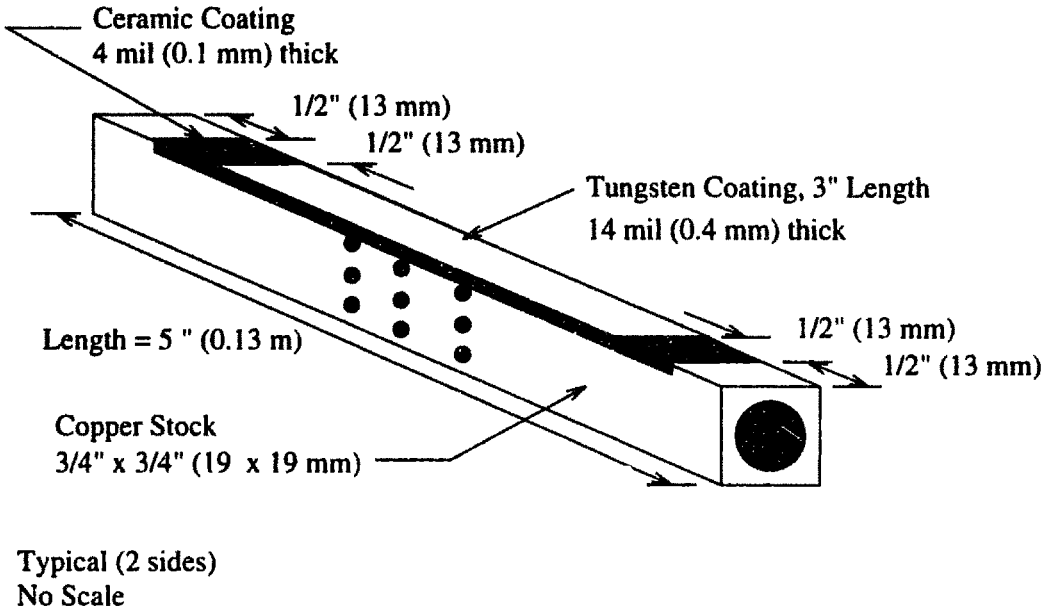

Figure 3-4: Test Section Specifications

Table 3.3: Average Coating Thicknesses Measured with Micrometer

Test Section Number	Alumina μm	Tungsten μm
6	71	207
9	123	197
11	126	248
14	89	259
15	109	161
16	80	146
17	65	230
26	74	406
27	109	406
28	79	457
29	102	432

3.1.3 Data Acquisition Components

A computerized data acquisition system capable of reading and storing 6 thermocouple voltages, the flowmeter signal, and voltages from the shunt resistor and across the heater was set up within one meter of the test section. The name of the software package which accompanied the data acquisition board is Daqware. Daqware provides a mouse controlled environment with measurements appearing on the screen in a real time recorder plot. Two Fortran codes (drf.for and cn6.f listed in Appendix C) were written by the author to convert logged measurements to the parameters of interest, e.g., voltage to temperature. A clear Lexan shield covered the higher pressure area between the pump exit and the needle valve to protect equipment from spraying water or tube rupture under pressure. A 3 x 3 array of dimples about 2 mm wide and 2 mm deep were drilled into the non-coated side of each test section. K-type thermocouples were placed into five of these slots according to Figure 3-5 such that three thermocouples measured the wall temperature close to the heater and three thermocouples measured the midsection wall. A thermocouple was also placed on the entrance-length pipe far enough from the heater to measure the inlet bulk temperature. Note: all thermocouples used in the present study are K-type.

3.2 Test Matrix and Experimental Procedure

This section details the experimental procedure for gathering, and method of calculating, thermal hydraulic parameters such as the coolant velocity and incident heat flux level. The subsequent chapter will incorporate computer modeling into the data reduction procedure to evaluate heat transfer coefficients and local heat fluxes as well as inferring nucleation mechanisms. Table 3.1 contains the test matrix used in the present study. The coolant velocity was the main parameter which was varied and high velocities (about 20 m/s) required the system pressure to drop as low as 1.5 MPa. As discussed in Chapter 1, various categories or windows of similar thermal hydraulic conditions are useful to compare results. The parameters in Table 3.1 correspond to Categories VI and IX (i.e., high subcooling with intermediate pressure).

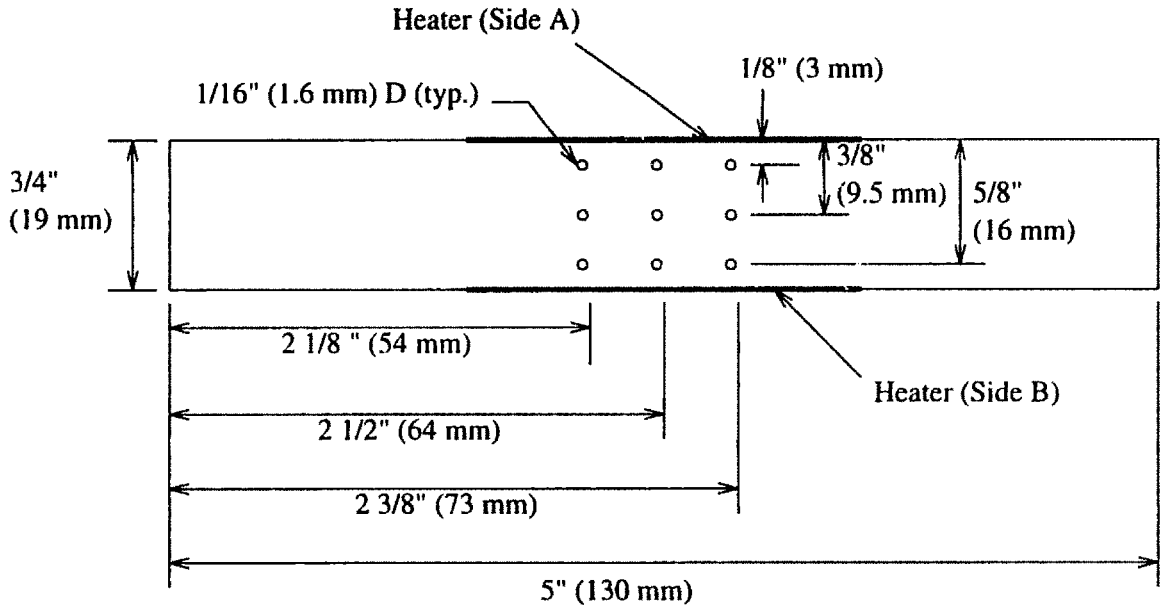

Scale: Full

Figure 3-5: Location of Thermocouples on Test Section

The experiment required only one operator (although two were typically present) since most of the data were logged using the data acquisition scanner which eventually creates text files of the data for the thermocouple, flow meter, heater and shunt resistor voltage measurements. The operator controlled the power supply and pump and manually logged the current and voltage reading from the power supply, the shunt resistor voltage from the voltmeter, and the pressure from the test gauge. The precise procedures are delineated in the following subsections.

3.2.1 Power Controlled Tests - Setup

The following step-by-step procedure was performed by the operator(s). It typically took 10 to 15 minutes to perform and resulted in a steady flow established with known pressure, velocity and inlet bulk coolant temperature.

1. The test section was labelled (to correspond to notebook and file labels) and affixed to the entrance and exit length pipes using flare unions (already existing

on the test sections).

2. The thermocouples were placed in their respective dimples on the wall of the test section.

3. The test section was clamped to the nichrome electrodes to establish an electrical connection. (Ceramic fibers were used to insulate the test section thermally and electrically).

4. The Power Supply coolant was turned on and flow established.

5. The electrical connection of the heater was tested by supplying a small voltage from the Power Supply and noting if current was flowing. If current was not flowing, the connection was checked and fixed.

6. Once the heater electrical connection was established, all hydraulic loop valves were appropriately opened or closed to give desired flow path.

7. The Lexan cover was placed over the high-pressure zone of the Test Section.

8. The data acquisition system was reset and Daqware software was loaded. The "Strip Chart and Data Logger" Instrument was selected; and, Channels 0 to 6 were engaged under "Chan Setup" to give visual readout of all seven channels.

9. The pump was started and ramped to full power.

10. The needle valve was adjusted to the desired pressure which established the desired flow. A pressure measurement was taken (Note: the pressure was never observed to deviate throughout an experiment and therefore only one pressure was sometimes recorded and then typically verified at the end of the run).

11. The Daqware sampling rate was adjusted to allow reasonable accuracy of the flow meter's frequency (about 5000 samples/second with a square wave length of about 2 inches on the monitor). A measurement of the inlet bulk temperature and flow velocity were taken by setting the Channel 0 switchbox to location 2 ("TB") and the Channel 1 switchbox to "Flowmeter".

12. Once the switches were set and the flowmeter square wave (i.e., pulse) was discernible, data were saved to a text file using the "Save to File" option on the Daqware screen. No more than 4000 samples were saved to ensure ample memory to complete the experimental measurements.

3.2.2 Power Controlled Tests

The following step-by-step procedure was performed by the operator(s). It took about 5 to 10 minutes to perform and the result was component failure. This failure was usually associated with the destruction of the heater or local melting of a nichrome electrode. The resulting data were manual readings of Power Supply voltage and current, shunt resistance voltage and tank water levels versus incremental power levels; and, a computer file containing the heater, shunt resistor and five thermocouple voltage measurements versus time.

1. The Daqware sampling rate was reset to 100 samples/second, the Channel 0 switchbox was set to 1 ("TC1"), and the Channel 1 switchbox was set to "Power Supply".

2. The current to the Test Section was stepped up slowly in increments of about 100 amps. This prevented circuit breakers from tripping within the Power Supply.

3. At a given power level (e.g., at each 100 amp current increment), the test section heating was allowed to stabilize (which took on the order of a second). At this time, the Power Supply current and Shunt Resistor voltage were logged. Then the Power Supply voltage was logged. If legible, the tank water levels were noted with time of day.

4. Measurements were taken until component failure (usually accompanied by flashing or arcing on the test section heater).

5. A second pressure, flow velocity, and inlet bulk temperature measurement were taken using the procedure outlined in the previous section.

3.2.3 Flow Controlled CHF Measurements

Flow Controlled experiments were not used as widely in the present study as Power Controlled experiments because the flow decrease was accompanied by a decrease in pressure. However a few experiments have been carried out using this technique as follows:

1. Experiment was set up as delineated in Power Controlled Tests - Setup, above.
2. As the pump power was increased to full power, pressure versus flow rate were calibrated for the needle valve setting (the needle valve setting was not changed for the remainder of this test run). This was done by correlating the flow meter data to pressure, for various flows.
3. The Channel 0 switchbox was set to 1 ("TC1") and the Channel 1 switchbox was set to "Power Supply".
4. Power Supply voltage was increased to obtain desired CHF power level.
5. The pump power was slowly ramped down (with one or two decrements of the pump controller button) and the test section heating was allowed to stabilize (which takes on the order of a second). At this time, the pressure, Power Supply current, and Shunt Resistor voltage were logged. Then the Power Supply voltage was logged.
6. Measurements were taken until component failure (usually accompanied by flashing or arcing on the test section heater).

3.3 Data Reduction

All thermocouples are standard 20 or 28 gauge chromel-alumel (K-type) thermocouples. Thermocouple voltages were measured via a Daqware conditioning module which outputs a voltage between 0 and 5 V. These voltages were linearly calibrated with temperature according to the following equation:

$$T = 1200V - 100 \tag{3.1}$$

where

T = Temperature (°C)

V = Daqware thermocouple voltage measurement (V)

The Daqware flow measurements (e.g., recorded at the beginning and end of a test run for the Power Controlled Tests) were converted into frequency using a Fortran code, drf.for, written by the author and listed in Appendix C.1. The inputs to the code were:

1. Flow data file from Daqware with first 5 lines of text moved to end of file
2. Sample rate
3. Number of samples taken (in multiples of 1000 if more than 1000 points)

The code output gave:

1. Average flow meter frequency (Hz)
2. Volumetric flow rate (gallons per minute)
3. Velocity (m/s)
4. Percent standard error of flow meter data (to evaluate if enough pulses were measured or if the flow rate varied)
5. Inlet bulk temperature (°C)

3.3.1 Thermal Hydraulic Parameters

Incident heat flux, q''_0

The incident heat flux (defined in the present study as the power input to the tungsten per unit area) is simply determined using the following expression:

$$q_0'' = IV/A_h \tag{3.2}$$

where

q_0'' = Incident heat flux (W/m^2)

I = Power Supply current (A)

V = Electrode voltage potential (V)

A_h = Heater area (m^2)

Equilibrium Quality, X_e

The equilibrium quality is used to represent the degree of coolant subcooling. It is calculated using the following expression:

$$X_e = -C_p(T_{sat} - T_{bulk})/H_{fg} \tag{3.3}$$

where

X_e = Subcooled equilibrium quality

C_p = Specific heat at constant pressure (J/kgK)

T_{sat} = Saturation temperature (^oC)

T_{bulk} = Bulk temperature (^oC)

H_{fg} = Heat of vaporization (J/kg)

Exit Bulk Temperature, T_{bulk}^{exit}

T_{bulk}^{exit} is calculated using the following energy balance:

$$T_{bulk}^{exit} = T_{inlet} + \mathcal{P}/GA_{flow}C_p \tag{3.4}$$

where

T_{inlet} = Inlet bulk temperature (^oC)

$\mathcal{P}$ = Power (W)

G = Mass flux (kg/m^2s)

A_{flow} = Coolant cross sectional flow area (m^2)

C_p = Specific heat at constant pressure (J/kgK)

Mass Flux, G

The mass flux is calculated from the flow velocity by the relation:

$$G = \rho v \tag{3.5}$$

where

G = Mass flux (kg/m^2s)

ρ = Coolant density (kg/m^3)

v = Flow velocity (m/s)

Other hydraulic parameters such as pressure and inlet and outlet temperatures were measured directly with no further manipulation. The heat transfer coefficient and the coolant side heat fluxes, on the other hand, were not directly measured and are discussed in the next chapter.

3.4 Calibrations and Instrument Range

Most instruments were new and, when supplied, the manufacturer's calibration and uncertainty were used. However, several instruments (such as those for which a data reduction program were written) had either complicated data manipulation (e.g., the flow meter frequency measurement) or had properties that had to be determined for each test run (such as the test section resistance). In this situation, several calibrations can be performed to validate measurement accuracy and precision.

3.4.1 Flow Meter Calibration

The flow meter contains a calibration curve supplied by the manufacturer [50]:

$$GPM = k(Hz + Offset) \tag{3.6}$$

where:

GPM = Flow rate (gpm)

k = 0.6266 (gpm/Hz)

Hz = Flow meter signal frequency (Hz)

$Offset$ = 0.0314 (Hz)

The range of frequencies for accuracy within ± 1 percent are 4.450 to 89.589 Hz. The mass flux range for accuracy within ± 1 percent is within 3.00 to 59.9 Mg/m^2s. Since a portion of the mass flux range used in the present study falls below 3 Mg/m^2s, it was necessary to calibrate the flow meter at the lower end of the measurements which extrapolate from the above equation. The flow meter impeller is made from standard PVDF [50]; operating temperature should be below 104 °C and the pressure below 1 MPa. Since the flow meter is located downstream of the test section exit needle valve, the pressure will be substantially below 1 MPa. The bulk exit temperature should remain below the 104 °C temperature limit although encroached upon at the lowest flows (about 0.5 Mg/m^2s).

The low flow rate calibration utilized a graduated five gallon plastic tank with 0.25-gallon divisions and a digital clock from a Hewlett Packard 48GX calculator. The tank level versus time was noted once the flow became steady and the Daqware Data Logger was used as if in a typical experimental run. The mass flux rate range of interest for this calibration was 0.5 to 3.0 Mg/m^2s. The data are plotted in Figure 3-6 and listed in Appendix D. The calibration range was 0.25-2.5 Mg/m^2s in order to cover the range of interest. The flow meter versus hand-timed measurements show good agreement (i.e., within about a 10 percent experimental uncertainty in hand measurements) after a flow meter measured mass flux rate of about 1 Mg/m^2s. Below 1 Mg/m^2s, the flow meter deviation can be estimated by the following equation:

$$f_{correction} = 0.475(1 + G) \tag{3.7}$$

where:

$f_{correction}$ = Corrected Mass flux rate/Flow meter measurement

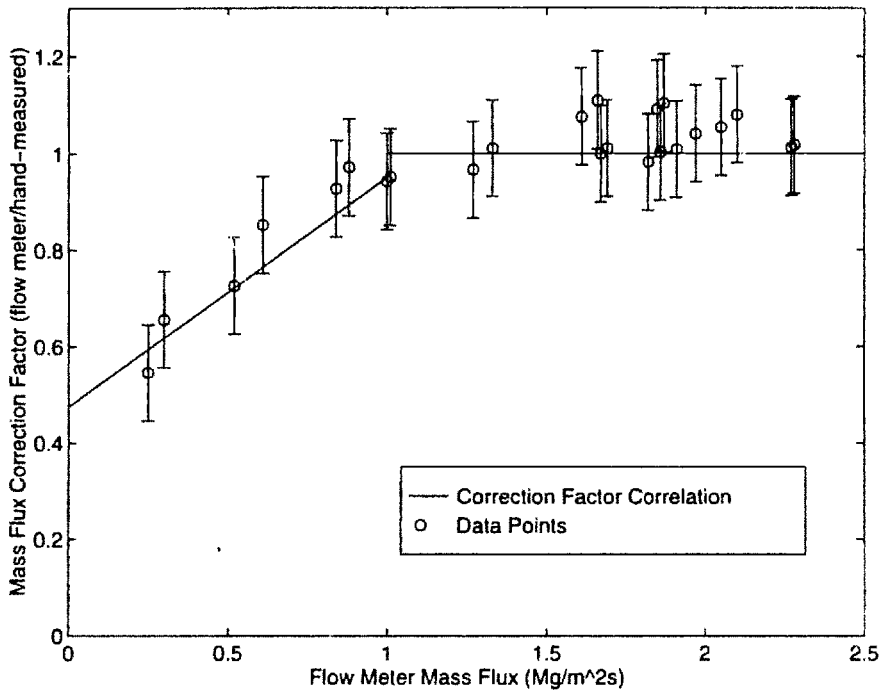

Figure 3-6: Flow Meter Calibration at Low Flow Rate

G = Mass flux rate (Mg/m^{2}s)

$0 \leq G \leq 1.0$ Mg/m^{2}s

3.4.2 Data Acquisition Component Calibrations

The National Instrument signal conditioning modules and Daqware software are assumed to be accurate to the catalog accuracy of $\pm$ 0.05 percent [54]. This accuracy is negligible to other experimental uncertainties not involving the computerized data acquisition system, e.g., the resolution and location of the thermocouples or the standard error in voltage and frequency measurements.

However, a voltage reduction circuit was made by Minh [53] to reduce the heater voltage (maximum of 22 volts) to within the signal conditioning module range of $\pm$ 5 volts and to allow the same module to condition the flow meter signal when the heater power is not being logged. Minh used the Fluke digital multimeter (see Table 3.2) to calibrate the voltage over the power supply range of 5 to 22 volts and a Fortran code (written by the author and contained in Appendix C.2) to measure the mean voltage and standard deviation as logged by Daqware. Minh's results are shown in

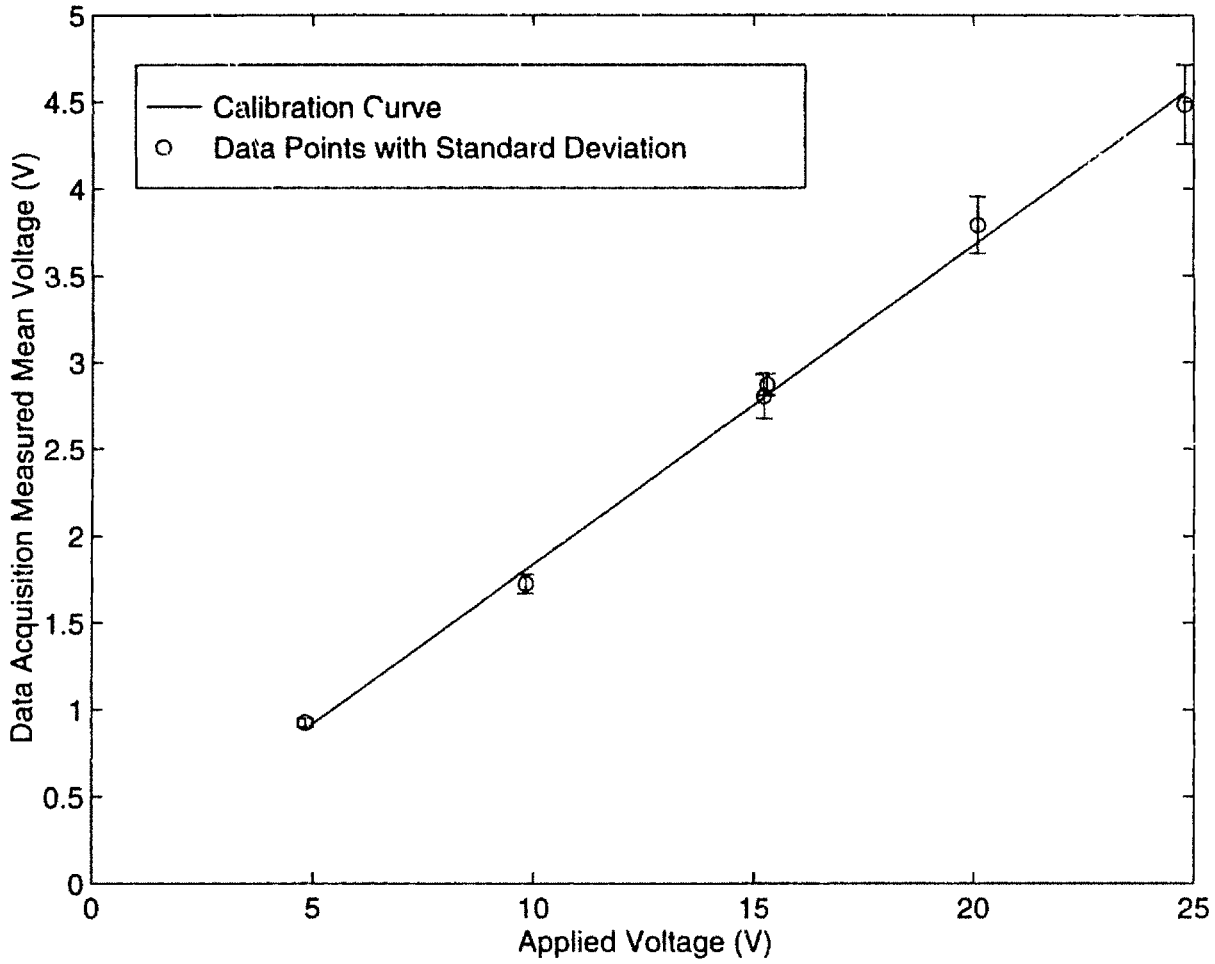

Figure 3-7: Heater Voltage Measurement Calibration Curve

Figure 3-7 and listed in Appendix D. The Daqware voltage was found to correspond to the applied voltage using the following linear relationship:

$$V^{applied} = 5.444V^{logged} \tag{3.8}$$

where V^{logged} has been logged by Daqware

3.5 Water Chemistry

Reporting water purity (and probably quantifying water purity) has been neglected by most experimenters and has been propounded by some as a possible significant parameter in critical heat flux levels. It is clear that the presence of particulates in the flow near homogeneous nucleation may cause nucleation at lower heat fluxes. For the sake of experimental characterization and completeness, conductivity measurements of coolant samples have been taken (typically after an experimental run) and logged. A Cole-Parmer conductivity meter [55] is used to measure the water conductivity in $\mu\Omega$/cm.

The measurements are quick and can be performed at any time after the experiment since the water samples were logged and saved in sterile vials. The manufacturer's instructions [55] are as follows:

1. Turn Range switch to position x1k
2. Center Cal knob
3. Rinse probe in distilled water
4. Insert probe in sample
5. Decrease range switch until reading is between 10 and 90 percent of scale
6. Choose calibration standard for that range
7. Rinse probe in distilled water
8. Measure calibration standard, and adjust Cal knob for correct reading
9. Rinse probe in distilled water
10. Measure sample

The conductivity is given digitally in $\mu\Omega$ with an accuracy of $\pm$ 2 percent of full scale [55].

Chapter 4

Computational Modeling

This chapter details the computational modeling aspect of the method of solution used in the present study. First, the problem is described and outlined using a flow chart. Subsequently, the details of the analysis is delineated and the files used in the iterative solution are defined. Finally, the resulting parameters of interest to the present study are discussed.

4.1 Problem Definition and Flow Chart

Heat transfer phenomena and representative quantitities, such as the heat transfer coefficient, applicable to the coolant side of the test section cannot be directly calculated from the measurements determined in the previous chapter. However, with the aid of a heat conduction code and heat transfer correlations for single phase water and subcooled nucleate boiling, the measured heat deposition at the channel surface can be used to calculate the inner wall heat transfer. In addition, the outer wall temperature profile can be used to validate the computed inner wall temperature profile. The outline of this computer modeling is shown in a descriptive flow chart in Figure 4-1.

The coolant-side heat transfer characteristics are calculated by linking several Fortran codes (written by the author and discussed later in the chapter) to form an executable file referred to as Program 1 in Figure 4-1. As indicated in the flow

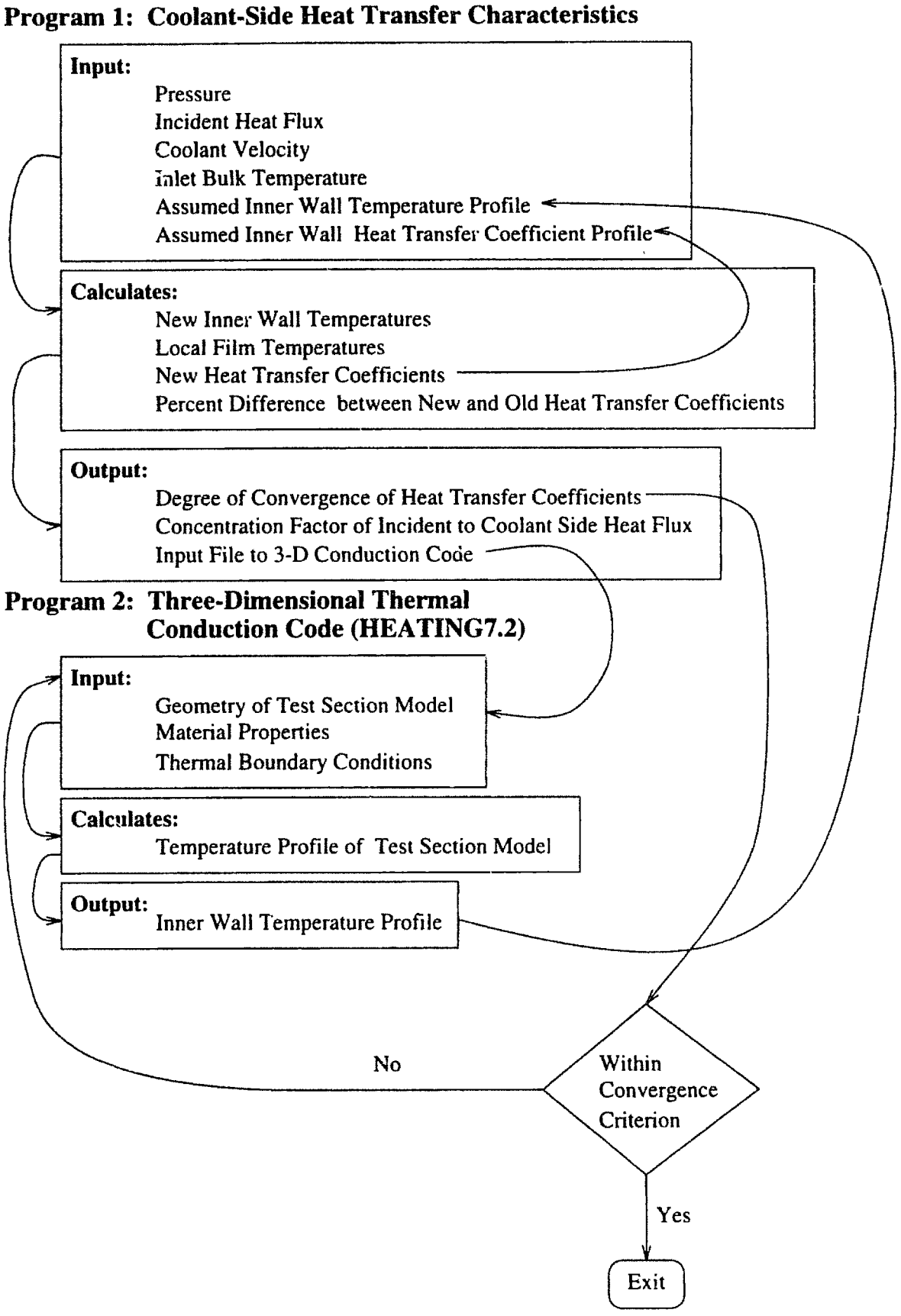

Figure 4-1: Descriptive Flow Chart of Computer Modeling Solution

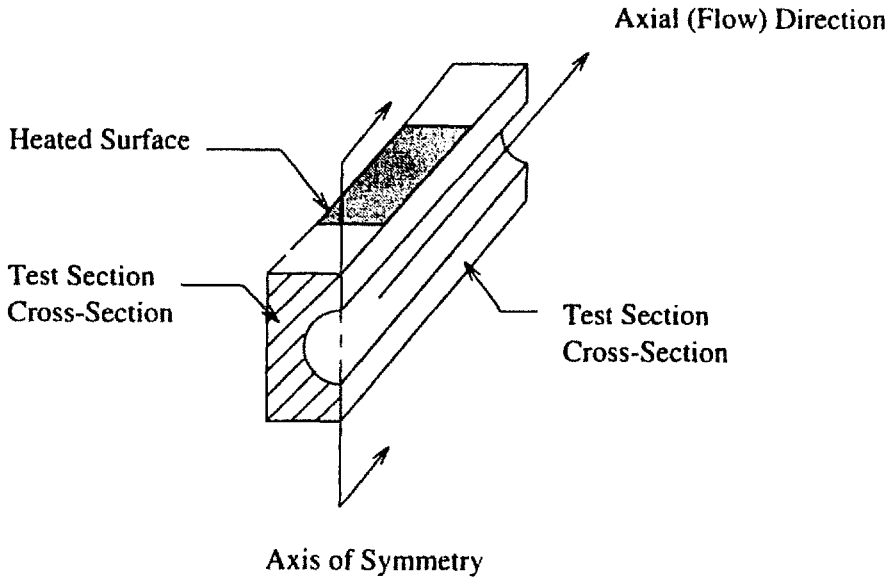

Figure 4-2: Test Section Model Showing Axis of Symmetry

chart, the computational method requires an iterative solution since heat transfer correlations, such as the Petukhov single-phase liquid heat transfer correlation, require film temperatures.

A multi-dimensional heat conduction code with temperature-dependent thermal properties entitled HEATING7.2 [56], referred to as Program 2 in Figure 4-1, was used to calculate temperature profiles for a three-dimensional model of the test section.

The model of the test section can take advantage of only one axis of symmetry because of the nonuniform axial and circumferential heat flux, and the consideration of the increase in bulk temperature along the axial direction. This axis of symmetry is illustrated in Figure 4-2.

HEATING7.2 requires a single heat transfer coefficient as the boundary condition on a region of the coolant side defined as follows:

$$h = \frac{q''}{(T_{wall} - T_{bulk})} \tag{4.1}$$

where:

q'' = Heat flux (W/m^2)

h = Heat transfer coefficient (W/m^2K)

T_{wall} = Wall temperature (^oC)

T_{bulk} = Bulk temperature (^oC)

Due to the nonuniform heating, the heat transfer coefficient will vary axially and azimuthally around the coolant channel. To approximate the actual conditions, the model was broken up azimuthally into several regions varying from 2.5^o to 10^o (shown as wedges in Figure 4-3). The non-boiling (or liquid-only) heat transfer coefficient is approximated using the Petukhov single-phase heat transfer correlation, Equation 2.10, with all properties evaluated at the average film temperature as explained by Boyd and Meng [41]. When the wall temperature is predicted to be above the saturation temperature of the coolant, a subcooled nucleate boiling correlation developed by Shah [45] or a suppression of nucleate boiling correlation developed by Chen [46] was used to predict the heat transfer coefficient. The Shah subcooled nucleate boiling and the Chen nucleate boiling correlations were presented in Chapter 2 and will not be discussed further. Once the heat transfer coefficients have been determined, HEATING7.2 is updated with these coefficients and new wall temperatures are calculated. The iteration is continued until the heat transfer coefficients are within the convergence criterion of five percent of their previous value.

Once the temperatures and the heat transfer coefficients are estimated, then the local heat flux profile at the coolant side can be readily calculated from Equation 4.1 as follows:

$$q''(\theta, z) = h(\theta, z)(T_{wall}(\theta, z) - T_{bulk}(z)) \tag{4.2}$$

where:

$q''(\theta, z)$ = Local heat flux (W/m^2)

$h(\theta, z)$ = Local heat transfer coefficient (W/m^2K)

$T_{wall}(\theta, z)$ = Local wall temperature (^oC)

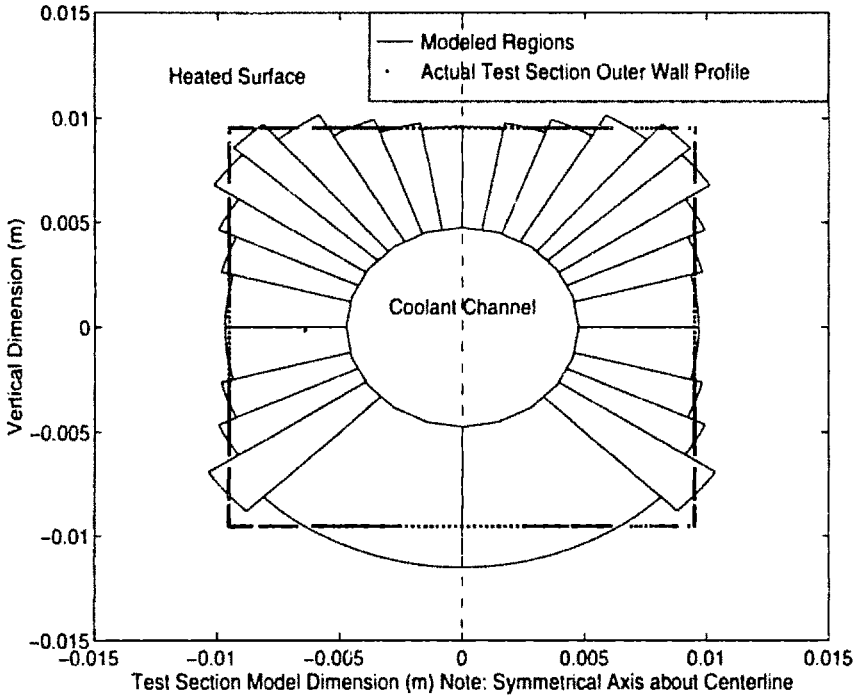

Figure 4-3: Axial Cross Section of Test Section Model with Polar Coordinates

$T_{bulk}(z)$ = Bulk temperature (°C)

θ = Azimuthal location ($\theta = 0$ is strikepoint location)

z = Axial location (m)

4.1.1 Program 1 Components and Input Files

The first part of the iteration, including Program 1, was run as a batch file. The files composing the executable Program 1 file can include three Fortran files depending on the heat transfer correlations of choice. Samples of the Fortran files are contained in Appendix C and listed in Table 4.1.

4.1.2 Program 2 (HEATING7.2) Input File Parameters

The input file to HEATING7.2 must be updated with new values for the heat transfer coefficient for each iteration. All other parameters in the input file are held constant. These parameters are defined in the following subsections.

Table 4.1: List of Fortran Files Written for the Present Study

File Name	Location in App. C	Description
sh2.for	C.4	Main program to call subroutines and generate HEATING7.2 input file
dr2s.for	C.5	Shah Subcooled Nucleate Boiling Corr. subroutine
dr1s.for	C.6	Subroutine to calculate water properties
drch.for	C.7	Chen Suppressed Nucleate Boiling Corr. subroutine
fh7	C.8	Sample input file to HEATING7.2
htc.dat	C.9	Sample boundary condition input file to sh2.for
input.one	C.10	Sample file containing initial temperature profile
ho.one	C.11	Sample file containing initial heat transfer coefficients

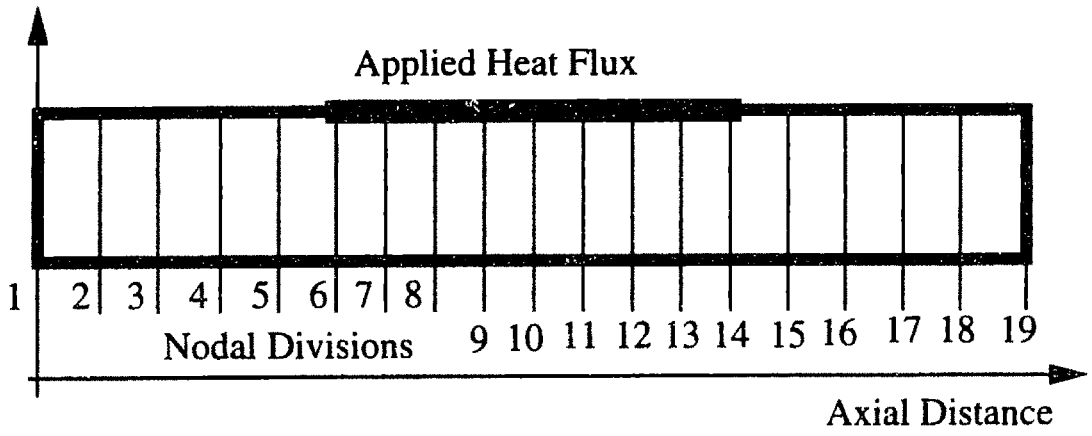

Figure 4-4: Axial Nodal Planes of Test Section Model

4.1.3 Geometry

The three-dimensional model of the test section consists of 19 axial segments, 15 azimuthal segments and 12 radial segments in an (r,θ,z) coordinate system, thus, there are 3420 nodes. The specifications of the actual test section are shown in Figure 3-4. The axial view of the model is shown in Figure 4-4.

Figure 4-3 illustrates the polar effects compared to the actual test section geometry. Figure 4-5 shows Figure 4-3 in rectilinear coordinates to illustrate the axial cross sectional nodes.

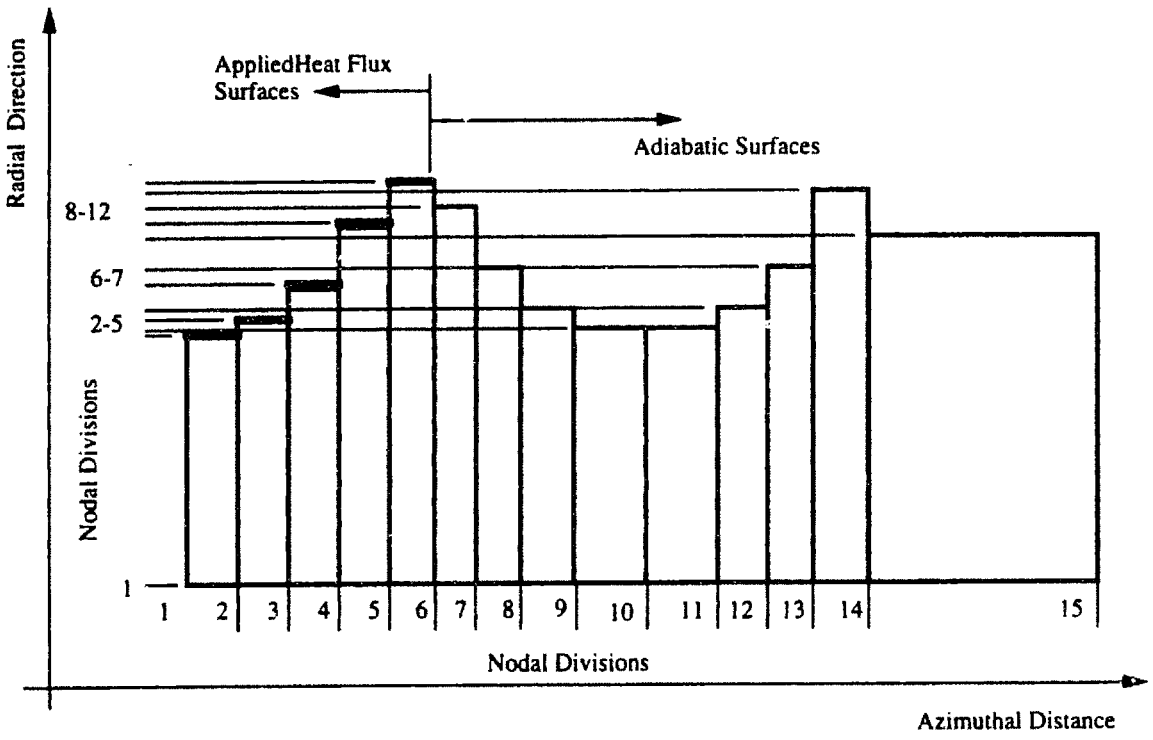

Node locations drawn to scale in relation to other nodes in their respective direction.

Figure 4-5: Axial Cross Sectional Nodes of Test Section Model in Rectilinear Coordinates

4.1.4 Boundary and Initial Conditions

Figures 4-4 and 4-5 also show the location of the applied heat flux boundary condition. There are 140 regions with a local convective heat transfer coefficient determined using the aforementioned correlations (e.g. the Petukhov correlation Equation 2.10 when $T_{wall} \leq T_{sat}$ and the Shah correlation [45] when $T_{wall} \geq T_{sat}$). The Shah and Chen correlations are convenient to use in HEATING7.2 iterations because they have a smooth transition at T_{sat}, in other words:

$h_{Shah}(\theta, z) = h_{Chen}(\theta, z) = h_{Petukhov}(\theta, z)$ @ $T_{wall} = T_{sat}$

This convective heat transfer boundary condition is applied along the coolant side of the test section which corresponds to the plane r = 4.75 mm in Figure 4-5.

The test section model surfaces not mentioned above are considered to be adiabatic.

The HEATING7.2 calculations are run to steady state which takes about a minute in real time using a Pentium computer. The initial temperature is arbitrarily set as the inlet bulk temperature of the coolant. The local bulk temperature is updated after each axial segment using a heat balance in the heated zones as follows:

$$T_{bulk}(z) = T_{inlet} + \frac{q_0'' L_h(z)}{A_{channel} G C_{pl}} \tag{4.3}$$

where:

$T_{bulk}(z)$ = Coolant bulk temperature along axial direction (°C)

T_{inlet} = Inlet bulk temperature (°C)

q_0'' = Incident heat flux (W/m^2)

$L_h(z)$ = Portion of length along axial direction that has been heated (m)

$A_{channel}$ = Cross sectional coolant channel area (m^2)

G = Mass flux (kg/m^{2}s)

C_{pl} = Liquid specific heat at constant pressure (J/kgK)

Table 4.2: Conductivity of Copper versus Temperature

Temperature °C	Conductivity W/mK
0	401
200	389
400	378
600	366
800	352
1000	336

4.1.5 Properties

The only input properties to HEATING7.2 are the material properties of the test section. The test section is assumed to be pure copper and the properties are from textbook [57]. A constant (i.e., temperature independent) density of 8933 kg/m^3 and constant specific heat of 385 J/kgK are input into HEATING7.2. The conductivity of copper (which is temperature dependent) is the only property to affect the steady state solution and is given as a table to HEATING7.2 as shown in Table 4.2.

4.2 Input File Code

Program 1 was written to interface between HEATING7.2 iterations. The main code, referred to as *sh2.for* in Table 4.1, reads the coolant-side wall temperatures from the previous steady state solution and calculates a new heat transfer coefficient using correlations. The new heat transfer coefficient is compared to the old value and if the two compare within five percent in all 140 regions, then the solution is considered to have converged. Otherwise, the average of the two heat transfer coefficients is placed into a new input file (called *fh7*) for HEATING7.2. Some subroutines for *sh2.for* were also written by the author and are contained in files *dr1s.for*, *dr2s.for* and *drch.for*. The code files and sample files are listed in Appendix C as referenced in Table 4.1.

The input values that define the rest of the problem are placed in a small (five-line) file called *htc.dat* and contains the information in Table 4.3. A sample *htc.dat* file is listed in Appendix C.9.

Table 4.3: Problem Definition File *htc.dat* contents for *sh2.for*

Power to Heated Section	kW
Coolant Velocity	m/s
Inlet Bulk Temperature	^oC
Pressure	MPa
Test Section Identification Number	TS#

Since the Petukhov, hence Shah and Chen, correlation is evaluated at the film temperature (as intended [41]), a water properties code is contained in the subroutine *dr2s.for*. The code is part of a larger French water properties subroutine called *Fpeau* and was obtained from the Thermal Hydraulic Research Division of the Water Reactor Department of the *Commissariat à l'Engergie Atomique* in Grenoble, France [58]. The code is valid for subcooled water properties and only the part relevant to water and steam (i.e., no gases other than vapor) has been extracted for use in the present study.

Clearly, the initial wall temperature profile and heat transfer coefficients are required to begin the HEATING7.2 iterations. These somewhat arbitrary files are called *input.one* and *ho.one* and are listed in Appendix C.10 and C.11, respectively.

4.3 Parameters of Interest from Modeling

The goal of the computational modeling is twofold. First, the modeling supplies wall temperature distributions at all nodal points in the test section. The calculated outer wall temperatures can be compared to the thermocouple-measured temperatures to validate the operational thermal hydraulic regime at the inner wall (i.e., transition from single phase to subcooled boiling to critical heat flux). Obviously, if measured temperatures do not predict a superheated wall on the coolant side, then it is doubtful that subcooled boiling or critical heat flux had occurred. The measured temperatures will also shed light on the possibility of failure of test section components due to phenomena other than critical heat flux or nonuniformity in the heated area.

Secondly, the computational model contains local values of the heat transfer coefficient from which the local heat flux can be determined using Equation 4.2. The local

heat flux is of interest to thermal hydraulists since the incident heat flux is apparatus specific while heat transfer models should be independent of geometry outside of the coolant-wall interface. Thus, the present study reports the local heat flux using a concentration factor, Φ, defined as follows:

$$\Phi = \frac{q''(\theta, z)}{q_0''} \tag{4.4}$$

where:

$q''(\theta, z)$ = Local heat flux (W/m^2)

q_0'' = Incident heat flux (W/m^2)

Other output files from Program 1 (such as *dot.dat* and *reg.dat*) are formatted for a packaged graphics application called Matlab. Matlab is used to generate all the output plots given in Appendices E to H which include Power and Temperature Profiles, Thermal Hydraulic Regions, Concentration Factor Profiles, and Measured and Calculated Temperatures, respectively.

Chapter 5

Results

5.1 Synopsis

Thirty-three high heat flux experimental runs are presented in this chapter. In each run, power was increased in steps until the test section heater failed at the end of each trial. Failure occurred by destruction of the heater while reaching elevated temperatures as power was increased to the test section. The aggregate measured and deducted data will be presented first. Particular runs will be discussed in detail to illustrate the approach used for determining the deducted values. Table 5.1 lists the measured parameters as recorded by hand. The test sections are identified by a number corresponding to the test specimen. Each test specimen has two sides (A and B) coated with alumina and tungsten. Data acquired by the automated recording system are plotted in figures presented in this chapter or in Appendices E to H. Table 5.2 lists the test sections and major thermal hydraulic parameters deduced from measurements and the computer model analysis. All raw data for each test run are contained in Appendix E, including hand noted data.

Except where noted by ^{ch} in Table 5.2, the Shah Correlation [45] for Subcooled Nucleate Boiling is used in the computer model analysis to determine the heat flux concentration factor, Φ, defined in Equation 4.4. The Chen Correlation for Suppressed Nucleate Boiling with saturated bulk temperature (i.e., without the subcooled bulk modification) is used to calculate the heat transfer coefficient for the low mass flux

Table 5.1: Measured Parameters

Test Section ID	Velocity m/s	Inlet T $_{bulk}$ °C	Exit Pressure MPa	Current[a] A	Voltage[a] V
TS6A	9.03	20	2.65	900	18.1
TS9B	4.66	20	2.93	700	17.2
TS11A	7.21	20	2.77	600	19
TS14B	10.42	20	2.50	800	20
TS15A	5.90	20	2.86	850	16.5
TS15B	5.73	20	2.90	625	15.5
TS16B	0.63	20	3.07	415	20
TS17A	2.55	20	3.00	500	13.2
TS17B	3.68	20	2.96	625	17
TS18A	.395	20	3.08	600	12.75
TS18B	.265	20	3.07	600	12.5
TS19A	3.54	20	3.00	925	16.5
TS19B	11.28	16	2.55	1100	17.4
TS20A	6.68	20	2.86	960	14.4
TS20B	10.3	18.9	2.58	825	14.5
TS21A	5.00	22.5	2.96	1000	17.5
TS21B	3.66	23.25	3.01	825	14.6
TS22A	9.20	20.35	2.69	1500	12.75
TS22B	9.73	17.45	2.65	1150	10.0
TS23A	8.70	21.05	2.72	1170	11.5
TS23B	10.2	21.1	2.62	1060	13.0
TS24A	10.55	21.1	2.58	1170	14.0
TS24B	10.64	23.25	2.55	1460	10.75
TS25A	8.25	24.7	2.76	1100	8.9
TS25B	7.41	24.7	2.79	1170	11.0
TS26A	5.74	21.8	2.92	1300	12.4
TS26B	4.5	23.25	2.95	900	11.25
TS27A	5.94	21.8	2.91	1350	9.74
TS27B	19.38	18.9	1.79	1400	12.5
TS28A	5.53	21.8	2.94	1300	10.28
TS28B	4.35	24.7	2.98	1200	10.61
TS29A	15.2	18.9	2.17	1300	12.35
TS29B	13.6	18.9	2.31	1400	12.38

[a] = Last noted value

Table 5.2: Synopsis of Reduced Data: Major Thermal Hydraulic Parameters

Test Section ID	G Mg/m^2s	Equil. Quality	Power kW	Exit Pressure MPa	Concentration Factor, Φ	$q"_{local}$ MW/m^2
TS6A	9.02	-.472	16.3	2.65	1.373	23.5
TS9B	4.65	-.486	12.0	2.93	1.298	16.4
TS11A	7.2	-.478	12.9	2.77	1.241	16.8
TS14B	10.4	-.460	18.5	2.50	1.432	27.8
TS15A	5.89	-.479	14.0	2.86	1.358	20.0
TS15B	5.72	-.486	11.3	2.90	1.187	14.1
TS16B^{ch}	0.63	-.398	9.3	3.07	1.598	15.6
TS17A	2.55	-.480	9.4	3.00	1.264	12.5
TS17B	3.68	-.468	12.5	2.96	1.363	17.9
TS18A^{ch}	.394	-.269	12.3	3.08	1.598	17.8
TS18B^{ch}	.265	-.197	10.6	3.07	1.598	20.6
TS19A	3.54	-.472	16.9	3.00	1.498	26.6
TS19B	11.3	-.472	19.1	2.55	1.417	28.4
TS20A	6.67	-.470	16.2	2.86	1.415	24.1
TS20B	10.3	-.469	15.3	2.58	1.279	20.5
TS21A	4.99	-.473	22.3	2.96	1.581	37.0
TS21B	3.65	-.476	12.0	3.01	1.353	17.0
TS22A	9.19	-.467	22.5	2.69	1.532	36.2
TS22B	9.72	-.480	11.5	2.65	0.997	12.0
TS23A	8.68	-.472	15.6	2.72	1.356	22.2
TS23B	10.2	-.468	13.9	2.62	1.214	17.7
TS24A	10.5	-.464	19.7	2.58	1.475	30.5
TS24B	10.6	-.452	15.7	2.55	1.320	21.8
TS25A	8.23	-.472	9.8	2.76	0.967	10.0
TS25B	7.39	-.461	14.4	2.79	1.351	20.4
TS26A	5.73	-.469	16.1	2.92	1.427	24.1
TS26B	4.49	-.469	12.8	2.95	1.354	18.2
TS27A	5.93	-.488	13.1	2.91	1.306	18.0
TS27B	19.38	-.410	17.5	1.79	1.188	21.8
TS28A	5.52	-.471	13.7	2.94	1.364	19.6
TS28B	4.34	-.474	12.7	2.98	1.357	18.1
TS29A	15.2	-.441	16.1	2.17	1.209	20.4
TS29B	13.6	-.450	17.3	2.31	1.340	24.3

^{ch} = Used Chen Correlation for Nucleate Boiling

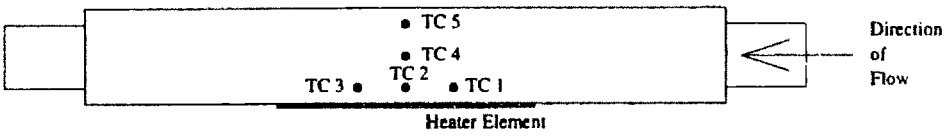

Figure 5-1: Test Section Thermocouple Locations for TS14B and Higher (Note: drawn to full relative scale with respect to test section)

($\leq$ 1.0 Mg/m^{2}s) experiments; the other correlations (Shah ~~and Modified Chen~~, see Chapter 2) did not lead to convergent solutions using HEATING7.2 (Note: in the case of the Shah correlation, this may be due to a mistake in the low subcooled boiling region part of the code).

Table 5.3 gives nondimensional thermal hydraulic parameters such as those employed in the Saha-Zuber bubble departure correlation [39] discussed in Chapter 2.

5.2 Wall Temperature Measurements

Table 5.4 contains the maximum thermocouple measured wall temperatures (before spiking if applicable). Blanks in the columns under thermocouple numbers indicates that either no thermocouple was placed at that location or the thermocouple moved out from that location during the course of the experiment. The locations of TC 1-5 are shown in Figure 5.4 for test sections TS14B and higher, see Appendix E.2 for locations of TS6A, TS9B and TS11A.

Table 5.3: Synopsis of Reduced Data: Dimensionless Numbers

Test Section ID	Re[a]	Pr[b]	Pe[c]	St[d]	Nu[e]
TS18B[ch]	18400	0.902	16600	0.11938	991.
TS18A[ch]	25200	0.954	24000	0.06831	822.
TS15A	264000	1.300	344000	0.00288	495.
TS24B	464000	1.333	618000	0.00185	573.
TS19A	166000	1.247	207000	0.00593	613.
TS25B	334000	1.291	431000	0.00241	520.
TS28A	252000	1.281	322000	0.00301	485.
TS26B	207000	1.267	262000	0.00350	459.
TS26A	262000	1.278	334000	0.00343	575.
TS16B[ch]	33700	1.105	37200	0.02177	405.
TS11A	318000	1.320	420000	0.00217	455.
TS19B	481000	1.370	659000	0.00205	675.
TS21A	235000	1.243	292000	0.00561	818.
TS21B	170000	1.254	213000	0.00404	431.
TS22A	408000	1.315	536000	0.00302	811.
TS24A	459000	1.334	612000	0.00233	714.
TS28B	202000	1.256	254000	0.00361	458.
TS20B	444000	1.353	600000	0.00181	545.
TS27A	269000	1.289	247000	0.00268	463.
TS17A	118000	1.264	149000	0.00450	335.
TS15B	256000	1.303	334000	0.00237	395.
TS20A	300000	1.299	389000	0.00294	573.
TS17B	169000	1.273	215000	0.00414	445.
TS23A	384000	1.320	506000	0.00220	556.
TS23B	444000	1.339	595000	0.00167	497.
TS29A	625000	1.417	886000	0.00135	597.
TS29B	569000	1.392	793000	0.00160	633.
TS9B	210000	1.290	271000	0.00311	422.
TS6A	395000	1.333	526000	0.00221	582.
TS14B	449000	1.351	606000	0.00221	671.
TS25A	367000	1.307	480000	0.00146	351.
TS22B	417000	1.359	566000	0.00142	402.
TS27B	758000	1.485	1130000	0.00121	682.

[ch] = Used Chen Correlation for Nucleate Boiling
[a]Re = GD_e/μ
[b]Pr = μ C_{pl}/k
[c]Pe = $RePr$
[d]St = $q''/(GC_{pl}(T_{sat} - T_{bulk}))$
[e]Nu = $q''D_h/(k_l(T_{sat} - T_{bulk}))$
(Note: q'' are peak values. Water properties are evaluated at film temperatures.)

Table 5.4: Maximum measured wall temperatures listed in order of highest observed temperature (before spiking if applicable)

Test Section ID	TC1 (°C)	TC2 (°C)	TC3 (°C)	TC4 (°C)	TC5 (°C)
TS26B	423	258	228	154	96
TS24B	385	298	300	160	117
TS15A	350	350	400		
TS21A		321	366	220	
TS26A	168	305	355	163	134
TS18B		350			
TS19A	342	313			
TS25B	260	250	334	170	140
TS19B	332	333	332	200	
TS29B	324	289	314	168	121
TS28B	231	293	323	173	132
TS16B	320	265			
TS21B	318		314	198	
TS24A	243	193	309	150	
TS28A	299	306	289	179	136
TS22A	277	304	207	150	104
TS11A[a]	240	135	105		
	215	146	90		
	213	128	117		
	296	117	110		
	202	150	78		
	175	142	108		
TS20A	290	283			
TS18A		285			
TS23B	285	178	252	138	111
TS17A	285	234			
TS23A	246	283	246	178	130
TS17B	283	78			
TS27A	275	237	280	189	145
TS15B	196	273			
TS27B	268	262	262	143	132
TS20B	235	227	262	185	137
TS29A	255	255	260	129	96

[a] Temperature plateaus: TCs switched in mid-experiment using switchboxes

Table 5.4 (Continued) Maximum measured wall temperatures listed in order of highest observed temperature (before spiking if applicable)

Test Section ID	TC1 (°C)	TC2 (°C)	TC3 (°C)	TC4 (°C)	TC5 (°C)
TS22B	237	242	245	130	78
TS25A	241	221	153	132	97
TS6A[a]	235	187	123		
	155	126	87		
TS9B[a]	145	232	150		
	101	150	120		
	73	115	107		
TS14B	207	181	228		

[a] Temperature plateaus: TCs switched in mid-experiment using switchboxes

5.3 Sample of Data Acquisition Plots

The raw data plots from the computerized data acquisition system are contained in Appendix E, Figures E-1 to E-87. For illustration, the power and temperature histories for trial TS28A are shown in Figures 5-2 to 5-4. TC 1, 2, and 3 in Figure 5-3 are located the same distance from the heater but at various axial positions. TC 2, 4, and 5 in Figure 5-4 are all located at the axial midplane of the test section but vary in distance from the heater (see Figure 5-1 for a scaled drawing showing the relative locations of the thermocouples with respect to the heater).

5.4 Sample of HEATING7.2 Results: Thermal Regions and Concentration Factor

The results of HEATING7.2 for the thermal region and concentration factor, Φ, profiles are presented graphically in Appendices F and G, respectively. For illustration, the thermal region and concentration factor profiles for trial TS28A are shown in Figures 5-5 to 5-8. The Thermal Region Profile illustrates the thermal-hydraulic phenomena at the coolant-side wall. At low wall temperatures, the Petukhov [41]

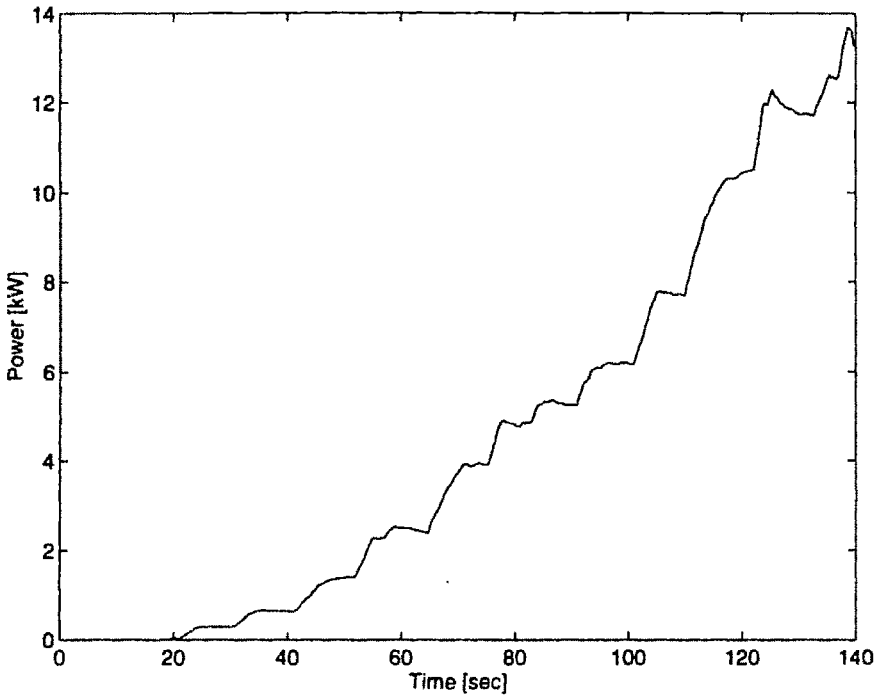

Figure 5-2: Test Section 28A Power History

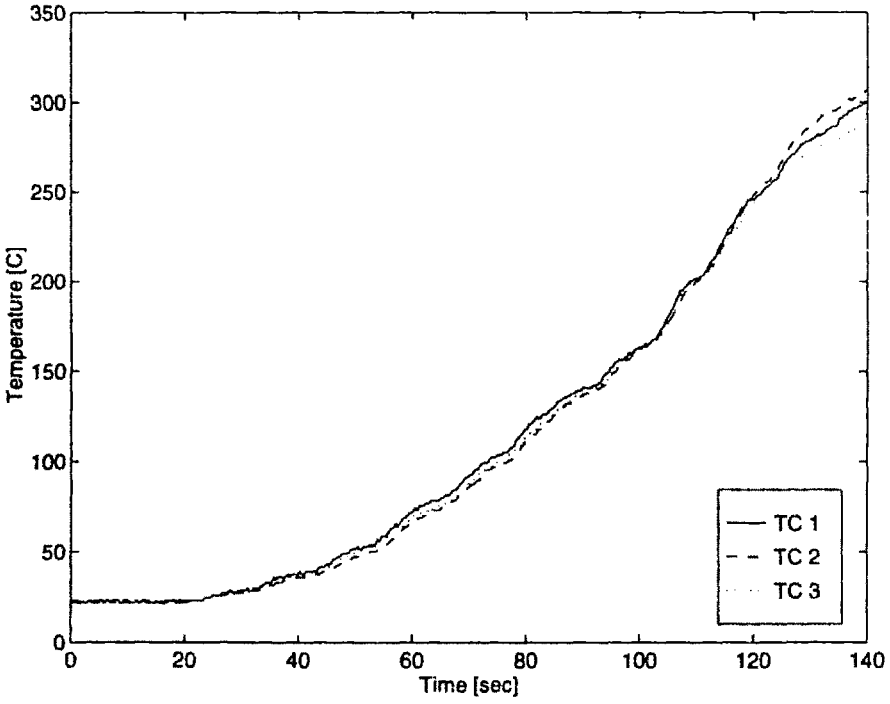

Figure 5-3: Test Section 28A Outer Wall Temperature History

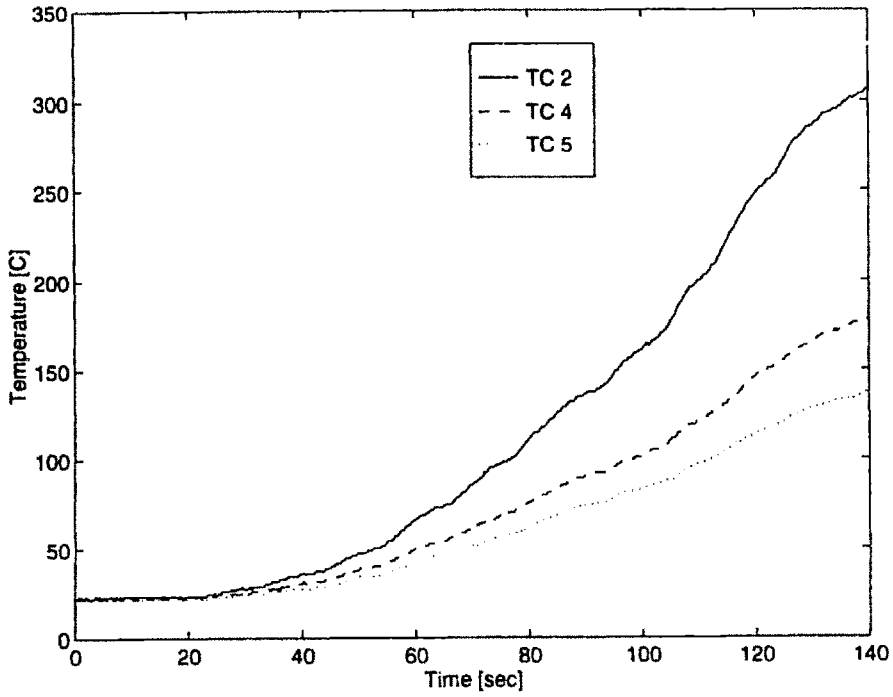

Figure 5-4: Test Section 28A Outer Wall Temperature History

single phase heat transfer correlation is used. When the wall temperature reaches saturation, the Shah [45] or Chen [46] nucleate boiling correlations are employed at the corresponding node locations. In other words, in Figures 5-5 and 5-6, the points where the Heat Transfer Regime equals 2 along the test section imply that the wall temperature is above saturation. Similarly, the points plotted in Figures 5-7 and 5-8 illustrate the distribution of concentration factors. The azimuthal and axial node numbers can be correlated to find a unique value for Φ. However, the maximum Φ is reported in Table 5.2 which corresponds to the maximum local heat flux.

5.5 Sample of Temperature Comparison Plots

Measured temperatures in Table 5.4 are compared to HEATING7.2 calculations for all runs and the results are given in Appendix H. For illustration, the measured temperatures in run TS28A are compared to HEATING7.2 results in Figures 5-9 and 5-10. The lateral scatter of the measurements reflects the uncertainty in thermocouple location and is not indicative of the number of thermocouples. In the latter

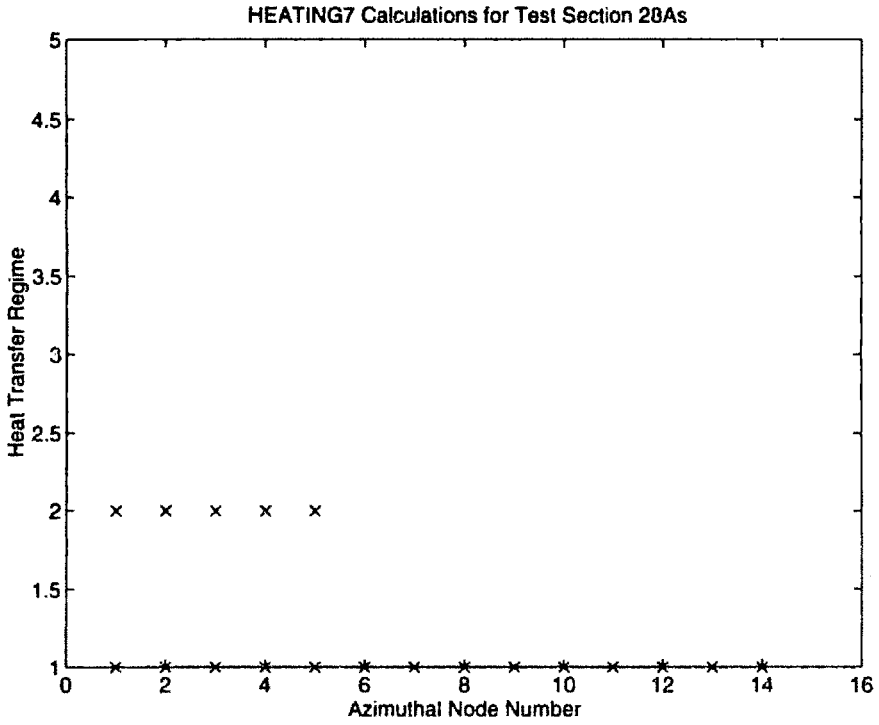

Figure 5-5: Test Section 28A Azimuthal Thermal Region Profile
1: Single Phase Liquid; 2: Boiling; 3: T $\geq$ T (homogeneous nucl.); 4: T $\geq$ T (crit)

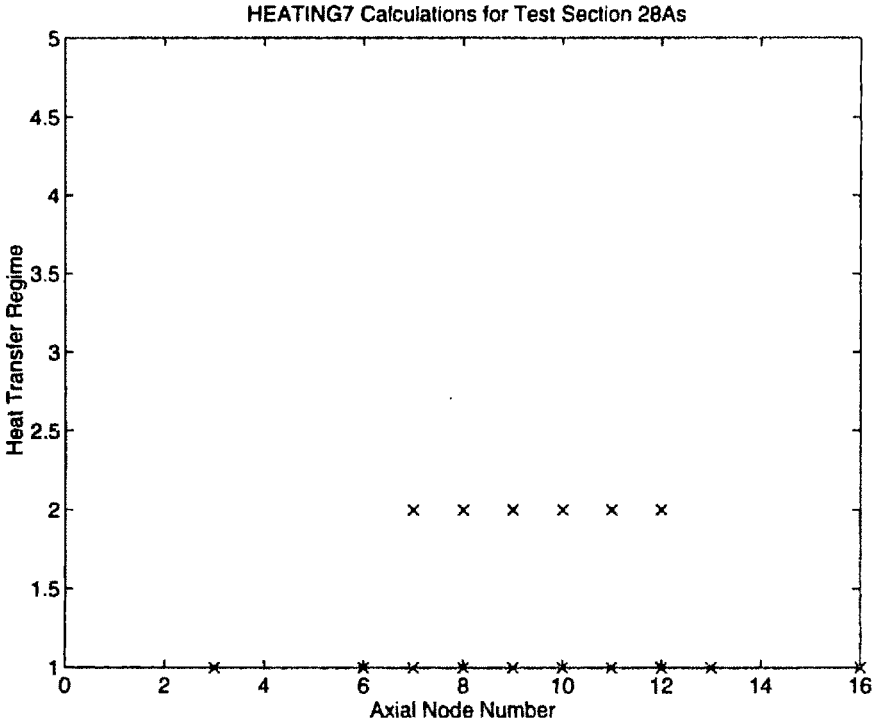

Figure 5-6: Test Section 28A Axial Thermal Region Profile
1: Single Phase Liquid; 2: Boiling; 3: T $\geq$ T (homogeneous nucl.); 4: T $\geq$ T (crit)

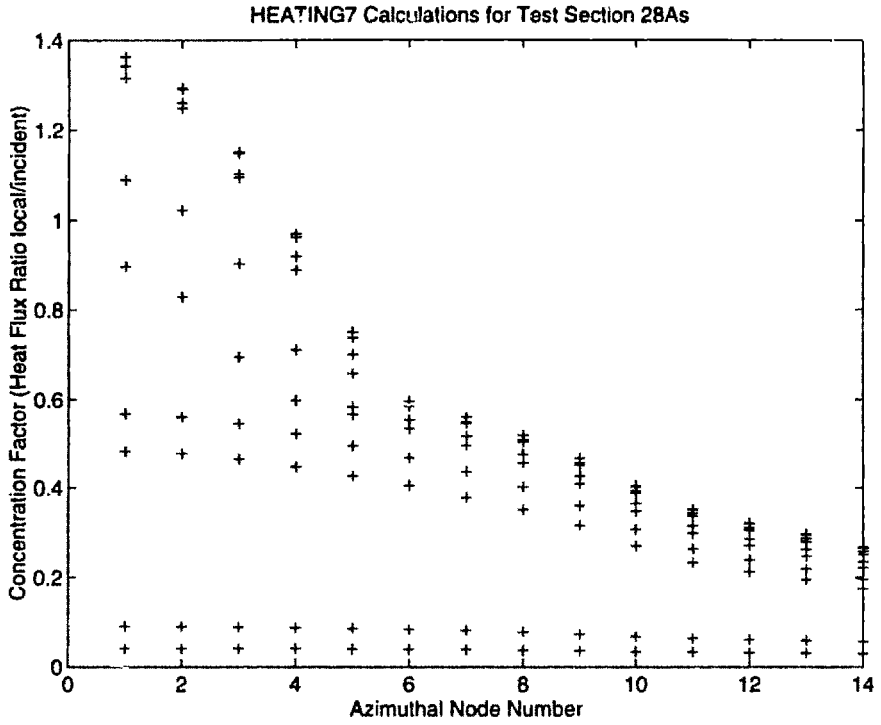

Figure 5-7: Test Section 28A Azimuthal Concentration Factor Profile

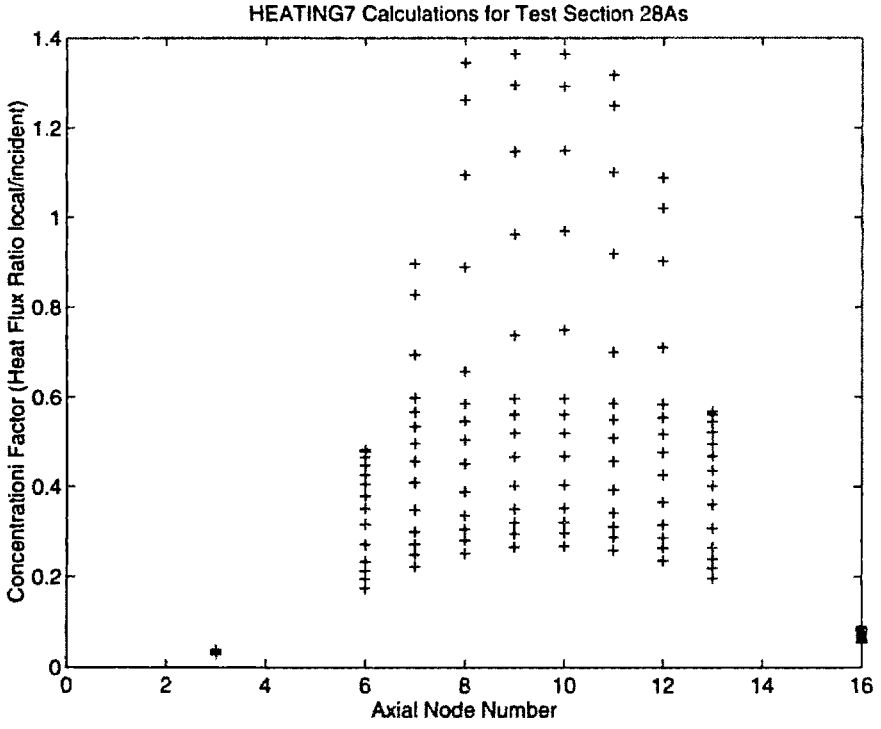

Figure 5-8: Test Section 28A Axial Concentration Factor Profile

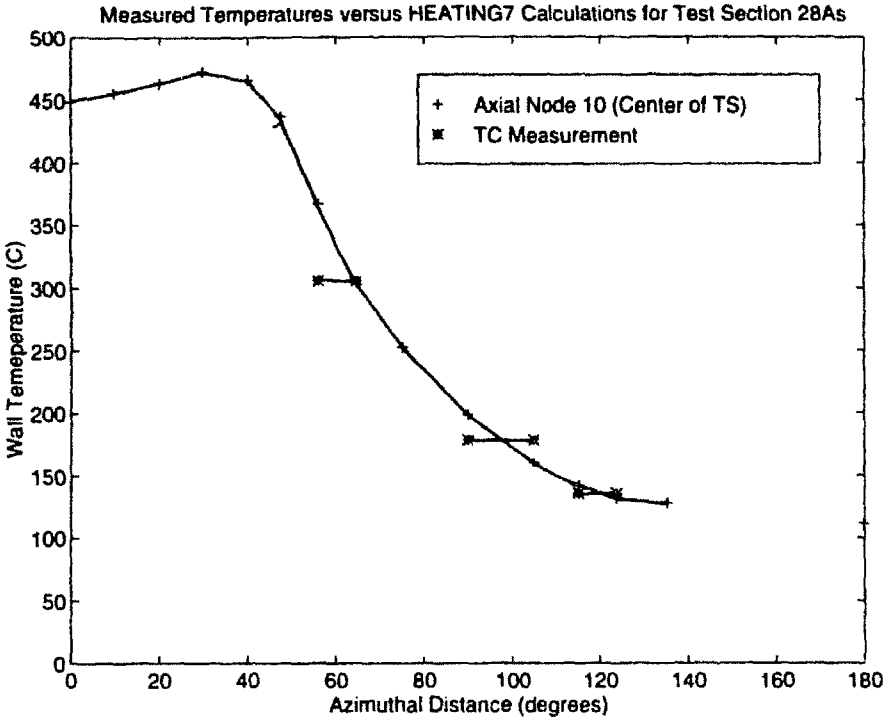

Figure 5-9: Test Section 28A Comparison of Measured to Calculated Temperatures (Azimuthal Direction)

experiments (those conducted after TS19B), five thermocouples were used. For three tests (TS19B, 21A and 21B), four thermocouples were used. And earlier test runs used two or three thermocouples. The number of temperatures reported may not be consistent with the number used if the thermocouples were observed to have moved from their appointed location.

5.6 Water Purity

Throughout the course of experimentation, the coolant water had to be recirculated from the downstream tank to the upstream tank. Typically, the water was filtered as described in Chapter 3. After each test run, the water remaining in the Test Section was saved in a sterile vial and its electrical conductivity was measured. The results of the conductivity measurements corresponding to each test run are shown in Figure 5-11. The electrical conductivity of the water is proportional to the number of charged particles in the sample and can be used as a gauge of water purity as indicated in Table 5.5 from [55]. Thus, although the filtering system did not produce

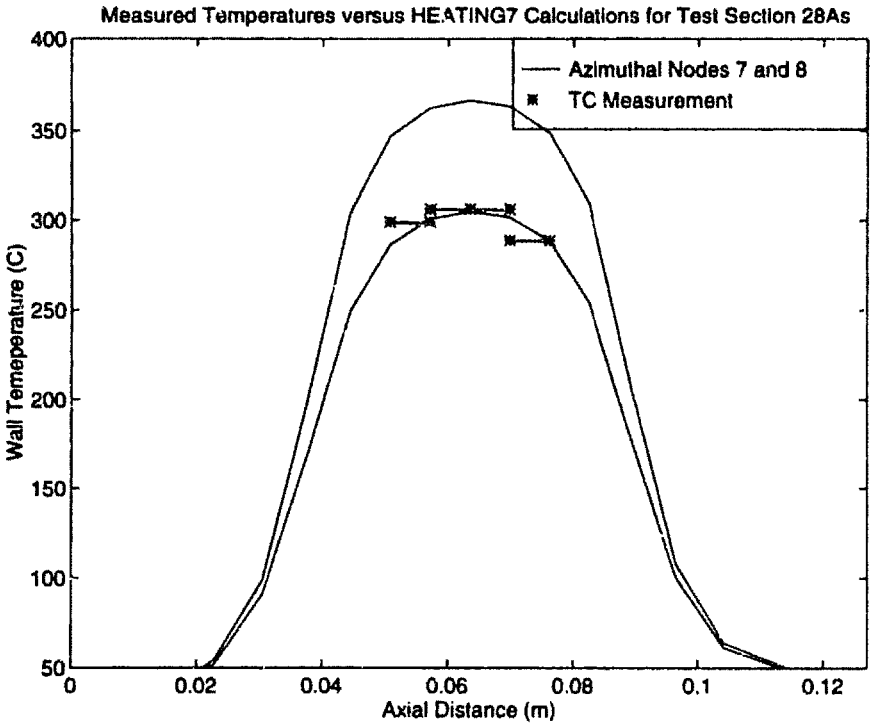

Figure 5-10: Test Section 28A Comparison of Measured to Calculated Temperatures (Axial Direction)

Table 5.5: Conductivity and Water Purity

Conductivity $\mu\Omega$/cm	Description
0.5 to 2.0	Freshly Distilled Water
50 to 1500	Potable Water
18,400	Normal Saline Solution

freshly distilled water, the water used in the present study is on the lower end of the potable water range. This analysis allows the water purity used in the experimental runs to be quantified in case of inquiry.

5.7 Uncertainty Analyses

The uncertainties in the evaluation of the critical heat flux (q''_{CHF}), temperatures, and mass flux (G) are calculated using a method presented by Kline and McClintock and described by Holman (1984) [59] in which the uncertainty in a measurement is estimated by the experimenter and given odds depending on the experimenter's

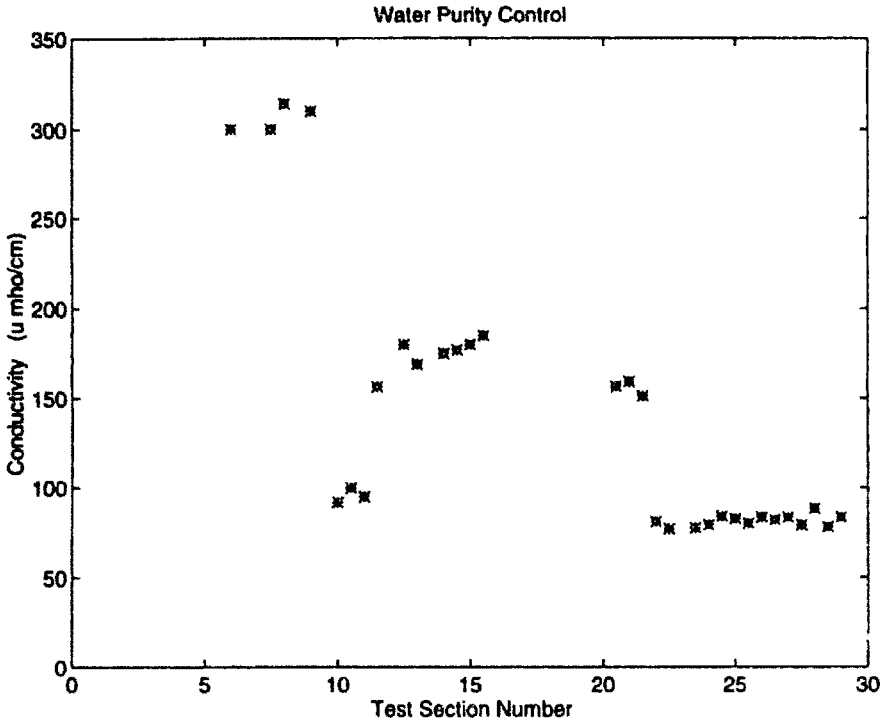

Figure 5-11: Electrical Conductivity of Coolant Water

confidence. In the present study, uncertainties were estimated with odds of 20-1. If w_R is the uncertainty in a result R which is a function of i independent variables, x_i, with an uncertainty of w_i, then w_R is given as:

$$w_R = [\sum_i (\frac{\partial R}{\partial x_i} \bullet w_i)^2]^{1/2} \tag{5.1}$$

Table 5.6 lists typical uncertainties assigned to measurements which were determined from equipment manufacturers' specifications and experience. Table 5.7 summarizes typical uncertainties in the important parameters considered in the present study.

Table 5.6 indicates that the uncertainties in two parameters significantly affect the total uncertainties given in Table 5.7: the heated area of the spiked heat flux and low-flow mass flux, which account for 12.5 and 10 percent uncertainty, respectively.

The heated area uncertainty is large due to the large relative size of the electrodes. Figure 5-12 illustrates the relative size of the electrodes with respect to heated length and width. The uncertainty in the axial heated length (also shown in Figure 5-12) is based on two independent observations: first, the variation in the observed

Table 5.6: Typical Uncertainties in Independent Variables

Measurement	Symbol (units)	w_i	x_i	Percent, $\frac{w_i}{x_i}$
Heated Area	A (m^2)	1.21 x 10^{-4}	9.68 x 10^{-4}	12.5
Current	I (A)	10	1000	1.0
Voltage	V (V)			0.3
Concentration Factor	Φ			5.0
Coolant Velocity	v $\geq$ 2.5 m/s			0.15
	v $\leq$ 2.5 m/s			10.0
Temperature	T (K)	3.0	300	1.0
Pressure	P (MPa)	0.03	3.00	1.0

Table 5.7: Typical Uncertainties in Important Parameters

Parameter, R	Symbol (units)	w	x	Percent, $\frac{w}{x}$
Critical Heat Flux	q''_{CHF} (MW/m^2)			13.5
Bulk Temperature	T_{bulk} (K)	3	293	1.0
Wall Temperature	T_{wall} (K)	3	500	0.6
$Pe = \frac{GDC_{pl}}{k_l}$	$\geq$ 1.56 x 10^5	240	160,000	0.15
	$\leq$ 1.56 x 10^5	15,000	150,000	10.0
$St_{CHF} = \frac{q''_{CHF}}{GC_{pl}(T_{sat}-T_{bulk})}$	Pe $\geq$ 1.56 x 10^5	0.00056	0.00414	13.6
	Pe $\leq$ 1.56 x 10^5	0.00076	0.00450	16.9

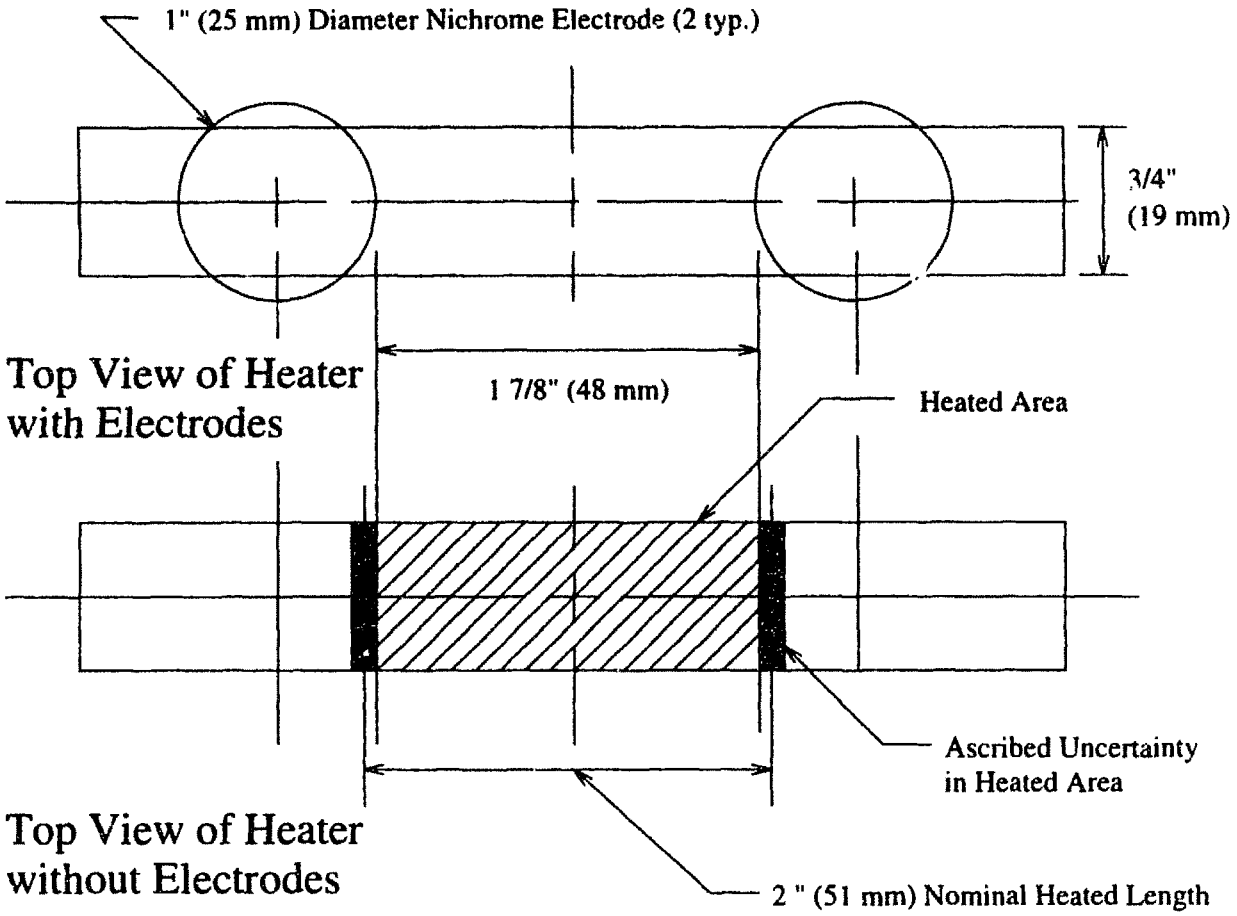

Figure 5-12: Two Views of Heater: Top showing location of electrodes and bottom illustrating ascribed heated area and uncertainty

discoloration of the test sections (i.e., where the heater is discolored or the tungsten has oxidized to yellow); and, secondly, the approximate surface connection between the nichrome electrode and the tungsten heater. Both of these considerations give about the same uncertainty of $\pm$ 6 mm.

The low-flow region of the mass flux measurements are outside of the manufacturer's recommended range of accuracy. Thus, a low-flow calibration was carried out and data fell within 10 percent of the reported correlation (as discussed in Chapter 3).

The K-type thermocouple voltages were measured using the Daqware system (also

discussed in Chapter 3) with a sensitivity of 1.5 K. Therefore, a ± 3 K uncertainty due to this sensitivity appears reasonable. This translates to about 1 percent of the bulk temperature and 0.6 percent of the wall temperature. The uncertainties ascribed to the wall temperatures, however, are more difficult to quanitify since the thermocouples were essentially pressed to the walls of the test sections. Dimples were made to aid in their placement, however, alumina and tungsten sprayed particles may have caused unexpected temperature drops. Thus, although the measured temperatures may be fairly accurate, the precise location of the thermocouple and the copper wall temperature have a higher uncertainty. This uncertainy is not reflected in the present section but is considered in the comparison of the calculated wall temperatures as shown in Section 5.5. The range of computed temperatures and the spread of measured points are meant to illustrate uncertainty due to the inexact geometry of the conduction model and the inexact location of the thermocouples, respectively, without rigorously quantifying these for each test section. The measured temperatures and the code calculated temperatures were meant as a tool to validate the heat flux characteristics (e.g., uniformity of the heat flux spike and reliability of the power measurement), not to determine the correlation between important thermal hydraulic parameters such as Pe and St_{CHF} which will be discussed in the next chapter.

The conduction code calculations are required, however, in determining the concentration factor, Φ, which relates the incident heat deposition to the local heat flux values at the coolant-side wall. The solution to the iterative process was considered to converge when the heat transfer coefficients on all 140 surfaces of the model fell within five percent of the previous value (as discussed in Chapter 4). In addition, a large variation in the heat transfer coefficient (e.g., Shah versus Chen) produced a variation in Φ of about half the percent difference. Considering that all the bench mark data heat fluxes were validated using independent temperature measurements, an uncertainty of ± 5 percent is used in the present analyses.

Chapter 6

A Framework For CHF Prediction

This chapter analyzes the results contained in the previous chapter. First, power-based heat flux estimates are validated using thermocouple measurements. Next, a parametric investigation of the bench mark critical heat flux data is performed and compared to some CHF correlations. Finally, a new CHF correlation is developed based upon phenomenological relations, with certain coefficients and exponents determined empirically using the bench mark data. The correlation is further validated using the data base described in Chapter 1.

6.1 Interpretation of the Results

The previous chapter presented the results of all the test runs which resulted in failure of the test section (i.e., overheating and destruction of the heater). This section divides the results into subgroups suitable for further analysis.

First, although visualization of the failure mechanism, such as burnout at the coolant-side wall, is beyond the scope of this study, inference can be made given the consistency of the measured thermal hydraulic parameters. For example, it is generally accepted that the critical heat flux is a result of excessive vapor generation on the wall. Several CHF mechanisms further explain the phenomena in the literature. Three theories considered in this chapter are: 1) vapor bubbles grow and depart the surface to form a vapor blanket and CHF occurs as a result of vaporizing the thin

Table 6.1: Cases with Premature Heater Failure

Test Section ID	Pressure MPa	Mass Flux Mg/m^2s	Heat Flux MW/m^2	T_{SAT} ^oC	Max. $T_{wall}^{Coolant}$ ^oC
TS22B	2.65	9.72	12.0	227	202
TS25A	2.76	8.23	18.0	229	202
TS27B	1.79	19.38	21.8	207	196

liquid film attached to the wall, see Celata et al. [36]; 2) the vapor bubbles remain attached to the surface and CHF occurs when the bubble density is so high that transition to film boiling occurs; and, 3) suppression of nucleate boiling on the coolant wall surface allows CHF based on homogeneous nucleation. Thus, the coolant-side wall temperature must be above the saturation temperature at the point of CHF for any of these theories. If this is not the case, then the most probable mechanism leading to heater failure might be a fault in the manufacturing of the heater (e.g., uneven surface coating) or in the electrode connection (e.g., poor contact).

The three-dimensional conduction code HEATING7.2 was combined with certain heat transfer correlations and used to determine coolant-side wall temperatures, as discussed in Chapter 4. Results of this modeling are shown in Appendix F (Figures F-1 to F-66) which contain thermal region profiles. These thermal analyses include the forced convection mechanism such as single-phase liquid, nucleate boiling, or homogeneous nucleation based on the calculated wall temperature. In addition, temperature flags would also be noted in the thermal region profile when the coolant-side wall temperature is calculated to be above the critical temperature of water or below the bulk temperature (note: such cases do not appear in the final results presented in Figures F-1 to F-66). The non-boiling results are summarized in Table 6.1.

A second measure of confidence is found in the comparison between the measured copper wall temperatures and those calculated by the conduction model. These comparisons are shown in Appendix H (Figures H-1 to H-67). The temperature calculations from the conduction code are based on the incident power and boiling heat transfer correlations. The thermocouple measured temperatures are, essentially, independent measurements and are a means of verifying the consistency of the power

Table 6.2: Cases with Inconsistent Temperature Analysis

Test Section ID	Mass Flux Mg/m^2s	Max. Heat Flux MW/m^2	Pe	St
TS6A	9.02	23.5	526000	0.00221
TS9B	4.65	16.4	271000	0.00311
TS11A	7.20	16.8	420000	0.00217
TS14B	10.4	27.8	606000	0.00221
TS17B	3.68	17.9	215000	0.00414
TS18A	0.394	17.8	24000	0.06831
TS19A	3.54	26.6	207000	0.00593
TS20A	6.67	24.1	389000	0.00294
TS21A	4.99	37.0	292000	0.00561
TS22A	9.19	36.2	536000	0.00302
TS23A	8.68	22.2	506000	0.00220
TS24A	10.5	30.5	612000	0.00233
TS26B	4.49	18.2	262000	0.00350

measurements. When the power-based temperature calculations and the thermocouple measurements do not agree within the uncertainty ranges ascribed in the figures, the accuracy of the data are at issue. The disagreement can be caused by non-uniform heating, i.e., the spiked heat flux is not properly emulated; or, by premature failure due to arcing in the heater which is misinterpreted as a larger than realized heat flux. Either of these plausible reasons are grounds to reduce the confidence in the data. Thirteen data points fall into this category of inconsistant temperature analysis as summarized in Table 6.2. Although these data are suspect, the inconsistency could also be caused by poor thermocouple placement, the uncertainty in the ascribed heat flux, or an error in the extrapolation of the heat transfer correlations. In these cases, the Pe and St numbers may be valid. However, there remain 17 data points which appear consistent and will be considered bench mark cases for reliable CHF (or near CHF) data. The bench mark data is given in Table 6.3.

Table 6.3: Bench Mark Cases for Critical Heat Flux Data

Test Section ID	Mass Flux Mg/m^2s	$q"_{CHF}$ MW/m^2	Pe	St_{CHF}
TS15A	5.89	20.0	344000	0.00288
TS15B	5.72	14.1	334000	0.00237
TS16B	0.63	15.6	37200	0.02177
TS17A	2.55	12.5	149000	0.00450
TS18B	0.265	20.6	16600	0.11938
TS19B	11.3	28.4	659000	0.00205
TS20B	10.3	20.5	600000	0.00181
TS21B	3.65	17.0	213000	0.00404
TS23B	10.2	17.7	595000	0.00167
TS24B	10.6	21.8	618000	0.00185
TS25B	7.39	20.2	431000	0.00241
TS26A	5.73	24.1	334000	0.00343
TS27A	4.49	18.0	247000	0.00268
TS28A	5.52	19.6	322000	0.00301
TS28B	4.34	18.1	254000	0.00361
TS29A	15.2	20.4	886000	0.00135
TS29B	13.6	24.3	793000	0.00160

6.2 Discussion of Critical Heat Flux Data

The data of Table 6.3 is plotted in Figures 6-1 to 6-3 for St_{CHF} versus Pe using differently scaled axes. St_{CHF} is defined as $q"_{CHF}/(G\ c_{pl}\ (T_{sat}\text{-}T_{bulk}))$ and Pe is defined as Re Pr = $G\ D_e\ C_{pl}/k_l$, where C_{pl} and k_l are the properties of water at the film average temperature. St_{CHF} appears to decrease monotonically versus Pe. For contrast, Nu_{CHF}, defined as $q"_{CHF}D_h/(k_l(T_{sat}\text{-}T_{bulk}))$ is also plotted against Pe in Figures 6-4 to 6-6. In these plots, a U-shaped curve is evident, separating the low mass flux region from the high flux region.

The Peclet number is a non-dimensionalization of the mass flux which, compared to the Reynolds number, is insensitive to large variations in bulk fluid properties. Recall that Saha and Zuber [39] used Pe to distinguish between the thermally-controlled and hydrodynamically-controlled mechanisms of bubble departure from the heated surface. Two regions also appear to exist from both the St_{CHF} and Nu_{CHF} plots above. In the case of Nu_{CHF}, Figure 6-4 suggests the notion that one mechanism

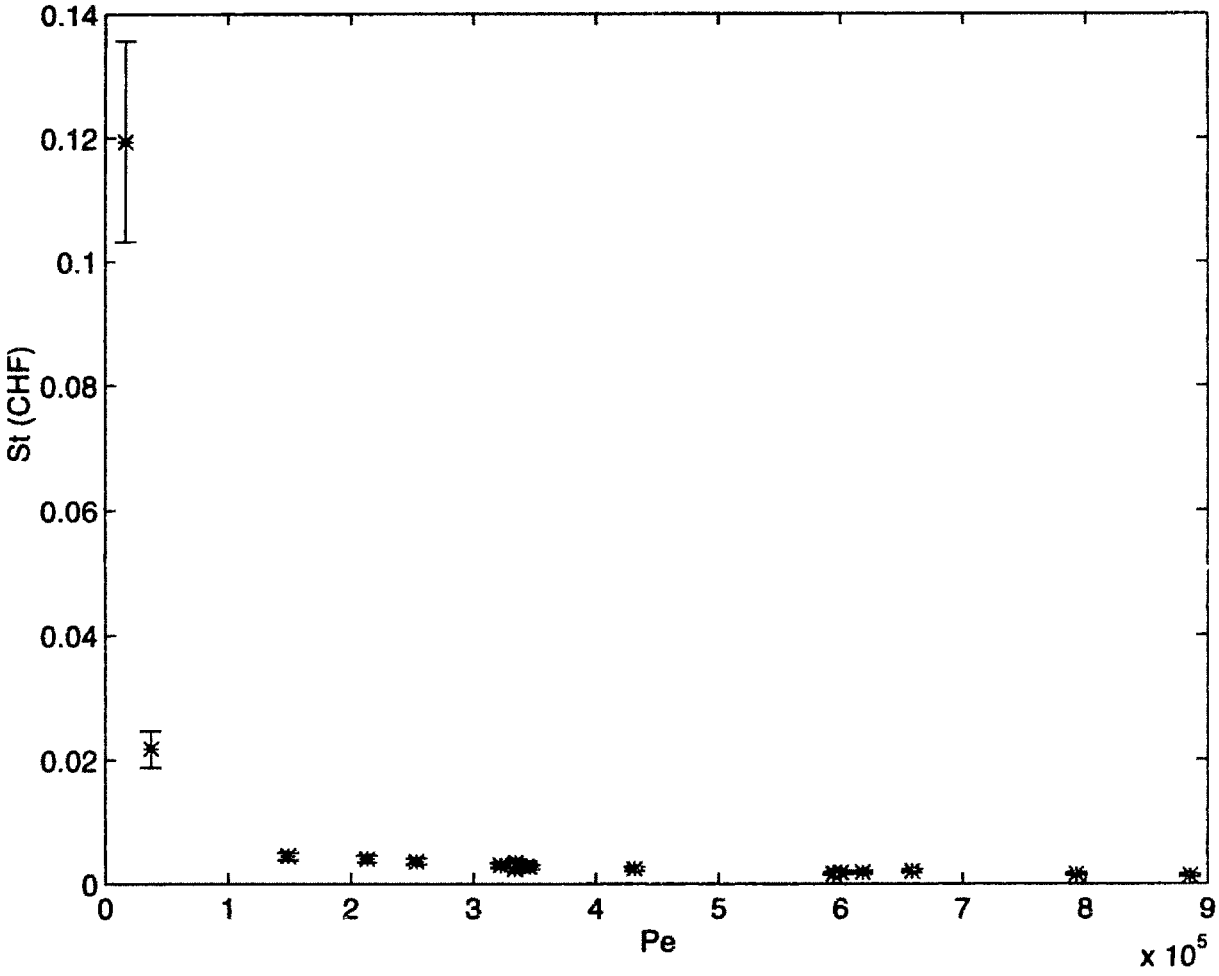

Figure 6-1: Stanton$_{CHF}$ versus Peclet using Bench Mark Data

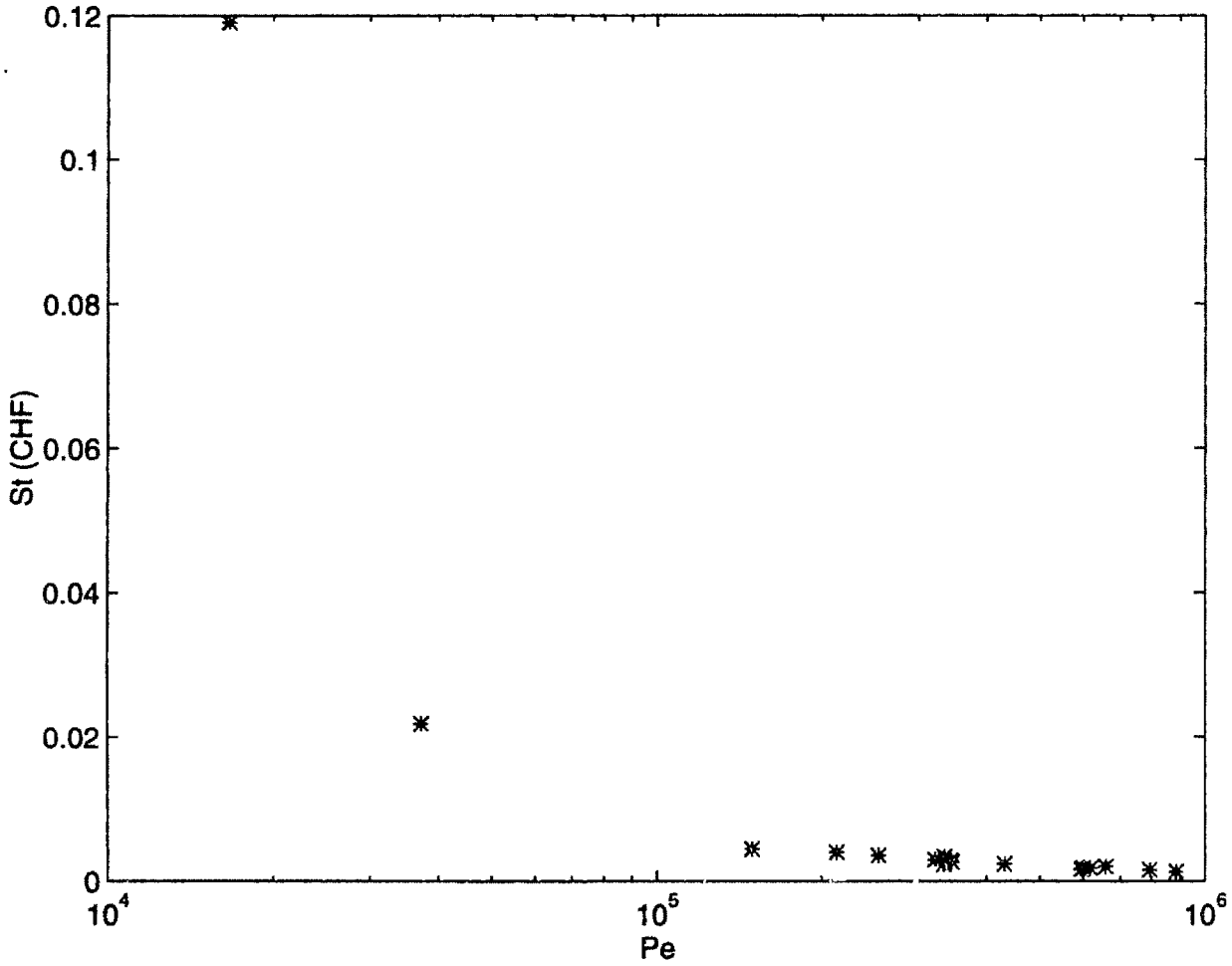

Figure 6-2: Stanton$_{CHF}$ versus Peclet using Bench Mark Data on Semi-Log Scale

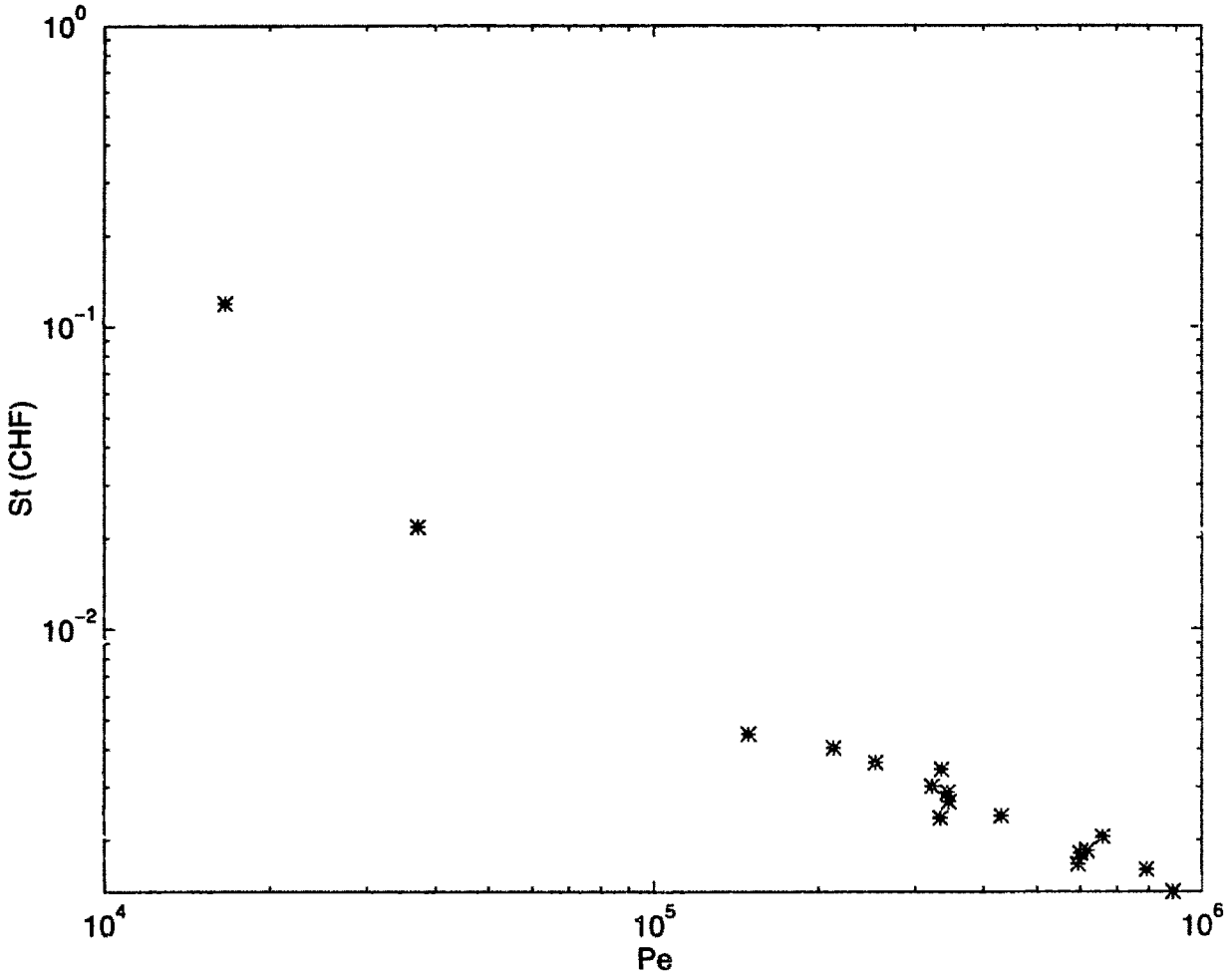

Figure 6-3: Stanton$_{CHF}$ versus Peclet using Bench Mark Data on Log-Log Scale

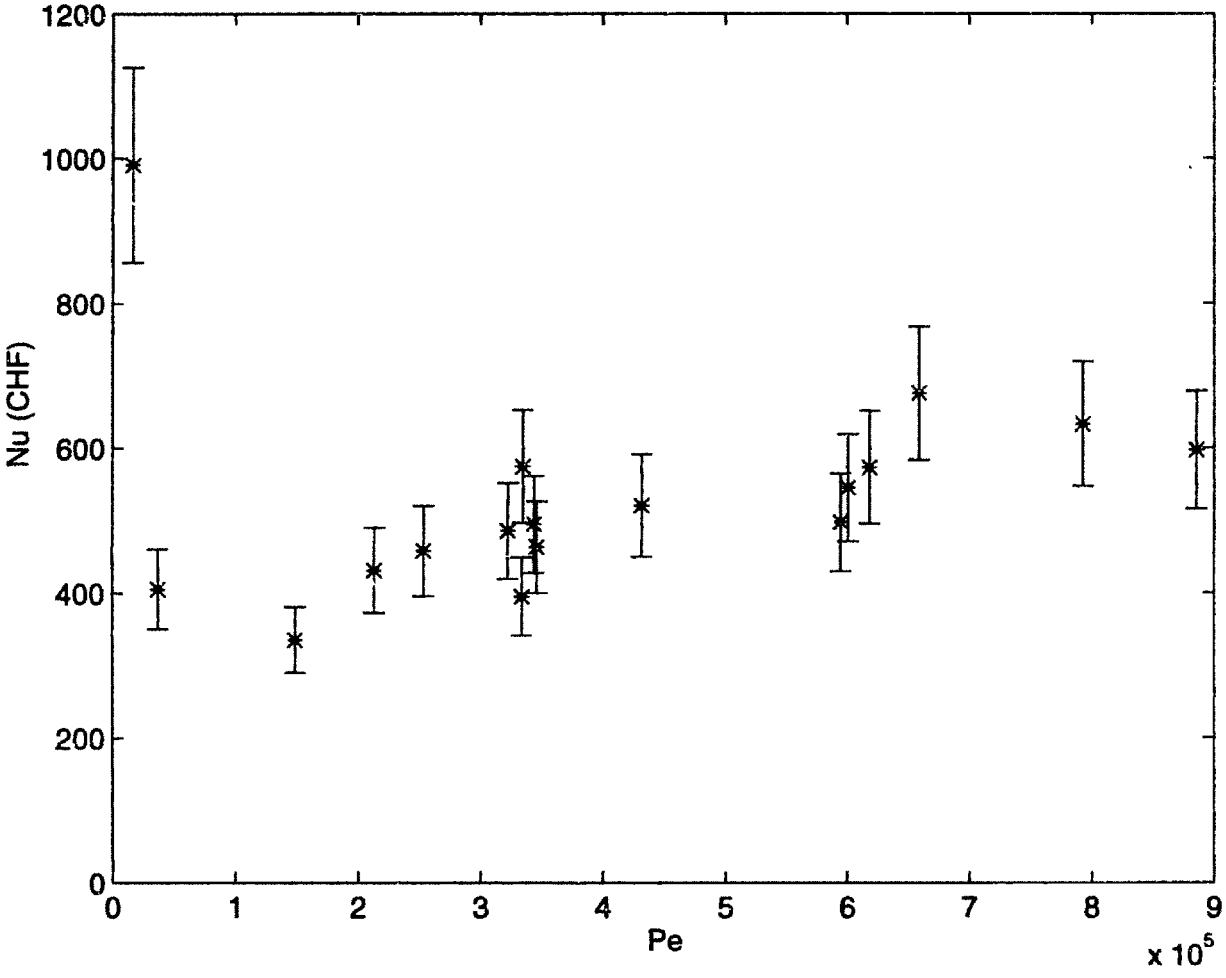

Figure 6-4: Nusselt$_{CHF}$ versus Peclet using Bench Mark Data

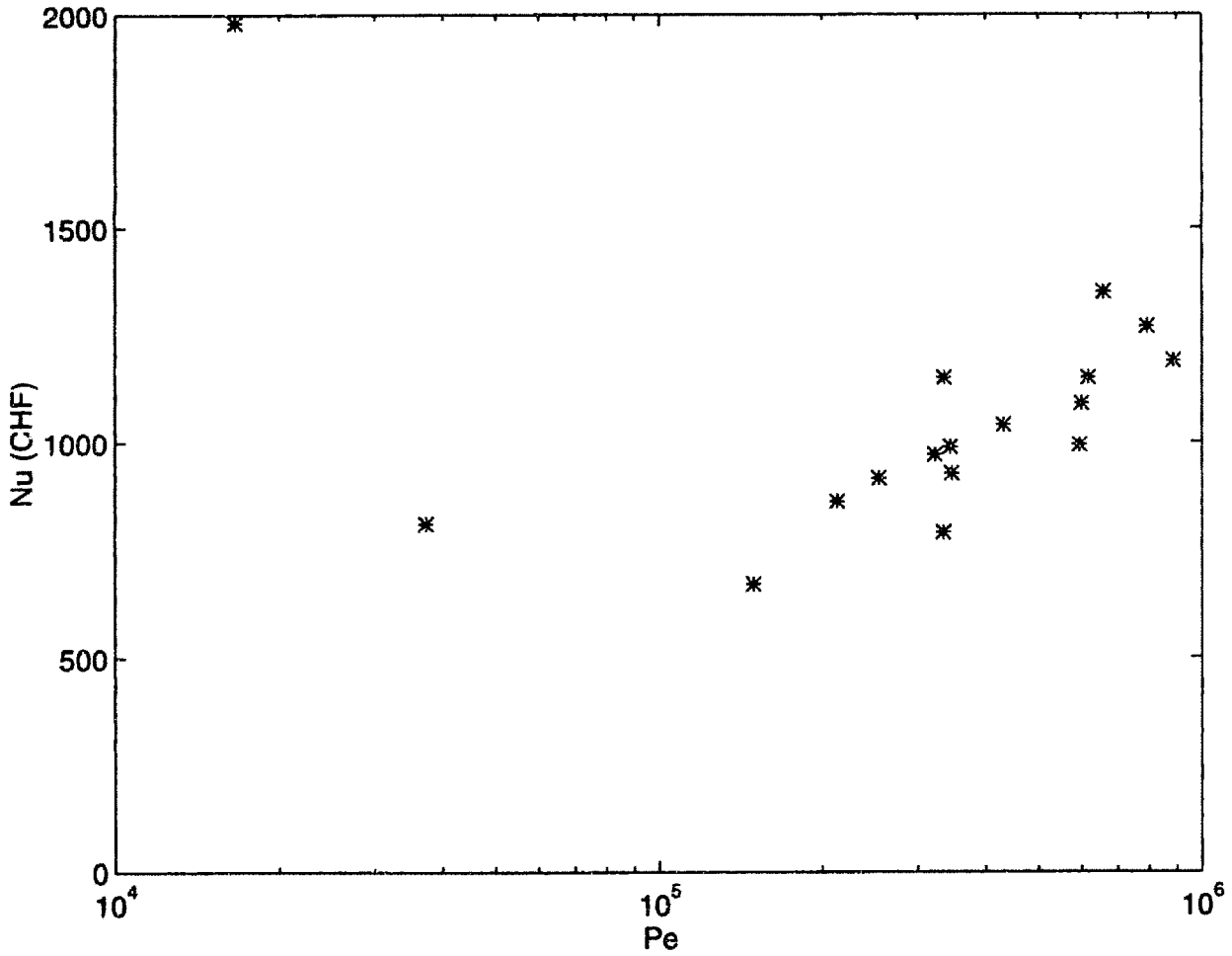

Figure 6-5: Nusselt$_{CHF}$ versus Peclet using Bench Mark Data on Semi-Log Scale

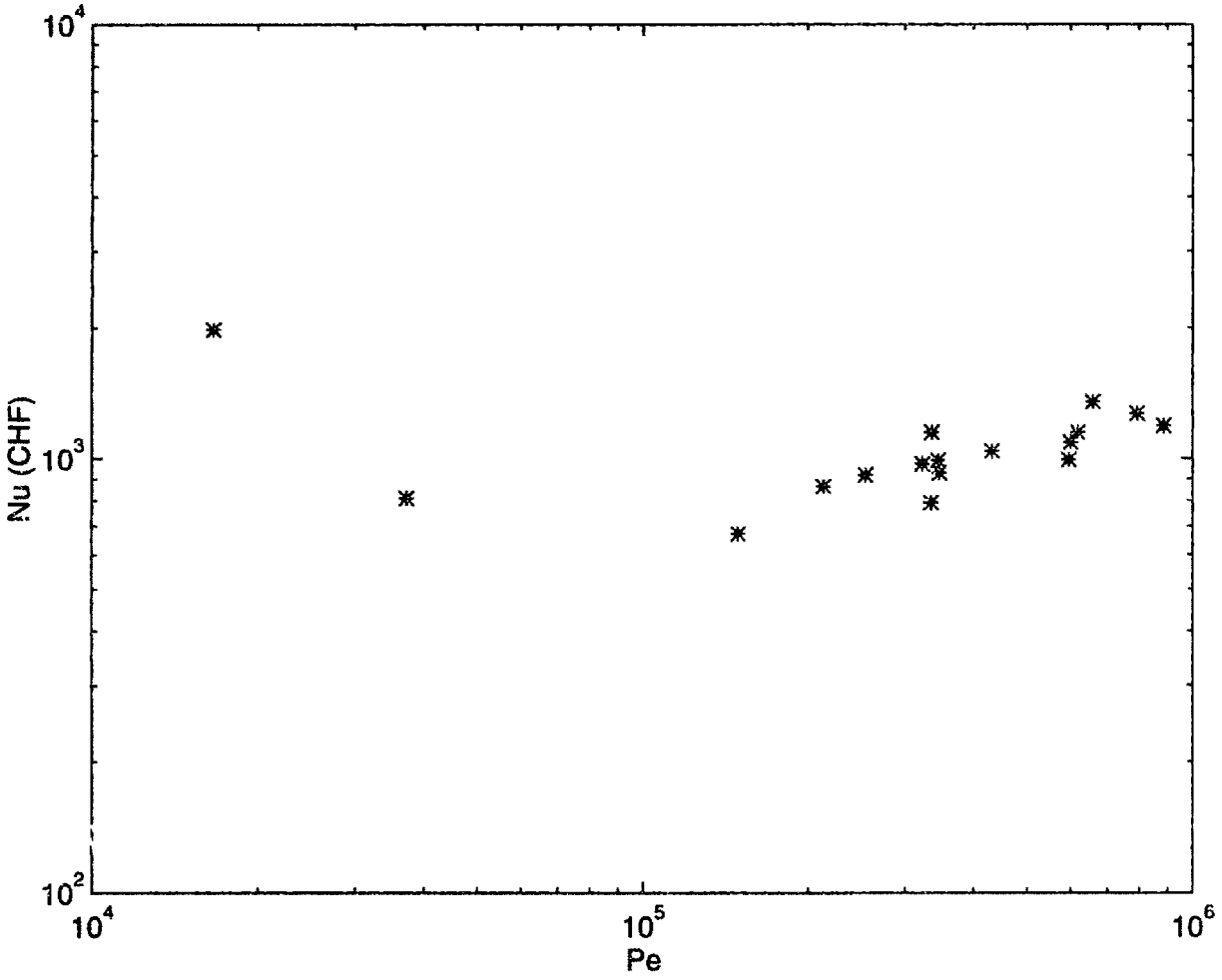

Figure 6-6: Nusselt_{CHF} versus Peclet using Bench Mark Data on Log-Log Scale

may dictate the behavior at low flows and another mechanism at high flows. The data also agree with the criterion of Saha and Zuber, namely a transition point between the two regions in the vicinity of Peclet equal to 70,000. However, the linearity of the data in the log-log plot of St_{CHF} versus Pe in Figure 6-3 suggests that the transition may not be very sharp.

The Stanton number is directly related to the mass flux, G, in contrast to the Nusselt number. The monotonic decrease in St_{CHF} versus Pe suggests that the suppression of nucleate boiling overcomes the enhanced heat transfer usually associated with increased flow velocity and turbulence. This is not a new idea since the Reynolds number typically has a negative exponent in heat transfer coefficient correlations such as the Chen correlation for suppressed nucleate boiling and the Tong-75 critical heat flux correlation (both discussed in Chapter 2).

The following subsections will investigate the critical heat flux correlations introduced in Chapter 2 and discuss the validity of their extrapolation for divertor CHF applications.

6.2.1 Tong Critical Heat Flux Correlations

In 1975, Tong [32] developed a critical heat flux correlation based on phenomenological effects and the existing CHF data base, as discussed in Chapter 2. The effects of local subcooling, turbulent mixing, bubble layer shielding, spacer grid, and two-phase flow friction on CHF were evaluated individually. Recall that the data used by Tong (see Table 2.1) were for much higher pressure and lower mass fluxes than in the present study. However, Figure 6-7 illustrates that the Tong-75 CHF correlation fares much better than the Modified Tong-68 correlation suggested by Inasaka and Nariai (1993) [34] which endeavored to account for the effect of lower pressures. The Modified Tong-68 correlation apparently does not extrapolate well since it is based on data with equilibrium exit qualities greater than -0.2 versus the equilibrium exit qualities of the present data which were typically less than -0.45.

However, the Tong-75 CHF correlation appears to greatly under-predict CHF in the low mass flux region (Pe $\leq$ 70,000) in Figures 6-7 and 6-8. Some explanations

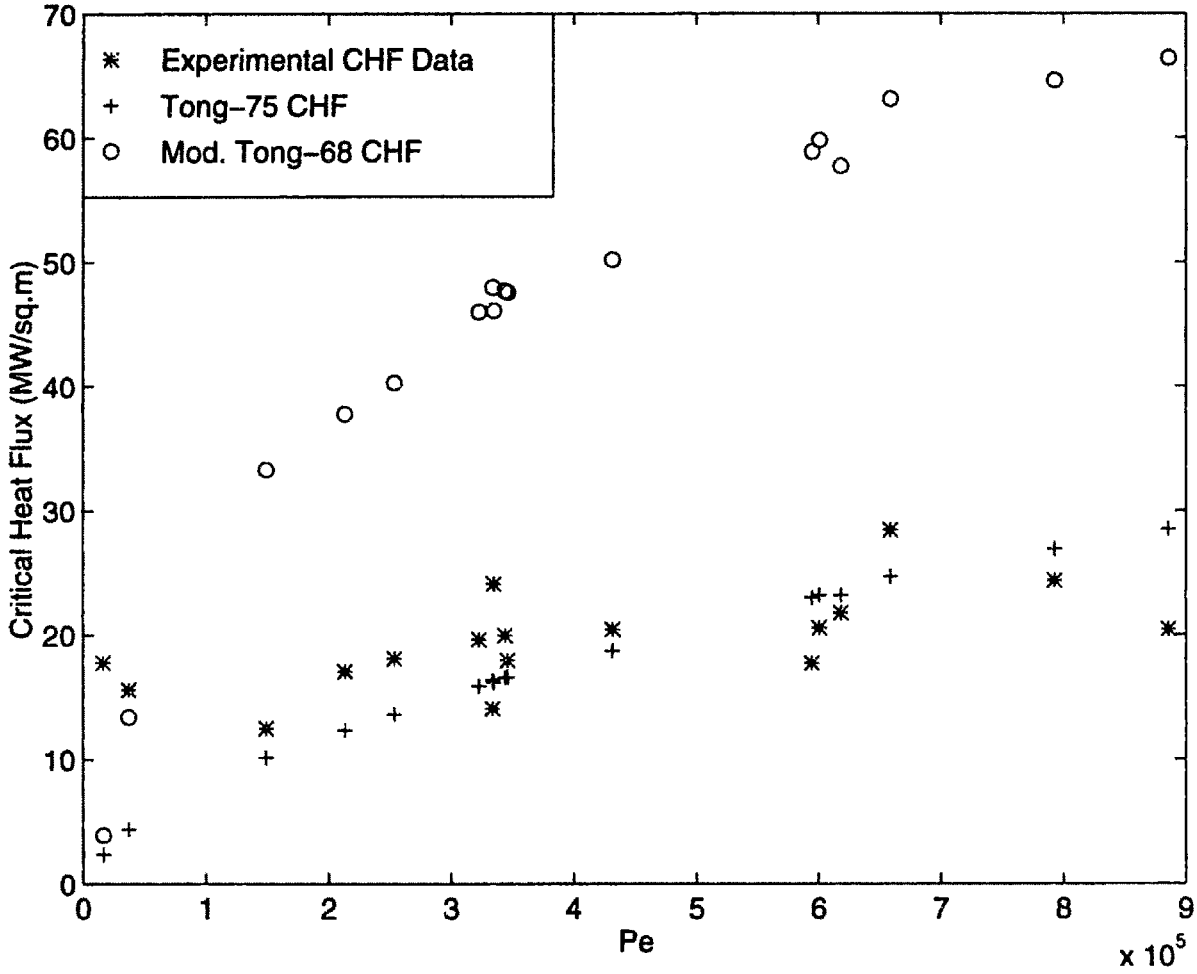

Figure 6-7: Comparison of Tong CHF correlations with Bench Mark Data

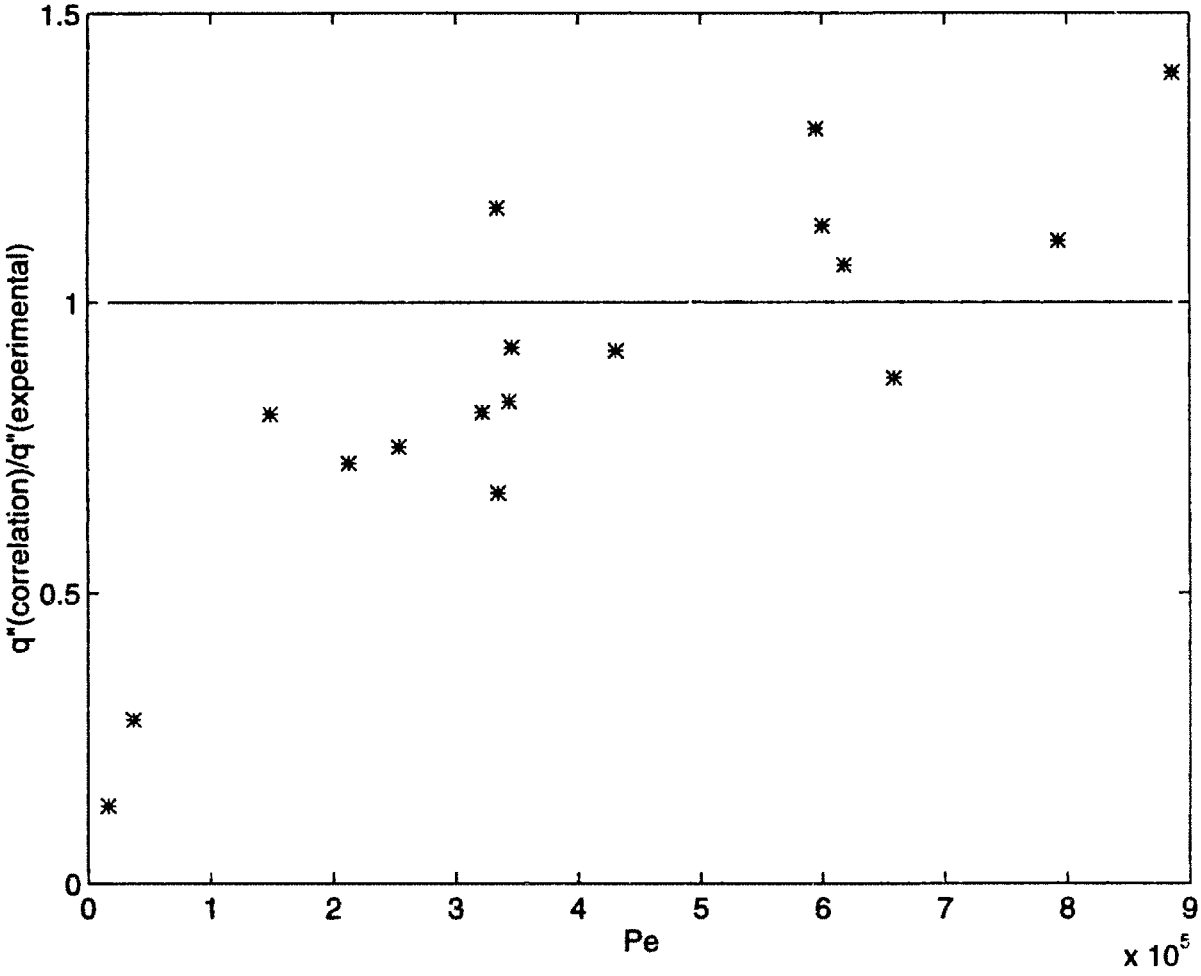

Figure 6-8: Ratio of Predicted to Bench Mark Data Using Tong-75 CHF correlation

seem evident, since the present data assume a spiked heat flux profile (heated length about 0.05 m), the thermal boundary layer does not develop symmetrically and the coolant-side wall is sensing a much greater subcooling effect than anticipated in the Tong-75 CHF correlation. In addition, bubble departure is more apt to occur at low mass fluxes which allows re-wetting of the surface and, consequently, very efficient heat transfer.

6.2.2 Celata et al. Critical Heat Flux Correlation

A recent mechanistic model for the prediction of water subcooled flow boiling critical heat flux was delineated by Celata et al. (1994) [36]. The model assumes that the dryout of a thin liquid layer beneath an intermittent vapor blanket due to the coalescence of small bubbles leads to CHF. The model is complex and requires the determination of the geometry of a vapor blanket and its velocity for an evaluation of CHF as follows:

$$q''_{CHF} = \frac{\rho_l \delta H_{fg}}{L_B} v_B \tag{6.1}$$

where:

q''_{CHF} = Critical heat flux (W/m^2)

ρ_l = Liquid density (kg/m^3)

δ = Liquid sublayer initial thickness (m)

H_{fg} = Latent heat of vaporization (J/kg)

L_B = Length of vapor blanket (m)

v_B = Vapor blanket velocity (m/s)

Further details of the model can be found in [36]. Thannickal [60] performed the prescribed calculations for 9 of the CHF data points given in Table 6.3. The results of the calculations are shown in Figures 6-9 and 6-10.

It is interesting to note from Figures 6-9 and 6-10 that, unlike the previous Tong-75 CHF correlation, the Celata et al. CHF model agrees well with the data at low mass fluxes (Pe $\leq$ 70,000) to within 20 percent; but, the model greatly overpredicts CHF

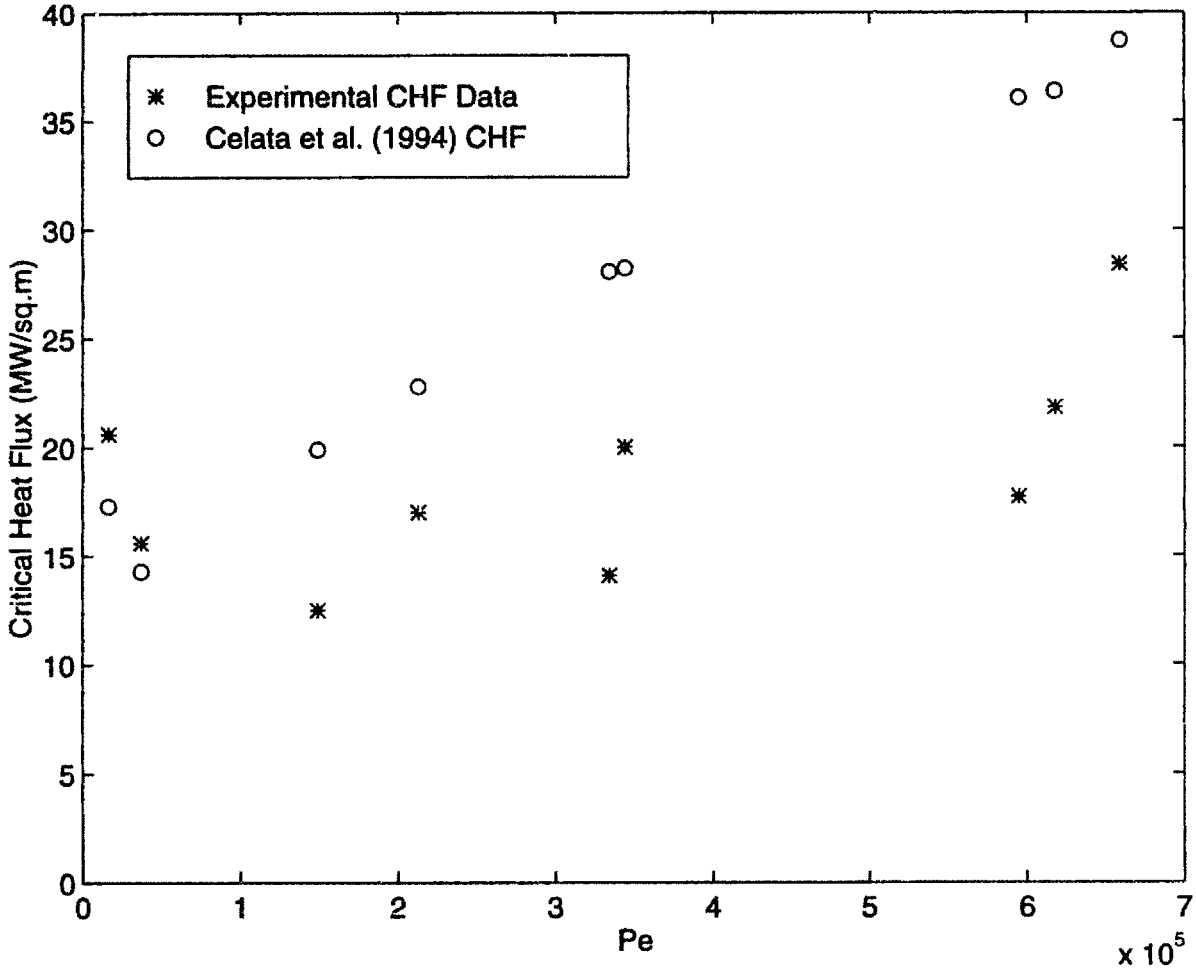

Figure 6-9: Comparison of Celata et al. (1994) CHF Model with some Bench Mark Data

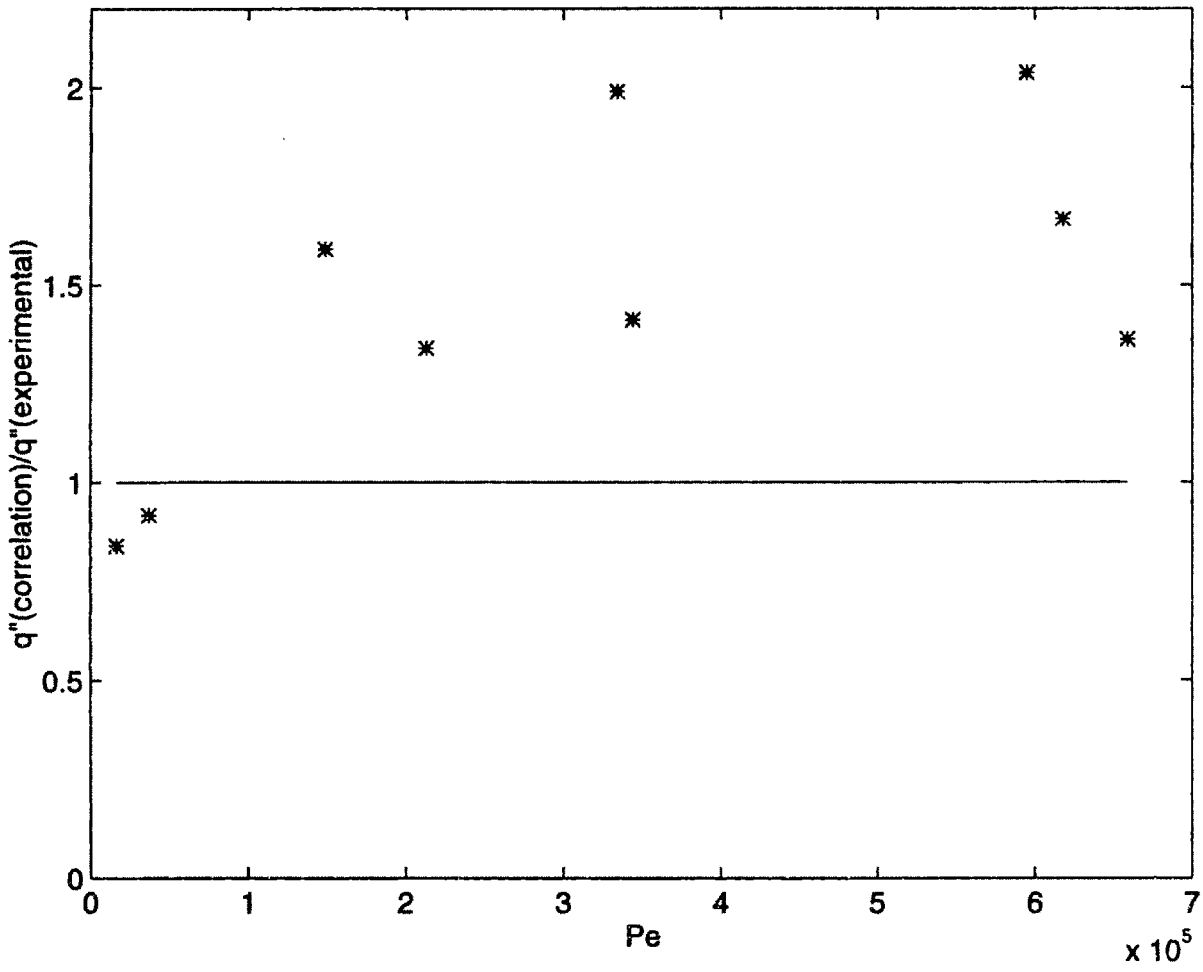

Figure 6-10: Ratio of Predicted to Bench Mark Data Using Celata et al. (1994) Model

at high mass fluxes. According to Thannickal's calculations [60], there are nuances about the model that did not make physical sense, specifically, the wall temperature superheat went markedly over the homogeneous nucleation temperature. In such an event, the dryout mechanism of a liquid existing beneath a bubble layer would not be realized. However, according to the modified Saha and Zuber bubble departure criterion discussed in Chapter 2, at the high mass flux (Pe $\geq$ 70,000) conditions of the present study, the bubbles are not expected to leave the surface. Furthermore, in such a highly subcooled bulk ($X_{eq}^{exit} \sim$ -0.45) with little thermal boundary layer development, the ability of a bubble layer to exist away from the wall is doubtful since any vapor that forms should condense very close to the wall.

On the other hand, the bubble departure criterion is surpassed in the low flow data. The thermal boundary layer has a much better opportunity to develop and agreement with the Celata et al. [36] CHF prediction suggests that the mechanism assumed is plausible, provided a different temperature profile is assumed.

6.3 Development of Critical Heat Flux Correlations

The preceding subsections indicate that different CHF mechanisms may be controlling at low mass fluxes from that at high mass fluxes. Assuming this to be true, then a transitional region may exist between the two regions of the St_{CHF} verse Pe relationship illustrated in Figures 6-1 to 6-3. If that transition occurs around Pe equal to 70,000, then the two bench mark data in the low mass flux region are not enough to characterize the low mass flux phenomena, especially since the low coolant flow measurements have a much larger uncertainty than the high flow ones. However, the corresponding velocity at Pe equal to 70,000 is 1 m/s. As illustrated in Chapter 2, CHF may no longer be the first failure mechanism encountered at such a low flow. Therefore, CHF values for the high mass flux regions are more significant to divertor design because CHF will probably be the limiting criterion.

Since the Tong-75 CHF correlation appears to fit the data best, it seems prudent to revist its formulation. Equation 2.1 defined the Tong-75 correlation as given in [32]. It can be rewritten in the form:

$$St_{CHF} = 8C_oC_1\frac{\rho_l}{\rho_v}(\frac{1}{Ja} + 0.00216p_r^{1.8}Re_m^{0.5})(\frac{D_h}{D_o})^{0.32}(\frac{D_e}{D_h})^{0.6}Pr^{0.6}Pe^{-0.6} \qquad (6.2)$$

For the present bench mark CHF data, there are small variations with respect to Pe in the values of the five terms preceding $Pe^{-0.6}$ in Equation 6.2. The rearrangement, however, indicates exponential decay of St_{CHF} with respect to Pe. A plot of St_{CHF} versus $Pe^{-0.6}$ is shown in Figure 6-11. The data appears to agree with the use of $Pe^{-0.6}$ for such a correlation. The curvefit from Figure 6-11 is shown on regular axes in Figure 6-12 and was found to be:

$$St_{CHF} = 5.8Pe^{-0.6} \qquad (6.3)$$

Equation 6.3 is recommended for conditions reflecting those upon which the correlation was based, indicated in Table 6.4. The closest comparative study is, unfortunately, an unpublished study that was conducted in Russia. The range of parameters of the Russian study, as reported by Lekakh [61], is also given in Table 6.4. The data from both studies are plotted in Figure 6-13 and show good agreement with Equation 6.3. A similar comparison with the complete subcooled CHF data base discussed in Chapter 1 does not show such agreement.

The subcooled CHF data base, however, will be used to broaden the applicability of the present data and aid in the formulation of a more general correlation than

Table 6.4: Range of Parameters Used by Present Study for CHF Correlation Equation 6.3 and Comparative Unpublished Russian Study with Single-Sided Heating

Group	D_i mm	L_h mm	X_e^{exit}	Pressure MPa	Mass Flux Mg/m^2s	Heat Flux MW/m^2
Present Study	9.5	50	-0.44 to -0.49	2.2 to 3.0	2.6 to 15	13 to 28
Russian Data [61]	6	60	-0.46	3.5	3.2 to 6.9	15 to 23

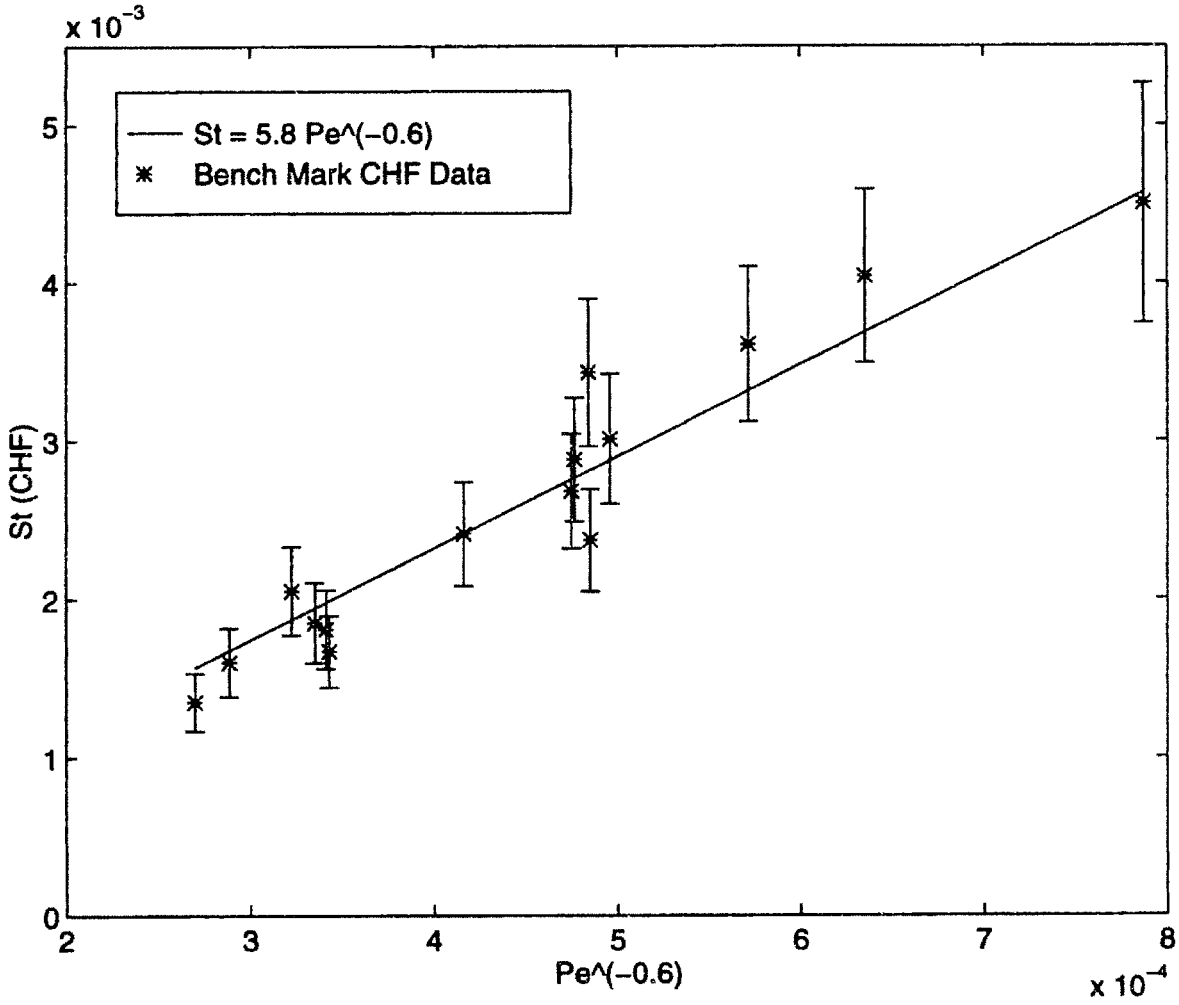

Figure 6-11: St_{CHF} plotted against $Pe^{-0.6}$

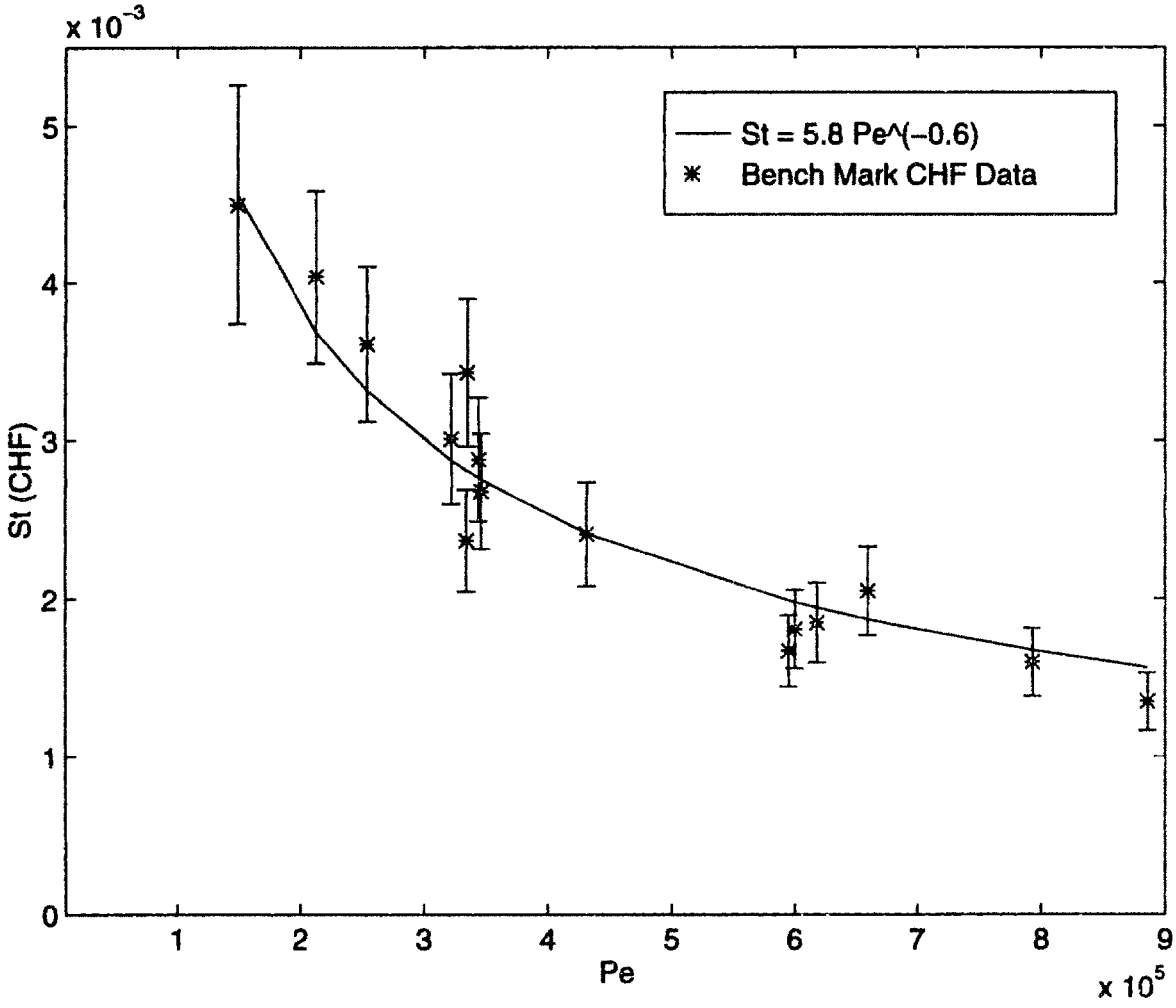

Figure 6-12: St_{CHF} plotted against Pe

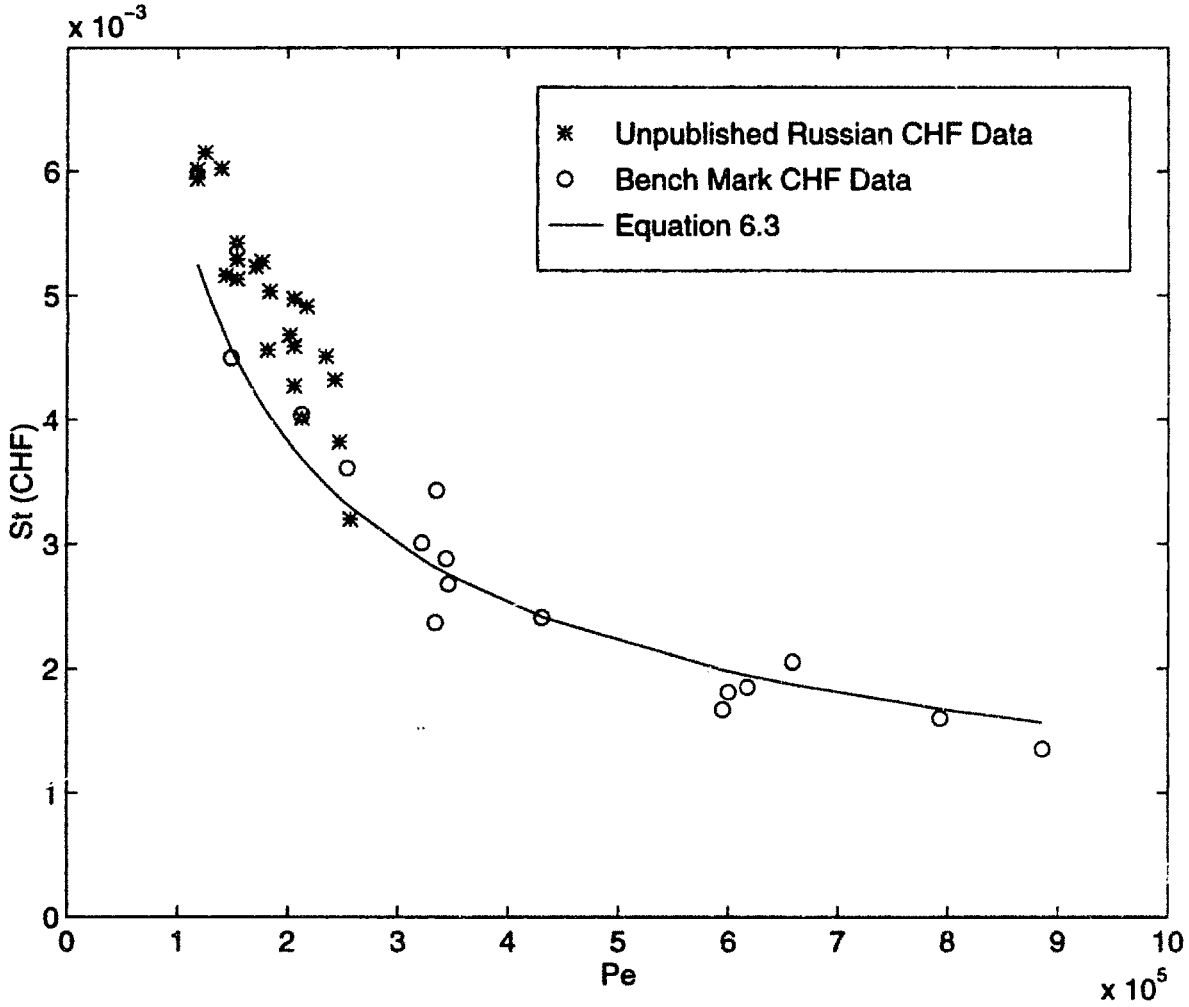

Figure 6-13: Comparative Data Base versus Correlation Equation 6.3

Equation 6.3. Returning to Tong's phenomenological correlation [32] Equation 6.2, several terms are less important under the present conditions and some terms seem to be lacking.

Tong [32] suggested the use of the heated diameter as reflected in Equation 6.2. However, in single-sided heating with significant deviation from the uniform thermal boundary layer development, the CHF occurrence is expected to be highly localized. Recall, the data base of interest to the present study includes only tube diameters of 5 mm or larger. Therefore, the effects of the diameter in a functional relationship will be neglected except in terms of the thermal boundary layer development. Kays and Crawford [62] investigated the thermal entry length effect for single-phase turbulent flow in a circular tube. They found a form that captures this effect similar to the following:

$$\frac{St_m}{St_\infty} = 1 + \frac{A \ln(Pe)}{B + L_h/D} \tag{6.4}$$

where St_m/St_∞ is the ratio of the under-developed to the fully-developed Stanton number and L_h is the axially heated length. Since the mass flux is already represented twice in Equation 6.2 in the form of Re and Pe; and, the variation in the log of Pe is small for the region of interest, the ln(Pe) term in Equation 6.4 will be dropped. Equation 6.4 assumes a uniformly heated diameter which is another topic of difference between the present study and much of the CHF data. To account for this effect, the D assumed for Equation 6.4 will be the heated diameter (D_h = Heated Perimeter). The relational form of St_{CHF} can now be expressed with the above modifications as:

$$St_{CHF} = C\frac{\rho_l}{\rho_v}\left(\frac{1}{Ja} + 0.0022 p_r^{1.8} Re^{0.5}\right)\left(1 + \frac{E}{F + L_h/D_h}\right) Pr^{0.6} Pe^n \tag{6.5}$$

where the variables are defined as before except for constants C, E, F, and n which will be determined next. The constants C and n are determined by curvefitting the bench mark data and consider the effects of the error bars. They are found to be n equal to -0.9 and C as follows:

$$C(1 + \frac{E}{F + 10.5}) = 65 \tag{6.6}$$

The terms preceding Pe^n in Equation 6.5 will be defined as follows to ease plotting:

Term 1 = ρ_l/ρ_v

Term 2 = $\frac{1}{Ja} + 0.0022 p_r^{1.8} Re^{0.5}$

Term 3 = $1 + \frac{E}{F + L_h/D_h}$

Term 4 = $Pr^{0.6}$

The fit of n and Equation 6.6 to the bench mark data is shown in Figure 6-14. For comparison, the fit to n equal to -0.8 is also illustrated. The lowering in the value of the Pe exponent from n equals -0.6 in the Tong-75 [32] correlation to n equals -0.9 in Equation 6.5 may account for the increased effect of nucleate boiling suppression for high mass fluxes. Recall, Tong's data are based on mass fluxes up to only 4 Mg/m^2s which is less than half of the reference mass flux of the present study.

Since Equation 6.4 was derived for single-phase flow, the constants E and F in Equation 6.5 are determined using the CHF data base described in Chapter 1 in order to verify the relationship from the CHF data. In order to limit the effect of the L_h/D_h term in Equation 6.5, the ratio of E/F was set to 0.5; i.e., the term is not allowed to account for more than about a 25 percent effect for the L_h/D_h range in the CHF Data Base ($10 \geq L_h/D_h \geq 80$).

A Partial CHF Data Base consisting of the uniformly heated, smooth flow data for pressures greater than 1 MPa, Pe greater than 70,000, and St_{CHF} less than 0.0065, was taken from the CHF data base discussed in Chapter 1 in order to validate the functional relationship with as few confounding parameters as possible. The results of fitting the 175 points from the Partial CHF Data Base are shown in Table 6.5. The merit of fit shown is the percent standard deviation of the data from the mean fit of the Partial CHF Data Base. Also given in Table 6.5 is the mean deviation from Equation 6.5 (with n = -0.9 and C satisfying Equation 6.6). It would be optimal to minimize both deviations, but the fitting of the L_h/D_h effect is the main point of using the Partial CHF Data Base. This effect shows the best fit based on the

Table 6.5: Determination of Heated Length Effect Constants Using Partial CHF Data Base (Uniform Circumferential Heating, Smooth Flow, Pe $\geq$ 70,000, $St_{CHF} \leq 0.0065$, $r \geq 5$ mm, p $\geq$ 1 MPa)

E	F	% MD[a]	% SD[b]
0		+17.3	21.5
1	2	+21.2	20.7
5	10	+26.0	19.7
10	20	+26.0	19.5
15	30	+25.2	19.6
20	40	+24.4	19.7

[a] MD = Mean deviation from Bench Mark Data Fit using Equation 6.6
[b] SD = Standard deviation from Mean of Partial CHF Data Base

standard deviation of the data base at E equal to 10 (thus, F equals 20 and C equals 50). This fit to the Partial CHF Data Base is shown in Figures 6-15 and 6-16.

The constants in Equation 6.5 have been determined and the proposed CHF correlation for extrapolation of Equation 6.3 outside of the range of parameters in Table 6.4 is:

$$St_{CHF} = 50\frac{\rho_l}{\rho_v}\left(\frac{1}{Ja} + 0.0022 p_r^{1.8} Re^{0.5}\right)\left(1 + \frac{10}{20 + L_h/D_h}\right) Pr^{0.6} Pe^{-0.9} \qquad (6.7)$$

For the bench mark CHF data, only Terms 1, 2, and 4 of Equation 6.7 varied with respect to Pe as shown in Figures 6-17 to 6-19, respectively, to elucidate the possible inter-relationship between effects. As mentioned above, the partial CHF data base includes 175 points from the data base described in Chapter 1 for uniformly heated, smooth flow, pressures greater than 1 MPa, Pe greater than 70,000, and St_{CHF} less than 0.0065 conditions. The range of L_h/D_h in the partial CHF data base is shown in Figure 6-20 along with the variation in the heat length term. Figure 6-20 indicates that the current heated length term has a small effect in Term 3 and, thus, Equation 6.7. More data is required to confidently extrapolate the heated length dependency into the "spiked" realm, e.g., $5 \leq L_h/D \leq 10$ or $L_h \sim 0.05$ m. In addition, there is

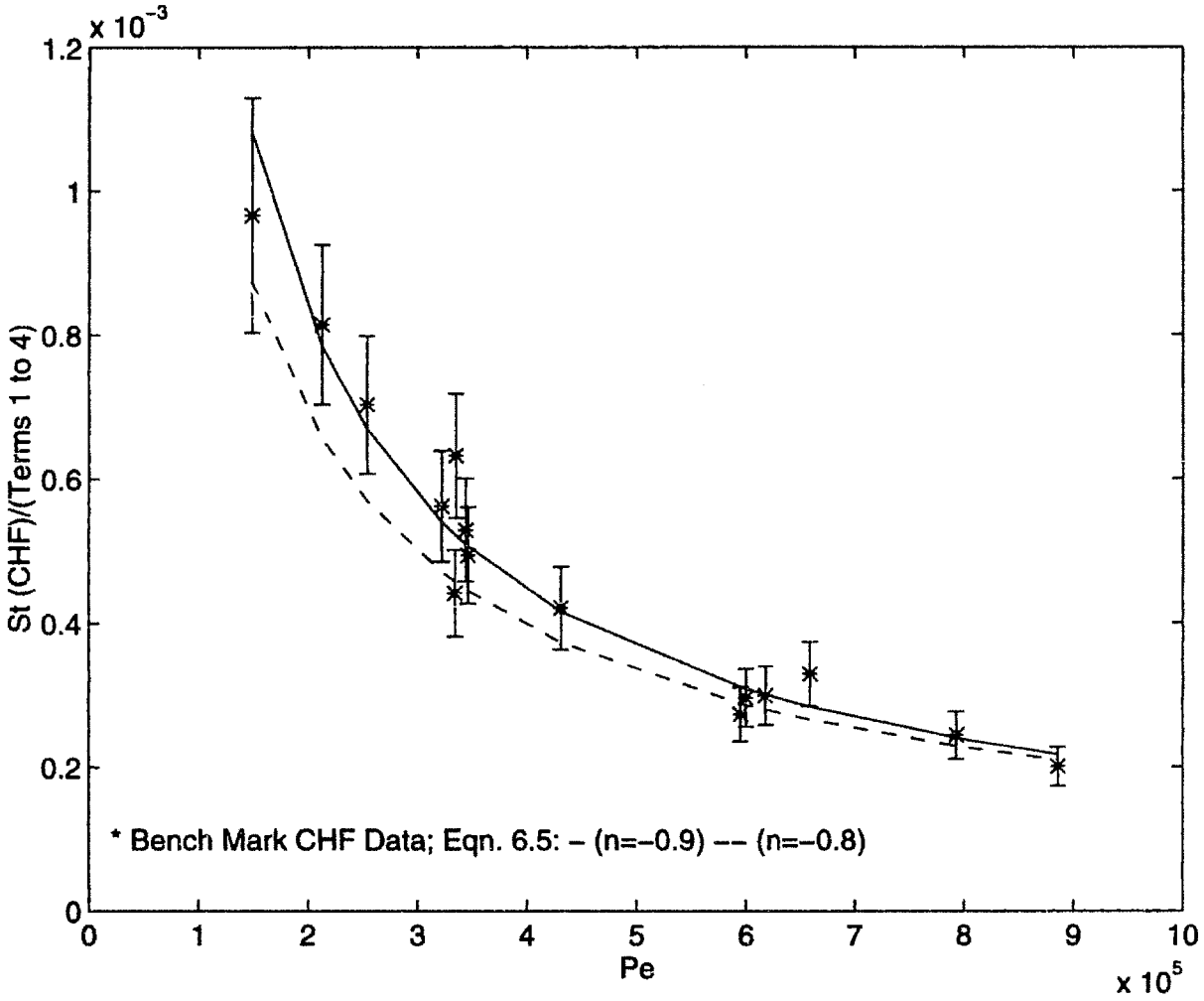

Figure 6-14: Determination of Exponent, n, of CHF Correlation using Bench Mark Data

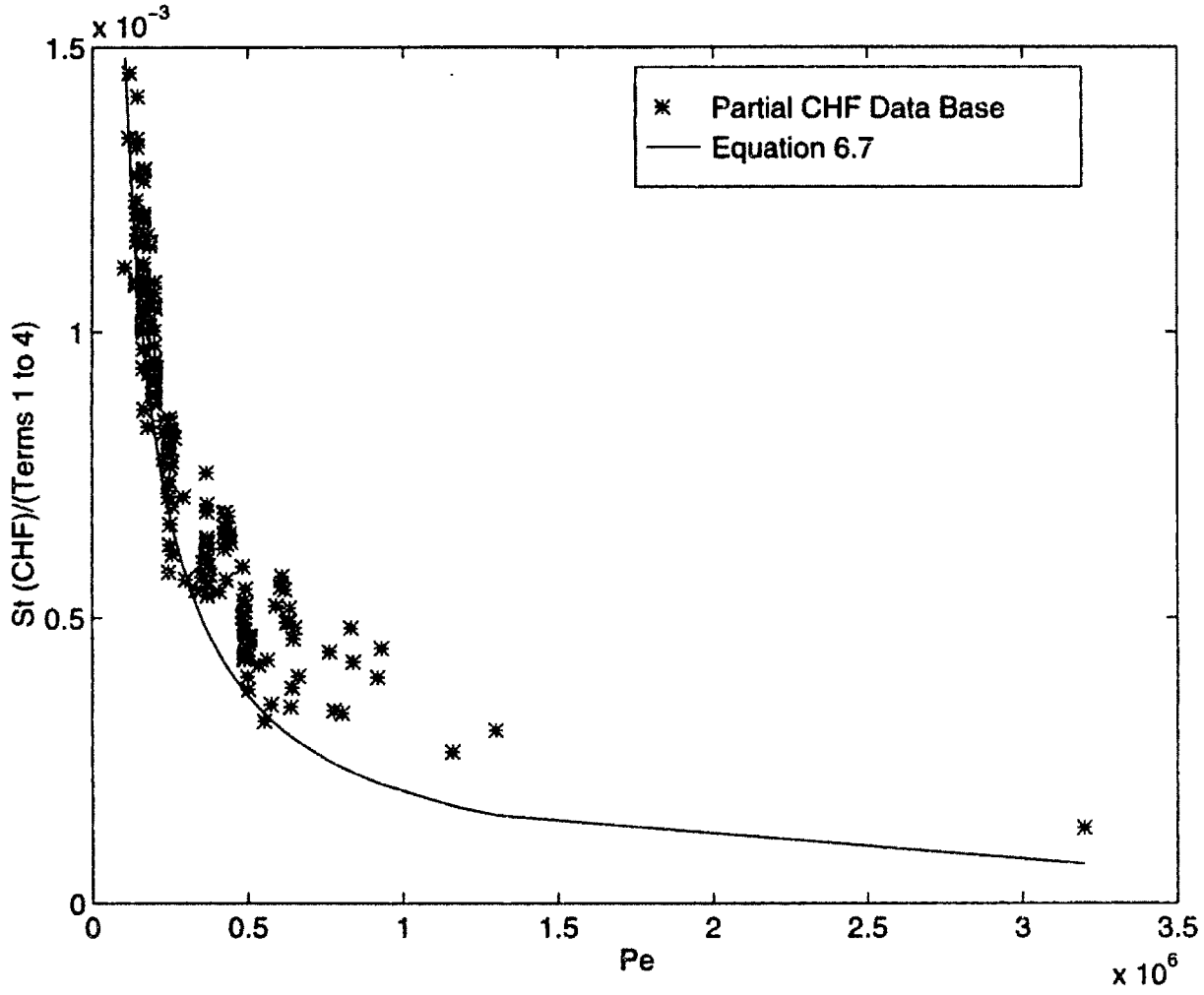

Figure 6-15: Determination of CHF Correlation using Partial CHF Data Base

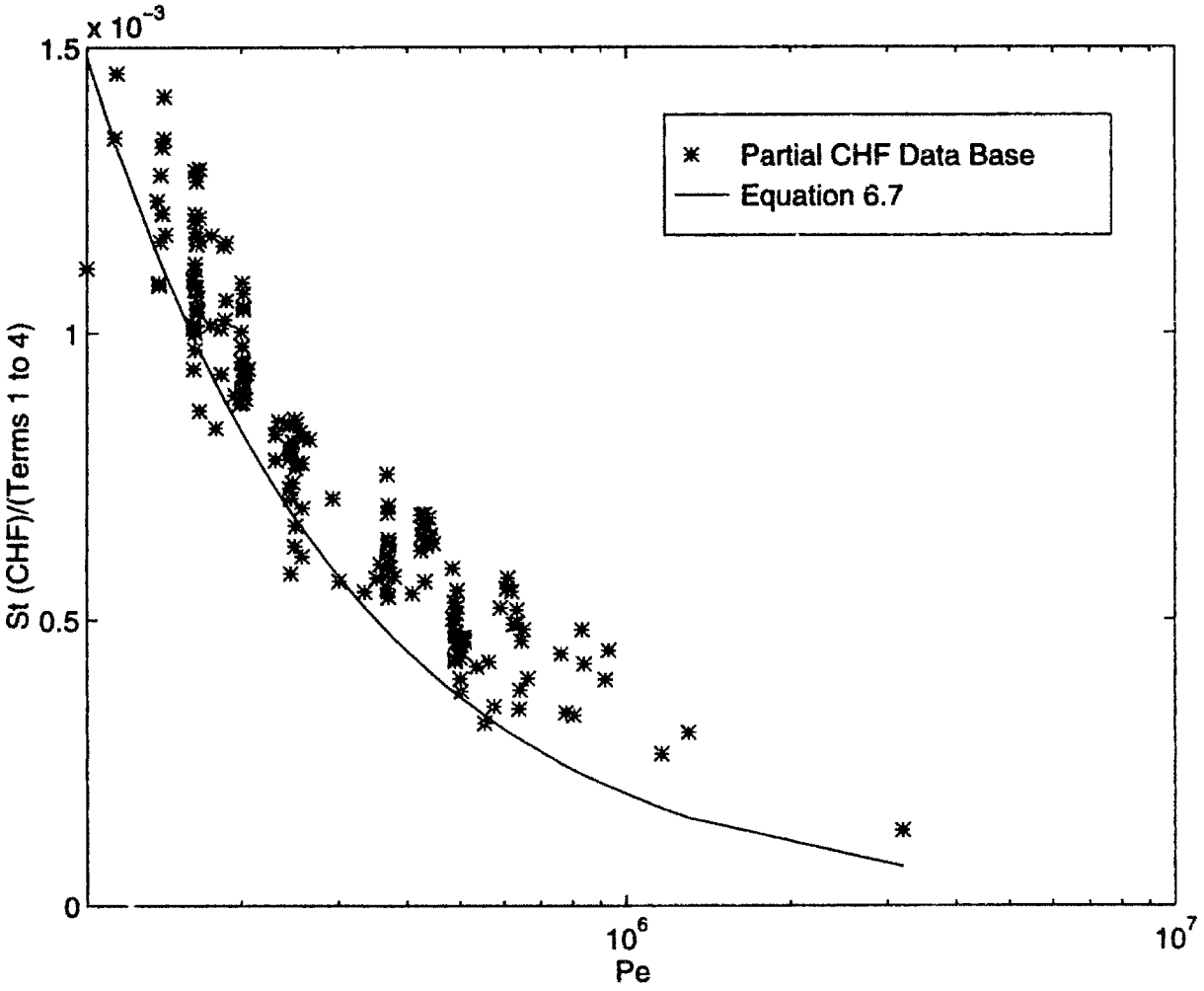

Figure 6-16: Determination of CHF Correlation using Partial CHF Data Base

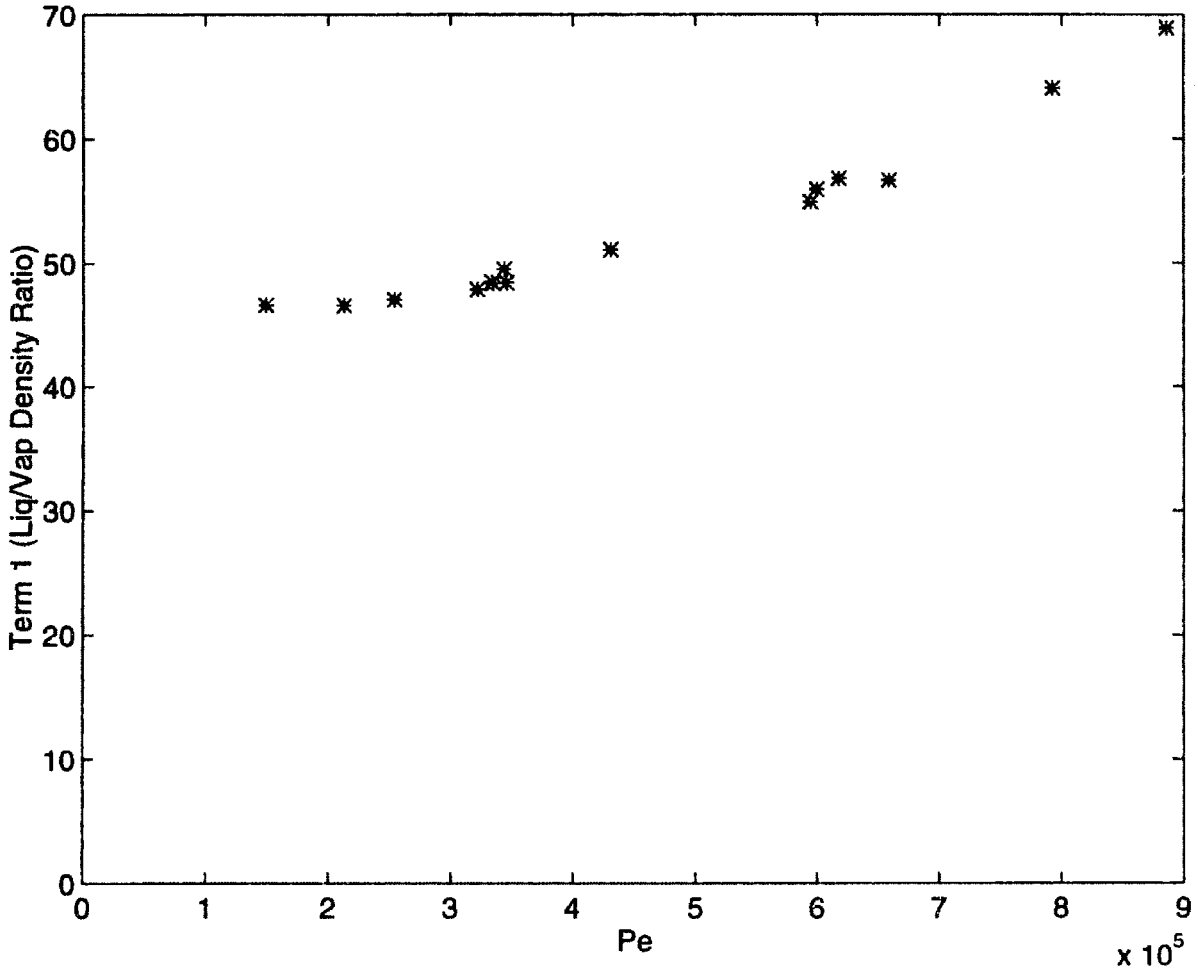

Figure 6-17: Variation in Term 1 (Liquid to Vapor Density Ratio) with respect to Pe for Bench Mark Data

not enough data on non-uniform circumferential heating to separately account for the heated diameter effect.

6.4 Critical Heat Flux Correlation Applied to Data Base

The data base described in Chapter 1 will inevitably include experiments in which the crisis mechanism will differ from that suggested for application of Equation 6.7. The transition from nucleation or vapor generation at the wall to film boiling is

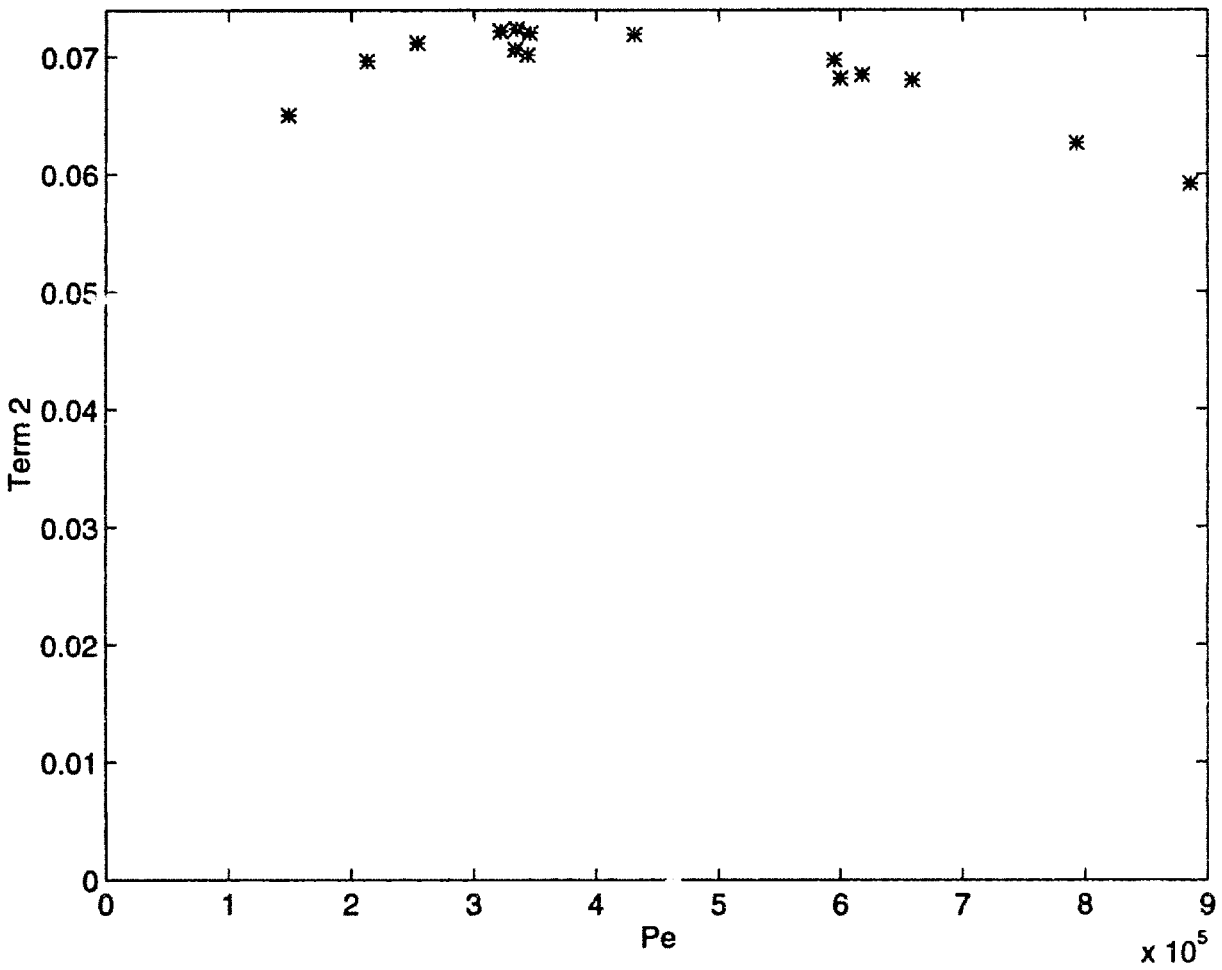

Figure 6-18: Variation in Term 2 with respect to Pe for Bench Mark Data

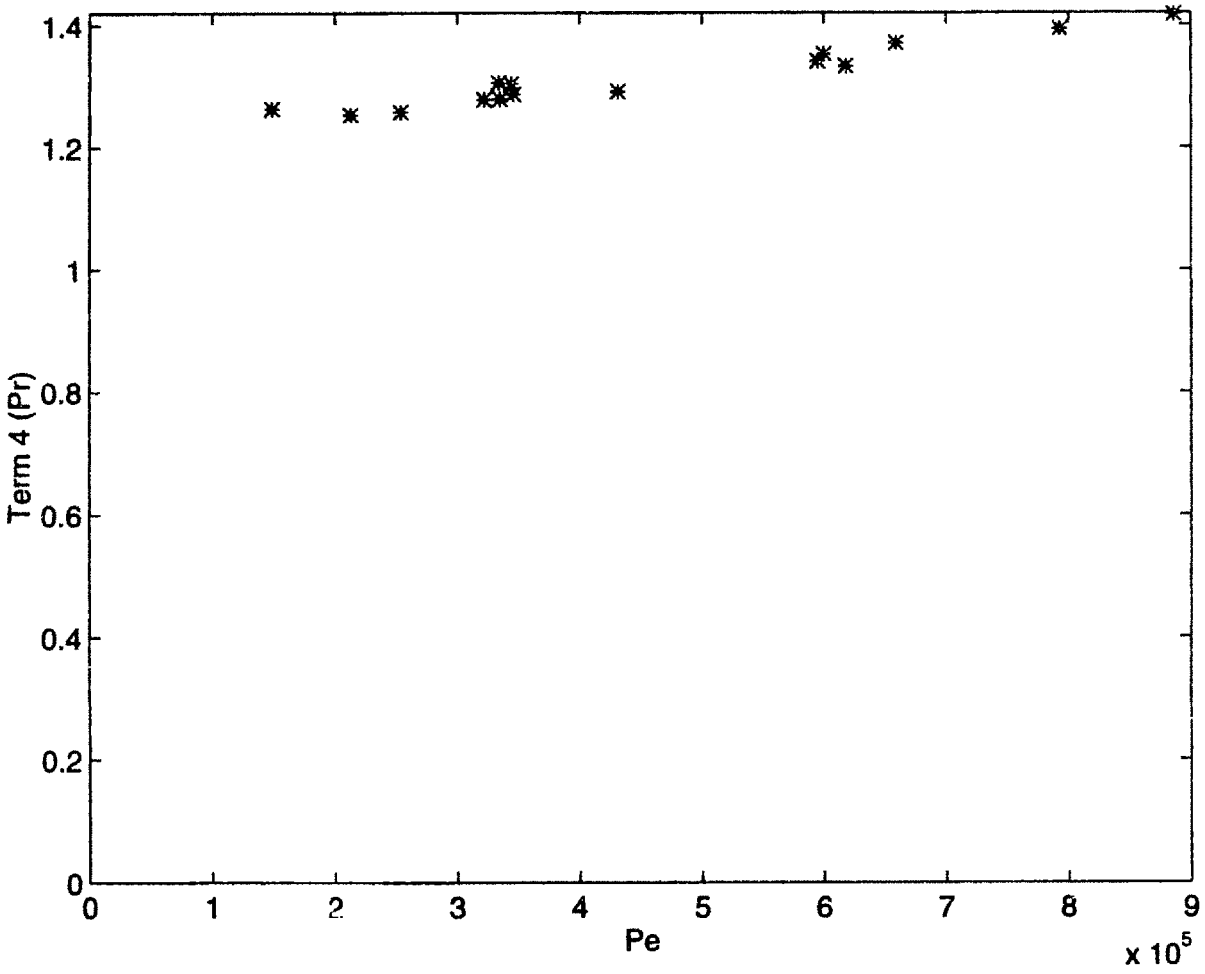

Figure 6-19: Variation in Term 4 ($Pr^{0.6}$) with respect to Pe for Bench Mark Data

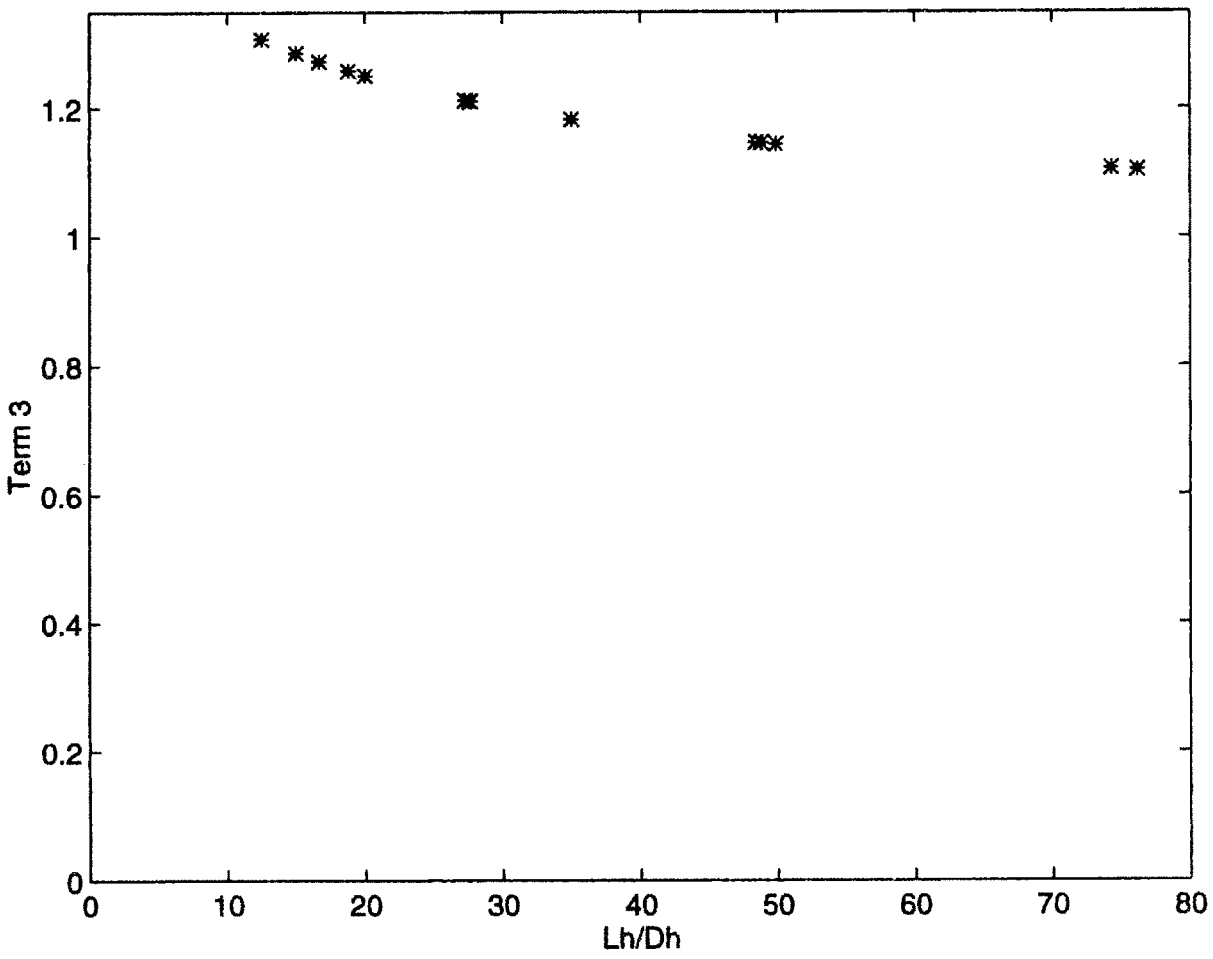

Figure 6-20: Range in Term 3 $(1 + \frac{10}{20+L_h/D_h})$ with respect to L_h/D_h for the Partial CHF Data Base

assumed to be the CHF transition. The relevant thermal hydraulic conditions are: 1) under-development of the thermal boundary layer, 2) subcooled and fully-developed hydraulic flow, and 3) large diameter (D $\geq$ 5 mm) pipe. Since many data points lie above the bubble departure criterion of the Modified Saha-Zuber correlation (St_{BD} = 0.0065), a vastly different mechanism which accounts for bubble departure, such as that suggested by Celata et al. [36] above, may apply. In addition, the under-development of the thermal boundary layer suggests that if any vapor were to depart, it would quickly condense due to the subcooled core being able to effectively penetrate into the boundary layers. Therefore, the data having Pe less than 70,000 or St greater than 0.0065 may not be valid for comparison. A modified data base (hereafter referred to as the Comprehensive CHF Data Base) is plotted in Figures 6-21 and 6-23 which excludes such data (as well as swirl or annular flow data) and includes the bench mark data of the present study. The Comprehensive CHF Data Base includes 289 points. The points appear to follow the correlation of Equation 6.7 with noticeable scatter on both sides. However, it is noteworthy to indicate that 217 points had pressures greater than 1 MPa and are shown in Figure 6-24. These data appear to follow the correlation of Equation 6.7 and most points appear bound by it. Figures 6-25 and 6-26 show the same data between the Pe range in which Equation 6.7 was based. The lower bounding of the data indicates that Equation 6.7 is a conservative prediction of CHF, appropriate for design applications. In addition, at pressures lower than 1 MPa, there is much scatter on both sides of Equation 6.7 (this is later illustrated in Figure 6-31) suggesting possible large vapor density effects producing large fluctuations in the measured values of CHF. Thus, component design using pressures lower than 1 MPa may need to consider large uncertainty in the expected value of CHF.

The variation in Terms 1 to 4 (as defined in the previous section) are shown in Figures 6-27 to 6-30 to show the large ranges in which these parameters varied over the range of Pe for pressures greater than 1 MPa.

In order to uncover parametric trends unaccounted for in Equation 6.7, the ratio of the correlation Equation 6.7 to St_{CHF} will be defined as follows:

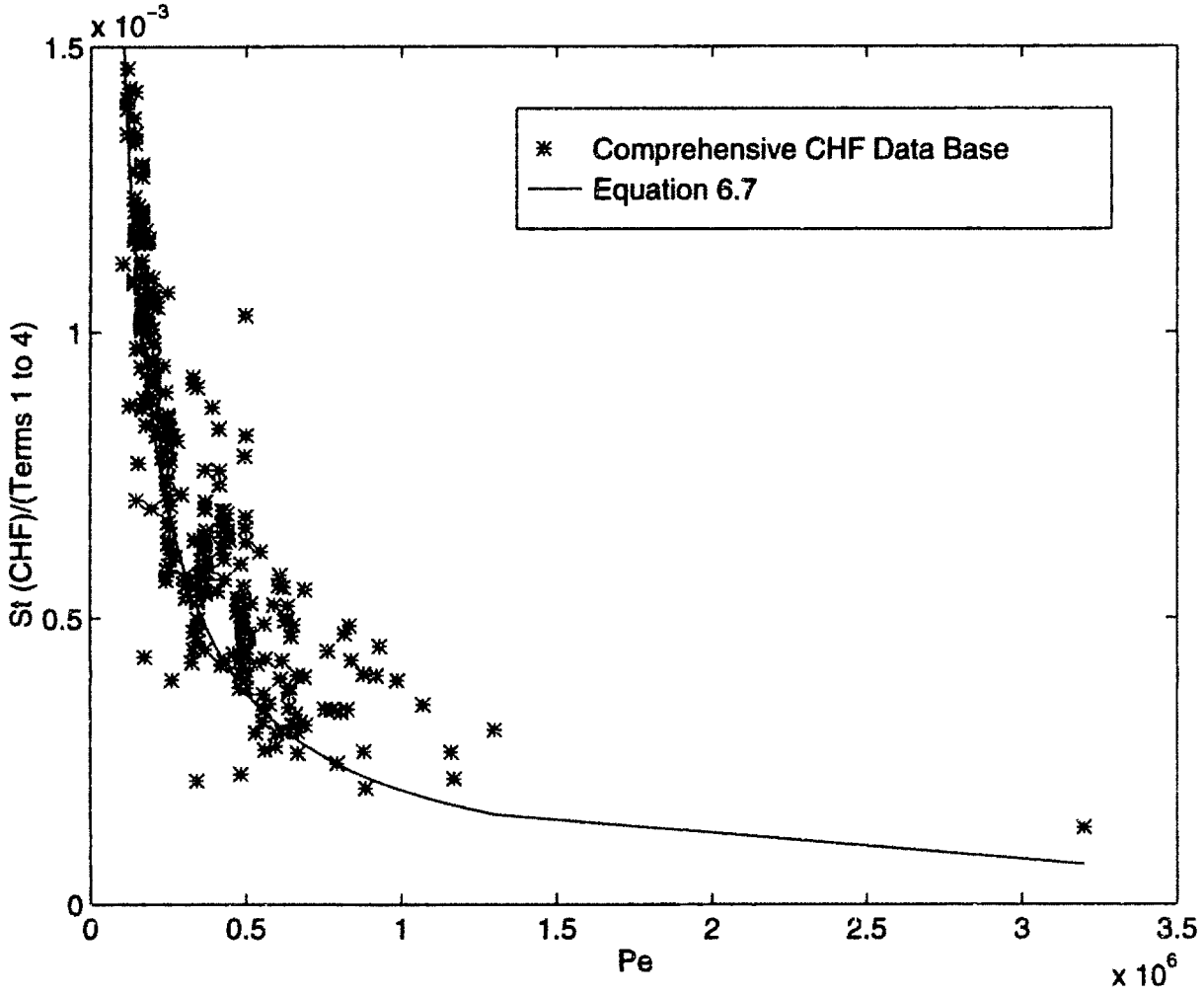

Figure 6-21: Comparison of Equation 6.7 with Comprehensive Data Base of D $\geq$ 5 mm, Pe $\geq$ 70,000 and $St_{CHF} \leq 0.0065$ CHF Experiments

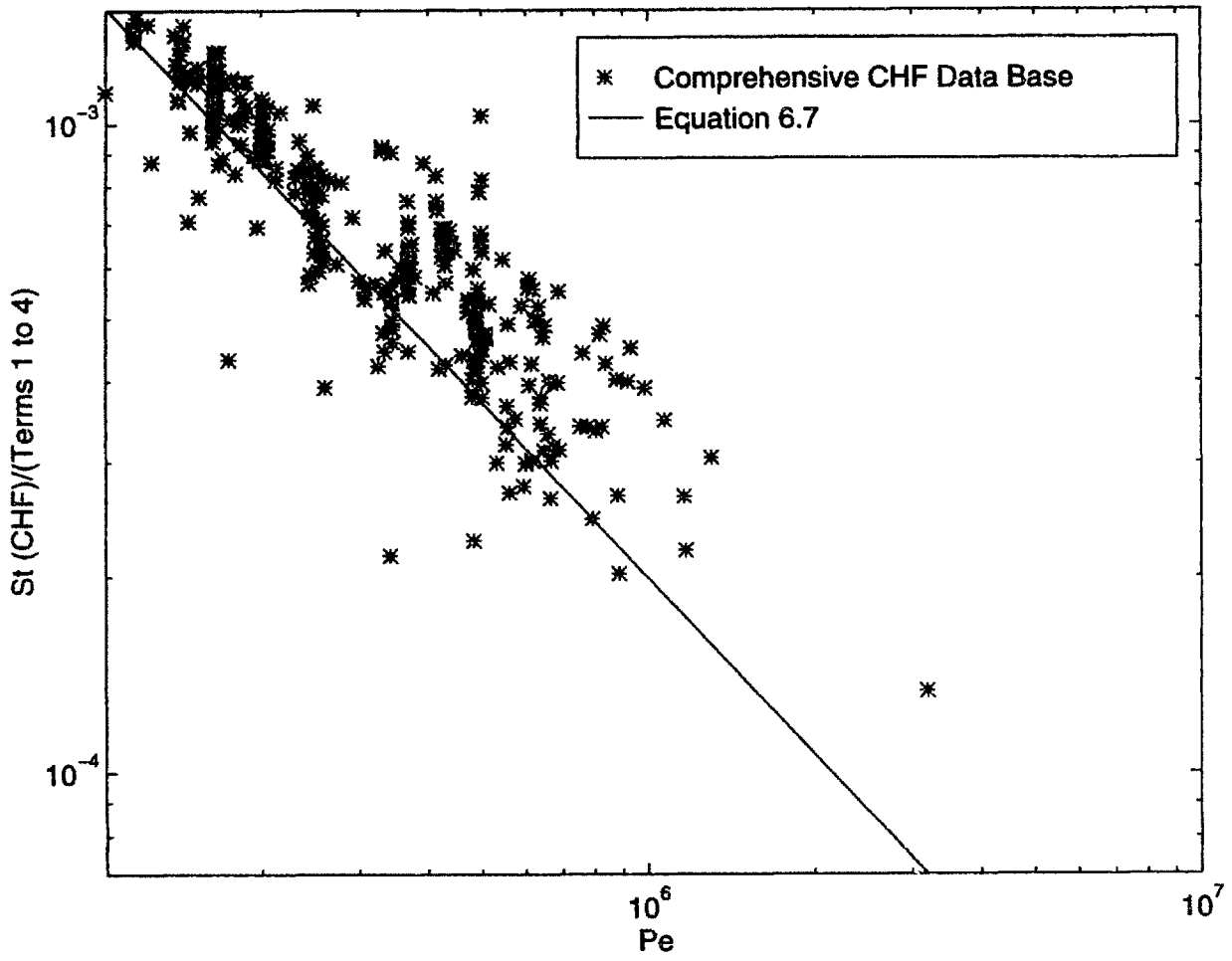

Figure 6-22: Comparison of Equation 6.7 with Comprehensive Data Base of D $\geq$ 5 mm, Pe $\geq$ 70,000 and $St_{CHF} \leq 0.0065$ CHF Experiments on Log-Log Scale

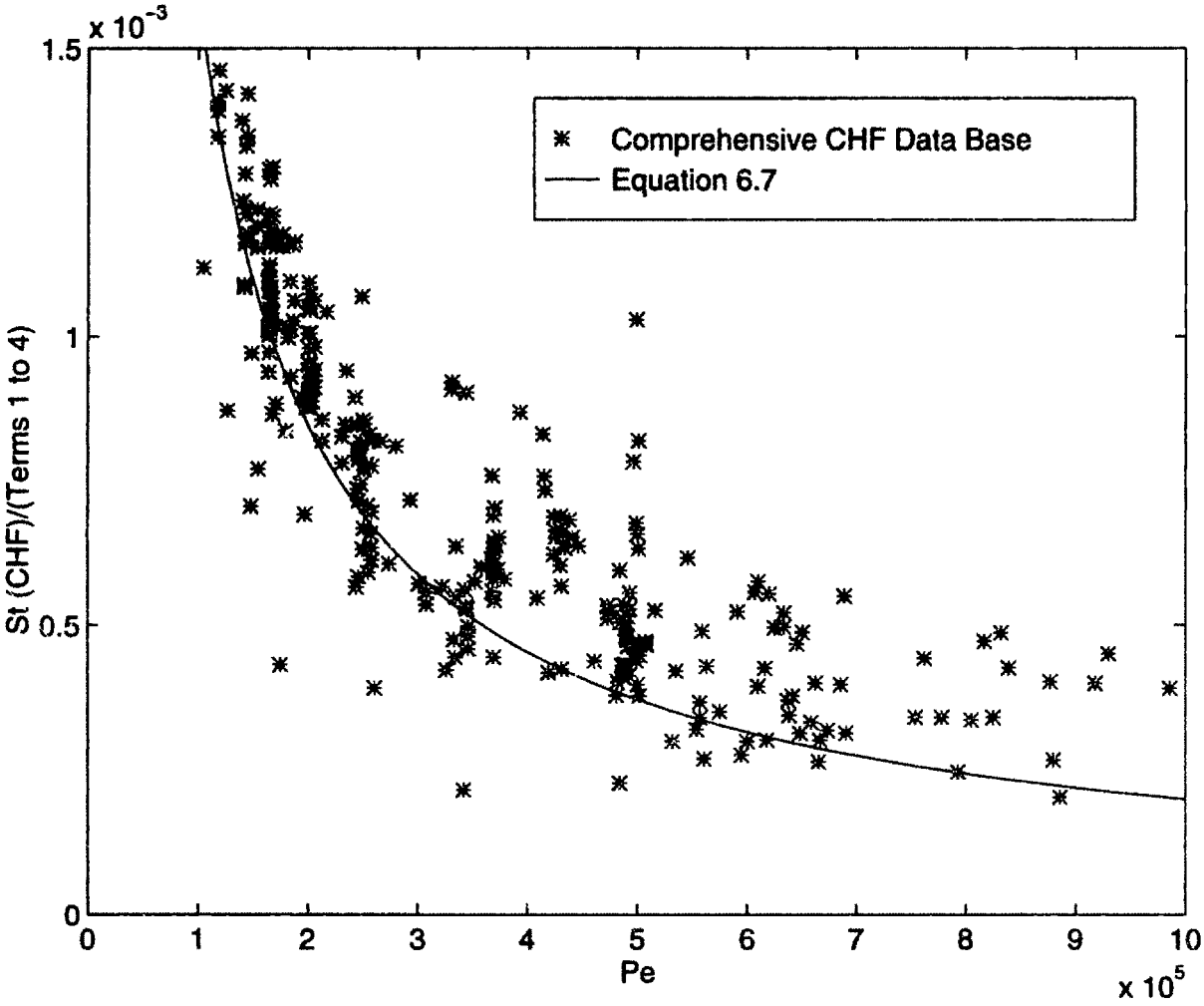

Figure 6-23: Comprehensive Data Base of D $\geq$ 5 mm, Pe $\geq$ 70,000 and $St_{CHF} \leq$ 0.0065 CHF Experiments with $10^5 \geq$ Pe $\geq 10^6$

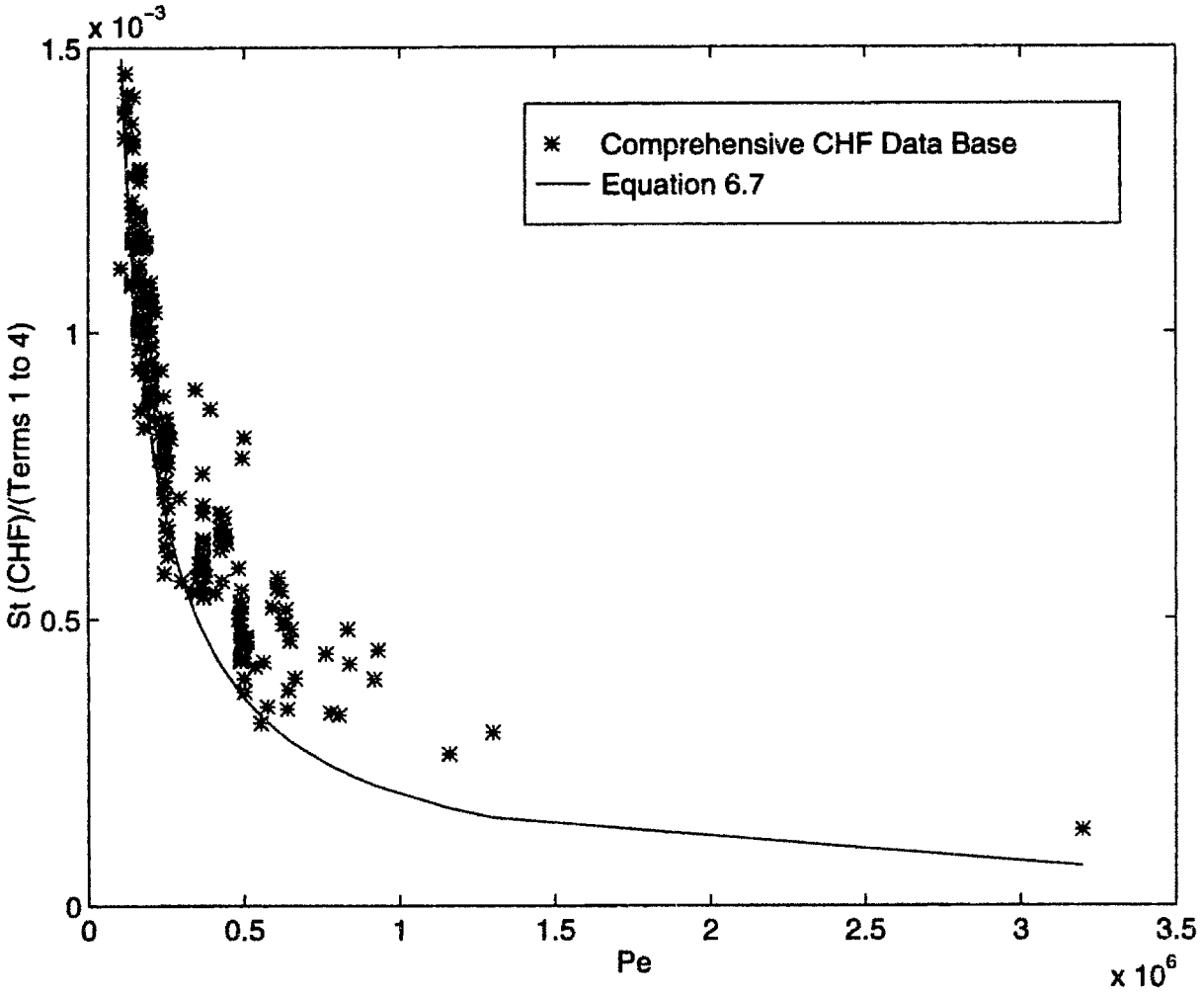

Figure 6-24: Comparison of Equation 6.7 with Comprehensive Data Base of D $\geq$ 5 mm, Pe $\geq$ 70,000 and $St_{CHF} \leq 0.0065$ CHF Experiments (with p $\geq$ 1 MPa)

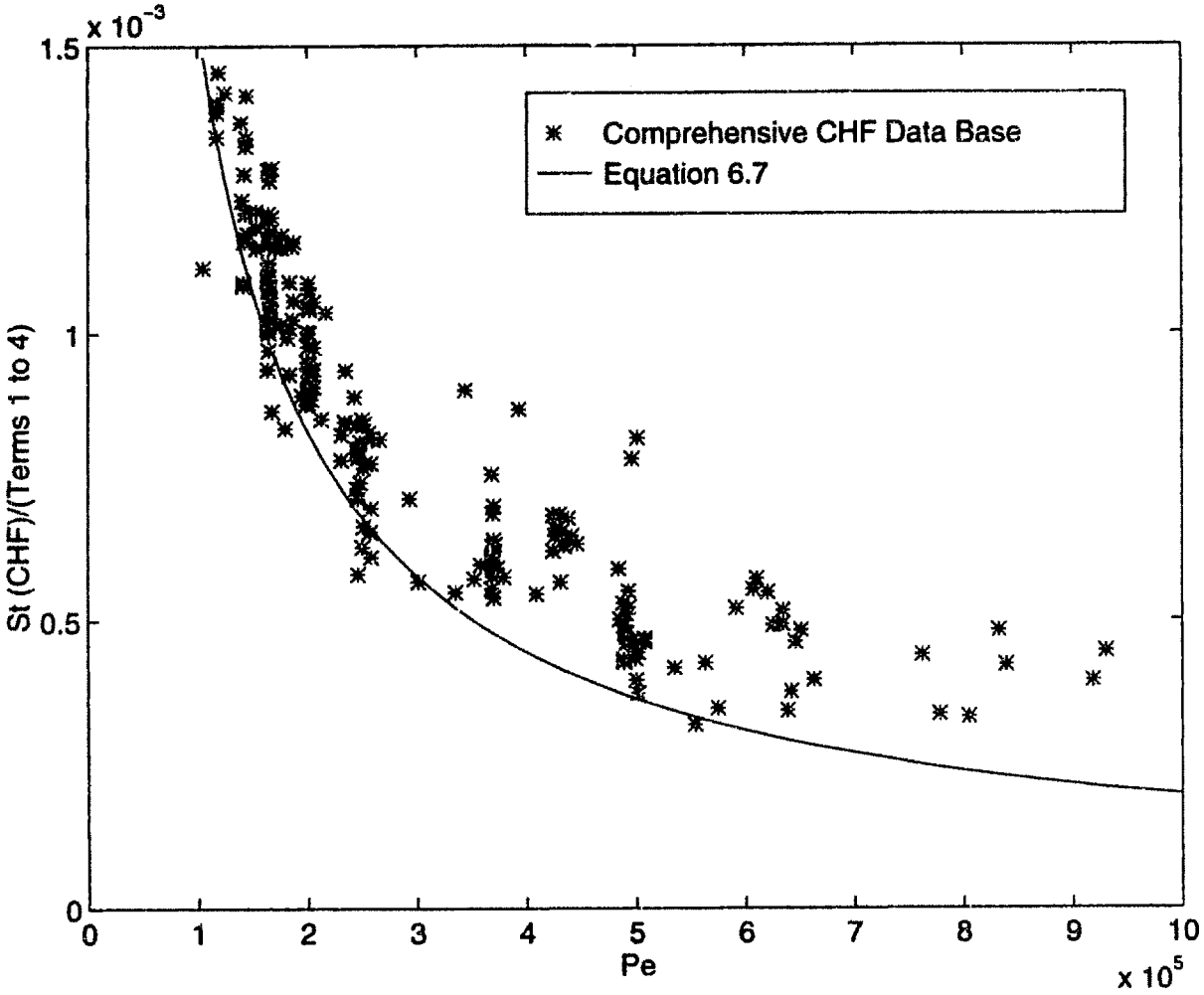

Figure 6-25: Comprehensive Data Base of D $\geq$ 5 mm, Pe $\geq$ 70,000 and $St_{CHF} \leq$ 0.0065 CHF Experiments with $10^5 \geq$ Pe $\geq 10^6$ (with p $\geq$ 1 MPa)

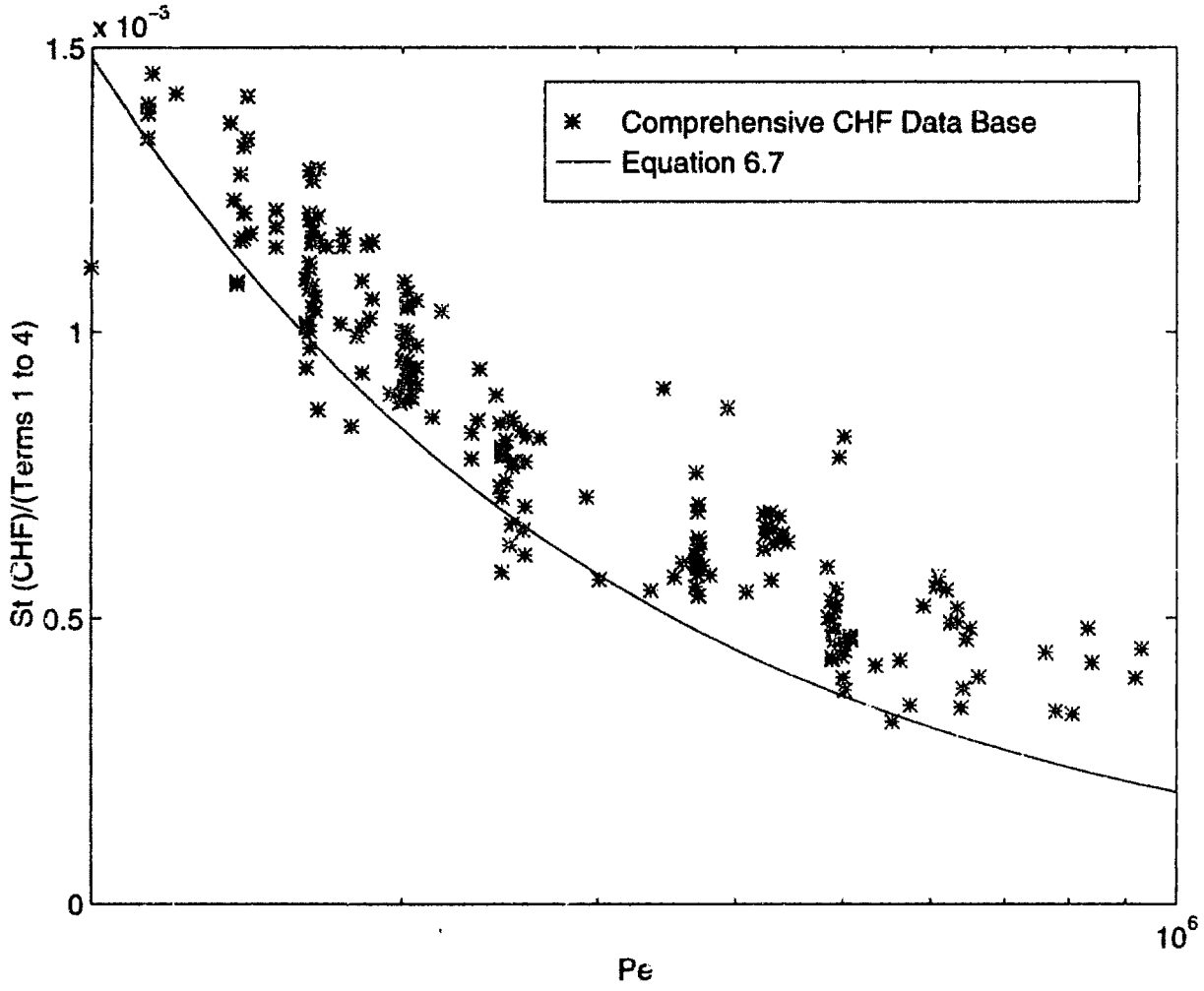

Figure 6-26: Comprehensive Data Base of D $\geq$ 5 mm, Pe $\geq$ 70,000 and $St_{CHF} \leq$ 0.0065 CHF Experiments with $10^5 \geq$ Pe $\geq 10^6$ (with p $\geq$ 1 MPa)

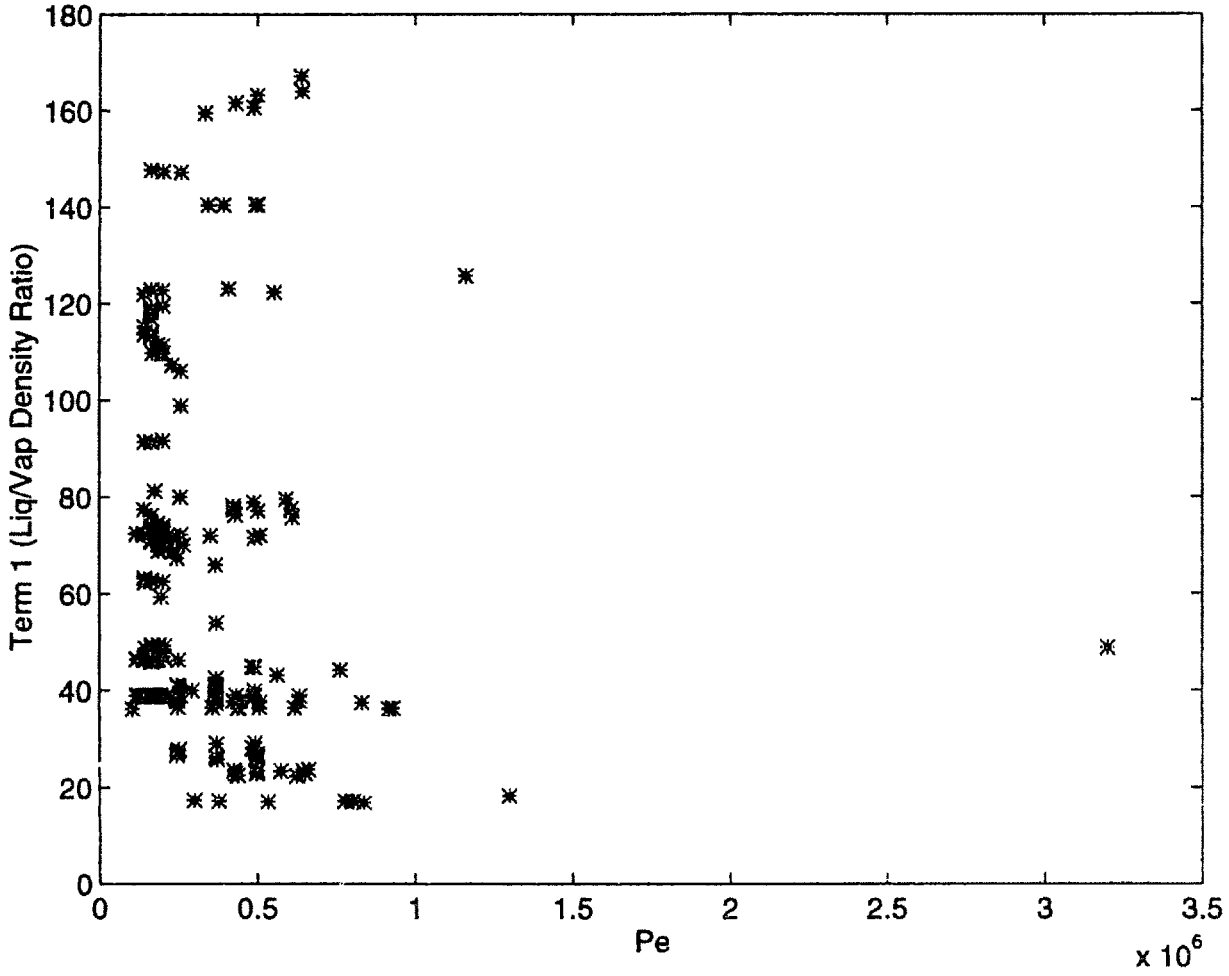

Figure 6-27: Variation in Term 1 (Liquid to Vapor Density Ratio) with respect to Pe for the Comprehensive Data Base (with p $\geq$ 1 MPa)

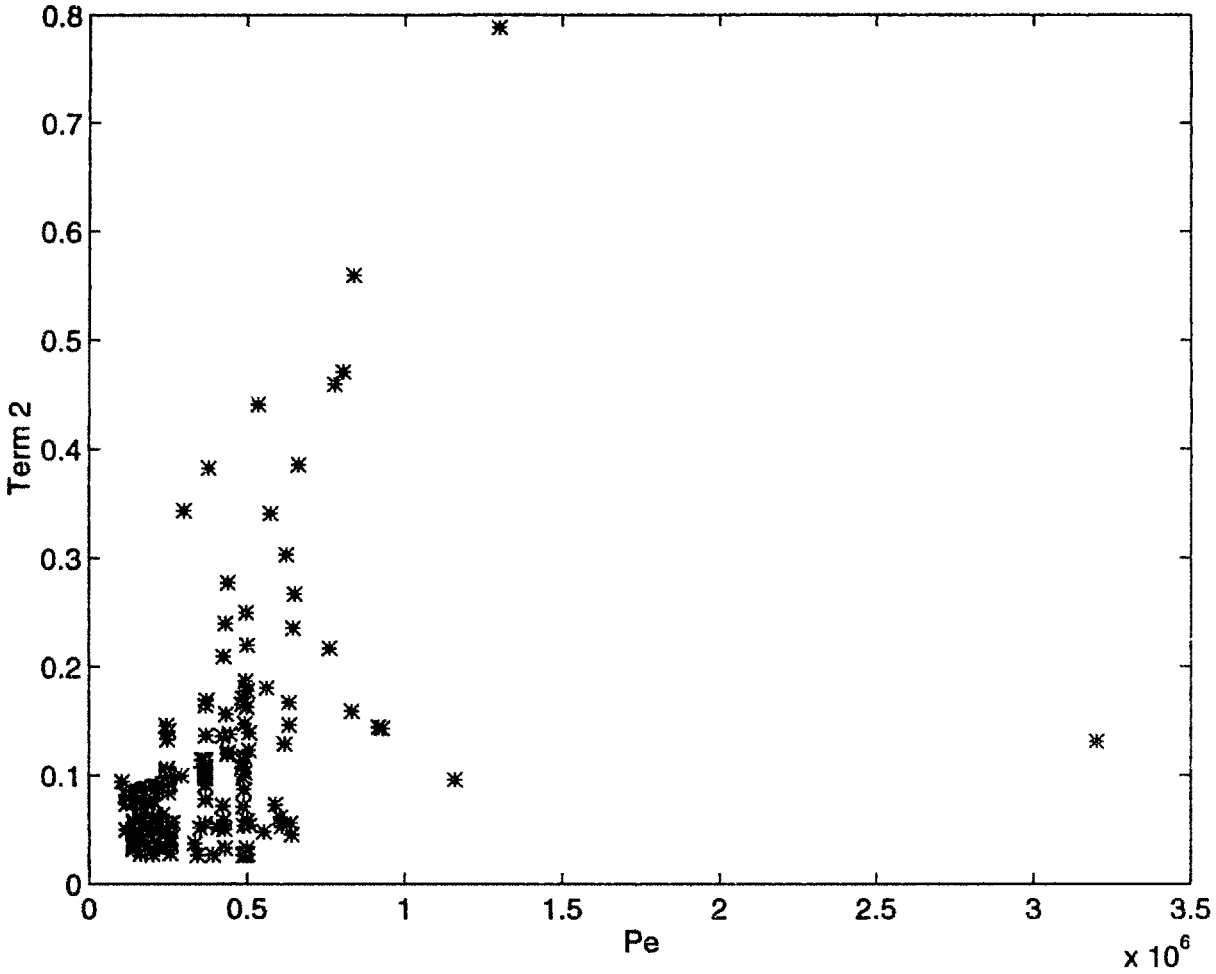

Figure 6-28: Variation in Term 2 with respect to Pe for the Comprehensive Data Base (with $p \geq 1$ MPa)

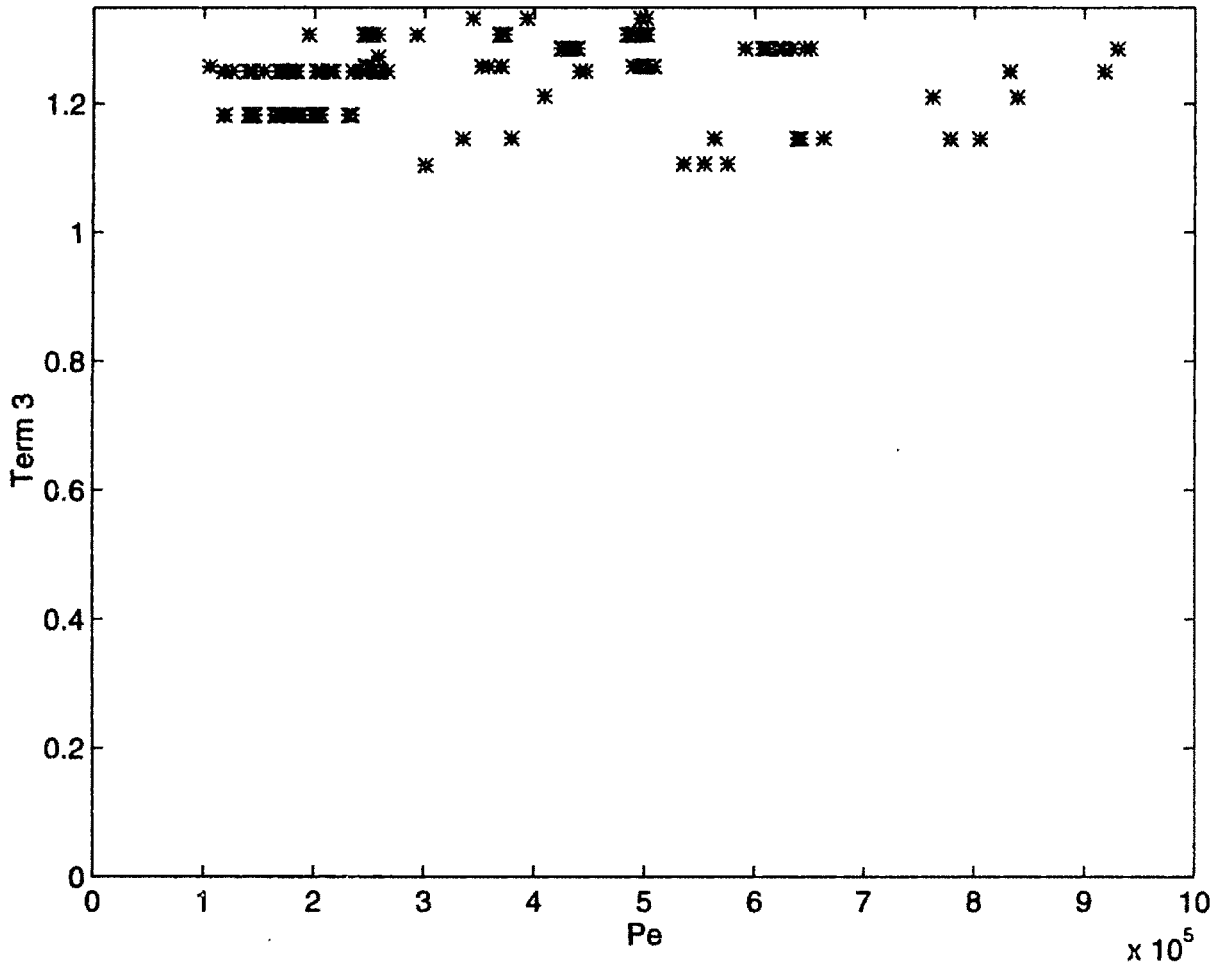

Figure 6-29: Variation in Term 3 $(1 + \frac{10}{20+L_h/D_h})$ with respect to Pe for the Comprehensive Data Base (with p $\geq$ 1 MPa)

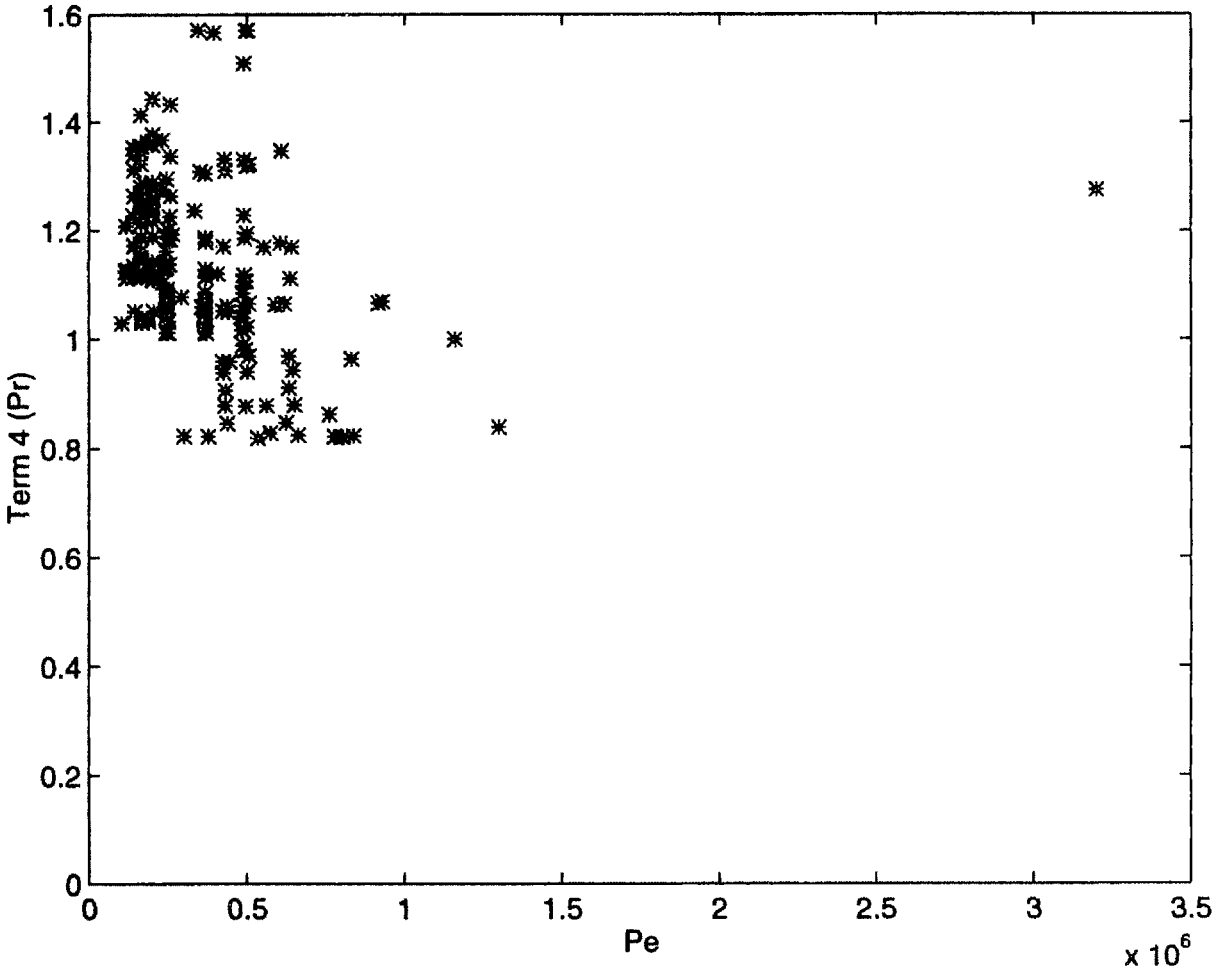

Figure 6-30: Variation in Term 4 ($Pr^{0.6}$) with respect to Pe for the Comprehensive Data Base (with $p \geq 1$ MPa)

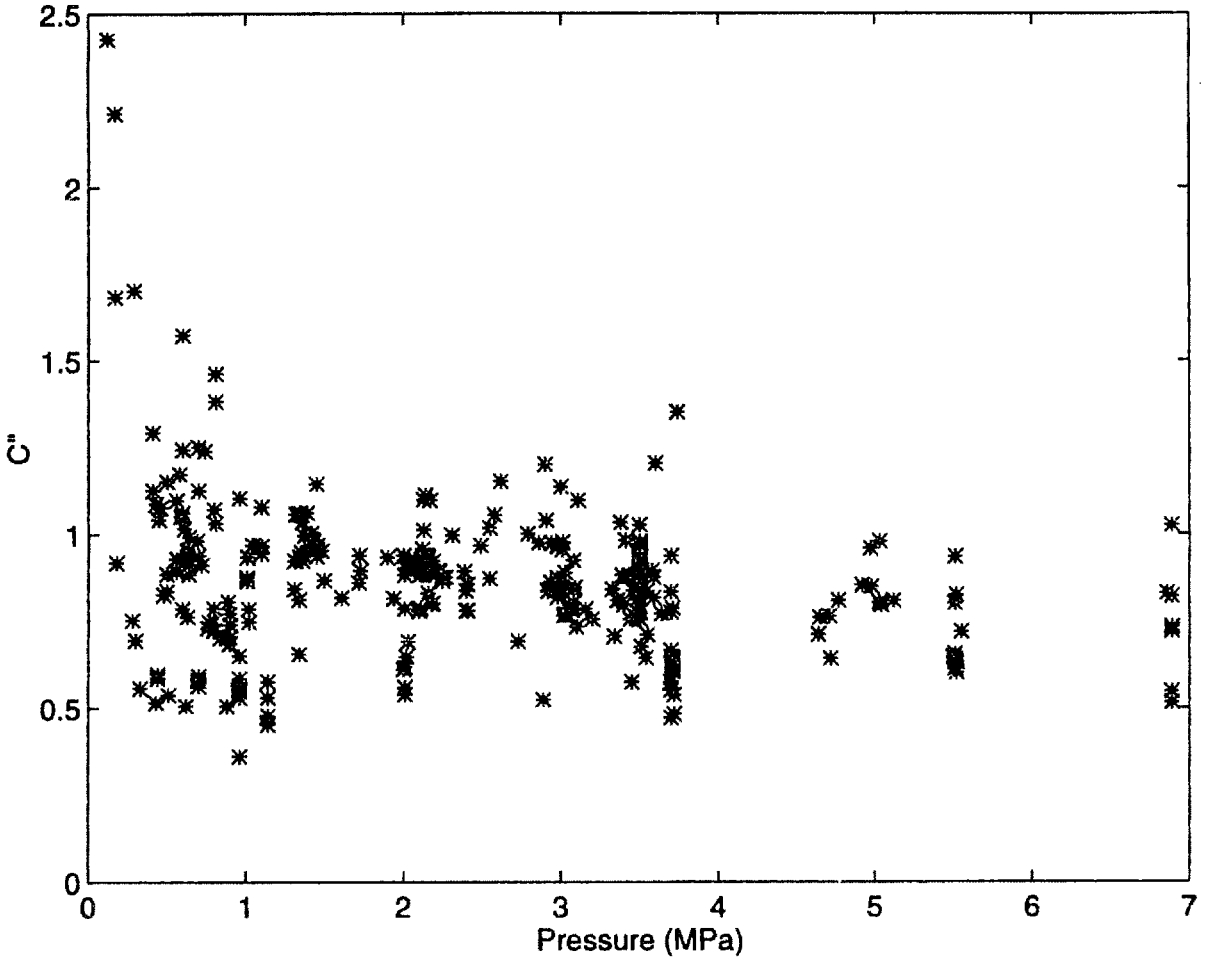

Figure 6-31: Variation in C" with respect to Pressure for the Comprehensive Data Base

$$C'' = \frac{50\frac{\rho_l}{\rho_v}(\frac{1}{Ja} + 0.0022 p_r^{1.8} Re^{0.5})(1 + \frac{10}{20+L_h/D_h})Pr^{0.6}Pe^{-0.9}}{St_{CHF}} \tag{6.8}$$

The ranges of the important thermal hydraulic parameters: pressure, L_h/D_h, Pe, and St_{CHF} are shown in Figures 6-31 to 6-34, respectively, with the variation in C" shown for the Comprehensive Data Base. The uniform scatter in C" indicates that the functional relationship of the parameters appear to be properly represented.

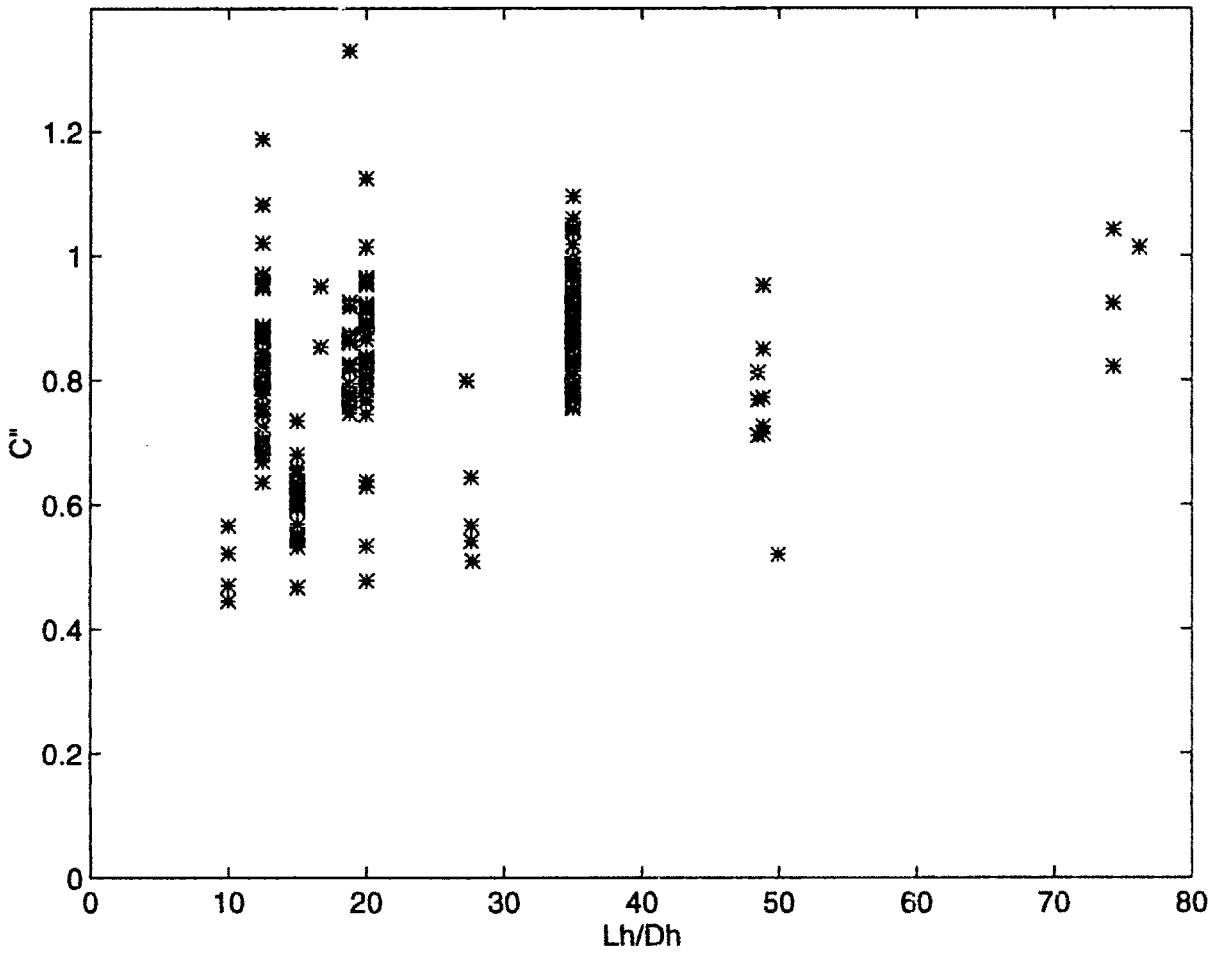

Figure 6-32: Variation in C" with respect to L_h/D_h for the Comprehensive Data Base (with p $\geq$ 1 MPa)

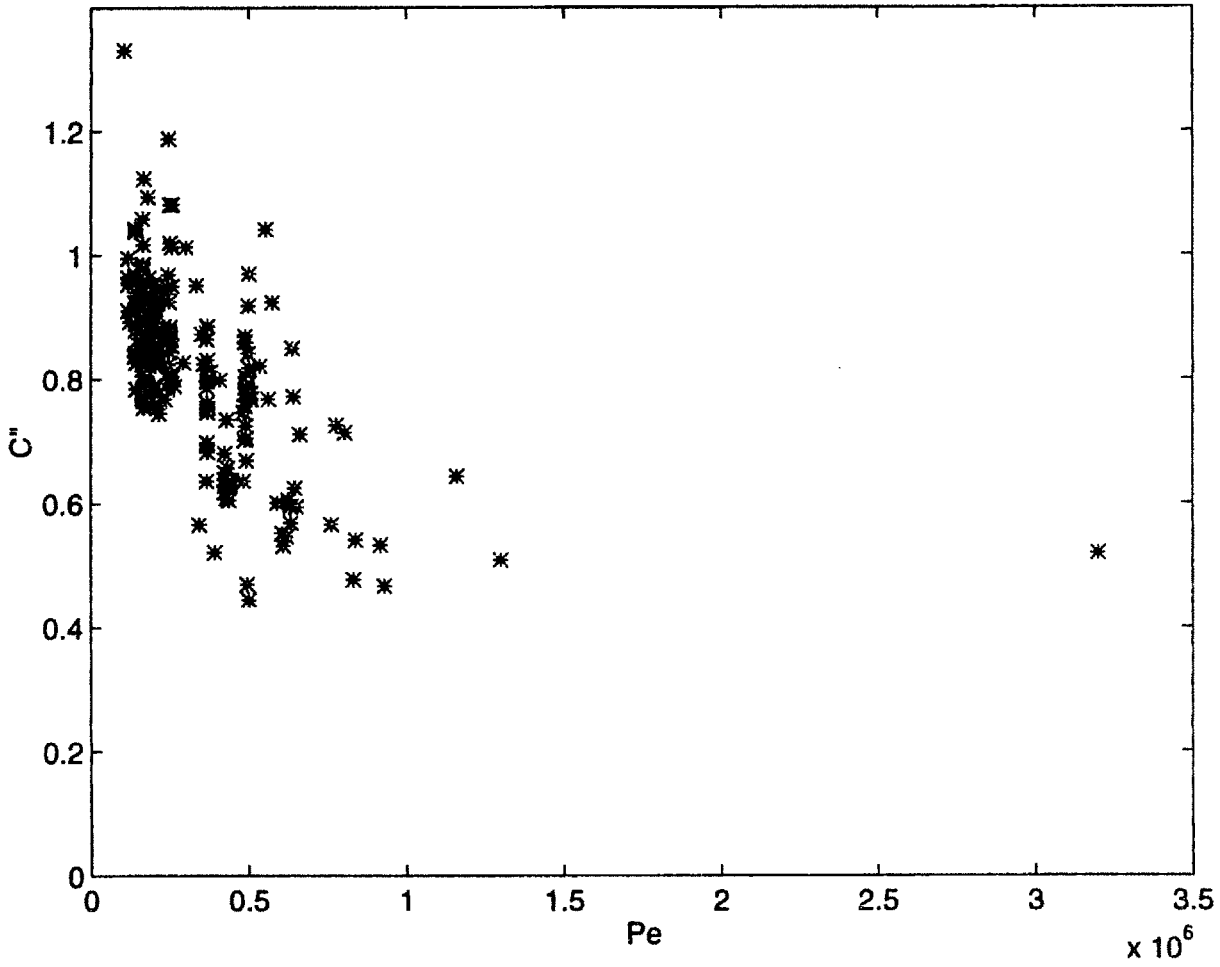

Figure 6-33: Variation in C" with respect to Peclet number for the Comprehensive Data Base (with p $\geq$ 1 MPa)

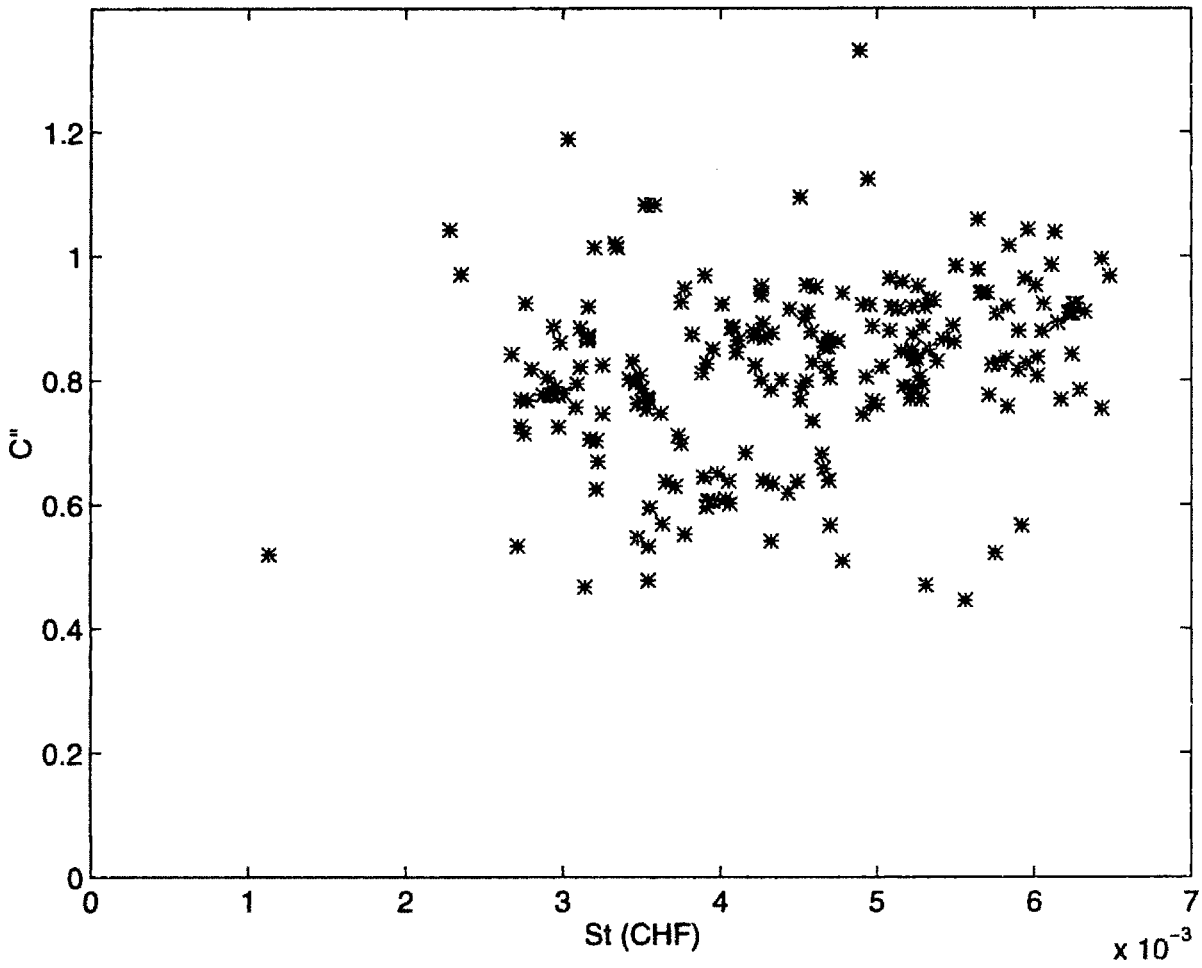

Figure 6-34: Variation in C" with respect to St_{CHF} for the Comprehensive Data Base (with p $\geq$ 1 MPa)

6.4.1 Critical Heat Flux Correlation Applied to Swirl Flow Data Base

Thus far, comparisons have been for smooth flow data. However, the additions of twisted tapes to enhance heat transfer at the divertor strike points were discussed in Chapter 2. All 81 of the swirl flow data from the data base described in Chapter 1 are shown in Figure 6-35. Figure 6-36 shows 32 out of 81 swirl flow points having pressure greater than 1 MPa. Figure 6-37 shows the 17 out of 81 swirl flow points which fulfill the criteria of Pe greater than 70,000 and St_{CHF} less than 0.0065. Finally, of the latter 17 data points, Figures 6-38 and 6-39 divide the points into low pressure data (less than 1 MPa) and the higher pressure data, respectively. This last comparison is to indicate that there appears to be agreement for low pressure cases within the undetached bubble criteria.

Clearly, the inclusion of swirl flow enhances turbulence and further suppresses nucleate boiling. In cases where bubbles may detach, the CHF mechanism is not prescribed and Equation 6.7 may not be appropriate. In cases of higher pressure, Equation 6.7 shows marked under-prediction for the nine points with pressures over 1 MPa. as illustrated in Figure 6-39. However, the opposite is noted in Figure 6-38 in which the eight data points are over-predicted by Equation 6.7. This would not bode well in the case of lost pressure which could occur in a loss of flow accident. Clearly, an insufficient amount of points exist in the swirl flow data base to make definitive conclusions. This section was meant as a preliminary comparison.

6.4.2 Critical Heat Flux Correlation Applied to All Data of the Present Experiments

Several data points were neglected during the development of Equation 6.7 due to the discrepancy when the computed outside wall temperatures disagreed with the measured temperatures as described at the beginning of this chapter. The boiling data points, i.e., those points for which the coolant-side wall temperatures are calculated to be higher than saturation, are shown in Figure 6-40 without error bars while

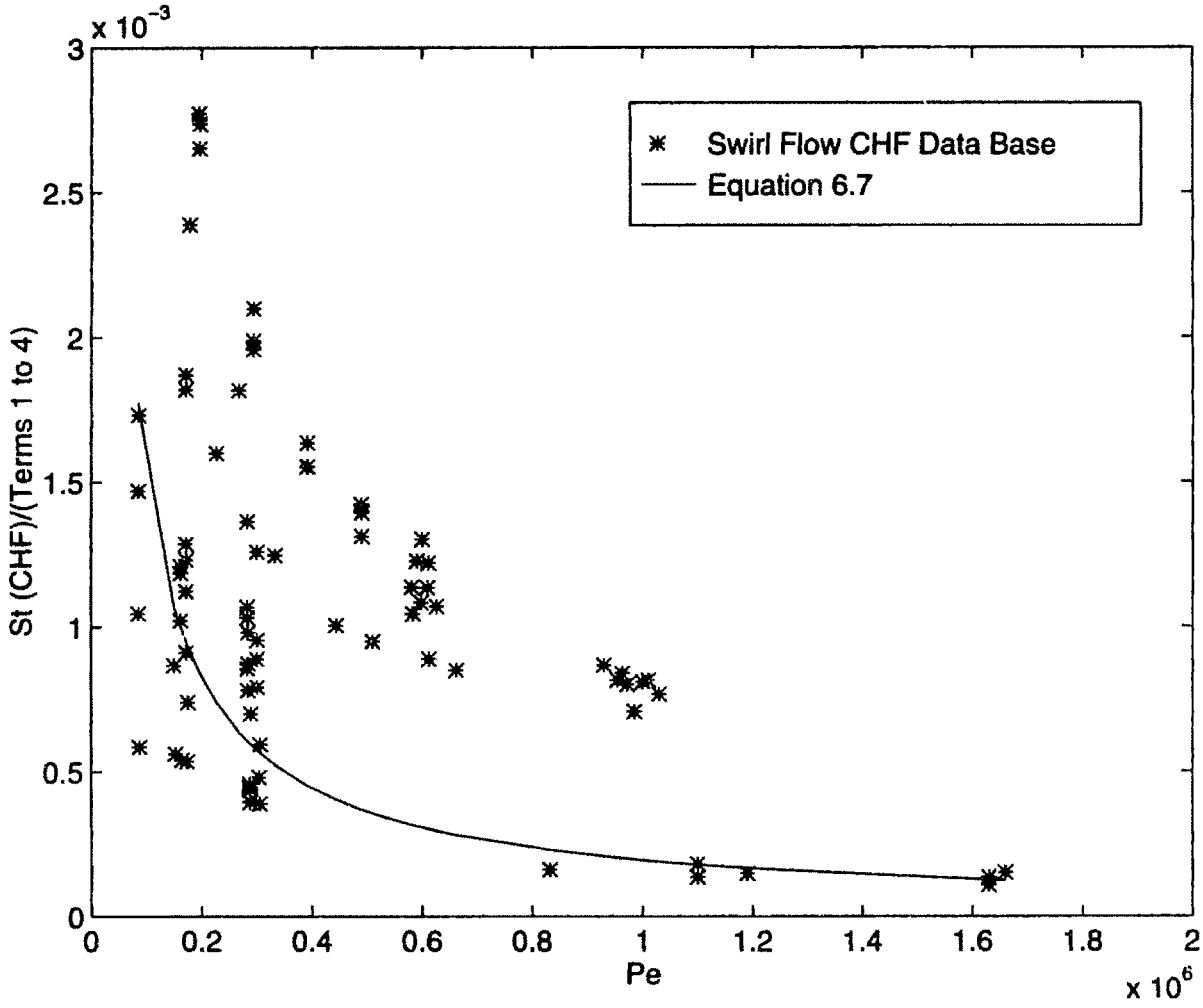

Figure 6-35: Swirl Flow Data of Data Base compared to Correlation.

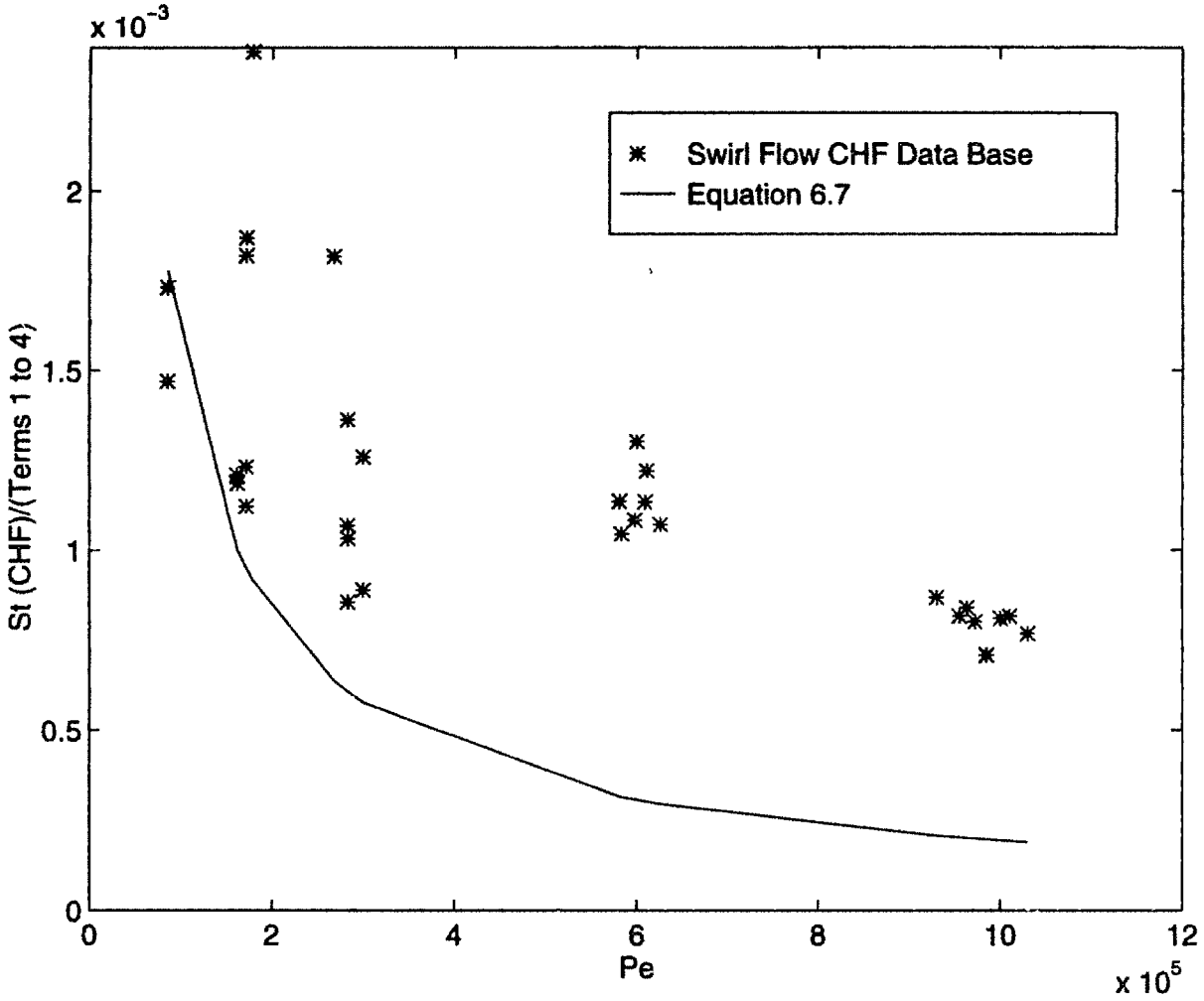

Figure 6-36: Swirl Flow Data of Data Base compared to Correlation ($p \geq 1$ MPa).

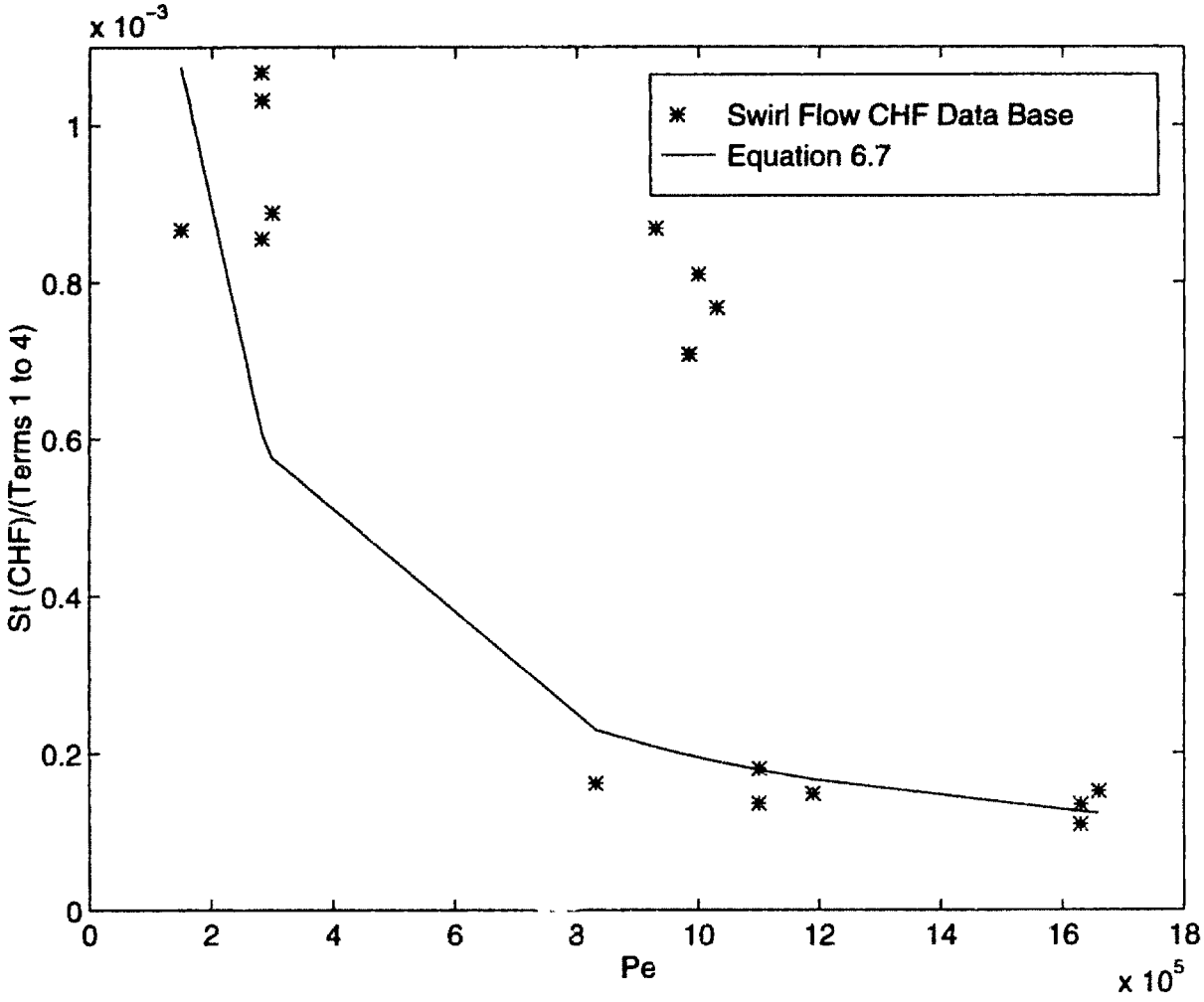

Figure 6-37: Swirl Flow Data of Data Base compared to Correlation (Pe $\geq$ 70,000 and $St_{CHF} \leq 0.0065$).

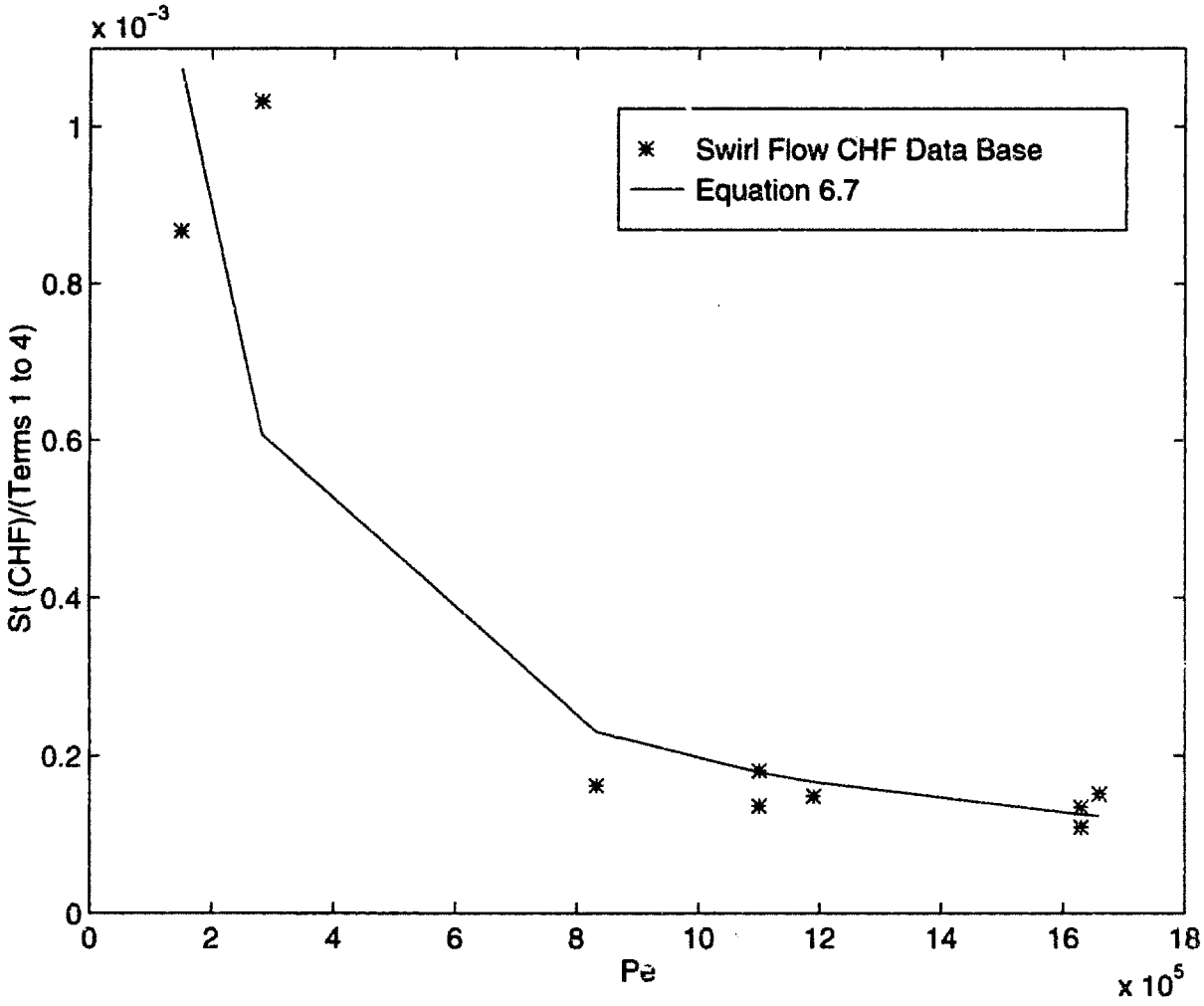

Figure 6-38: Swirl Flow Data of Data Base compared to Correlation (Pe $\geq$ 70,000, $St_{CHF} \leq 0.0065$, and p $\leq$ 1 MPa).

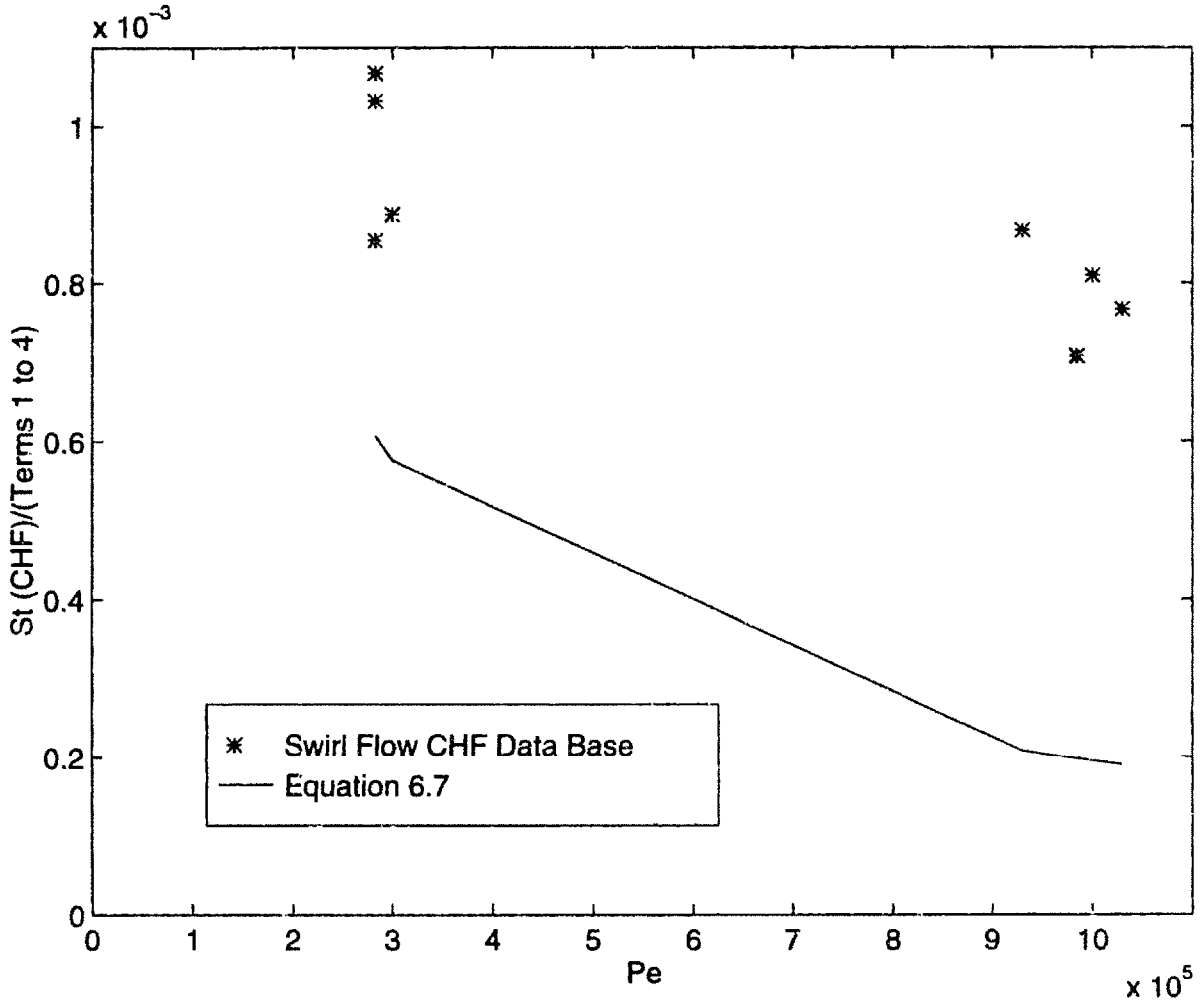

Figure 6-39: Swirl Flow Data of Data Base compared to Correlation (Pe $\geq$ 70,000, $St_{CHF} \leq 0.0065$, and p $\geq$ 1 MPa).

the bench mark data include the bars. The trend of the 27 data points show good agreement with Equation 6.7. The data shown in Figures 6-40 and 6-41 have Pe greater than 70,000 and St_{CHF} less than 0.0065. The three data points with Pe less than 70,000 are included in Figure 6-42 on a log-log scale. Recall, the data in the low flux region have conditions in which detachment of bubbles from the surface are expected. This mechanism would be very different from the mechanism in which the phenomenological correlation Equation 6.7 was conceived. For this reason and the high uncertainties ascribed to the low mass flux measurements, no further discussion will be given explaining the three data points with Pe less than 70,000.

The next chapter will summarize the important findings of the present study and suggest improvements to experimental technique, refinement of parameter-space relationships, and extension of thermal hydraulic boundary phenomena.

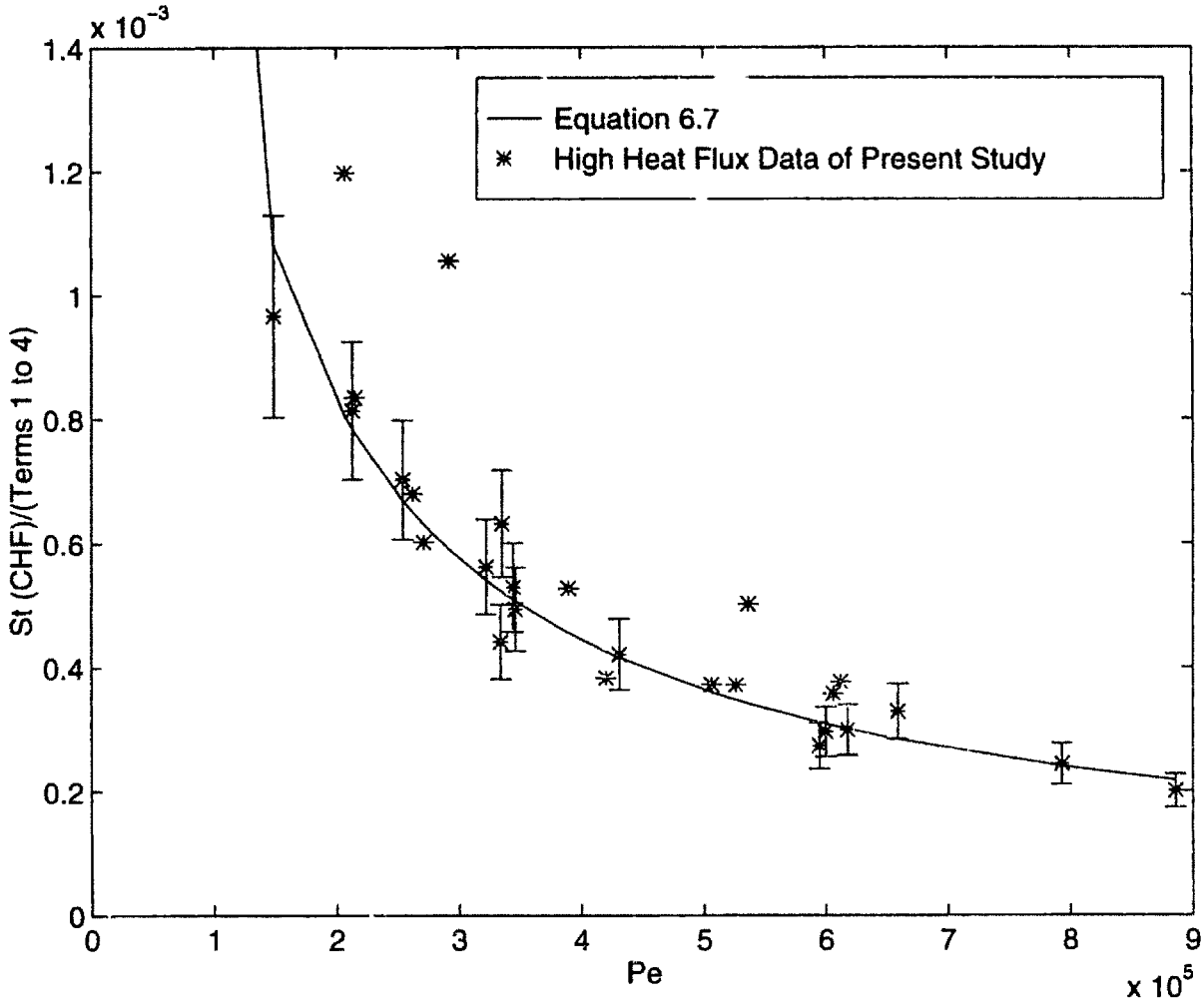

Figure 6-40: Data of Present Study in which Boiling is Expected, Pe $\geq$ 70,000 and $St_{CHF} \leq 0.0065$, compared to Correlation. Note: points with error bars represent bench mark CHF data.

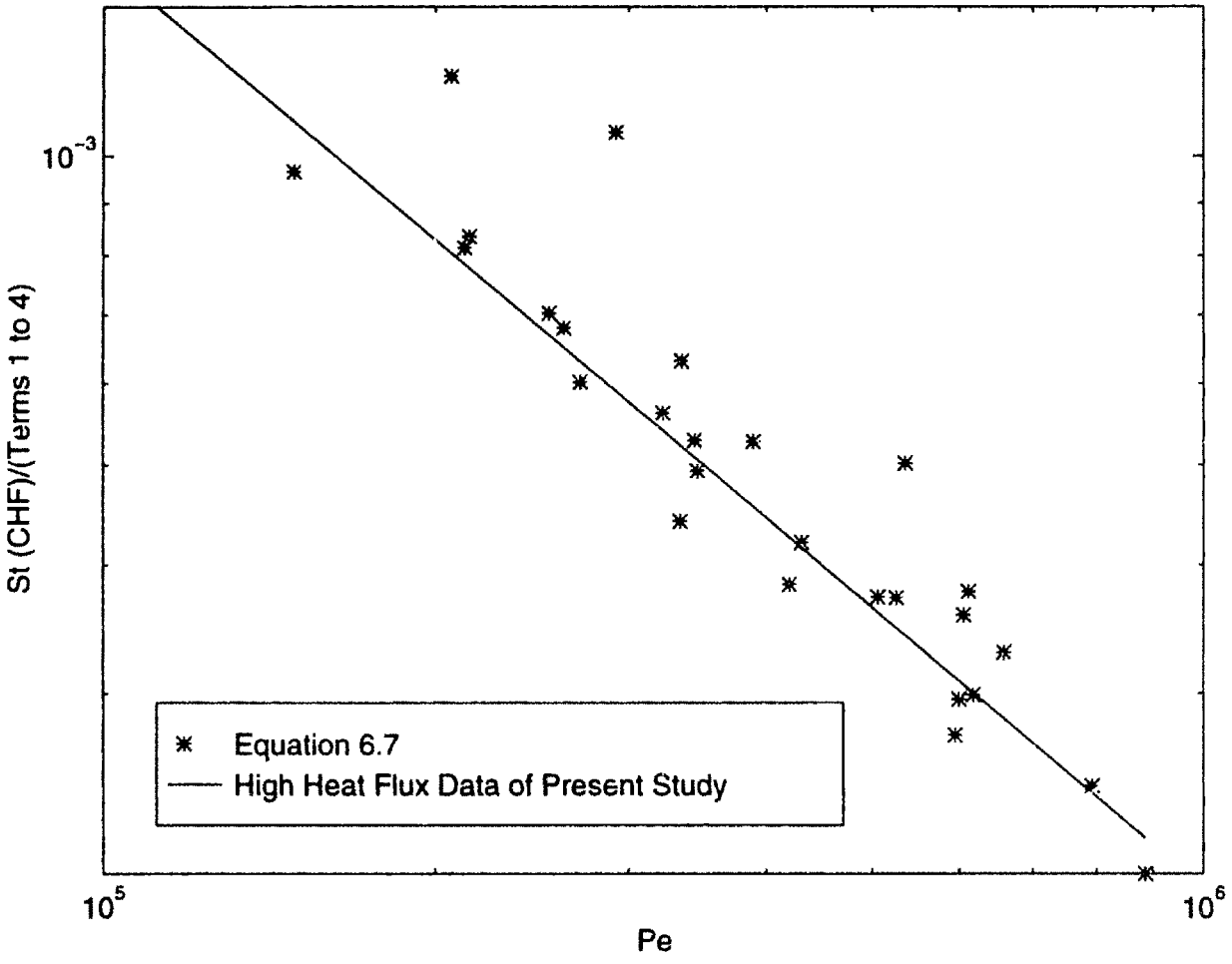

Figure 6-41: Data of Present Study in which Boiling is Expected, Pe $\geq$ 70,000 and $St_{CHF} \leq 0.0065$, compared to Correlation on Log-Log Axes

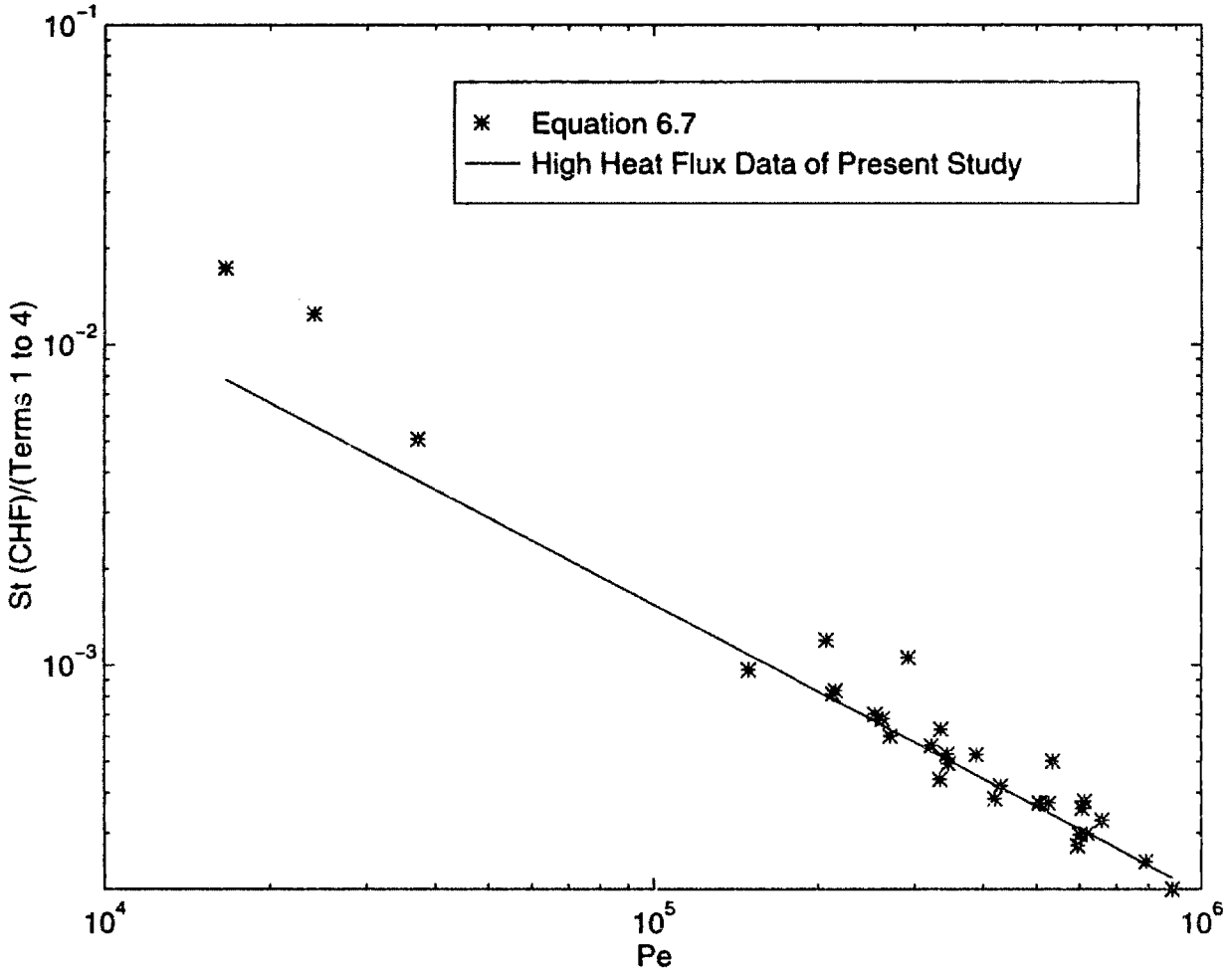

Figure 6-42: Data of Present Study in which Boiling is Expected

Chapter 7

Conclusion and Recommendations

7.1 Summary of Major Findings

1. An experimental technique of single-sided heating using direct current heating was developed to reach local heat fluxes of 37 MW/m^2.

2. For subcooled water flow, critical heat flux values above 10 MW/m^2 were consistently obtained for all 33 data measurements with mass flow rates ranging from 0.27 to 19 Mg/m^2s and equilibrium exit thermodynamic qualities ranging from -0.2 to -0.49.

3. At least two regimes of critical heat flux (defined herein as departure from nucleate boiling) have been identified in the present study. One regime appears more likely in low flow cases where bubbles are expected to depart the surface and possibly allow a thin liquid sublayer to exist. These conditions are favorable according to a modified Saha-Zuber bubble departure correlation when the Peclet number is less than 70,000 or the Stanton number is greater than 0.0065. The second CHF regime seems to be associated with local transition from nucleate to film boiling, which would be expected for Pe greater than 70,000 and St less than 0.0065. The latter condition is expected to appear under the fusion divertor thermal hydraulic conditions of interest for the present study.

4. A CHF correlation was developed based upon experiments having low to high mass fluxes (1 to 10 Mg/m^2s), very high subcooling (an exit equilibrium quality typically less than -0.45), moderate pressures (about 3 MPa), and single-sided heating. Data reduction relied on a three-dimensional conduction code to infer the heat transfer at the coolant-side of the channel. The outer wall temperature profile was used to validate the computer simulation and only upon agreement were data points deemed bench mark.

   Fifteen bench mark CHF data points were used to determine the parameters of a phenomenological equation partly based upon the method of Tong (1975) [32]. The correlation was tested against a database containing 202 points having comparable thermal hydraulic parameters. The correlation, below, was found to predict the trend of the data and even appears to be a lower bound; and thus, may be an appropriate conservative limit for design applications.

$$St_{CHF} = 50\frac{\rho_l}{\rho_v}\left(\frac{1}{Ja} + 0.00216 p_r^{1.8} Re^{0.5}\right)\left(1 + \frac{10}{20 + L_h/D_h}\right) Pr^{0.6} Pe^{-0.9} \qquad (7.1)$$

   The heated length term and the increased dependency on Pe were added in the present study to consider the under-development of the thermal boundary layer and the suppression of nucleate boiling, respectively. The main parameter-space constraints are Pe greater than 70,000 St_{CHF} less than 0.0065 for hydraulically fully-developed, smooth tube flows in large (greater than 5 mm) diameter tubes. The recommended range of main parameters are Pe [7.0 x 10^4, 1.0 x 10^6], pressure [1, 7 MPa], coolant channel diameter [5, 25 mm], and heated length to heated diameter ratio [5, 80].

5. The predicted critical heat flux for the ITER thermal hydraulic conditions, as mentioned in Table 1.2 (except without swirl tapes), is shown in Figure 7-1 along with the limiting heat fluxes from Figure 2-5. The Tong-75 CHF correlation in Figure 2-5 has been replaced by Equation 7.1 for comparison in Figure

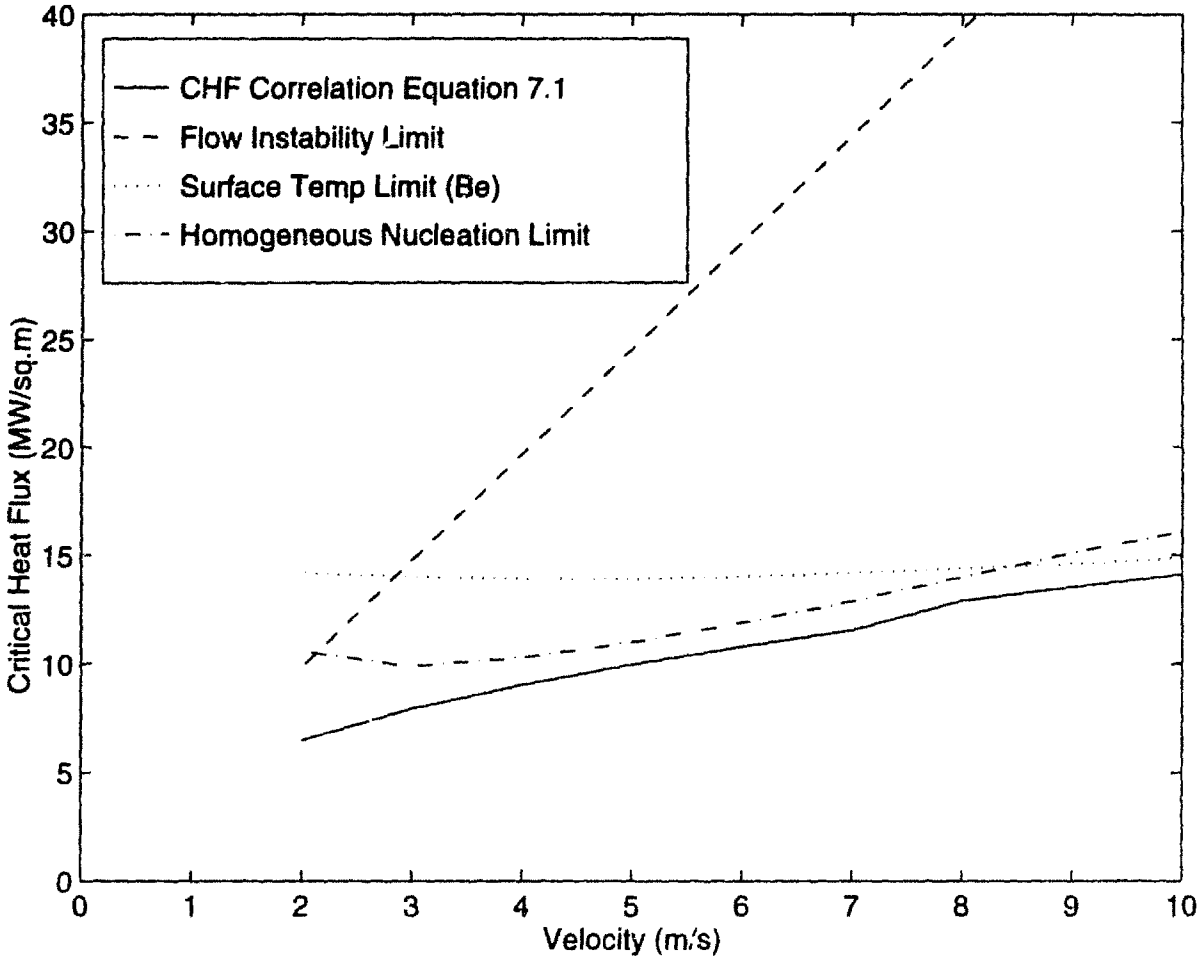

Figure 7-1: Comparison of Limiting Heat Fluxes including Homogeneous Nucleation for ITER Conditions with Unobstructed Flow

7-1. Equation 7.1 predicts that the CHF limit will be the most restrictive thermal limit and, in addition, suggests that it may slightly preempt homogeneous nucleation. The latter conclusion adds credibility to the use of nucleate boiling correlations applied to the coolant-side wall for heat transfer modeling prior to CHF. A comparison of Figures 2-5 and 7-1 also suggests that the extrapolation of the Tong-75 CHF correlation to fusion divertor thermal hydraulic conditions is unwarranted and the proposed CHF correlation (Equation 7.1) appears to the conservative choice for the limiting heat flux.

7.2 Recommendations

The present study has addressed an area where few other studies exist, namely, high heat flux thermal hydraulics experimentation. Therefore, many areas of expansion and refinement are worthy of pursuit.

First, of the major parameters (mass flux, pressure, subcooling, and diameter) only the mass flux was sufficiently varied to formulate a relation (Pe $\geq$ 70,000). A similar parametric study of the others as well as an extended study at low mass fluxes, i.e., Pe $\leq$ 70,000, would add confidence to interdependent terms in the proposed CHF correlation. Particularly, a study to better describe the heated length effect for short or spiked profiles, e.g.: L_h about 0.05 m or L_h/D_h ranging from 5 to 10: or, to investigate the non-uniform heated diameter effect for non-uniform circumferential heat fluxes.

Second, methods of heat transfer enhancement such as twisted tapes or novel channel designs would be the next logical step in increasing heat transfer performance. The present study only touched upon the question of swirl flow since the added complexity and sparse data base do not warrant full comparison to the smooth flow case in the above phenomenological endeavor. Nevertheless, within the attached bubble criteria it was noted in Chapter 6 that at pressures less than 1 MPa, Equation 7.1 slightly over-predicted the sparse data. On the other hand, at pressures above 1 MPa, Equation 7.1 greatly under-predicted the data.

Finally, refinement of the experimental method would entail more instrumentation such as larger thermocouple arrays to aid in characterizing the actual heat flux profile; or, a differential pressure transducer across the heated section to identify significant vapor formation. In addition, more modern state-of-the-art computational codes would have made the analysis much less time consuming.

Bibliography

[1] Draft Report for ITER Concept Definition Phase. Technical report, 1989.

[2] ITER Concept Definition, International Atomic Energy Agency, Vienna. *ITER Documentation Series*, 2(3), 1989.

[3] R.D. Watson, editor, et al. ITER Divertor Engineering Design, Summary of Joint Working Session, Garching, Germany, Max Planck Institute for Plasma Physics. October 1989.

[4] R.T. McGrath, J.A. Koski, R.D. Watson, R.A Causey, C.D. Croessmann, J.F. Dempsey, M. Hosking, K.A. Neimer, A.J. Russo, J.C. Salmonson, J. Stephens, M.F. Smith, J.G. Watkins, and J.B. Whitley. Design Considerations for ITER Plasma Facing Components, Sandia National Laboratory. *Report SAND89-0901 UC-420*, July 1989.

[5] J.A. Koski. Divertor Fabrication Issues, Sandia National Laboratory. *Report SAND89-0901 UC-420*, July 1989.

[6] T.E. Hechanova. Thermo-Mechanical Performance of Beryllium-Coated Copper Divertors, S.M. Thesis, Massachusetts Institute of Technology. September 1990.

[7] J.A. Koski, R.D. Watson, P.L. Goranson, A.M. Hassanein, and J.C. Salmonson. Thermal-Hydraulic Design Issues and Analysis For The ITER Divertor. *Fusion Technology*, 19, May 1991.

[8] C.L. Vandervort, A.E. Bergles, and M.K. Jensen. Ultimate Limits of Boiling Heat Fluxes. *Proc. 8th Symp. on Energy Engineering Sci., CONF-9005183*, 1990.

[9] C.L. Vandervort, A.E. Bergles, and M.K. Jensen. An experimental study of critical heat flux in very high heat flux subcooled boiling. *Int. J. Heat Mass Transfer, Suppl. 1*, 27, 1994.

[10] G.P. Celata, M. Cumo, and A. Mariani. Burnout in Highly Subcooled Water-Flow Boiling in Small-Diameter Tubes. In [63]. *Trans. Am. Nuc. Soc.*, 64, 1991.

[11] H.D. Falter, G.H. Deschamps, R.S. Hemsworth, P. Massmann, H. Altmann, D. Martin, and R. Tivey. Tests of High-Heat-Flux Target Plates for the JET Divertor. *Trans. Am. Nuc. Soc.*, 64, 1991.

[12] R.D. Boyd. Subcooled Water Flow Boiling at 1.66 MPa Under Uniform High Heat Flux Conditions. *ASME HTD-Vol 119*, 1989.

[13] R.D. Boyd. Subcooled Water Flow Boiling Experiment Under Uniform High Heat Flux Conditions. *Fusion Technology*, 13, January 1988.

[14] Y.A. Zeigarnik, N.P. Privalov, and A.I. Klimov. Critical heat flux with boiling of subcooled water in rectangular channels with one-sided supply of heat. *Thermal Eng. (Teploenergetika)*, 28(1), 1981.

[15] M.-R.M. Drizius, R.K. Skema, and A.A. Slanciauskas. Boiling Crisis in Swirled Flow of Water in Pipes. *Heat Transfer - Sov. Res.*, 10, 1978.

[16] A.P. Ornatskii and L.S. Vinyarski. Heat Transfer Crisis in a Forced Flow of Underheated Water in Small-Bore Tubes. *Terplofizika Vysokikh Temperatur*, 3(3), 1965.

[17] A. Achilli, G. Cattadori, and G.P. Gaspari. Subcooled Burnout in Uniformly and Non-Uniformly Heated Tubes. In [63], European Two-Phase Flow Group Meeting, Stockholm, Paper C2. June 1992.

[18] M. Araki, M. Akiba, and S. Suzuki. Recent Activities on Developing Plasma Facing Components at JAERI, Second Specialists' Workshop on High Heat Flux Components Thermal-Hydraulics, Rome, Italy. September 1992.

[19] A. Cardella. Progress in Divertor Development (NET), Second Specialists' Workshop on High Heat Flux Components Thermal-Hydraulics, Rome, Italy. September 1992.

[20] G.P. Celata, M. Cumo, and A. Mariani. Subcooled Water Flow Boiling CHF with Very High Heat Fluxes. In [63]. *Revue Generale de Thermique*, (361), 1992.

[21] G.P. Celata, M. Cumo, and A. Mariani. CHF in Highly Subcooled Flow Boiling With and Without Turbulence Promoters. In [63], European Two-Phase Flow Group Meeting, Stockholm, Paper C1. June 1992.

[22] H. Nariai, F. Inasaka, A. Ishikawa, and W. Fujisaki. Critical heat flux of subcooled flow boiling in tube with internal twisted tape under non-uniform heating condition. *Proceedings of the 2nd JSME-KSME Thermal Engineering Conference*, October 1992.

[23] J. Schlosser. Tests of NET divertor thermal hydraulic mock-ups water cooled by circular swirl tubes, Divertor Thermohydraulics Workshop, Rome, Italy. September 1992.

[24] M. Araki, M. Dairaku, T. Inoue, M. Komata, M. Kuriyama, M. Shinzaburo, M. Ogawa, Y. Ohara, M. Seki. and K Yokoyama. Burnout experiments on the externally-finned swirl tube for steady-state and high-heat flux beam stops. *Fusion Engineering and Design*, 9, 1989.

[25] J.A. Koski, A.G. Beattie, J.B. Whitley, and C.D. Croessmann. Experimental Verification of Subcooled Flow Boiling for Tokamak Pump Limiter Designs. *ASME 87-HT-45*, 1987.

[26] E. Burck and W. Hufschmidt. EUR-2432. In [63]. *EURATOM*, 1965.

[27] J. Mayersak, S.D. Raezer, and E.A. Bundt. Confirmation of Gambill-Green Straight Flow Burnout Heat Flux Equation at Higher Flow Velocity. In [63]. *J. of Heat Transfer*, 86, 1964.

[28] D.F. Babcock. Heavy Water Moderated Power Reactors. In [63], E.I. Dupont de Nemours and Company. *DP-725*, 1962.

[29] W.R. Gambill, R.D. Bundy, and R.W. Wansbrough. Heat transfer, burnout, and pressure drop for water in swirl flow through tubes with internal tapes. In [63]. *Chem. Engng. Prog. Symp. Ser.*, 57(32), 1961.

[30] S. Mirshak, W.S. Durant, and R.H. Towell. Heat Flux at Burnout. In [63], E.I. Dupont de Nemours and Company. *DP-355*, 1959.

[31] W.R. Gambill and N.D. Greene. Boiling Burnout with Water in Vortex Flow. In [63]. *Chem. Eng. Prog.*, 54(10), 1958.

[32] L.S. Tong. A Phenomenological Study of Critical Heat Flux. *ASME75-HT-68*, pages 1–4, 1975.

[33] ITER Conceptual Design: Interim Report, International Atomic Energy Agency, Vienna. *ITER Documentation Series*, (7), 1990.

[34] F. Inasaka and H. Nariai. Critical heat flux of subcooled flow boiling with water for high heat flux application. *High Heat Flux Engineering II (preprint)*, 1997, July 1993.

[35] L.S. Tong. Boundary-layer analysis of the flow boiling crisis. *Int. J. of Heat Mass Transfer*, 11:1208–1211, 1968.

[36] G.P. Celata, M. Cumo, A. Mariani, M. Simoncini, and G. Zummo. Rationalization of existing mechanistic models for the prediction of water subcooled flow boiling critical heat flux. *Int. J. Heat Mass Transfer, Suppl. 1*, 37, 1994.

[37] Z.H. Qureshi, T. Dougherty, C. Fighetti, E. McAssey, and T. Jafri. Subcooled Boiling in Vertical Down-Flow, Poster Session, ANS Winter Meeting. 1989.

[38] T. Dougherty, C.F. Fighetti, G. Reddy, B. Yang, E. Jr. McAssey, and Z. Qureshi. Boiling Channel Flow Instability. *ASME/JSME Thermal Engineering Proceedings*, 2, March 1991.

[39] P. Saha and N. Zuber. Point of net vapor operation and vapor void fraction in subcooled boiling. In [64], Proceedings 5th International Heat Transfer Conference. Tokyo. 1974.

[40] R.F. Lopina and A.E. Bergles. Heat Transfer and Pressure Drop in Tape Generated Swirl Flow, Department of Mechanical Engineering, Massachusetts Institute of Technology. *DSR 70281-47*, 1967.

[41] R.D. Boyd and X. Meng. Local Heat Transfer For Subcooled Flow Boiling With Water. *Fusion Technology*, 22, December 1992.

[42] S.T. Yin, A. Cardella, A.H. Abdelmessih, Z. Jin, and B.P. Bromley. Prediction of Highly Subcooled Flow Boiling For Cooling of High-Flux Components in Fusion Reactors, NURETH-6 proceedings, Grenoble, France. October 1993.

[43] A.E. Bergles and W.M. Rohsenow. The Determination of Forced-Convection Surface-Boiling Heat Transfer. *Journal of Heat Transfer*, (86):365–372, 1964.

[44] S.T. Yin, A. Cardella, A.H. Abdelmessih, Z. Jin, and B.P. Bromley. Assessment of a heat transfer correlations package for water-cooled plasma-facing components in fusion reactors. NURETH-5 proceedings, Salt Lake City, Utah. September 1992.

[45] M.M. Shah. A general correlation for heat transfer during subcooled boiling in pipes and annuli. *ASHRAE Transactions, Part I*, 83, 1997.

[46] J.C. Chen. A Correlation for Boiling Heat Transfer to Saturated Fluids in Convective Flow. *ASME63-HT-34*, 1963.

[47] R. Watson. Effect of New Heat Flux on ITER Divertor Design, Sandia National Laboratories, Memo, March 28. 1990.

[48] B. Lekakh, J.E. Meyer, and M.S. Kazimi. Mechanisms for Extreme Heat Transfer Conditions in Water-Cooling of Fusion Reactor Components. Third International

Symposium on Fusion Nuclear Technology (ISFNT-3), Los Angeles, California. July 1994.

[49] J.G. Collier. *Convective Boiling and Condensation.* McGraw-Hill, 1981.

[50] Data Industrial. Series 4000 owner's manual. 1990.

[51] S. Davila. Undergraduate Research Opportunity Program intern, Massachusetts Institute of Techonology. 1994.

[52] J.-P. Folch. Undergraduate Research Opportunity Program intern, Massachusetts Institute of Techonology. 1994.

[53] Thai T. Minh. Research Science Institute intern, Massachusetts Institute of Techonology. 1994.

[54] National Instruments. IEEE 488 and VXIbus Control, Data Acquisition, and Analysis. 1993.

[55] Cole-Parmer Instrument Company. Conductivity Meter Model 1500-10 Instruction Manual.

[56] HEATING Version 7.2b. *Heat Conduction Code: 3D Conduction Profile.* Computing Applications Division, Oak Ridge National Laboratory, February 1993.

[57] F.M. White. *Heat Transfer.* Addison-Wesley Publishing Company, 1984.

[58] T.E. Hechanova. Heat Transfer Modeling of Saturated Steam Condensing on a Subcooled Liquid for use in the CATHARE Code with Geometry and Validation from the COSI Test Facility High Pressure Safety Injection Experiments. *Commissariat à l'Energie Atomique, Centre d'Etudes Nucléaires de Grenoble. Final Report,* August 1989.

[59] J.P. Holman. *Experimental Methods For Engineers.* McGraw-Hill Book Company, 1984.

[60] V.M. Thannickal. Personal Communication of Celata et al. [36] model calculations, Massachusetts Institute of Technology. 1994.

[61] B. Lekakh. Personal Communication of Russian Data, Massachusetts Institute of Technology. 1994.

[62] W.M. Kays and M.E. Crawford. *Convective Heat and Mass Transfer*. McGraw-Hill Book Company, 1980.

[63] G.P. Celata and A. Mariani. A data set of critical heat flux in water subcooled flow boiling, Specialists' Workshop on the Thermal-Hydraulics of High Heat Flux Components in Fusion Reactors. 1993.

[64] N.E. Todreas and M.S. Kazimi. *Nuclear Systems I: Thermal Hydraulic Fundamentals*. Hemisphere Publishing Corporation. 1990.

[65] G.P. Celata, M. Cumo, and A. Mariani. A Data Set of Critical Heat Flux in Water Subcooled Flow Boiling. In [63]. *ENEA report - not published*, 1993.

[66] D.H. Knoebel, S.D. Harris, B. Crain Jr., and R.M. Biderman. Forced-Convection Subcooled Critical Heat Flux. In [63]. E.I. Dupont de Nemours and Company. *DP-1306*, February 1973.

[67] E.J. Thorgerson. Hydrodynamic Aspect of the Critical Heat Flux in Subcooled Convection Boiling. In [63], Ph.D. Thesis, Univ. of South Carolina. 1969.

Appendix A

Nomenclature

	Variables	Units
A	Area	m^2
C_p	Specific Heat at Constant Pressure	J/kgK
D	Diameter	m
G	Mass Flux	kg/m^2s
GPM	Gallons Per Minute	gal/min
H_{fg}	Heat of Vaporization	J/kg
h_{sp}	Single-Phase Heat Transfer Coefficient	W/m^2K
$h(\theta)$	Local Heat Transfer Coefficient	W/m^2K
Hz	Flow Meter Signal Frequency	Hz
I	Power Supply Current	A
k	Thermal Conductivity	W/m K
L	Length	m
$\dot{m}$	Flow Rate	kg/s
$\mathcal{P}$	Power	W
p	Pressure	Pa
q''_0	Incident Heat Flux	W/m^2
q''	Heat Flux	W/m^2
r	Radial Location	m
T	Temperature	°C or K
v	Velocity	m/s
V	Voltage	V
X	Quality	
Y	Twist Ratio	D per 180° twist
z	Axial Location	m

	Greek Symbols	
α	Void Fraction	
β	Fluid Coefficient of Thermal Expansion	K^{-1}
δ	Liquid sublayer initial thickness	m
δf	Thickness of Twisted Tape Insert	m
ΔT	Temperature Difference	K
$\Delta T*$	Nondimensional Subcooling Parameter	
γ	Fraction of total heated length (0.7 to 1.0)	Eqn. 2.16
μ	Viscosity	kg/m s
σ	Surface Tension	N/m
θ	Azimuthal Location	degrees
	$\theta = 0$ is strikepoint on divertor plate	
ρ	Density	kg/m^3
Φ	Heat Flux Concentration Factor	Eqn. 4.4
ψ	Nondimensional Heat Flux Parameter [45]	Eqn. 2.18
ψ_o	Nondimensional Parameter [45]	Eqn. 2.18
σ	Surface Tension	N/m
	Subscripts	
B	Vapor Blanket	
$bulk$	Bulk (or Mixing Cup)	
c	Convective Term	
cc	Centrifugal Convection Term	
e	Electric	
e	Equivalent or equilibrium	
ex	Exit	
f	Fluid (or Liquid)	
$flow$	Pertaining to Coolant Flow	
g	Gas (or Vapor)	
h	Heated	
∞	Pertaining to Fully Developed Conditions	
i	Inner	
l	Liquid (or Fluid)	
lo	Liquid Only	
m	Mean	
nb	Nucleate Boiling Term	
r	Reduced	Absolute/Critical
sat	Saturation	
sp	Single Phase Term	
sub	Subcooled	
$swirl$	Swirl Flow Term	
w	Wall	

	Dimensionless Parameters	
Bo	Boiling number	$q''Gh_{fg}$
F	Reynolds number factor (Eqn. 2.22)	
Gr	Grashof number (Eqn. 2.12)	
Ja	Jakob number (Eqn. 2.1)	$C_p\Delta T/H_{fg}$
Nu	Nusselt number (Eqn. 2.5)	$q''D_h/(k_l(T_{sat}-T_{bulk}))$
Pe	Peclet number	GDC_{pl}/k_l
Pr	Prandtl number	$\mu C_{pl}/k_l$
Re	Reynolds number	GD/μ
Re_m	Reynolds number (Eqn. 2.1)	$GD_h/\mu(1-\alpha)$
$Re_{2\phi}$	Re Two-Phase number (Eqn. 2.22)	$Re_lF^{1.25}$
Re_l	Re Liquid in 2ϕ number (Eqn. 2.22)	$G(1-x)D/\mu_f$
S	Suppression factor (Eqn. 2.22)	
St	Stanton number (Eqn. 2.6)	$q''/(GC_{pl}(T_{sat}-T_{bulk}))$
Y	Twist Ratio	D per 180° twist
	Acronyms	
BD	Bubble Departure	
CHF	Critical Heat Flux	W/m^2
FWHM	Full-Width at Half-Maximum	
HEATING7.2	3-D Conduction Code	
ITER	Internationl Thermonuclear Experimental Reactor	
OFI	Onset of Flow Instability	
ONB	Onset of Nucleate Boiling	
OSV	Onset of Significant Voids	
PF	Plasma Facing	
TC	Thermocouple	k-type
	Constants	
A	Undetermined Constant	
B	Undetermined Constant	
E	10 Eqn. 6.5	
F	20 Eqn. 6.5	
C	50 Eqn. 6.5	
C_oC_1	0.23 [32] Eqn. 2.1	
D_o	0.0127 [32] Eqn. 2.1	m
k	0.6266 [50] Eqn. 3.6	gpm/Hz
n	Exponent -0.9 Eqn. 6.5	
$Offset$	0.0314 [50] Eqn. 3.6	Hz

Appendix B

Critical Heat Flux Database

Total number in data base = 972

1 Researchers: Celata et al. [20] UN SF LC PB[a]

d mm	tsub K	p MPa	G kg/m^{2}s	chf MW/m^2	Tong-75 MW/m^2	Tong-75(mod) MW/m^2
5.00	34.	0.11	2166.	5.3	14.9	5.9
5.00	72.	1.45	5471.	16.6	14.1	19.0
5.00	61.	0.96	5561.	17.4	14.8	15.3
5.00	38.	0.17	5606.	11.1	20.0	9.0
5.00	79.	1.90	5727.	20.5	14.0	21.9
5.00	73.	1.94	8282.	24.3	16.0	23.2
5.00	47.	0.50	8288.	18.4	18.8	12.6
5.00	68.	1.61	8417.	24.2	16.3	21.4
5.00	45.	0.29	8430.	14.0	21.6	12.1
5.00	75.	2.18	8596.	25.2	16.2	24.7
5.00	44.	0.46	11244.	20.4	21.3	13.2

2 Researchers: Celata et al. [21] UN SF LC PB[a]

d mm	tsub K	p MPa	G kg/m^{2}s	chf MW/m^2	Tong-75 MW/m^2	Tong-75(mod) MW/m^2
8.00	63.	0.81	2019.	8.4	9.0	7.7
8.00	80.	3.79	2096.	9.6	6.8	11.3
8.00	83.	3.74	2100.	7.4	6.9	11.7
8.00	87.	2.82	2160.	13.9	7.7	12.6
8.00	90.	2.49	3952.	13.9	10.8	16.9
8.00	37.	0.40	3983.	9.8	12.2	5.6
8.00	63.	0.74	4001.	11.0	12.3	10.1
8.00	96.	4.97	4863.	15.3	11.1	18.8
8.00	79.	3.41	4904.	13.1	10.6	15.6

2 Researchers: Celata et al. [21] (Continued) UN SF LC PB[a]

d mm	tsub K	p MPa	G kg/m^{2}s	chf MW/m^2	Tong-75 MW/m^2	Tong-75(mod) MW/m^2
8.00	82.	3.59	4913.	14.4	10.7	16.3
8.00	85.	3.39	4930.	15.2	11.0	16.9
8.00	87.	3.60	4932.	11.3	11.0	17.5
8.00	98.	3.54	4944.	17.6	11.8	20.1
8.00	85.	3.70	4949.	13.7	10.8	17.0
8.00	63.	0.70	4961.	11.4	13.7	11.0
8.00	109.	4.92	4985.	19.2	12.2	22.3
8.00	76.	3.11	4995.	11.6	10.7	15.2
8.00	88.	2.23	4997.	15.8	12.1	17.9
8.00	85.	3.50	5018.	15.1	11.0	17.2
8.00	99.	3.36	5071.	18.3	12.0	20.6
8.00	44.	0.59	5575.	12.6	13.3	7.9
8.00	85.	3.46	5873.	16.9	12.0	18.2
8.00	44.	0.56	6972.	14.8	14.8	8.5
8.00	97.	5.03	7322.	21.4	14.2	22.5
8.00	80.	3.59	7346.	17.9	13.1	18.7
8.00	78.	3.33	7356.	17.1	13.0	18.2
8.00	85.	3.64	7373.	18.8	13.4	19.8
8.00	80.	3.44	7383.	18.7	13.2	18.8
8.00	86.	3.40	7384.	19.1	13.6	20.1
8.00	84.	3.51	7396.	16.8	13.5	19.8
8.00	60.	0.56	7471.	14.1	16.9	11.9
8.00	98.	3.34	7474.	23.6	14.8	23.9
8.00	108.	4.65	7475.	24.6	15.5	26.3
8.00	90.	2.27	7488.	18.1	15.0	21.6
8.00	93.	4.72	9608.	28.5	16.2	24.1
8.00	74.	3.20	9657.	20.3	14.8	19.4
8.00	88.	4.71	9657.	22.9	15.7	22.7
8.00	42.	0.61	9776.	13.8	16.5	9.5
8.00	47.	0.63	9807.	15.1	16.9	10.6
8.00	84.	3.16	9853.	21.0	15.9	22.3
8.00	57.	0.62	9887.	16.8	18.2	12.7
8.00	52.	0.64	9889.	16.8	17.5	11.7
8.00	109.	4.64	9946.	29.5	18.4	29.7
8.00	98.	3.10	9962.	25.0	17.5	27.1
8.00	62.	0.63	9988.	17.6	18.8	14.1
8.00	88.	2.11	9998.	21.6	17.3	23.7
8.00	93.	4.77	5004.	17.9	11.2	18.6
8.00	78.	3.44	5042.	14.6	10.6	15.6
8.00	100.	3.38	5078.	14.5	12.1	20.9
8.00	73.	2.13	5223.	11.8	11.5	14.8

2 Researchers: Celata et al. [21] (Continued) UN SF LC PB[a]

d	tsub	p	G	chf	Tong-75	Tong-75(mod)
mm	K	MPa	kg/m^{2}s	MW/m^2	MW/m^2	MW/m^2
8.00	78.	3.54	7314.	22.4	12.9	18.2
8.00	97.	5.12	7393.	21.4	14.2	22.5
8.00	79.	2.73	7448.	21.2	13.6	18.7
8.00	101.	3.58	7490.	19.1	15.0	24.7
8.00	79.	3.49	9779.	19.6	15.2	20.8
8.00	90.	5.04	9780.	22.8	16.1	23.2
8.00	88.	3.55	9792.	23.8	16.0	23.1
8.00	101.	3.51	9993.	27.8	17.6	27.7
8.00	99.	5.03	9996.	20.1	17.3	26.0
8.00	111.	4.98	10046.	25.7	18.9	30.5

3 Researchers: Celata et al. [65] UN SF LC NP[a]

d	tsub	p	G	chf	Tong-75	Tong-75(mod)
mm	K	MPa	kg/m^{2}s	MW/m^2	MW/m^2	MW/m^2
5.00	61.	0.81	4121.	13.0	13.6	13.2
5.00	62.	0.81	5032.	14.2	14.8	14.4
5.00	59.	0.80	10019.	19.9	19.5	18.0
5.00	64.	0.81	10023.	21.4	20.1	19.8
5.00	62.	0.72	14971.	26.0	24.4	22.2
5.00	60.	0.80	19863.	30.6	26.6	24.4
5.00	65.	0.80	20041.	34.7	27.6	26.8

4 Researchers: Celata et al. [65] UN SF LC NP[a]

d	tsub	p	G	chf	Tong-75	Tong-75(mod)
mm	K	MPa	kg/m^{2}s	MW/m^2	MW/m^2	MW/m^2
5.00	33.	0.10	2923.	6.9	17.1	6.5
5.00	62.	0.62	22356.	51.3	30.0	25.6
5.00	66.	0.88	26581.	52.0	30.8	30.7

5 Researchers: Achilli et al. [17] UN SF LC PB[a]

d	tsub	p	G	chf	Tong-75	Tong-75(mod)
mm	K	MPa	kg/m^{2}s	MW/m^2	MW/m^2	MW/m^2
8.00	86.	3.70	7162.	17.4	13.3	20.0
8.00	86.	2.11	7162.	16.7	14.5	20.2
8.00	52.	1.01	10146.	14.3	15.9	12.6
8.00	67.	1.01	9947.	17.0	17.4	16.3
8.00	87.	3.70	10146.	21.2	16.1	23.2
8.00	69.	3.71	9947.	18.0	14.3	18.2
8.00	53.	2.01	9748.	14.1	13.9	14.0
8.00	87.	2.10	10345.	21.1	17.6	23.8
8.00	71.	2.01	10146.	18.5	15.9	18.7
8.00	86.	5.52	9748.	20.8	15.6	21.9
8.00	67.	5.51	9350.	17.4	13.2	16.9
10.00	52.	1.02	7003.	14.2	12.8	9.4
10.00	52.	3.70	6621.	14.3	10.0	10.8
10.00	86.	3.71	7003.	20.7	12.7	17.3
10.00	67.	3.71	6621.	17.2	11.0	13.1
10.00	52.	2.03	6748.	14.1	11.0	10.5
10.00	86.	2.01	7003.	20.7	13.9	17.4
10.00	69.	2.02	6876.	17.4	12.4	13.5
10.00	52.	5.50	6366.	14.2	9.2	10.5
10.00	86.	5.51	6621.	20.0	12.1	16.4
10.00	67.	5.51	6494.	17.0	10.5	12.9
10.00	53.	3.71	9677.	17.9	12.3	12.8
10.00	87.	3.70	9931.	26.1	15.6	20.2
10.00	69.	3.70	9931.	21.7	13.9	15.8
10.00	53.	2.00	9422.	17.5	13.1	12.1
10.00	87.	2.01	9931.	26.1	16.6	20.4
10.00	69.	2.01	9804.	22.0	14.8	15.6
10.00	52.	5.51	9040.	16.8	11.2	12.0
10.00	87.	5.52	10059.	24.8	15.8	19.6
10.00	68.	5.52	9804.	21.3	13.5	15.4
10.00	88.	3.70	14897.	35.6	19.8	23.9
15.00	87.	3.72	9790.	20.1	14.8	15.8
15.00	68.	3.72	8677.	18.3	12.2	11.6
15.00	85.	3.71	4697.	12.8	9.6	11.3
15.00	66.	3.71	4640.	11.0	8.6	8.9

6 Researchers: Gambill and Greene [31] UN SW LC PB[a]

d mm	tsub K	p MPa	G kg/m^{2}s	chf MW/m^2	Tong-75 MW/m^2	Tong-75(mod) MW/m^2
7.80	45.	0.10	25712.	27.1	44.8	18.2
7.80	45.	0.10	17294.	24.9	38.0	15.4
7.80	46.	0.10	26139.	33.1	45.6	18.8
7.80	44.	0.10	17294.	17.3	37.6	14.9
7.80	43.	0.10	13146.	15.8	33.6	13.3
7.80	44.	0.10	18758.	21.4	39.1	15.7
7.80	31.	0.10	26078.	19.8	39.5	12.5

7 Researchers: Knoebel et al. [66] UN AN LC PB[a]

d mm	tsub K	p MPa	G kg/m^{2}s	chf MW/m^2	Tong-75 MW/m^2	Tong-75(mod) MW/m^2
9.50	26.	0.21	8577.	5.8	17.2	5.2
9.50	21.	0.22	8520.	5.3	16.5	4.6
9.50	46.	0.21	4431.	5.2	15.3	6.6
9.50	42.	0.20	4327.	4.8	15.0	6.0
9.50	39.	0.22	4283.	4.3	14.1	5.4
9.50	33.	0.21	4339.	3.8	13.8	4.8
9.50	27.	0.20	8707.	6.2	17.7	5.5
9.50	24.	0.20	8795.	5.8	17.4	5.1
9.50	17.	0.20	8711.	5.3	16.6	4.2
9.50	38.	0.20	8845.	7.8	19.3	7.1
9.50	35.	0.20	8831.	7.3	19.0	6.8
9.50	28.	0.20	8764.	6.5	17.9	5.7
9.50	39.	0.21	4525.	4.2	14.6	5.5
9.50	34.	0.20	4441.	3.7	14.2	5.0
9.50	29.	0.20	4371.	3.3	13.6	4.4
9.50	17.	0.26	13102.	7.0	18.4	5.0
9.50	32.	0.21	8732.	6.5	18.2	6.2
9.50	24.	0.21	8792.	5.9	17.2	5.1
9.50	20.	0.21	8826.	5.3	16.8	4.6
9.50	36.	0.21	8912.	6.9	18.9	6.9
9.50	33.	0.21	8795.	6.3	18.4	6.3
9.50	29.	0.21	8806.	5.7	17.8	5.7
9.50	20.	0.21	8609.	5.2	16.6	4.5
9.50	46.	0.21	4534.	5.2	15.4	6.6
9.50	41.	0.21	4517.	4.7	14.8	5.9
9.50	36.	0.21	4449.	4.2	14.3	5.2
9.50	28.	0.21	8831.	5.0	17.8	5.6
9.50	45.	0.21	4409.	4.7	15.1	6.4
9.50	38.	0.19	4391.	4.2	14.8	5.5

7 Researchers: Knoebel et al. [66] (Continued) UN AN LC PB[a]

d	tsub	p	G	chf	Tong-75	Tong-75(mod)
mm	K	MPa	kg/m^{2}s	MW/m^2	MW/m^2	MW/m^2
9.50	35.	0.21	4393.	3.7	14.1	5.1
9.50	48.	0.21	4516.	4.6	15.7	7.0
9.50	42.	0.21	4495.	4.2	15.0	6.1
9.50	37.	0.21	4429.	3.7	14.3	5.3
9.50	49.	0.38	8858.	9.7	17.7	9.1
9.50	46.	0.37	8788.	9.1	17.4	8.4
9.50	38.	0.39	8694.	7.6	16.3	7.2
9.50	28.	0.38	8599.	5.8	15.3	5.7
9.50	29.	0.38	8610.	5.9	15.3	5.8
9.50	19.	0.39	8454.	4.7	14.3	4.7
9.50	51.	0.39	8850.	9.7	17.9	9.4
9.50	48.	0.38	8825.	9.0	17.5	8.8
9.50	51.	0.38	4311.	5.6	13.4	7.2
9.50	37.	0.39	4216.	4.2	12.0	5.2
9.50	33.	0.38	4325.	3.8	11.9	4.8
9.50	54.	0.39	8919.	9.8	18.3	10.0
9.50	49.	0.41	8897.	9.8	17.5	9.2
9.50	45.	0.39	8863.	9.0	17.1	8.3
9.50	37.	0.38	8802.	7.7	16.4	7.0
9.50	27.	0.39	8697.	5.8	15.2	5.6
9.50	24.	0.40	8659.	5.3	14.7	5.2
9.50	17.	0.39	8530.	4.8	14.1	4.4
9.50	34.	0.38	13139.	9.8	18.9	7.7
9.50	32.	0.38	13126.	9.0	18.6	7.3
9.50	22.	0.37	12812.	7.8	17.4	5.8
9.50	16.	0.37	12724.	6.7	16.7	5.0
9.50	48.	0.37	8903.	10.1	17.8	8.9
9.50	46.	0.38	8879.	9.5	17.4	8.5
9.50	38.	0.39	13219.	10.9	19.4	8.5
9.50	35.	0.38	13173.	10.1	19.0	7.8
9.50	32.	0.38	13132.	9.3	18.6	7.3
9.50	30.	0.39	13150.	8.9	18.3	7.1
9.50	33.	0.40	13129.	9.2	18.5	7.5
9.50	22.	0.38	12881.	7.9	17.4	5.9
9.50	29.	0.39	13007.	8.7	18.1	6.9
9.50	19.	0.39	12802.	7.4	16.9	5.4
9.50	53.	0.38	4293.	6.1	13.6	7.4
9.50	48.	0.39	4339.	5.6	13.1	6.7
9.50	42.	0.39	4241.	5.0	12.4	5.8
9.50	37.	0.39	4218.	4.6	12.0	5.2
9.50	30.	0.38	4285.	4.1	11.6	4.5

7 Researchers: Knoebel et al. [66] (Continued) UN AN LC PB[a]

d mm	tsub K	p MPa	G kg/m^{2}s	chf MW/m^2	Tong-75 MW/m^2	Tong-75(mod) MW/m^2
9.50	20.	0.39	4128.	3.4	10.7	3.5
9.50	49.	0.38	9005.	10.0	17.9	9.2
9.50	47.	0.38	8912.	9.4	17.5	8.6
9.50	54.	0.41	8979.	10.2	18.1	10.1
9.50	49.	0.39	8848.	9.5	17.6	9.0
9.50	46.	0.39	8802.	8.9	17.2	8.4
9.50	42.	0.39	8745.	8.3	16.7	7.8
9.50	39.	0.39	8722.	7.7	16.4	7.3
9.50	35.	0.39	8680.	7.1	15.9	6.7
9.50	30.	0.39	8793.	6.3	15.5	6.0
9.50	29.	0.38	8712.	6.1	15.4	5.8
9.50	24.	0.39	8669.	5.3	14.9	5.2
9.50	41.	0.40	13144.	10.9	19.5	8.9
9.50	36.	0.39	13173.	9.9	19.1	8.1
9.50	34.	0.39	13213.	9.5	18.8	7.8
9.50	31.	0.39	13065.	8.5	18.3	7.2
9.50	29.	0.39	13078.	8.0	18.1	6.9
9.50	52.	0.39	4119.	5.6	13.2	7.2
9.50	44.	0.39	4077.	4.8	12.4	6.0
9.50	40.	0.40	4207.	4.5	12.1	5.5
9.50	28.	0.39	4004.	3.8	11.1	4.2
9.50	54.	0.38	8916.	9.8	18.4	10.1
9.50	51.	0.39	8921.	9.3	17.9	9.4
9.50	47.	0.39	8898.	8.7	17.4	8.8
9.50	45.	0.39	8636.	8.0	16.9	8.2
9.50	41.	0.39	8605.	7.6	16.5	7.6
9.50	38.	0.39	8477.	7.0	16.0	7.0
9.50	33.	0.40	8637.	6.4	15.6	6.4
9.50	29.	0.38	8602.	5.8	15.3	5.8
9.50	51.	0.39	8844.	9.8	17.9	9.5
0.61	55.	0.38	8870.	9.1	38.9	53.3
0.61	52.	0.38	8616.	8.3	37.9	50.1
0.61	48.	0.38	8419.	7.7	36.5	45.6
0.61	62.	0.41	8857.	9.7	40.1	62.0
0.61	56.	0.38	8889.	9.0	39.5	55.4
0.61	51.	0.40	8840.	8.2	37.3	49.0
0.61	48.	0.41	8811.	7.6	36.4	46.4
0.61	61.	0.41	8929.	9.8	40.1	61.7
0.61	58.	0.40	8884.	9.0	39.3	57.4
0.61	53.	0.41	8853.	8.3	37.7	52.0
0.61	48.	0.39	8821.	7.7	36.9	46.4

7 Researchers: Knoebel et al. [66] (Continued) UN AN LC PB[a]

d mm	tsub K	p MPa	G kg/m^{2}s	chf MW/m^2	Tong-75 MW/m^2	Tong-75(mod) MW/m^2
0.61	59.	0.40	8836.	9.8	39.6	58.7
0.61	55.	0.40	8881.	9.0	38.3	53.1
0.61	51.	0.40	8833.	8.4	37.3	48.9
0.61	46.	0.40	8791.	7.7	36.0	44.0
0.61	61.	0.41	8895.	9.8	39.8	60.6
0.61	60.	0.40	8894.	9.7	39.8	59.5
0.61	60.	0.40	8776.	9.8	39.7	59.5
0.61	56.	0.41	8819.	9.0	38.4	54.8
0.61	51.	0.40	8834.	8.3	37.3	49.0
0.61	47.	0.40	8798.	7.7	36.2	44.8
0.61	61.	0.41	8951.	9.8	40.0	61.1
0.61	52.	0.41	8882.	8.3	37.3	50.0
0.61	60.	0.40	8924.	9.8	40.0	60.1
0.61	62.	0.41	8981.	9.8	40.4	62.9
0.61	57.	0.41	8973.	9.1	39.0	56.9
0.61	53.	0.40	8944.	8.4	37.9	51.2
0.61	48.	0.41	8897.	7.7	36.4	46.0
0.61	62.	0.41	9004.	9.9	40.4	62.7
0.61	52.	0.41	8932.	8.4	37.6	51.0
0.61	62.	0.39	8915.	9.8	40.7	62.0
0.61	57.	0.39	8885.	9.0	39.3	56.2
0.61	53.	0.39	8850.	8.3	38.0	50.9
0.61	48.	0.39	8812.	7.6	36.7	45.8
0.61	70.	0.38	4644.	6.4	33.7	57.2
0.61	64.	0.38	4547.	5.9	31.9	49.9
0.61	59.	0.39	4381.	5.3	29.9	43.8
0.61	53.	0.39	4366.	4.8	28.8	39.1
0.61	62.	0.39	8677.	9.8	40.5	62.0
0.61	46.	0.39	13250.	10.5	42.7	51.4
0.61	51.	0.40	13558.	11.4	44.3	58.0
0.61	43.	0.39	13494.	9.8	42.3	48.9
0.61	40.	0.39	13470.	9.1	41.4	45.5
0.61	36.	0.39	13444.	8.4	40.5	42.5
0.61	33.	0.39	13396.	7.7	39.6	39.1
0.61	65.	0.39	8888.	9.9	41.6	65.9
0.61	63.	0.39	8881.	9.8	41.2	64.3
0.61	54.	0.39	8815.	8.3	38.2	51.9
0.61	36.	0.38	8727.	5.8	34.1	35.2
0.61	60.	0.38	8859.	9.7	40.6	60.4
0.61	57.	0.38	8841.	9.1	39.5	56.0
0.61	52.	0.38	8807.	8.3	38.1	50.3

7 Researchers: Knoebel et al. [66] (Continued) UN AN LC PB[a]

d mm	tsub K	p MPa	G kg/m²s	chf MW/m²	Tong-75 MW/m²	Tong-75(mod) MW/m²
0.61	47.	0.38	8767.	7.6	36.8	45.1
0.61	61.	0.38	8872.	9.8	40.9	61.8
0.61	51.	0.39	13332.	11.4	44.5	58.3
0.61	47.	0.39	13282.	10.6	43.3	53.6
0.61	43.	0.38	13427.	9.8	42.4	48.5
0.61	39.	0.38	13429.	9.1	41.5	45.0
0.61	37.	0.39	13370.	8.5	40.5	42.7
0.61	32.	0.38	13292.	7.7	39.6	38.7
0.61	63.	0.38	8904.	9.8	41.3	63.3
0.61	60.	0.38	8887.	9.5	40.6	60.2
0.61	57.	0.39	8851.	9.0	39.2	55.6
0.61	52.	0.38	8847.	8.4	38.1	49.9
0.61	47.	0.39	8834.	7.7	36.7	45.4
0.61	49.	0.39	13538.	11.4	44.2	56.2
0.61	46.	0.39	13523.	10.6	43.2	52.4
0.61	43.	0.39	13485.	9.8	42.2	48.7
0.61	39.	0.39	13418.	9.0	41.2	45.2
0.61	36.	0.39	13380.	8.4	40.4	42.1
0.61	31.	0.39	13477.	7.3	39.3	37.9
0.61	63.	0.38	8857.	9.9	41.5	64.1
0.61	58.	0.38	8823.	9.1	39.8	56.9
0.61	35.	0.38	8711.	5.8	33.9	34.4
0.61	31.	0.39	8666.	5.3	32.9	31.8
0.61	62.	0.38	8995.	9.8	41.2	62.3
0.61	69.	0.39	8978.	9.7	43.3	73.0
0.61	61.	0.39	9033.	9.8	40.8	61.6
0.61	57.	0.39	9009.	9.1	39.6	56.8
0.61	52.	0.39	8976.	8.4	38.2	51.1
0.61	48.	0.39	8944.	7.7	37.1	46.7
0.61	62.	0.39	9039.	9.8	41.1	62.9
0.61	51.	0.39	13507.	11.4	44.8	58.7
0.61	48.	0.39	13460.	10.6	43.6	54.0
0.61	44.	0.39	13419.	9.9	42.5	49.9
0.61	41.	0.39	13370.	9.1	41.5	46.4
0.61	37.	0.39	13394.	8.3	40.6	42.9
0.61	34.	0.39	13347.	7.7	39.7	39.7
0.61	64.	0.38	8940.	9.8	41.8	64.9
0.61	63.	0.39	8937.	9.5	41.2	63.9
0.61	21.	0.35	8274.	4.8	31.3	24.7
0.61	63.	0.38	8894.	9.5	41.5	64.1
0.61	66.	0.38	8910.	9.8	42.5	68.3

7 Researchers: Knoebel et al. [66] (Continued) UN AN LC PB[a]

d	tsub	p	G	chf	Tong-75	Tong-75(mod)
mm	K	MPa	kg/m^{2}s	MW/m^2	MW/m^2	MW/m^2
0.61	60.	0.38	8977.	9.7	40.6	59.8
0.61	56.	0.38	8972.	9.0	39.4	54.7
0.61	52.	0.38	8944.	8.4	38.3	50.1
0.61	47.	0.38	8905.	7.7	37.0	45.1
0.61	49.	0.39	13539.	11.4	44.2	56.4
0.61	46.	0.39	13486.	10.6	43.3	52.8
0.61	43.	0.39	13462.	9.8	42.2	48.6
9.50	33.	0.39	13424.	9.1	18.8	7.6
9.50	30.	0.39	13285.	8.3	18.4	7.1
9.50	51.	0.38	8923.	9.8	18.1	9.6
9.50	52.	0.38	8926.	9.8	18.1	9.6
9.50	51.	0.38	8993.	9.7	18.1	9.5
9.50	56.	0.38	4544.	6.4	14.2	8.1
9.50	51.	0.38	4502.	5.8	13.6	7.2
9.50	46.	0.38	4406.	5.3	13.1	6.5
9.50	41.	0.38	4358.	4.7	12.5	5.7
9.50	36.	0.38	4336.	4.2	12.1	5.2
9.50	31.	0.38	4375.	3.8	11.8	4.6
9.50	53.	0.38	8871.	9.7	18.3	9.9
9.50	50.	0.39	8940.	9.6	17.8	9.2
9.50	48.	0.39	8953.	8.9	17.6	8.9
9.50	43.	0.39	8965.	8.2	17.0	8.1
9.50	40.	0.39	8953.	7.5	16.6	7.4
9.50	55.	0.38	4525.	6.3	14.1	7.9
9.50	54.	0.38	4291.	5.8	13.6	7.5
9.50	46.	0.39	43[illegible]	5.2	12.9	6.4
9.50	36.	0.39	13657.	9.7	19.3	8.1
9.50	33.	0.39	13430.	8.9	18.8	7.6
9.50	57.	0.38	4405.	6.3	14.1	8.1
9.50	52.	0.39	4381.	5.8	13.4	7.3
9.50	52.	0.38	8903.	9.6	18.2	9.8
9.50	53.	0.39	8894.	10.5	18.2	9.9
9.50	49.	0.39	8865.	9.7	17.7	9.2
9.50	45.	0.39	8829.	9.0	17.1	8.3
9.50	41.	0.39	8793.	8.2	16.6	7.6
9.50	38.	0.39	8767.	7.6	16.3	7.1
9.50	34.	0.39	8727.	7.0	15.8	6.5
9.50	56.	0.38	4398.	6.4	14.0	8.0
9.50	50.	0.38	4393.	5.8	13.3	6.9
9.50	47.	0.39	4351.	5.2	13.0	6.6
9.50	55.	0.39	8909.	10.5	18.4	10.3

7 Researchers: Knoebel et al. [66] (Continued) UN AN LC PB[a]

d mm	tsub K	p MPa	G kg/m^{2}s	chf MW/m^2	Tong-75 MW/m^2	Tong-75(mod) MW/m^2
9.50	50.	0.38	8881.	9.7	17.9	9.3
9.50	39.	0.39	13367.	10.5	19.5	8.6
9.50	36.	0.39	13346.	9.7	19.1	8.0
9.50	33.	0.39	13268.	9.0	18.7	7.5
9.50	30.	0.39	13203.	8.3	18.3	7.0
9.50	53.	0.39	8903.	9.7	18.2	10.0
9.50	24.	0.44	12949.	7.0	17.0	6.3
9.50	21.	0.39	8665.	4.7	14.6	4.9
9.50	55.	0.38	9060.	10.4	18.7	10.4
9.50	50.	0.38	9019.	9.7	18.0	9.3
9.50	45.	0.38	8983.	9.0	17.4	8.4
9.50	42.	0.38	8828.	8.2	16.8	7.7
9.50	38.	0.39	8889.	7.6	16.4	7.2
9.50	34.	0.38	8849.	6.9	16.0	6.6
9.50	56.	0.38	4378.	6.4	13.9	7.9
9.50	50.	0.38	4358.	5.8	13.4	7.0
9.50	45.	0.38	4460.	5.3	13.0	6.3
9.50	39.	0.39	4467.	4.7	12.4	5.6
9.50	56.	0.38	8919.	10.4	18.7	10.5
9.50	42.	0.39	13467.	11.2	20.1	9.3
9.50	39.	0.39	13396.	10.4	19.6	8.7
9.50	36.	0.39	13420.	9.7	19.2	8.1
9.50	33.	0.39	13352.	9.0	18.8	7.6
9.50	30.	0.39	13275.	8.2	18.4	7.1
9.50	53.	0.39	8834.	9.7	18.2	9.9
9.50	43.	0.40	13513.	11.3	20.1	9.5
9.50	19.	0.40	12990.	7.0	16.9	5.5
9.50	29.	0.38	8689.	5.8	15.4	5.8
9.50	26.	0.38	8602.	5.2	15.0	5.4
9.50	18.	0.38	8435.	4.7	14.2	4.5
9.50	28.	0.38	4231.	3.8	11.4	4.3
9.50	30.	0.39	13240.	7.6	18.3	7.1
9.50	26.	0.39	13268.	6.9	17.9	6.5
9.50	17.	0.39	13000.	6.3	16.8	5.3
9.50	27.	0.38	8694.	5.2	15.2	5.6
9.50	24.	0.39	8631.	4.9	14.9	5.3
9.50	15.	0.36	8504.	4.2	14.3	4.2
9.50	37.	0.39	4321.	4.2	12.1	5.3
9.50	31.	0.38	4191.	3.8	11.6	4.5
9.50	53.	0.38	9016.	10.4	18.4	10.0
9.50	49.	0.38	9014.	9.6	17.9	9.2

7 Researchers: Knoebel et al. [66] (Continued) UN AN LC PB[a]

d mm	tsub K	p MPa	G kg/m^{2}s	chf MW/m^2	Tong-75 MW/m^2	Tong-75(mod) MW/m^2
9.50	47.	0.38	8987.	9.4	17.6	8.7
9.50	46.	0.38	8985.	9.5	17.5	8.6
9.50	56.	0.38	9066.	10.5	18.9	10.7
9.50	24.	0.38	8752.	5.2	15.0	5.2
9.50	43.	0.39	13568.	11.2	20.2	9.5
9.50	27.	0.38	13112.	7.5	18.0	6.5
9.50	45.	0.40	10661.	9.9	18.4	9.0
9.50	49.	0.38	8863.	9.8	17.8	9.1
9.50	23.	0.38	8543.	5.1	14.7	5.0
9.50	50.	0.38	8917.	9.9	17.9	9.2
9.50	45.	0.39	8897.	9.0	17.2	8.3
9.50	23.	0.39	8681.	5.3	14.8	5.1
9.50	50.	0.39	8944.	9.8	17.9	9.4
9.50	17.	0.37	13134.	7.1	17.0	5.2
9.50	24.	0.38	8506.	5.4	14.8	5.1
9.50	36.	0.38	4189.	4.4	11.9	5.0
9.50	54.	0.39	8966.	10.7	18.4	10.2
9.50	50.	0.38	8942.	10.0	17.9	9.2
9.50	23.	0.38	8616.	5.4	14.8	5.1
9.50	50.	0.39	8945.	9.9	17.9	9.4
9.50	42.	0.38	4392.	5.3	12.7	5.9
9.50	54.	0.40	8989.	9.9	18.2	10.1
9.50	56.	0.39	9034.	10.6	18.8	10.7
9.50	53.	0.39	9011.	9.8	18.2	9.9
9.50	38.	0.39	4318.	4.3	12.2	5.4
9.50	39.	0.40	8810.	7.0	16.4	7.4
9.50	26.	0.40	8726.	3.7	15.0	5.6
9.50	28.	0.39	8659.	5.2	15.2	5.7
9.50	56.	0.39	9038.	10.4	18.7	10.7
9.50	54.	0.40	8920.	9.6	18.2	10.1
9.50	51.	0.40	8906.	8.9	17.8	9.4
9.50	59.	0.40	8961.	10.4	18.9	11.2
9.50	29.	0.39	8757.	5.7	15.4	5.9
9.50	26.	0.39	8725.	5.2	15.1	5.5
9.50	18.	0.38	8550.	4.7	14.3	4.5
9.50	56.	0.41	4474.	5.7	13.8	8.0
9.50	50.	0.39	4455.	5.2	13.3	7.0
9.50	44.	0.40	4349.	4.7	12.6	6.2
9.50	39.	0.40	4438.	4.2	12.3	5.5
9.50	56.	0.40	8943.	9.6	18.5	10.6
9.50	29.	0.40	13271.	7.5	18.2	7.0

7 Researchers: Knoebel et al. [66] (Continued) UN AN LC PB[a]

d mm	tsub K	p MPa	G kg/m^{2}s	chf MW/m^2	Tong-75 MW/m^2	Tong-75(mod) MW/m^2
9.50	26.	0.40	13262.	6.9	17.8	6.6
9.50	23.	0.39	13219.	6.3	17.6	6.1
9.50	16.	0.39	13023.	4.6	16.7	5.1
9.50	46.	0.40	4405.	4.7	12.8	6.4
9.50	40.	0.40	4356.	4.2	12.3	5.7
9.50	34.	0.40	4304.	3.7	11.8	5.0
9.50	58.	0.40	8989.	9.6	18.9	11.2
9.50	32.	0.40	8759.	5.7	15.6	6.3
9.50	29.	0.40	8728.	5.2	15.3	5.9
9.50	16.	0.34	8544.	4.7	14.5	4.2
9.50	50.	0.40	9010.	9.6	17.7	9.3
9.50	46.	0.40	8954.	8.9	17.2	8.6
9.50	22.	0.39	13091.	7.6	17.4	5.9
9.50	29.	0.40	13204.	8.2	18.1	6.9
9.50	51.	0.39	8904.	9.7	17.9	9.4
9.50	26.	0.38	8697.	5.7	15.2	5.5
9.50	23.	0.39	8610.	5.2	14.7	5.1
9.50	51.	0.39	8953.	9.7	17.9	9.4
9.50	51.	0.40	4357.	6.4	13.3	7.2
9.50	40.	0.41	4245.	4.7	12.1	5.6
9.50	49.	0.40	8840.	9.7	17.6	9.2
9.50	46.	0.40	8839.	9.0	17.1	8.5
9.50	27.	0.40	8630.	5.8	15.0	5.6
9.50	23.	0.39	8584.	5.2	14.7	5.1
9.50	24.	0.41	13101.	7.6	17.4	6.2
9.50	50.	0.39	8849.	9.7	17.7	9.2
9.50	45.	0.40	4293.	5.2	12.6	6.3
9.50	39.	0.40	13328.	10.6	19.3	8.6
9.50	32.	0.40	13233.	9.0	18.5	7.4
9.50	29.	0.40	13208.	8.3	18.1	7.0
9.50	21.	0.40	12915.	7.0	17.0	5.7
9.50	27.	0.38	8705.	5.8	15.2	5.6
9.50	24.	0.40	8685.	5.2	14.7	5.2
9.50	45.	0.40	4379.	5.2	12.7	6.3
9.50	41.	0.40	4280.	4.7	12.3	5.7
9.50	52.	0.40	8935.	9.8	17.9	9.7
9.50	63.	0.65	4357.	7.1	12.6	9.3
9.50	51.	0.64	4358.	5.9	11.7	7.4
9.50	40.	0.65	4195.	4.7	10.8	5.9
9.50	36.	0.65	4011.	4.3	10.3	5.4
9.50	32.	0.65	4017.	4.3	10.1	5.0

7 Researchers: Knoebel et al. [66] (Continued) UN AN LC PB[a]

d	tsub	p	G	chf	Tong-75	Tong-75(mod)
mm	K	MPa	kg/m^{2}s	MW/m^2	MW/m^2	MW/m^2
9.50	28.	0.72	8164.	5.8	12.9	6.2
9.50	43.	0.67	4328.	8.1	11.0	6.3
9.50	65.	0.67	4504.	7.5	12.8	9.8
9.50	48.	0.68	4303.	6.0	11.3	7.0
9.50	43.	0.68	4102.	5.1	10.7	6.2
9.50	36.	0.74	3915.	4.5	9.9	5.4
9.50	38.	0.69	4035.	4.8	10.3	5.7
9.50	41.	0.65	4229.	4.8	10.9	6.1
9.50	38.	0.66	4111.	4.3	10.5	5.7
9.50	30.	0.68	4277.	3.8	10.1	5.0
9.50	52.	0.66	8829.	9.6	15.8	10.1
9.50	44.	0.66	8740.	8.3	14.9	8.5
9.50	55.	0.66	8826.	10.5	16.1	10.7
9.50	60.	0.66	8817.	11.3	16.6	11.6
9.50	56.	0.65	8806.	10.6	16.2	10.8
9.50	62.	0.66	8882.	11.3	16.9	12.1
9.50	57.	0.66	8887.	10.5	16.4	11.1
9.50	31.	0.68	8329.	6.5	13.5	6.7
9.50	23.	0.56	12985.	5.7	16.1	6.5

11 Researchers: Mirshak et al. [30] UN RC LC PB[a]

d	tsub	p	G	chf	Tong-75	Tong-75(mod)
mm	K	MPa	kg/m^{2}s	MW/m^2	MW/m^2	MW/m^2
6.30	45.	0.26	5558.	5.0	17.6	8.9
6.30	41.	0.26	5562.	4.8	17.1	8.1
6.30	45.	0.25	5500.	5.0	17.8	8.9
6.30	42.	0.26	5485.	4.6	17.1	8.2
6.30	36.	0.28	5601.	4.6	16.2	7.1
6.30	41.	0.29	5642.	4.7	16.8	8.2
6.30	28.	0.29	5106.	4.0	14.7	5.7
6.30	26.	0.30	4928.	4.2	14.2	5.4
6.30	22.	0.28	5467.	4.2	14.7	5.2
6.30	38.	0.29	5743.	5.3	16.5	7.7
6.30	39.	0.27	5605.	5.5	16.8	7.8
6.30	38.	0.27	5455.	5.2	16.4	7.5
6.30	48.	0.26	5098.	5.6	17.4	9.2
6.30	33.	0.28	5401.	4.7	15.7	6.7
6.30	40.	0.27	5517.	5.6	16.7	7.8

11 Researchers: Mirshak et al. [30] (Continued) UN RC LC PB[a]

d	tsub	p	G	chf	Tong-75	Tong-75(mod)
mm	K	MPa	kg/m^{2}s	MW/m^2	MW/m^2	MW/m^2
11.70	36.	0.34	5491.	5.3	12.9	4.9
11.90	36.	0.34	5520.	5.6	12.9	4.9
11.80	36.	0.35	5518.	5.7	12.9	5.0
11.60	44.	0.35	5583.	6.8	13.7	6.0
11.60	48.	0.35	5611.	6.8	14.1	6.6
11.50	55.	0.35	5729.	7.9	15.0	7.7
11.80	55.	0.35	5615.	7.7	14.8	7.5
6.20	44.	0.35	9804.	8.0	20.4	10.8
6.10	52.	0.41	9889.	9.3	20.9	13.2
6.30	34.	0.34	9897.	6.8	19.2	8.7
6.20	41.	0.34	9942.	7.6	20.2	10.2
6.50	48.	0.35	9580.	8.7	20.5	11.4
6.50	50.	0.34	9706.	8.9	21.2	12.2
6.10	40.	0.41	9613.	7.3	19.0	10.0
6.50	32.	0.34	9524.	7.6	18.6	8.1
6.40	51.	0.34	9932.	8.6	21.6	12.6
6.30	52.	0.35	9999.	8.4	21.7	13.0
6.30	56.	0.36	10017.	9.3	22.2	14.2
8.50	27.	0.28	4672.	3.9	13.1	4.5
8.50	39.	0.28	5124.	4.9	14.7	6.2
8.50	48.	0.27	5392.	5.5	16.2	7.9
8.50	50.	0.28	5201.	6.1	16.0	8.0
8.50	40.	0.27	5315.	5.1	15.2	6.5
6.10	42.	0.17	9916.	6.7	24.7	11.1
6.40	39.	0.17	9827.	6.8	23.7	9.9
6.10	33.	0.38	12061.	7.4	20.4	9.5
6.10	36.	0.38	12098.	7.9	20.8	10.2
6.00	48.	0.38	12285.	9.3	22.8	13.4
6.50	49.	0.38	11346.	10.0	21.7	12.5
6.50	46.	0.38	11250.	8.9	21.2	11.7
6.60	47.	0.38	11228.	9.2	21.2	11.8
6.70	54.	0.59	9721.	9.8	18.7	13.2

12 Researchers: Babcock [28] UN SF LC PB[a]

d mm	tsub K	p MPa	G kg/m^{2}s	chf MW/m^2	Tong-75 MW/m^2	Tong-75(mod) MW/m^2
8.20	41.	6.86	8731.	10.5	10.0	11.3
8.00	51.	6.89	5222.	8.3	8.3	10.7
8.20	38.	5.51	9730.	9.5	10.8	11.6
8.20	48.	1.34	10891.	10.4	15.2	12.7
8.20	37.	0.60	11119.	9.2	16.8	8.9
8.20	44.	0.58	10555.	10.2	17.3	9.8
12.60	46.	6.89	4101.	6.9	6.6	6.9
12.50	46.	6.89	8493.	10.1	10.0	9.3
12.50	45.	6.89	8746.	10.2	10.0	9.3
12.60	32.	5.55	7143.	8.0	8.2	7.3
12.60	38.	3.48	6668.	8.1	8.9	7.8
12.40	59.	0.64	7302.	9.1	14.3	9.0
14.20	40.	0.45	4794.	6.9	11.2	4.7
12.50	38.	0.56	8770.	9.1	13.9	6.3
12.50	38.	0.89	8266.	9.2	12.3	6.7
12.50	29.	0.43	8669.	7.4	13.9	5.0
12.50	30.	0.70	8412.	7.8	12.4	5.6
12.50	36.	1.02	8289.	9.2	11.9	6.8
12.50	40.	0.50	8990.	9.5	14.6	6.5
12.50	33.	0.50	11452.	9.9	15.5	6.2
12.50	29.	0.63	8660.	7.8	12.8	5.4
12.50	28.	1.01	8191.	7.8	11.2	5.8
12.50	49.	0.84	8927.	11.8	13.8	8.5
12.50	36.	0.41	4241.	6.0	11.0	4.4
12.50	50.	0.41	4477.	7.6	12.3	6.0
12.50	34.	0.70	4321.	6.1	9.6	4.6
12.50	55.	0.69	4489.	8.1	11.1	6.9
12.50	45.	1.04	4338.	7.1	9.4	6.1
22.10	32.	6.89	4892.	6.5	5.9	4.4
22.00	18.	6.89	7095.	6.1	6.2	4.1
22.10	30.	3.45	5050.	6.5	6.6	4.5
22.30	42.	1.34	2946.	4.9	6.4	3.7
22.10	22.	1.34	8283.	6.2	9.0	4.1
22.40	21.	0.60	8417.	5.7	10.4	3.2
22.50	43.	0.76	3414.	6.1	7.8	3.6
22.50	48.	0.77	3528.	6.2	8.1	3.9
22.50	48.	0.78	3437.	6.2	8.0	3.9
22.50	47.	0.63	3421.	6.2	8.3	3.7
22.50	48.	0.48	3604.	6.1	9.1	3.7

13 Researchers: Burck and Hufschmidt [26] UN SF LC PB[a]

d	tsub	p	G	chf	Tong-75	Tong-75(mod)
mm	K	MPa	kg/m^{2}s	MW/m^2	MW/m^2	MW/m^2
10.00	73.	2.39	1884.	9.6	6.6	8.6
10.00	78.	2.41	2330.	9.8	7.5	10.1
10.00	66.	1.10	3285.	9.9	9.8	9.0
10.00	65.	1.10	2674.	8.3	8.9	8.1
10.00	63.	1.10	1910.	7.0	7.7	6.9
10.00	86.	2.94	2674.	10.3	8.0	11.8
10.00	82.	2.94	2674.	10.1	7.9	11.2
10.00	81.	2.94	1910.	9.0	6.6	9.7
10.00	79.	2.94	1362.	7.1	5.6	8.2
10.00	70.	1.34	3272.	9.9	9.6	9.8
10.00	69.	1.37	2674.	8.9	8.7	8.9
10.00	65.	1.35	1884.	7.3	7.3	7.3
10.00	62.	1.35	3272.	9.3	9.1	8.7
10.00	60.	1.36	2674.	8.1	8.3	7.8
10.00	57.	1.33	1910.	6.7	7.1	6.5
10.00	65.	2.12	3209.	9.4	8.3	9.4
10.00	64.	2.12	2687.	8.4	7.6	8.7
10.00	62.	2 12	1897.	7.0	6.5	7.4
10.00	63.	2.13	2674.	8.5	7.6	8.5
10.00	80.	2.17	3272.	10.5	9.1	11.8
10.00	79.	2.16	2674.	9.5	8.3	10.8
10.00	76.	2.13	1910.	8.0	7.0	9.0
10.00	73.	2.12	1350.	6.1	5.9	7.5
10.00	82.	2.19	3272.	10.5	9.2	12.1
10.00	63.	2.15	3272.	8.9	8.3	9.3
10.00	86.	3.08	2852.	11.2	8.2	12.2
10.00	87.	3.09	2674.	10.5	8.0	12.0
10.00	84.	3.08	2330.	10.1	7.4	11.0
10.00	83.	3.08	1910.	8.7	6.6	10.0
10.00	78.	3.07	1350.	7.6	5.5	8.1
10.00	64.	1.38	1350.	6.0	6.3	6.3
10.00	67.	1.40	1910.	7.5	7.4	7.6
10.00	67.	1.41	2330.	8.6	8.0	8.2
10.00	66.	1.36	2674.	9.4	8.5	8.5
10.00	64.	2.12	2674.	8.4	7.6	8.6
10.00	63.	2.19	1884.	7.0	6.4	7.4
10.00	69.	1.61	1859.	7.7	7.1	7.9
10.00	55.	1.10	929.	4.8	5.4	4.5
10.00	58.	1.10	1222.	5.5	6.2	5.3
10.00	73.	2.21	1592.	8.0	6.2	8.0
10.00	75.	2.22	1846.	8.6	6.7	8.7

13 Researchers: Burck and Hufschmidt [26] (Continued) UN SF LC PB[a]

d mm	tsub K	p MPa	G kg/m^{2}s	chf MW/m^2	Tong-75 MW/m^2	Tong-75(mod) MW/m^2
10.00	62.	1.59	929.	5.1	5.1	5.3
10.00	65.	1.59	1222.	6.1	5.8	6.3
10.00	66.	1.58	1464.	6.8	6.3	6.8
10.00	66.	1.59	1592.	7.3	6.5	7.0
10.00	82.	3.07	1592.	7.9	6.1	9.1
10.00	69.	2.55	929.	6.0	4.7	6.2
10.00	74.	2.57	1222.	6.9	5.4	7.3
10.00	75.	2.58	1451.	7.7	5.8	8.0
10.00	76.	2.58	1592.	8.1	6.1	8.4
10.00	79.	2.67	1846.	8.6	6.6	9.3
10.00	68.	2.17	929.	5.5	4.8	6.0
10.00	72.	2.18	1222.	6.2	5.6	7.2
10.00	73.	2.20	1464.	7.3	6.0	7.7
10.00	71.	3.04	929.	6.1	4.5	6.4
10.00	78.	3.05	1210.	7.0	5.2	7.7
10.00	80.	3.05	1464.	7.8	5.8	8.6
10.00	78.	3.05	1553.	8.7	5.9	8.6
10.00	82.	3.05	1808.	8.9	6.4	9.6
10.00	74.	3.07	929.	6.0	4.5	6.6
10.00	80.	3.08	1553.	8.2	5.9	8.8
10.00	70.	2.98	2992.	9.8	7.7	10.0
10.00	69.	2.99	2674.	9.4	7.3	9.5
10.00	67.	2.97	2330.	9.0	6.8	8.7
10.00	67.	2.96	1910.	7.9	6.2	8.0
10.00	69.	2.98	2674.	9.7	7.3	9.5
10.00	65.	2.08	1910.	7.3	6.6	7.7
10.00	67.	2.14	2317.	8.4	7.2	8.5
10.00	66.	2.19	2674.	8.8	7.7	8.9
10.00	67.	2.25	3005.	9.5	8.1	9.5
10.00	66.	2.22	3259.	9.4	8.4	9.6
10.00	66.	2.25	3756.	10.0	8.9	10.2
10.00	72.	2.98	3285.	9.8	8.2	10.7
10.00	69.	1.39	2317.	8.1	8.1	8.4
10.00	71.	1.41	2674.	8.9	8.7	9.2
10.00	72.	1.43	2992.	9.3	9.2	9.8
10.00	72.	1.45	3272.	9.9	9.5	10.2
10.00	74.	1.48	3756.	10.1	10.2	11.1
10.00	61.	1.45	3234.	8.9	8.9	8.5
10.00	58.	1.42	2674.	8.2	8.1	7.6
10.00	60.	1.38	1910.	6.5	7.1	6.7
10.00	86.	3.03	3285.	10.5	8.8	12.8

13 Researchers: Burck and Hufschmidt [26] (Continued) UN SF LC PB[a]

d mm	tsub K	p MPa	G kg/m^{2}s	chf MW/m^2	Tong-75 MW/m^2	Tong-75(mod) MW/m^2
10.00	73.	1.45	3272.	9.8	9.6	10.4
10.00	81.	2.07	3272.	10.1	9.3	12.0
10.00	83.	2.12	3756.	10.9	10.0	13.0
10.00	81.	2.08	3285.	10.3	9.3	11.9
10.00	79.	2.06	2992.	10.1	8.8	11.3
10.00	77.	2.02	2674.	9.7	8.3	10.4
10.00	76.	2.00	2292.	9.0	7.7	9.6
10.00	74.	1.97	1910.	8.0	7.0	8.7
10.00	68.	1.37	1910.	7.3	7.4	7.7
10.00	67.	1.31	3247.	10.8	9.5	9.4
10.00	67.	1.31	2674.	9.5	8.6	8.6
10.00	67.	1.32	2305.	8.1	8.1	8.1
10.00	66.	1.30	1974.	7.4	7.5	7.4
10.00	87.	3.03	3247.	12.2	8.8	13.0
10.00	77.	2.40	1923.	8.4	6.8	9.2
10.00	78.	2.39	2317.	9.4	7.5	10.0
10.00	80.	2.40	2674.	10.5	8.1	10.9
10.00	81.	2.41	3272.	11.8	8.9	11.9
10.00	77.	2.40	2674.	11.0	8.0	10.5
10.00	66.	1.61	2317.	9.8	7.7	8.1
10.00	66.	1.59	1833.	8.7	6.9	7.4
10.00	70.	1.70	1910.	8.0	7.1	8.1
10.00	72.	1.72	2343.	9.0	7.9	9.0
10.00	72.	1.73	2674.	9.8	8.4	9.6
10.00	74.	1.72	3272.	10.7	9.3	10.7
10.00	42.	1.60	929.	5.3	4.6	4.0
10.00	47.	1.62	1222.	5.4	5.3	4.8
10.00	51.	1.61	1464.	6.1	5.8	5.4
10.00	51.	1.62	1617.	6.3	6.1	5.6
10.00	40.	1.10	929.	4.5	5.0	3.5
10.00	44.	1.10	1235.	5.0	5.7	4.2
10.00	45.	1.10	1464.	5.4	6.2	4.6
10.00	44.	1.10	1617.	5.7	6.4	4.7
10.00	45.	1.10	1859.	6.2	6.8	5.0
10.00	44.	1.59	917.	4.5	4.6	4.0
10.00	48.	1.59	1235.	5.6	5.3	4.8
10.00	47.	1.59	1451.	6.3	5.7	5.1
10.00	50.	1.60	1630.	6.5	6.1	5.6
10.00	59.	1.10	1210.	5.4	6.2	5.3
10.00	60.	1.10	1451.	6.1	6.7	5.9
10.00	60.	1.10	1592.	6.5	7.0	6.1

13 Researchers: Burck and Hufschmidt [26] (Continued) UN SF LC PB[a]

d mm	tsub K	p MPa	G kg/m^{2}s	chf MW/m^2	Tong-75 MW/m^2	Tong-75(mod) MW/m^2
10.00	62.	1.10	1846.	6.8	7.5	6.7
10.00	61.	1.10	1579.	6.2	7.0	6.2
10.00	60.	1.10	1464.	6.3	6.7	5.9
10.00	66.	1.59	1604.	7.4	6.6	7.1
10.00	66.	2.14	2890.	7.4	8.0	9.2
10.00	78.	2.18	3272.	11.5	9.0	11.5
10.00	77.	2.16	2674.	10.5	8.2	10.5
10.00	74.	2.13	1910.	8.7	6.9	8.7
10.00	71.	2.12	1350.	6.7	5.8	7.3
10.00	80.	2.19	3272.	11.6	9.1	11.8
10.00	76.	3.04	1350.	7.7	5.4	7.9
10.00	80.	3.05	1910.	9.9	6.5	9.5
10.00	84.	3.06	2330.	10.6	7.3	10.9
10.00	85.	3.07	2674.	11.2	7.9	11.7
10.00	86.	3.07	2992.	11.7	8.4	12.4
10.00	70.	3.04	2992.	10.7	7.7	10.1
10.00	70.	3.02	2674.	10.5	7.3	9.6
10.00	72.	3.01	2330.	8.3	6.9	9.3
10.00	67.	3.01	1910.	8.6	6.1	8.0
10.00	60.	3.00	1350.	7.5	5.0	6.3

15 Researchers: Mayersak et al. [27] UN SF LC PB[a]

d mm	tsub K	p MPa	G kg/m^{2}s	chf MW/m^2	Tong-75 MW/m^2	Tong-75(mod) MW/m^2
11.70	99.	2.89	44428.	42.8	41.8	39.9

16 Researchers: Thorgerson [67] UN AN LC PB[a]

d mm	tsub K	p MPa	G kg/m^{2}s	chf MW/m^2	Tong-75 MW/m^2	Tong-75(mod) MW/m^2
8.40	49.	0.45	8857.	7.2	17.5	9.8
8.40	44.	0.45	8725.	7.8	16.8	8.8
8.40	46.	0.45	8790.	7.6	17.1	9.2
8.40	40.	0.45	8744.	6.5	16.4	8.0
8.40	40.	0.45	8744.	6.6	16.4	8.0
8.40	63.	0.45	8900.	8.6	19.4	13.1
8.40	43.	0.45	8757.	7.6	16.8	8.7
8.40	43.	0.45	8757.	7.6	16.8	8.7
8.40	40.	0.45	13109.	9.8	19.4	9.4
8.40	40.	0.45	13119.	9.9	19.5	9.6
8.40	30.	0.45	8646.	5.6	15.4	6.6
8.40	31.	0.45	12824.	8.2	18.3	7.9

16 Researchers: Thorgerson [67] (Continued) UN AN LC PB[a]

d mm	tsub K	p MPa	G kg/m^{2}s	chf MW/m^2	Tong-75 MW/m^2	Tong-75(mod) MW/m^2
8.40	52.	0.45	4325.	5.4	13.3	7.9
8.40	36.	0.45	4336.	4.2	12.0	5.6
8.40	52.	0.45	4383.	5.5	13.4	7.9
8.40	40.	0.45	4322.	4.7	12.3	6.1
8.40	31.	0.45	8646.	5.9	15.5	6.7
8.40	29.	0.45	12973.	7.6	18.1	7.6
8.40	28.	0.45	12951.	7.5	18.0	7.4
8.40	52.	0.45	13103.	12.0	21.1	12.1
8.40	53.	0.45	13280.	12.4	21.4	12.5
8.40	36.	0.45	4175.	4.4	11.8	5.5
8.40	49.	0.45	4209.	5.8	12.9	7.3
8.40	48.	0.45	8599.	8.6	17.2	9.6
8.40	40.	0.45	8519.	6.0	16.3	8.0
8.40	41.	0.45	8552.	5.8	16.4	8.2
7.80	58.	0.45	8867.	9.6	19.0	12.3
7.80	53.	0.45	13420.	11.5	21.9	13.1
7.80	52.	0.45	13401.	11.5	21.7	12.9
7.80	57.	0.45	8880.	9.7	18.9	12.0
7.80	46.	0.45	8828.	7.4	17.6	9.7
7.80	42.	0.45	8786.	7.1	17.0	8.8
7.80	54.	0.45	4395.	6.3	13.9	8.7
7.80	43.	0.45	8871.	6.3	17.2	9.1
7.80	43.	0.45	8835.	7.3	17.1	9.0
7.80	46.	0.45	13108.	7.9	20.7	11.3
7.80	44.	0.45	12957.	10.8	20.2	10.7
7.80	43.	0.45	13283.	10.7	20.3	10.6
7.80	46.	0.45	8770.	8.3	17.5	9.7
7.80	55.	0.45	4525.	5.9	14.2	9.0
7.80	41.	0.45	4427.	4.7	12.8	6.6
7.80	30.	0.45	8700.	5.7	15.7	6.8

17 Researchers: Gambill et al. [29] UN SF LC PB[a]

d	tsub	p	G	chf	Tong-75	Tong-75(mod)
mm	K	MPa	kg/m^2s	MW/m^2	MW/m^2	MW/m^2
7.70	45.	0.17	10002.	10.1	23.7	10.2
7.70	55.	0.28	15671.	24.7	26.9	14.8
7.70	67.	0.51	22411.	37.8	29.5	21.9
7.70	65.	0.43	20579.	41.6	29.2	20.4
7.70	38.	0.12	7058.	7.0	21.4	7.9
7.70	45.	0.18	11531.	20.0	24.8	10.9
7.70	57.	0.30	17157.	28.9	28.0	16.2
7.70	61.	0.33	18237.	38.7	28.7	17.8

18 Researchers: Koski et al. [25] NU SF LC PB[a]

d	tsub	p	G	chf	Tong-75	Tong-75(mod)
mm	K	MPa	kg/m^2s	MW/m^2	MW/m^2	MW/m^2
8.00	77.	1.14	5000.	23.0	15.6	22.1
8.00	77.	1.14	7000.	27.0	18.1	25.4
8.00	77.	1.14	8000.	30.0	19.2	26.8
8.00	77.	1.14	10100.	35.0	21.3	29.5
8.00	77.	1.14	10200.	37.0	21.4	29.5
8.00	77.	1.14	9300.	39.5	20.5	28.4

19 Researchers: Koski et al. [25] NU SW LC PB[a]

d	tsub	p	G	chf	Tong-75	Tong-75(mod)
mm	K	MPa	kg/m^2s	MW/m^2	MW/m^2	MW/m^2
7.62	73.	1.14	3000.	36.0	13.8	19.2
7.62	74.	1.14	4500.	42.5	16.5	23.0
7.62	75.	1.14	9800.	58.0	23.4	32.1

20 Researchers: Nariai et al. [22] UN SF LC PB[a]

d	tsub	p	G	chf	Tong-75	Tong-75(mod)
mm	K	MPa	kg/m^2s	MW/m^2	MW/m^2	MW/m^2
6.00	24.	0.10	4000.	8.5	17.2	5.3
6.00	53.	0.60	4000.	10.6	13.1	9.7
6.00	62.	1.08	4000.	14.5	11.9	12.4
6.00	68.	1.47	4000.	16.7	11.4	14.1
6.00	28.	0.12	7000.	13.5	21.0	7.0
6.00	53.	0.60	7000.	17.0	16.6	12.2
6.00	65.	1.10	7000.	18.0	15.4	16.4
6.00	72.	1.50	7000.	20.0	14.9	18.8

21 Researchers: Nariai et al. [22] UN SW IN PB[a]

d mm	tsub K	p MPa	G kg/m^{2}s	chf MW/m^2	Tong-75 MW/m^2	Tong-75(mod) MW/m^2
6.00	24.	0.10	4000.	9.5	18.2	5.5
6.00	51.	0.60	4000.	12.5	13.9	10.0
6.00	63.	1.10	4000.	14.6	12.7	13.3
6.00	69.	1.50	4000.	15.8	12.2	15.3
6.00	25.	0.10	7000.	12.3	23.0	7.2
6.00	24.	0.10	7000.	15.0	22.9	7.0
6.00	52.	0.60	7000.	19.5	17.6	12.7
6.00	64.	1.10	7000.	21.2	16.4	17.1

22 Researchers: Araki et al. [24] UN SF LC PB[a]

d mm	tsub K	p MPa	G kg/m^{2}s	chf MW/m^2	Tong-75 MW/m^2	Tong-75(mod) MW/m^2
7.00	44.	0.90	4400.	13.5	11.2	8.3
7.00	51.	0.90	6500.	16.0	13.8	10.9
7.00	55.	0.90	8700.	18.0	16.1	13.2
7.00	56.	0.90	10000.	19.5	17.2	14.3
7.00	58.	0.90	12000.	21.0	18.9	16.0
7.00	60.	0.90	13000.	21.5	19.7	16.8

23 Researchers: Araki et al. [24] UN SW IN PB[a]

d mm	tsub K	p MPa	G kg/m^{2}s	chf MW/m^2	Tong-75 MW/m^2	Tong-75(mod) MW/m^2
7.00	35.	0.90	4400.	17.0	11.5	7.6
7.00	42.	0.90	6500.	21.0	14.1	10.1
7.00	47.	0.90	8700.	24.0	16.5	12.4
7.00	49.	0.90	10000.	26.5	17.6	13.4
7.00	50.	0.90	12000.	30.5	19.2	14.7
7.00	51.	0.90	13000.	32.0	20.1	15.4

24 Researchers: Schlosser [23] NU SW LC PB[a]

d mm	tsub K	p MPa	G kg/m²s	chf MW/m²	Tong-75 MW/m²	Tong-75(mod) MW/m²
14.00	87.	3.30	8400.	49.2	17.1	25.6
14.00	67.	3.30	8900.	43.3	15.7	20.3
14.00	87.	3.30	8900.	43.3	17.7	26.4
14.00	63.	1.30	9150.	39.8	17.8	18.1
14.00	88.	3.30	8900.	46.2	17.8	26.8
14.00	67.	3.30	9100.	41.8	15.9	20.5
14.00	65.	1.40	5300.	30.8	13.9	15.1
14.00	46.	1.40	8700.	34.4	15.5	13.7
14.00	46.	1.40	5400.	26.0	12.5	11.2
14.00	100.	3.40	5700.	41.3	14.9	26.0
14.00	88.	3.40	5500.	38.5	13.6	22.0
14.00	68.	3.40	5400.	35.6	12.1	16.8
14.00	46.	3.60	8100.	32.9	12.9	14.7
14.00	43.	3.40	5100.	29.2	10.2	11.8
14.00	58.	2.30	8700.	37.0	15.4	17.6

25 Researchers: Nariai et al. Dh=.5De [22] NU SW IN PB[a]

d mm	tsub K	p MPa	G kg/m²s	chf MW/m²	Tong-75 MW/m²	Tong-75(mod) MW/m²
6.00	26.	0.10	4000.	12.5	22.4	8.8
6.00	54.	0.60	4000.	16.8	17.0	16.0
6.00	65.	1.10	4000.	22.5	15.3	20.9
6.00	72.	1.50	4000.	23.0	14.7	24.2
6.00	27.	0.10	7000.	17.7	28.2	11.3
6.00	55.	0.60	7000.	22.5	21.5	20.5
6.00	67.	1.10	7000.	28.6	19.7	27.0

26 Researchers: Araki et al. [24] (external fin) NU SW IN PB[a]

d mm	tsub K	p MPa	G kg/m^{2}s	chf MW/m^2	Tong-75 MW/m^2	Tong-75(mod) MW/m^2
7.00	44.	0.96	3850.	24.8	13.4	12.9
7.00	51.	0.96	5780.	30.0	16.5	17.0
7.00	55.	0.96	7700.	33.1	19.2	20.8
7.00	57.	0.96	9630.	38.2	21.4	23.5
7.00	59.	0.96	11600.	41.8	23.5	26.2
7.00	36.	0.70	3850.	25.8	13.9	10.4
7.00	43.	0.70	5780.	31.5	17.1	13.9
7.00	48.	0.70	7700.	34.6	19.9	17.2
7.00	50.	0.70	9630.	39.0	22.1	19.7
7.00	25.	0.44	3850.	27.0	14.7	7.7
7.00	34.	0.44	5780.	30.7	18.3	11.0
7.00	39.	0.44	7700.	34.0	21.2	13.7
7.00	42.	0.44	9630.	37.2	23.7	16.0

27 Researchers: Araki et al. [24] (external fin) NU SF IN PB[a]

d mm	tsub K	p MPa	G kg/m^{2}s	chf MW/m^2	Tong-75 MW/m^2	Tong-75(mod) MW/m^2
7.00	47.	0.96	3850.	22.7	12.7	12.7
7.00	56.	0.96	5780.	24.2	15.9	17.5
7.00	60.	0.96	7700.	27.1	18.4	21.0
7.00	62.	0.96	9630.	29.5	20.5	23.9
7.00	65.	0.96	11600.	30.6	22.6	26.8
7.00	40.	0.70	3850.	23.0	13.3	10.5
7.00	49.	0.70	5780.	24.6	16.6	14.7
7.00	54.	0.70	7700.	26.5	19.2	18.0
7.00	55.	0.70	9630.	30.6	21.3	20.2
7.00	31.	0.44	3850.	23.2	14.1	8.1
7.00	40.	0.44	5780.	25.1	17.6	11.5
7.00	45.	0.44	7700.	26.2	20.5	14.4
7.00	46.	0.44	9630.	30.1	22.7	16.3

28 Researchers: Araki et al. [24] (internal fin) NU FN IN PB[a]

d mm	tsub K	p MPa	G kg/m^{2}s	chf MW/m^2	Tong-75 MW/m^2	Tong-75(mod) MW/m^2
7.00	65.	0.96	3850.	10.0	14.1	17.3
7.00	66.	0.96	5780.	13.4	16.9	20.9
7.00	67.	0.96	7700.	17.2	19.2	23.7
7.00	67.	0.96	9630.	20.8	21.2	26.1
7.00	67.	0.96	11600.	24.5	23.0	28.2
7.00	68.	0.96	13500.	28.0	24.6	30.1
7.00	59.	0.70	3850.	9.5	14.9	15.0
7.00	59.	0.70	5780.	13.8	17.6	17.8
7.00	60.	0.70	7700.	16.9	20.0	20.4
7.00	61.	0.70	9630.	19.8	22.1	22.7
7.00	61.	0.70	11600.	24.0	23.9	24.4
7.00	50.	0.44	3850.	9.5	16.0	12.2
7.00	52.	0.44	5780.	12.3	19.1	14.9
7.00	52.	0.44	7700.	16.8	21.4	16.6
7.00	53.	0.44	9630.	19.1	23.7	18.5
7.00	52.	0.44	11600.	23.5	25.5	19.9

29 Researchers: Araki et al. [24] NU SF IN PB[a]

d mm	tsub K	p MPa	G kg/m^{2}s	chf MW/m^2	Tong-75 MW/m^2	Tong-75(mod) MW/m^2
7.00	58.	0.96	3850.	14.5	13.6	15.5
7.00	65.	0.96	5780.	15.1	16.8	20.4
7.00	66.	0.96	7700.	17.9	19.1	23.5
7.00	67.	0.96	9630.	20.7	21.2	26.1
7.00	69.	0.96	11600.	21.0	23.2	29.0
7.00	70.	0.96	12700.	21.2	24.3	30.5
7.00	53.	0.70	3850.	13.5	14.4	13.5
7.00	58.	0.70	5780.	15.5	17.5	17.3
7.00	60.	0.70	7700.	17.9	19.9	20.1
7.00	62.	0.70	9630.	19.2	22.2	22.8
7.00	63.	0.70	11600.	20.5	24.2	25.1
7.00	45.	0.44	3850.	13.2	15.4	10.9
7.00	48.	0.44	5780.	16.2	18.6	13.8
7.00	51.	0.44	7700.	17.9	21.3	16.3
7.00	53.	0.44	9630.	19.2	23.7	18.5
7.00	54.	0.44	11600.	20.3	25.8	20.5

30 Researchers: Mirshak et al. [30] UN AN LC PB[a]

d mm	tsub K	p MPa	G kg/m^{2}s	chf MW/m^2	Tong-75 MW/m^2	Tong-75(mod) MW/m^2
6.40	49.	0.29	5942.	5.5	18.1	9.9
6.40	52.	0.29	5948.	5.7	18.4	10.5
6.40	48.	0.28	5856.	5.9	17.9	9.6
6.40	29.	0.26	5798.	4.9	16.0	6.2
6.40	52.	0.43	5791.	6.6	16.4	10.4
6.40	43.	0.29	5915.	5.5	17.2	8.6
6.40	45.	0.34	9799.	8.1	20.6	11.0
6.40	41.	0.34	9748.	7.7	20.0	10.0
6.40	36.	0.34	9699.	7.3	19.3	9.0

31 Researchers: Babcock [28] UN AN LC PB[a]

d mm	tsub K	p MPa	G kg/m^{2}s	chf MW/m^2	Tong-75 MW/m^2	Tong-75(mod) MW/m^2
9.50	55.	0.61	9269.	10.3	16.8	10.8
12.70	48.	0.61	7043.	9.6	13.2	7.1
12.70	38.	0.43	9973.	9.4	15.6	6.4
12.70	47.	0.45	10205.	10.5	16.5	7.7
12.70	40.	3.62	6069.	7.4	8.5	7.7
12.70	54.	3.58	6653.	9.4	9.8	9.6
12.70	71.	3.62	2856.	6.5	7.0	8.6
12.70	48.	3.58	2373.	5.2	5.6	5.9
12.70	53.	8.41	6683.	9.7	9.3	9.0
19.10	42.	0.43	6279.	7.7	11.8	4.5
19.10	52.	0.62	6669.	9.8	11.9	5.9
19.10	52.	0.45	3546.	6.6	9.8	4.4
19.10	58.	0.76	3463.	7.2	8.9	5.2
19.10	57.	0.70	3466.	7.0	9.0	5.0
19.10	45.	3.58	3536.	6.5	6.3	5.2
19.10	63.	7.85	2190.	6.2	5.0	5.2
25.40	45.	0.41	4859.	7.6	10.1	3.6
25.40	46.	0.52	5669.	8.8	10.4	4.0

32 Researchers: Nariai et al. [22] UN SW IN PB[a]

d	tsub	p	G	chf	Tong-75	Tong-75(mod)
mm	K	MPa	kg/m^{2}s	MW/m^2	MW/m^2	MW/m^2
6.00	24.	0.10	4000.	9.0	17.8	5.4
6.00	51.	0.60	4000.	13.2	13.5	9.7
6.00	63.	1.10	4000.	14.5	12.4	13.0
6.00	70.	1.50	4000.	14.6	12.0	15.1
6.00	26.	0.10	7000.	11.8	22.5	7.1
6.00	25.	0.10	7000.	13.2	22.4	7.0
6.00	25.	0.10	7000.	13.6	22.4	6.9
6.00	53.	0.60	7000.	18.2	17.2	12.6
6.00	65.	1.10	7000.	19.3	16.0	16.9

33 Researchers: Nariai et al. Dh=0.25De [22] NU SW IN PB[a]

d	tsub	p	G	chf	Tong-75	Tong-75(mod)
mm	K	MPa	kg/m^{2}s	MW/m^2	MW/m^2	MW/m^2
6.00	28.	0.10	4000.	9.5	27.8	14.3
6.00	57.	0.60	4000.	13.0	20.9	25.8
6.00	69.	1.10	4000.	17.0	18.9	34.1
6.00	76.	1.50	4000.	19.5	17.9	39.2
6.00	28.	0.10	7000.	15.9	34.8	17.9
6.00	58.	0.60	7000.	19.1	26.3	32.5

34 Researchers: Nariai et al. Dh=0.5De [22] NU SW IN PB[a]

d	tsub	p	G	chf	Tong-75	Tong-75(mod)
mm	K	MPa	kg/m^{2}s	MW/m^2	MW/m^2	MW/m^2
6.00	28.	0.10	7000.	12.5	27.8	11.3
6.00	56.	0.60	7000.	19.5	21.1	20.2
6.00	68.	1.10	7000.	22.3	19.4	26.9
6.00	75.	1.50	7000.	23.2	18.6	31.0
6.00	26.	0.10	7000.	19.5	27.5	10.9
6.00	55.	0.60	7000.	21.8	21.0	20.1
6.00	67.	1.10	7000.	29.1	19.2	26.3

35 Researchers: Russian Data, Lekakh [61] NU SF LC NP[a]

d	tsub	p	G	chf	Tong-75	Tong-75(mod)
mm	K	MPa	kg/m^{2}s	MW/m^2	MW/m^2	MW/m^2
6.00	93.	3.50	3160.	15.0	11.0	28.3
6.00	93.	3.50	3360.	16.5	11.3	28.9
6.00	93.	3.50	3860.	16.0	12.1	30.8
6.00	93.	3.50	4900.	18.0	13.6	34.1
6.00	93.	3.50	4950.	20.0	13.6	34.1
6.00	93.	3.50	5440.	20.5	14.3	35.5
6.00	93.	3.50	6330.	23.0	15.4	37.8
6.00	94.	3.50	6630.	20.5	15.8	38.7
6.00	94.	3.50	6920.	18.0	16.1	39.6
6.00	92.	3.50	2970.	17.4	10.6	27.3
6.00	92.	3.50	3960.	20.5	12.2	30.8
6.00	93.	3.50	5540.	22.1	14.4	35.7
6.00	93.	3.50	5840.	23.1	14.8	36.5
6.00	93.	3.50	3760.	18.1	11.9	30.3
6.00	93.	3.50	4750.	20.1	13.3	33.5
6.00	93.	3.50	5540.	22.1	14.4	35.7
6.00	94.	3.50	6530.	22.8	15.6	38.3
6.00	92.	3.50	2970.	16.9	10.6	27.3
6.00	93.	3.50	4150.	17.1	12.5	31.8
6.00	93.	3.50	5540.	20.5	14.4	35.8
6.00	92.	3.50	2970.	17.0	10.6	27.3
6.00	93.	3.50	4150.	18.0	12.5	31.7
6.00	94.	3.50	5540.	19.1	14.4	35.9
6.00	93.	3.50	3160.	15.2	11 0	28.3
6.00	93.	3.50	4150.	17.6	12.5	31.7
6.00	93.	3.50	4600.	19.3	13.1	33.1
6.00	94.	3.50	5740.	18.6	14.7	36.5

[a] Legend:

UN = Uniform Heat Flux; NU = Nonuniform Heat Flux

SF = Smooth Flow; SW = Swirl Flow; AN = Annular Flow; RC = Rectangular Channel; FN = Internal Fin

LC = Local Heat Flux; IN = Incident Heat Flux

PB = Published Data; NP = Non-published Data

Appendix C

Codes Written for Present Study

Note: column locations are not accounted for in the following Fortran code listings.

C.1 Fortran Code *drf.for* for Flow Meter and Inlet Bulk Temperature Conversion

```
c Data Reduction Code for Flow Meter and Inlet Bulk Temperature
      c
      c Last Updated by Anthony Hechanova 10-10-94
      c
      implicit real*8(a-h,o-z)
      character*64 finp,fout
      real*8 ch1(1000),f(1000)
      c
      write(*,*)' Enter input file name —≫'
      read(*,10) finp
      10 format(a)
      write(*,*)' Enter sample rate —≫'
      read(*,110) samp
      samp=samp/7.
      write(*,*)' Enter samples taken (multiples of 1000) —≫'
      read(*,115) nsamp
      110 format(f8.0)
      115 format(i5)
      open(unit=5,file=finp,status='old')
      ch1o=0.
      i=1
```

```
icount=0
k1=0
k=nsamp/1000
if(nsamp.lt.1000) k=0
140 continue
do 60 i2=1,1000
read(5,30)ch1(i2),ch2
d1=ch1o-ch1(i2)
if(abs(d1).le.0.5) then
icount=icount+1
else
f(i)=icount
i=i+1
icount=0
endif
30 format(2(f6.3))
ch1o=ch1(i2)
80 format(2x,f5.0))
85 format(2x,'avg freq = ',f8.2,' gpm = ',f8.2,' vel = ',f8.2,' m/s'
1,' percent Std Error = ',f8.0/' T inlet = ',f8.2,' C')
86 format(2x,'i = ',i5)
if(i2.eq.nsamp)goto 160
60 continue
k1=k1+1
if(k1.eq.k) goto 160
goto 140
160 continue
i4=i-2
itot=i4-1
ftot=0.0
do 100 i3=2,i4
ftot=ftot+f(i3)
100 continue
favg=ftot/real(itot)
c
c Standard Error
c
fsd=0.
do 120 i3=2,i4
fsd=fsd+(favg-f(i3))**2.
120 continue
sde=(fsd/(i4-3))**.5
freq=samp/favg/2.
sde=100.*sde/favg
gpm=0.6266*(freq+0.0314)
```

```
vel=0.89*gpm
t2=290.*ch2-100.
c
c write(6,85)freq
write(*,85)freq,gpm,vel,sde,t2
stop
end
```

C.2 A Sample Fortran Code *cn6.f* for Thermocouple and Voltage Conversion

```
c
    c Data Reduction Code
    c
    implicit real*8(a-h,o-z)
    character*64 finp,fout
    real*8 a(1000),b(1000),c(1000)
    c
    finp='in.txt'
    fout='prog3.dat'
    c sam=sample rate/no. of channels
    sam=20./4.
    open(unit=6,file=fout,status='new')
    c do 20 i2=1,20
    open(unit=5,file=finp,status='old')
    timtot=0.
    timcs=0.
    c
    ikount=0
    j1=1
    dtim=0.
    c
    c
    icn=1
    k=0
    290 continue
    do 120 i=1,1000
    c if(timtot.le.142.)goto 50
    c if(timtot.ge.152.)goto 2700
    j1=0
    do 40 j=1,icn
    30 format(7(f6.3,1x))
    read(5,30)voi,ch1,ch2,ch3,ch4,chi,ch5
    timtot=timtot+1./sam
    timcs=timcs+1.
    c if(timcs.le.1700.)goto 50
    c if(timcs.ge.2200.)goto 2700
    curm=chi/5./(0.000112)
    if(voi.eq.-100.)goto 2700
    j1=j1+1
    a(j1)=voi
```

```
b(j1)=curm
c(j1)=voi*chi
40 continue
voi2=0.
chi2=0.
p2=0.
do 10 j=1,j1
voi2=voi2+a(j)
chi2=chi2+b(j)
p2=p2+c(j)
10 continue
voi=voi2/float(j1)
curm=chi2/float(j1)
p2=p2/float(j1)
pow=p2*5.444/5./0.000112
c Screen Current Signal
c curm=(290.*chi-84.)*.0406/.112
vo2=5.444*voi
vmean=vo2
c
cvvvvvvvvvvvvvv Voltage Specified vvvvvvvvvvvvvvv
c
c if(timtot.gt.363.)vmean=10.
c if(timtot.ge.125.and.timtot.le.142.)vmean=12.
c if(vmean.ge.8.3)cur=600.
c
c************** Power Supply Curve Fit ***********
c
c if(timtot.ge.135..and.timtot.le.148)vmean=14.5
cur=0.
c if(vmean.ge.4.)then
cur=-136.+vmean*75.259
c ts19b cur=-107.+vmean*70.921
c ts21a cur=-53.7+vmean*62.284
c else
c endif
c*************************************************
pow3=curm*vmean
pow2=cur*vmean
c
t1=0.
c t1=290.*ch1-100.
t2=290.*ch2-100.
t3=290.*ch3-100.
t4=290.*ch4-100.
```

```
c t5=0.
t5=290.*ch5-100.
if(cur.eq.0.)then
cfi=0.
else
cfi=curm/cur
endif
135 format(14(g12.4,1x))
130 format(i3,1x,3(g12.3,1x))
c write(6,130)icn,pow,pow2,pow3
write(6,135)t1,t2,t3,t4,t5,vmean,vo2,timcs,cur,curm,pow,pow2
pow3,cfi
50 continue
120 continue
k=k+1
c
goto 290
2700 continue
close(unit=5)
c
20 continue
close(unit=6)
stop
end
```

C.3 A Sample Matlab Code *pcn7.m* for Plotting Temperature, Power and Other Data Reduction Graphs

```
load prog3.dat
    t1=prog3(:,1);
    t2=prog3(:,2);
    t3=prog3(:,3);
    t4=prog3(:,4);
    t5=prog3(:,5);
    v=prog3(:,6);
    vo=prog3(:,7);
    tim=prog3(:,8);
    i=prog3(:,9);
    io=prog3(:,10);
    po=prog3(:,11);
    p=prog3(:,12);
    p3=prog3(:,13);
    cf=prog3(:,14);
    %
    % Figure 2
    %
    figure
    plot(tim,t2,'-',tim,t4,'-',tim,t5,':')
    axis
    xmin=ans(1)
    xmax=ans(2)
    ymin=ans(3)
    ymax=ans(4)
    %axis([xmin xmax ymin ymax])
    axis([xmin xmax 0 ymax])
    legend('TC 2','TC 4','TC 5')
    title('Temperature Profile TS20B (increments of n=1)')
    xlabel('Time [data no.]')
    ylabel('Temperature [C]')
    %
    % Figure 3
    %
    figure
    plot(po,t3,'o',po,t2,'x')
    axis
    xmin=ans(1)
```

```
xmax=ans(2)
ymin=ans(3)
ymax=ans(4)
axis([0 xmax 0 ymax])
legend('TC 3','TC 2')
title('Temperature vs Power Profile TS20B (increments of n=1)')
xlabel('Power [W]')
ylabel('Temperature [C]')
%
% Figure 4
%
figure
plot(v,i,'o',vo,io,'x')
axis
xmin=ans(1)
xmax=ans(2)
ymin=ans(3)
ymax=ans(4)
axis([0 xmax 0 ymax])
legend('Notebook Fit','Module')
title('Current Profile TS20B (increments of n=1)')
xlabel('Voltage [V]')
ylabel('Current [Amps]')
%
% Figure 6
%
figure
%plot(tim,v,'-',tim,vo,'-')
plot(tim,vo,'-')
axis
xmin=ans(1)
xmax=ans(2)
ymin=ans(3)
ymax=ans(4)
axis([xmin xmax 0 ymax])
%axis([xmin xmax ymin ymax])
title('Voltage Profile TS20B (increments of n=1)')
xlabel('Time [data no.]')
ylabel('Volts')
%
% Figure 7
%
figure
plot(tim,i,'-',tim,io,'-')
axis
```

```
xmin=ans(1)
xmax=ans(2)
ymin=ans(3)
ymax=ans(4)
%axis([xmin xmax ymin ymax])
axis([xmin xmax 0 ymax])
title('Current Profile TS20B (increments of n=1)')
legend('Notebook Fit','Module')
xlabel('Time [data no.]')
ylabel ('Current [Amps]')
%
% Figure 8
%
figure
plot(tim,po,'-',tim,p,'-',tim,p3,':')
axis
xmin=ans(1)
xmax=ans(2)
ymin=ans(3)
ymax=ans(4)
axis([2000 2500 ymin ymax])
axis([xmin xmax ymin ymax])
legend('Module Power','Notebook Fit','Module V*I')
title('Power Profile TS20B (increments of n=1)')
xlabel('Time [data no.]')
%
figure
% Figure 9
%
plot(tim,t1,'-',tim,t2,'-',tim,t3,':')
axis
xmin=ans(1)
xmax=ans(2)
ymin=ans(3)
ymax=ans(4)
axis([xmin xmax 0 ymax])
%axis([2030 2120 0 ymax])
legend('TC 1','TC 2','TC 3')
title('Temperature Profile TS20B (increments of n=1)')
xlabel('Time [data no.]')
ylabel('Temperature [C]')
%
% Figure 10
%
figure
```

```
plot(tim,cf,'-')
axis
xmin=ans(1)
xmax=ans(2)
ymin=ans(3)
ymax=ans(4)
%axis([xmin xmax ymin ymax])
axis([xmin xmax 0 ymax])
title('TS20B Ratio of Current: Module/Notebook Fit (increments of n=1)')
xlabel('Time [data no.]')
```

C.4 Fortran Code *sh2.for* for calculation and evaluation of heat transfer coefficients, and HEATING7.2 input file generation

```
c sh2.for
      c
      c Data Reduction Code
      c
      implicit real*8(a-h,o-z)
      character*64 finp,fout,crap,desc,deso,des2,fh7,hodat
      real*8 t(20,20),h1(50,50),tb(18)
      2,ta(20,20),x(20),x2(20)
      3,y1(20,20),y2(20,20)
      c
      Data ts1 /+0.010293 d0/
      Data ts2 /+0.38048 d0/
      Data ts3 /+1.7934 d0/
      Data ts4 /+28.553 d0/
      Data ts5 /+99.63 d0/
      c
      hmlt=1.0
      c write(*,*)' Enter h Multiplication Factor'
      c read(*,2000)hmlt
      2000 format(f9.3)
      if(hmlt.le.1.0)hmlt=1.0
      c
      write(*,*)' Enter "input.one" if first iteration or "plot.out"'
      read(*,10) finp
      c finp='h7.out'
      10 format(a)
      c write(*,*)' Enter output file name -->>'
      c read(*,10) fout
      npass=1
      1200 continue
      open(unit=5,file=finp,status='old')
      open(unit=4,file='htc.dat',status='old')
      c Inputs
      c
      read(4,200)pow
      read(4,200)vel
      read(4,200)tin
      read(4,200)p
```

```
read(4,202)fout
diam=0.0095
qdp=pow*1000./(0.75*0.0254*2.*0.0254)
200 format(f7.3)
202 format(a9)
c if(finp.eq.'input.one') then
c hodat='ho.one'
c else
hodat='ho.dat'
c endif
c
open(unit=7,file='dot.dat',status='new')
open(unit=8,file='reg.dat',status='new')
open(unit=3,file=hodat,status='old')
open(unit=9,file=fout,status='new')
do 220 i=1,14
read(3,230)(h1(i,j),j=1,18)
c write(*,230)(h1(i,j),j=1,18)
230 format(18(f8.0,2x))
220 continue
close(unit=3)
c
c
read(5,20)desc
read(5,20)desc
read(5,20)desc
c
90 format(' ',a)
20 format(a)
c
do 1970 i=15,1,-1
read(5,1830)t(i,1),ta(i,1)
c write(*,1830)t(i,1),ta(i,1)
1830 format(17x,f7.2,1x,f7.2)
1970 continue
do 1850 j=2,19
do 1840 i=1,6
read(5,20)desc
1840 continue
do 1980 i=15,1,-1
read(5,1830)t(i,j),ta(i,j)
c write(*,1830)t(i,j),ta(i,j)
c write(*,1845)i,j
1845 format(' i = ',i2,' j = ',i2)
1980 continue
```

```
1850 continue
close(unit=5)
c
c Temperature of Homogeneous Nucleation from Collier, p 115
c
p=p*1.0d6
pbar=p/100000.
pt=log(pbar)
tsatp=(((ts1*pt+ts2)*pt+ts3)*pt+ts4)*pt+ts5
tho=647.29*(0.905+0.095*(tsatp/647.29)**8.)-273.15
c
c use T crit
c
tcrit=376.
write(9,1010)tsatp,tho
1010 format(' T sat = ',f6.1,' T hn = ',f6.1)
c
do 1100 i=1,5
tb(i)=tin
tb(i+13)=tin+pow*1000.*4./(3.14159*(0.0095)**2.*4190.*vel*900.0)
1100 continue
c
do 760 j=6,13
tb(j)=tin+float(j-5)*pow*1000.*4./(8.*3.14159*(0.0095)
1**2.*4190.*vel*900.0)
c tb=tin+pow*4./(3.14159*(0.0095)**2.*4190.*vel*900.0)
760 continue
do 764 j=1,18
write(9,762)j,tb(j)
write(*,762)j,tb(j)
764 continue
762 format(' T bulk (',i2,') = ',f5.1)
c
c HEAT TRANSFER COEFFICIENT EQUATION
c
c regions: 1 = single phase
c 2 = subcooled nucleate boiling
c 3 = homogeneous nucleation temp reached
c 4 = critical temperature reached
c 5 = temperature drops below tsat
c 6 = wall temperature drops below tbulk
c
c Heat Flux Calculations
c
nend=0
```

```
icount=0
c
c
do 1110 j=6,13
c
do 80 i=1,14
tavg=(2.*t(i,j)+t(i+1,j)+t(i,j+1))/4.
if(tavg.le.tb(j)) then
qa=1.
h12=7000.
ireg=6
goto 3030
else
qa=h1(i,j)*(tavg-tb(j))
endif
c
qa1=qa/qdp
tw=tavg
c
if(tw.gt.tho) then
ireg=4
c tl=tsatp
h12=qa/(tw-tb(j))
else
tl=(tw+tb(j))/2.
c
tbk=tb(j)
call heau(qdp,vel,p,tl,qa,h,hsh,tbk,hdb,tw)
ireg=1
h12=h
c
if(tw.gt.tsatp) then
ireg=2
h12=hsh
hmin=qa/(tcrit-tb(j))
if(h12.lt.hmin) then
h12=hmin
ireg=6
else
endif
c hmax=qa/(tsatp-tb(j))
c if(h12.gt.hmax) then
c h12=hmax
c ireg=5
write(9,3032)tw,h,hdb,h12
```

```
if(tw.gt.tho) ireg=3
else
endif
endif
3032 format(' T w = ',f6.0,' h pet = ',f8.0,
1' h db =',f8.0,' h shah = ',f8.0)
3030 continue
h12=hmlt*h12
dh=h12-h1(i,j)
if(h1(i,j).eq.0) goto 3010
dh=dh/h1(i,j)
if(abs(dh).le..05) icount=icount+1
3010 continue
write(*,210)i,j,h12,h1(i,j),qa1,icount,ireg
write(8,211)i,j,h1(i,j),qa1,ireg
write(9,210)i,j,h12,h1(i,j),qa1,icount,ireg
h1(i,j)=(h1(i,j)+h12)/2.
80 continue
210 format(2x,i2,2x,i2,f9.0,f9.0,1x,f6.3,1x,i3,2x,i2)
211 format(2x,i3,i3,f9.0,1x,f6.3,1x,i2)
c
1110 continue
c
c z = 1,5
c
j=3
3000 continue
do 81 i=1,14
tw=(t(i,j)+t(i+1,j))/2.
if(tw.gt.tho) then
ireg=4
h12=qa/(tw-tb(j))
c tl=tsatp
else
tl=(tw+tb(j))/2
c
if(tw.le.tb(j)) then
qa=1.
h12=7000
ireg=6
goto 3040
else
qa=h1(i,j)*(tw-tb(j))
endif
c
```

```
qa1=qa/qdp
c if(tw.le.tsatp)then
tbk=tb(j)
call heau(qdp,vel,p,tl,qa,h,hsh,tbk,hdb,tw)
ireg=1
h12=h
if(tw.gt.tsatp) then
h12=hsh
ireg=2
c hmax=qa/(tsatp-tb(j))
c if(h12.gt.hmax) then
c h12=hmax
c ireg=5
c else
c endif
write(9,3032)tw,h,hdb,h12
if(tw.gt.tho) ireg=3
else
endif
3040 continue
endif
h12=hmlt*h12
if(h1(i,j).eq.0) goto 3020
dh=h12-h1(i,j)
dh=dh/h1(i,j)
if(abs(dh).le..05) icount=icount+1
3020 continue
write(*,210)i,j,h12,h1(i,j),qa1,icount,ireg
write(8,211)i,j,h1(i,j),qa1,ireg
write(9,210)i,j,h12,h1(i,j),qa1,icount,ireg
h1(i,j)=(h1(i,j)+h12)/2.
81 continue
c
c z = 14-19
c
if(j.eq.3) then
j=16
goto 3000
else
endif
open(unit=3,file='ho.dat',status='new')
do 430 i=1,14
write(3,440)(h1(i,j),j=1,18),i
440 format(18(f8.0,2x),i2)
430 continue
```

```
c
if(icount.eq.140.)then
write(9,505)tsatp
write(*,500)fout
500 format(' Iteration Completed. Output in ',a9)
505 format(' T sat = ',f7.1)
goto 70
else
open(unit=2,file='fh7',status='new')
260 format(a)
write(2,261)fout
261 format('3D Conduction Profile of Test Section',a12)
write(2,260)'* Copper structure, water coolant'
write(2,260)'* Units: J, kg, s, m, C'
write(2,260)'* Iteration using heating7'
write(2,260)'* htc.dat defines thermal parameters'
280 format(i5,2x,i2,2x,i2,2x,i2)
write(2,280)10000,1,0,1
write(2,260)'REGIONS'
290 format(i3,2x,i2,2x,f7.5,2x,f8.6,2x,f8.6,2x,f8.6,2x,f6.5,2x,f6.5)
310 format(8(i3,2x))
c z6
write(2,290)1,1,0.00475,0.009598,0.0,0.174532,0.0381,.04445
write(2,310)1,0,1,141,0,0,0,0
write(2,290)2,1,0.00475,0.009904,0.174532,0.349065,0.0381,.04445
write(2,310)1,0,2,141,0,0,0,0
write(2,290)3,1,0.00475,0.010567,0.349065,0.523598,0.0381,.04445
write(2,310)1,0,3,141,0,0,0,0
write(2,290)4,1,0.00475,0.011716,0.523598,0.698131,0.0381,.04445
write(2,310)1,0,4,141,0,0,0,0
write(2,290)5,1,0.00475,0.012676,0.698131,0.829030,0.0381,.04445
write(2,310)1,0,5,141,0,0,0,0
c
write(2,290)6,1,0.00475,0.012184,0.829030,0.982619,0.0381,0.04445
write(2,310)1,0,6,0,0,0,0,0
write(2,290)7,1,0.00475,0.010979,0.982619,1.134463,0.0381,0.04445
write(2,310)1,0,7,0,0,0,0,0
write(2,290)8,1,0.00475,0.010185,1.134463,1.308995,0.0381,0.04445
write(2,310)1,0,8,0,0,0,0,0
write(2,290)9,1,0.00475,0.009693,1.308995,1.570795,0.0381,0.04445
write(2,310)1,0,9,0,0,0,0,0
write(2,290)10,1,0.00475,0.009693,1.570795,1.832594,0.0381,0.04445
write(2,310)1,0,10,0,0,0,0,0
write(2,290)11,1,0.00475,0.010185,1.832594,2.007126,0.0381,0.04445
write(2,310)1,0,11,0,0,0,0,0
```

```
write(2,290)12,1,0.00475,0.010979,2.007126,2.158970,0.0381,0.04445
write(2,310)1,0,12,0,0,0,0,0
write(2,290)13,1,0.00475,0.012459,2.158970,2.356192,0.0381,0.04445
write(2,310)1,0,13,0,0,0,0,0
write(2,290)14,1,0.00475,0.011497,2.356192,3.141590,0.0381,0.04445
write(2,310)1,0,14,0,0,0,0,0
c
c z7
write(2,290)15,1,0.00475,0.009598,0.0,0.174532,.04445,.0508
write(2,310)1,0,15,141,0,0,0,0
write(2,290)16,1,0.00475,0.009904,0.174532,0.349065,.04445,.0508
write(2,310)1,0,16,141,0,0,0,0
write(2,290)17,1,0.00475,0.010567,0.349065,0.523598,.04445,.0508
write(2,310)1,0,17,141,0,0,0,0
write(2,290)18,1,0.00475,0.011716,0.523598,0.698131,.04445,.0508
write(2,310)1,0,18,141,0,0,0,0
write(2,290)19,1,0.00475,0.012676,0.698131,0.829030,.04445,.0508
write(2,310)1,0,19,141,0,0,0,0
c
write(2,290)20,1,0.00475,0.012184,0.829030,0.982619,0.04445,.0508
write(2,310)1,0,20,0,0,0,0,0
write(2,290)21,1,0.00475,0.010979,0.982619,1.134463,0.04445,.0508
write(2,310)1,0,21,0,0,0,0,0
write(2,290)22,1,0.00475,0.010185,1.134463,1.308995,0.04445,.0508
write(2,310)1,0,22,0,0,0,0,0
write(2,290)23,1,0.00475,0.009693,1.308995,1.570795,0.04445,.0508
write(2,310)1,0,23,0,0,0,0,0
write(2,290)24,1,0.00475,0.009693,1.570795,1.832594,0.04445,.0508
write(2,310)1,0,24,0,0,0,0,0
write(2,290)25,1,0.00475,0.010185,1.832594,2.007126,0.04445,.0508
write(2,310)1,0,25,0,0,0,0,0
write(2,290)26,1,0.00475,0.010979,2.007126,2.158970,0.04445,.0508
write(2,310)1,0,26,0,0,0,0,0
write(2,290)27,1,0.00475,0.012459,2.158970,2.356192,0.04445,.0508
write(2,310)1,0,27,0,0,0,0,0
write(2,290)28,1,0.00475,0.011497,2.356192,3.141590,0.04445,.0508
write(2,310)1,0,28,0,0,0,0,0
c
c z8
write(2,290)29,1,0.00475,0.009598,0.0,0.174532,.0508,.05715
write(2,310)1,0,29,141,0,0,0,0
write(2,290)30,1,0.00475,0.009904,0.174532,0.349065,.0508,.05715
write(2,310)1,0,30,141,0,0,0,0
write(2,290)31,1,0.00475,0.010567,0.349065,0.523598,.0508,.05715
write(2,310)1,0,31,141,0,0,0,0
```

```
write(2,290)32,1,0.00475,0.011716,0.523598,0.698131,.0508,.05715
write(2,310)1,0,32,141,0,0,0,0
write(2,290)33,1,0.00475,0.012676,0.698131,0.829030,.0508,.05715
write(2,310)1,0,33,141,0,0,0,0
c
write(2,290)34,1,0.00475,0.012184,0.829030,0.982619,0.0508,.05715
write(2,310)1,0,34,0,0,0,0,0
write(2,290)35,1,0.00475,0.010979,0.982619,1.134463,0.0508,.05715
write(2,310)1,0,35,0,0,0,0,0
write(2,290)36,1,0.00475,0.010185,1.134463,1.308995,0.0508,.05715
write(2,310)1,0,36,0,0,0,0,0
write(2,290)37,1,0.00475,0.009693,1.308995,1.570795,0.0508,.05715
write(2,310)1,0,37,0,0,0,0,0
write(2,290)38,1,0.00475,0.009693,1.570795,1.832594,0.0508,.05715
write(2,310)1,0,38,0,0,0,0,0
write(2,290)39,1,0.00475,0.010185,1.832594,2.007126,0.0508,.05715
write(2,310)1,0,39,0,0,0,0,0
write(2,290)40,1,0.00475,0.010979,2.007126,2.158970,0.0508,.05715
write(2,310)1,0,40,0,0,0,0,0
write(2,290)41,1,0.00475,0.012459,2.158970,2.356192,0.0508,.05715
write(2,310)1,0,41,0,0,0,0,0
write(2,290)42,1,0.00475,0.011497,2.356192,3.141590,0.0508,.05715
write(2,310)1,0,42,0,0,0,0,0
c
c z9
write(2,290)43,1,0.00475,0.009598,0.0,0.174532,.05715,.0635
write(2,310)1,0,43,141,0,0,0,0
write(2,290)44,1,0.00475,0.009904,0.174532,0.349065,.05715,0.0635
write(2,310)1,0,44,141,0,0,0,0
write(2,290)45,1,0.00475,0.010567,0.349065,0.523598,.05715,.0635
write(2,310)1,0,45,141,0,0,0,0
write(2,290)46,1,0.00475,0.011716,0.523598,0.698131,.05715,.0635
write(2,310)1,0,46,141,0,0,0,0
write(2,290)47,1,0.00475,0.012676,0.698131,0.829030,.05715,.0635
write(2,310)1,0,47,141,0,0,0,0
c
write(2,290)48,1,0.00475,0.012184,0.829030,0.982619,0.05715,.0635
write(2,310)1,0,48,0,0,0,0,0
write(2,290)49,1,0.00475,0.010979,0.982619,1.134463,0.05715,.0635
write(2,310)1,0,49,0,0,0,0,0
write(2,290)50,1,0.00475,0.010185,1.134463,1.308995,0.05715,.0635
write(2,310)1,0,50,0,0,0,0,0
write(2,290)51,1,0.00475,0.009693,1.308995,1.570795,0.05715,.0635
write(2,310)1,0,51,0,0,0,0,0
write(2,290)52,1,0.00475,0.009693,1.570795,1.832594,0.05715,.0635
```

```
write(2,310)1,0,52,0,0,0,0,0
write(2,290)53,1,0.00475,0.010185,1.832594,2.007126,0.05715,.0635
write(2,310)1,0,53,0,0,0,0,0
write(2,290)54,1,0.00475,0.010979,2.007126,2.158970,0.05715,.0635
write(2,310)1,0,54,0,0,0,0,0
write(2,290)55,1,0.00475,0.012459,2.158970,2.356192,0.05715,.0635
write(2,310)1,0,55,0,0,0,0,0
write(2,290)56,1,0.00475,0.011497,2.356192,3.141590,0.05715,.0635
write(2,310)1,0,56,0,0,0,0,0
c
c z10
write(2,290)57,1,0.00475,0.009598,0.0,0.174532,.0635,.06985
write(2,310)1,0,57,141,0,0,0,0
write(2,290)58,1,0.00475,0.009904,0.174532,0.349065,.0635,.06985
write(2,310)1,0,58,141,0,0,0,0
write(2,290)59,1,0.00475,0.010567,0.349065,0.523598,.0635,.06985
write(2,310)1,0,59,141,0,0,0,0
write(2,290)60,1,0.00475,0.011716,0.523598,0.698131,.0635,.06985
write(2,310)1,0,60,141,0,0,0,0
write(2,290)61,1,0.00475,0.012676,0.698131,0.829030,.0635,.06985
write(2,310)1,0,61,141,0,0,0,0
c
write(2,290)62,1,0.00475,0.012184,0.829030,0.982619,0.0635,.06985
write(2,310)1,0,62,0,0,0,0,0
write(2,290)63,1,0.00475,0.010979,0.982619,1.134463,0.0635,.06985
write(2,310)1,0,63,0,0,0,0,0
write(2,290)64,1,0.00475,0.010185,1.134463,1.308995,0.0635,.06985
write(2,310)1,0,64,0,0,0,0,0
write(2,290)65,1,0.00475,0.009693,1.308995,1.570795,0.0635,.06985
write(2,310)1,0,65,0,0,0,0,0
write(2,290)66,1,0.00475,0.009693,1.570795,1.832594,0.0635,.06985
write(2,310)1,0,66,0,0,0,0,0
write(2,290)67,1,0.00475,0.010185,1.832594,2.007126,0.0635,.06985
write(2,310)1,0,67,0,0,0,0,0
write(2,290)68,1,0.00475,0.010979,2.007126,2.158970,0.0635,.06985
write(2,310)1,0,68,0,0,0,0,0
write(2,290)69,1,0.00475,0.012459,2.158970,2.356192,0.0635,.06985
write(2,310)1,0,69,0,0,0,0,0
write(2,290)70,1,0.00475,0.011497,2.356192,3.141590,0.0635,.06985
write(2,310)1,0,70,0,0,0,0,0
c
c z11
write(2,290)71,1,0.00475,0.009598,0.0,0.174532,.06985,.0762
write(2,310)1,0,71,141,0,0,0,0
write(2,290)72,1,0.00475,0.009904,0.174532,0.349065,.06985,.0762
```

```
write(2,310)1,0,72,141,0,0,0,0
write(2,290)73,1,0.00475,0.010567,0.349065,0.523598,.06985,.0762
write(2,310)1,0,73,141,0,0,0,0
write(2,290)74,1,0.00475,0.011716,0.523598,0.698131,.06985,.0762
write(2,310)1,0,74,141,0,0,0,0
write(2,290)75,1,0.00475,0.012676,0.698131,0.829030,.06985,.0762
write(2,310)1,0,75,141,0,0,0,0
c
write(2,290)76,1,0.00475,0.012184,0.829030,0.982619,0.06985,.0762
write(2,310)1,0,76,0,0,0,0,0
write(2,290)77,1,0.00475,0.010979,0.982619,1.134463,0.06985,.0762
write(2,310)1,0,77,0,0,0,0,0
write(2,290)78,1,0.00475,0.010185,1.134463,1.308995,0.06985,.0762
write(2,310)1,0,78,0,0,0,0,0
write(2,290)79,1,0.00475,0.009693,1.308995,1.570795,0.06985,.0762
write(2,310)1,0,79,0,0,0,0,0
write(2,290)80,1,0.00475,0.009693,1.570795,1.832594,0.06985,.0762
write(2,310)1,0,80,0,0,0,0,0
write(2,290)81,1,0.00475,0.010185,1.832594,2.007126,0.06985,.0762
write(2,310)1,0,81,0,0,0,0,0
write(2,290)82,1,0.00475,0.010979,2.007126,2.158970,0.06985,.0762
write(2,310)1,0,82,0,0,0,0,0
write(2,290)83,1,0.00475,0.012459,2.158970,2.356192,0.06985,.0762
write(2,310)1,0,83,0,0,0,0,0
write(2,290)84,1,0.00475,0.011497,2.356192,3.141590,0.06985,.0762
write(2,310)1,0,84,0,0,0,0,0
c
c z12
write(2,290)85,1,0.00475,0.009598,0.0,0.174532,.0762,.08255
write(2,310)1,0,85,141,0,0,0,0
write(2,290)86,1,0.00475,0.009904,0.174532,0.349065,.0762,.08255
write(2,310)1,0,86,141,0,0,0,0
write(2,290)87,1,0.00475,0.010567,0.349065,0.523598,.0762,.08255
write(2,310)1,0,87,141,0,0,0,0
write(2,290)88,1,0.00475,0.011716,0.523598,0.698131,.0762,.08255
write(2,310)1,0,88,141,0,0,0,0
write(2,290)89,1,0.00475,0.012676,0.698131,0.829030,.0762,.08255
write(2,310)1,0,89,141,0,0,0,0
c
write(2,290)90,1,0.00475,0.012184,0.829030,0.982619,0.0762,.08255
write(2,310)1,0,90,0,0,0,0,0
write(2,290)91,1,0.00475,0.010979,0.982619,1.134463,0.0762,.08255
write(2,310)1,0,91,0,0,0,0,0
write(2,290)92,1,0.00475,0.010185,1.134463,1.308995,0.0762,.08255
write(2,310)1,0,92,0,0,0,0,0
```

```
write(2,290)93,1,0.00475,0.009693,1.308995,1.570795,0.0762,.08255
write(2,310)1,0,93,0,0,0,0,0
write(2,290)94,1,0.00475,0.009693,1.570795,1.832594,0.0762,.08255
write(2,310)1,0,94,0,0,0,0,0
write(2,290)95,1,0.00475,0.010185,1.832594,2.007126,0.0762,.08255
write(2,310)1,0,95,0,0,0,0,0
write(2,290)96,1,0.00475,0.010979,2.007126,2.158970,0.0762,.08255
write(2,310)1,0,96,0,0,0,0,0
write(2,290)97,1,0.00475,0.012459,2.158970,2.356192,0.0762,.08255
write(2,310)1,0,97,0,0,0,0,0
write(2,290)98,1,0.00475,0.011497,2.356192,3.141590,0.0762,.08255
write(2,310)1,0,98,0,0,0,0,0
c
c z13
write(2,290)99,1,0.00475,0.009598,0.0,0.174532,.08255,.0889
write(2,310)1,0,99,141,0,0,0,0
write(2,290)100,1,0.00475,0.009904,0.174532,0.349065,.08255,.0889
write(2,310)1,0,100,141,0,0,0,0
write(2,290)101,1,0.00475,0.010567,0.349065,0.523598,.08255,.0889
write(2,310)1,0,101,141,0,0,0,0
write(2,290)102,1,0.00475,0.011716,0.523598,0.698131,.08255,.0889
write(2,310)1,0,102,141,0,0,0,0
write(2,290)103,1,0.00475,0.012676,0.698131,0.829030,.08255,.0889
write(2,310)1,0,103,141,0,0,0,0
c
write(2,290)104,1,0.00475,0.012184,0.829030,0.982619,0.08255,.0889
write(2,310)1,0,104,0,0,0,0,0
write(2,290)105,1,0.00475,0.010979,0.982619,1.134463,0.08255,.0889
write(2,310)1,0,105,0,0,0,0,0
write(2,290)106,1,0.00475,0.010185,1.134463,1.308995,0.08255,.0889
write(2,310)1,0,106,0,0,0,0,0
write(2,290)107,1,0.00475,0.009693,1.308995,1.570795,0.08255,.0889
write(2,310)1,0,107,0,0,0,0,0
write(2,290)108,1,0.00475,0.009693,1.570795,1.832594,0.08255,.0889
write(2,310)1,0,108,0,0,0,0,0
write(2,290)109,1,0.00475,0.010185,1.832594,2.007126,0.08255,.0889
write(2,310)1,0,109,0,0,0,0,0
write(2,290)110,1,0.00475,0.010979,2.007126,2.158970,0.08255,.0889
write(2,310)1,0,110,0,0,0,0,0
write(2,290)111,1,0.00475,0.012459,2.158970,2.356192,0.08255,.0889
write(2,310)1,0,111,0,0,0,0,0
write(2,290)112,1,0.00475,0.011497,2.356192,3.141590,0.08255,.0889
write(2,310)1,0,112,0,0,0,0,0
c
c z1-6
```

```
write(2,290)113,1,0.00475,0.009598,0.0,0.174532,0.0,0.0381
write(2,310)1,0,113,0,0,0,0,0
write(2,290)114,1,0.00475,0.009904,0.174532,0.349065,0.0,0.0381
write(2,310)1,0,114,0,0,0,0,0
write(2,290)115,1,0.00475,0.010567,0.349065,0.523598,0.0,0.0381
write(2,310)1,0,115,0,0,0,0,0
write(2,290)116,1,0.00475,0.011716,0.523598,0.698131,0.0,0.0381
write(2,310)1,0,116,0,0,0,0,0
write(2,290)117,1,0.00475,0.012676,0.698131,0.829030,0.0,0.0381
write(2,310)1,0,117,0,0,0,0,0
c
write(2,290)118,1,0.00475,0.012184,0.829030,0.982619,0.0,0.0381
write(2,310)1,0,118,0,0,0,0,0
write(2,290)119,1,0.00475,0.010979,0.982619,1.134463,0.0,0.0381
write(2,310)1,0,119,0,0,0,0,0
write(2,290)120,1,0.00475,0.010185,1.134463,1.308995,0.0,0.0381
write(2,310)1,0,120,0,0,0,0,0
write(2,290)121,1,0.00475,0.009693,1.308995,1.570795,0.0,0.0381
write(2,310)1,0,121,0,0,0,0,0
write(2,290)122,1,0.00475,0.009693,1.570795,1.832594,0.0,0.0381
write(2,310)1,0,122,0,0,0,0,0
write(2,290)123,1,0.00475,0.010185,1.832594,2.007126,0.0,0.0381
write(2,310)1,0,123,0,0,0,0,0
write(2,290)124,1,0.00475,0.010979,2.007126,2.158970,0.0,0.0381
write(2,310)1,0,124,0,0,0,0,0
write(2,290)125,1,0.00475,0.012459,2.158970,2.356192,0.0,0.0381
write(2,310)1,0,125,0,0,0,0,0
write(2,290)126,1,0.00475,0.011497,2.356192,3.141590,0.0,0.0381
write(2,310)1,0,126,0,0,0,0,0
c
c z14-19
write(2,290)127,1,0.00475,0.009598,0.0,0.174532,0.0889,0.127
write(2,310)1,0,127,0,0,0,0,0
write(2,290)128,1,0.00475,0.009904,0.174532,0.349065,0.0889,0.127
write(2,310)1,0,128,0,0,0,0,0
write(2,290)129,1,0.00475,0.010567,0.349065,0.523598,0.0889,0.127
write(2,310)1,0,129,0,0,0,0,0
write(2,290)130,1,0.00475,0.011716,0.523598,0.698131,0.0889,0.127
write(2,310)1,0,130,0,0,0,0,0
write(2,290)131,1,0.00475,0.012676,0.698131,0.829030,0.0889,0.127
write(2,310)1,0,131,0,0,0,0,0
c
write(2,290)132,1,0.00475,0.012184,0.829030,0.982619,0.0889,0.127
write(2,310)1,0,132,0,0,0,0,0
write(2,290)133,1,0.00475,0.010979,0.982619,1.134463,0.0889,0.127
```

```
write(2,310)1,0,133,0,0,0,0,0
write(2,290)134,1,0.00475,0.010185,1.134463,1.308995,0.0889,0.127
write(2,310)1,0,134,0,0,0,0,0
write(2,290)135,1,0.00475,0.009693,1.308995,1.570795,0.0889,0.127
write(2,310)1,0,135,0,0,0,0,0
write(2,290)136,1,0.00475,0.009693,1.570795,1.832594,0.0889,0.127
write(2,310)1,0,136,0,0,0,0,0
write(2,290)137,1,0.00475,0.010185,1.832594,2.007126,0.0889,0.127
write(2,310)1,0,137,0,0,0,0,0
write(2,290)138,1,0.00475,0.010979,2.007126,2.158970,0.0889,0.127
write(2,310)1,0,138,0,0,0,0,0
write(2,290)139,1,0.00475,0.012459,2.158970,2.356192,0.0889,0.127
write(2,310)1,0,139,0,0,0,0,0
write(2,290)140,1,0.00475,0.011497,2.356192,3.141590,0.0889,0.127
write(2,310)1,0,140,0,0,0,0,0
c
write(2,260)'MATERIALS'
320 format(i2,2x,a6,2x,i2,2x,f5.0,2x,f4.0,2x,i2,2x,i2,2x,i2,2x,i2)
write(2,320)1,'Copper',0,8933.,385.,-1,0,0,0
write(2,260)'INITIAL TEMPERATURES'
330 format(i2,2x,f5.2)
write(2,330)1,tin
write(2,260)'BOUNDARY CONDITIONS'
350 format(i3,2x,i2,2x,f9.1)
360 format(f9.0)
inum=0
do 1150 j=6,13
do 370 i=1,14
inum=inum+1
write(2,350)inum,1,tb(j)
write(2,360)h1(i,j)
370 continue
1150 continue
c do 1160 j=1,5
do 374 i=1,14
inum=inum+1
write(2,350)inum,1,tb(3)
write(2,360)h1(i,3)
374 continue
c1160 continue
c do 1170 j=14,18
do 376 i=1,14
inum=inum+1
write(2,350)inum,1,tb(16)
write(2,360)h1(i,16)
```

```
376 continue
c1170 continue
c
write(2,280)141,1
390 format(i2,2x,i2,2x,i2,2x,i2,2x,g9.3)
write(2,390)0,0,0,0,qdp
write(2,260)'XGRID'
400 format(8(f8.6,1x))
401 format('@',8(f8.6,1x))
410 format(8(i2,2x))
411 format('@',8(i2,2x))
412 format(8(i2,2x)/'@',2(i2,2x))
413 format(8(f8.6,1x)/'@',8(f8.6,1x))
r1=.00475
r2=.009598
r3=.009693
r4=.009904
r5=.010185
r6=.010567
r7=.010979
r8=.011497
write(2,400)r1,r2,r3,r4,r5,r6,r7,r8
write(2,401).0117160,.0121840,.0124590,.0126760
write(2,410)1,1,1,1,1,1,1,1
write(2,411)1,1,1,1
write(2,260)'YGRID'
s1=0.
s2=.174532
s3=.349065
s4=.523598
s5=.698131
s6=.829030
s7=.982619
s8=1.134463
write(2,400)s1,s2,s3,s4,s5,s6,s7,s8
s9=1.308995
s10=1.570795
s11=1.832594
s12=2.007126
s13=2.15897
s14=2.356192
s15=3.14159
write(2,401)s9,s10,s11,s12,s13,s14,s15
write(2,410)1,1,1,1,1,1,1,1
write(2,411)1,1,1,1,1,1,1,1
```

```
write(2,260)'ZGRID'
write(2,413)0.0,0.0381,0.04445,0.0508,0.05715,.0635,.06985,.0762,
10.08255,0.0889,0.127
write(2,412)5,1,1,1,1,1,1,1,1,5
write(2,260)'TABULAR FUNCTIONS'
write(2,410)1
420 format(f2.1,11(1x,f5.0))
write(2,420)0.,401.,200.,389.,400.,378.,600.,366.,800.,352.,1000.,
1336.
write(2,260)'STEADY-STATE'
write(2,460)1,10000
460 format(i2,2x,i5)
write(2,260)'%'
c
c rerun heat5
if(npass.eq.0)then
npass=1
goto 1200
else
endif
write(*,510)
510 format(' Please run "h7 -i fh7" to continue iteration')
write(*,520)
520 format(' Then run "h7map" using plot000 and plot.out')
write(*,530)
530 format(' Then rerun "drh7" using plot.out')
endif
70 continue
c
open(unit=5,file=finp,status='old')
do 822 i=1,3
read(5,20)desc
822 continue
do 970 i3=15,1,-1
read(5,830)y1(1,i3)
970 continue
do 850 j=2,19
830 format(17x,f7.2)
do 840 i=1,6
read(5,20)desc
840 continue
do 980 i3=15,1,-1
read(5,830)y1(j,i3)
980 continue
850 continue
```

```
close(unit=5)
c
open(unit=5,file=finp,status='old')
do 890 i=1,3
read(5,20)desc
890 continue
c
read(5,905)y2(1,15)
read(5,910)y2(1,14)
read(5,910)y2(1,13)
read(5,915)y2(1,12)
read(5,920)y2(1,11)
read(5,925)y2(1,10)
read(5,920)y2(1,9)
read(5,915)y2(1,8)
read(5,930)y2(1,7)
read(5,935)y2(1,6)
read(5,935)y2(1,5)
read(5,955)y2(1,4)
read(5,940)y2(1,3)
read(5,942)y2(1,2)
read(5,945)y2(1,1)
905 format(17x,7(8x),f7.2)
910 format(17x,10(8x),f7.2)
915 format(17x,6(8x),f7.2)
920 format(17x,4(8x),f7.2)
925 format(17x,2(8x),f7.2)
930 format(17x,9(8x),f7.2)
935 format(17x,11(8x),f7.2)
940 format(17x,5(8x),f7.2)
942 format(17x,3(8x),f7.2)
945 format(17x,1(8x),f7.2)
955 format(17x,8(8x),f7.2)
c
do 990 j=2,19
do 1000 i=1,6
read(5,20)desc
1000 continue
read(5,905)y2(j,15)
read(5,910)y2(j,14)
read(5,910)y2(j,13)
read(5,915)y2(j,12)
read(5,920)y2(j,11)
read(5,925)y2(j,10)
read(5,920)y2(j,9)
```

```
read(5,915)y2(j,8)
read(5,930)y2(j,7)
read(5,935)y2(j,6)
read(5,935)y2(j,5)
read(5,955)y2(j,4)
read(5,940)y2(j,3)
read(5,942)y2(j,2)
read(5,945)y2(j,1)
990 continue
c
close(unit=5)
do 960 i=1,15
ang=180.*x2(i)/3.14159
do 860 i=1,19
write(7,810)x(j),ang,y1(j,i),y2(j,i)
860 continue
960 continue
810 format(6(f12.6,1x))
c
stop
end
```

C.5 Fortran Code *dr2s.for* subroutine called by *sh2.for*

```
subroutine heau(qdp,vel,p,tl,q,h,hsh,tbk,hdb,tw)
    implicit double precision (a-h,o-z)
    c
    dimension progaz(18)
    c
    c Physical Constant or Unit Change
    c
    Data chhiv/1.7196904 d-06/
    c
    c Constants For TSAT Calculation and its Derivatives
    c
    Data ts1 /+0.010293 d0/
    Data ts2 /+0.38048 d0/
    Data ts3 /+1.7934 d0/
    Data ts4 /+28.553 d0/
    Data ts5 /+99.63 d0/
    Data dts1 /+0.041172 d0/
    Data dts2 /+1.14144 d0/
    Data dts3 /+3.5868 d0/
    Data dts4 /+28.553 d0/
    c
    c Constants for HLSAT Calculation and its Derivatives
    c
    Data hl1 /+0.18637 d-02/
    Data hl2 /-0.50352 d+05/
    Data hl3 /+0.3654 d-12/
    Data hl4 /-0.30413 d-05/
    Data hl5 /+0.40047 d+04/
    Data hl6 /-0.95261 d-08/
    Data hl7 /-0.25785 d0/
    Data hl8 /+0.20641 d+08/
    c
    c Constants for TV, CPV Calculation and their Derivatives
    c
    Data a10 /-22. d0/
    Data a11 /1.093 d-5/
    Data b10 /-1. d-5/
    Data b11 /6.75 d-13/
    Data b13 /-0.7 d-27/
    Data c13 /-.18 d-25/
```

```
Data c12 /0.748 d-18/
Data c11 /-0.104 d-10/
Data c10 /+4.6 d-04/
c
c Constants for ROLIQ Calculation and its Derivatives
c
Data r41 /+0.50507 d-30/
Data r42 /-0.58821 d-22/
Data r31 /-0.83829 d-24/
Data r32 /+0.17239 d-15/
Data r21 /+0.85471 d-18/
Data r22 /-0.29179 d-09/
Data r11 /+0.48157 d-06/
Data r12 /+0.99916 d+03/
c
c Constants for ROVAP Calculation and its Derivatives
c
Data a1 /-5.102602362 d-05/
Data a2 /+1.120801432 d-10/
Data a3 /-4.450559764 d+05/
Data b1 /-1.689303841 d-10/
Data b2 /-3.398017873 d-17/
Data b3 /+2.305760761 d-01/
c
c Constants for CONLIQ Calculation and its Derivatives
c
Data ak0 /5.73738622 d-01/
Data ak1 /2.536103551 d-01/
Data ak2 /-1.45468269 d-01/
Data ak3 /1.387472485 d-02/
c
c Constants for the convergence of hvet of pv
c
Data epsh,epsp /1.d0,1.d3/
c
c Molar mass of vapor
c
Data xmv /18.d0/
c
c Bounds given as an indication (defined in ALOCOM)
c
c For Pressure:
Data xpm,xpp /0.01d05,221d05/
c For Liquid enthalpy:
Data xhlm,xhlp /42100.,2.0d6/
```

```
c For Steam enthalpy:
Data xhvm,xhvp /1.,1.d8/
c
c Reset common drivo
dlalsp=0.0d0
dsighl=0.0d0
c
9900 format(2x,' >>>>>>> Out of bounds in fpeau: P = ',d15.7,' Pa')
9910 format(2x,' >>>>>>> Out of bounds in fpeau: hl = ',d15.7,' J/k
1g hv = ',d15.7,' J/kg')
9920 format(2x,' >>>>>>> Out of bounds in fpeau: tg = ',d15.7)
9930 format(2x,' >>>>>>> Out of bounds in fpeau: tsat = ',d15.7,'
1 sigmal = ',d15.7)
9940 format(2x,' >>>>>>> Out of bounds in fpeau: The value of pv is
1 ',d15.7,' Pa')
9950 format(2x,' >>> No convergence after 50 iterations in fpeau',/,2
1x,'P = ',d15.7,' Pa hg = ',d15.7,' J/kg')
c
c-------------------------------------------------
c BETWEEN LINE IS MAKESHIFT DATA ENTRY
c
x1=0.d0
x2=0.d0
incond=0
indic=0
ider=0
c
tcrit=376.
c tdum=0.
pbar=p/100000.
pv=p
diam=0.0095
q0=q
pt=log(pbar)
tsatp=(((ts1*pt+ts2)*pt+ts3)*pt+ts4)*pt+ts5
100 continue
npass=0
if(ncpass.eq.1)goto 666
nfilm=0
nwall=0
nho=0
nonb=0
ncrit=0
c
c Assuming minimum temperature is 10 C:
```

```
hl=40000.
c
c-------------------------------------------------------
c
if(p.gt.xpp.or.p.le.xpm)then
limite=1
write(*,9900)p
goto 9999
endif
umx1x2=1.d0-x1-x2
ifin=0
pv=p*umx1x2
c
c LABEL 70 IS A LOOP TO INCREMENTALLY FIND LIQUID ENTHALPY
c
c Calculation of TSAT(P) HLSAT(P) HVSAT(P) TL
c Unit Change
c
pmeg=p/1.0d6
tsatp=(((ts1*pt+ts2)*pt+ts3)*pt+ts4)*pt+ts5
c
if(npass.eq.0) then
npass=1
else
endif
ph1=hl1*p+hl2
ph2=(hl3*p+hl4)*p+hl5
ph3=(hl6*p+hl7)*p+hl8
ph4=1.d0/(399.98d0-tsatp)
hlsp=ph1+ph2*tsatp+ph3*ph4
cha1=-0.17638d-2*hlsp+0.68525d+4
cha2=(221.2d05-p)**0.35d0
hvsp=hlsp+cha1*cha2
c
70 continue
2000 continue
c
adet=hl-ph1+399.98d0*ph2
det=adet*adet+4.d0*ph2*((ph1-hl)*399.98d0+ph3)
tl2=(adet-sqrt(det))/(2.d0*ph2)
c
if(abs(tl2-tl).le.0.25)goto 60
if(tl2.ge.tl)goto 60
hl=hl+1000.
goto 70
```

```
c
60 continue
c
ph5=1.d0/(399.98d0-tl)
dtssp=(((dts1*pt+dts2)*pt+dts3)*pt+dts4)/p
dph1=hl1
dph2=2.d0*hl3*p+hl4
dph3=2.d0*hl6*p+hl7
dhlsp=(ph2+ph3*ph4*ph4)*dtssp+dph1+dph2*tsatp+dph3*ph4
dhvsp=dhlsp+cha2*(-0.17638d-02*dhlsp-0.35d0*cha1/(221.2d+05-p))
dtldhl=1.d0/(ph2+ph3*ph5*ph5)
dtldp=-dtldhl*(dph1+dph2*tl+dph3*ph5)
c
c Routine to calculate HV from TL using TSATP=TL add 7 to var
c Works because no condensible gases for now (11-8-91)
c
hlsp7=ph1+ph2*tl+ph3*ph4
cha17=-0.17638d-2*hlsp7+0.68525d+4
c cha2=(221.2d05-p)**0.35d0
hg=hlsp7+cha17*cha2
c
c Initialization of HV for beginning of iterations
c
if(incond.eq.0)then
hv=hg
else
c
pbar=pv*1.d-5
if(pbar.gt.1.d-1)then
pt=log(pbar)
tsatpv=(((ts1*pt+ts2)*pt+ts3)*pt+ts4)*pt+ts5
else
pt=log(1.d-1)
xxk=(((ts1*pt+ts2)*pt+ts3)*pt+ts4)*pt+ts5
xxks=(((dts1*pt+dts2)*pt+dts3)*pt+dts4)/1.d-1
xxc=1.d-1
xxa=(xxks*.1-xxk+xxc)/1.d-2
xxb=-xxks+20.d0*(xxk-xxc)
tsatpv=xxa*pbar*pbar+xxb*pbar+xxc
endif
c
ph1=hl1*pv+hl2
ph2v=(hl3*pv+hl4)*pv+hl5
ph3v=(hl6*pv+hl7)*pv+hl8
ph4=1.d0/(399.98d0-tsatpv)
```

```
hlspv=ph1+ph2v*tsatpv+ph3v*ph4
cha1=-0.17638d-2*hlspv+0.68525d+4
cha2=(221.2d05-pv)**0.35d0
hvspv=hlspv+cha1+cha2
acpv=2000.d0+pv*1.d-4
deltg=273.16d0
zerhvs=hvspv-acpv*deltg
zdeno=x1*c1ic+x2*c2ic+umx1x2*acpv
atv=(hg-zerhvs*umx1x2-deltg*(x1*c1ic+x2*c2ic))/zdeno
hv=acpv*atv+zerhvs
endif
c
c Calculation of TSAT(PV), HLSAT(PV), HVSAT(PV),TV=TG
c Calculation of PV HV by iteration in case of incondensables
c
valh=epsh
valp=epsp*umx1x2
valp=max(valp,5.d0)
c
c Verification of PV value
c
if(pv.gt.221.d+5)then
write(*,9940)pv
c goto 9999
endif
if(pv.gt.p)pv=p
if(pv.lt.0.d0)pv=0.d0
if(incond.eq.0)then
tsatpv=tsatp
hlspv=hlsp
hvspv=hvsp
dtsspv=dtssp
dhlspv=dhlsp
dhvspv=dhvsp
endif
hvmhvs=hv-hvspv
c
c Calculation of TG and derivatives
c
a=a10+a11*pv
b=b10+b11*pv+b13*pv*pv*pv
c=((c13*pv+c12)*pv+c11)*pv+c10
db=b11+3.d0*b13*pv*pv
dc=(3.d0*c13*pv+2.d0*c12)*pv+c11
if(hvmhvs.gt.0.d0)then
```

```
ebdh=exp(b*hvmhvs)
tg=tsatpv+a*(ebdh-1.d0)+c*hvmhvs
dtgdpv=dtsspv-(c+a*b*ebdh)*dhvspv+a11*(ebdh-1.d0)+a*ebdh*
1hvmhvs*db+dc*hvmhvs
dtgdhv=a*b*ebdh+c
else
dtgdhv=a*b+c
tg=tsatpv+hvmhvs*dtgdhv
d2dhdp=a11*b+db*a+dc
dtgdpv=dtsspv-dtgdhv*dhvspv+hvmhvs*d2dhdp
endif
c
c Calculation of ROVAP and derivatives
c
if(pv.ne.0.d0)then
pinv=1.d0/pv
auxv=b1+b2*pv+b3*pinv
if(hv.ge.hvspv)then
rovap=1.d0/(a1+a2*pv+a3*pinv+hv*auxv)
drvspv=-(a2+b2*hv-(a3+b3*hv)*pinv*pinv)*rovap*rovap
drvshv=-auxv*rovap*rovap
else
rovaps=1.d0/(a1+a2*pv+a3*pinv+hvspv*auxv)
rovap=(1.d0-hvmhvs*auxv*rovaps)*rovaps
drvshv=-auxv*rovaps*rovaps
drvs=-(a2+b2*hvspv-(a3+b3*hvspv)*pinv*pinv)*rovaps*rovaps
drvdhs=rovaps*((-b2+b3*pinv*pinv)*rovaps-2.d0*auxv*(drvs+
1dhvspv*drvshv))
drvspv=drvs+hvmhvs*drvdhs
endif
else
rovap=zero
drvspv=1.d0/a3+hv*b3
drvshv=zero
endif
tgkp1=tg+273.16d0
tgkp2=tg+273.16d0
tgk=tg+273.16d0
c
c Control of parameters HL and HV
c rev5
c
xhlm=100.00
if(hl.gt.xhlp.or.hl.le.xhlm.or.hv.gt.xhvp.or.hv.le.xhvm)then
limite=1
```

```
write(*,9910)hl,hv
hdb=10000
h=10000
hsh=10000
goto 9999
endif
c
c Control of TG (greater than 0K and less than 2000C)
c
if(tg.le.-273.d0.or.tg.gt.2000.d0)then
write(*,9920)tg
limite=1
endif
c
c Calculation of ROGAZ and derivatives
c
rogaz=rovap
c
c Calculation of ROLIQ and derivatives and ROLS
c
r4=r41*p+r42
r3=r31*p+r32
r2=r21*p+r22
r1=r11*p+r12
roliq=((r4*hl+r3)*hl+r2)*hl*hl+r1
rols=((r4*hlsp+r3)*hlsp+r2)*hlsp*hlsp+r1
c
c Calculation of the Water Surface Tension
c
sigmal = 0.78078d-01 - 0.2104809d-03*tsatp
if(sigmal.le.0.d0)then
limite=1
write(*,9930)tsatp,sigmal
c goto 9999
endif
c
c Calculation of the Water Dynamic Viscosity TMULIQ
c Calculation of the Water Conductivity CONLIQ
c
auxmu1=1.d0/(tl+133.15d0)
tmuliq=2.414d-5*exp(570.58058d0*auxmu1)
c Calculation of water saturated viscosity tmuls
auxmus1=1.d0/(tsatp+133.15d0)
tmuls=2.414d-5*exp(570.58058d0*auxmus1)
xk=hl*chhiv
```

```
conliq=((ak3*xk+ak2)*xk+ak1)*xk+ak0
ph42=ph5*ph5
cpliq=ph2+ph3*ph42
c
c Calculation of TMUGAZ CPGAZ CONGAZ
c
ala=al0+al1*pv
bla=bl0+bl1*pv
cla=cl0+cl1*pv
convap=ala*tg*tg+bla*tg+cla
tmuvap=(3.85d-8*tg+1.0d-5)
if(incond.eq.0)then
congaz=convap
tmugaz=tmuvap
endif
if(tmugaz.lt.1.d-6)tmugaz=1.d-6
if(congaz.lt.0.005d0)congaz=0.005d0
c
c For CPGAZ
if(hvmhvs.gt.0.d0)then
cpvap=1.d0/(a*b*ebdh+c)
else
cpvap=1.d0/(a*b+c)
endif c
cpgaz=x1*c1ic+x2*c2ic+umx1x2*cpvap
c 666 bypass
666 continue
c
c Dittus-Boelter single phase liquid
c re=roliq*vel*diam/tmuliq
pr=tmuliq*cpliq/conliq
spnu=0.023*re**.8*pr**.4
hdb=spnu*conliq/diam
c
c Petukhov single phase liquid
c
pec=pr*re
fpet=1/((0.7904*log(re)-1.64)**2)
petk1=1+3.4*fpet
petk2=11.7+1.8/pr**(1/3)
hpet=conliq*fpet*pec/(diam*8.)
h=hpet/(petk1+petk2*(fpet/8.)**.5*(pr**(2/3)-1))
c
c Thom Correlation for Fully Developed Subcooled Boiling
c
```

```
c tnb=tsatp+22.65*exp(-pbar/87.)*(q0*1.d-6)**.5
c
c Yin Correlation for SNB
c
c gamma=1.
c tnb=7.195*q0*1.d-6*gamma**1.82*(pbar/10.)**(-0.072)
c tnb=tsatp+tnb
c
c Shah Correlation (1977) for SCB
c
gi=(vel*roliq*(hvsp-hlsp))
if(tw.le.tsatp) then
hsh=h
goto 9999
else
rdt=(tsatp-tbk)/(tw-tsatp)
endif
c
q1=hdb*(tw-tbk)
15 continue
bo=q1/gi
if(bo.lt.0.3d-4)then
phio=1.+46.*bo**.5
else
phio=230.*bo**.5
endif
c
if(rdt.le.2.)then
hsh=bo*gi/(tw-tbk)
else
hsh=(hdb*(tw-tbk)+hdb*(phio-1.)*(tw-tsatp))/(tw-tbk)
endif
q2=hsh*(tw-tbk)
if(abs(q2/q1-1.).le.0.05) goto 200
q1=(q1+q2)/2.
goto 15
c
200 continue
write(*,10)bo,gi,tw,tbk,hsh,rdt
10 format(' bo = ',g10.3,' gi = ',g10.3,' tw = ',f5.0,
/' tbk = ',f4.0,' hsh = ',f8.0,' DT = ',f4.1)
9999 continue
return
end
```

C.6 Fortran file *dr1s.for* Containing Subroutine to Calculate Water Properties

```
subroutine prop(dumb,p,tl)
    implicit double precision (a-h,o-z)
    c
    dimension progaz(18)
    c
    common/eauprops/hlsp,hvsp,roliq,rovap,cpliq,conliq,tmuliq,
    1sigmal
    c
    c Physical Constant or Unit Change
    c
    Data chhiv/1.7196904 d-06/
    c
    c Constants For TSAT Calculation and its Derivatives
    c
    Data ts1 /+0.010293 d0/
    Data ts2 /+0.38048 d0/
    Data ts3 /+1.7934 d0/
    Data ts4 /+28.553 d0/
    Data ts5 /+99.63 d0/
    Data dts1 /+0.041172 d0/
    Data dts2 /+1.14144 d0/
    Data dts3 /+3.5868 d0/
    Data dts4 /+28.553 d0/
    c
    c Constants for HLSAT Calculation and its Derivatives
    c
    Data hl1 /+0.18637 d-02/
    Data hl2 /-0.50352 d+05/
    Data hl3 /+0.3654 d-12/
    Data hl4 /-0.30413 d-05/
    Data hl5 /+0.40047 d+04/
    Data hl6 /-0.95261 d-08/
    Data hl7 /-0.25785 d0/
    Data hl8 /+0.20641 d+08/
    c
    c Constants for TV, CPV Calculation and their Derivatives
    c
    Data a10 /-22. d0/
    Data a11 /1.093 d-5/
    Data b10 /-1. d-5/
```

```
Data b11 /6.75 d-13/
Data b13 /-0.7 d-27/
Data c13 /-.18 d-25/
Data c12 /0.748 d-18/
Data c11 /-0.104 d-10/
Data c10 /+4.6 d-04/
c
c Constants for ROLIQ Calculation and its Derivatives
c
Data r41 /+0.50507 d-30/
Data r42 /-0.58821 d-22/
Data r31 /-0.83829 d-24/
Data r32 /+0.17239 d-15/
Data r21 /+0.85471 d-18/
Data r22 /-0.29179 d-09/
Data r11 /+0.48157 d-06/
Data r12 /+0.99916 d+03/
c
c Constants for ROVAP Calculation and its Derivatives
c
Data a1 /-5.102602362 d-05/
Data a2 /+1.120801432 d-10/
Data a3 /-4.450559764 d+05/
Data b1 /-1.689303841 d-10/
Data b2 /-3.398017873 d-17/
Data b3 /+2.305760761 d-01/
c
c Constants for CONLIQ Calculation and its Derivatives
c
Data ak0 /5.73738622 d-01/
Data ak1 /2.536103551 d-01/
Data ak2 /-1.45468269 d-01/
Data ak3 /1.387472485 d-02/
c
c Constants for the convergence of hvet of pv
c
Data epsh,epsp /1.d0,1.d3/
c
c Molar mass of vapor
c
Data xmv /18.d0/
c
c Bounds given as an indication (defined in ALOCOM)
c
c For Pressure:
```

```
Data xpm,xpp /0.01d05,221d05/
c For Liquid enthalpy:
Data xhlm,xhlp /42100.,2.0d6/
c For Steam enthalpy:
Data xhvm,xhvp /1.,1.d8/
c
c Reset common drivo
c dlalsp=0.0d0
c dsighl=0.0d0
c
9900 format(2x,' >>>>>>> Out of bounds in fpeau: P = ',d15.7,' Pa')
9910 format(2x,' >>>>>>> Out of bounds in fpeau: hl = ',d15.7,' J/k
1g hv = ',d15.7,' J/kg')
9920 format(2x,' >>>>>>> Out of bounds in fpeau: tg = ',d15.7)
9930 format(2x,' >>>>>>> Out of bounds in fpeau: tsat = ',d15.7,'
1 sigmal = ',d15.7)
9940 format(2x,' >>>>>>> Out of bounds in fpeau: The value of pv is
1 ',d15.7,' Pa')
9950 format(2x,' >>> No convergence after 50 iterations in fpeau',/,2
1x,'P = ',d15.7,' Pa hg = ',d15.7,' J/kg')
c
c-------------------------------------------------
c BETWEEN LINE IS MAKESHIFT DATA ENTRY
c
c subroutine heau(qdp,vel,p,tl,q,h,hsh,tbk,hdb,tw)
c
c write(*,95)p,tl
c95 format(' p = ',g8.0,' tl = ',g8.3)
x1=0.d0
x2=0.d0
incond=0
indic=0
ider=0
c
tcrit=376.
c tdum=0.
pbar=p/100000.
pv=p
pt=log(pbar)
tsatp=(((ts1*pt+ts2)*pt+ts3)*pt+ts4)*pt+ts5
100 continue
npass=0
c
c Assuming minimum temperature is 10 C:
hl=40000.
```

```
c
c-----------------------------------------------------
c
if(p.gt.xpp.or.p.le.xpm)then
limite=1
write(*,9900)p
goto 9999
endif
umx1x2=1.d0-x1-x2
ifin=0
pv=p*umx1x2
c
c LABEL 70 IS A LOOP TO INCREMENTALLY FIND LIQUID ENTHALPY
c
c Calculation of TSAT(P) HLSAT(P) HVSAT(P) TL
c Unit Change
c
pmeg=p/1.0d6
tsatp=(((ts1*pt+ts2)*pt+ts3)*pt+ts4)*pt+ts5
c
if(npass.eq.0) then
npass=1
else
endif
ph1=hl1*p+hl2
ph2=(hl3*p+hl4)*p+hl5
ph3=(hl6*p+hl7)*p+hl8
ph4=1.d0/(399.98d0-tsatp)
hlsp=ph1+ph2*tsatp+ph3*ph4
cha1=-0.17638d-2*hlsp+0.68525d+4
cha2=(221.2d05-p)**0.35d0
hvsp=hlsp+cha1*cha2
c
70 continue
2000 continue
c
adet=hl-ph1+399.98d0*ph2
det=adet*adet+4.d0*ph2*((ph1-hl)*399.98d0+ph3)
tl2=(adet-sqrt(det))/(2.d0*ph2)
c
if(abs(tl2-tl).le.0.25)goto 60
if(tl2.ge.tl)goto 60
hl=hl+1000.
goto 70
c
```

```
60 continue
c
ph5=1.d0/(399.98d0-tl)
dtssp=(((dts1*pt+dts2)*pt+dts3)*pt+dts4)/p
dph1=hl1
dph2=2.d0*hl3*p+hl4
dph3=2.d0*hl6*p+hl7
dhlsp=(ph2+ph3*ph4*ph4)*dtssp+dph1+dph2*tsatp+dph3*ph4
dhvsp=dhlsp+cha2*(-0.17638d-02*dhlsp-0.35d0*cha1/(221.2d+05-p))
dtldhl=1.d0/(ph2+ph3*ph5*ph5)
dtldp=-dtldhl*(dph1+dph2*tl+dph3*ph5)
c
c Routine to calculate HV from TL using TSATP=TL add 7 to var
c Works because no condensible gases for now (11-8-91)
c
hlsp7=ph1+ph2*tl+ph3*ph4
cha17=-0.17638d-2*hlsp7+0.68525d+4
c cha2=(221.2d05-p)**0.35d0
hg=hlsp7+cha17*cha2
c
c Initialization of HV for beginning of iterations
c
if(incond.eq.0)then
hv=hg
else
c
pbar=pv*1.d-5
if(pbar.gt.1.d-1)then
pt=log(pbar)
tsatpv=(((ts1*pt+ts2)*pt+ts3)*pt+ts4)*pt+ts5
else
pt=log(1.d-1)
xxk=(((ts1*pt+ts2)*pt+ts3)*pt+ts4)*pt+ts5
xxks=(((dts1*pt+dts2)*pt+dts3)*pt+dts4)/1.d-1
xxc=1.d-1
xxa=(xxks*.1-xxk+xxc)/1.d-2
xxb=-xxks+20.d0*(xxk-xxc)
tsatpv=xxa*pbar*pbar+xxb*pbar+xxc
endif
c
ph1=hl1*pv+hl2
ph2v=(hl3*pv+hl4)*pv+hl5
ph3v=(hl6*pv+hl7)*pv+hl8
ph4=1.d0/(399.98d0-tsatpv)
hlspv=ph1+ph2v*tsatpv+ph3v*ph4
```

```
cha1=-0.17638d-2*hlspv+0.68525d+4
cha2=(221.2d05-pv)**0.35d0
hvspv=hlspv+cha1+cha2
acpv=2000.d0+pv*1.d-4
deltg=273.16d0
zerhvs=hvspv-acpv*deltg
zdeno=x1*c1ic+x2*c2ic+umx1x2*acpv
atv=(hg-zerhvs*umx1x2-deltg*(x1*c1ic+x2*c2ic))/zdeno
hv=acpv*atv+zerhvs
endif
c
c Calculation of TSAT(PV), HLSAT(PV), HVSAT(PV),TV=TG
c Calculation of PV HV by iteration in case of incondensables
c
valh=epsh
valp=epsp*umx1x2
valp=max(valp,5.d0)
c
c Verification of PV value
c
if(pv.gt.221.d+5)then
write(*,9940)pv
c goto 9999
endif
if(pv.gt.p)pv=p
if(pv.lt.0.d0)pv=0.d0
if(incond.eq.0)then
tsatpv=tsatp
hlspv=hlsp
hvspv=hvsp
dtsspv=dtssp
dhlspv=dhlsp
dhvspv=dhvsp
endif
hvmhvs=hv-hvspv
c
c Calculation of TG and derivatives
c
a=a10+a11*pv
b=b10+b11*pv+b13*pv*pv*pv
c=((c13*pv+c12)*pv+c11)*pv+c10
db=b11+3.d0*b13*pv*pv
dc=(3.d0*c13*pv+2.d0*c12)*pv+c11
if(hvmhvs.gt.0.d0)then
ebdh=exp(b*hvmhvs)
```

```
tg=tsatpv+a*(ebdh-1.d0)+c*hvmhvs
dtgdpv=dtsspv-(c+a*b*ebdh)*dhvspv+a11*(ebdh-1.d0)+a*ebdh*
1hvmhvs*db+dc*hvmhvs
dtgdhv=a*b*ebdh+c
else
dtgdhv=a*b+c
tg=tsatpv+hvmhvs*dtgdhv
d2dhdp=a11*b+db*a+dc
dtgdpv=dtsspv-dtgdhv*dhvspv+hvmhvs*d2dhdp
endif
c
c Calculation of ROVAP and derivatives
c
if(pv.ne.0.d0)then
pinv=1.d0/pv
auxv=b1+b2*pv+b3*pinv
if(hv.ge.hvspv)then
rovap=1.d0/(a1+a2*pv+a3*pinv+hv*auxv)
drvspv=-(a2+b2*hv-(a3+b3*hv)*pinv*pinv)*rovap*rovap
drvshv=-auxv*rovap*rovap
else
rovaps=1.d0/(a1+a2*pv+a3*pinv+hvspv*auxv)
rovap=(1.d0-hvmhvs*auxv*rovaps)*rovaps
drvshv=-auxv*rovaps*rovaps
drvs=-(a2+b2*hvspv-(a3+b3*hvspv)*pinv*pinv)*rovaps*rovaps
drvdhs=rovaps*((-b2+b3*pinv*pinv)*rovaps-2.d0*auxv*(drvs+
1dhvspv*drvshv))
drvspv=drvs+hvmhvs*drvdhs
endif
else
rovap=zero
drvspv=1.d0/a3+hv*b3
drvshv=zero
endif
tgkp1=tg+273.16d0
tgkp2=tg+273.16d0
tgk=tg+273.16d0
c
c Control of parameters HL and HV
c rev5
c
xhlm=100.00
if(hl.gt.xhlp.or.hl.le.xhlm.or.hv.gt.xhvp.or.hv.le.xhvm)then
limite=1
write(*,9910)hl,hv
```

```
goto 9999
endif
c
c Control of TG (greater than 0K and less than 2000C)
c
if(tg.le.-273.d0.or.tg.gt.2000.d0)then
write(*,9920)tg
limite=1
endif
c
c Calculation of ROGAZ and derivatives
c
rogaz=rovap
c
c Calculation of ROLIQ and derivatives and ROLS
c
r4=r41*p+r42
r3=r31*p+r32
r2=r21*p+r22
r1=r11*p+r12
roliq=((r4*hl+r3)*hl+r2)*hl*hl+r1
rols=((r4*hlsp+r3)*hlsp+r2)*hlsp*hlsp+r1
c
c Calculation of the Water Surface Tension
c
sigmal = 0.78078d-01 - 0.2104809d-03*tsatp
if(sigmal.le.0.d0)then
limite=1
write(*,9930)tsatp,sigmal
c goto 9999
endif
c
c Calculation of the Water Dynamic Viscosity TMULIQ
c Calculation of the Water Conductivity CONLIQ
c
auxmu1=1.d0/(tl+133.15d0)
tmuliq=2.414d-5*exp(570.58058d0*auxmu1)
c Calculation of water saturated viscosity tmuls
auxmus1=1.d0/(tsatp+133.15d0)
tmuls=2.414d-5*exp(570.58058d0*auxmus1)
xk=hl*chhiv
conliq=((ak3*xk+ak2)*xk+ak1)*xk+ak0
ph42=ph5*ph5
cpliq=ph2+ph3*ph42
c
```

```
c Calculation of TMUGAZ CPGAZ CONGAZ
c
ala=al0+al1*pv
bla=bl0+bl1*pv
cla=cl0+cl1*pv
convap=ala*tg*tg+bla*tg+cla
tmuvap=(3.85d-8*tg+1.0d-5)
if(incond.eq.0)then
congaz=convap
tmugaz=tmuvap
endif
if(tmugaz.lt.1.d-6)tmugaz=1.d-6
if(congaz.lt.0.005d0)congaz=0.005d0
c
c For CPGAZ
if(hvmhvs.gt.0.d0)then
cpvap=1.d0/(a*b*ebdh+c)
else
cpvap=1.d0/(a*b+c)
endif
c
cpgaz=x1*c1ic+x2*c2ic+umx1x2*cpvap
c
9999 continue
return
end
```

C.7 Fortran file *drch.for* Containing Chen Suppressed Nucleate Boiling Correlation Subroutine

```
c Chen Correlation for Suppressed Nucleate Boiling
      subroutine hsat(qdp,vel,p,tfilm,q,tw,sdum,tonb,tnb,hnb)
      implicit double precision (a-h,o-z)
      c
      dimension progaz(18)
      c
      c Physical Constant or Unit Change
      c
      Data chhiv/1.7196904 d-06/
      c
      c Constants For TSAT Calculation and its Derivatives
      c
      Data ts1 /+0.010293 d0/
      Data ts2 /+0.38048 d0/
      Data ts3 /+1.7934 d0/
      Data ts4 /+28.553 d0/
      Data ts5 /+99.63 d0/
      Data dts1 /+0.041172 d0/
      Data dts2 /+1.14144 d0/
      Data dts3 /+3.5868 d0/
      Data dts4 /+28.553 d0/
      c
      c Constants for HLSAT Calculation and its Derivatives
      c
      Data hl1 /+0.18637 d-02/
      Data hl2 /-0.50352 d+05/
      Data hl3 /+0.3654 d-12/
      Data hl4 /-0.30413 d-05/
      Data hl5 /+0.40047 d+04/
      Data hl6 /-0.95261 d-08/
      Data hl7 /-0.25785 d0/
      Data hl8 /+0.20641 d+08/
      c
      c Constants for TV, CPV Calculation and their Derivatives
      c
      Data a10 /-22. d0/
      Data a11 /1.093 d-5/
      Data b10 /-1. d-5/
```

```
Data b11 /6.75 d-13/
Data b13 /-0.7 d-27/
Data c13 /-.18 d-25/
Data c12 /0.748 d-18/
Data c11 /-0.104 d-10/
Data c10 /+4.6 d-04/
c
c Constants for ROLIQ Calculation and its Derivatives
c
Data r41 /+0.50507 d-30/
Data r42 /-0.58821 d-22/
Data r31 /-0.83829 d-24/
Data r32 /+0.17239 d-15/
Data r21 /+0.85471 d-18/
Data r22 /-0.29179 d-09/
Data r11 /+0.48157 d-06/
Data r12 /+0.99916 d+03/
c
c Constants for ROVAP Calculation and its Derivatives
c
Data a1 /-5.102602362 d-05/
Data a2 /+1.120801432 d-10/
Data a3 /-4.450559764 d+05/
Data b1 /-1.689303841 d-10/
Data b2 /-3.398017873 d-17/
Data b3 /+2.305760761 d-01/
c
c Constants for CONLIQ Calculation and its Derivatives
c
Data ak0 /5.73738622 d-01/
Data ak1 /2.536103551 d-01/
Data ak2 /-1.45468269 d-01/
Data ak3 /1.387472485 d-02/
c
c Constants for the convergence of hvet of pv
c
Data epsh,epsp /1.d0,1.d3/
c
c Molar mass of vapor
c
Data xmv /18.d0/
c
c Bounds given as an indication (defined in ALOCOM)
c
c For Pressure:
```

```
Data xpm,xpp /0.01d05,221d05/
c For Liquid enthalpy:
Data xhlm,xhlp /42100.,2.0d6/
c For Steam enthalpy:
Data xhvm,xhvp /1.,1.d8/
c
c Reset common drivo
dlalsp=0.0d0
dsighl=0.0d0
c
9900 format(2x,' !!!!!!!!!! Out of bounds in fpeau: P = ',d15 7,' Pa')
9910 format(2x,' !!!!!!!!!! Out of bounds in fpeau: hl = ',d15.7,' J/k
1g hv = ',d15.7,' J/kg')
9920 format(2x,' !!!!!!!!!! Out of bounds in fpeau: tg = ',d15.7)
9930 format(2x,' !!!!!!!!!! Out of bounds in fpeau: tsat = ',d15.7,'
1 sigmal = ',d15.7)
9940 format(2x,' !!!!!!!!!! Out of bounds in fpeau: The value of pv is
1 ',d15.7,' Pa')
9950 format(2x,' !!!!! No convergence after 50 iterations in fpeau',/,2
1x,'P = ',d15.7,' Pa hg = ',d15.7,' J/kg')
c
c-----------------------------------------------
c BETWEEN LINE IS MAKESHIFT DATA ENTRY
c
x1=0.d0
x2=0.d0
incond=0
indic=0
ider=0
c
tcrit=374.
pbar=p/100000.
pv=p
diam=0.0095
q0=q
pt=log(pbar)
tsatp=(((ts1*pt+ts2)*pt+ts3)*pt+ts4)*pt+ts5
tl=tsatp
100 continue
npass=0
if(ncpass.eq.1)goto 666
nfilm=0
nwall=0
nho=0
nonb=0
```

```
ncrit=0
c
c Assuming minimum temperature is 10 C:
hl=40000.
c
c-------------------------------------------------------
c
if(p.gt.xpp.or.p.le.xpm)then
limite=1
write(*,9900)p
goto 9999
endif
umx1x2=1.d0-x1-x2
ifin=0
pv=p*umx1x2
c
c LABEL 70 IS A LOOP TO INCREMENTALLY FIND LIQUID ENTHALPY
c
c Calculation of TSAT(P) HLSAT(P) HVSAT(P) TL
c Unit Change
c
pmeg=p/1.0d6
tsatp=(((ts1*pt+ts2)*pt+ts3)*pt+ts4)*pt+ts5
c
if(npass.eq.0) then
npass=1
else
endif
ph1=hl1*p+hl2
ph2=(hl3*p+hl4)*p+hl5
ph3=(hl6*p+hl7)*p+hl8
ph4=1.d0/(399.98d0-tsatp)
hlsp=ph1+ph2*tsatp+ph3*ph4
cha1=-0.17638d-2*hlsp+0.68525d+4
cha2=(221.2d05-p)**0.35d0
hvsp=hlsp+cha1*cha2
c
70 continue
2000 continue
c
c adet=hl-ph1+399.98d0*ph2
c det=adet*adet+4.d0*ph2*((ph1-hl)*399.98d0+ph3)
c tl2=(adet-sqrt(det))/(2.d0*ph2)
c tl2=tl
hl=hlsp
```

```
c goto 70
c
60 continue
c
ph5=1.d0/(399.98d0-tl)
dtssp=(((dts1*pt+dts2)*pt+dts3)*pt+dts4)/p
dph1=hl1
dph2=2.d0*hl3*p+hl4
dph3=2.d0*hl6*p+hl7
dhlsp=(ph2+ph3*ph4*ph4)*dtssp+dph1+dph2*tsatp+dph3*ph4
dhvsp=dhlsp+cha2*(-0.17638d-02*dhlsp-0.35d0*cha1/(221.2d+05-p))
dtldhl=1.d0/(ph2+ph3*ph5*ph5)
dtldp=-dtldhl*(dph1+dph2*tl+dph3*ph5)
c
c Routine to calculate HV from TL using TSATP=TL add 7 to var
c Works because no condensible gases for now (11-8-91)
c
hlsp7=ph1+ph2*tl+ph3*ph4
cha17=-0.17638d-2*hlsp7+0.68525d+4
c cha2=(221.2d05-p)**0.35d0
hg=hlsp7+cha17*cha2
c
c Initialization of HV for beginning of iterations
c
if(incond.eq.0)then
hv=hg
else
c
pbar=pv*1.d-5
if(pbar.gt.1.d-1)then
pt=log(pbar)
tsatpv=(((ts1*pt+ts2)*pt+ts3)*pt+ts4)*pt+ts5
else
pt=log(1.d-1)
xxk=(((ts1*pt+ts2)*pt+ts3)*pt+ts4)*pt+ts5
xxks=(((dts1*pt+dts2)*pt+dts3)*pt+dts4)/1.d-1
xxc=1.d-1
xxa=(xxks*.1-xxk+xxc)/1.d-2
xxb=-xxks+20.d0*(xxk-xxc)
tsatpv=xxa*pbar*pbar+xxb*pbar+xxc
endif
c
ph1=hl1*pv+hl2
ph2v=(hl3*pv+hl4)*pv+hl5
ph3v=(hl6*pv+hl7)*pv+hl8
```

```
ph4=1.d0/(399.98d0-tsatpv)
hlspv=ph1+ph2v*tsatpv+ph3v*ph4
cha1=-0.17638d-2*hlspv+0.68525d+4
cha2=(221.2d05-pv)**0.35d0
hvspv=hlspv+cha1+cha2
acpv=2000.d0+pv*1.d-4
deltg=273.16d0
zerhvs=hvspv-acpv*deltg
zdeno=x1*c1ic+x2*c2ic+umx1x2*acpv
atv=(hg-zerhvs*umx1x2-deltg*(x1*c1ic+x2*c2ic))/zdeno
hv=acpv*atv+zerhvs
endif
c
c Calculation of TSAT(PV), HLSAT(PV), HVSAT(PV),TV=TG
c Calculation of PV HV by iteration in case of incondensables
c
valh=epsh
valp=epsp*umx1x2
valp=max(valp,5.d0)
c
c Verification of PV value
c
if(pv.gt.221.d+5)then
write(*,9940)pv
c goto 9999
endif
if(pv.gt.p)pv=p
if(pv.lt.0.d0)pv=0.d0
if(incond.eq.0)then
tsatpv=tsatp
hlspv=hlsp
hvspv=hvsp
dtsspv=dtssp
dhlspv=dhlsp
dhvspv=dhvsp
endif
hvmhvs=hv-hvspv
c
c Calculation of TG and derivatives
c
a=a10+a11*pv
b=b10+b11*pv+b13*pv*pv*pv
c=((c13*pv+c12)*pv+c11)*pv+c10
db=b11+3.d0*b13*pv*pv
dc=(3.d0*c13*pv+2.d0*c12)*pv+c11
```

```
if(hvmhvs.gt.0.d0)then
ebdh=exp(b*hvmhvs)
tg=tsatpv+a*(ebdh-1.d0)+c*hvmhvs
dtgdpv=dtsspv-(c+a*b*ebdh)*dhvspv+a11*(ebdh-1.d0)+a*ebdh*
1hvmhvs*db+dc*hvmhvs
dtgdhv=a*b*ebdh+c
else
dtgdhv=a*b+c
tg=tsatpv+hvmhvs*dtgdhv
d2dhdp=a11*b+db*a+dc
dtgdpv=dtsspv-dtgdhv*dhvspv+hvmhvs*d2dhdp
endif
c
c Calculation of ROVAP and derivatives
c
if(pv.ne.0.d0)then
pinv=1.d0/pv
auxv=b1+b2*pv+b3*pinv
if(hv.ge.hvspv)then
rovap=1.d0/(a1+a2*pv+a3*pinv+hv*auxv)
drvspv=-(a2+b2*hv-(a3+b3*hv)*pinv*pinv)*rovap*rovap
drvshv=-auxv*rovap*rovap
else
rovaps=1.d0/(a1+a2*pv+a3*pinv+hvspv*auxv)
rovap=(1.d0-hvmhvs*auxv*rovaps)*rovaps
drvshv=-auxv*rovaps*rovaps
drvs=-(a2+b2*hvspv-(a3+b3*hvspv)*pinv*pinv)*rovaps*rovaps
drvdhs=rovaps*((-b2+b3*pinv*pinv)*rovaps-2.d0*auxv*(drvs+
1dhvspv*drvshv))
drvspv=drvs+hvmhvs*drvdhs
endif
else
rovap=zero
drvspv=1.d0/a3+hv*b3
drvshv=zero
endif
tgkp1=tg+273.16d0
tgkp2=tg+273.16d0
tgk=tg+273.16d0
c
c Control of parameters HL and HV
c rev5
c
xhlm=100.00
if(hl.gt.xhlp.or.hl.le.xhlm.or.hv.gt.xhvp.or.hv.le.xhvm)then
```

```
limite=1
write(*,9910)hl,hv
tonb=tsatp
tnb=tonb
h=10000
goto 9999
endif
c
c Control of TG (greater than 0K and less than 2000C)
c
if(tg.le.-273.d0.or.tg.gt.2000.d0)then
write(*,9920)tg
limite=1
endif
c
c Calculation of ROGAZ and derivatives
c
rogaz=rovap
c
c Calculation of ROLIQ and derivatives and ROLS
c
r4=r41*p+r42
r3=r31*p+r32
r2=r21*p+r22
r1=r11*p+r12
roliq=((r4*hl+r3)*hl+r2)*hl*hl+r1
rols=((r4*hlsp+r3)*hlsp+r2)*hlsp*hlsp+r1
c
c Calculation of the Water Surface Tension
c sigmal = 0.78078d-01 - 0.2104809d-03*tsatp
if(sigmal.le.0.d0)then
limite=1
write(*,9930)tsatp,sigmal
c goto 9999
endif
c
c Calculation of the Water Dynamic Viscosity TMULIQ
c Calculation of the Water Conductivity CONLIQ
c
auxmul=1.d0/(tl+133.15d0)
tmuliq=2.414d-5*exp(570.58058d0*auxmul)
c Calculation of water saturated viscosity tmuls
auxmusl=1.d0/(tsatp+133.15d0)
tmuls=2.414d-5*exp(570.58058d0*auxmusl)
xk=hl*chhiv
```

```
conliq=((ak3*xk+ak2)*xk+ak1)*xk+ak0
ph42=ph5*ph5
cpliq=ph2+ph3*ph42
c
c Calculation of TMUGAZ CPGAZ CONGAZ
c
ala=al0+al1*pv
bla=bl0+bl1*pv
cla=cl0+cl1*pv
convap=ala*tg*tg+bla*tg+cla
tmuvap=(3.85d-8*tg+1.0d-5)
if(incond.eq.0)then
congaz=convap
tmugaz=tmuvap
endif
if(tmugaz.lt.1.d-6)tmugaz=1.d-6
if(congaz.lt.0.005d0)congaz=0.005d0
c
c For CPGAZ
if(hvmhvs.gt.0.d0)then
cpvap=1.d0/(a*b*ebdh+c)
else
cpvap=1.d0/(a*b+c)
endif
c
cpgaz=x1*c1ic+x2*c2ic+umx1x2*cpvap
c 666 bypass
666 continue
c
c Yin Correlation for Onset of Nucleate Boiling
c
twonb=1800.*q0*sigmal*(tsatp+273.15)/((hvsp-hlsp)*rovap*conliq)
c
c Davis-Anderson Correlation for onb
c twonb=8.*q0*sigmal*(tsatp+273.15)/((hvsp-hlsp)*rovap*conliq)
c
tonb=tsatp+twonb**.5
c tnb=tsatp+twonb**.5
c
c Dittus-Boelter single phase liquid
c
re=roliq*vel*diam/tmuliq
pr=tmuliq*cpliq/conliq
spnu=0.023*re**.8*pr**.4
c
```

```
c Petukhov single phase liquid
c
pec=pr*re
fpet=1/((0.7904*log(re)-1.64)**2)
petk1=1+3.4*fpet
petk2=11.7+1.8/pr**(1/3)
hpet=conliq*fpet*pec/(diam*8.)
hpet=hpet/(petk1+petk2*(fpet/8.)**.5*(pr**(2/3)-1))
c
c Thom Correlation for Fully Developed Subcooled Boiling
c
c tnb=tsatp+22.65*exp(-pbar/87.)*(q0*1.d-6)**.5
c
c Yin Correlation for SNB
c
c gamma=1.
c tnb=7.195*q0*1.d-6*gamma**1.82*(pbar/10.)**(-0.072)
c tnb=tsatp+tnb
c
c Chen Correlation for NB
c
psatt=-1.1482d5+5632.*tw-83.773*tw*tw+0.53707*tw*tw*tw
1-7.4056d-4*tw*tw*tw*tw+2.4798d-6*tw**5.
sdum=1/(1.+2.53e-6*re**1.17)
hnb=0.00122*conliq**.79*cpliq**0.45*roliq**0.49
1*(tw-tsatp)**0.24*(psatt-p)**.75/(sigmal**.5*tmuliq**.29*
2(hvsp-hlsp)**.24*rovap**.24)
200 continue
9999 continue
return
end
```

C.8 A Sample *fh7* Input File to HEATING7.2

```
3D Conduction Profile of Test SectionTS17B
   * Copper structure, water coolant
   * Units: J, kg, s, m, C
   * Iteration using heating7
   * htc.dat defines thermal parameters
   10000 1 0 1
   REGIONS
   1 1 .00475 .009598 .000000 .174532 .03810 .04445
   1 0 1 141 0 0 0 0
   2 1 .00475 .009904 .174532 .349065 .03810 .04445
   1 0 2 141 0 0 0 0
   3 1 .00475 .010567 .349065 .523598 .03810 .04445
   1 0 3 141 0 0 0 0
   4 1 .00475 .011716 .523598 .698131 .03810 .04445
   1 0 4 141 0 0 0 0
   5 1 .00475 .012676 .698131 .829030 .03810 .04445
   1 0 5 141 0 0 0 0
   6 1 .00475 .012184 .829030 .982619 .03810 .04445
   1 0 6 0 0 0 0 0
   7 1 .00475 .010979 .982619 1.134463 .03810 .04445
   1 0 7 0 0 0 0 0
   8 1 .00475 .010185 1.134463 1.308995 .03810 .04445
   1 0 8 0 0 0 0 0
   9 1 .00475 .009693 1.308995 1.570795 .03810 .04445
   1 0 9 0 0 0 0 0
   10 1 .00475 .009693 1.570795 1.832594 .03810 .04445
   1 0 10 0 0 0 0 0
   11 1 .00475 .010185 1.832594 2.007126 .03810 .04445
   1 0 11 0 0 0 0 0
   12 1 .00475 .010979 2.007126 2.158970 .03810 .04445
   1 0 12 0 0 0 0 0
   13 1 .00475 .012459 2.158970 2.356192 .03810 .04445
   1 0 13 0 0 0 0 0
   14 1 .00475 .011497 2.356192 3.141590 .03810 .04445
   1 0 14 0 0 0 0 0
   15 1 .00475 .009598 .000000 .174532 .04445 .05080
   1 0 15 141 0 0 0 0
   16 1 .00475 .009904 .174532 .349065 .04445 .05080
   1 0 16 141 0 0 0 0
   17 1 .00475 .010567 .349065 .523598 .04445 .05080
   1 0 17 141 0 0 0 0
   18 1 .00475 .011716 .523598 .698131 .04445 .05080
```

1 0 18 141 0 0 0 0
19 1 .00475 .012676 .698131 .829030 .04445 .05080
1 0 19 141 0 0 0 0
20 1 .00475 .012184 .829030 .982619 .04445 .05080
1 0 20 0 0 0 0 0
21 1 .00475 .010979 .982619 1.134463 .04445 .05080
1 0 21 0 0 0 0 0
22 1 .00475 .010185 1.134463 1.308995 .04445 .05080
1 0 22 0 0 0 0 0
23 1 .00475 .009693 1.308995 1.570795 .04445 .05080
1 0 23 0 0 0 0 0
24 1 .00475 .009693 1.570795 1.832594 .04445 .05080
1 0 24 0 0 0 0 0
25 1 .00475 .010185 1.832594 2.007126 .04445 .05080
1 0 25 0 0 0 0 0
26 1 .00475 .010979 2.007126 2.158970 .04445 .05080
1 0 26 0 0 0 0 0
27 1 .00475 .012459 2.158970 2.356192 .04445 .05080
1 0 27 0 0 0 0 0
28 1 .00475 .011497 2.356192 3.141590 .04445 .05080
1 0 28 0 0 0 0 0
29 1 .00475 .009598 .000000 .174532 .05080 .05715
1 0 29 141 0 0 0 0
30 1 .00475 .009904 .174532 .349065 .05080 .05715
1 0 30 141 0 0 0 0
31 1 .00475 .010567 .349065 .523598 .05080 .05715
1 0 31 141 0 0 0 0
32 1 .00475 .011716 .523598 .698131 .05080 .05715
1 0 32 141 0 0 0 0
33 1 .00475 .012676 .698131 .829030 .05080 .05715
1 0 33 141 0 0 0 0
34 1 .00475 .012184 .829030 .982619 .05080 .05715
1 0 34 0 0 0 0 0
35 1 .00475 .010979 .982619 1.134463 .05080 .05715
1 0 35 0 0 0 0 0
36 1 .00475 .010185 1.134463 1.308995 .05080 .05715
1 0 36 0 0 0 0 0
37 1 .00475 .009693 1.308995 1.570795 .05080 .05715
1 0 37 0 0 0 0 0
38 1 .00475 .009693 1.570795 1.832594 .05080 .05715
1 0 38 0 0 0 0 0
39 1 .00475 .010185 1.832594 2.007126 .05080 .05715
1 0 39 0 0 0 0 0
40 1 .00475 .010979 2.007126 2.158970 .05080 .05715
1 0 40 0 0 0 0 0

41 1 .00475 .012459 2.158970 2.356192 .05080 .05715
1 0 41 0 0 0 0 0
42 1 .00475 .011497 2.356192 3.141590 .05080 .05715
1 0 42 0 0 0 0 0
43 1 .00475 .009598 .000000 .174532 .05715 .06350
1 0 43 141 0 0 0 0
44 1 .00475 .009904 .174532 .349065 .05715 .06350
1 0 44 141 0 0 0 0
45 1 .00475 .010567 .349065 .523598 .05715 .06350
1 0 45 141 0 0 0 0
46 1 .00475 .011716 .523598 .698131 .05715 .06350
1 0 46 141 0 0 0 0
47 1 .00475 .012676 .698131 .829030 .05715 .06350
1 0 47 141 0 0 0 0
48 1 .00475 .012184 .829030 .982619 .05715 .06350
1 0 48 0 0 0 0 0
49 1 .00475 .010979 .982619 1.134463 .05715 .06350
1 0 49 0 0 0 0 0
50 1 .00475 .010185 1.134463 1.308995 .05715 .06350
1 0 50 0 0 0 0 0
51 1 .00475 .009693 1.308995 1.570795 .05715 .06350
1 0 51 0 0 0 0 0
52 1 .00475 .009693 1.570795 1.832594 .05715 .06350
1 0 52 0 0 0 0 0
53 1 .00475 .010185 1.832594 2.007126 .05715 .06350
1 0 53 0 0 0 0 0
54 1 .00475 .010979 2.007126 2.158970 .05715 .06350
1 0 54 0 0 0 0 0
55 1 .00475 .012459 2.158970 2.356192 .05715 .06350
1 0 55 0 0 0 0 0
56 1 .00475 .011497 2.356192 3.141590 .05715 .06350
1 0 56 0 0 0 0 0
57 1 .00475 .009598 .000000 .174532 .06350 .06985
1 0 57 141 0 0 0 0
58 1 .00475 .009904 .174532 .349065 .06350 .06985
1 0 58 141 0 0 0 0
59 1 .00475 .010567 .349065 .523598 .06350 .06985
1 0 59 141 0 0 0 0
60 1 .00475 .011716 .523598 .698131 .06350 .0698
1 0 60 141 0 0 0 0
61 1 .00475 .012676 .698131 .829030 .06350 .06985
1 0 61 141 0 0 0 0
62 1 .00475 .012184 .829030 .982619 .06350 .06985
1 0 62 0 0 0 0 0
63 1 .00475 .010979 .982619 1.134463 .06350 .06985

1 0 63 0 0 0 0 0
64 1 .00475 .010185 1.134463 1.308995 .06350 .06985
1 0 64 0 0 0 0 0
65 1 .00475 .009693 1.308995 1.570795 .06350 .06985
1 0 65 0 0 0 0 0
66 1 .00475 .009693 1.570795 1.832594 .06350 .06985
1 0 66 0 0 0 0 0
67 1 .00475 .010185 1.832594 2.007126 .06350 .06985
1 0 67 0 0 0 0 0
68 1 .00475 .010979 2.007126 2.158970 .06350 .06985
1 0 68 0 0 0 0 0
69 1 .00475 .012459 2.158970 2.356192 .06350 .06985
1 0 69 0 0 0 0 0
70 1 .00475 .011497 2.356192 3.141590 .06350 .06985
1 0 70 0 0 0 0 0
71 1 .00475 .009598 .000000 .174532 .06985 .07620
1 0 71 141 0 0 0 0
72 1 .00475 .009904 .174532 .349065 .06985 .07620
1 0 72 141 0 0 0 0
73 1 .00475 .010567 .349065 .523598 .06985 .07620
1 0 73 141 0 0 0 0
74 1 .00475 .011716 .523598 .698131 .06985 .07620
1 0 74 141 0 0 0 0
75 1 .00475 .012676 .698131 .829030 .06985 .07620
1 0 75 141 0 0 0 0
76 1 .00475 .012184 .829030 .982619 .06985 .07620
1 0 76 0 0 0 0 0
77 1 .00475 .010979 .982619 1.134463 .06985 .07620
1 0 77 0 0 0 0 0
78 1 .00475 .010185 1.134463 1.308995 .06985 .07620
1 0 78 0 0 0 0 0
79 1 .00475 .009693 1.308995 1.570795 .06985 .07620
1 0 79 0 0 0 0 0
80 1 .00475 .009693 1.570795 1.832594 .06985 .07620
1 0 80 0 0 0 0 0
81 1 .00475 .010185 1.832594 2.007126 .06985 .07620
1 0 81 0 0 0 0 0
82 1 .00475 .010979 2.007126 2.158970 .06985 .07620
1 0 82 0 0 0 0 0
83 1 .00475 .012459 2.158970 2.356192 .06985 .07620
1 0 83 0 0 0 0 0
84 1 .00475 .011497 2.356192 3.141590 .06985 .07620
1 0 84 0 0 0 0 0
85 1 .00475 .009598 .000000 .174532 .07620 .08255
1 0 85 141 0 0 0 0

86 1 .00475 .009904 .174532 .349065 .07620 .08255
1 0 86 141 0 0 0 0
87 1 .00475 .010567 .349065 .523598 .07620 .08255
1 0 87 141 0 0 0 0
88 1 .00475 .011716 .523598 .698131 .07620 .08255
1 0 88 141 0 0 0 0
89 1 .00475 .012676 .698131 .829030 .07620 .08255
1 0 89 141 0 0 0 0
90 1 .00475 .012184 .829030 .982619 .07620 .08255
1 0 90 0 0 0 0 0
91 1 .00475 .010979 .982619 1.134463 .07620 .08255
1 0 91 0 0 0 0 0
92 1 .00475 .010185 1.134463 1.308995 .07620 .08255
1 0 92 0 0 0 0 0
93 1 .00475 .009693 1.308995 1.570795 .07620 .08255
1 0 93 0 0 0 0 0
94 1 .00475 .009693 1.570795 1.832594 .07620 .08255
1 0 94 0 0 0 0 0
95 1 .00475 .010185 1.832594 2.007126 .07620 .08255
1 0 95 0 0 0 0 0
96 1 .00475 .010979 2.007126 2.158970 .07620 .08255
1 0 96 0 0 0 0 0
97 1 .00475 .012459 2.158970 2.356192 .07620 .08255
1 0 97 0 0 0 0 0
98 1 .00475 .011497 2.356192 3.141590 .07620 .08255
1 0 98 0 0 0 0 0
99 1 .00475 .009598 .000000 .174532 .08255 .08890
1 0 99 141 0 0 0 0
100 1 .00475 .009904 .174532 .349065 .08255 .08890
1 0 100 141 0 0 0 0
101 1 .00475 .010567 .349065 .523598 .08255 .08890
1 0 101 141 0 0 0 0
102 1 .00475 .011716 .523598 .698131 .08255 .08890
1 0 102 141 0 0 0 0
103 1 .00475 .012676 .698131 .829030 .08255 .08890
1 0 103 141 0 0 0 0
104 1 .00475 .012184 .829030 .982619 .08255 .08890
1 0 104 0 0 0 0 0
105 1 .00475 .010979 .982619 1.134463 .08255 .08890
1 0 105 0 0 0 0 0
106 1 .00475 .010185 1.134463 1.308995 .08255 .08890
1 0 106 0 0 0 0 0
107 1 .00475 .009693 1.308995 1.570795 .08255 .08890
1 0 107 0 0 0 0 0
108 1 .00475 .009693 1.570795 1.832594 .08255 .08890

1 0 108 0 0 0 0 0
109 1 .00475 .010185 1.832594 2.007126 .08255 .08890
1 0 109 0 0 0 0 0
110 1 .00475 .010979 2.007126 2.158970 .08255 .08890
1 0 110 0 0 0 0 0
111 1 .00475 .012459 2.158970 2.356192 .08255 .08890
1 0 111 0 0 0 0 0
112 1 .00475 .011497 2.356192 3.141590 .08255 .08890
1 0 112 0 0 0 0 0
113 1 .00475 .009598 .000000 .174532 .00000 .03810
1 0 113 0 0 0 0 0
114 1 .00475 .009904 .174532 .349065 .00000 .03810
1 0 114 0 0 0 0 0
115 1 .00475 .010567 .349065 .523598 .00000 .03810
1 0 115 0 0 0 0 0
116 1 .00475 .011716 .523598 .698131 .00000 .03810
1 0 116 0 0 0 0 0
117 1 .00475 .012676 .698131 .829030 .00000 .03810
1 0 117 0 0 0 0 0
118 1 .00475 .012184 .829030 .982619 .00000 .03810
1 0 118 0 0 0 0 0
119 1 .00475 .010979 .982619 1.134463 .00000 .03810
1 0 119 0 0 0 0 0
120 1 .00475 .010185 1.134463 1.308995 .00000 .03810
1 0 120 0 0 0 0 0
121 1 .00475 .009693 1.308995 1.570795 .00000 .03810
1 0 121 0 0 0 0 0
122 1 .00475 .009693 1.570795 1.832594 .00000 .03810
1 0 122 0 0 0 0 0
123 1 .00475 .010185 1.832594 2.007126 .00000 .03810
1 0 123 0 0 0 0 0
124 1 .00475 .010979 2.007126 2.158970 .00000 .03810
1 0 124 0 0 0 0 0
125 1 .00475 .012459 2.158970 2.356192 .00000 .03810
1 0 125 0 0 0 0 0
126 1 .00475 .011497 2.356192 3.141590 .00000 .03810
1 0 126 0 0 0 0 0
127 1 .00475 .009598 .000000 .174532 .08890 .12700
1 0 127 0 0 0 0 0
128 1 .00475 .009904 .174532 .349065 .08890 .12700
1 0 128 0 0 0 0 0
129 1 .00475 .010567 .349065 .523598 .08890 .12700
1 0 129 0 0 0 0 0
130 1 .00475 .011716 .523598 .698131 .08890 .12700
1 0 130 0 0 0 0 0

131 1 .00475 .012676 .698131 .829030 .08890 .12700
1 0 131 0 0 0 0 0
132 1 .00475 .012184 .829030 .982619 .08890 .12700
1 0 132 0 0 0 0 0
133 1 .00475 .010979 .982619 1.134463 .08890 .12700
1 0 133 0 0 0 0 0
134 1 .00475 .010185 1.134463 1.308995 .08890 .12700
1 0 134 0 0 0 0 0
135 1 .00475 .009693 1.308995 1.570795 .08890 .12700
1 0 135 0 0 0 0 0
136 1 .00475 .009693 1.570795 1.832594 .08890 .12700
1 0 136 0 0 0 0 0
137 1 .00475 .010185 1.832594 2.007126 .08890 .12700
1 0 137 0 0 0 0 0
138 1 .00475 .010979 2.007126 2.158970 .08890 .12700
1 0 138 0 0 0 0 0
139 1 .00475 .012459 2.158970 2.356192 .08890 .12700
1 0 139 0 0 0 0 0
140 1 .00475 .011497 2.356192 3.141590 .08890 .12700
1 0 140 0 0 0 0 0
MATERIALS
1 Copper 0 8933. 385. -1 0 0 0
INITIAL TEMPERATURES
1 20.00
BOUNDARY CONDITIONS
1 1 21.4
30113.
2 1 21.4
30172.
3 1 21.4
30312.
4 1 21.4
30531.
5 1 21.4
30805.
6 1 21.4
31078.
7 1 21.4
31427.
8 1 21.4
31821.
9 1 21.4
32334.
10 1 21.4
33034.

11 1 21.4
33633.
12 1 21.4
33994.
13 1 21.4
34288.
14 1 21.4
34641.
15 1 22.7
35872.
16 1 22.7
33402.
17 1 22.7
28396.
18 1 22.7
28738.
19 1 22.7
29029.
20 1 22.7
29326.
21 1 22.7
29715.
22 1 22.7
30161. 23 1 22.7
30750.
24 1 22.7
31558.
25 1 22.7
32259.
26 1 22.7
32689.
27 1 22.7
33043.
28 1 22.7 33477.
29 1 24.1
58182.
30 1 24.1
55214.
31 1 24.1
48626.
32 1 24.1
39487.
33 1 24.1
30233.
34 1 24.1

28671.
35 1 24.1
29018.
36 1 24.1
29432.
37 1 24.1
29997.
38 1 24.1
30790.
39 1 24.1
31484.
40 1 24.1
31918.
41 1 24.1
32277.
42 1 24.1
32724.
43 1 25.5
59502.
44 1 25.5
57121.
45 1 25.5
51627.
46 1 25.5
43770.
47 1 25.5
35083.
48 1 25.5
28745.
49 1 25.5
28775.
50 1 25.5
29153.
51 1 25.5
29683.
52 1 25.5
30436.
53 1 25.5
31103.
54 1 25.5
31518.
55 1 25.5
31870.
56 1 25.5
32303.

57 1 26.8
60339.
58 1 26.8
57967.
59 1 26.8
52506.
60 1 26.8
44710.
61 1 26.8
36094.
62 1 26.8
28492.
63 1 26.8
28697.
64 1 26.8
29062.
65 1 26.8
29576.
66 1 26.8
30307.
67 1 26.8
30956.
68 1 26.8
31364.
69 1 26.8
31705.
70 1 26.8
32128.
71 1 28.2
58127.
72 1 28.2
55696.
73 1 28.2
50131.
74 1 28.2
42282.
75 1 28.2
33627.
76 1 28.2
28314.
77 1 28.2
28742.
78 1 28.2
29112.
79 1 28.2

29633.
80 1 28.2
30365.
81 1 28.2
31010.
82 1 28.2
31414.
83 1 28.2
31751.
84 1 28.2
32170.
85 1 29.6
47998.
86 1 29.6
45448.
87 1 29.6
40044.
88 1 29.6
32658.
89 1 29.6
27700.
90 1 29.6
28685.
91 1 29.6
29017.
92 1 29.6
29410.
93 1 29.6
29946.
94 1 29.6
30683.
95 1 29.6
31325.
96 1 29.6
31721.
97 1 29.6
32051.
98 1 29.6
32460.
99 1 30.9
28601.
100 1 30.9
28658.
101 1 30.9
28791.

102 1 30.9
28997.
103 1 30.9
29252.
104 1 30.9
29516.
105 1 30.9
29859.
106 1 30.9
30248.
107 1 30.9
30768.
108 1 30.9
31460.
109 1 30.9
32046.
110 1 30.9
32403.
111 1 30.9
32698.
112 1 30.9
33063.
113 1 20.0
38489.
114 1 20.0
38491.
115 1 20.0
38497.
116 1 20.0
38507.
117 1 20.0
38519.
118 1 20.0
38535.
119 1 20.0
38558.
120 1 20.0
38584.
121 1 20.0
38623.
122 1 20.0
38668.
123 1 20.0
38701.
124 1 20.0

38720.
125 1 20.0
38738.
126 1 20.0
38763.
127 1 30.9
35438.
128 1 30.9
35447.
129 1 30.9
35463.
130 1 30.9
35491.
131 1 30.9
35524.
132 1 30.9
35564.
133 1 30.9
35616.
134 1 30.9
35681.
135 1 30.9
35774.
136 1 30.9
35883.
137 1 30.9
35966.
138 1 30.9
36018.
139 1 30.9
36065.
140 1 30.9
36133.
141 1
0 0 0 0 .111E+08
XGRID
.004750 .009598 .009693 .009904 .010185 .010567 .010979 .011497
@ .011716 .012184 .012459 .012676
1 1 1 1 1 1 1
@ 1 1 1 1
YGRID
.000000 .174532 .349065 .523598 .698131 .829030 .982619 1.134463
@1.308995 1.570795 1.832594 2.007126 2.158970 2.356192 3.141590
1 1 1 1 1 1 1
@ 1 1 1 1 1 1 1

ZGRID
.000000 .038100 .044450 .050800 .057150 .063500 .069850 .076200
@ .082550 .088900 .127000
5 1 1 1 1 1 1 1
@ 1 5
TABULAR FUNCTIONS
1
.0 401. 200. 389. 400. 378. 600. 366. 800. 352. 1000. 336.
STEADY-STATE
1 10000

C.9 A Sample *htc.dat* Input File to *sh2.for*

10.7	power(kW)
3.66	velocity(m/s)
20.00	t(bulk)
2.96	pressure(MPa)
TS17B	test section

C.10 *input.one* Initial Wall Temperature Input File to *sh2.for*

```
read
   this
   stuff
   15 3.14 — 36.93 41.12 41.14 41.19 41.24 41.29 41.32 41.34
   14 2.36 — 41.74 46.49 46.51 46.57 46.63 46.70 46.75 46.81 46.90 47.01 47.03
   13 2.16 — 44.92 49.74 49.72 49.65 49.54 49.36 49.12 48.69 48.58 48.45 48.43
   12 2.01 — 47.99 53.32 53.26 53.10 52.86 52.32 52.13
   11 1.83 — 52.28 59.12 59.05 58.74 58.59
   10 1.57 — 60.26 71.90 71.90
   9 1.31 — 69.80 89.53 89.71 90.48 90.84 8 1.13 — 76.58 103.12 103.52 104.38 105.50
107.88 108.76
   7 0.98 — 82.44 115.06 115.63 116.87 118.52 120.74 123.07 127.46 128.59 129.61
   6 0.83 — 88.09 126.49 127.21 128.79 130.89 133.74 136.82 140.71 142.33 145.74
149.81 152.59
   5 0.70 — 92.48 135.26 136.07 137.87 140.25 143.50 147.01 151.52 153.45 156.63
159.31 161.77
   4 0.52 — 97.53 145.23 146.12 148.09 150.69 154.21 157.30 162.37 164.89
   3 0.35 — 101.38 153.16 154.16 156.37 159.10 163.35
   2 0.17 — 103.80 158.41 159.48 161.95
   1 0.00 — 104.63 160.25
   +------------------------------------------------------------
   0.00 0.01 0.01 0.01 0.01 0.01 0.01 0.01 0.01 0.01 0.01 0.01
   1 2 3 4 5 6 7 8 9 10 11 12
   3D Conduction Profile of Test SectionTS4AP5 13-JUL-94 21:43:08
   Steady-State Temperature Distribution at Time 0.0000E+00
   Z = 3.1750E-03
   15 3.14 — 36.79 40.95 40.97 41.02 41.07 41.12 41.15 41.17
   14 2.36 — 41.58 46.29 46.32 46.37 46.43 46.50 46.55 46.61 46.70 46.81 46.83
   13 2.16 — 44.75 49.53 49.51 49.44 49.33 49.15 48.91 48.49 48.37 48.24 48.22
   12 2.01 — 47.81 53.10 53.04 52.88 52.64 52.10 51.91
   11 1.83 — 52.08 58.88 58.81 58.49 58.35
   10 1.57 — 60.03 71.61 71.61
   9 1.31 — 69.55 89.19 89.37 90.13 90.50
   8 1.13 — 76.31 102.75 103.14 104.00 105.11 107.49 108.37
   7 0.98 — 82.16 114.66 115.23 116.47 118.11 120.33 122.65 127.04 128.17 129.18
   6 0.83 — 87.79 126.08 126.79 128.37 130.46 133.31 136.38 140.28 141.89 145.30
149.37 152.15
   5 0.70 — 92.18 134.84 135.65 137.44 139.82 143.06 146.58 151.07 153.01 156.18
158.87 161.33
   4 0.52 — 97.21 144.80 145.69 147.65 150.25 153.77 156.86 161.93 164.45
```

3 0.35 — 101.06 152.72 153.72 155.94 158.66 162.91
2 0.17 — 103.48 157.97 159.05 161.52
1 0.00 — 104.31 159.82
+——
0.00 0.01 0.01 0.01 0.01 0.01 0.01 0.01 0.01 0.01 0.01 0.01
1 2 3 4 5 6 7 8 9 10 11 12
3D Conduction Profile of Test SectionTS4AP5 13-JUL-94 21:43:08
Steady-State Temperature Distribution at Time 0.0000E+00
Z = 6.3500E-03
15 3.14 — 36.38 40.44 40.46 40.51 40.55 40.60 40.64 40.65
14 2.36 — 41.10 45.69 45.72 45.77 45.83 45.89 45.95 46.00 46.10 46.20 46.22
13 2.16 — 44.22 48.89 48.87 48.80 48.69 48.51 48.28 47.85 47.74 47.61 47.59
12 2.01 — 47.25 52.42 52.35 52.20 51.96 51.42 51.24
11 1.83 — 51.48 58.13 58.06 57.75 57.60
10 1.57 — 59.34 70.72 70.72
9 1.31 — 68.76 88.12 88.30 89.06 89.42
8 1.13 — 75.46 101.57 101.96 102.82 103.92 106.28 107.15
7 0.98 — 81.27 113.41 113.97 115.20 116.84 119.04 121.35 125.71 126.83 127.85
6 0.83 — 86.86 124.77 125.47 127.04 129.13 131.96 135.03 138.91 140.52 143.92 147.99 150.76
5 0.70 — 91.22 133.49 134.30 136.08 138.46 141.69 145.19 149.68 151.61 154.79 157.47 159.93
4 0.52 — 96.23 143.44 144.32 146.28 148.87 152.38 155.47 160.53 163.05
3 0.35 — 100.05 151.35 152.35 154.57 157.28 161.53
2 0.17 — 102.46 156.61 157.68 160.15
1 0.00 — 103.29 158.46
+——
0.00 0.01 0.01 0.01 0.01 0.01 0.01 0.01 0.01 0.01 0.01 0.01
1 2 3 4 5 6 7 8 9 10 11 12
3D Conduction Profile of Test SectionTS4AP5 13-JUL-94 21:43:08
Steady-State Temperature Distribution at Time 0.0000E+00
Z = 9.5250E-03
15 3.14 — 35.68 39.58 39.60 39.64 39.69 39.74 39.77 39.78
14 2.36 — 40.27 44.68 44.70 44.75 44.81 44.87 44.92 44.97 45.06 45.17 45.18
13 2.16 — 43.32 47.79 47.77 47.71 47.60 47.42 47.19 46.77 46.66 46.54 46.52
12 2.01 — 46.28 51.23 51.17 51.02 50.79 50.26 50.08
11 1.83 — 50.41 56.82 56.75 56.44 56.30
10 1.57 — 58.11 69.14 69.14
9 1.31 — 67.35 86.21 86.39 87.13 87.49
8 1.13 — 73.94 99.45 99.83 100.67 101.76 104.08 104.94
7 0.98 — 79.65 111.13 111.68 112.90 114.51 116.69 118.97 123.29 124.40 125.41
6 0.83 — 85.17 122.37 123.07 124.62 126.69 129.50 132.54 136.40 138.01 141.40 145.46 148.23
5 0.70 — 89.47 131.03 131.83 133.60 135.96 139.17 142.66 147.14 149.06 152.23 154.91 157.37

4 0.52 — 94.42 140.93 141.80 143.75 146.34 149.84 152.91 157.96 160.47
3 0.35 — 98.21 148.83 149.83 152.03 154.74 158.99
2 0.17 — 100.60 154.09 155.16 157.62
1 0.00 — 101.41 155.94
+———
0.00 0.01 0.01 0.01 0.01 0.01 0.01 0.01 0.01 0.01 0.01 0.01
1 2 3 4 5 6 7 8 9 10 11 12
3D Conduction Profile of Test SectionTS4AP5 13-JUL-94 21:43:08
Steady-State Temperature Distribution at Time 0.0000E+00
Z = 1.2700E-02
15 3.14 — 34.68 38.37 38.39 38.43 38.48 38.52 38.55 38.56
14 2.36 — 39.07 43.22 43.24 43.29 43.34 43.40 43.45 43.50 43.58 43.68 43.70
13 2.16 — 42.00 46.21 46.18 46.12 46.01 45.84 45.62 45.22 45.11 44.99 44.98
12 2.01 — 44.84 49.50 49.44 49.30 49.07 48.57 48.39
11 1.83 — 48.81 54.86 54.80 54.51 54.37
10 1.57 — 56.23 66.73 66.73
9 1.31 — 65.16 83.23 83.40 84.12 84.47
8 1.13 — 71.55 96.10 96.47 97.28 98.34 100.60 101.44
7 0.98 — 77.10 107.50 108.04 109.23 110.81 112.94 115.18 119.43 120.52 121.51
6 0.83 — 82.48 118.54 119.22 120.75 122.78 125.56 128.56 132.38 133.98 137.35 141.40 144.17
5 0.70 — 86.68 127.07 127.86 129.61 131.94 135.12 138.58 143.04 144.96 148.12 150.80 153.25
4 0.52 — 91.52 136.87 137.74 139.67 142.24 145.72 148.77 153.81 156.32
3 0.35 — 95.24 144.73 145.72 147.92 150.62 154.86
2 0.17 — 97.58 149.98 151.05 153.51
1 0.00 — 98.39 151.83
+———
0.00 0.01 0.01 0.01 0.01 0.01 0.01 0.01 0.01 0.01 0.01 0.01
1 2 3 4 5 6 7 8 9 10 11 12
3D Conduction Profile of Test SectionTS4AP5 13-JUL-94 21:43:08
Steady-State Temperature Distribution at Time 0.0000E+00
Z = 1.5875E-02
15 3.14 — 33.39 36.82 36.84 36.88 36.92 36.96 36.99 37.00
14 2.36 — 37.47 41.31 41.34 41.38 41.43 41.48 41.52 41.57 41.65 41.74 41.76
13 2.16 — 40.20 44.09 44.07 44.01 43.91 43.75 43.54 43.17 43.07 42.96 42.94
12 2.01 — 42.85 47.17 47.11 46.98 46.77 46.29 46.13
11 1.83 — 46.57 52.18 52.12 51.85 51.72
10 1.57 — 53.54 63.30 63.31
9 1.31 — 61.97 78.88 79.04 79.72 80.05
8 1.13 — 68.01 91.11 91.47 92.24 93.25 95.41 96.22
7 0.98 — 73.30 102.04 102.56 103.70 105.22 107.28 109.45 113.57 114.63 115.59
6 0.83 — 78.42 112.69 113.36 114.85 116.83 119.54 122.48 126.24 127.82 131.16 135.19 137.95
5 0.70 — 82.44 120.99 121.76 123.47 125.76 128.90 132.32 136.74 138.66 141.80

144.47 146.93

4 0.52 — 87.10 130.58 131.43 133.34 135.89 139.35 142.37 147.39 149.89

3 0.35 — 90.68 138.33 139.31 141.50 144.19 148.42

2 0.17 — 92.95 143.53 144.59 147.05

1 0.00 — 93.72 145.37

+——

0.00 0.01 0.01 0.01 0.01 0.01 0.01 0.01 0.01 0.01 0.01 0.01

1 2 3 4 5 6 7 8 9 10 11 12

3D Conduction Profile of Test SectionTS4AP5 13-JUL-94 21:43:08

Steady-State Temperature Distribution at Time 0.0000E+00

Z = 1.9050E-02

15 3.14 — 31.80 34.96 34.98 35.02 35.06 35.09 35.12 35.13

14 2.36 — 35.45 38.98 39.00 39.04 39.08 39.13 39.17 39.21 39.29 39.37 39.38

13 2.16 — 37.90 41.46 41.44 41.39 41.31 41.16 40.98 40.65 40.56 40.46 40.44

12 2.01 — 40.29 44.21 44.17 44.04 43.86 43.43 43.29

11 1.83 — 43.63 48.70 48.65 48.40 48.29

10 1.57 — 49.90 58.71 58.71

9 1.31 — 57.51 72.80 72.95 73.57 73.86

8 1.13 — 63.01 83.97 84.29 85.01 85.94 87.92 88.67

7 0.98 — 67.82 94.05 94.53 95.59 97.01 98.94 100.98 104.86 105.86 106.78

6 0.83 — 72.52 103.98 104.61 106.02 107.91 110.50 113.34 116.99 118.53 121.81 125.79 128.54

5 0.70 — 76.22 111.78 112.52 114.17 116.39 119.43 122.78 127.15 129.06 132.18 134.84 137.29

4 0.52 — 80.51 120.89 121.73 123.60 126.10 129.53 132.51 137.50 140.00

3 0.35 — 83.84 128.35 129.33 131.50 134.16 138.38

2 0.17 — 85.95 133.39 134.45 136.90

1 0.00 — 86.67 135.17

+——

0.00 0.01 0.01 0.01 0.01 0.01 0.01 0.01 0.01 0.01 0.01 0.01

1 2 3 4 5 6 7 8 9 10 11 12

3D Conduction Profile of Test SectionTS4AP5 13-JUL-94 21:43:08

Steady-State Temperature Distribution at Time 0.0000E+00

Z = 2.2225E-02

15 3.14 — 29.99 32.86 32.88 32.91 32.95 32.98 33.01 33.02

14 2.36 — 33.08 36.29 36.31 36.35 36.39 36.43 36.47 36.51 36.57 36.64 36.65

13 2.16 — 35.15 38.39 38.37 38.33 38.26 38.14 37.99 37.72 37.65 37.57 37.55

12 2.01 — 37.16 40.70 40.66 40.56 40.41 40.05 39.93

11 1.83 — 39.98 44.48 44.43 44.23 44.13

10 1.57 — 45.26 52.90 52.90

9 1.31 — 51.66 64.76 64.89 65.41 65.66

8 1.13 — 56.27 74.18 74.46 75.07 75.86 77.55 78.18

7 0.98 — 60.32 82.72 83.14 84.06 85.29 86.96 88.73 92.12 93.00 93.81

6 0.83 — 64.27 91.19 91.75 93.00 94.68 97.00 99.56 102.90 104.33 107.44 111.29 114.00

5 0.70 — 67.39 97.91 98.58 100.07 102.09 104.89 108.01 112.17 114.03 117.03 119.63 122.06

4 0.52 — 71.01 105.85 106.64 108.39 110.77 114.06 116.87 121.70 124.18

3 0.35 — 73.83 112.49 113.44 115.57 118.17 122.33

2 0.17 — 75.62 117.00 118.05 120.48

1 0.00 — 76.24 118.60

+----------

0.00 0.01 0.01 0.01 0.01 0.01 0.01 0.01 0.01 0.01 0.01 0.01

1 2 3 4 5 6 7 8 9 10 11 12

3D Conduction Profile of Test SectionTS4AP5 13-JUL-94 21:43:08

Steady-State Temperature Distribution at Time 0.0000E+00

Z = 2.5400E-02

15 3.14 — 28.03 30.62 30.64 30.67 30.70 30.73 30.76 30.77

14 2.36 — 30.50 33.39 33.41 33.44 33.48 33.53 33.56 33.59 33.65 33.71 33.72

13 2.16 — 32.11 35.04 35.03 35.00 34.96 34.87 34.76 34.55 34.50 34.44 34.43

12 2.01 — 33.67 36.84 36.81 36.74 36.62 36.35 36.26

11 1.83 — 35.85 39.77 39.73 39.58 39.50

10 1.57 — 39.89 46.24 46.24

9 1.31 — 44.70 55.17 55.26 55.65 55.84

8 1.13 — 48.09 62.02 62.22 62.66 63.22 64.42 64.87

7 0.98 — 51.00 67.99 68.28 68.91 69.73 70.84 72.00 74.17 74.73 75.23

6 0.83 — 53.77 73.65 74.01 74.79 75.82 77.22 78.72 80.59 81.35 82.95 84.82 86.08

5 0.70 — 55.91 77.94 78.34 79.21 80.37 81.93 83.61 85.71 86.60 88.08 89.31 90.42

4 0.52 — 58.36 82.74 83.16 84.10 85.33 86.97 88.44 90.78 91.92

3 0.35 — 60.22 86.48 86.94 87.96 89.21 91.15

2 0.17 — 61.39 88.92 89.41 90.52

1 0.00 — 61.79 89.77

+----------

0.00 0.01 0.01 0.01 0.01 0.01 0.01 0.01 0.01 0.01 0.01 0.01

1 2 3 4 5 6 7 8 9 10 11 12

3D Conduction Profile of Test SectionTS4AP5 13-JUL-94 21:43:08 Steady-State Temperature Distribution at Time 0.0000E+00

Z = 2.9210E-02

15 3.14 — 25.67 27.91 27.92 27.95 27.98 28.01 28.03 28.04

14 2.36 — 27.38 29.89 29.91 29.94 29.98 30.02 30.05 30.08 30.12 30.16 30.17

13 2.16 — 28.45 31.00 31.00 30.99 30.97 30.93 30.86 30.74 30.70 30.67 30.66

12 2.01 — 29.48 32.19 32.18 32.14 32.06 31.90 31.84

11 1.83 — 30.90 34.10 34.08 33.99 33.94

10 1.57 — 33.46 38.26 38.26

9 1.31 — 36.41 43.73 43.79 44.02 44.13

8 1.13 — 38.38 47.62 47.73 47.98 48.29 48.93 49.17

7 0.98 — 40.00 50.60 50.83 51.14 51.54 52.05 52.55 53.44 53.67 53.85

6 0.83 — 41.46 53.25 53.40 53.70 54.09 54.57 55.02 55.49 55.65 55.89 56.05 56.09

5 0.70 — 42.52 54.95 55.07 55.35 55.68 56.07 56.40 56.68 56.73 56.87 56.92 56.94

4 0.52 — 43.68 56.50 56.59 56.78 56.98 57.17 57.42 57.60 57.62

3 0.35 — 44.52 57.37 57.41 57.48 57.59 57.66
2 0.17 — 45.01 57.79 57.81 57.83
1 0.00 — 45.18 57.92
+———
0.00 0.01 0.01 0.01 0.01 0.01 0.01 0.01 0.01 0.01 0.01 0.01
1 2 3 4 5 6 7 8 9 10 11 12
3D Conduction Profile of Test SectionTS4AP5 13-JUL-94 21:43:08
Steady-State Temperature Distribution at Time 0.0000E+00
Z = 3.3020E-02
15 3.14 — 23.51 25.39 25.40 25.42 25.45 25.48 25.50 25.50
14 2.36 — 24.60 26.70 26.72 26.75 26.78 26.82 26.84 26.87 26.90 26.93 26.94
13 2.16 — 25.26 27.39 27.39 27.39 27.39 27.38 27.34 27.28 27.27 27.25 27.25
12 2.01 — 25.88 28.10 28.10 28.08 28.04 27.95 27.92
11 1.83 — 26.73 29.24 29.22 29.17 29.15
10 1.57 — 28.24 31.69 31.69
9 1.31 — 29.92 34.83 34.86 34.99 35.06
8 1.13 — 31.01 36.94 37.01 37.15 37.32 37.67 37.80
7 0.98 — 31.87 38.52 38.60 38.77 38.98 39.25 39.50 39.95 40.06 40.15
6 0.83 — 32.61 39.73 39.80 39.96 40.16 40.40 40.62 40.84 40.91 41.01 41.07 41.08
5 0.70 — 33.13 40.44 40.51 40.65 40.81 41.00 41.16 41.28 41.30 41.36 41.38 41.39
4 0.52 — 33.68 40.99 41.04 41.14 41.24 41.34 41.46 41.54 41.55
3 0.35 — 34.05 41.19 41.21 41.25 41.32 41.35
2 0.17 — 34.27 41.21 41.22 41.23
1 0.00 — 34.33 41.20
+———
0.00 0.01 0.01 0.01 0.01 0.01 0.01 0.01 0.01 0.01 0.01 0.01
1 2 3 4 5 6 7 8 9 10 11 12
3D Conduction Profile of Test SectionTS4AP5 13-JUL-94 21:43:08
Steady-State Temperature Distr ution at Time 0.0000E+00
Z = 3.6830E-02
15 3.14 — 21.67 23.20 23.21 23.23 23.26 23.28 23.29 23.30
14 2.36 — 22.34 24.02 24.03 24.06 24.09 24.12 24.14 24.16 24.18 24.20 24.21
13 2.16 — 22.72 24.41 24.42 24.43 24.44 24.44 24.43 24.40 24.40 24.39 24.39
12 2.01 — 23.07 24.81 24.81 24.80 24.79 24.74 24.73
11 1.83 — 23.56 25.44 25.44 25.41 25.40
10 1.57 — 24.41 26.82 26.82
9 1.31 — 25.34 28.58 28.60 28.67 28.71
8 1.13 — 25.94 29.74 29.78 29.86 29.96 30.16 30.23
7 0.98 — 26.39 30.58 30.63 30.73 30.85 31.00 31.15 31.39 31.46 31.51
6 0.83 — 26.78 31.19 31.24 31.33 31.45 31.59 31.72 31.84 31.88 31.93 31.97 31.97
5 0.70 — 27.04 31.52 31.56 31.65 31.75 31.86 31.96 32.03 32.05 32.09 32.11 32.11
4 0.52 — 27.30 31.72 31.75 31.82 31.88 31.95 32.03 32.09 32.10
3 0.35 — 27.47 31.73 31.75 31.77 31.82 31.84
2 0.17 — 27.57 31.66 31.67 31.68
1 0.00 — 27.60 31.63

+----------
0.00 0.01 0.01 0.01 0.01 0.01 0.01 0.01 0.01 0.01 0.01 0.01
1 2 3 4 5 6 7 8 9 10 11 12
3D Conduction Profile of Test SectionTS4AP5 13-JUL-94 21:43:08
Steady-State Temperature Distribution at Time 0.0000E+00
Z = 4.0640E-02
15 3.14 — 20.21 21.41 21.42 21.44 21.46 21.48 21.49 21.49
14 2.36 — 20.59 21.90 21.91 21.93 21.95 21.97 21.99 22.01 22.02 22.04 22.04
13 2.16 — 20.80 22.11 22.11 22.13 22.14 22.15 22.15 22.14 22.14 22.14 22.14
12 2.01 — 21.00 22.32 22.32 22.32 22.31 22.30 22.29
11 1.83 — 21.27 22.65 22.65 22.63 22.63
10 1.57 — 21.74 23.40 23.40
9 1.31 — 22.25 24.38 24.39 24.43 24.46
8 1.13 — 22.58 25.03 25.05 25.10 25.16 25.27 25.31
7 0.98 — 22.82 25.49 25.52 25.58 25.65 25.74 25.83 25.97 26.01 26.04
6 0.83 — 23.02 25.81 25.84 25.90 25.97 26.06 26.13 26.21 26.23 26.27 26.29 26.29
5 0.70 — 23.15 25.97 26.00 26.05 26.12 26.19 26.25 26.30 26.31 26.34 26.35 26.35
4 0.52 — 23.28 26.05 26.07 26.11 26.15 26.19 26.25 26.29 26.30
3 0.35 — 23.36 26.01 26.02 26.03 26.07 26.08
2 0.17 — 23.41 25.93 25.94 25.94
1 0.00 — 23.42 25.90
+----------
0.00 0.01 0.01 0.01 0.01 0.01 0.01 0.01 0.01 0.01 0.01 0.01
1 2 3 4 5 6 7 8 9 10 11 12
3D Conduction Profile of Test SectionTS4AP5 13-JUL-94 21:43:08
Steady-State Temperature Distribution at Time 0.0000E+00
Z = 4.4450E-02
15 3.14 — 19.09 20.02 20.03 20.04 20.05 20.07 20.08 20.08
14 2.36 — 19.30 20.29 20.30 20.32 20.33 20.35 20.37 20.38 20.39 20.40 20.40
13 2.16 — 19.42 20.40 20.40 20.42 20.43 20.44 20.44 20.45 20.45 20.45 20.45
12 2.01 — 19.52 20.50 20.50 20.51 20.51 20.50 20.50
11 1.83 — 19.67 20.66 20.66 20.66 20.66
10 1.57 — 19.92 21.06 21.06
9 1.31 — 20.21 21.61 21.61 21.64 21.65
8 1.13 — 20.38 21.98 21.99 22.02 22.05 22.12 22.15
7 0.98 — 20.51 22.24 22.25 22.29 22.34 22.39 22.44 22.53 22.55 22.57
6 0.83 — 20.62 22.41 22.43 22.47 22.51 22.57 22.62 22.66 22.68 22.70 22.71 22.71
5 0.70 — 20.69 22.49 22.51 22.54 22.59 22.63 22.67 22.70 22.71 22.73 22.74 22.74
4 0.52 — 20.75 22.52 22.53 22.55 22.58 22.61 22.65 22.68 22.68
3 0.35 — 20.79 22.47 22.48 22.49 22.51 22.52
2 0.17 — 20.81 22.41 22.41 22.41
1 0.00 — 20.81 22.38
+----------
0.00 0.01 0.01 0.01 0.01 0.01 0.01 0.01 0.01 0.01 0.01 0.01
1 2 3 4 5 6 7 8 9 10 11 12

3D Conduction Profile of Test SectionTS4AP5 13-JUL-94 21:43:08
Steady-State Temperature Distribution at Time 0.0000E+00
Z = 4.8260E-02
15 3.14 — 18.27 18.98 18.98 18.99 19.01 19.02 19.02 19.03
14 2.36 — 18.38 19.13 19.13 19.14 19.16 19.17 19.18 19.19 19.20 19.21 19.21
13 2.16 — 18.44 19.18 19.18 19.19 19.20 19.21 19.22 19.23 19.23 19.23 19.23
12 2.01 — 18.50 19.22 19.22 19.23 19.23 19.23 19.23
11 1.83 — 18.57 19.29 19.29 19.29 19.29
10 1.57 — 18.71 19.50 19.50
9 1.31 — 18.87 19.81 19.81 19.83 19.83
8 1.13 — 18.96 20.02 20.03 20.04 20.06 20.11 20.12
7 0.98 — 19.03 20.17 20.18 20.20 20.23 20.27 20.30 20.35 20.36 20.37
6 0.83 — 19.09 20.27 20.28 20.30 20.33 20.36 20.40 20.43 20.43 20.45 20.45 20.46
5 0.70 — 19.13 20.31 20.32 20.34 20.37 20.40 20.42 20.44 20.45 20.47 20.47 20.47
4 0.52 — 19.16 20.31 20.32 20.33 20.35 20.37 20.40 20.42 20.42
3 0.35 — 19.17 20.27 20.27 20.28 20.30 20.30
2 0.17 — 19.18 20.22 20.22 20.22
1 0.00 — 19.18 20.20
+----------
0.00 0.01 0.01 0.01 0.01 0.01 0.01 0.01 0.01 0.01 0.01 0.01
1 2 3 4 5 6 7 8 9 10 11 12
3D Conduction Profile of Test SectionTS4AP5 13-JUL-94 21:43:08
Steady-State Temperature Distribution at Time 0.0000E+00
Z = 5.2070E-02
15 3.14 — 17.69 18.24 18.24 18.25 18.26 18.27 18.27 18.28
14 2.36 — 17.75 18.32 18.32 18.33 18.34 18.35 18.36 18.36 18.37 18.37 18.38
13 2.16 — 17.78 18.33 18.34 18.35 18.36 18.36 18.37 18.38 18.38 18.39 18.39
12 2.01 — 17.81 18.35 18.35 18.36 18.36 18.36 18.37
11 1.83 — 17.85 18.38 18.38 18.38 18.38
10 1.57 — 17.92 18.48 18.48
9 1.31 — 18.01 18.65 18.66 18.67 18.67
8 1.13 — 18.06 18.78 18.78 18.80 18.81 18.84 18.84
7 0.98 — 18.10 18.87 18.87 18.89 18.91 18.93 18.95 18.98 18.99 19.00
6 0.83 — 18.13 18.92 18.93 18.95 18.97 18.99 19.01 19.03 19.04 19.04 19.05 19.05
5 0.70 — 18.15 18.95 18.95 18.97 18.99 19.01 19.02 19.04 19.04 19.05 19.06 19.06
4 0.52 — 18.16 18.94 18.95 18.9€ 18.97 18.98 19.00 19.02 19.02
3 0.35 — 18.17 18.91 18.91 18.92 18.93 18.93
2 0.17 — 18.17 18.87 18.87 18.87
1 0.00 — 18.17 18.86
+----------
0.00 0.01 0.01 0.01 0.01 0.01 0.01 0.01 0.01 0.01 0.01 0.01
1 2 3 4 5 6 7 8 9 10 11 12
3D Conduction Profile of Test SectionTS4AP5 13-JUL-94 21:43:08
Steady-State Temperature Distribution at Time 0.0000E+00
Z = 5.5880E-02

15 3.14 — 17.31 17.75 17.75 17.76 17.77 17.77 17.78 17.78
14 2.36 — 17.34 17.79 17.79 17.80 17.81 17.82 17.82 17.83 17.83 17.83 17.84
13 2.16 — 17.36 17.79 17.80 17.80 17.81 17.82 17.82 17.83 17.84 17.84 17.84
12 2.01 — 17.37 17.79 17.79 17.80 17.80 17.81 17.81
11 1.83 — 17.39 17.80 17.80 17.80 17.80
10 1.57 — 17.43 17.85 17.85
9 1.31 — 17.48 17.95 17.95 17.96 17.96
8 1.13 — 17.51 18.03 18.03 18.04 18.05 18.07 18.07
7 0.98 — 17.53 18.08 18.09 18.10 18.11 18.13 18.14 18.16 18.17 18.17
6 0.83 — 17.55 18.12 18.12 18.14 18.15 18.17 18.18 18.19 18.20 18.20 18.21 18.21
5 0.70 — 17.56 18.13 18.14 18.15 18.16 18.17 18.19 18.20 18.20 18.21 18.21 18.21
4 0.52 — 17.57 18.12 18.13 18.13 18.14 18.15 18.17 18.18 18.18
3 0.35 — 17.57 18.09 18.10 18.10 18.11 18.11
2 0.17 — 17.57 18.07 18.07 18.07
1 0.00 — 17.57 18.05
+----------
0.00 0.01 0.01 0.01 0.01 0.01 0.01 0.01 0.01 0.01 0.01 0.01
1 2 3 4 5 6 7 8 9 10 11 12
3D Conduction Profile of Test SectionTS4AP5 13-JUL-94 21:43:08
Steady-State Temperature Distribution at Time 0.0000E+00
Z = 5.9690E-02
15 3.14 — 17.10 17.48 17.48 17.48 17.49 17.50 17.50 17.50
14 2.36 — 17.12 17.49 17.50 17.50 17.51 17.52 17.52 17.53 17.53 17.53 17.53
13 2.16 — 17.12 17.49 17.49 17.50 17.51 17.51 17.52 17.53 17.53 17.53 17.53
12 2.01 — 17.13 17.48 17.49 17.49 17.49 17.50 17.50
11 1.83 — 17.14 17.48 17.48 17.48 17.48
10 1.57 — 17.17 17.51 17.51
9 1.31 — 17.20 17.57 17.57 17.58 17.58
8 1.13 — 17.22 17.63 17.63 17.64 17.64 17.66 17.66
7 0.98 — 17.23 17.67 17.67 17.68 17.69 17.70 17.71 17.73 17.73 17.74
6 0.83 — 17.24 17.69 17.69 17.70 17.71 17.73 17.74 17.75 17.75 17.76 17.76 17.76
5 0.70 — 17.25 17.70 17.70 17.71 17.72 17.73 17.74 17.75 17.75 17.76 17.76 17.76
4 0.52 — 17.25 17.69 17.69 17.70 17.70 17.71 17.73 17.73 17.73
3 0.35 — 17.25 17.66 17.67 17.67 17.68 17.68
2 0.17 — 17.25 17.64 17.64 17.64
1 0.00 — 17.25 17.63
+----------
0.00 0.01 0.01 0.01 0.01 0.01 0.01 0.01 0.01 0.01 0.01 0.01
1 2 3 4 5 6 7 8 9 10 11 12
3D Conduction Profile of Test SectionTS4AP5 13-JUL-94 21:43:08
Steady-State Temperature Distribution at Time 0.0000E+00
Z = 6.3500E-02 15 3.14 — 17.03 17.39 17.39 17.39 17.40 17.40 17.41 17.41
14 2.36 — 17.04 17.40 17.40 17.41 17.41 17.42 17.43 17.43 17.43 17.43 17.44
13 2.16 — 17.05 17.39 17.40 17.40 17.41 17.42 17.42 17.43 17.43 17.44 17.44
12 2.01 — 17.06 17.39 17.39 17.39 17.39 17.40 17.40

11 1.83 — 17.06 17.38 17.38 17.38 17.38
10 1.57 — 17.08 17.40 17.40
9 1.31 — 17.11 17.45 17.46 17.46 17.46
8 1.13 — 17.12 17.50 17.50 17.51 17.52 17.53 17.53
7 0.98 — 17.14 17.54 17.54 17.55 17.56 17.57 17.58 17.59 17.59 17.60
6 0.83 — 17.14 17.56 17.56 17.57 17.58 17.59 17.60 17.61 17.61 17.62 17.62 17.62
5 0.70 — 17.15 17.56 17.56 17.57 17.58 17.59 17.60 17.61 17.61 17.62 17.62 17.62
4 0.52 — 17.15 17.55 17.55 17.56 17.57 17.58 17.59 17.59 17.59
3 0.35 — 17.15 17.53 17.53 17.53 17.54 17.54
2 0.17 — 17.15 17.51 17.51 17.51
1 0.00 — 17.15 17.50
+———
0.00 0.01 0.01 0.01 0.01 0.01 0.01 0.01 0.01 0.01 0.01 0.01
1 2 3 4 5 6 7 8 9 10 11 12

C.11 *ho.one* Initial Heat Transfer Coefficients Input File to *sh2.for*

```
50006. 50006. 81311. 50000. 50000. 65580. 61295. 83822. 90592.
   90914. 87864. 70450. 62241. 50000. 50000. 77291. 50000. 50000. 1
   50006. 50006. 81314. 50000. 50000. 65732. 61474. 77958. 85770.
   86206. 83122. 65726. 62352. 50000. 50000. 77305. 50000. 50000. 2
   50006. 50006. 81323. 50000. 50000. 66099. 61895. 65543. 74610.
   75688. 72261. 56701. 62621. 50000. 50000. 77334. 50000. 50000. 3
   50006. 50006. 81339. 50000. 50000. 66663. 62550. 61101. 59272.
   60752. 57266. 61507. 63085. 50000. 50000. 77387. 50000. 50000. 4
   50006. 50006. 81361. 50000. 50000. 67374. 63365. 61853. 61395.
   61272. 61406. 62041. 63865. 50000. 50000. 77454. 50000. 50000. 5
   50006. 50006. 81390. 50000. 50000. 68076. 64192. 62641. 62129.
   62006. 62142. 62820. 64622. 50000. 50000. 77536. 50000. 50000. 6
   50006. 50006. 81426. 50000. 50000. 68977. 65255. 63681. 63119.
   62974. 63118. 63822. 65577. 50000. 50000. 77641. 50000. 50000. 7
   50006. 50006. 81474. 50000. 50000. 69984. 66470. 64885. 64280.
   64114. 64268. 64684. 66668. 50000. 50000. 77775. 50000. 50000. 8
   50006. 50006. 81540. 50000. 50000. 71288. 68063. 66503. 65862.
   65673. 65816. 66232. 68099. 50000. 50000. 77964. 50000. 50000. 9
   50006. 50006. 81619. 50000. 50000. 73041. 70219. 68732. 68059.
   67835. 67961. 68328. 69986. 50000. 50000. 78187. 50000. 50000. 10
   50006. 50006. 81675. 50000. 50000. 74512. 72064. 70659. 69973.
   69724. 69824. 70121. 71555. 50000. 50000. 78351. 50000. 50000. 11
   50006. 50006. 81709. 50000. 50000. 75376. 73170. 71835. 71151.
   70884. 70959. 71215. 72500. 50000. 50000. 78452. 50000. 50000. 12
   50006. 50006. 81738. 50000. 50000. 76061. 74067. 72803. 72121.
   71843. 71607. 72106. 73269. 50000. 50000. 78544. 50000. 50000. 13
   50006. 50006. 81783. 50000. 50000. 76859. 75121. 73954. 73290.
   72995. 72735. 73177. 74185. 50000. 50000. 78670. 50000. 50000. 14
```

Appendix D

Calibration Data

D.1 Flow Meter at Low Flow Rate Data

Calibration performed on October 19, 1994 by Anthony Hechanova, Philip LaFond, and Varghese Thannickal

Flow Rate Flow Meter Computed (gpm)	Flow Rate Hand-timed Measurement (gpm)
0.25	0.458
0.30	0.458
0.52	0.716
0.61	0.716
0.84	0.906
0.88	0.906
1.00	1.062
1.01	1.062
1.33	1.315
1.27	1.315
1.61	1.496
1.66	1.496
1.69	1.672
1.67	1.672
1.85	1.694

Flow Rate Flow Meter Computed (gpm)	Flow Rate Hand-timed Measurement (gpm)
1.87	1.694
1.97	1.893
1.91	1.893
2.10	1.945
2.05	1.945
1.86	1.854
1.82	1.854
2.28	2.240
2.27	2.240

D.2 Channel 0 Switchbox and *Daqware* Voltage Measurement Data

Calibration performed on July 8, 1994 by Thai Thanh Minh

Applied Voltage (V)	Mean Voltage (V)	Standard Deviation (V)
15.31	2.873	0.06330
9.82	1.722	0.05370
4.84	0.925	0.02350
20.10	3.791	0.1632
24.80	4.485	0.2262
15.23	2.803	0.1292

Appendix E

Experimental Data

E.1 Notebook Data and Comments

E.1.1 Data Files

Test Section ID	Pressure (psig)[a]	Flowmeter File	Flowmeter Sample Rate	Data File	Data Sample Rate
TS6A	370	t628a.txt	1000	t628c.txt	20
		t628b.txt	1000		
TS9B	410	f627b.txt	500	ts9b.dat	40
TS11A	387±5	t11a2.txt	4000	t11a.txt	20
TS14B	355	t14b16.txt	600	t14b17.txt	20
TS15A	400	t15a1.txt	300	t15a2.txt	20
TS15B	405	ts15b1.txt	300	ts15b2.txt	20
TS16B	430±3	t16b1.txt	100	t16b2.txt	100
TS17A	420±5	t17a1.txt	200	t17a2.txt	100
TS17B	415±5	t17b1.txt	300	t17b2.txt	100
TS18A	432	ts18a3.txt	100	ts18a4.txt	20
TS18B	430	t18b5.txt	300		20
		t18b6.txt	200		
TS19A	420	t19a1.txt	200	ts19a2.txt	20
		t19a3.txt	200		
TS19B	355±10	t19b1.txt	2000	t19b2.txt	20
		t19b3.txt	4000		
TS20A	400	ts20a1.txt	1000	ts20a2.txt	20
		ts20a3.txt	2000		
TS20B	360±5	t20b1.txt	5000	t20b2.txt	100
		t20b3.txt	5000		
TS21A	415-5	t21a3.txt	2000	t21a4.txt	100
		t21a5.txt	2000		
TS21B	422±3	ts21b1.txt	1800	ts21b2.txt	100
		ts21b3.txt	1800		
TS22A	375	t22a6.txt	5000	t22a5.txt	100
TS22B	370±5	t22b1.txt	5000	t22b2.txt	100

[a] ± Represents fast fluctuation in Bourdon Gauge measurement, not uncertainty.

Table E.1.1 (Continued)

Test Section ID	Pressure (psig)[a]	Flowmeter File	Flowmeter Samp. Rate	Data File	Data Samp. Rate
TS23A	380	t23a2.txt	5000	t23a3.txt	100
		t23a4.txt	5000		
TS23B	365±3	t23b2.txt	5000	t23b3.txt	100
		t23b4.txt	5000		
TS24A	360±2	t24a1.txt	5000	t24a2.txt	100
		t24a3.txt	6000		
TS24B	355±5	t24b1.txt	6000	t24b2.txt	100
		t24b3.txt	6000		
TS25A	385±2	t25a1.txt	5000	t25a2.txt	100
		t25a2.txt	5000		
TS25B	390±3	t25b1.txt	5000	t25b2.txt	100
		t25b3.txt	5000		
TS26A	409	t26a1.txt	5000	t26a2.txt	100
		t26a3.txt	5000		
TS26B	413	ts26b1.txt	4000	ts26b2.txt	100
		ts26b3.txt	4000		
TS27A	407	t27a1.txt	5000	t27a2.txt	100
		t27a3.txt	5000		
TS27B	245±5	t27b1.txt	8000	t27b2.txt	100
		t27b3.txt	9000		
		t27b4.txt	9000		
TS28A	411	t28a1.txt	5000	t28a2.txt	100
		t28a3.txt	5000		
TS28B	417	t28b1.txt	3000	t28b2.txt	100
		t28b3.txt	3000		
TS29A	300	t29a1.txt	6000	t29a2.txt	100
		t29a3.txt	7000		
TS29B	320±10	t29b1.txt	8000	t29b2.txt	100
		t29b3.txt	8000		

[a]± Represents fast fluctuation in Bourdon Gauge measurement, not uncertainty.

E.1.2 Power Measurements

Power Supply Current (A)	Power Supply Voltage (V)	Power (kW)	Observations and Comments
TS6A	TH, JP[a]		Date: 6-28-94
900	18.1	16.3	Time: 2:28 pm
850	18.2	15.5	TC Box Channels:
800	16.7	13.4	From 1 to 2 @ 2:29:45 pm
			Lost soon after channels were switched
TS9B	TH, JP		Date: 6-27-94
700	17.2	12.0	Time: 11:02 am
650	17.4	11.3	TC Box Channels switched:
600	17.5	10.5	from 3 to 2 @ 11:05:45 am
			from 2 to 1 @ 11:06:05 am
			TS burned out at 11:06:30 am.
			JP switching box 3 from 1 to 4
			but stopped at 3, thus, temp.
			increase may appear in data.
			f627b.txt @ 11:08 am
TS11A	TH, JP, TM		Date: 7-13-94
			@ 12:06 pm p=387±5
			Tank2 level = 340 gal
400	15	6.0	Time: 12:11 pm
425	17	7.2	Time: 12:12 pm
450	17	7.7	Time: 12:12 pm
500	19	9.5	TC's switched every 2 secs x 3
510	19	9.7	
575	19	10.9	
600	19	11.4	Time: 12:14 pm
			Tank2 level = 375 gal
TS14B	TH, JP		Date: 8-24-94
525	11.75	6.2	
500	12.	6.0	
600	14.75	8.9	
700	17.25	12.1	
800	~20	16.	

Table E.1.2 (Continued)

PS Current (A)	PS Voltage (V)	Power (kW)	Shunt Volt. (mV)	Shunt Resist. (mΩ)	Observations and Comments
TS15A	TH, JP[a]				Date: 8-24-94
500	12.6	6.3	59.1	.118	@ 12:43 pm
550	14.5	7.8	65.1	.118	steady p = 400 psig
650	16.5	10.7	79.6	.122	
710	16.5	11.7	84.4	.119	
760	16.5	12.5	89.8	.118	
800	16.5	13.2	93.6	.117	
850	16.5	14.0	96.8	.114	
300	8.5	2.6	37.1	.124	R_{shunt} in CH 3
400	10	4.0	48.4	.121	
500	12	6.0	58.2	.116	
625	15.5	9.7	71.8	.115	
TS15B	TH, JP				Date: 8-24-94
					Ch3 → Shunt Resistor
300	8.5	2.6	37.1	.124	
400	10.	4.0	48.4	.121	
500	12.	6.0	58.2	.116	
625	15.5	9.7	71.8	.115	
TS16B	TH, JP				Date: 8-25-94
100	4.5	0.45	13.8	.138	No cement on heater
175	8.75				Paused
200	10.5	2.1	25.4	.127	
300	13	3.9	36.9	.123	
415	20	8.3	49.1	.118	Burnt out
TS17A	TH, JP				Date: 8-25-94
110	2	0.22	15.2	.138	No felt (raised one connector)
200	3	.06	25.5	.128	No cement
200	4.2	0.84	23.0	.115	Jump down 100 A
300	8	2.4	36.8	.123	
400	11	4.4	47.4	.119	
500	13.2	6.6	57.2	.114	*Snap*
0	25.0	0.	0.	NA	Lost at 600 A
					@ 18V I = 0

Table E.1.2 (Continued)

PS Current (A)	PS Voltage (V)	Power (kW)	Shunt Volt. (mV)	Shunt Resist. (mΩ)	Observations and Comments
TS17B	TH, JP[a]				Date: 8-25-94
100	3.	0.3	14.3	.143	Tank1 Level = 375 gal
200	5.75	1.2	25.1	.126	
300	9.	2.7	36.1	.120	
410	12.75	5.2	48.6	.119	
530	15.5	8.2	60.2	.114	
625	17.	10.6	70.5	.113	*Snap* Tank1 Level = 340 gal
TS18A	TH				Date: 9-9-94 Using Ceramic Fiber to insulate top of TS No cement on heater
100	2.25	0.22	14.0	.140	Time: 9:55 am
200	4.6	0.92	24.8	.124	
325	7.5	2.44	38.6	.119	Increasing I
425	8.5	3.61	49.5	.116	
550	9.5	5.22	62.6	.114	
600	12.75	7.65	66.7	.111	TS is orange Steam from downstream joints Heat deformed PVC piping
TS18B	TH, BL				Date: 9-16-94
100	3.75	.38	13.9	.139	
200	7.5	1.5	25.6	.128	
350	9.3	3.3	41.2	.118	
460	10.	4.6	55.1	.120	
600	12.5	7.5	68.4	.114	*Snap* TC in CH 3 TC in Ch 2 not touching TS

Table E.1.2 (Continued)

PS Current (A)	PS Voltage (V)	Power (kW)	Shunt Volt. (mV)	Shunt Resist. (mΩ)	Observations and Comments
TS19A	TH[a]				Date: 9-21-94
					TC2 - Mid, close to heater
					TC3 - downstream
					A is upstream
100	3	0.3	14.7	.147	
200	5.5	1.1	23.4	.117	
300	8.5	2.6	35.7	.119	
425	10.5	4.5	50.0	.118	
575	11.3	6.5	65.9	.115	
725	15.	10.9	83.3	.115	TS is orange
925	16.5	15.3	100.3	.108	Burnt
TS19B	TH				Date: 10-8-94
100	2.2	0.2	14.3	.143	
200	4.0	0.8	24.6	.123	
300	6.75	2.0	35.6	.119	
400	8.6	3.4	48.8	.122	
510	9.1	4.6	60.2	.118	
600	9.6	5.8	69.3	.116	
700	10.5	7.4	80.4	.115	
800	13.2	10.6	93.4	.117	
950	14.0	13.3	108.3	.114	
1000	15.2	15.2	115.1	.115	
1100	17.4	19.1	124.4	.113	Time: 5:13 pm

Table E.1.2 (Continued)

PS Current (A)	PS Voltage (V)	Power (kW)	Shunt Volt. (mV)	Shunt Resist. (mΩ)	Observations and Comments
TS20A	TH, BL[a]				Date: 9-23-94
					Tank1 Level = 250 gal
					Pump - full power
100	2.5	.25	13.8	.138	
200	4.75	.95	25.4	.127	
300	6.0	1.8	34.4	.115	
400	8.2	3.3	47.4	.119	
525	9.0	4.7	60.2	.115	
610	9.5	5.8	69.7	.114	
700	10.2	7.1	79.9	.114	
760	12.5	9.5	87.4	.115	
900	13.5	12.2			
950	14.4	13.7			
960	14.4	13.8			Final Tank1 Level = 140 gal
TS20B	TH, BL,	SL			Date: 10-14-94
					Tank2 Level $\leq$ 50 gal
100	2.2	.22	13.4	.134	No flow, BL test TC's
150	3.5	.53	18.9	.126	No flow
200	4.7	.94	24.7	.124	Flow
300	7.7	2.3	35.7	.119	Tank2 = 92 gal @ 5:04:40
425	9.7	4.1	49.7	.117	
550	10.5	5.8	62.7	.114	
625	11.	6.9	72.9	.117	
700	11.75	8.2	81.6	.117	
750	13.2	9.9	85.0	.113	
825	14.5	12.0	96.3	.117	Time: 5:10 pm
					TC4/TC5 possibly out of TS
					Tank2 = 150 gal @ 5:10:15
					Tank2 $\sim$ 180 gal @ 5:14 pm

Table E.1.2 (Continued)

PS Current (A)	PS Voltage (V)	Power (kW)	Shunt Volt. (mV)	Shunt Resist. (mΩ)	Observations and Comments
TS21A	TH[a]				Date: 10-9-94
					Fixed current circuit
100	2.0	.20	14.0	.140	No file
200	4.25	.85	24.9	.125	To file
300	7.25	2.2	36.5	.122	Tank2 = 250 gal @ 12:14:10
400	8.5	3.4	48.9	.122	
500	9.25	4.6	58.5	.117	
600	10.	6.0	69.8	.116	
700	11.75	8.2	79.4	.113	
850	14.	11.9	96.5	.114	
925	15.	13.9	105.5	.114	
1000	17.5	17.5	115.9	.116	Tank2 = 275 gal @ 12:19:05
TS21B	TH, PL				Date: 10-9-94
					Note: CH1 TCs switched
100	2.5	.25	13.4	.134	now CH1 → TS
200	5.	1.0	24.6	.123	T_B → TS earlier
300	8.	2.4	36.2	.121	
400	9.	3.6	48.8	.122	
500	10.1	5.1	59.4	.119	
625	11.	6.9	71.8	.115	
700	13.4	9.4	81.6	.117	
825	14.6	12.	94.7	.115	
950					Blew between 850-950 A
					PL: TC1 (upstream) came out
TS22A	TH, BL,	VT			Date: 10-26-94
100			12.3		No flow, Time: 6:14 pm
200	4.75	.95	25.6	.128	Flow, Time: 6:16 pm
300	5.5	1.7	36.5	.122	
400	7.5	3.0	56.2	.141	
550	8.0	4.4	64.7	.118	
675	8.5	5.7	78.7	.117.	
700	8.5	6.0	81.8	117.	
900	9.0	8.1	104.7	.116	
975	9.75	9.5	113.5	.116	
1175	11.0	16.3			
1500	12.75	22.5			

Table E.1.2 (Continued)

PS Current (A)	PS Voltage (V)	Power (kW)	Shunt Volt. (mV)	Shunt Resist. (mΩ)	Observations and Comments
TS22B	TH, BL,	VT[a]			Date: 10-26-94
					May max PS at 2200A
					If so, then lower velocity
175	.5	.09	20.1	.115	
310	.5	.16	38.3	.124	
505	.75	.38	59.8	.118	
730	1.0	.73	84.2	.115	
900	1.25	1.1	102.3	.114	
1000	1.3	1.3	116.2	.116	
1100	1.5	1.7	126.5	.115	
1200	1.75	2.1	138.0	.115	
1340	1.75	2.3	156.5	.117	
1550	2	3.1	186.0	.120	
1770	2	3.5	.206V	.116	
2000	2.25	4.5	.235V	.118	↑ through Cu
525	5.6	2.9	63.4	.121	
600	7.2	4.3	72.4	.121	
725	7.75	5.6	86.0	.119	
900	8.2	7.4	108.4	.120	
1075	8.8	9.5	127.8	.119	Turned off prematurely by BL?
1150	10.	11.5	135.4	.118	←Artificially placed in txt file
TS23A	TH				Date: 10-26-94
					Tank1 = 300 gal @ 6:48:15
200	1.5	.30	23.0	.115	Time: 6:51 pm
300	2.2	.66	36.6	.122	
400	3.25	1.3	48.6	.122	
500	4.5	2.25	58.9	.118	
600	6.1	3.66	69.4	.116	
700	7.0	4.9	82.1	.117	
800	7.5	6.0	93.9	.117	
925	8.0	7.4	107.4	.116	
1000	8.5	8.5	117.6	.118	
1080	9.5	10.3	124.6	.115	
1120	10.5	11.8	128.8	.115	
1170	11.5	13.5	136.1	.116	
					Blew @ 12.5 V, lots of smoke
					Tank1 = 220 gal @ 6:57:50

Table E.1.2 (Continued)

PS Current (A)	PS Voltage (V)	Power (kW)	Shunt Volt. (mV)	Shunt Resist. (mΩ)	Observations and Comments
TS23B	TH, BL[a]				Date: 10-27-94
					Tank1 = 435 gal, 3:15 pm
200	1.75	.35	23.5	.118	Time: 3:31 pm
300	2.2	.66	35.3	.118	
400	3.0	1.2	47.8	.120	
400	4.5	1.8	46.6	.117	Dip in I as V increased
500	6.4	3.2	57.5	.115	
625	7.6	4.75	68.8	.110	
700	8.0	5.6	79.0	.113	
800	8.3	6.6	91.0	.114	
900	9.0	8.1	101.8	.113	
1000	10.2	10.2	112.8	.113	
1050	12.0	12.6	118.3	.113	
1060	13.0	13.8	119.4	.113	Smoked @ 3:36 pm
TS24A	TH, BL				Date: 10-27-94
175	1.5	.26	22.6	.129	Tank2 = 200 gal @ 3:56 pm
300	2.2	.66	39.1	.130	
405	3.0	1.2	53.0	.131	
405	3.5	1.4	66.0	.163	Dip in I
500	5.6	2.8	63.1	.126	
620	7.2	4.5	75.9	.122	
730	8.0	5.8	90.2	.124	
850	8.5	7.2	105.1	.124	
950	9.1	8.6	119.0	.125	
1050	10.3	10.8	130.5	.124	
1100	12.0	13.2	135.7	.123	
1110	13.0	14.4	137.5	.124	
1170	14.0	16.4	145.3	.124	Big blast, cables jiggle @ 4:01 pm

Table E.1.2 (Continued)

PS Current (A)	PS Voltage (V)	Power (kW)	Shunt Volt. (mV)	Shunt Resist. (mΩ)	Observations and Comments
TS24B	TH, VT[a]				Date: 10-27-94
160	1.5	.24	18.1	.113	
300	2.5	.75	35.6	.119	
400	3.0	1.2	47.1	.118	
500	5.0	2.5	59.1	.118	
600	6.0	3.6	69.7	.116	
700	7.0	4.9	80.5	.115	
850	7.2	6.1	96.4	.113	
1000	8.0	8.0	116	.116	
1100	9.0	9.9	125.7	.114	
1175	10.0	11.8	134	.114	
1275	11.0	14.0	146.8	.115	
1400	11.0	15.4	160.9	.115	
1460	10.75	15.7	166.9	.114	*Boom*, smoke
TS25A	TH, VT				Date: 10-27-94
200	1.6	.32	22.9	.115	
310	2.75	.85	37.1	.120	
400	3.75	1.5	47.7	.119	I dip
500	5.5	2.75	56.4	.113	
600	7.1	4.3	69.8	.116	
710	7.7	5.5	82.7	.116	
900	8.4	7.6	103.3	.115	
1100	8.9	9.8	126.3	.115	*Pop*, maybe too early Time: 5:45 pm
TS25B	TH, VT				Date: 10-27-94
200	2.5	.50	25.4	.127	
300	3.5	1.1	37.0	.123	
400	4.75	1.9	44.9	.112	
500	6.7	3.4	59.2	.118	
600	7.7	4.6	70.0	.117	
700	7.9	5.5	81.4	.116	
850	8.2	7.0	98.0	.115	
975	8.7	8.5	112.2	.115	
1050	9.25	9.7	121.8	.116	
1100	10.	11.0	126.5	.115	
1170	11.	12.9	135.0	.115	@ 12V I shot up, *snap*

Table E.1.2 (Continued)

PS Current (A)	PS (Voltmeter) Voltage (V)	Power (kW)	Observations and Comments
TS26A	TH, BL[a]		Date: 11-4-94
			TC's checked by BL
			Tank1 $\sim$ 450 gal
300	3.09	.93	
400	4.39	1.8	
500	5.83	2.9	
600	6.74	4.0	
700	7.14	5.0	
800	7.61	6.1	
900	8.56	7.7	
1050	10.7	11.3	
1200	11.53	13.8	
1300	12.4	16.1	
1400	?12.4?	(17.4)	
			Pump humming, very smooth run
TS26B	TH, FB		Date: 11-6-94
			TC visual check by TH
200	2.42	.48	
300	3.78	1.1	
400	5.29	2.1	
500	6.73	3.4	
600	7.66	4.6	
700	8.30	5.8	
800	9.50	7.6	
900	11.25	10.1	Lost @ 1000 A

Table E.1.2 (Continued)

PS Current (A)	PS (Voltmeter) Voltage (V)	Power (kW)	Observations and Comments
TS27A	TH, BL[a]		Date: 11-4-94
			Time: 3:20 pm
200	1.83	.37	BL: TC check
300	2.76	.83	
400	3.71	1.5	
500	5.01	2.5	
600	6.11	3.7	
700	6.64	4.6	
800	7.01	5.6	
900	7.77	7.0	
1000	9.57	9.6	
1350	9.74	13.1	Flash and spark
TS27B	TH		Date: 11-4-94
			TH: visual TC check
			Fully open needle valve
			"overwrite" error in "Save to File"
200	1.80	.36	
300	2.77	.83	
400	4.07	1.6	
500	5.52	2.8	
600	6.76	4.1	
700	7.35	5.1	
800	7.86	6.3	
900	8.65	7.8	
1000	9.99	10.0	
1100	11.3	12.4	
1200	11.67	14.0	
1300	11.58	15.1	
1400	12.5	17.5	Spark
			Same file error, read flow again

Table E.1.2 (Continued)

PS Current (A)	PS (Voltmeter) Voltage (V)	Power (kW)	Observations and Comments
TS28A	TH, BL[a]		Date: 11-4-94
200	1.68	.34	BL: TC check
300	2.48	.74	Flow read while TH was adjusting?
400	3.50	1.4	
500	4.74	2.4	
600	5.78	3.5	
700	6.38	4.5	
800	6.72	5.4	
900	7.25	6.5	
1000	8.15	8.2	
1100	9.39	10.3	
1200	10.03	12.0	
1300	10.28	13.4	Flash between 1400-1500 A
TS28B	TH, FB		Date: 11-6-94
			Note: TC centerline is not TS C.L.
100	1.05	.11	
200	1.82	.36	
300	2.77	.83	
400	3.91	1.6	
500	5.17	2.6	
600	6.22	3.7	
700	6.84	4.8	
800	7.29	5.8	
900	8.19	7.4	
1000	9.78	9.8	
1100	10.47	11.5	
1200	10.61	12.7	Smoke
			End of final experiment 1:50 am

Table E.1.2 (Continued)

PS Current (A)	PS (Voltmeter) Voltage (V)	Power (kW)	Observations and Comments
TS29A	TH, BL[a]		Date: 11-4-94
200	1.85	.38	TC check by BL
300	3.03	.91	
400	4.46	1.8	
500	5.96	3.0	
600	7.10	4.3	
700	7.57	5.3	
800	8.02	6.4	
900	8.95	8.1	
1000	10.87	10.9	
1150	11.6	13.3	
1200	11.7	14.0	
1300	12.35	16.1	Flash, gone
TS29B	TH		Date: 11-4-94
			TC visual check by TH
200	1.79	.36	
300	2.88	.86	
400	4.26	1.7	
500	5.59	2.8	
600	6.77	4.1	
700	7.32	5.1	
800	7.88	6.3	
900	8.82	7.9	
1000	10.52	10.5	
1100	11.11	12.2	
1200	11.69	14.0	
1300	12.27	16.0	
1400	12.38	17.3	Smoke

[a] Researcher's/Observer's Initials:
TH = Anthony Hechanova, Graduate Student
JP = Jean-Paul Folch, Undergraduate Student
TM = Thai Thanh Minh, Research Science Institute Intern
BL = Boris Lekakh, Graduate Student
SL = Bronislav Guimpelson, Graduate Student
PL = Philip LaFond, Undergraduate Student
VT = Varghese Thannickal, Graduate Student
FB = Frode Bloch, Research Affiliate

E.2 Power and Temperature Profiles

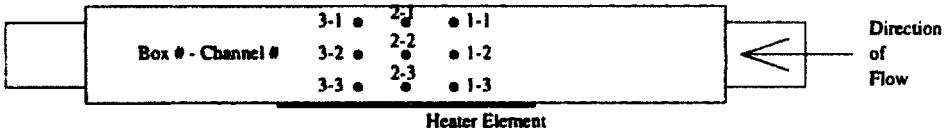

Figure E-1: Test Section 6A and 9B Thermocouple Locations

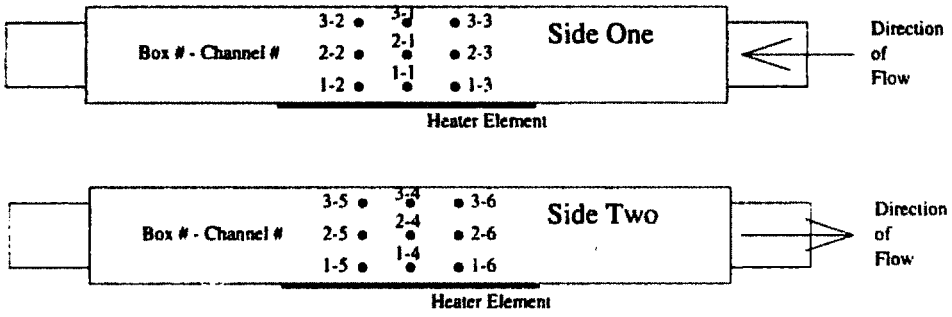

Figure E-2: Test Section 11A Thermocouple Locations

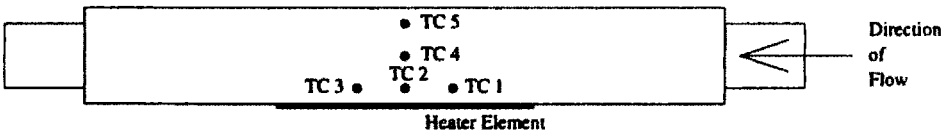

Figure E-3: Test Section Thermocouple Locations for TS14B and Higher

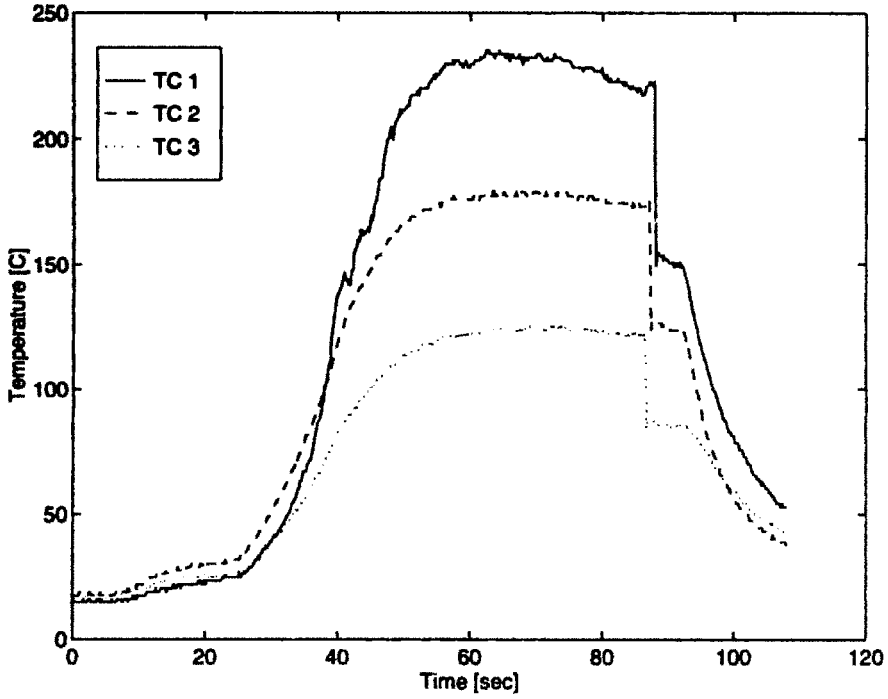

Figure E-4: Test Section 6A Temperature Profile

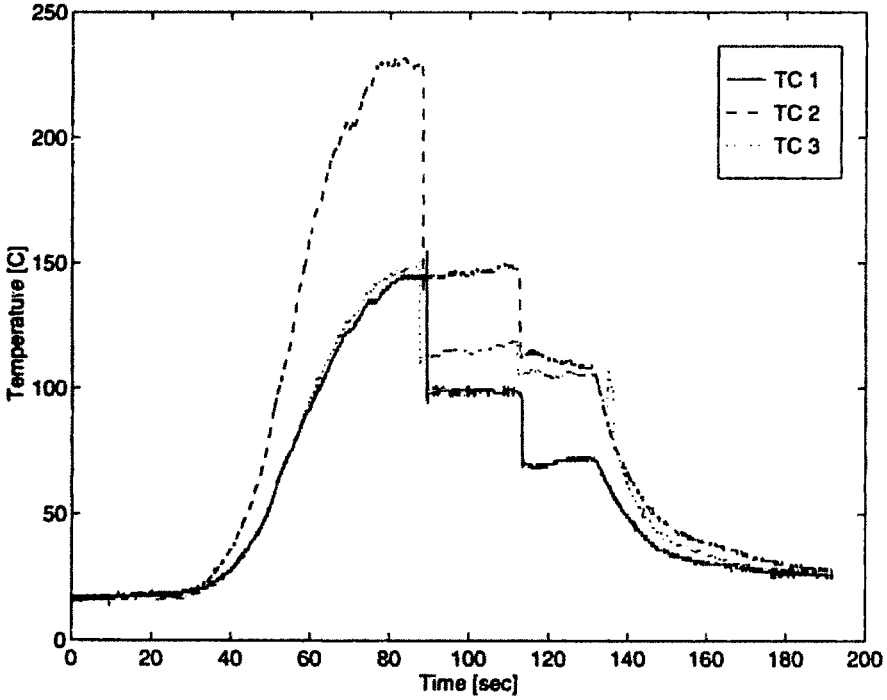

Figure E-5: Test Section 9B Temperature Profile

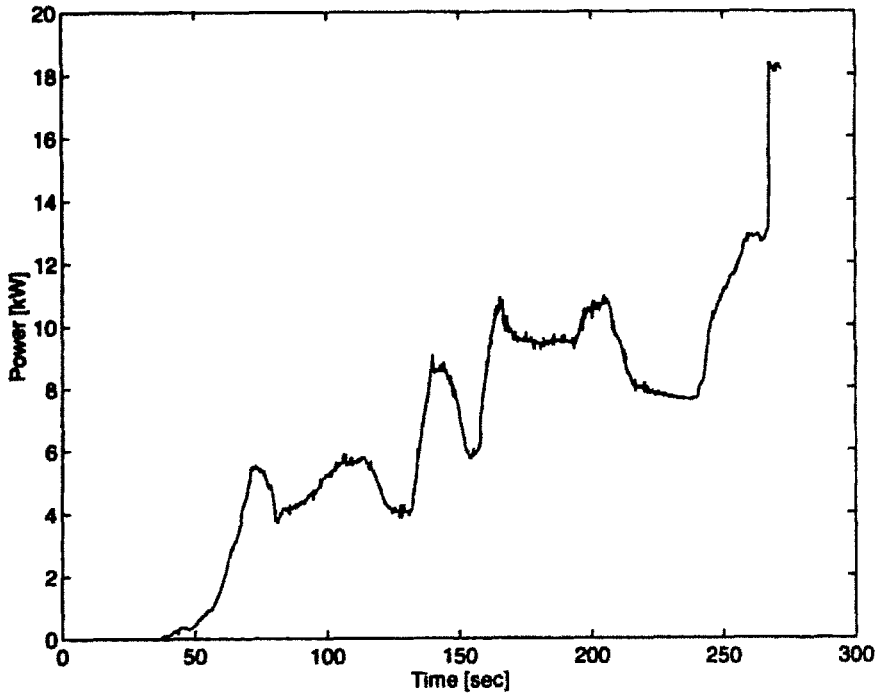

Figure E-6: Test Section 11A Power Profile

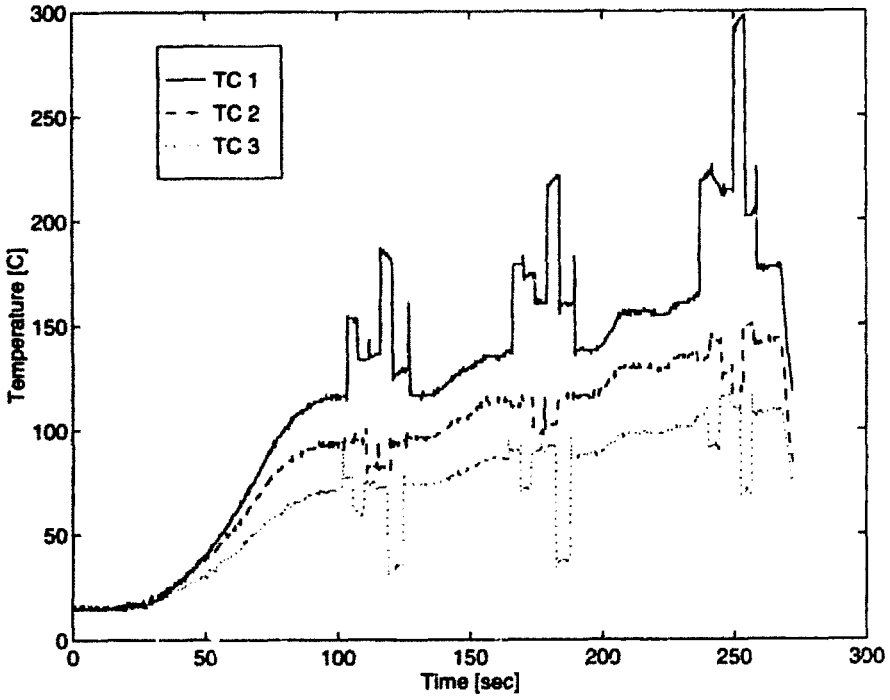

Figure E-7: Test Section 11A Temperature Profile

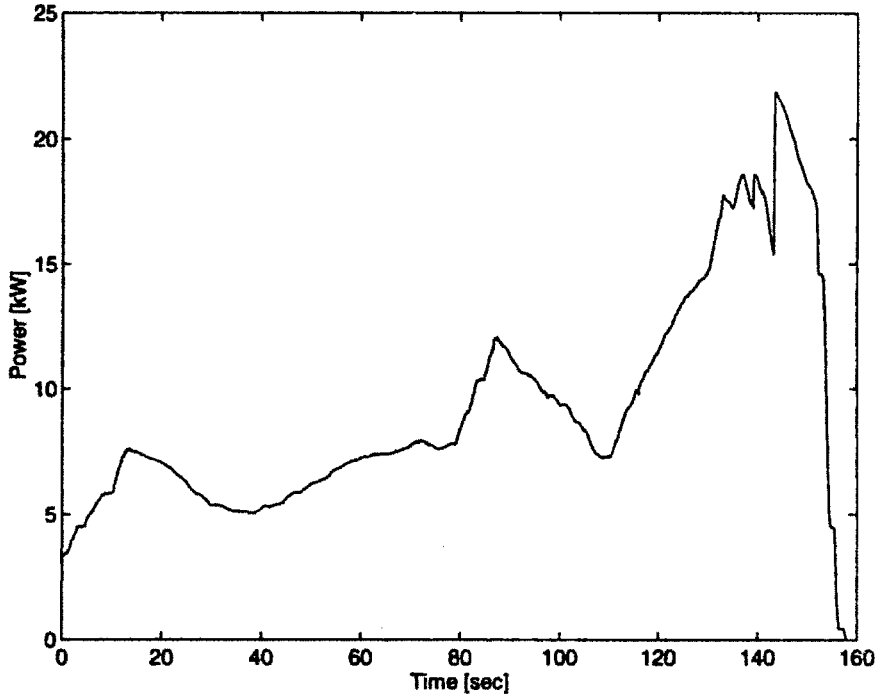

Figure E-8: Test Section 14B Power Profile

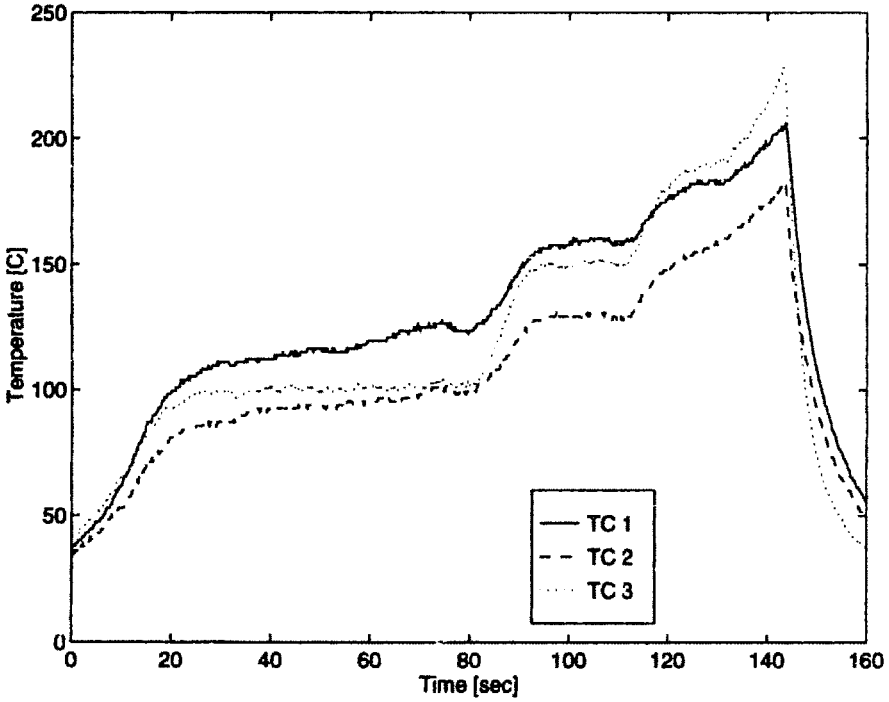

Figure E-9: Test Section 14B Temperature Profile

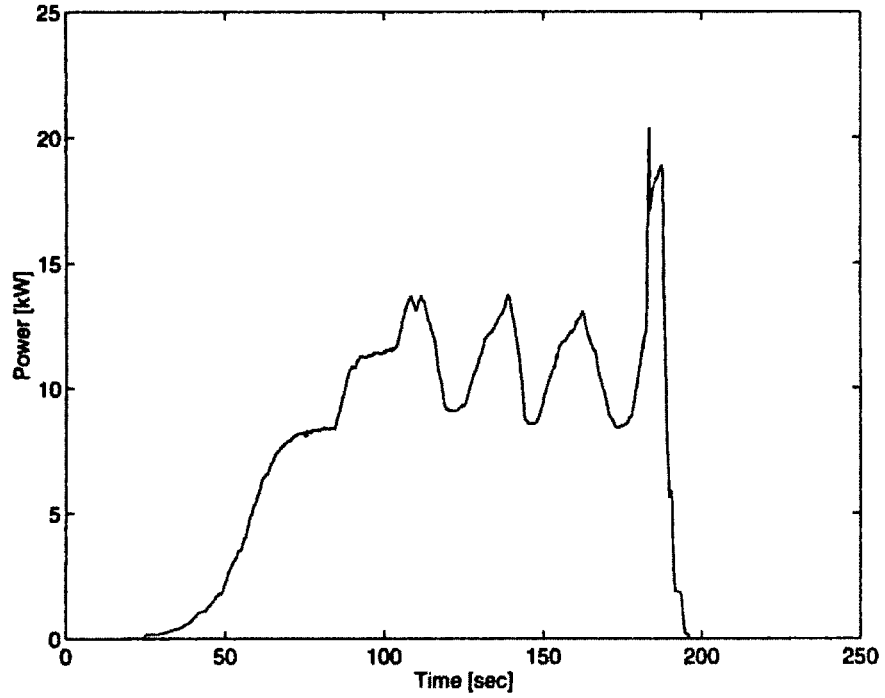

Figure E-10: Test Section 15A Power Profile

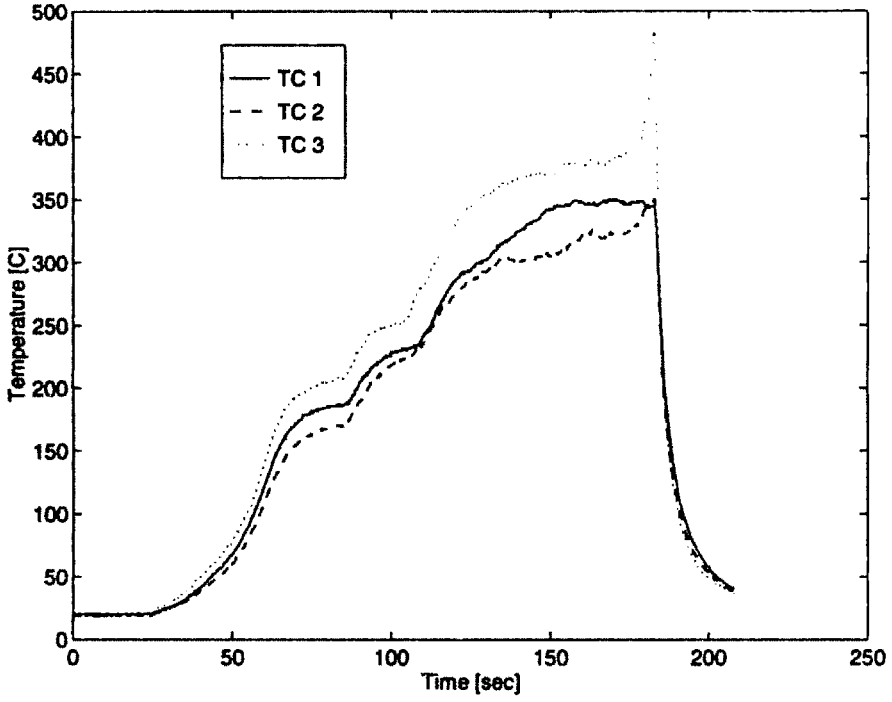

Figure E-11: Test Section 15A Temperature Profile

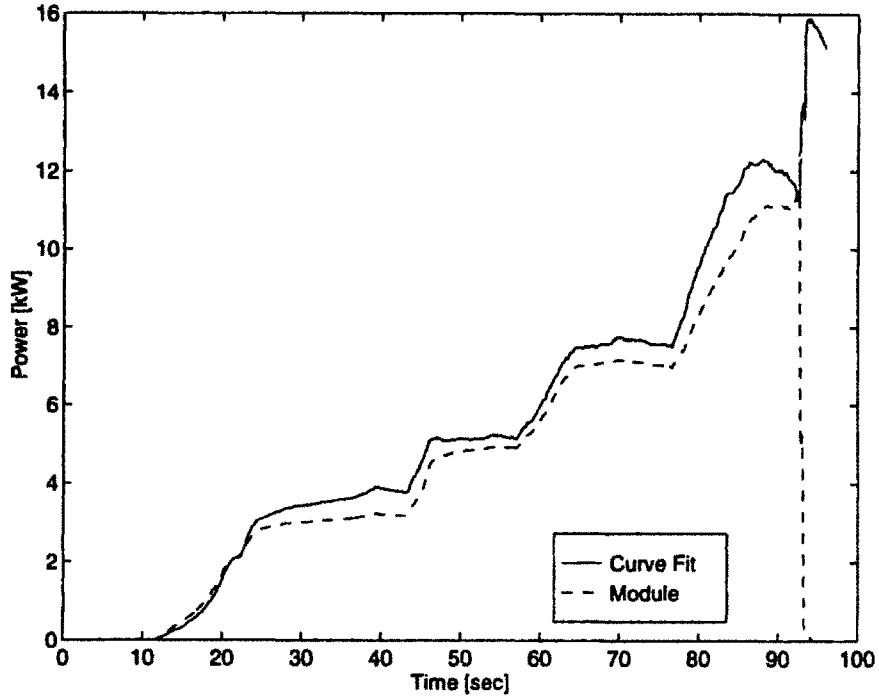

Figure E-12: Test Section 15B Power Profile

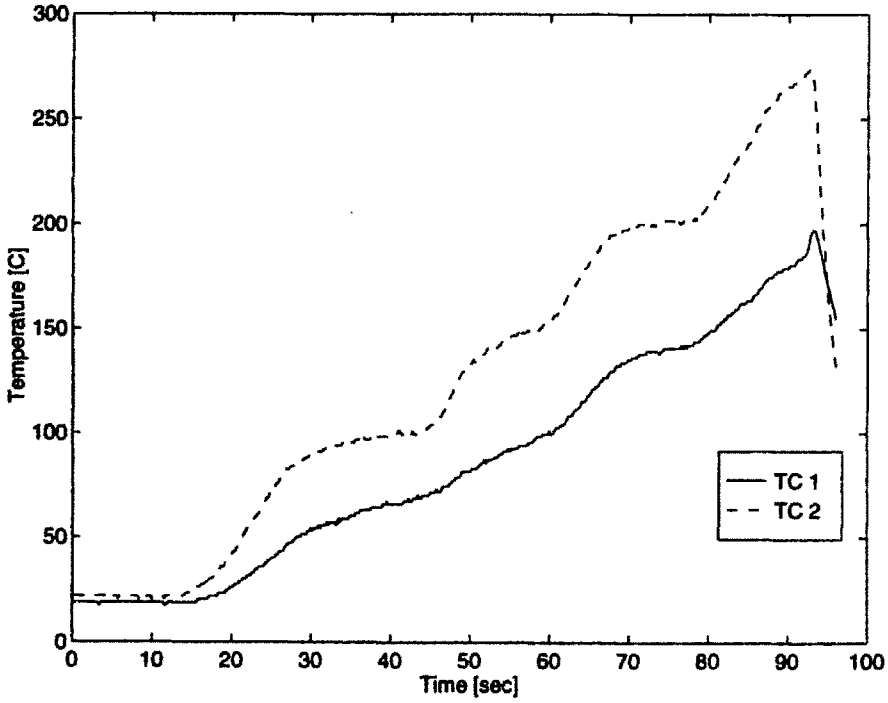

Figure E-13: Test Section 15B Temperature Profile

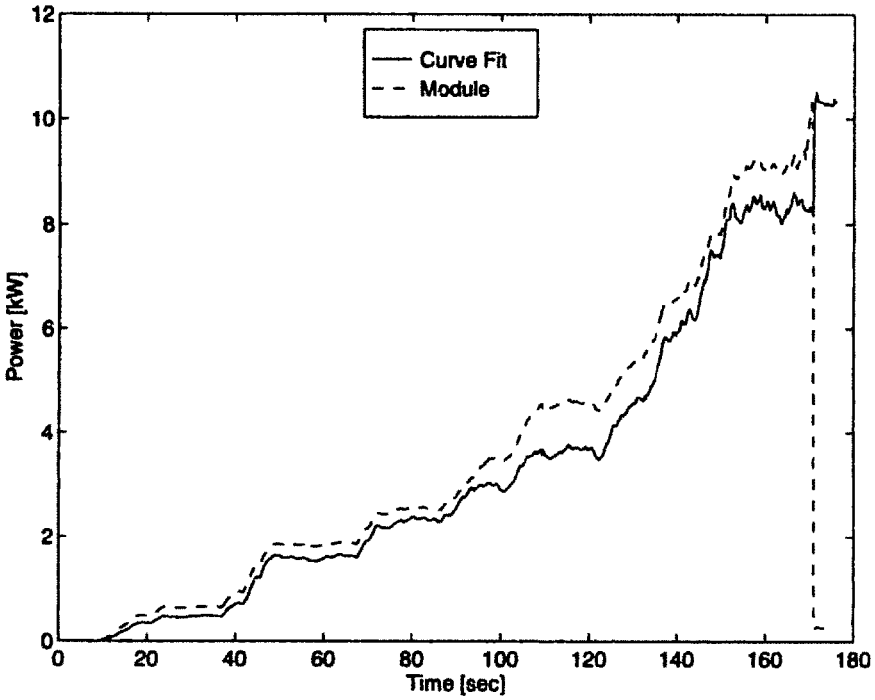

Figure E-14: Test Section 16B Power Profile

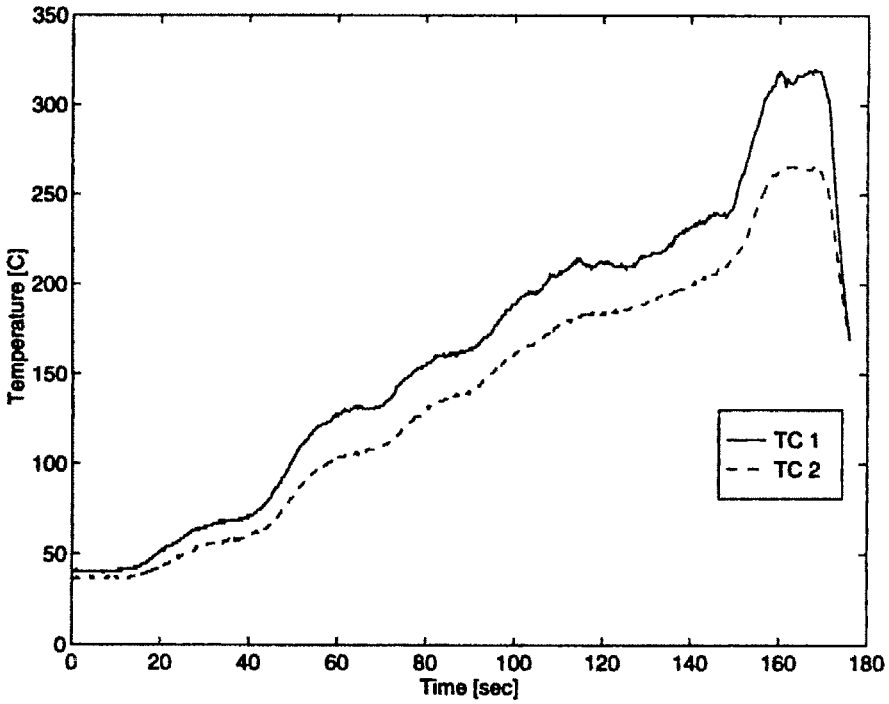

Figure E-15: Test Section 16B Temperature Profile

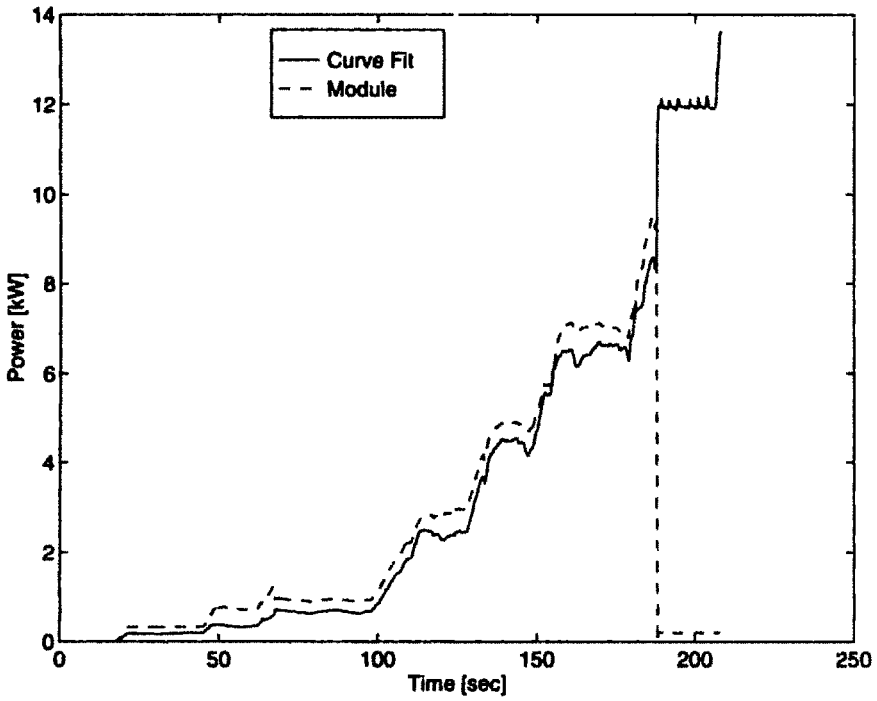

Figure E-16: Test Section 17A Power Profile

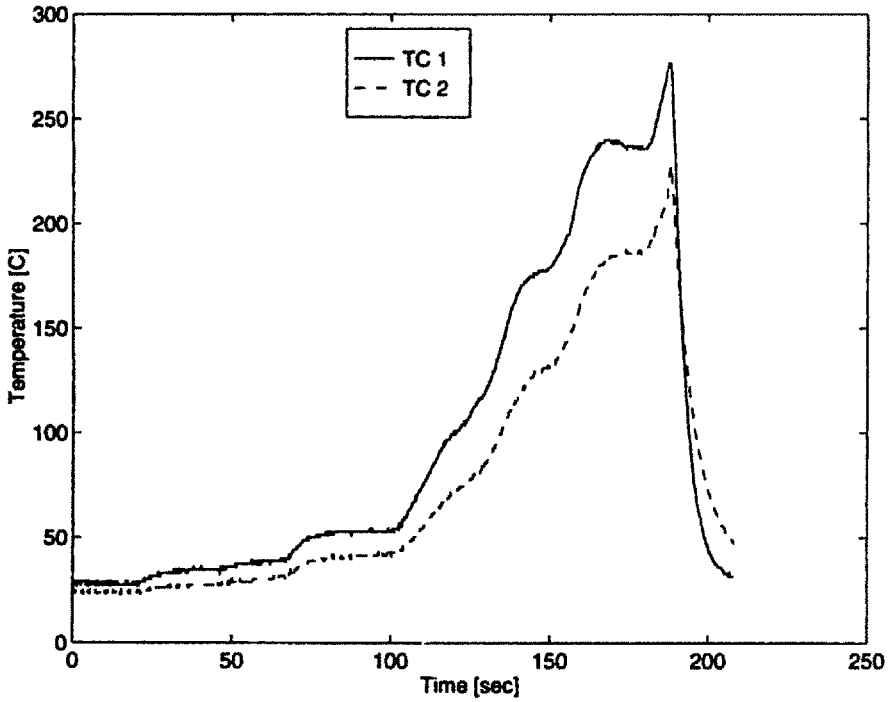

Figure E-17: Test Section 17A Temperature Profile

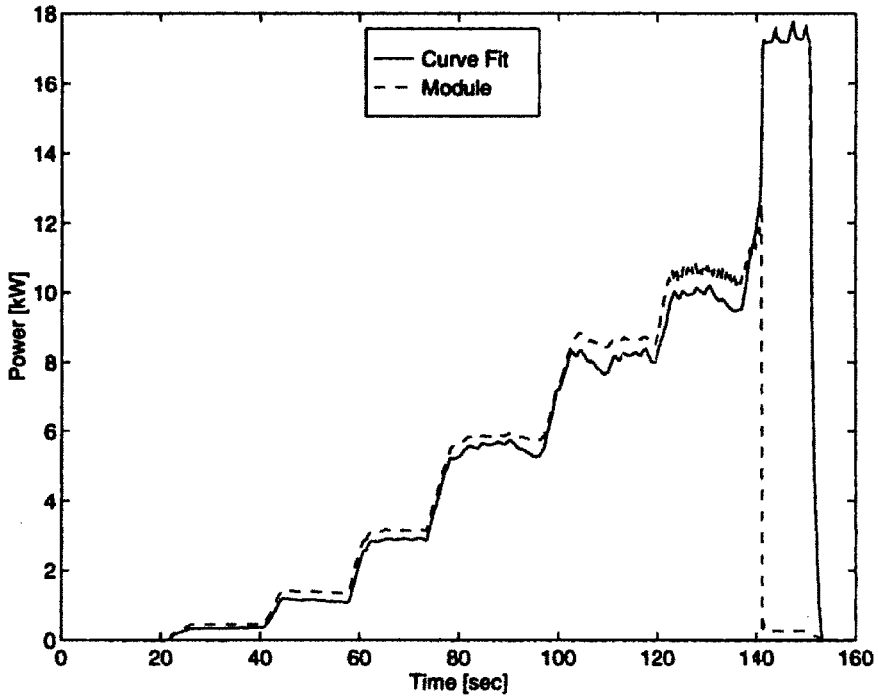

Figure E-18: Test Section 17B Power Profile

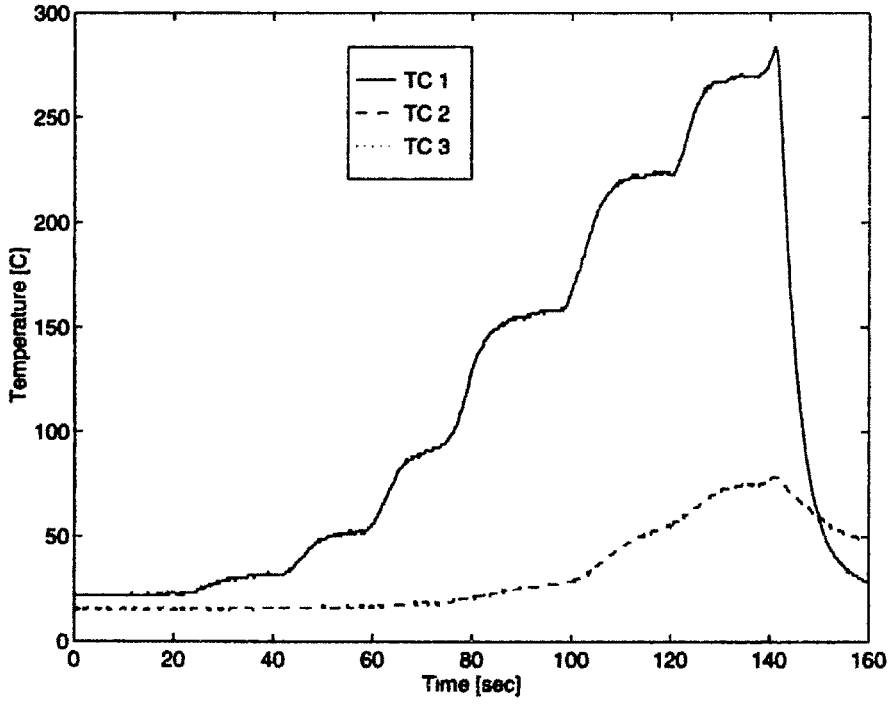

Figure E-19: Test Section 17B Temperature Profile

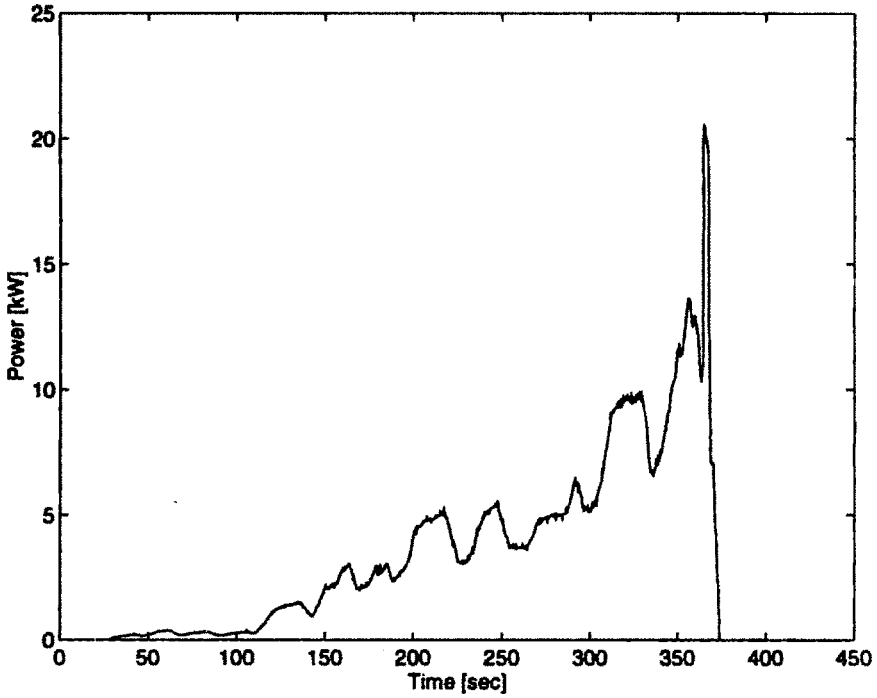

Figure E-20: Test Section 18A Power Profile

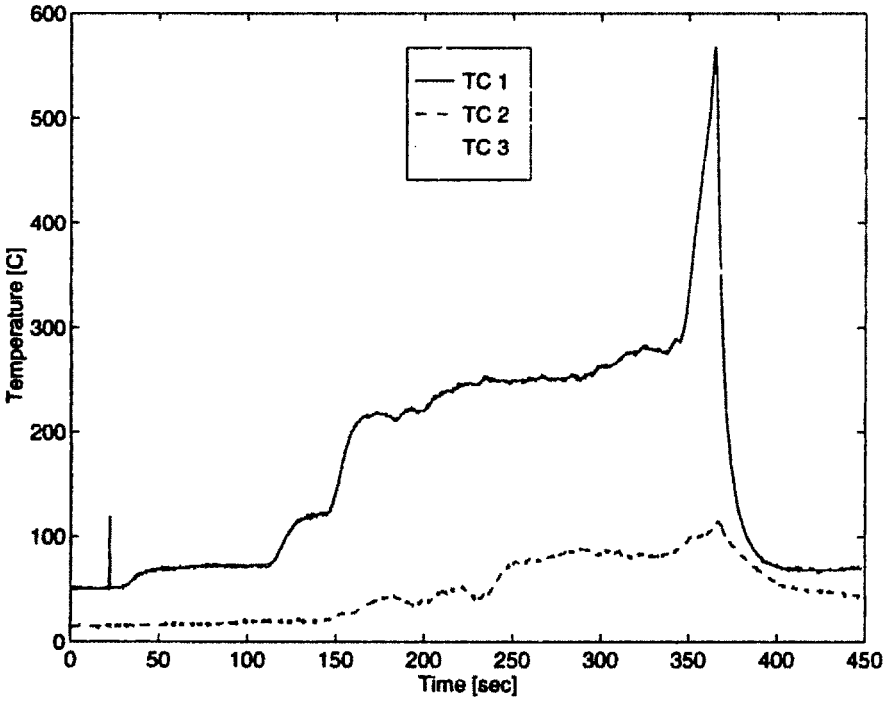

Figure E-21: Test Section 18A Temperature Profile

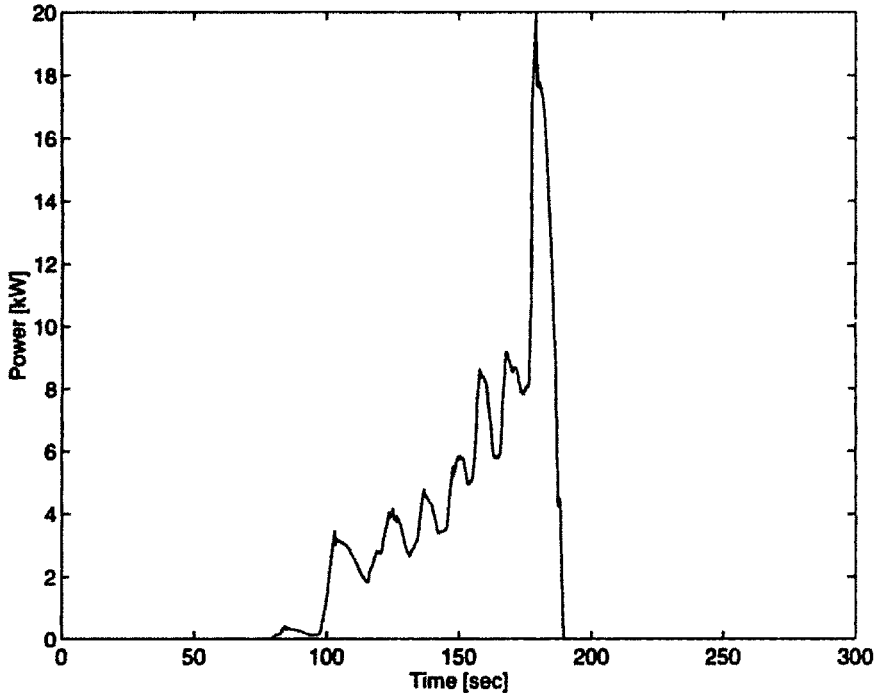

Figure E-22: Test Section 18B Power Profile

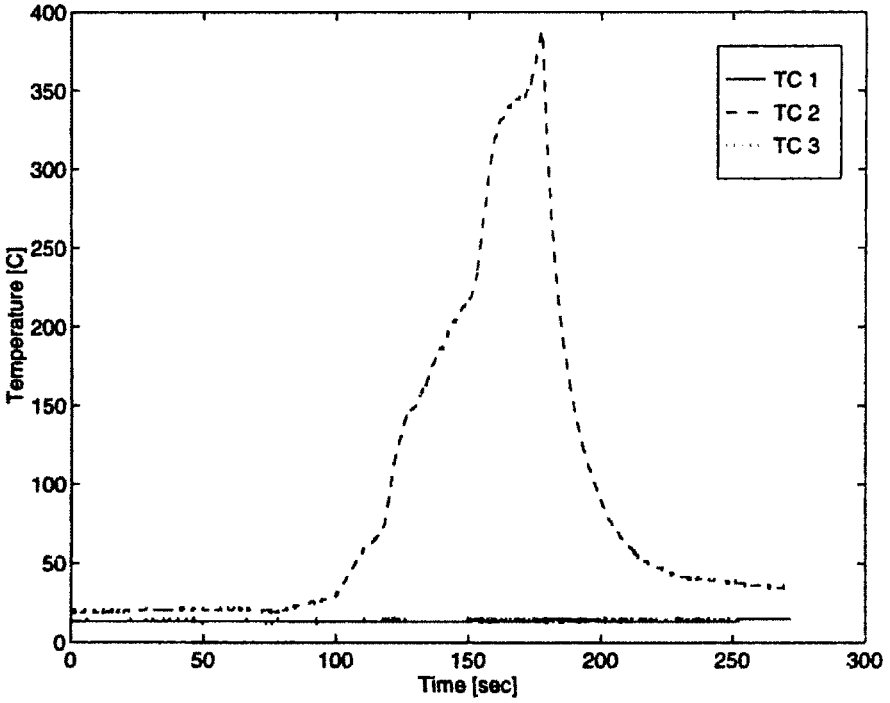

Figure E-23: Test Section 18B Temperature Profile

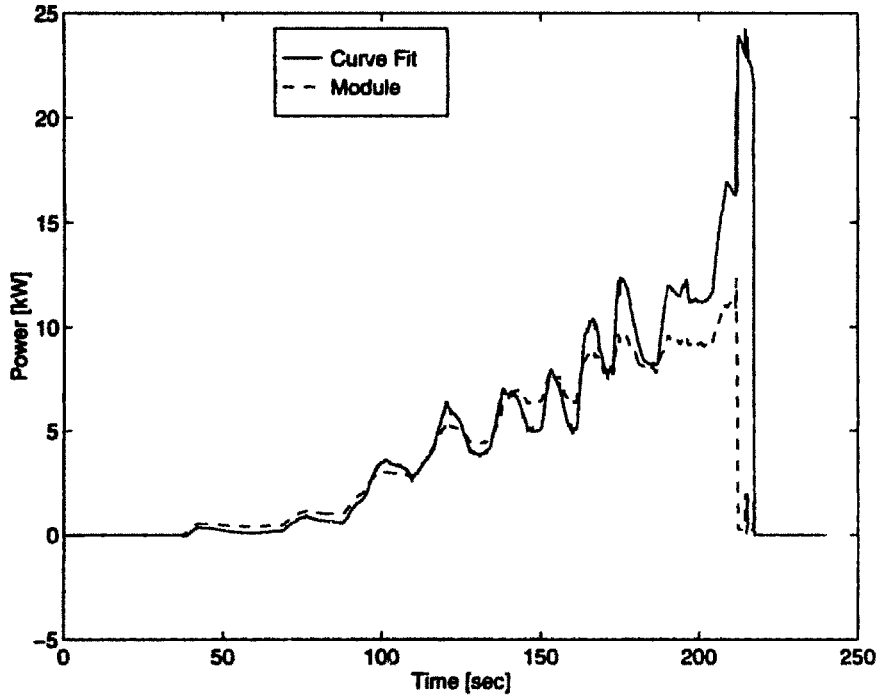

Figure E-24: Test Section 19A Power Profile

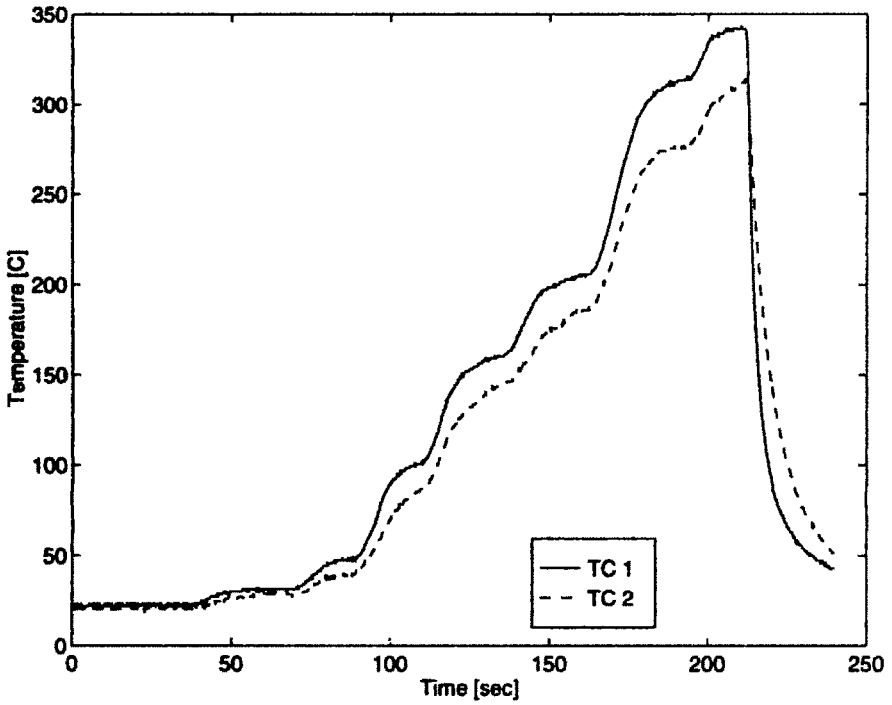

Figure E-25: Test Section 19A Temperature Profile

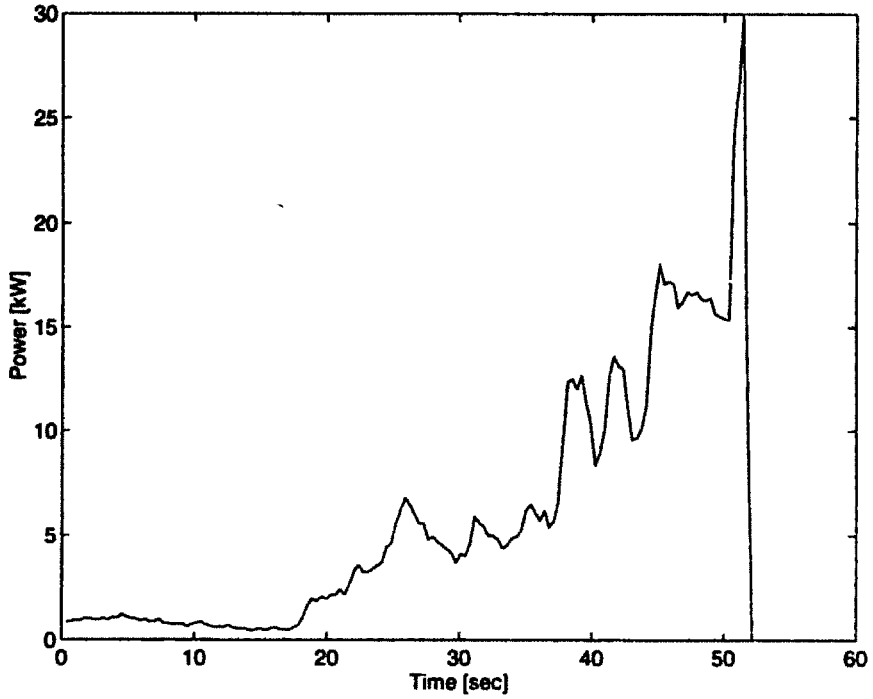

Figure E-26: Test Section 19B Power Profile

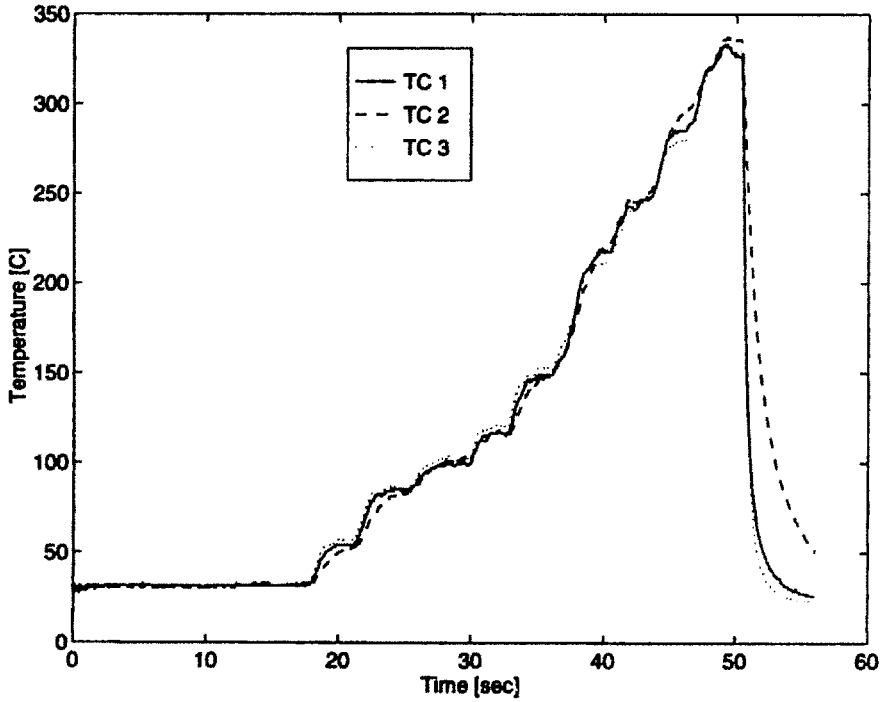

Figure E-27: Test Section 19B Temperature Profile

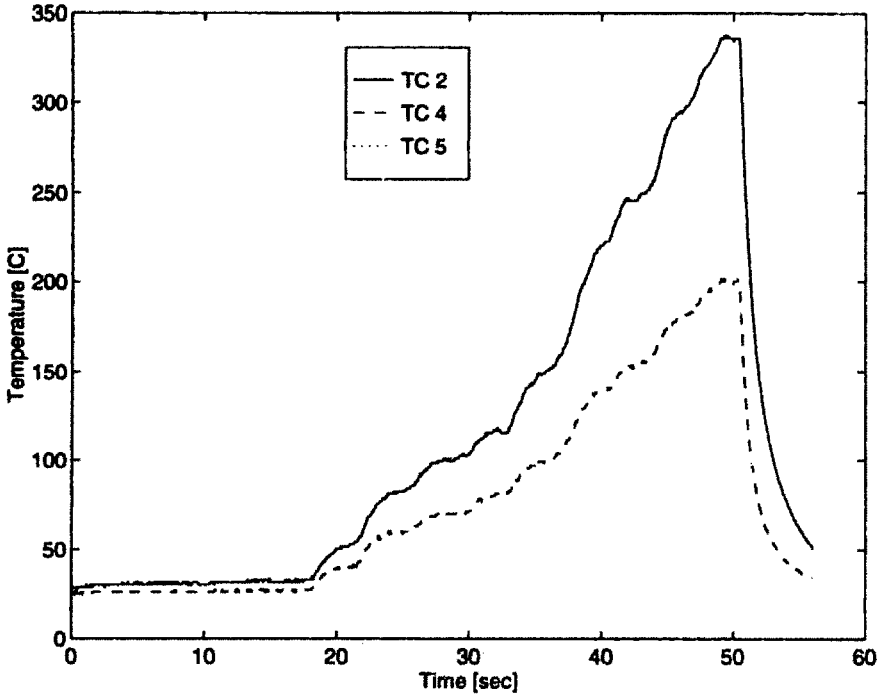

Figure E-28: Test Section 19B Temperature Profile

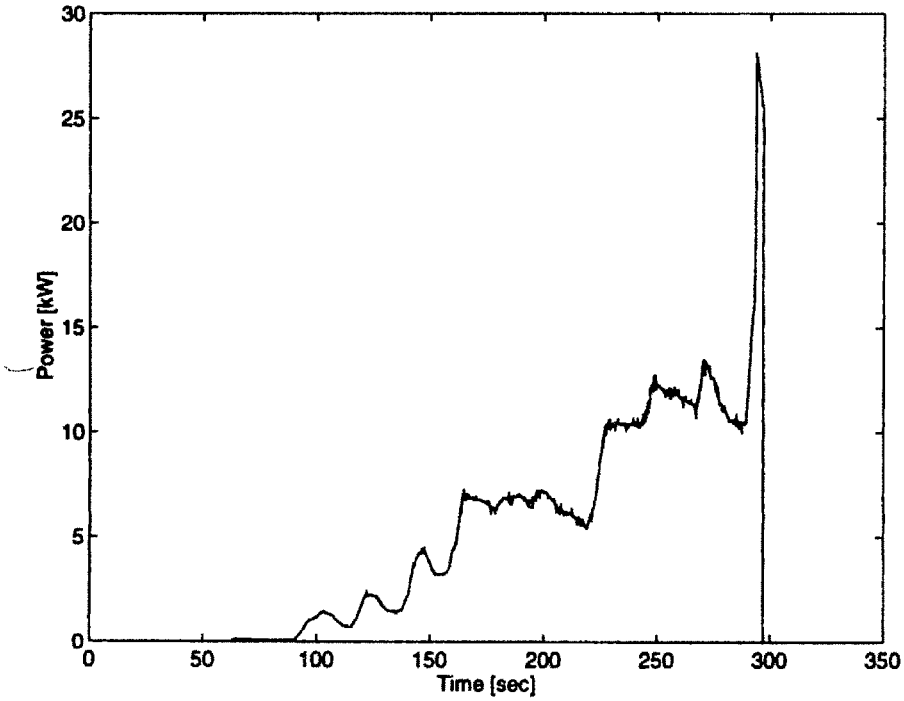

Figure E-29: Test Section 20A Power Profile

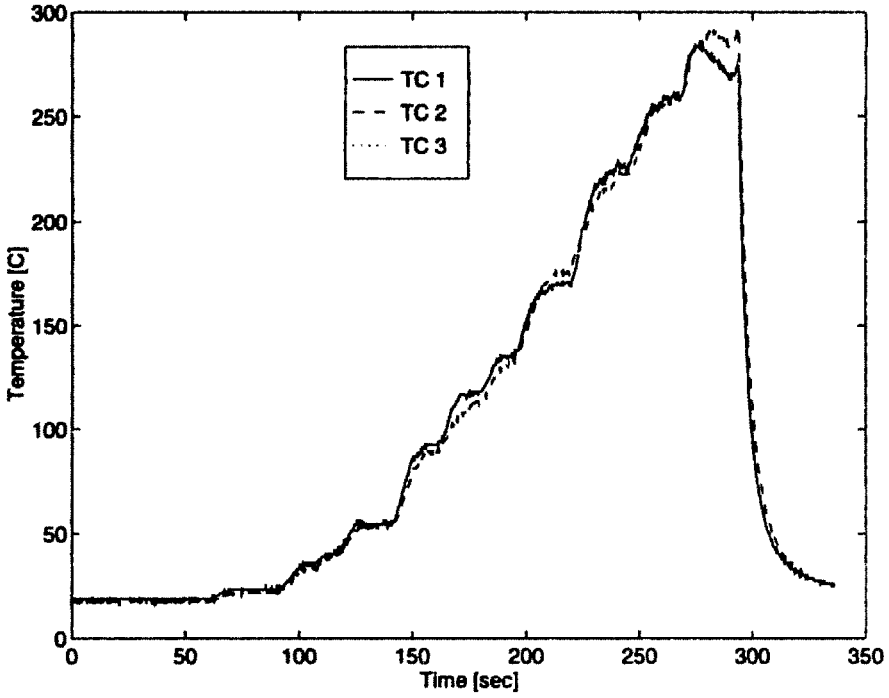

Figure E-30: Test Section 20A Temperature Profile

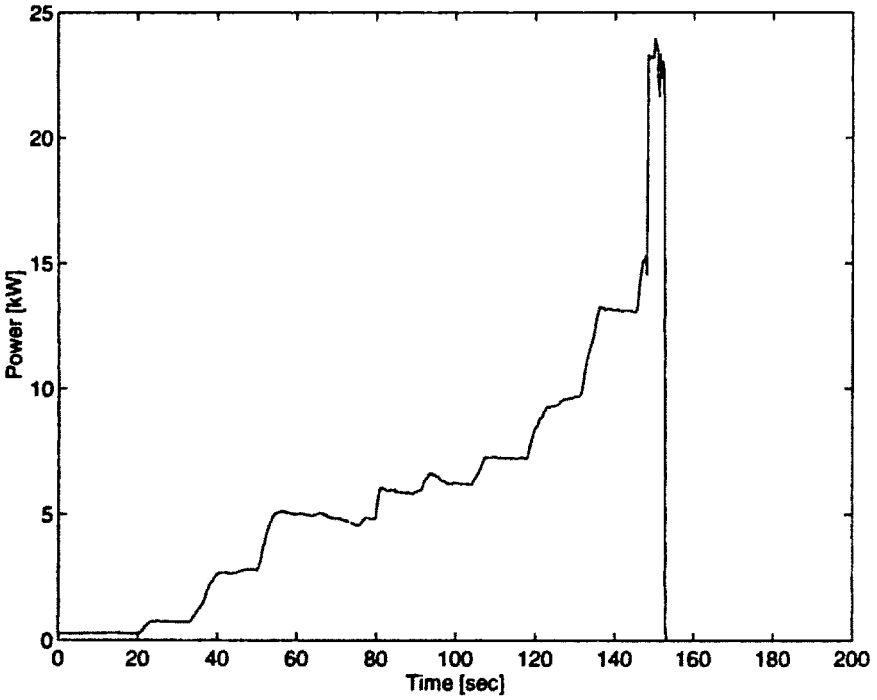

Figure E-31: Test Section 20B Power Profile

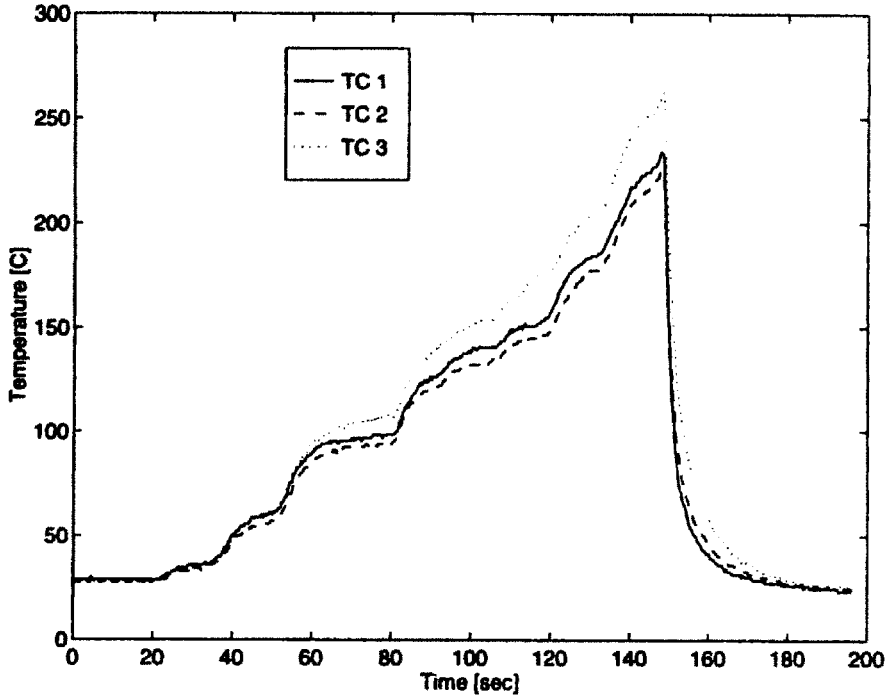

Figure E-32: Test Section 20B Temperature Profile

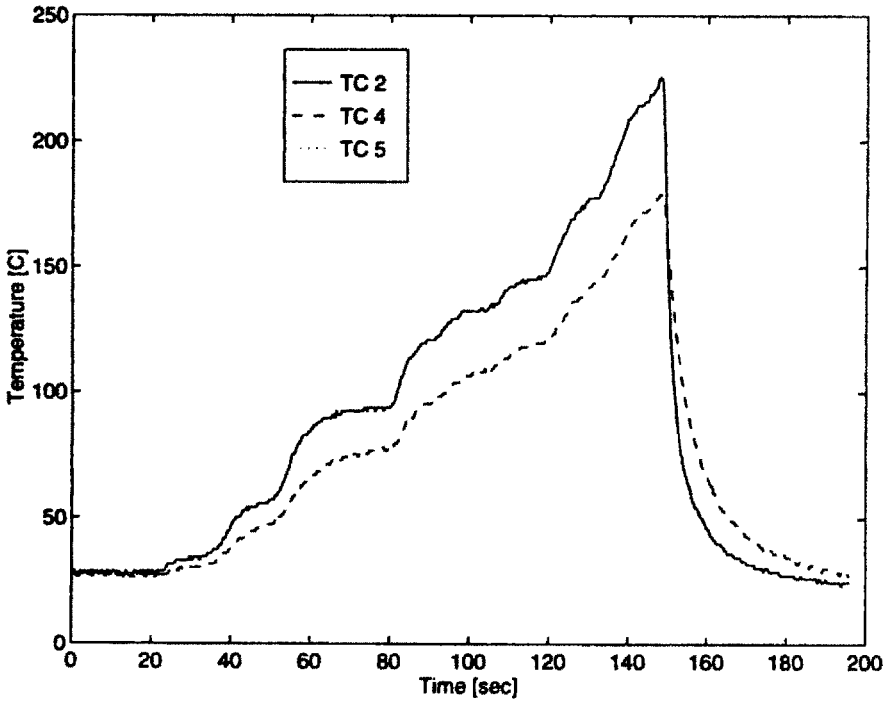

Figure E-33: Test Section 20B Temperature Profile

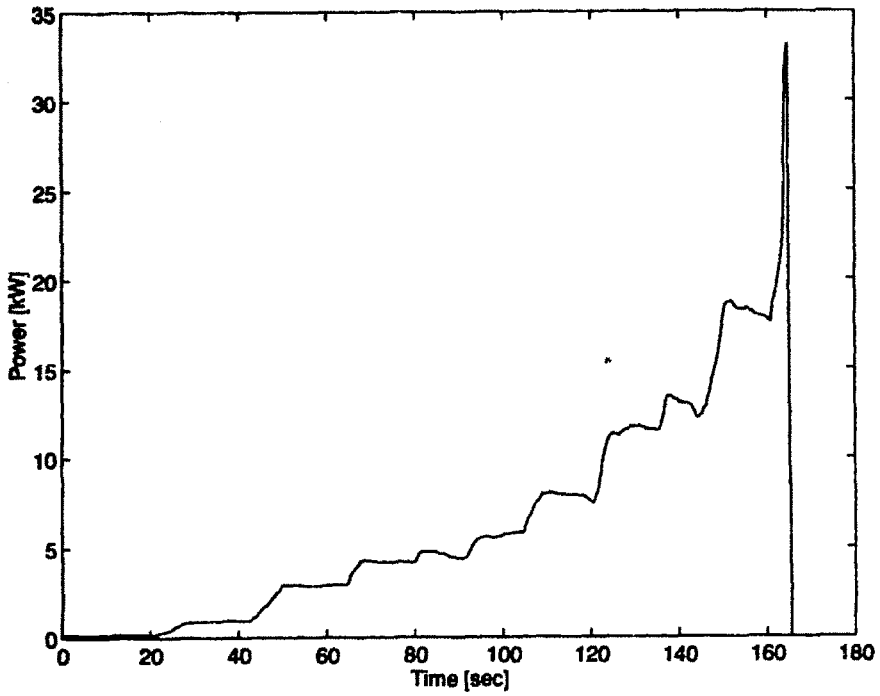

Figure E-34: Test Section 21A Power Profile

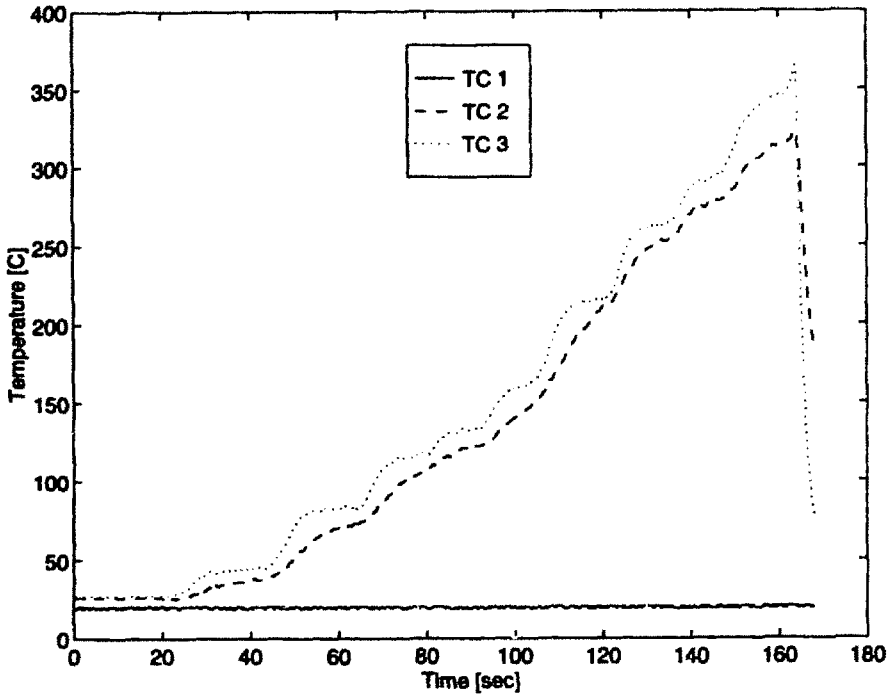

Figure E-35: Test Section 21A Temperature Profile

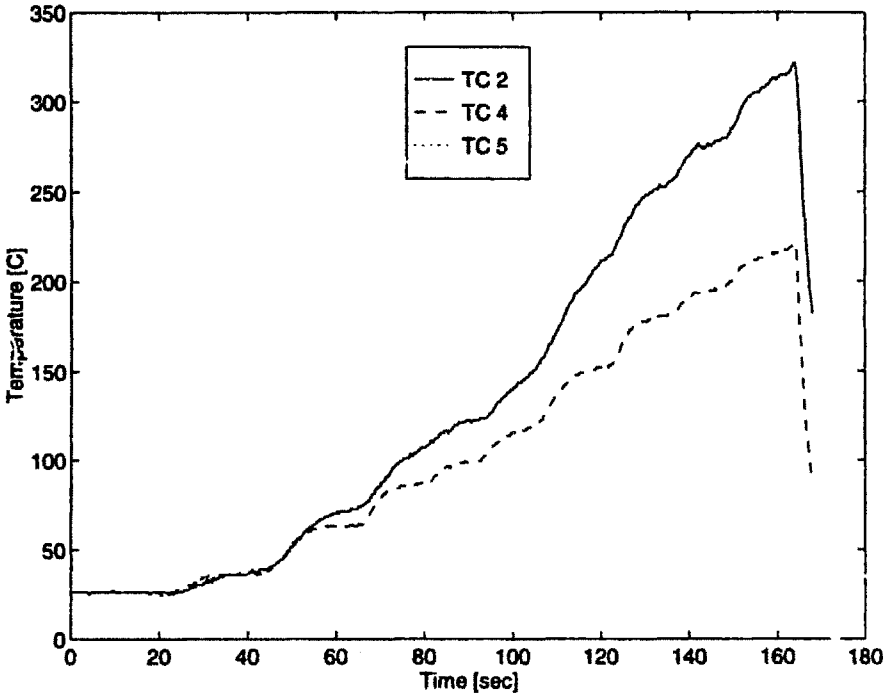

Figure E-36: Test Section 21A Temperature Profile

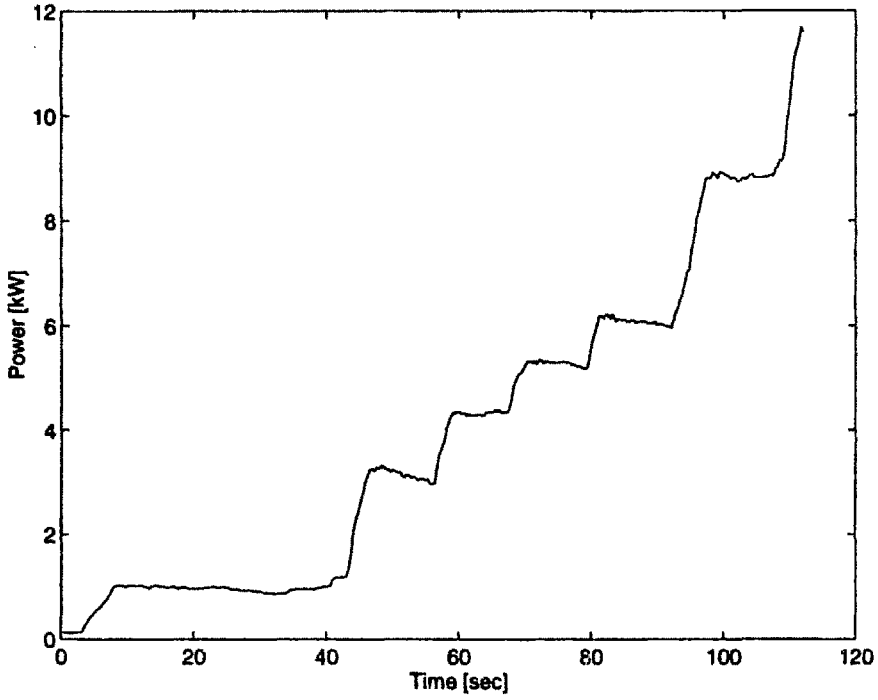

Figure E-37: Test Section 21B Power Profile

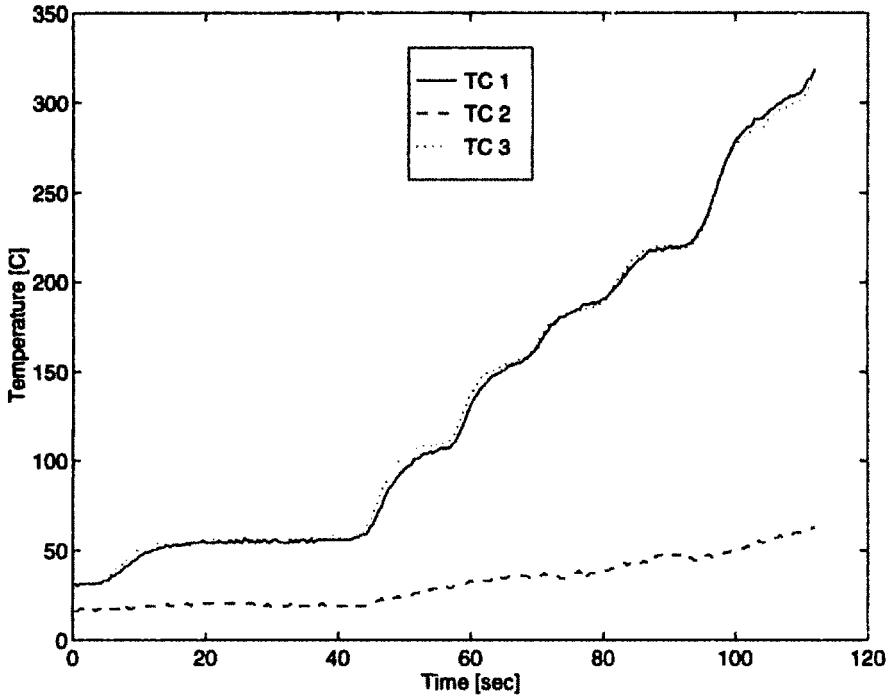

Figure E-38: Test Section 21B Temperature Profile

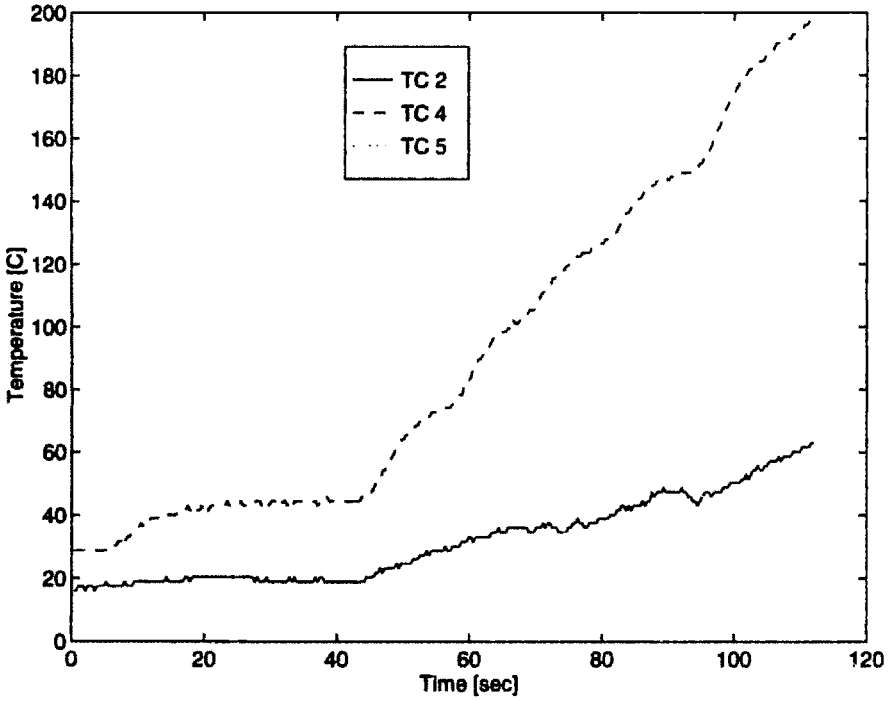

Figure E-39: Test Section 21B Temperature Profile

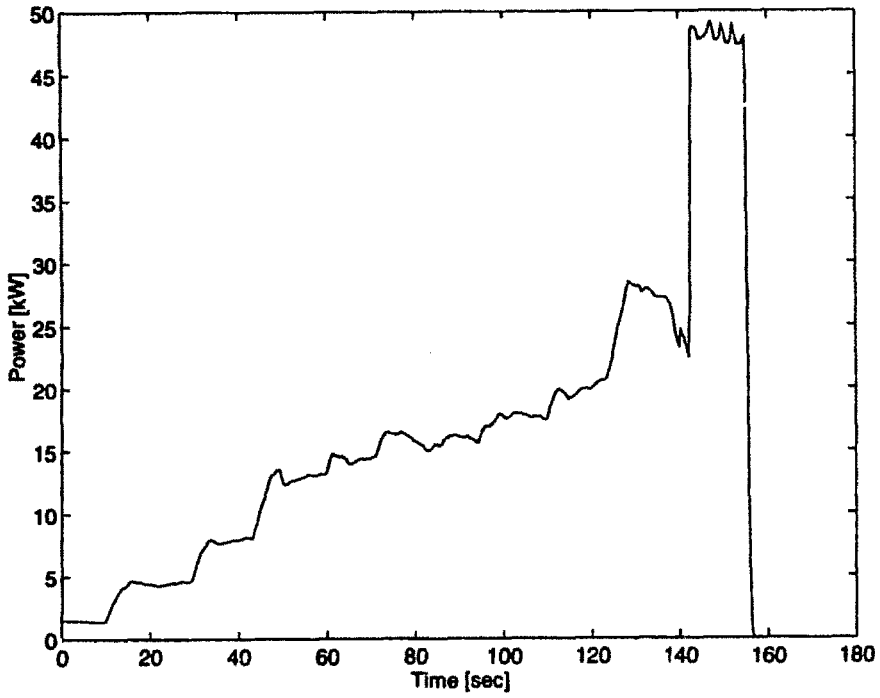

Figure E-40: Test Section 22A Power Profile

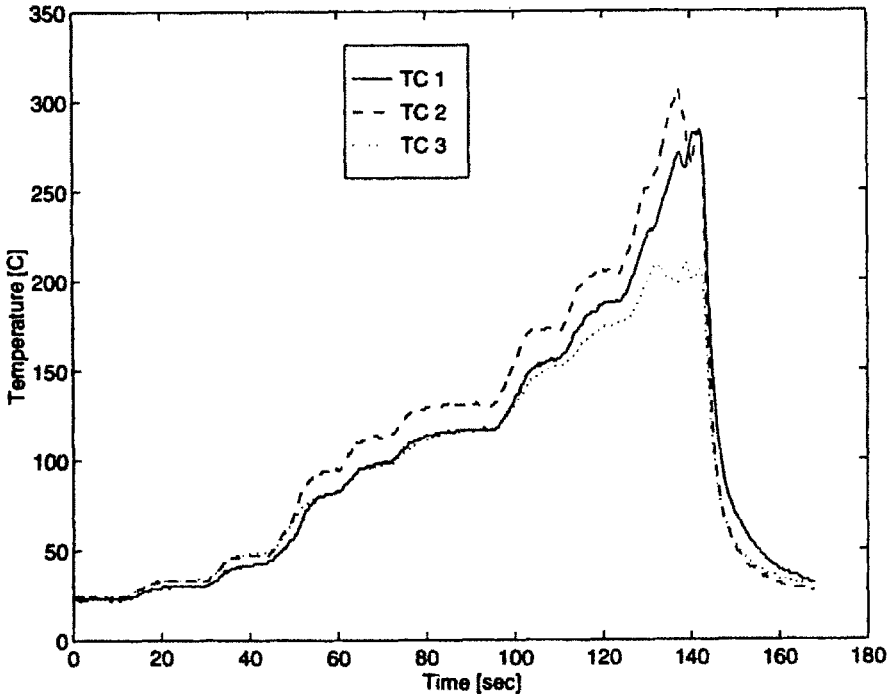

Figure E-41: Test Section 22A Temperature Profile

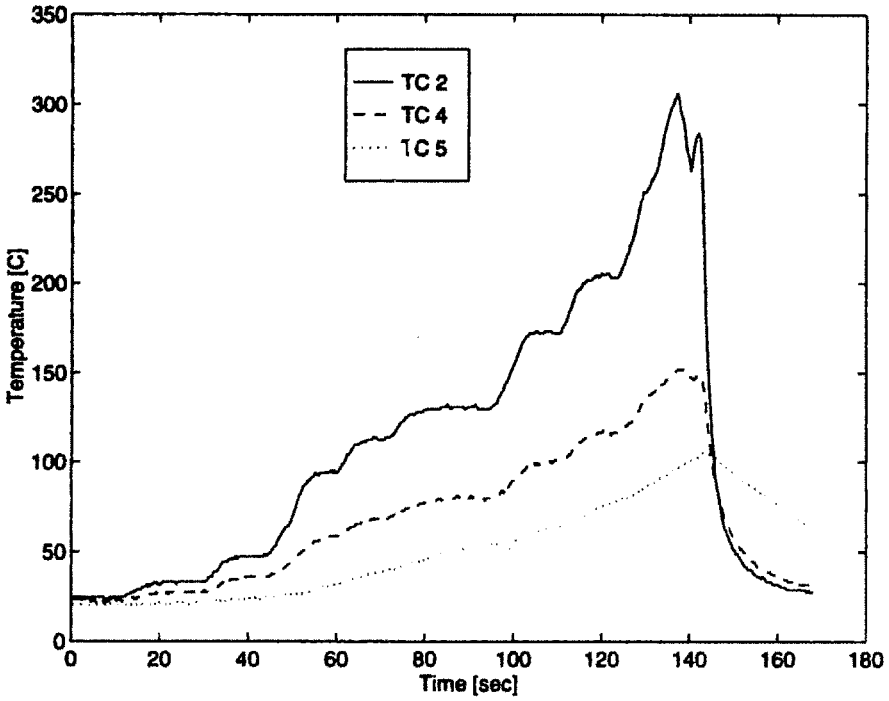

Figure E-42: Test Section 22A Temperature Profile

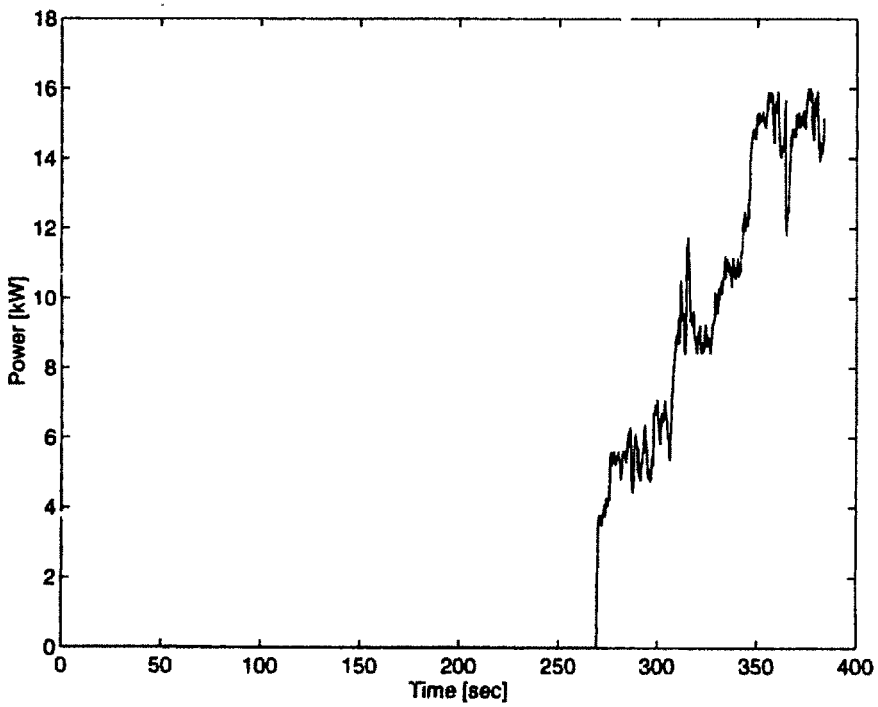

Figure E-43: Test Section 22B Power Profile

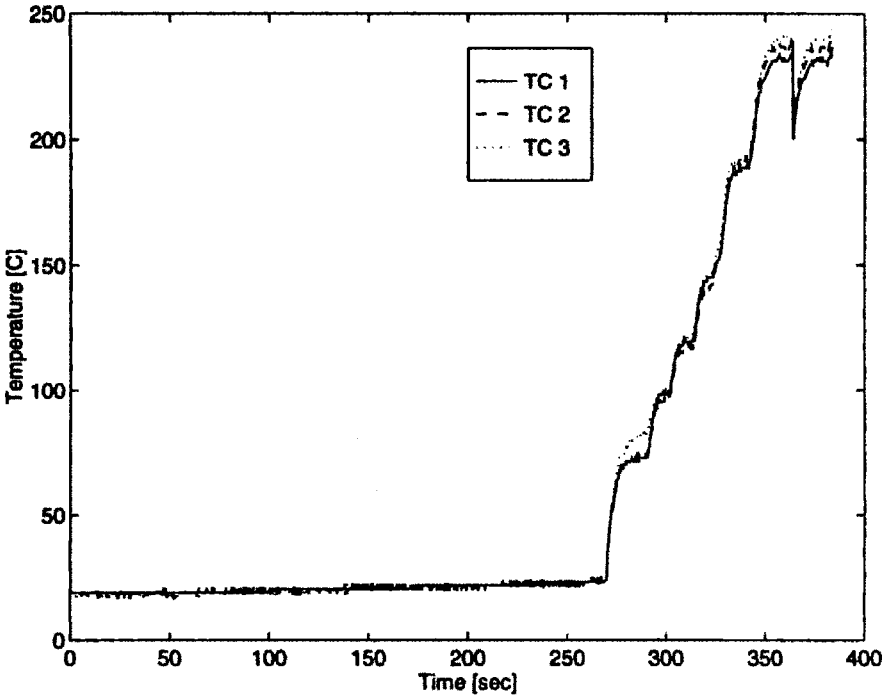

Figure E-44: Test Section 22B Temperature Profile

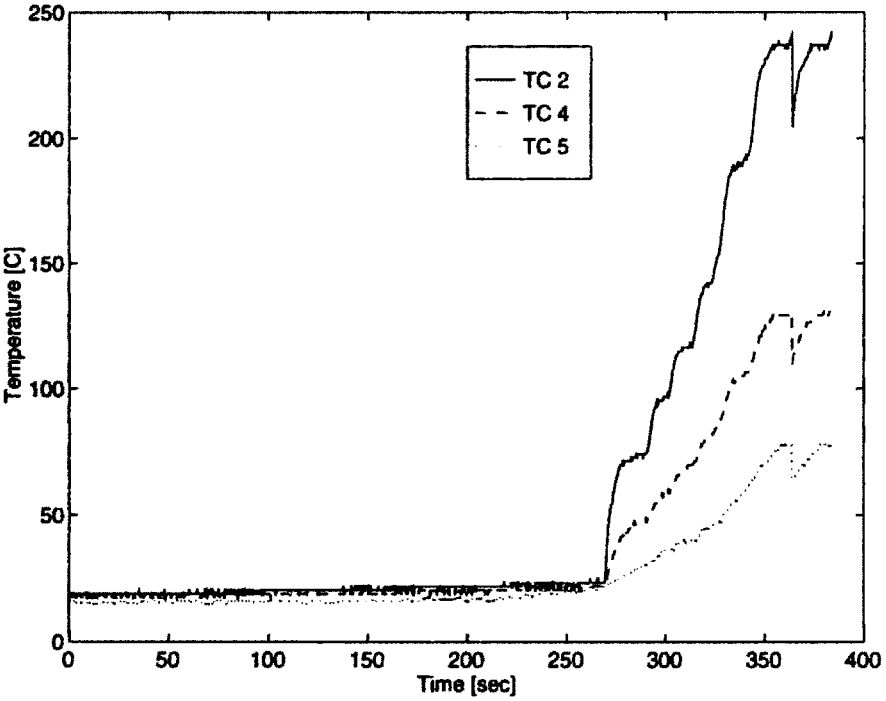

Figure E-45: Test Section 22B Temperature Profile

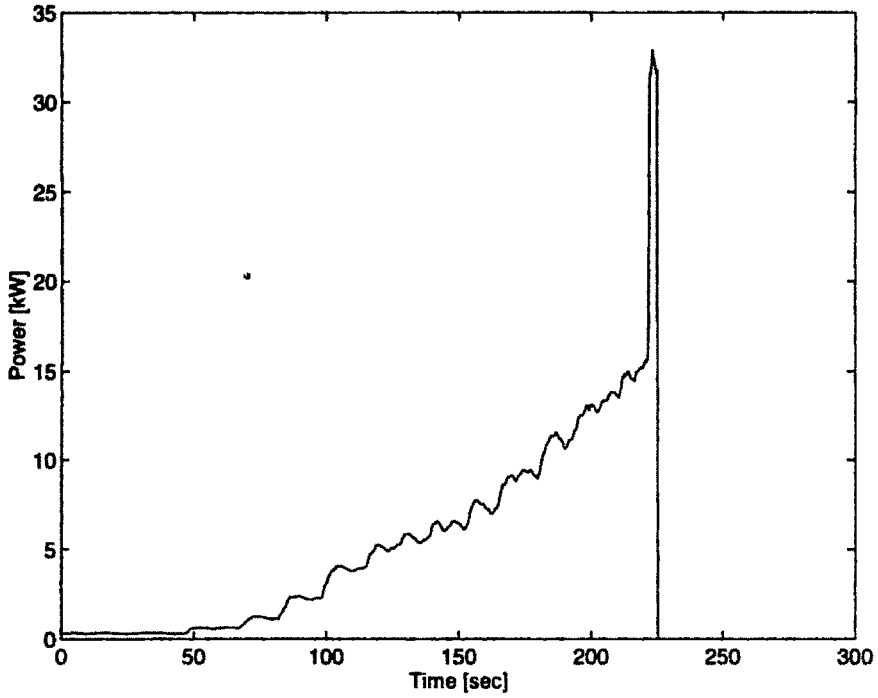

Figure E-46: Test Section 23A Power Profile

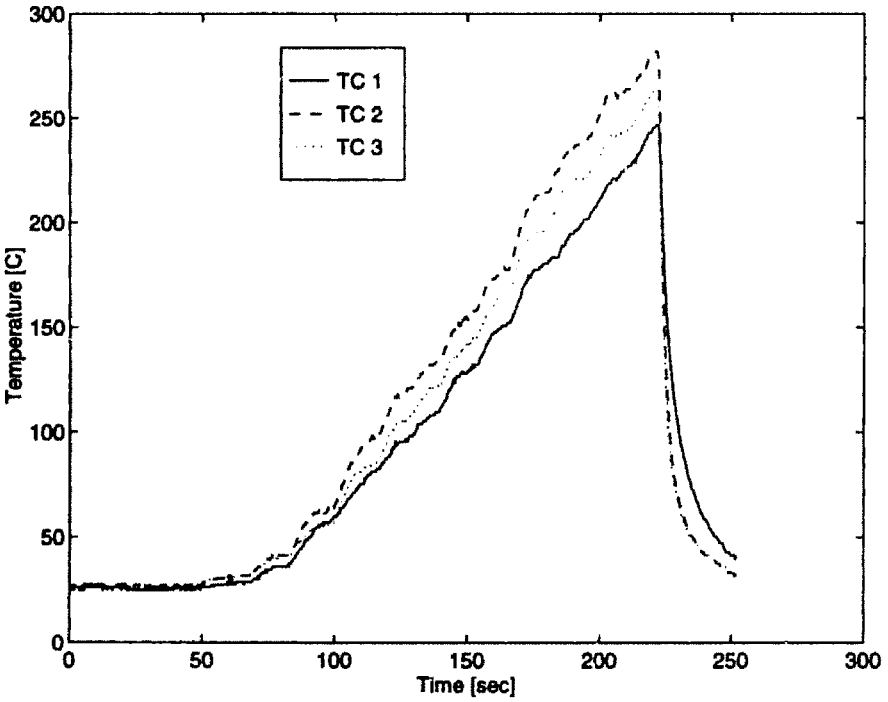

Figure E-47: Test Section 23A Temperature Profile

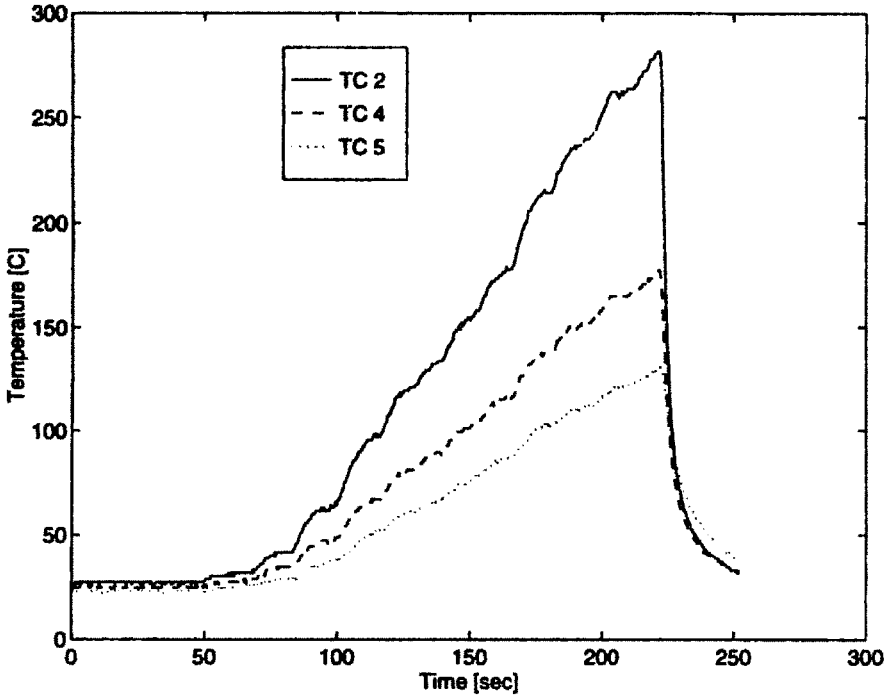

Figure E-48: Test Section 23A Temperature Profile

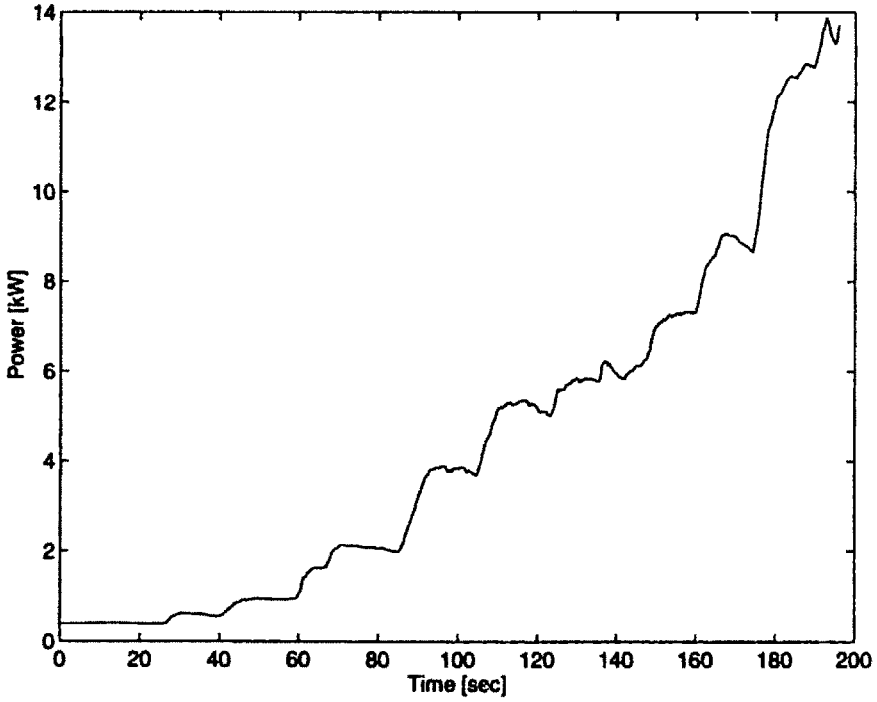

Figure E-49: Test Section 23B Power Profile

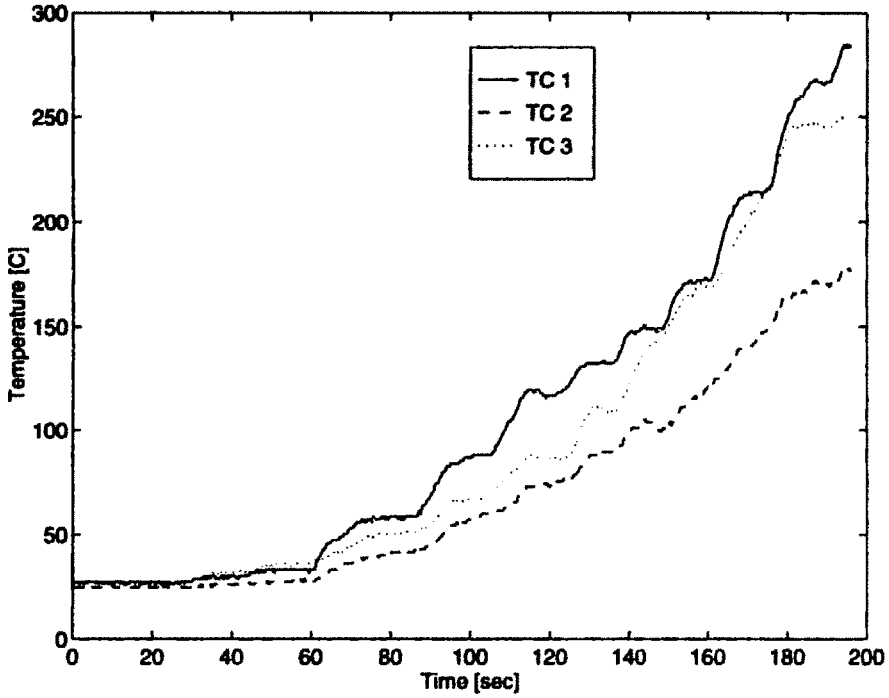

Figure E-50: Test Section 23B Temperature Profile

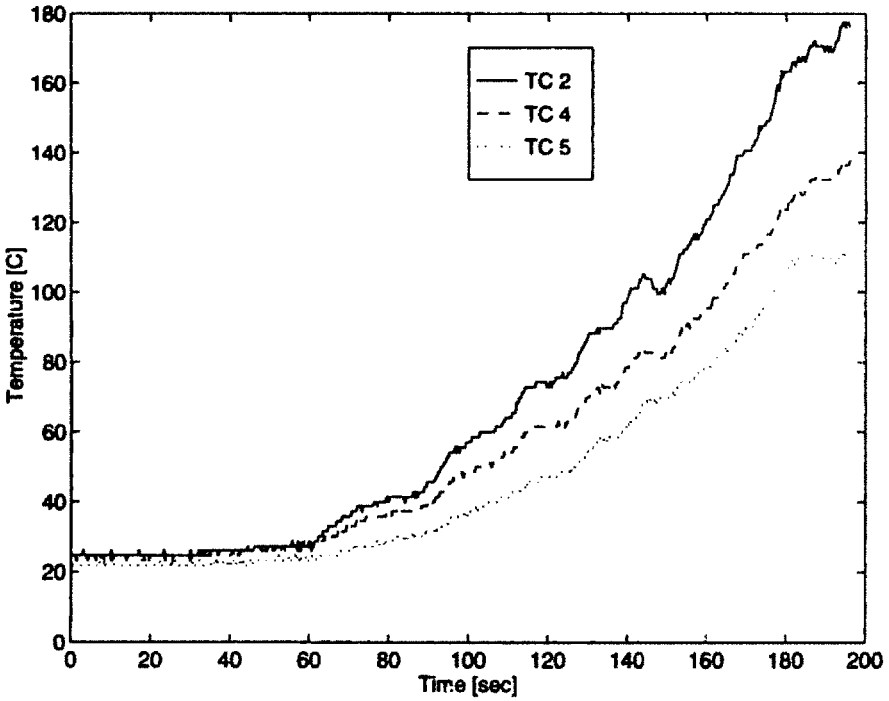

Figure E-51: Test Section 23B Temperature Profile

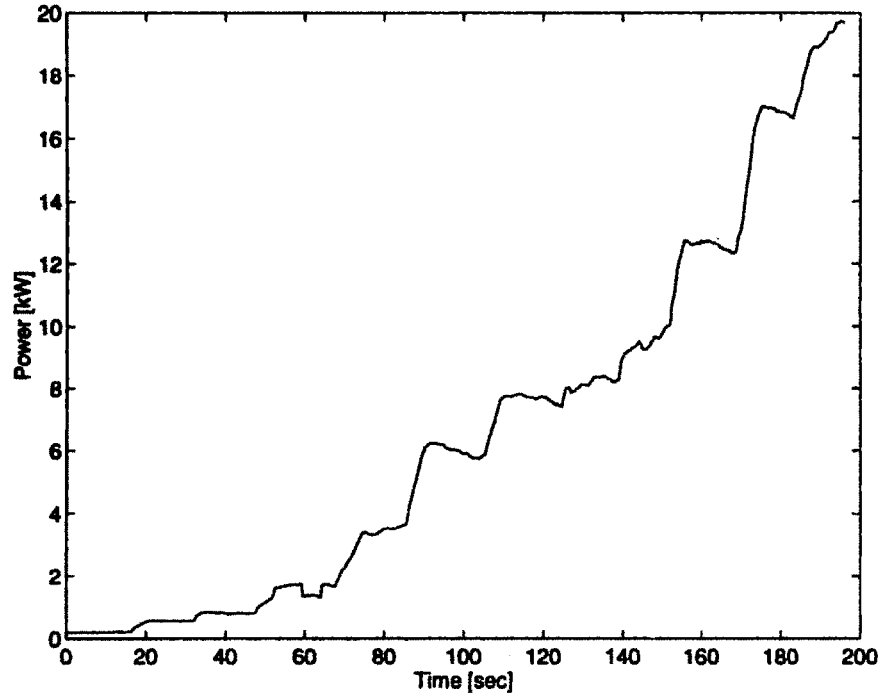

Figure E-52: Test Section 24A Power Profile

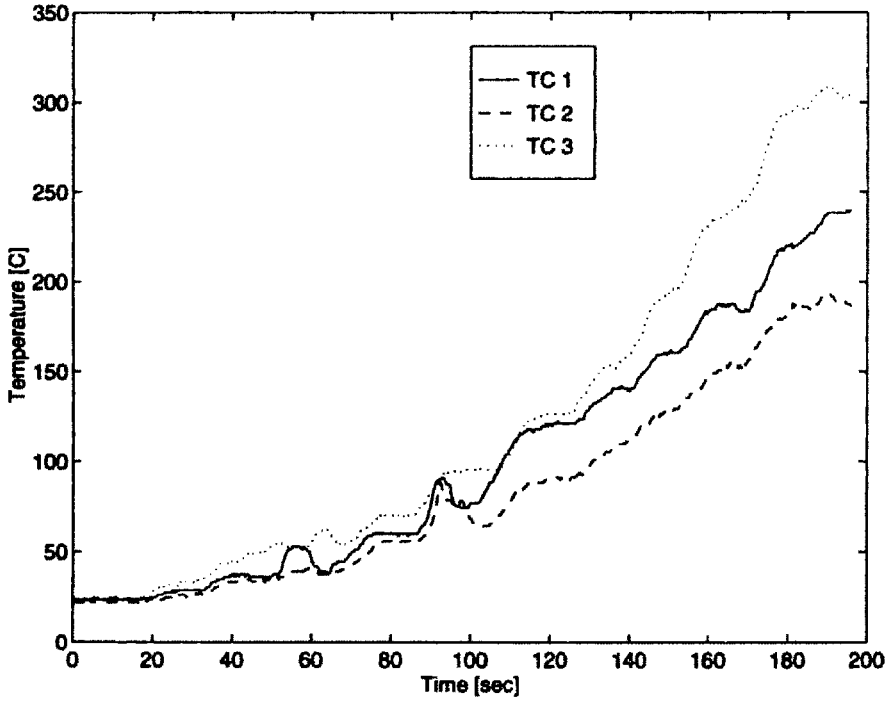

Figure E-53: Test Section 24A Temperature Profile

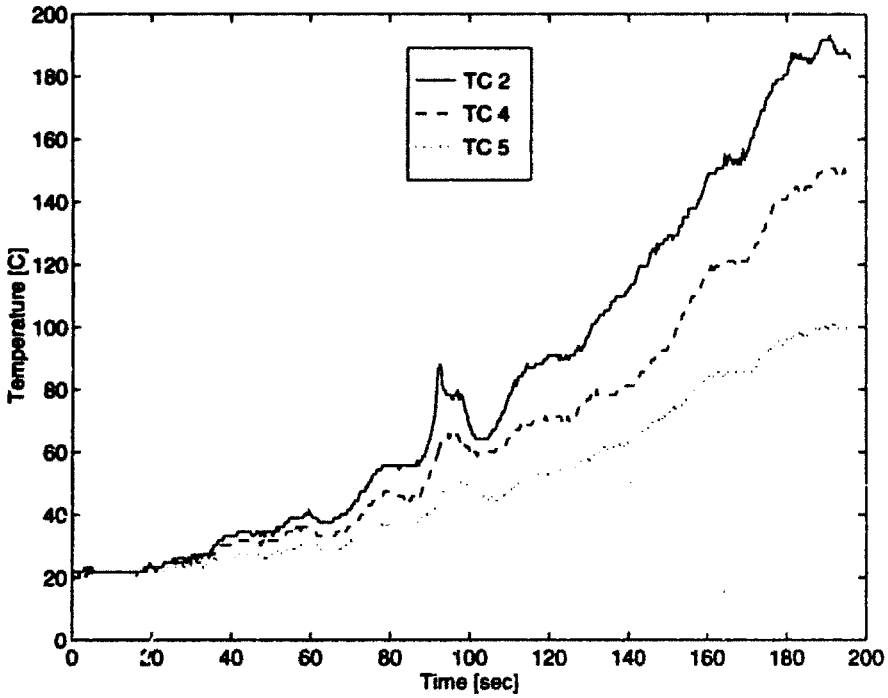

Figure E-54: Test Section 24A Temperature Profile

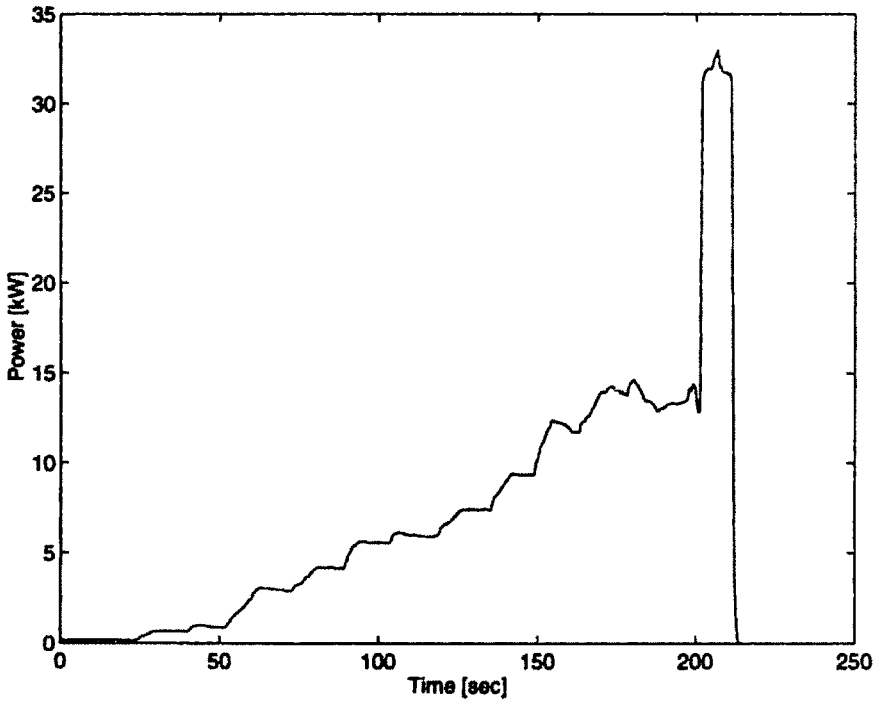

Figure E-55: Test Section 24B Power Profile

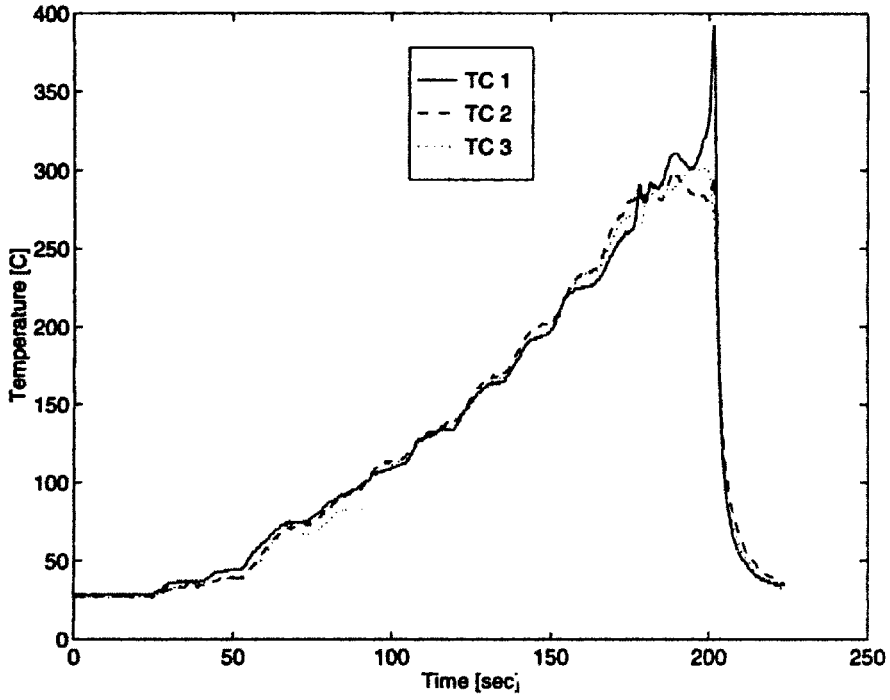

Figure E-56: Test Section 24B Temperature Profile

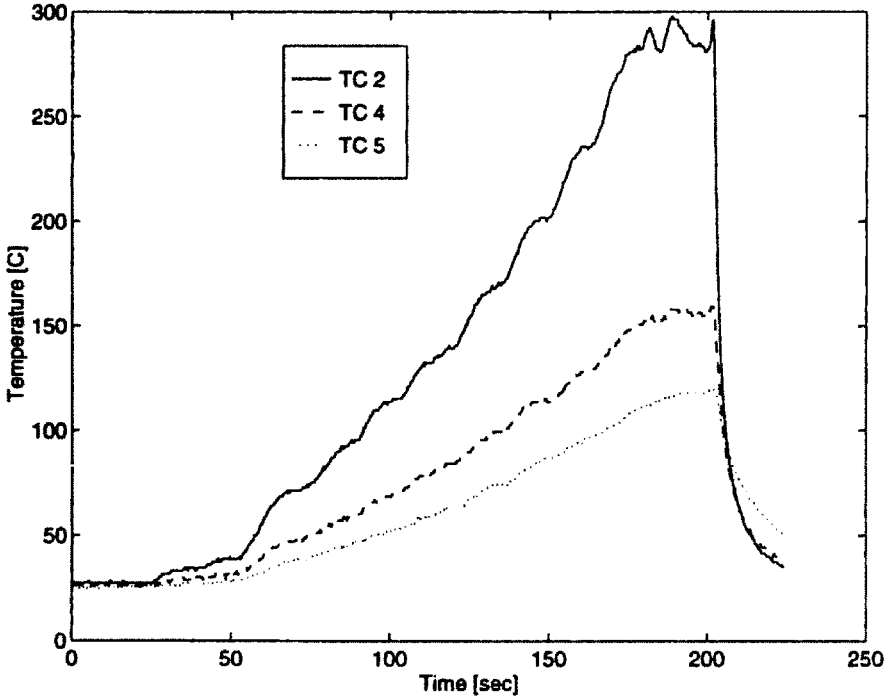

Figure E-57: Test Section 24B Temperature Profile

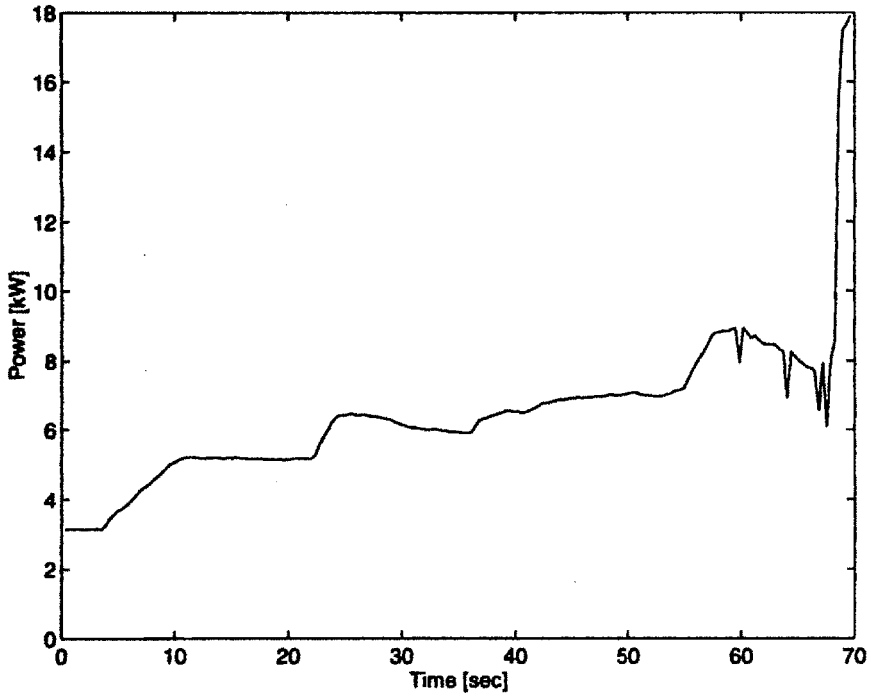

Figure E-58: Test Section 25A Power Profile

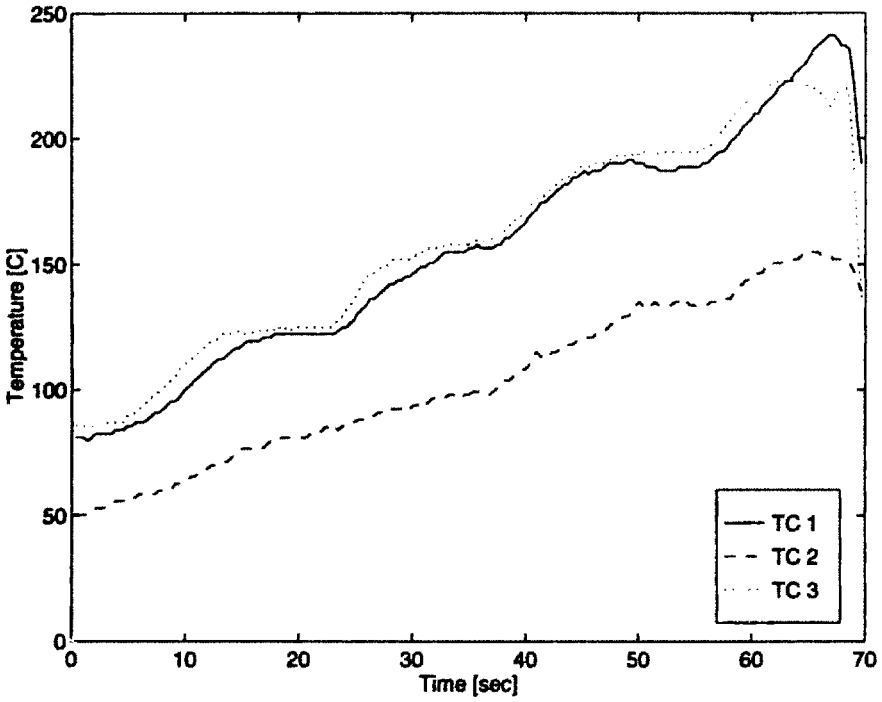

Figure E-59: Test Section 25A Temperature Profile

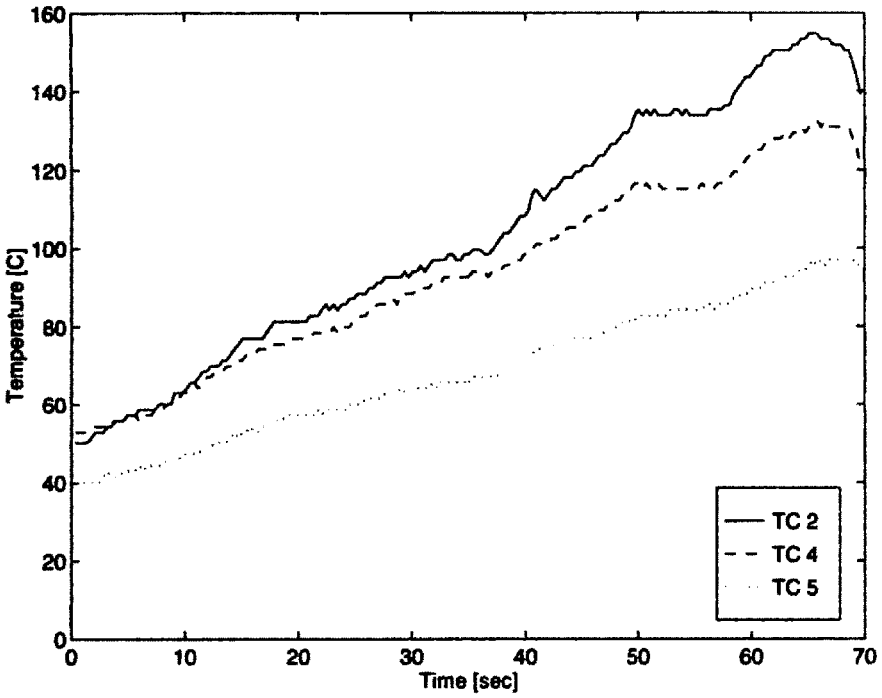

Figure E-60: Test Section 25A Temperature Profile

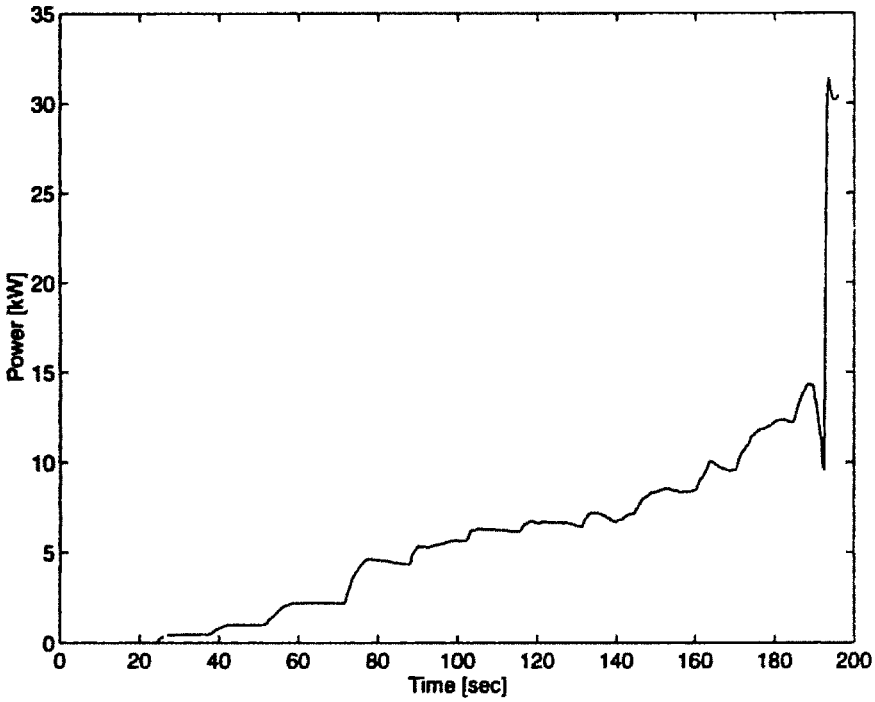

Figure E-61: Test Section 25B Power Profile

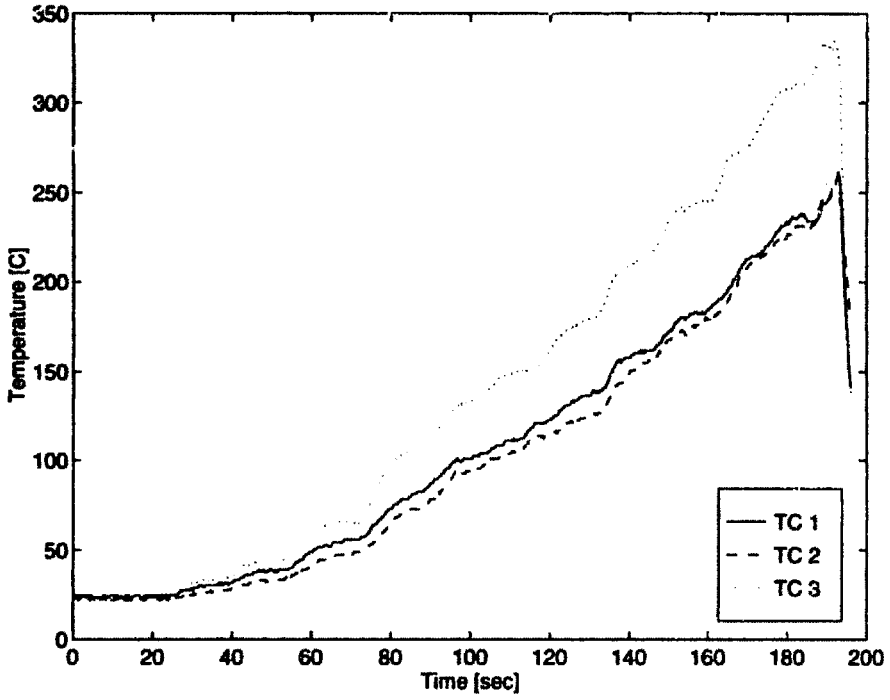

Figure E-62: Test Section 25B Temperature Profile

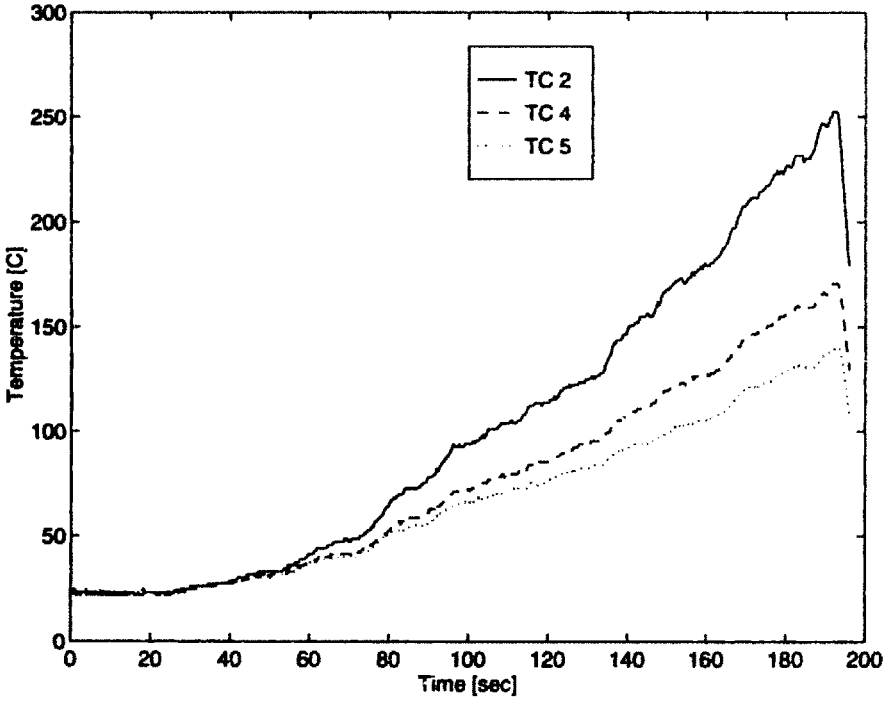

Figure E-63: Test Section 25B Temperature Profile

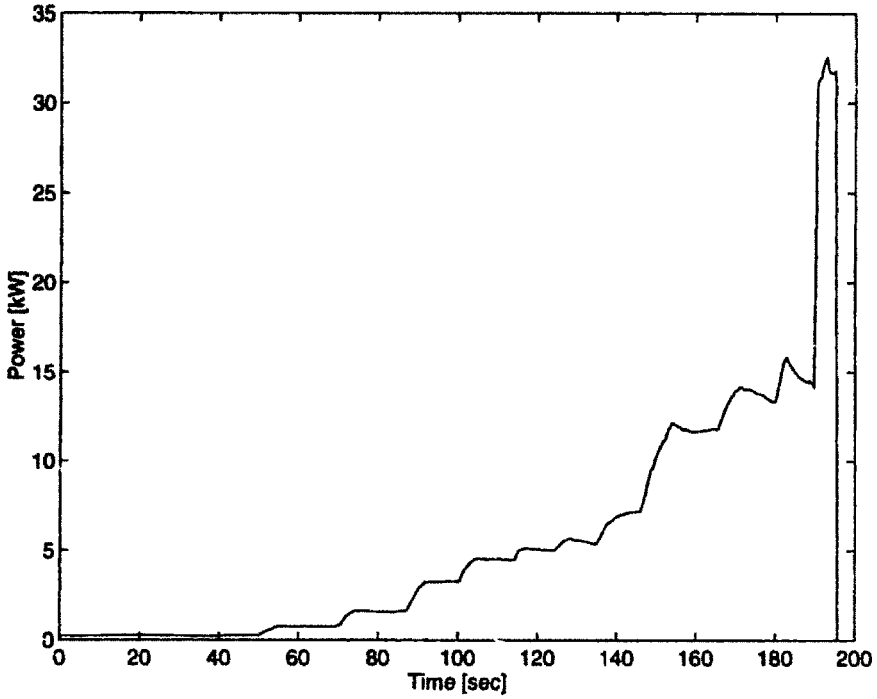

Figure E-64: Test Section 26A Power Profile

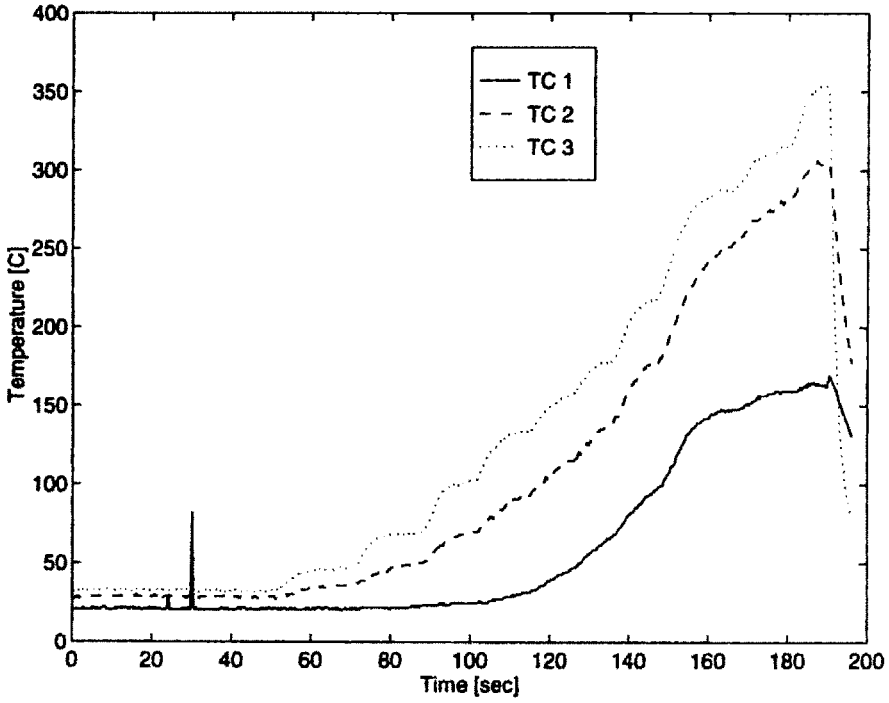

Figure E-65: Test Section 26A Temperature Profile

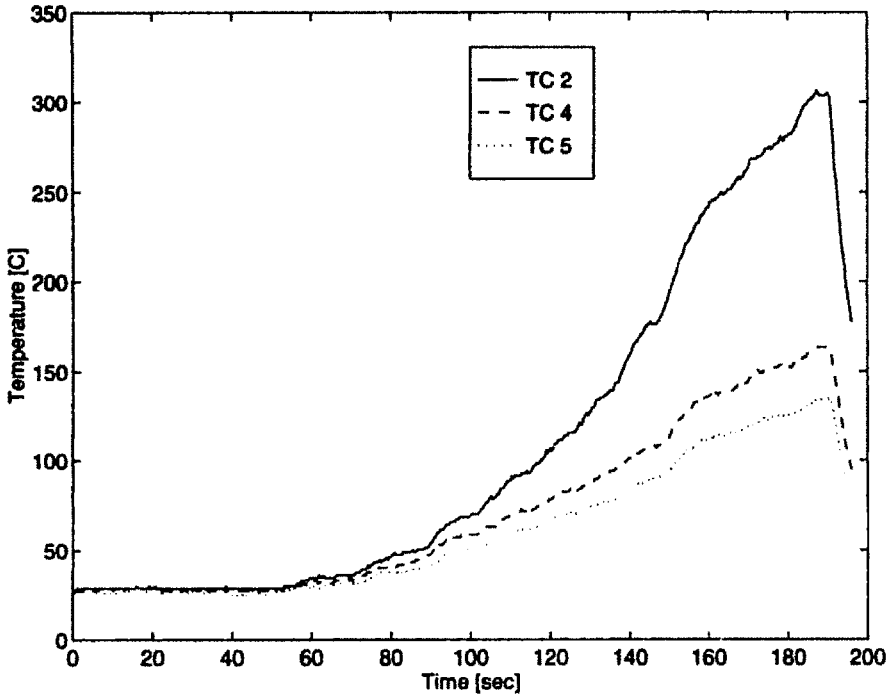

Figure E-66: Test Section 26A Temperature Profile

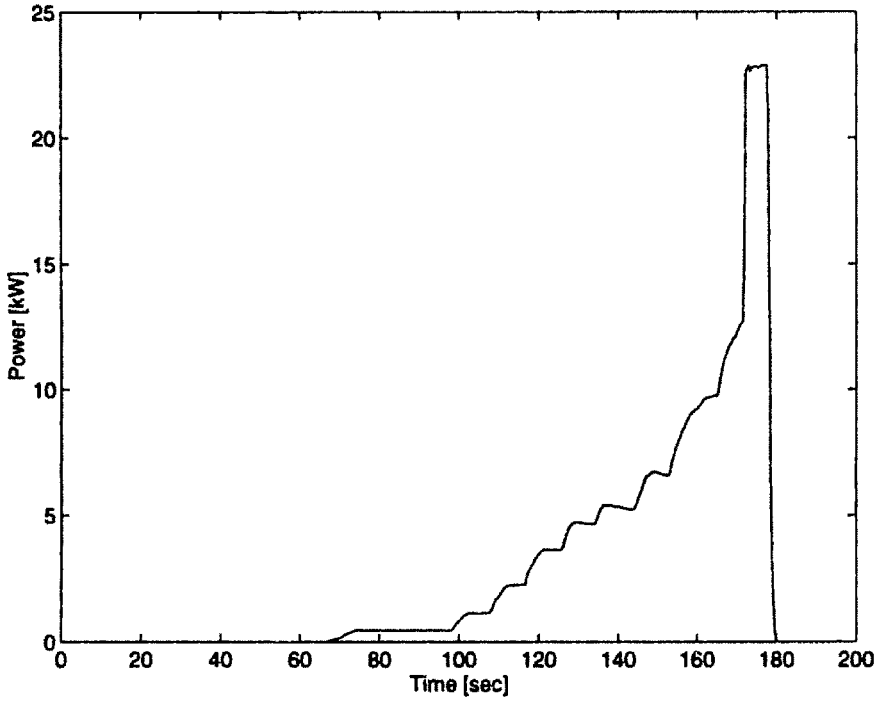

Figure E-67: Test Section 26B Power Profile

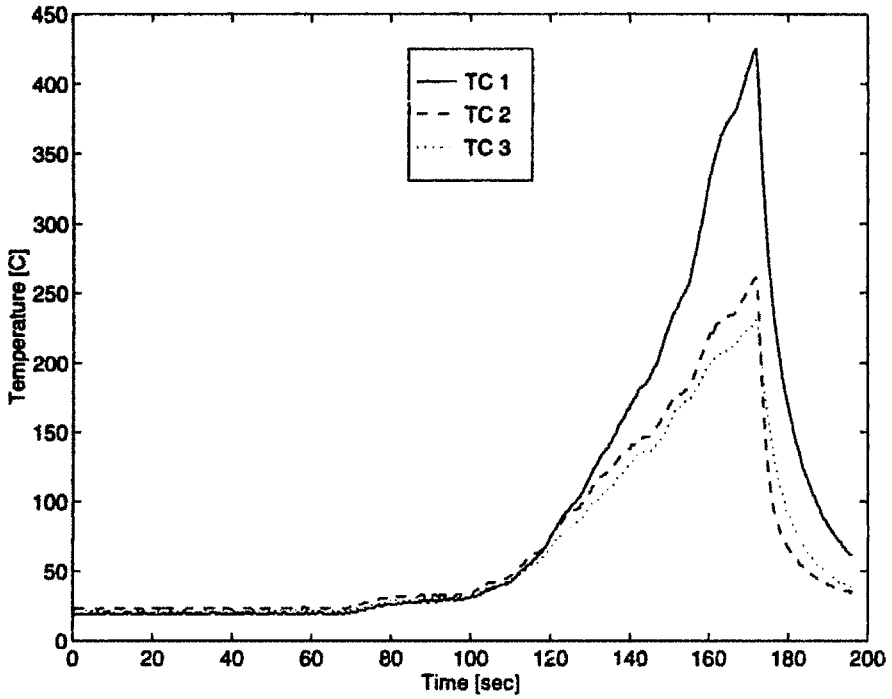

Figure E-68: Test Section 26B Temperature Profile

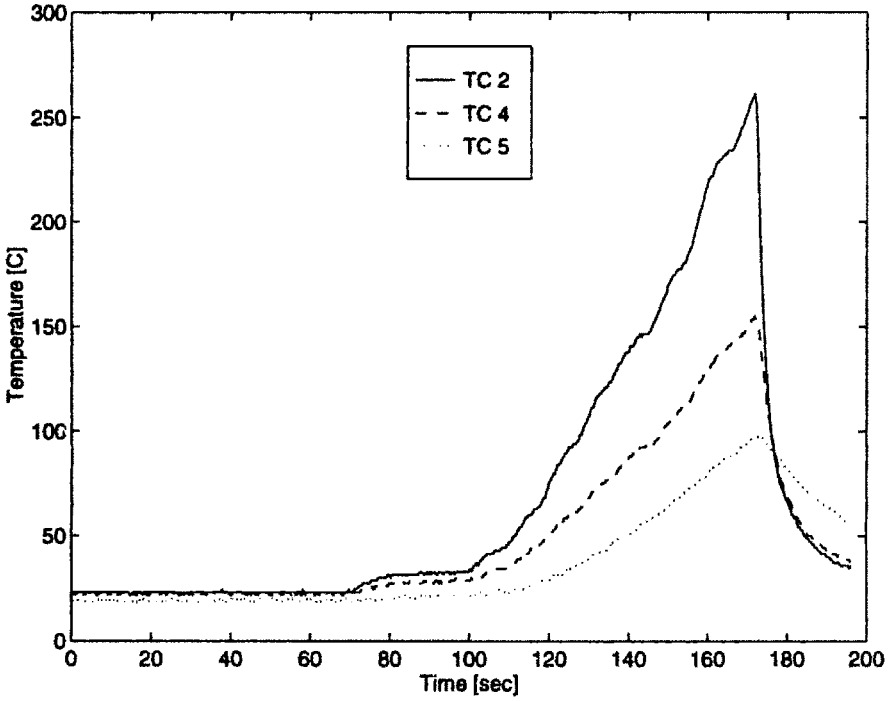

Figure E-69: Test Section 26B Temperature Profile

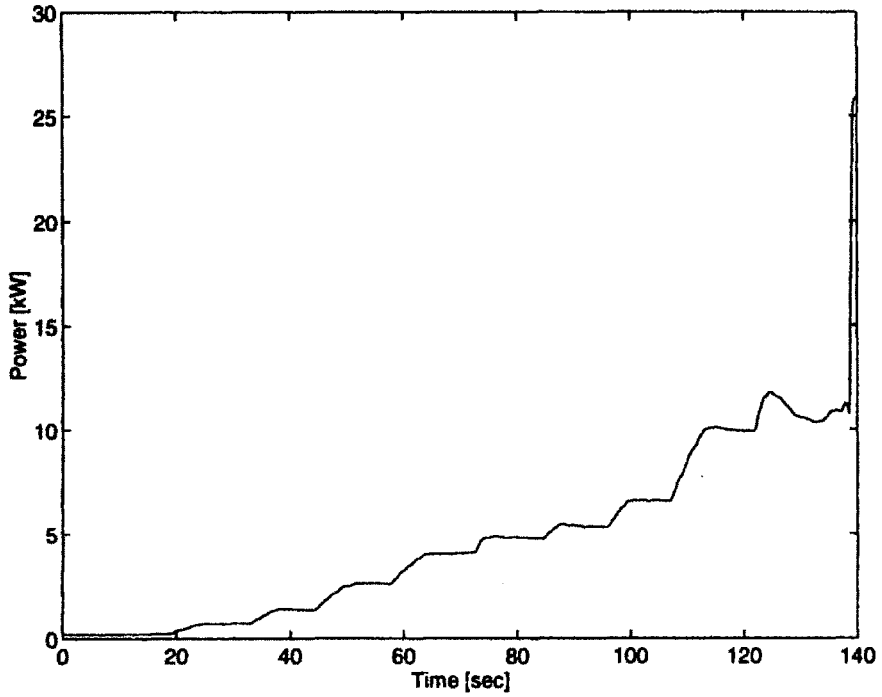

Figure E-70: Test Section 27A Power Profile

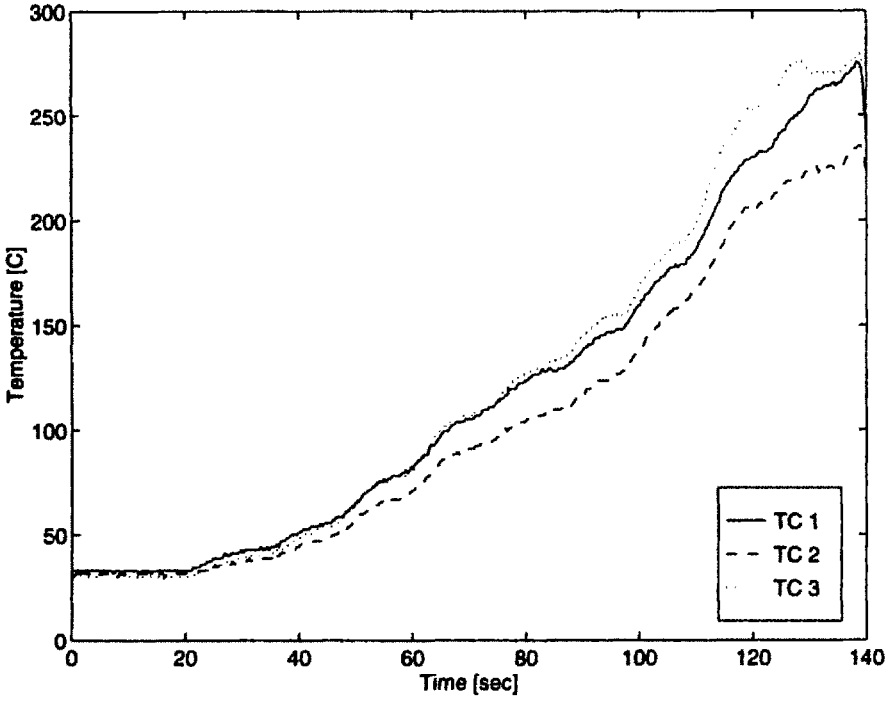

Figure E-71: Test Section 27A Temperature Profile

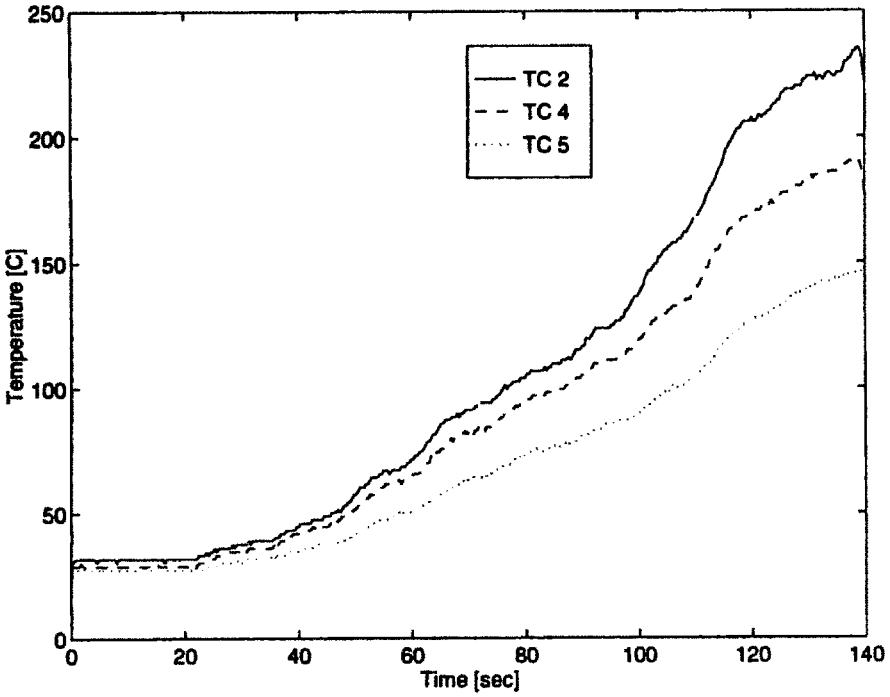

Figure E-72: Test Section 27A Temperature Profile

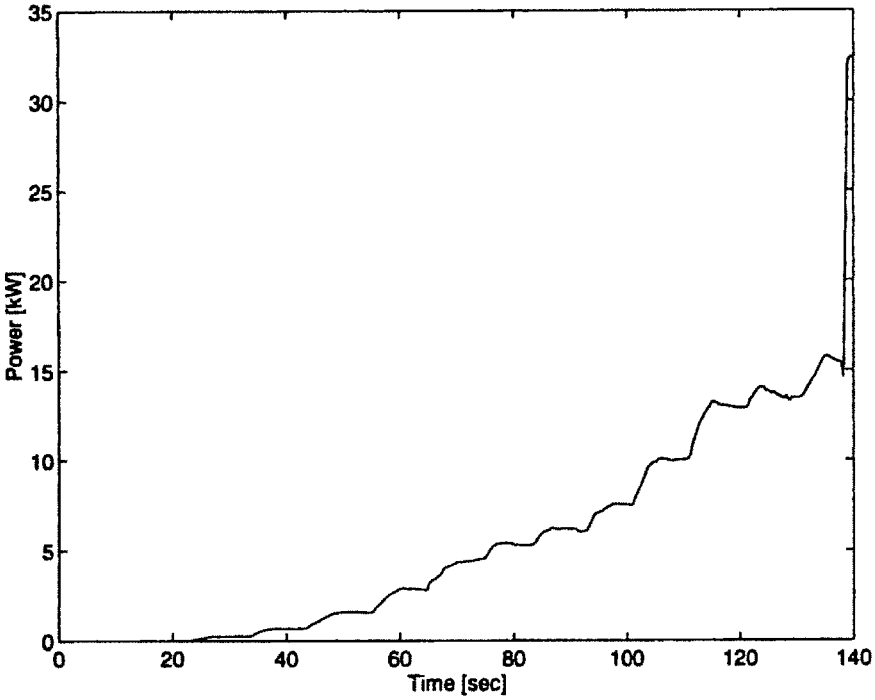

Figure E-73: Test Section 27B Power Profile

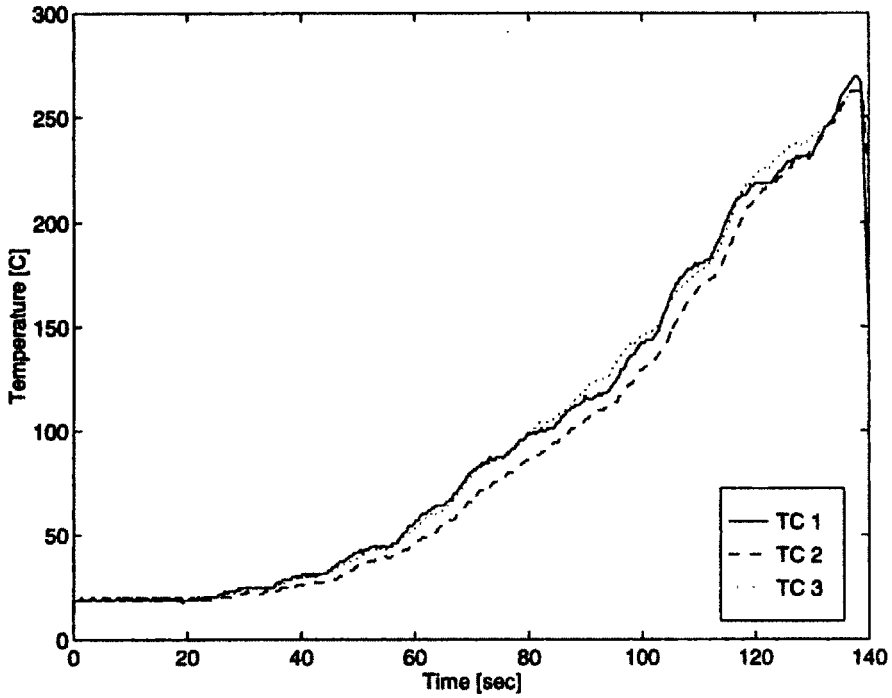

Figure E-74: Test Section 27B Temperature Profile

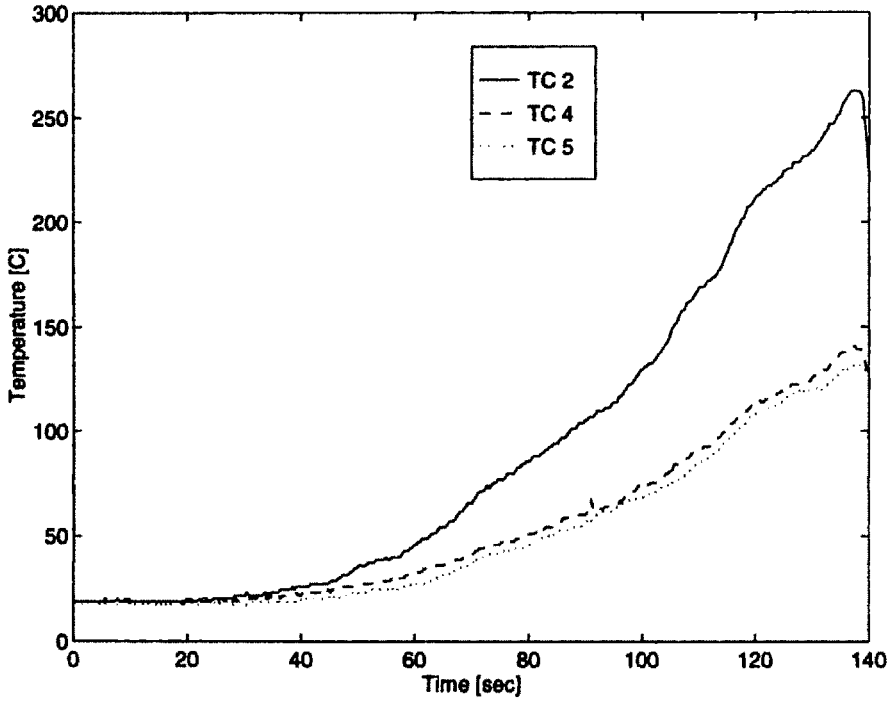

Figure E-75: Test Section 27B Temperature Profile

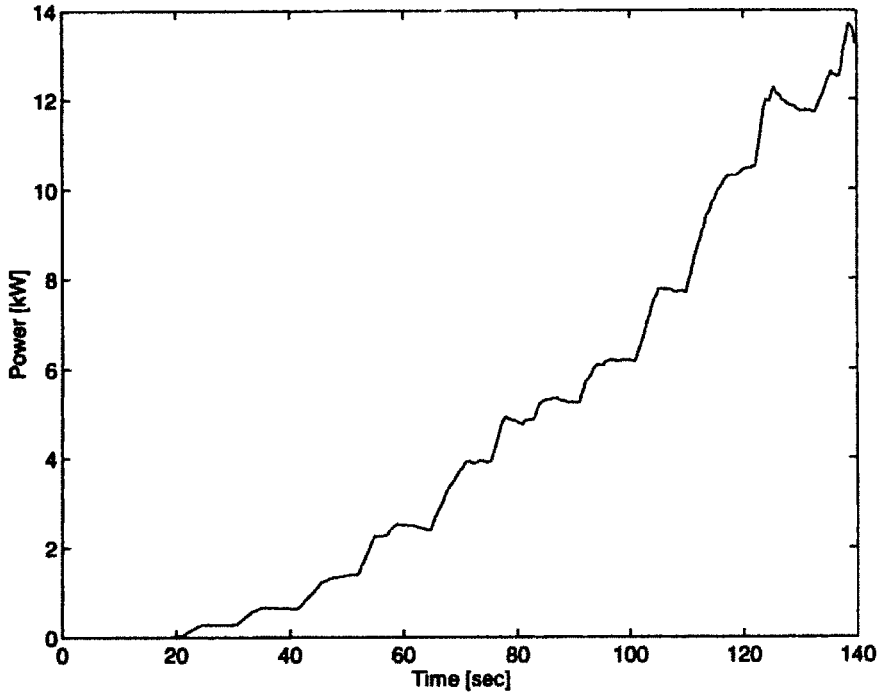

Figure E-76: Test Section 28A Power Profile

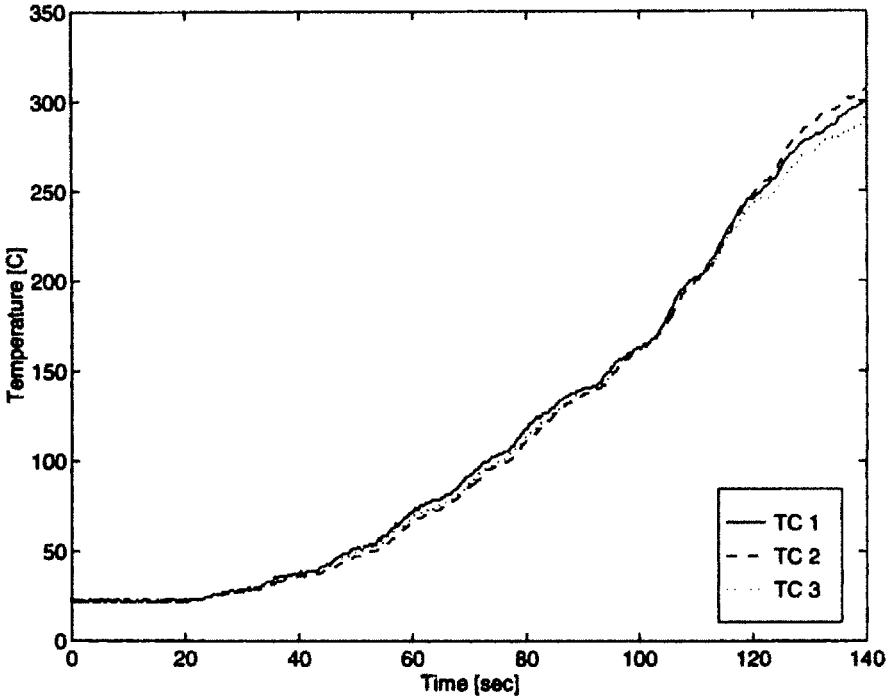

Figure E-77: Test Section 28A Temperature Profile

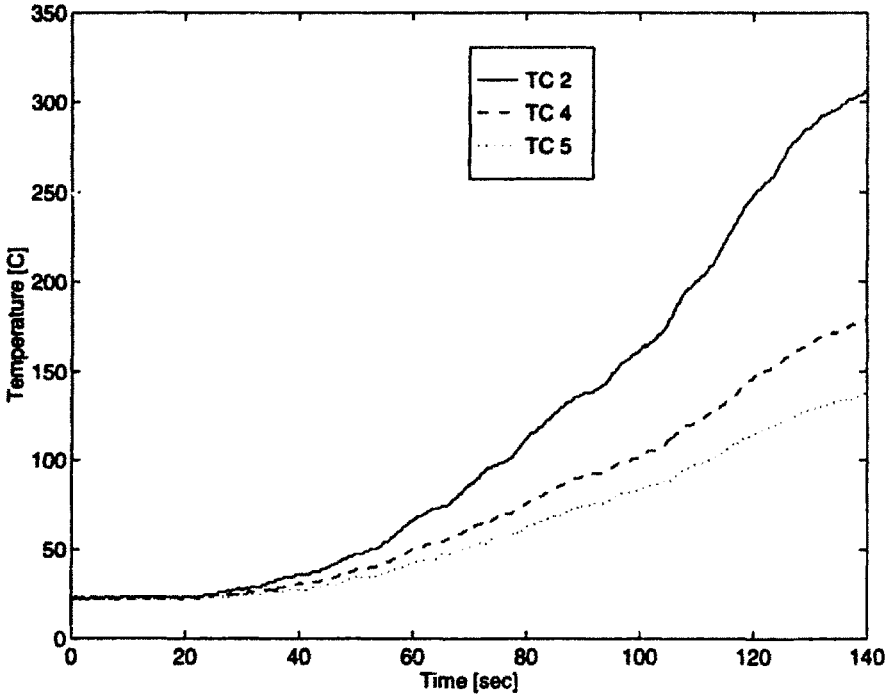

Figure E-78: Test Section 28A Temperature Profile

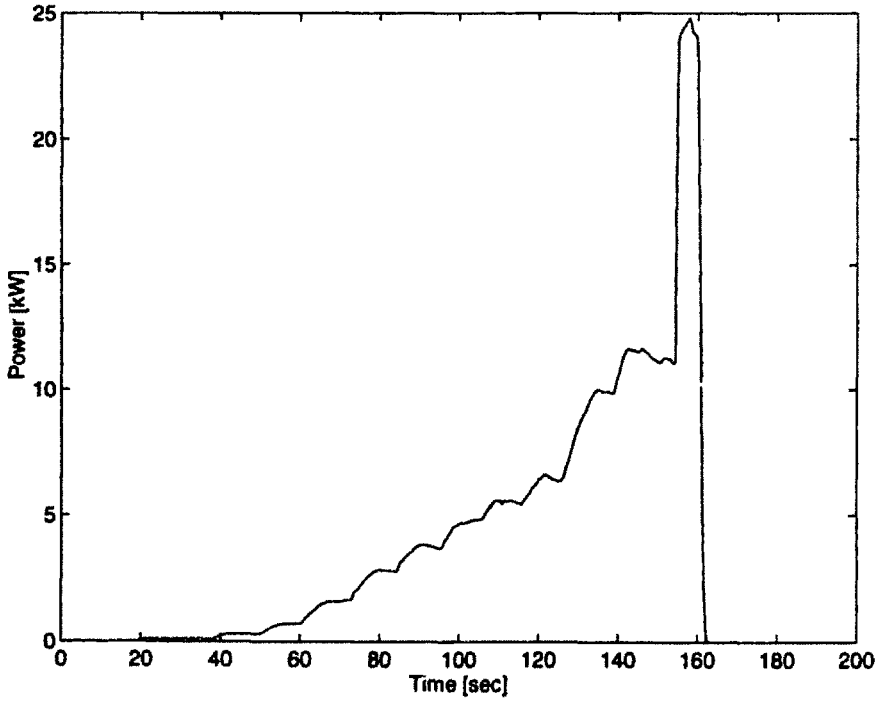

Figure E-79: Test Section 28B Power Profile

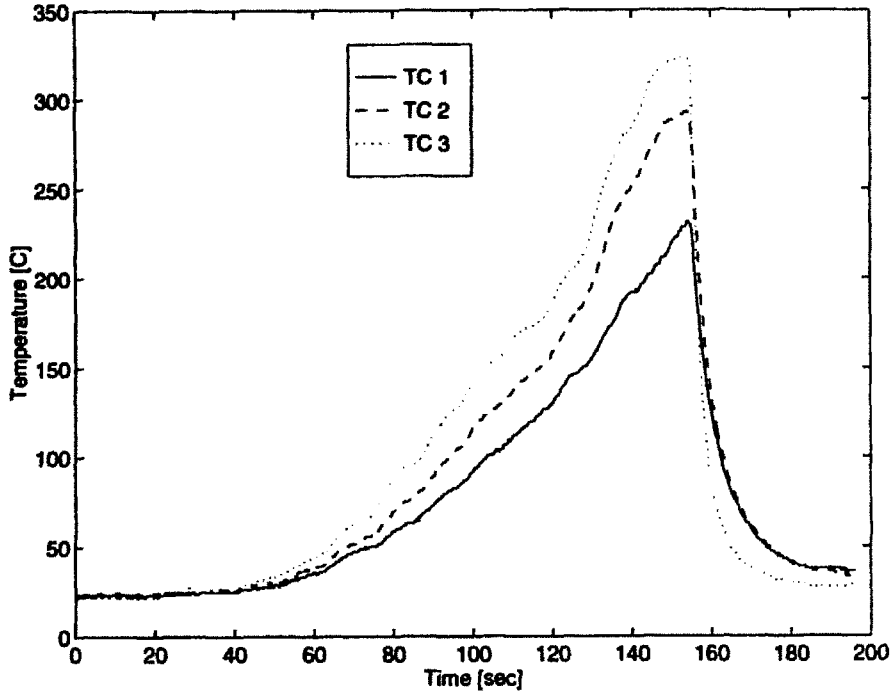

Figure E-80: Test Section 28B Temperature Profile

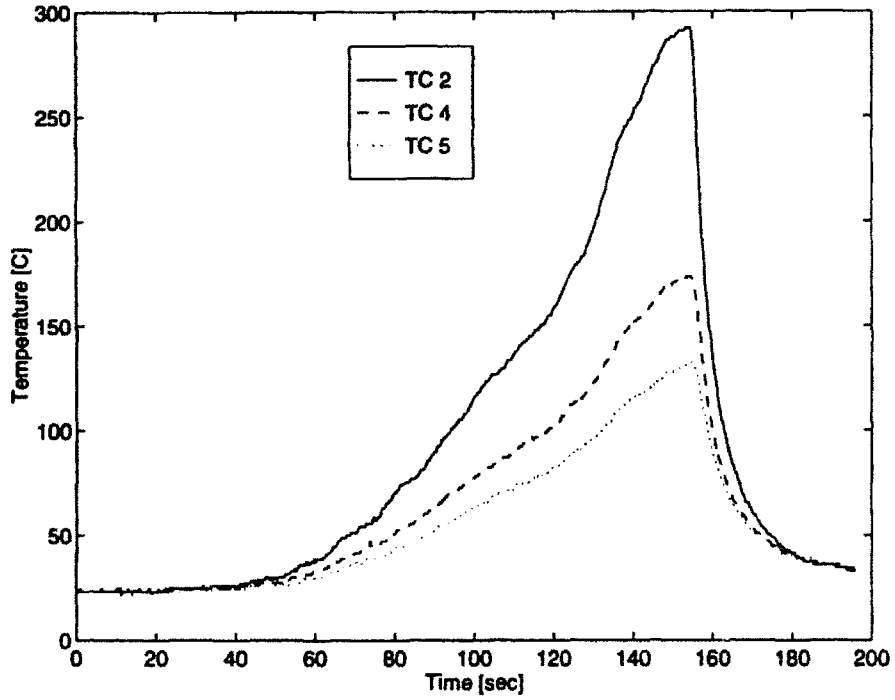

Figure E-81: Test Section 28B Temperature Profile

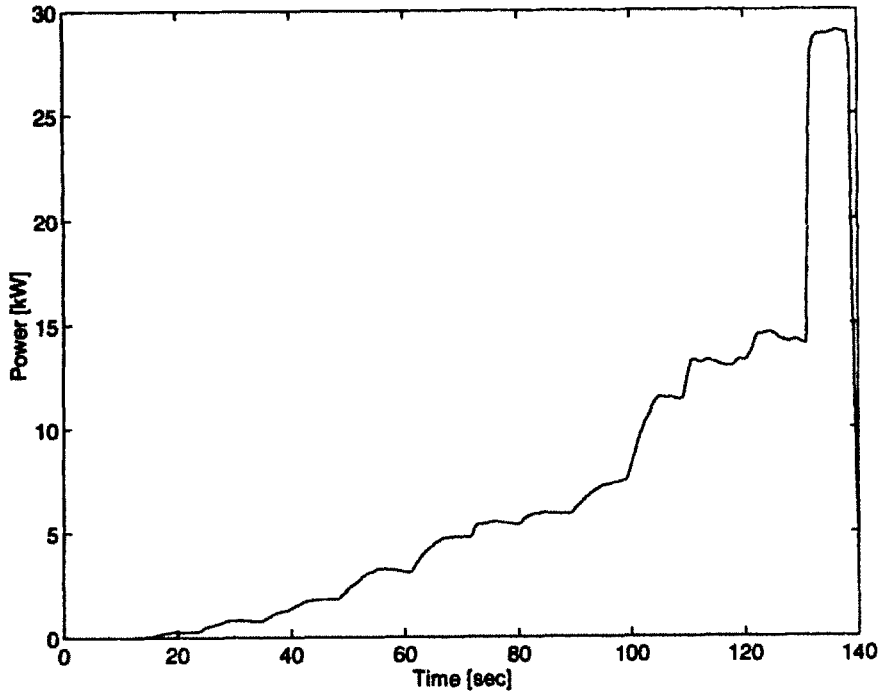

Figure E-82: Test Section 29A Power Profile

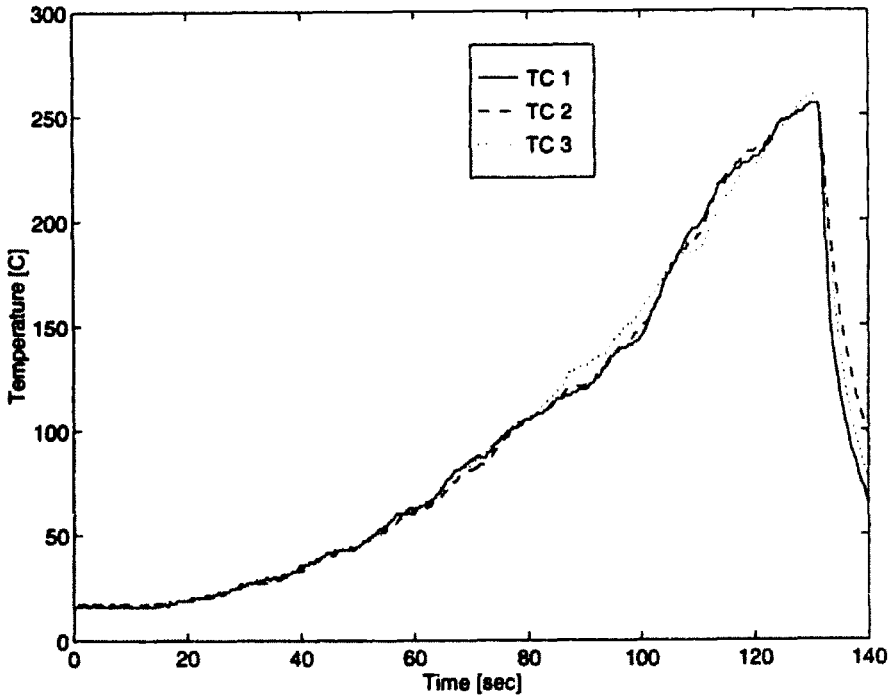

Figure E-83: Test Section 29A Temperature Profile

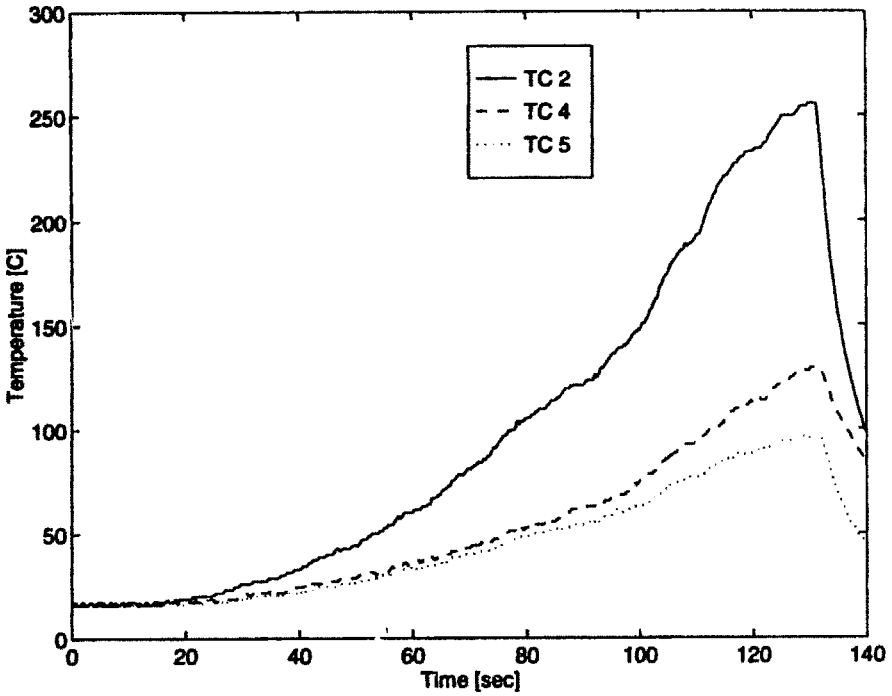

Figure E-84: Test Section 29A Temperature Profile

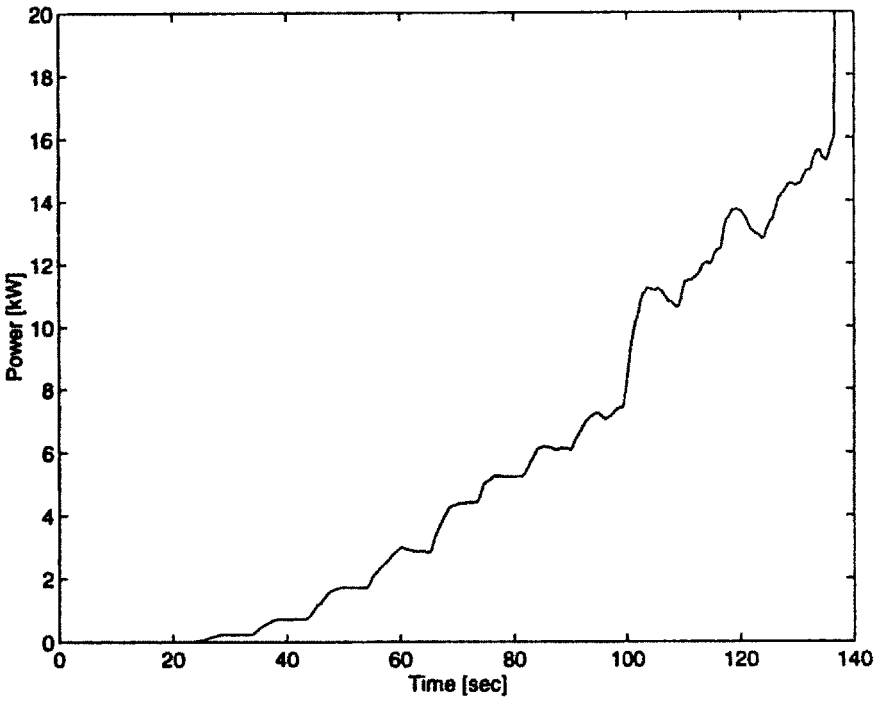

Figure E-85: Test Section 29B Power Profile

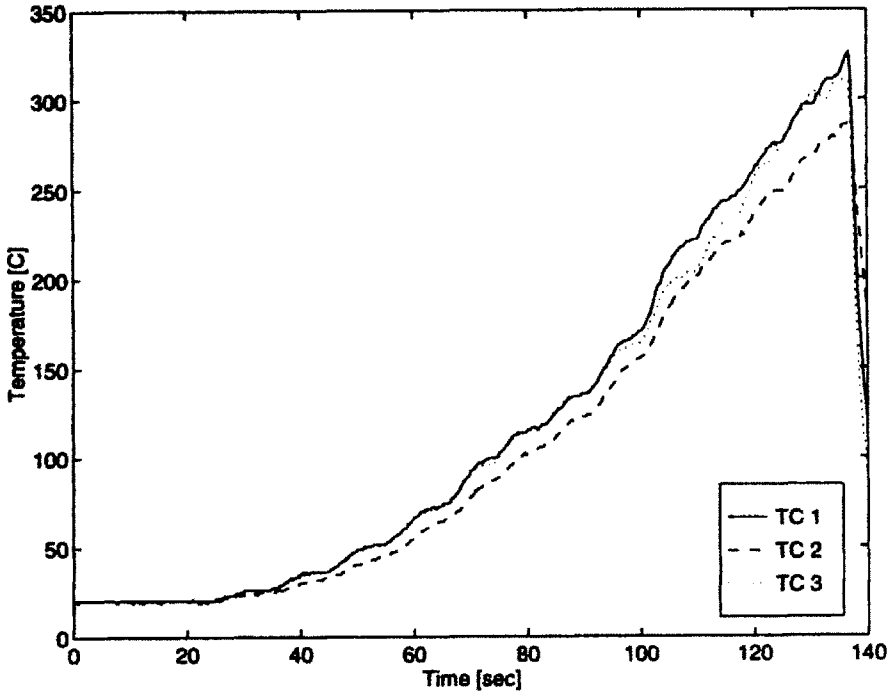

Figure E-86: Test Section 29B Temperature Profile

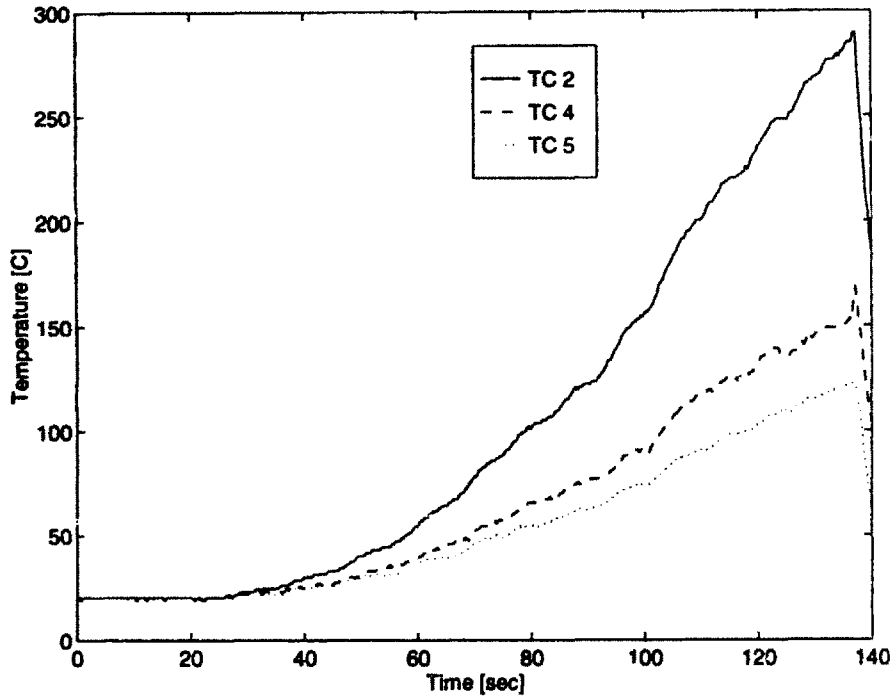

Figure E-87: Test Section 29B Temperature Profile

Appendix F

Data Reduction Results: Profiles of Thermal Hydraulic Regions

In the following figures, the Shah Correlation [45] (see Chapter 2) for Subcooled Nucleate Boiling is used except where noted by ^{ch} above the Test Section number. In these cases, the Chen Correlation [46] (see Chapter 2) for Suppressed Nucleate Boiling is used.

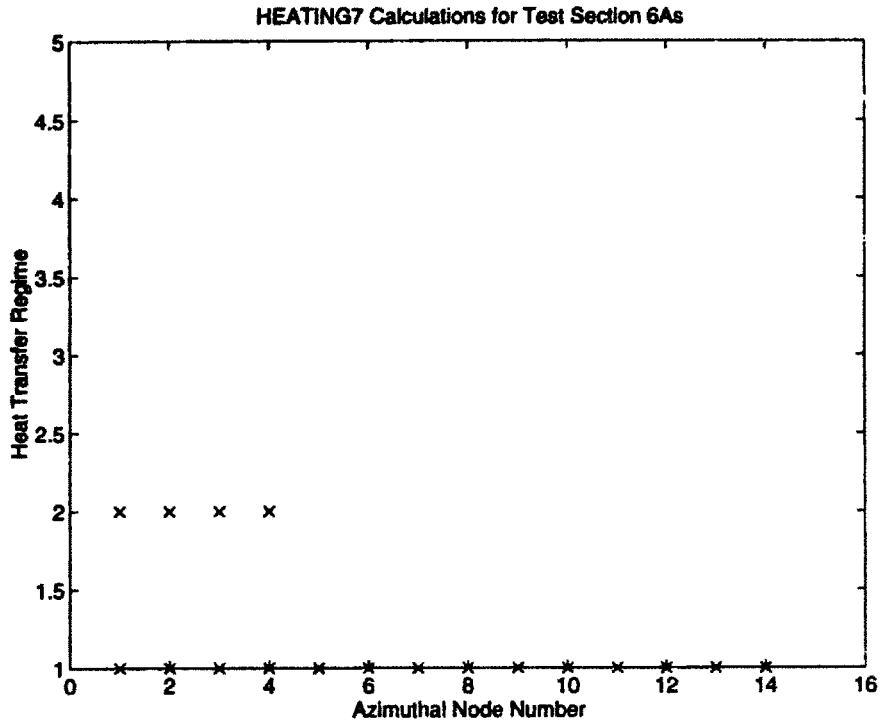

Figure F-1: Test Section 6A Azimuthal Thermal Region Profile
1: Single Phase Liquid; 2: Boiling; 3: T $\geq$ T (homogeneous nucl.); 4: T $\geq$ T (crit)

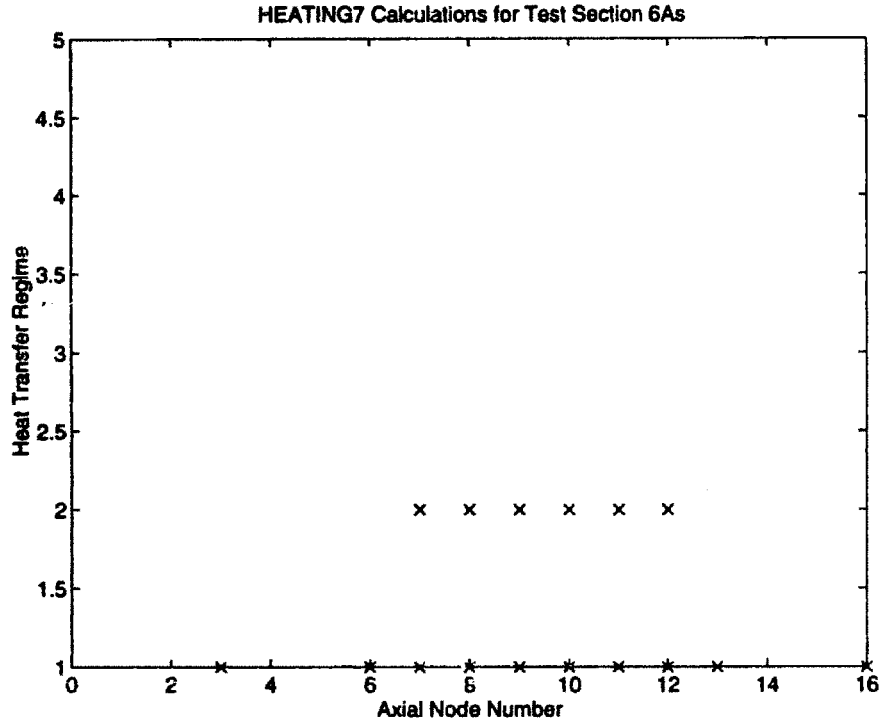

Figure F-2: Test Section 6A Axial Thermal Region Profile
1: Single Phase Liquid; 2: Boiling; 3: T $\geq$ T (homogeneous nucl.); 4: T $\geq$ T (crit)

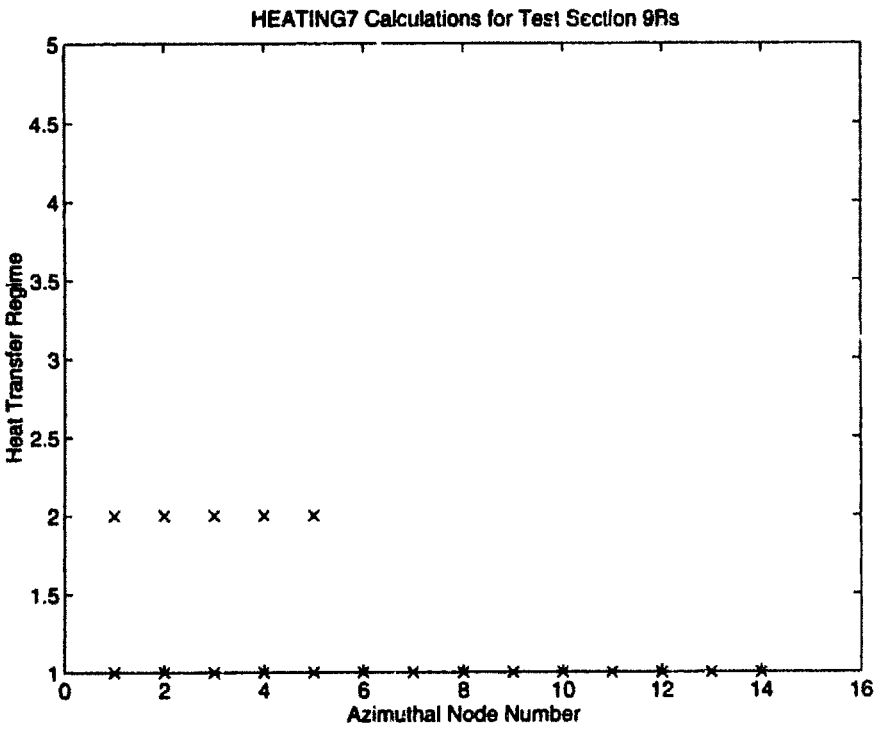

Figure F-3: Test Section 9B Azimuthal Thermal Region Profile
1: Single Phase Liquid; 2: Boiling; 3: T $\geq$ T (homogeneous nucl.); 4: T $\geq$ T (crit)

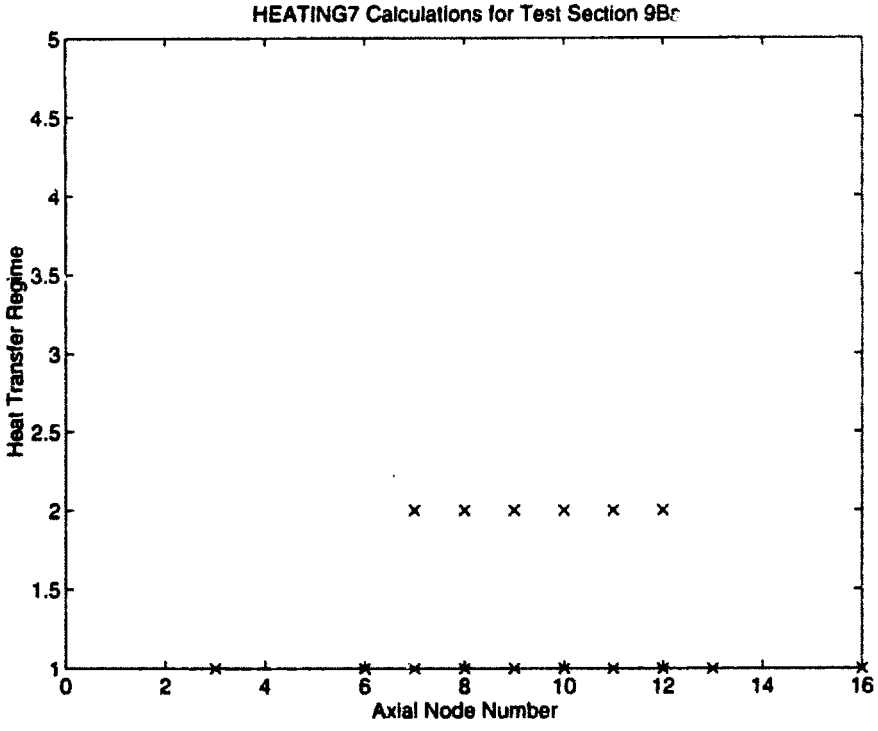

Figure F-4: Test Section 9B Axial Thermal Region Profile
1: Single Phase Liquid; 2: Boiling; 3: T $\geq$ T (homogeneous nucl.); 4: T $\geq$ T (crit)

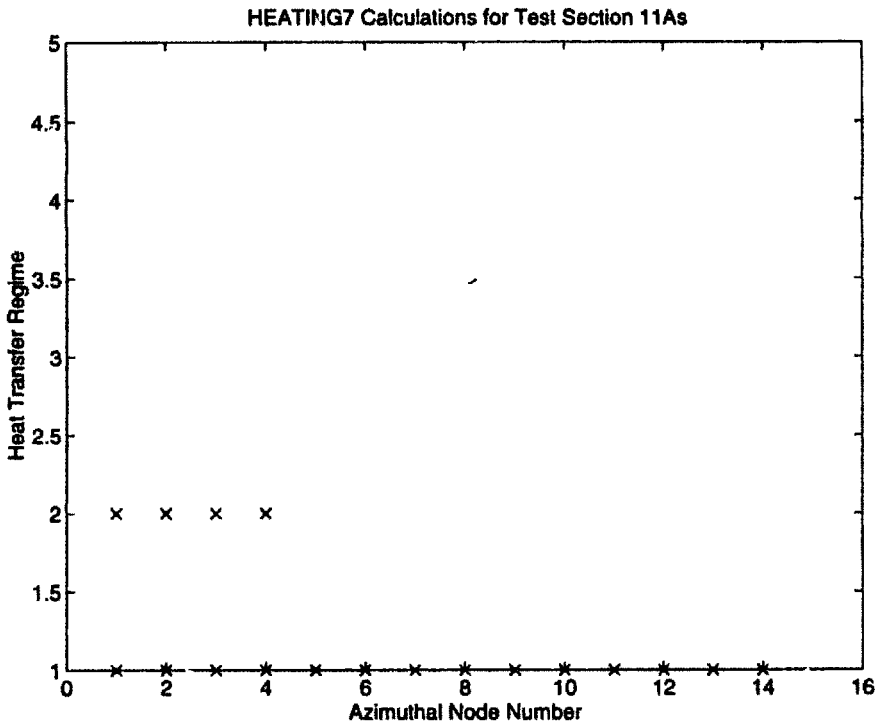

Figure F-5: Test Section 11A Azimuthal Thermal Region Profile
1: Single Phase Liquid; 2: Boiling; 3: T $\geq$ T (homogeneous nucl.); 4: T $\geq$ T (crit)

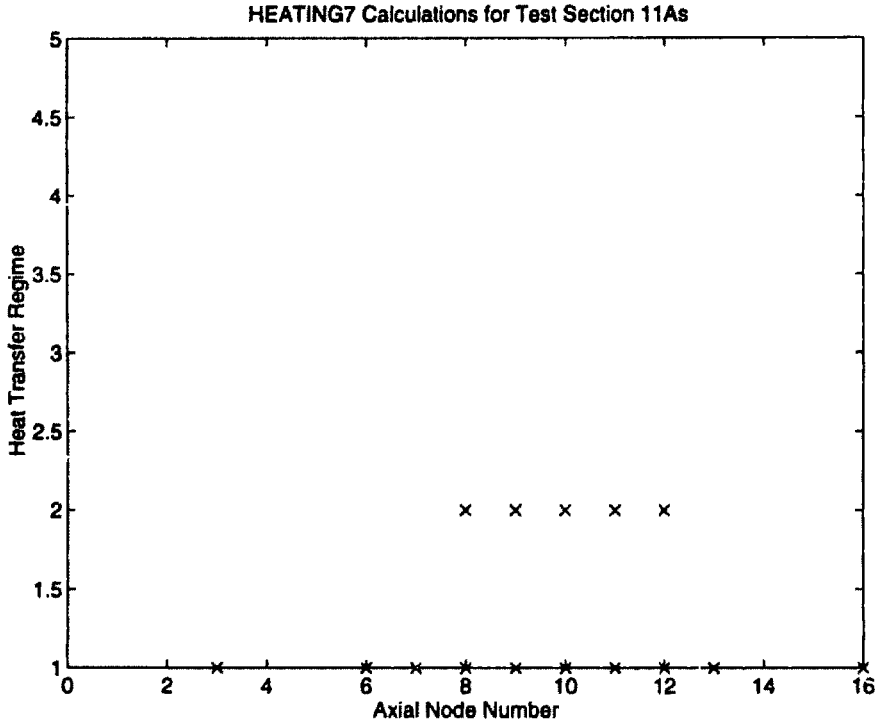

Figure F-6: Test Section 11A Axial Thermal Region Profile
1: Single Phase Liquid; 2: Boiling; 3: T $\geq$ T (homogeneous nucl.); 4: T $\geq$ T (crit)

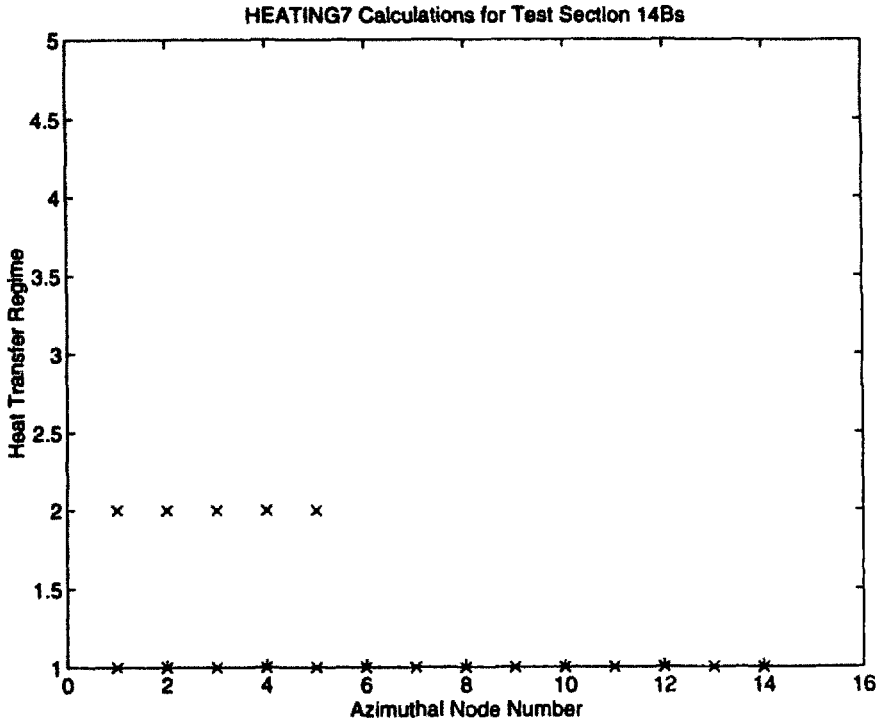

Figure F-7: Test Section 14B Azimuthal Thermal Region Profile
1: Single Phase Liquid; 2: Boiling; 3: T $\geq$ T (homogeneous nucl.); 4: T $\geq$ T (crit)

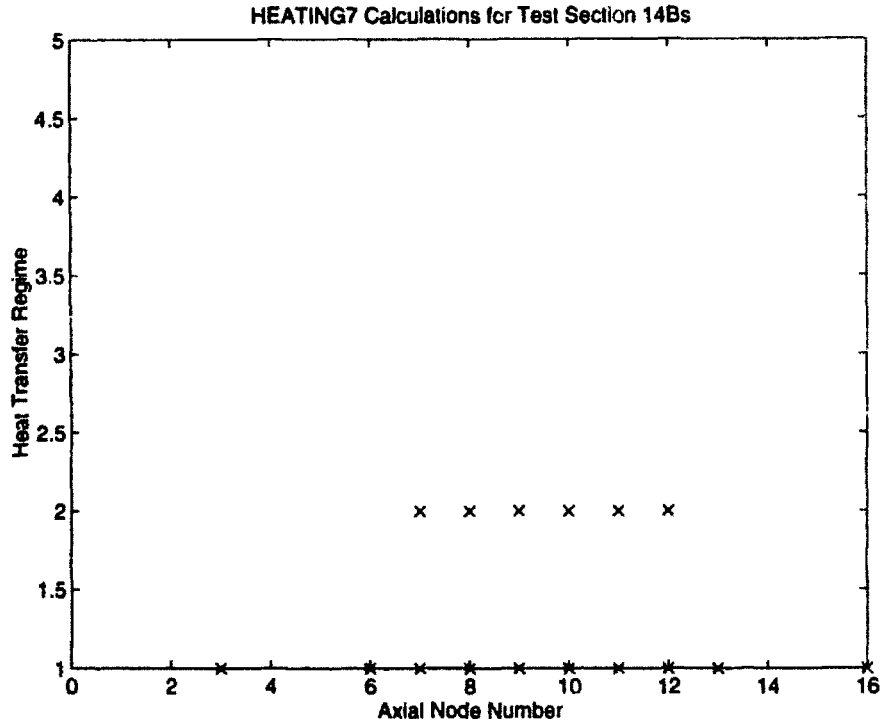

Figure F-8: Test Section 14B Axial Thermal Region Profile
1: Single Phase Liquid; 2: Boiling; 3: T $\geq$ T (homogeneous nucl.); 4: T $\geq$ T (crit)

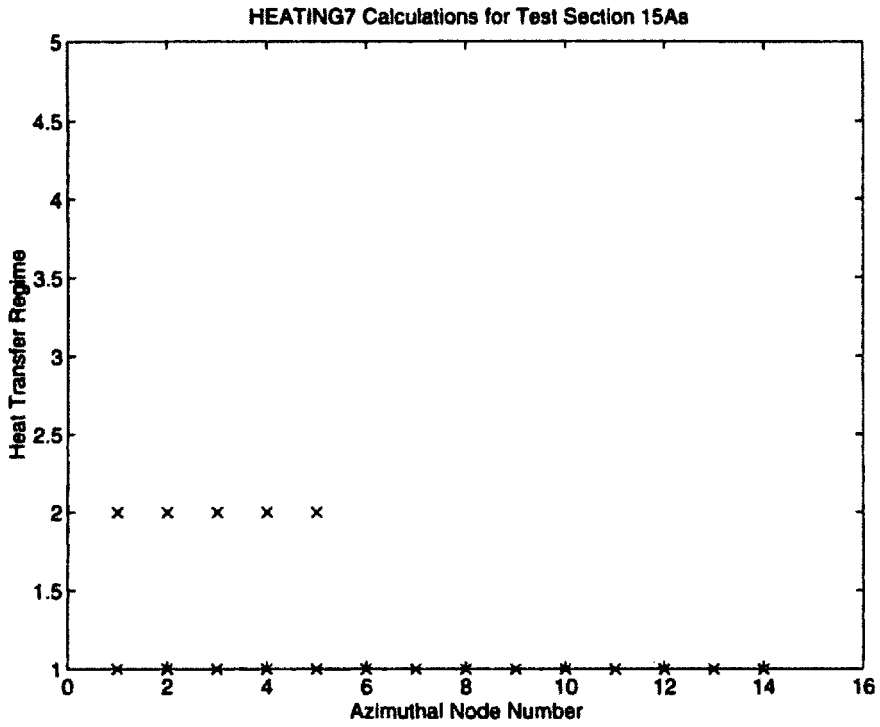

Figure F-9: Test Section 15A Azimuthal Thermal Region Profile
1: Single Phase Liquid; 2: Boiling; 3: T $\geq$ T (homogeneous nucl.); 4: T $\geq$ T (crit)

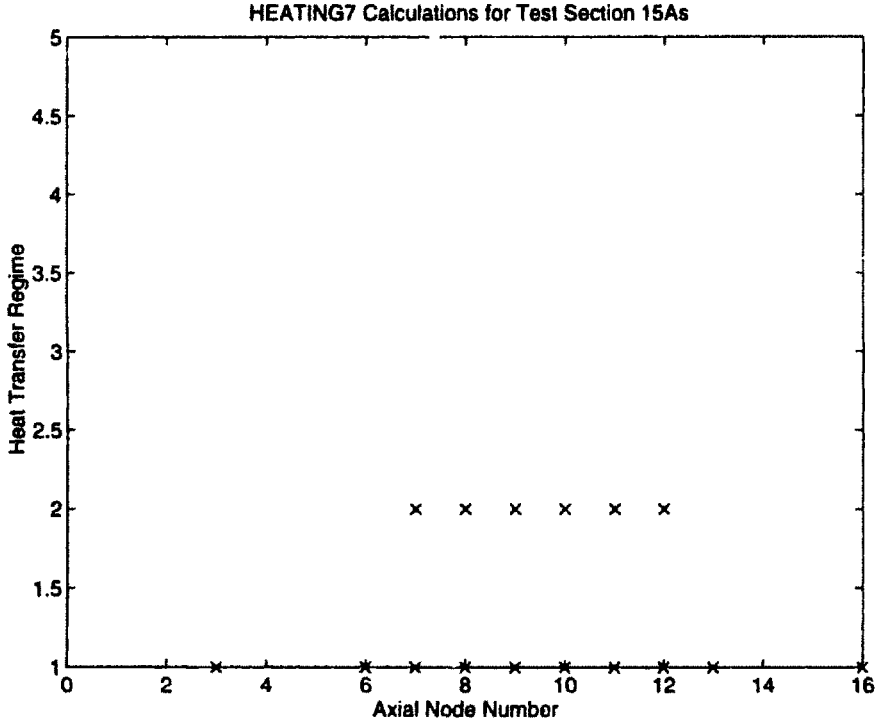

Figure F-10: Test Section 15A Axial Thermal Region Profile
1: Single Phase Liquid; 2: Boiling; 3: T $\geq$ T (homogeneous nucl.); 4: T $\geq$ T (crit)

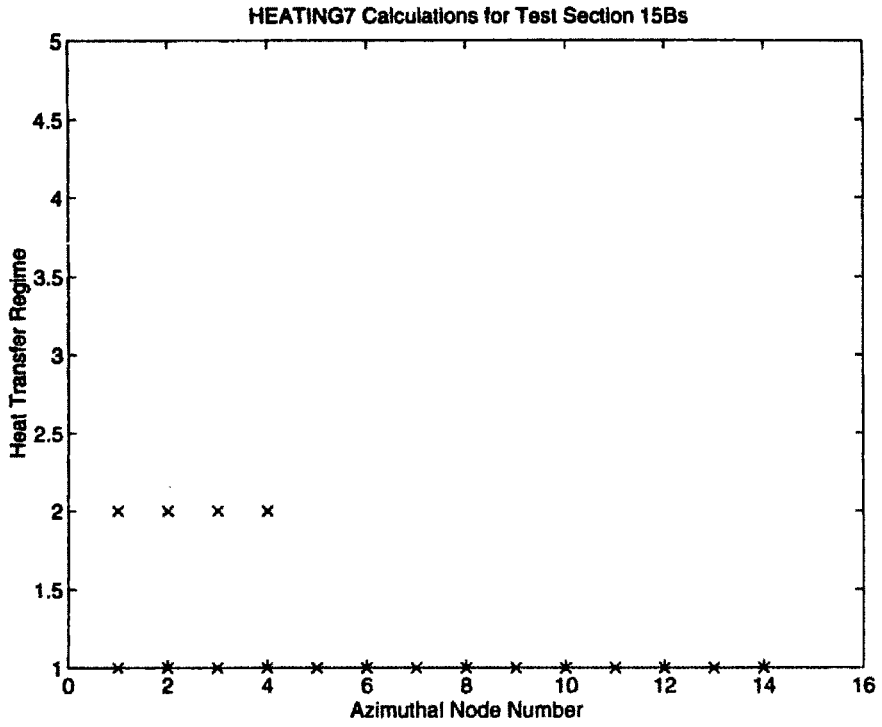

Figure F-11: Test Section 15B Azimuthal Thermal Region Profile
1: Single Phase Liquid; 2: Boiling; 3: T $\geq$ T (homogeneous nucl.); 4: T $\geq$ T (crit)

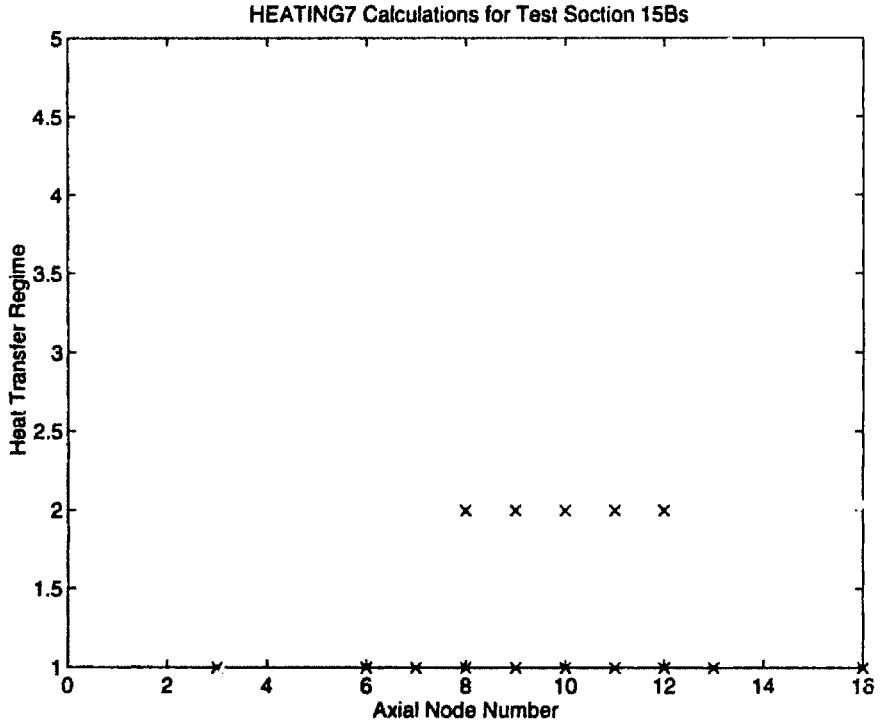

Figure F-12: Test Section 15B Axial Thermal Region Profile
1: Single Phase Liquid; 2: Boiling; 3: T $\geq$ T (homogeneous nucl.); 4: T $\geq$ T (crit)

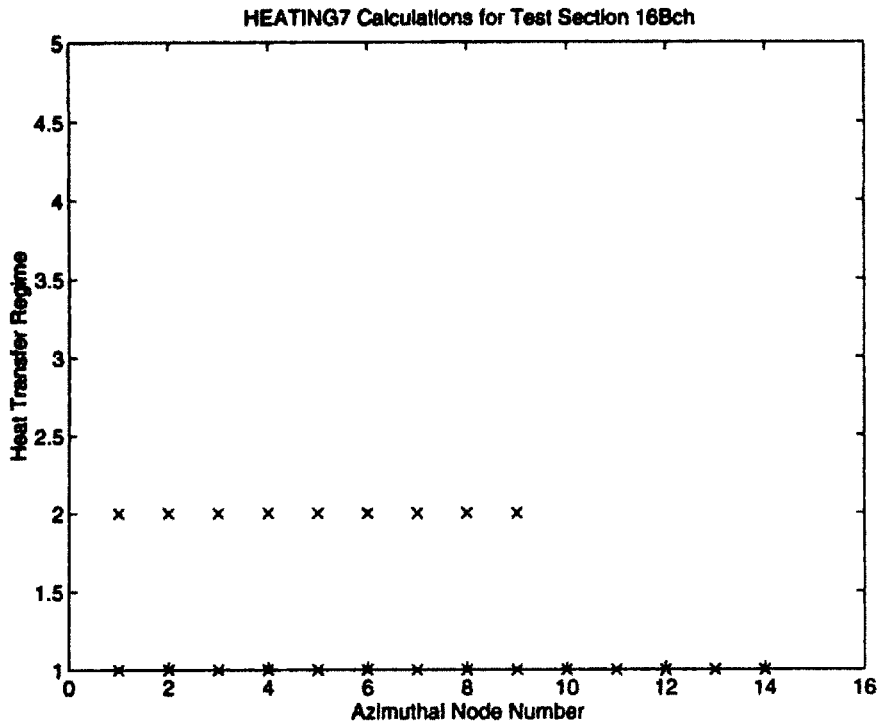

Figure F-13: Test Section $16B^{ch}$ Azimuthal Thermal Region Profile
1: Single Phase Liquid; 2: Boiling; 3: T $\geq$ T (homogeneous nucl.); 4: T $\geq$ T (crit)

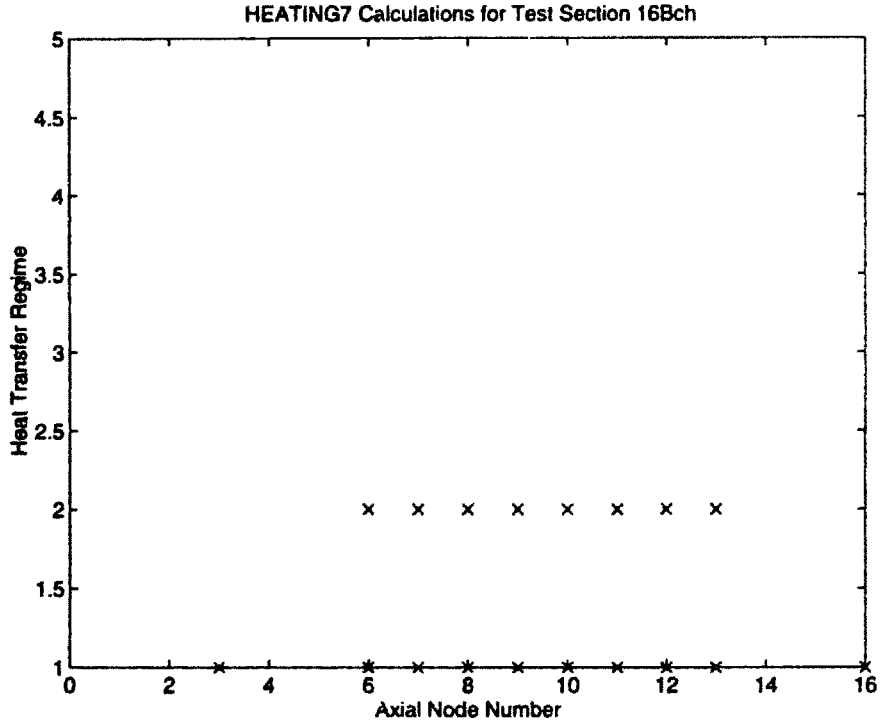

Figure F-14: Test Section $16B^{ch}$ Axial Thermal Region Profile
1: Single Phase Liquid; 2: Boiling; 3: T $\geq$ T (homogeneous nucl.); 4: T $\geq$ T (crit)

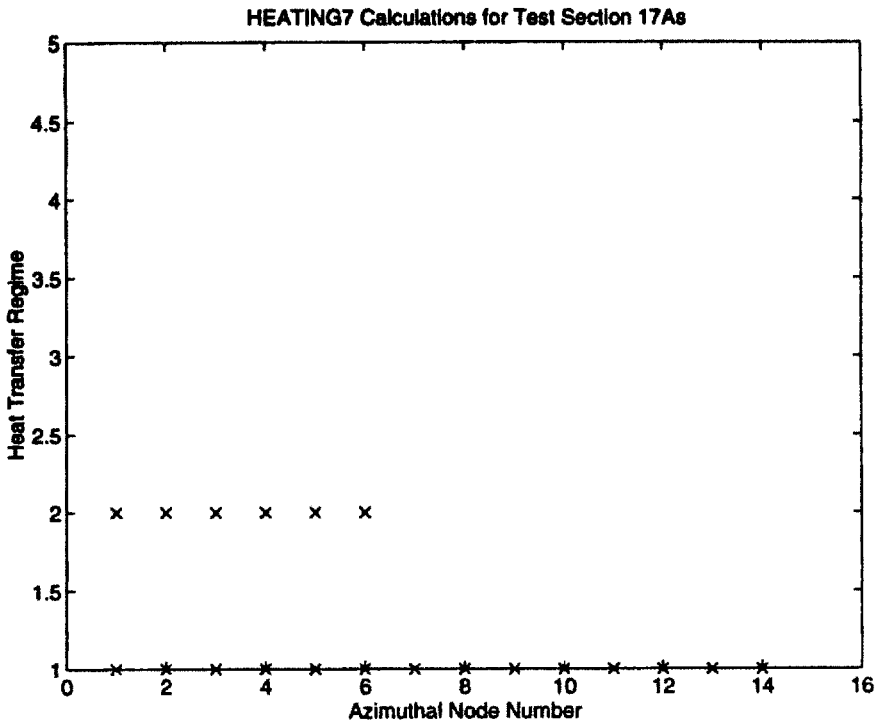

Figure F-15: Test Section 17A Azimuthal Thermal Region Profile
1: Single Phase Liquid; 2: Boiling; 3: T $\geq$ T (homogeneous nucl.); 4: T $\geq$ T (crit)

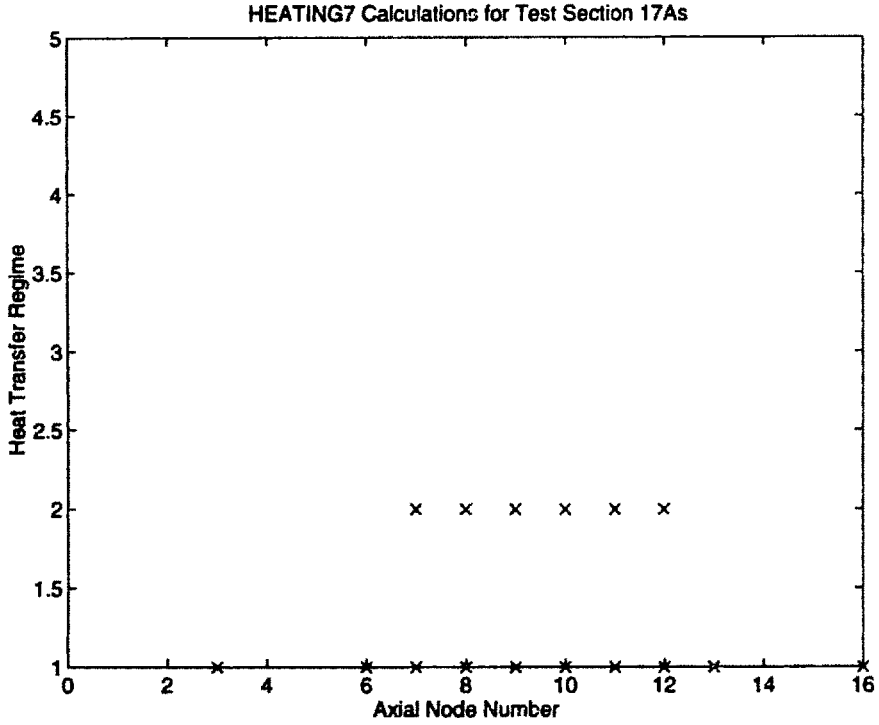

Figure F-16: Test Section 17A Axial Thermal Region Profile
1: Single Phase Liquid; 2: Boiling; 3: T $\geq$ T (homogeneous nucl.); 4: T $\geq$ T (crit)

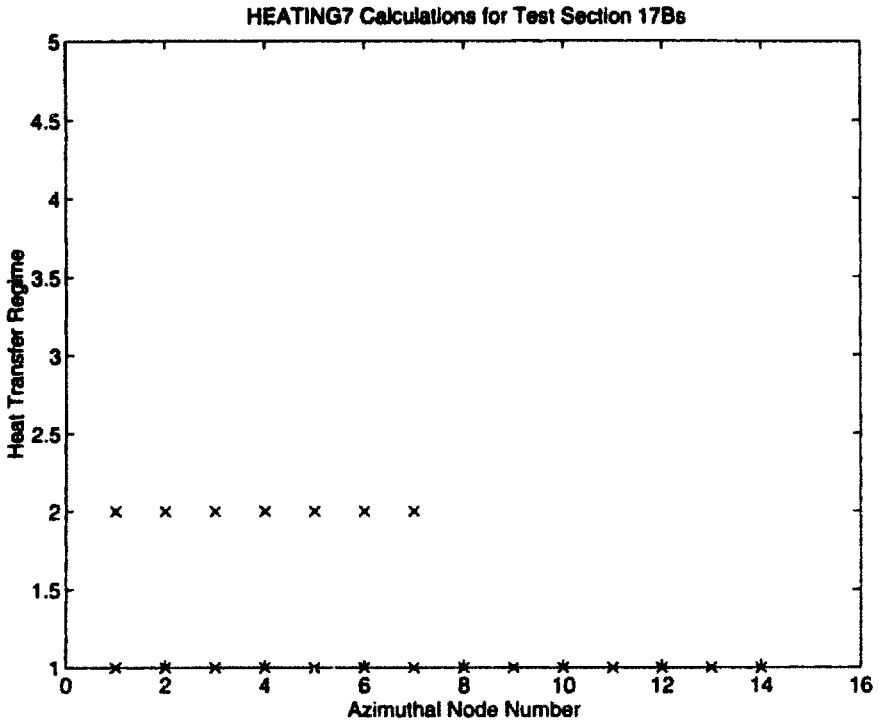

Figure F-17: Test Section 17B Azimuthal Thermal Region Profile
1: Single Phase Liquid; 2: Boiling; 3: T $\geq$ T (homogeneous nucl.); 4: T $\geq$ T (crit)

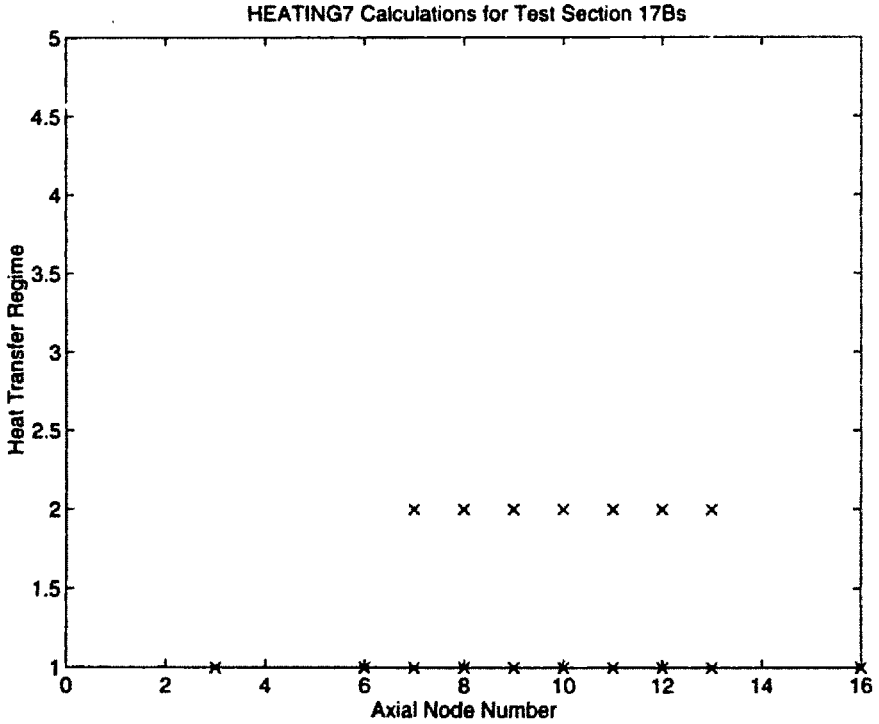

Figure F-18: Test Section 17B Axial Thermal Region Profile
1: Single Phase Liquid; 2: Boiling; 3: T $\geq$ T (homogeneous nucl.); 4: T $\geq$ T (crit)

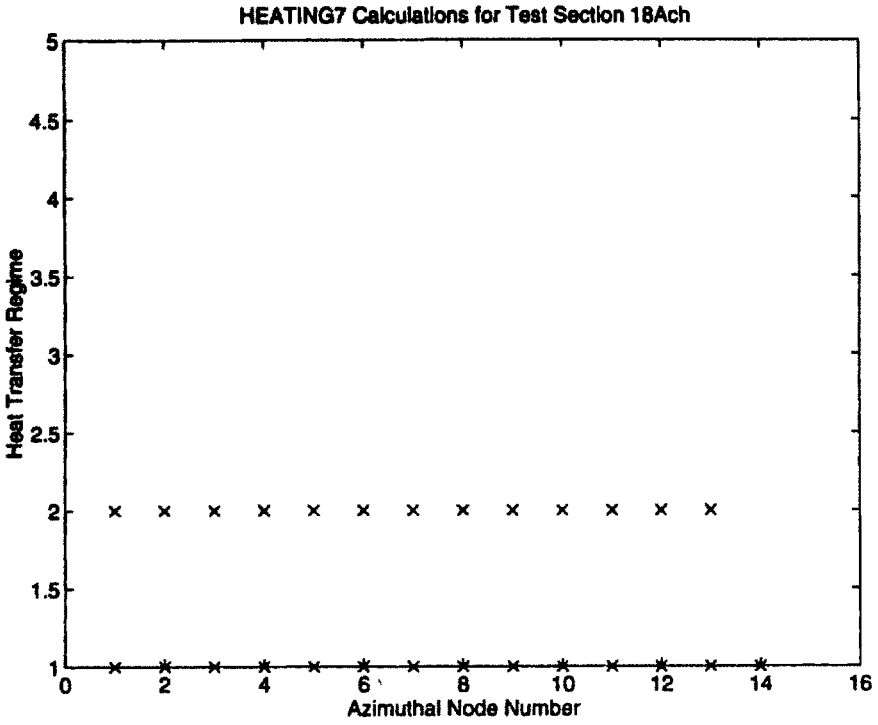

Figure F-19: Test Section 18A^{ch} Azimuthal Thermal Region Profile
1: Single Phase Liquid; 2: Boiling; 3: T $\geq$ T (homogeneous nucl.); 4: T $\geq$ T (crit)

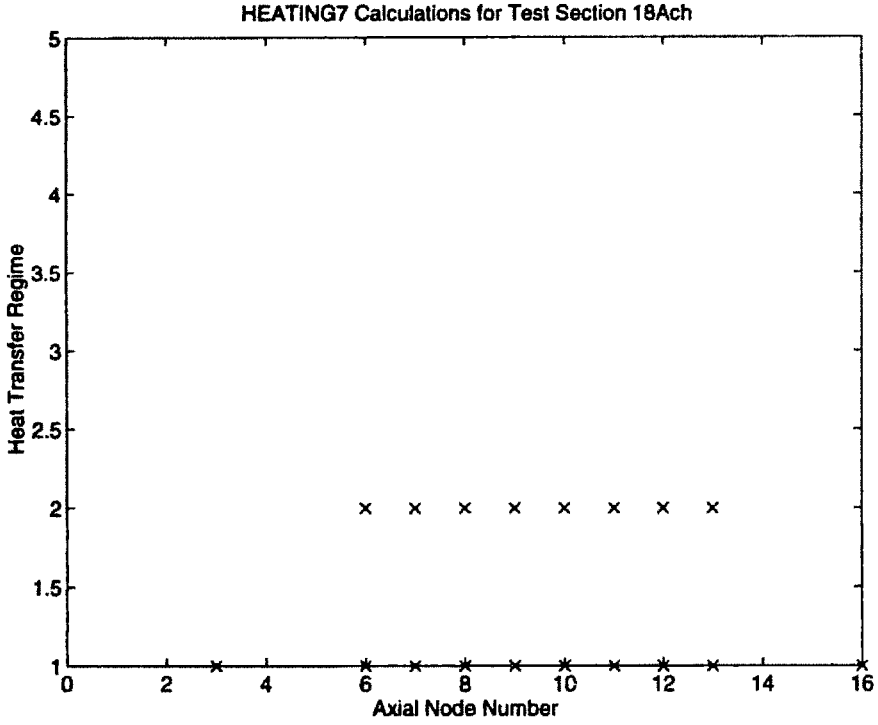

Figure F-20: Test Section 18A^{ch} Axial Thermal Region Profile
1: Single Phase Liquid; 2: Boiling; 3: T $\geq$ T (homogeneous nucl.); 4: T $\geq$ T (crit)

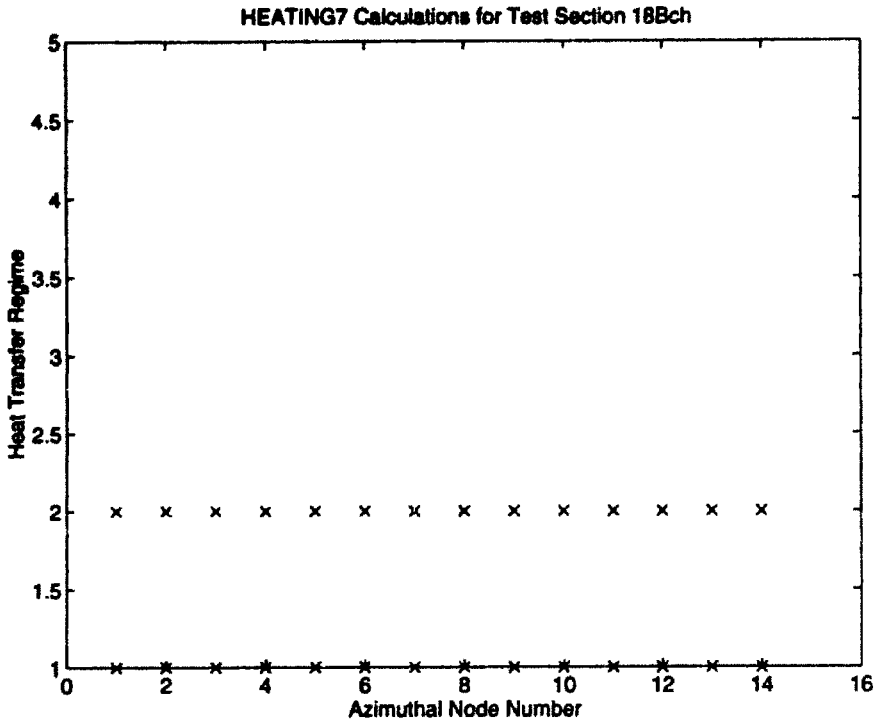

Figure F-21: Test Section 18B^{ch} Azimuthal Thermal Region Profile
1: Single Phase Liquid; 2: Boiling; 3: T $\geq$ T (homogeneous nucl.); 4: T $\geq$ T (crit)

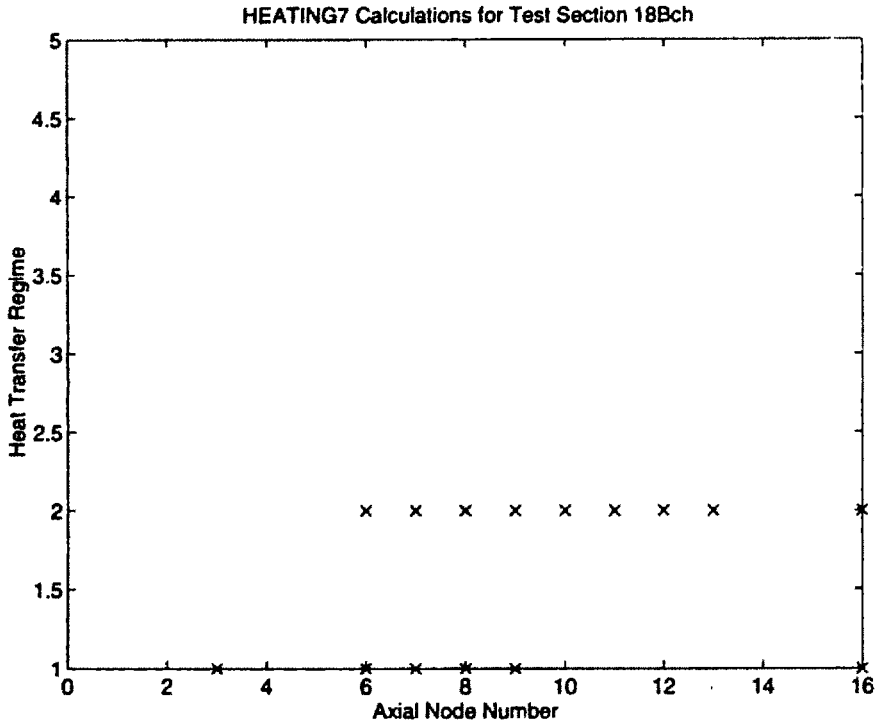

Figure F-22: Test Section 18B^{ch} Axial Thermal Region Profile
1: Single Phase Liquid; 2: Boiling; 3: T $\geq$ T (homogeneous nucl.); 4: T $\geq$ T (crit)

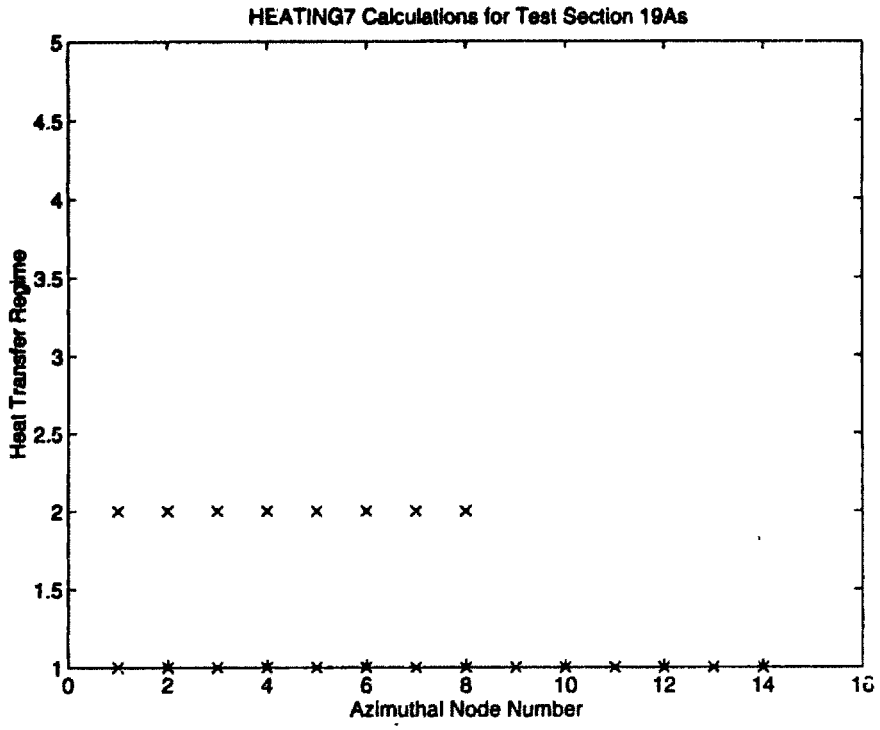

Figure F-23: Test Section 19A Azimuthal Thermal Region Profile
1: Single Phase Liquid; 2: Boiling; 3: T $\geq$ T (homogeneous nucl.); 4: T $\geq$ T (crit)

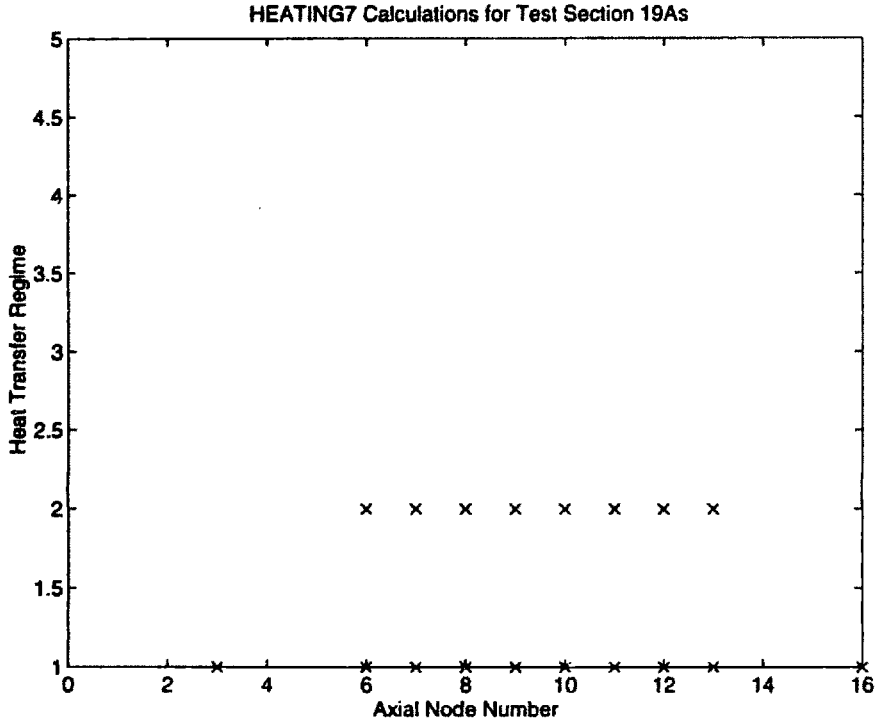

Figure F-24: Test Section 19A Axial Thermal Region Profile
1: Single Phase Liquid; 2: Boiling; 3: T $\geq$ T (homogeneous nucl.); 4: T $\geq$ T (crit)

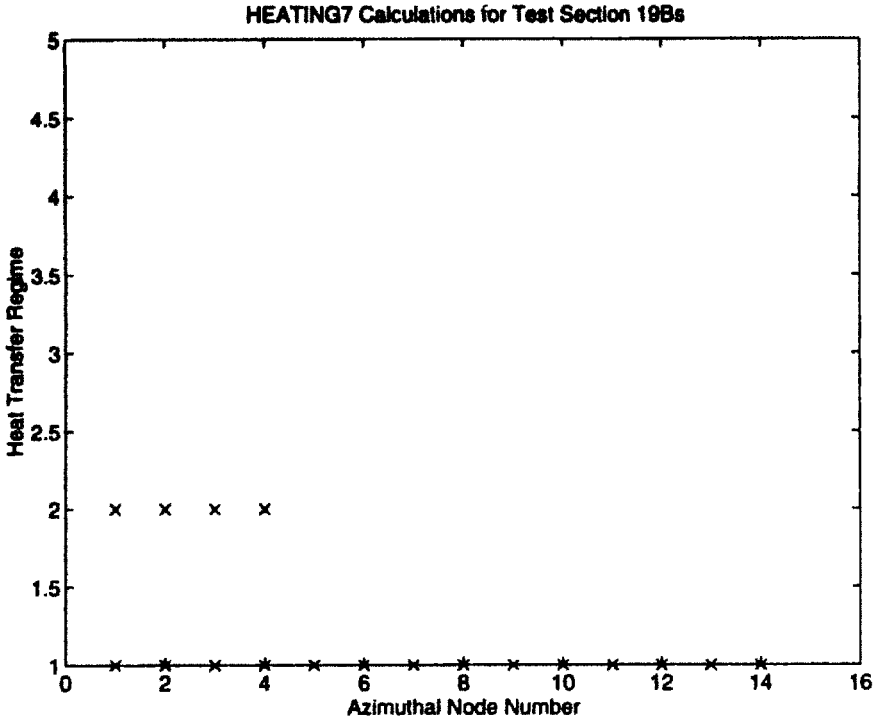

Figure F-25: Test Section 19B Azimuthal Thermal Region Profile
1: Single Phase Liquid; 2: Boiling; 3: T $\geq$ T (homogeneous nucl.); 4: T $\geq$ T (crit)

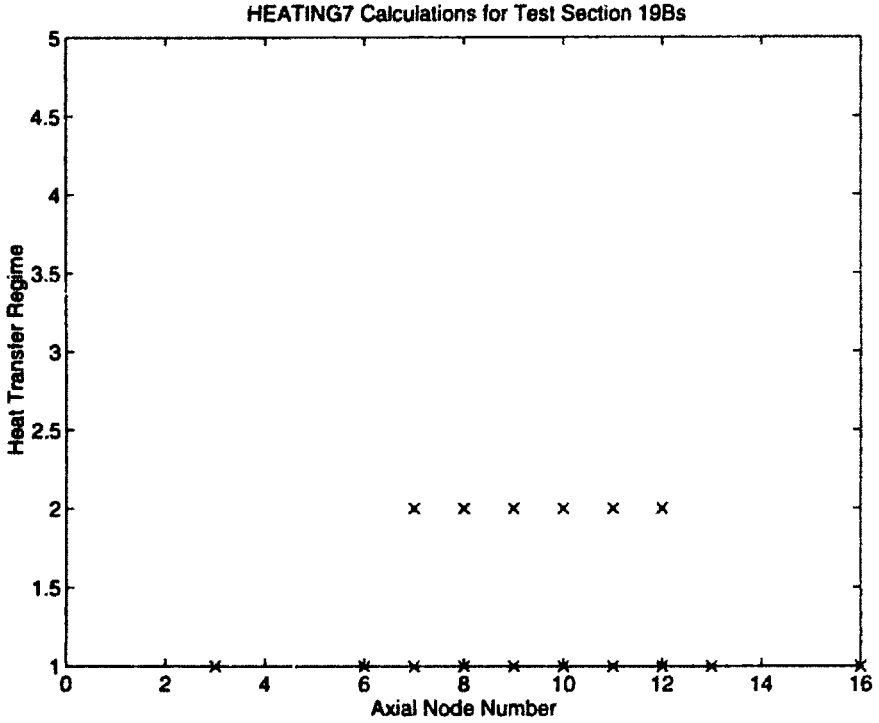

Figure F-26: Test Section 19B Axial Thermal Region Profile
1: Single Phase Liquid; 2: Boiling; 3: T $\geq$ T (homogeneous nucl.); 4: T $\geq$ T (crit)

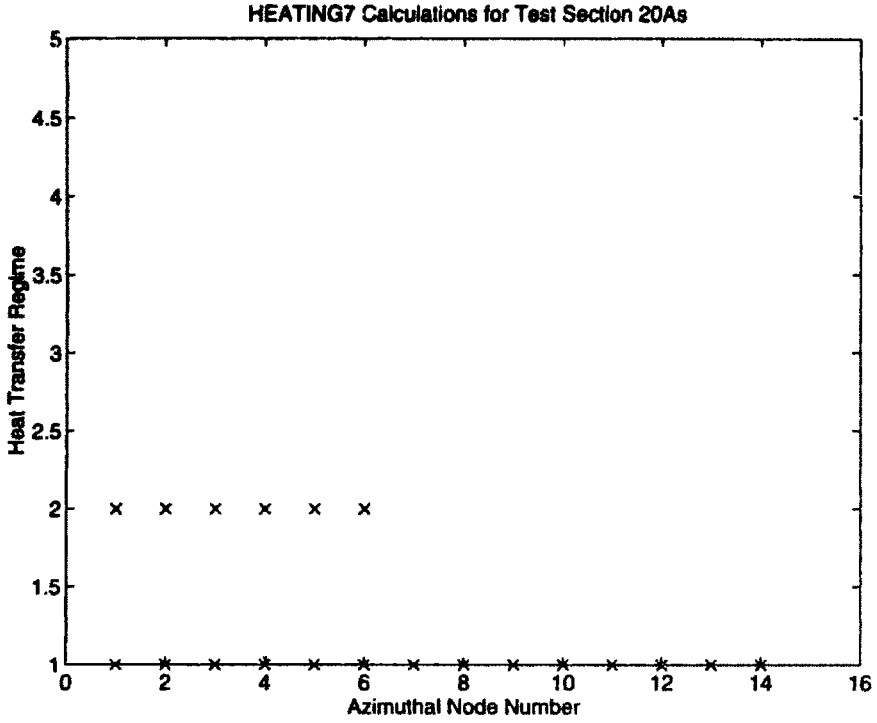

Figure F-27: Test Section 20A Azimuthal Thermal Region Profile
1: Single Phase Liquid; 2: Boiling; 3: T $\geq$ T (homogeneous nucl.); 4: T $\geq$ T (crit)

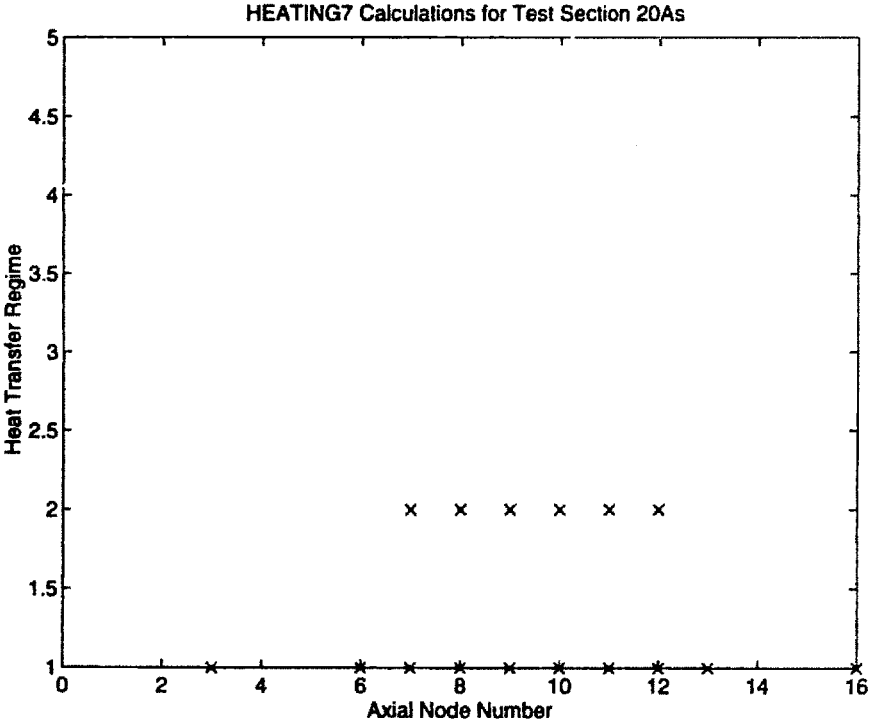

Figure F-28: Test Section 20A Axial Thermal Region Profile
1: Single Phase Liquid; 2: Boiling; 3: T $\geq$ T (homogeneous nucl.); 4: T $\geq$ T (crit)

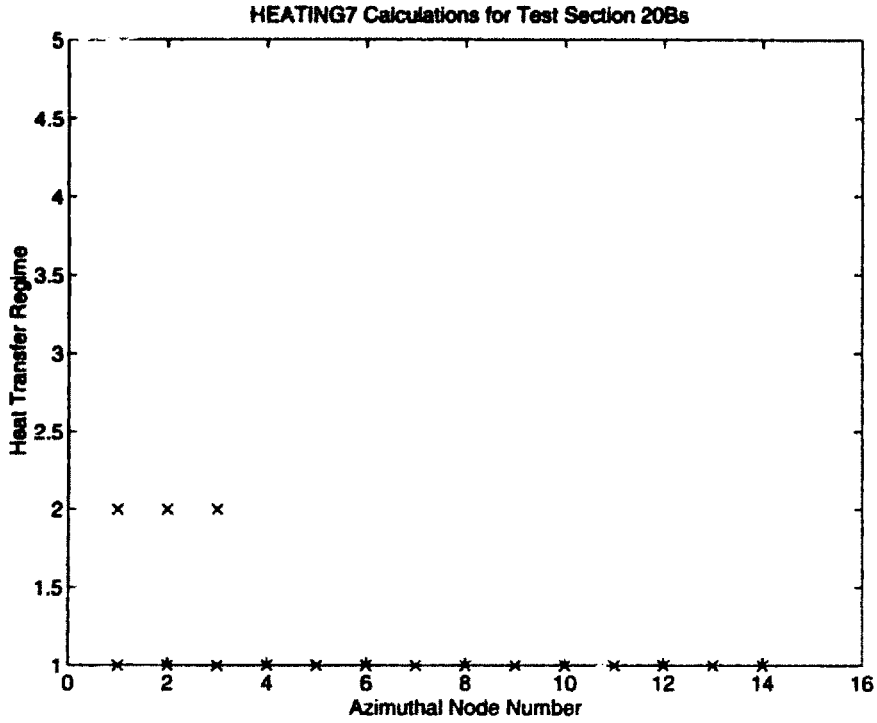

Figure F-29: Test Section 20B Azimuthal Thermal Region Profile
1: Single Phase Liquid; 2: Boiling; 3: T $\geq$ T (homogeneous nucl.); 4: T $\geq$ T (crit)

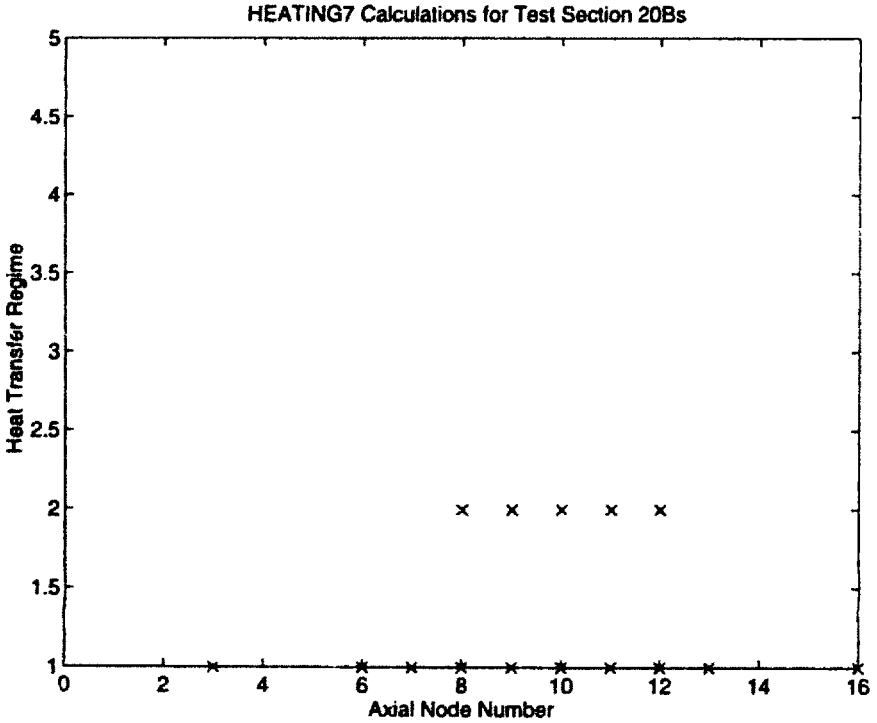

Figure F-30: Test Section 20B Axial Thermal Region Profile
1: Single Phase Liquid; 2: Boiling; 3: T $\geq$ T (homogeneous nucl.); 4: T $\geq$ T (crit)

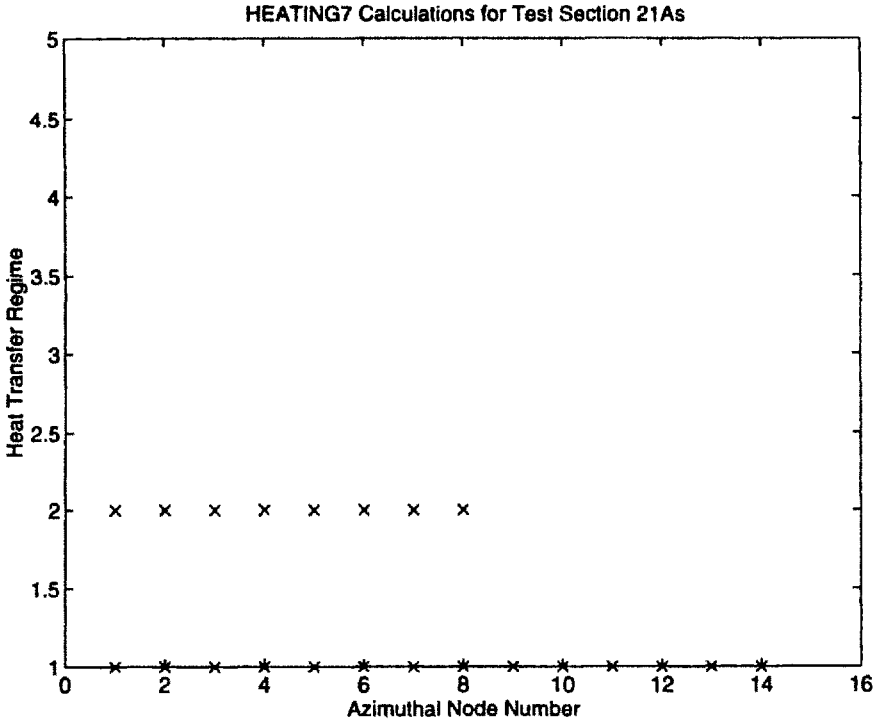

Figure F-31: Test Section 21A Azimuthal Thermal Region Profile
1: Single Phase Liquid; 2: Boiling; 3: T $\geq$ T (homogeneous nucl.); 4: T $\geq$ T (crit)

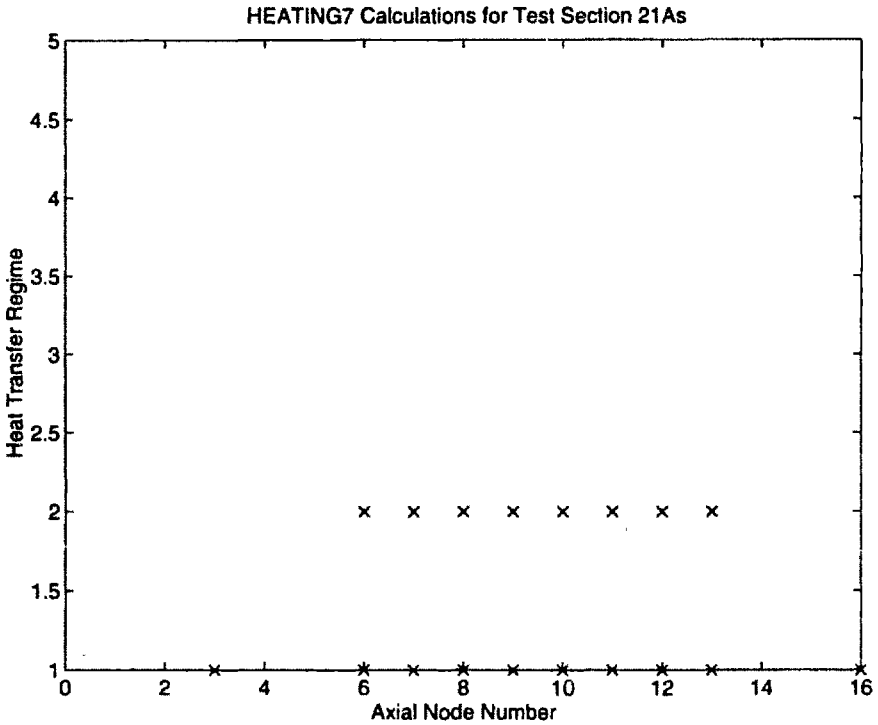

Figure F-32: Test Section 21A Axial Thermal Region Profile
1: Single Phase Liquid; 2: Boiling; 3: T $\geq$ T (homogeneous nucl.); 4: T $\geq$ T (crit)

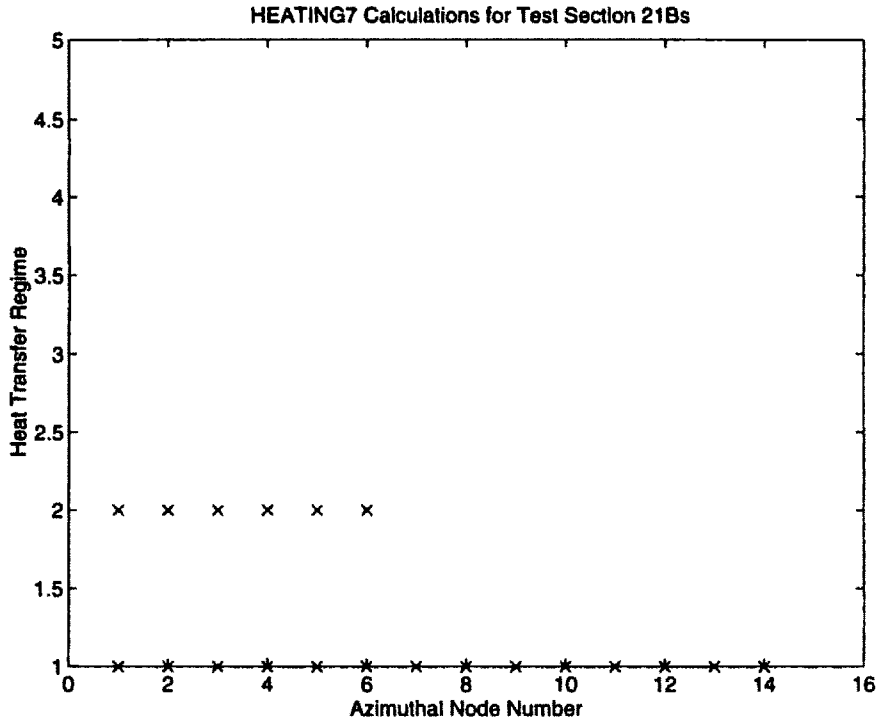

Figure F-33: Test Section 21B Azimuthal Thermal Region Profile
1: Single Phase Liquid; 2: Boiling; 3: T $\geq$ T (homogeneous nucl.); 4: T $\geq$ T (crit)

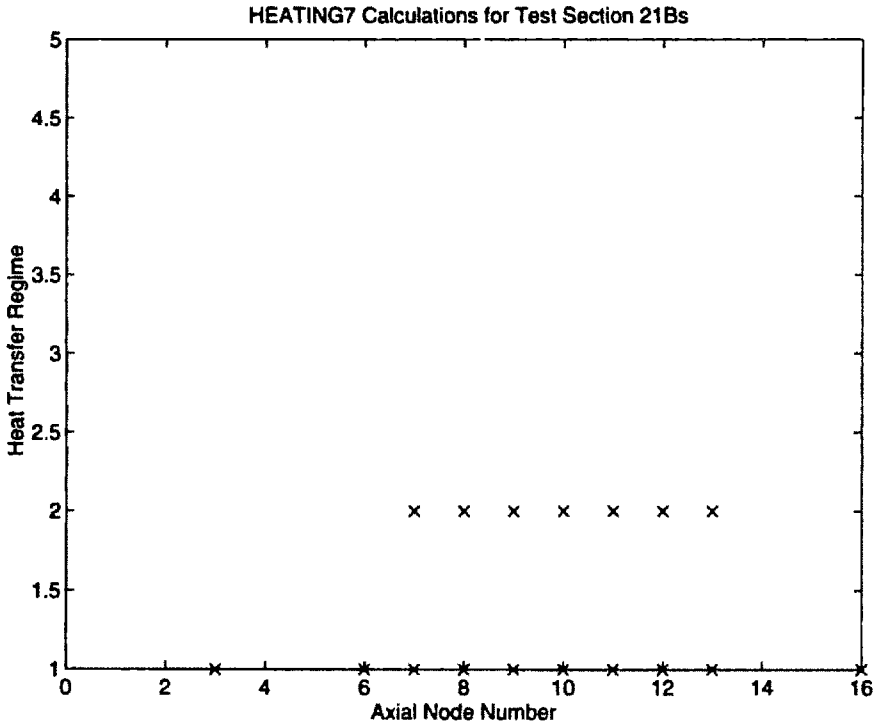

Figure F-34: Test Section 21B Axial Thermal Region Profile
1: Single Phase Liquid; 2: Boiling; 3: T $\geq$ T (homogeneous nucl.); 4: T $\geq$ T (crit)

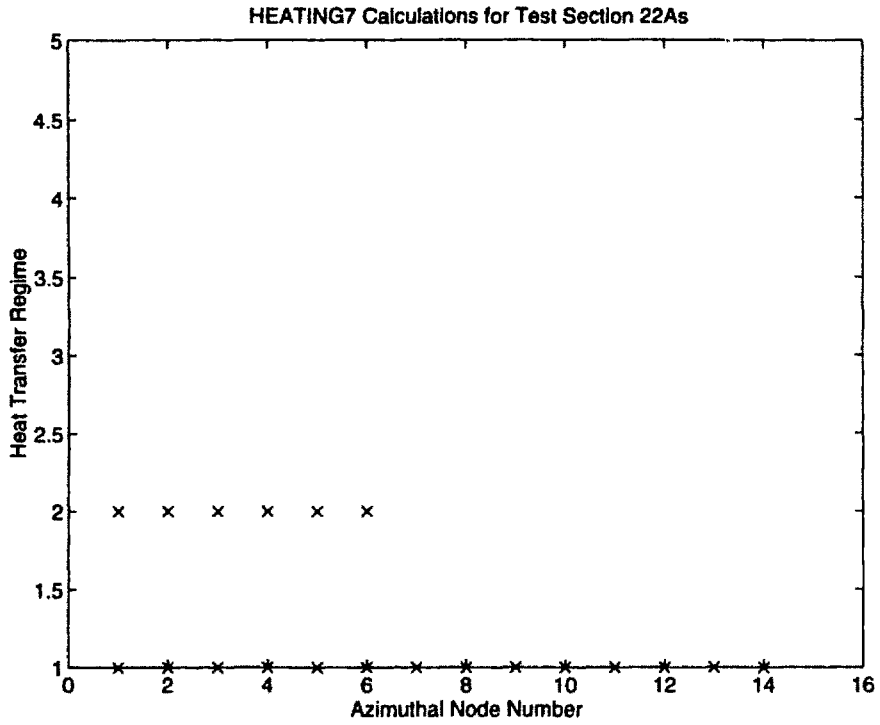

Figure F-35: Test Section 22A Azimuthal Thermal Region Profile
1: Single Phase Liquid; 2: Boiling; 3: T $\geq$ T (homogeneous nucl.); 4: T $\geq$ T (crit)

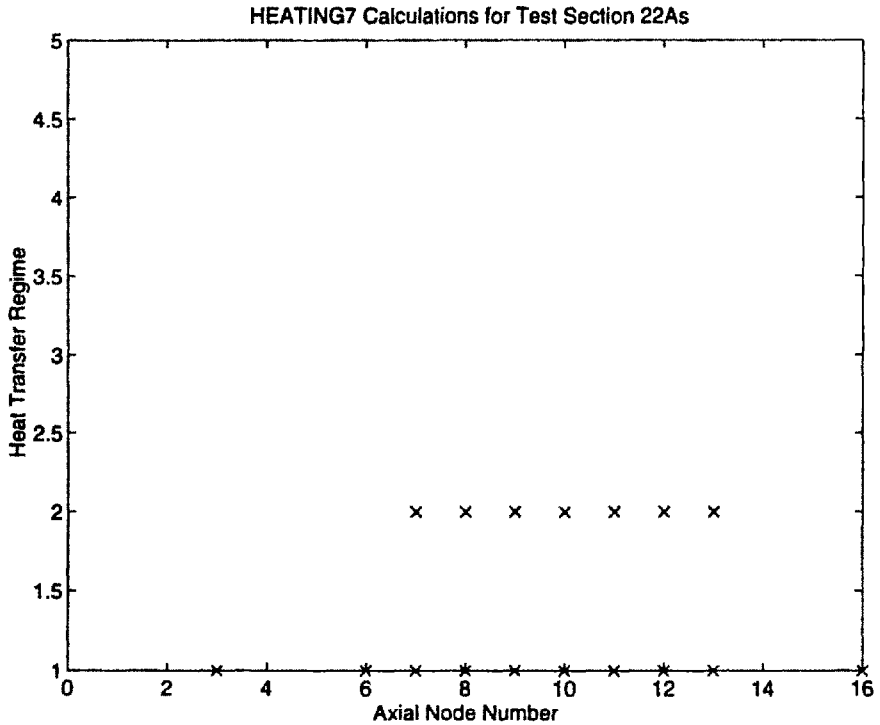

Figure F-36: Test Section 22A Axial Thermal Region Profile
1: Single Phase Liquid; 2: Boiling; 3: T $\geq$ T (homogeneous nucl.); 4: T $\geq$ T (crit)

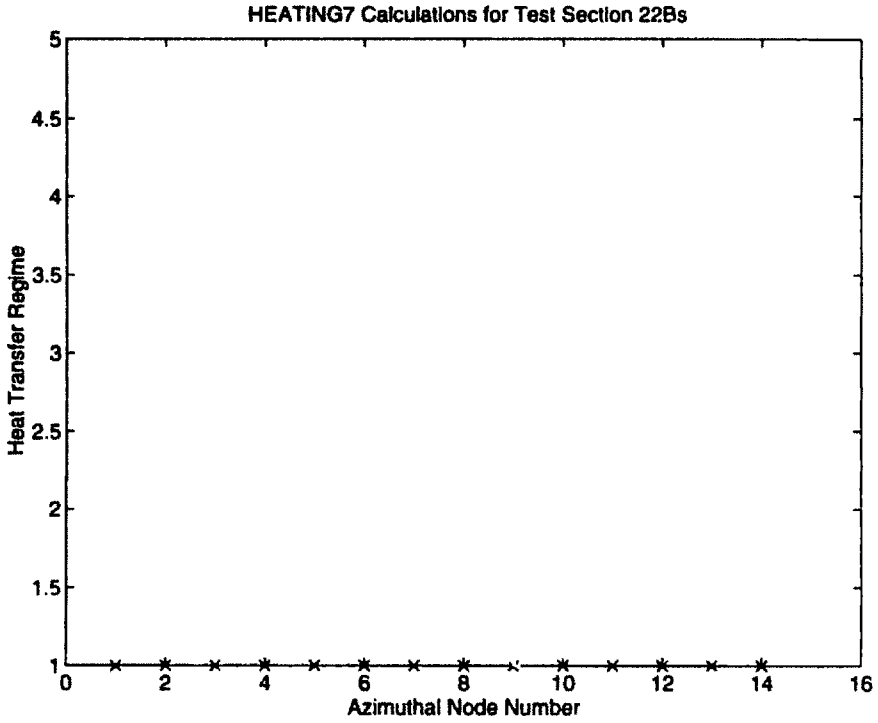

Figure F-37: Test Section 22B Azimuthal Thermal Region Profile
1: Single Phase Liquid; 2: Boiling; 3: T $\geq$ T (homogeneous nucl.); 4: T $\geq$ T (crit)

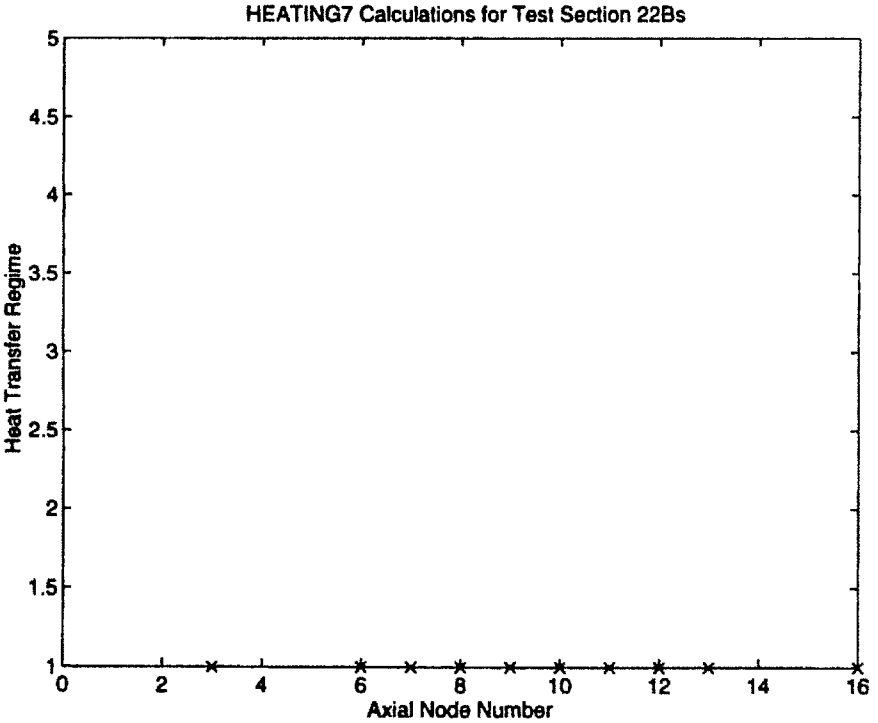

Figure F-38: Test Section 22B Axial Thermal Region Profile
1: Single Phase Liquid; 2: Boiling; 3: T $\geq$ T (homogeneous nucl.); 4: T $\geq$ T (crit)

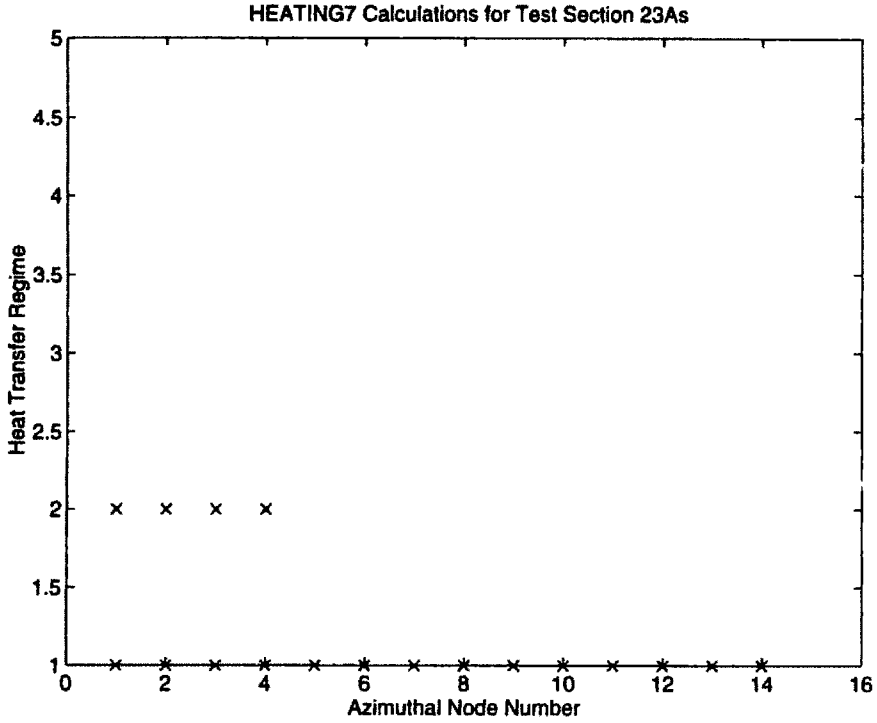

Figure F-39: Test Section 23A Azimuthal Thermal Region Profile
1: Single Phase Liquid; 2: Boiling; 3: T $\geq$ T (homogeneous nucl.); 4: T $\geq$ T (crit)

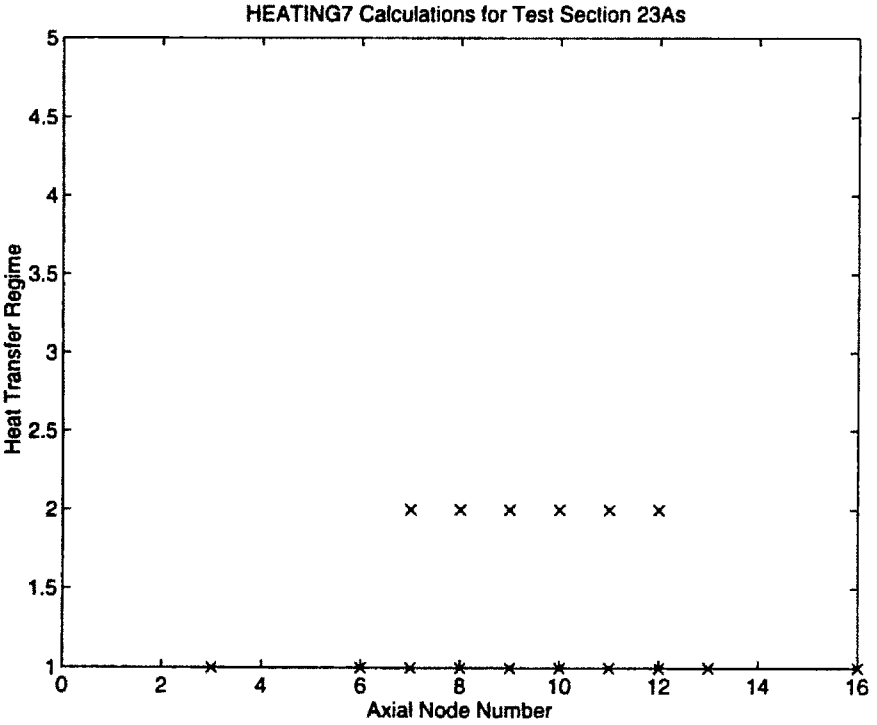

Figure F-40: Test Section 23A Axial Thermal Region Profile
1: Single Phase Liquid; 2: Boiling; 3: T $\geq$ T (homogeneous nucl.); 4: T $\geq$ T (crit)

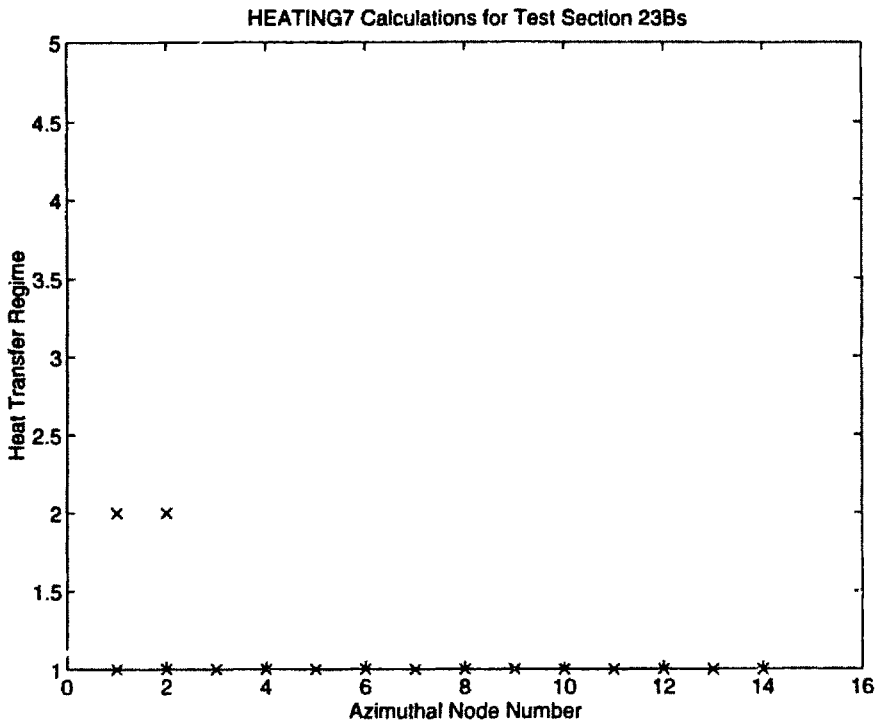

Figure F-41: Test Section 23B Azimuthal Thermal Region Profile
1: Single Phase Liquid; 2: Boiling; 3: T $\geq$ T (homogeneous nucl.); 4: T $\geq$ T (crit)

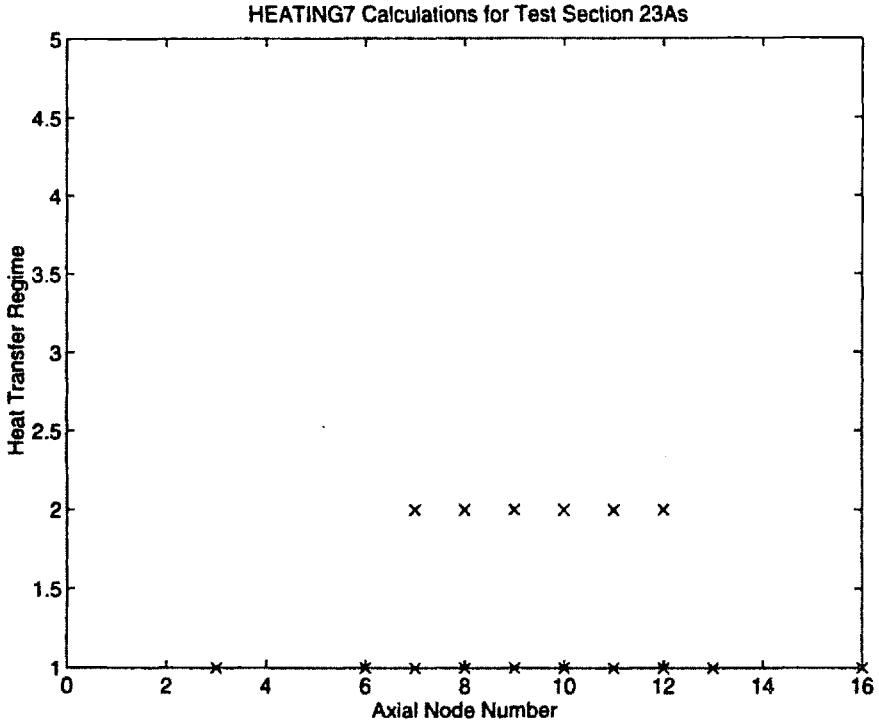

Figure F-42: Test Section 23B Axial Thermal Region Profile
1: Single Phase Liquid; 2: Boiling; 3: T $\geq$ T (homogeneous nucl.); 4: T $\geq$ T (crit)

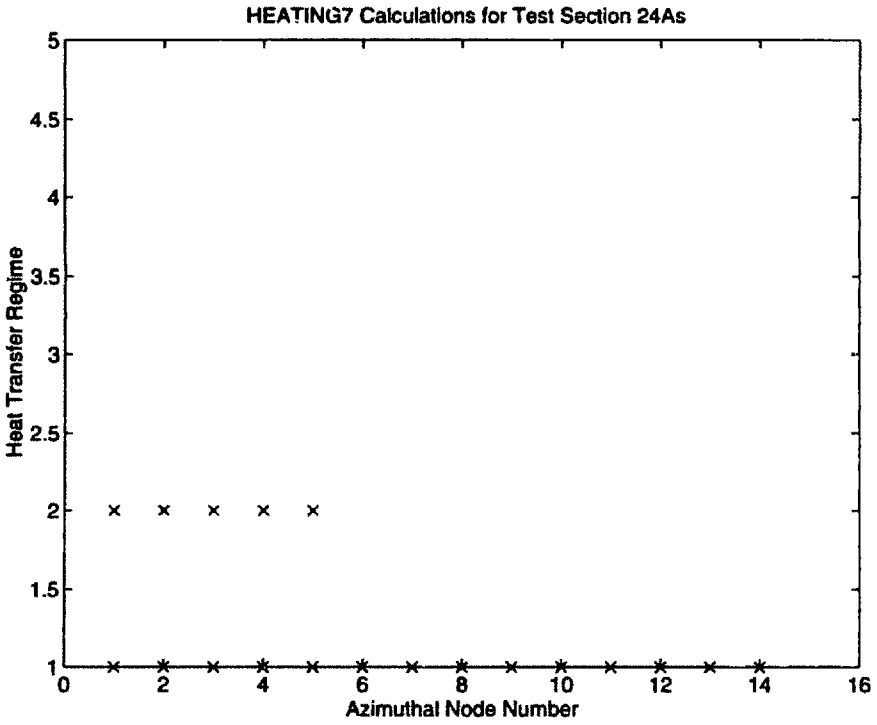

Figure F-43: Test Section 24A Azimuthal Thermal Region Profile
1: Single Phase Liquid; 2: Boiling; 3: T $\geq$ T (homogeneous nucl.); 4: T $\geq$ T (crit)

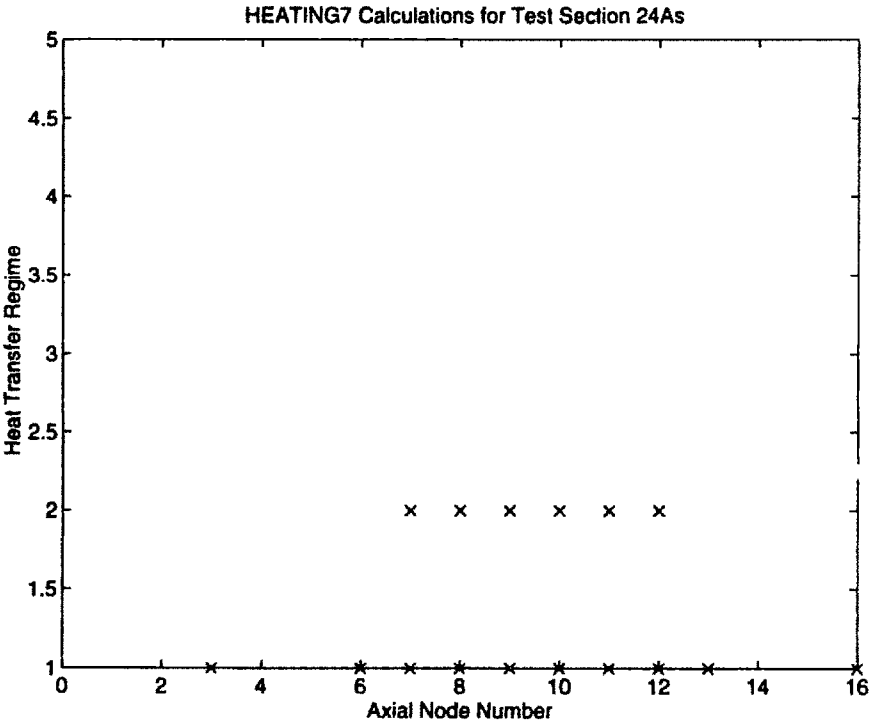

Figure F-44: Test Section 24A Axial Thermal Region Profile
1: Single Phase Liquid; 2: Boiling; 3: T $\geq$ T (homogeneous nucl.); 4: T $\geq$ T (crit)

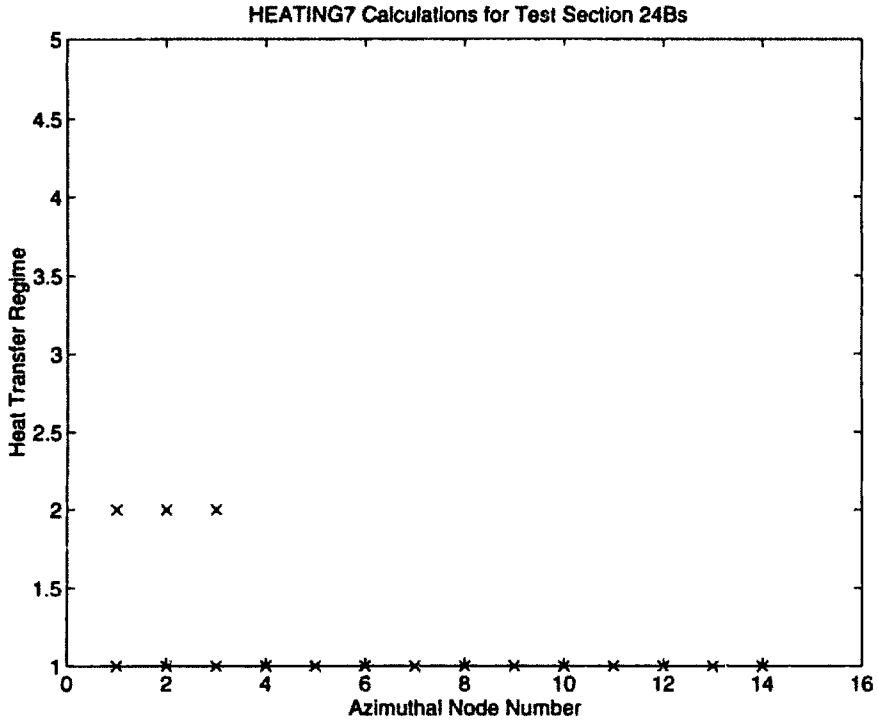

Figure F-45: Test Section 24B Azimuthal Thermal Region Profile
1: Single Phase Liquid; 2: Boiling; 3: T $\geq$ T (homogeneous nucl.); 4: T $\geq$ T (crit)

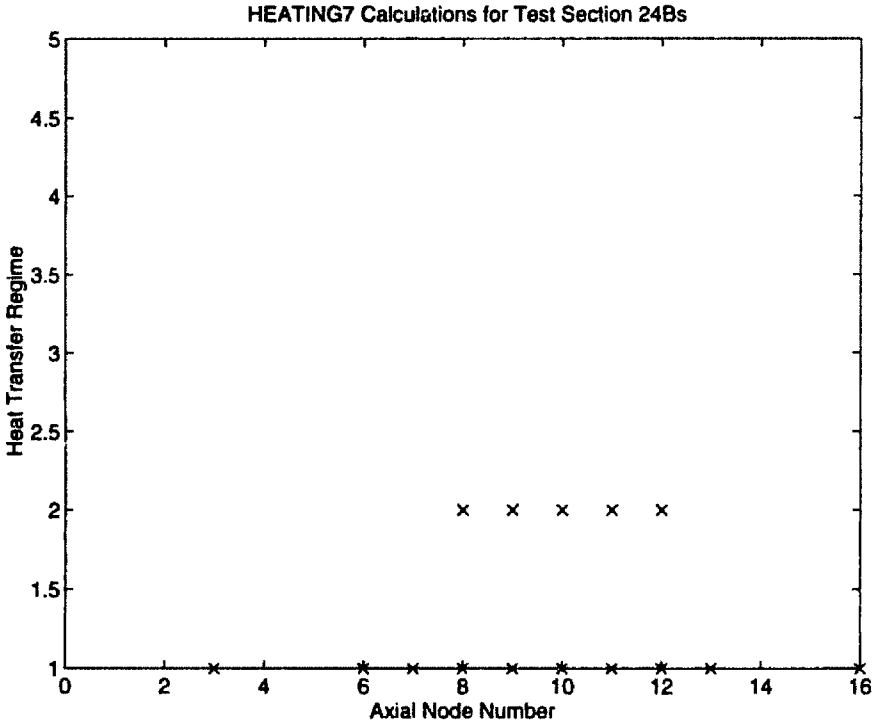

Figure F-46: Test Section 24B Axial Thermal Region Profile
1: Single Phase Liquid; 2: Boiling; 3: T $\geq$ T (homogeneous nucl.); 4: T $\geq$ T (crit)

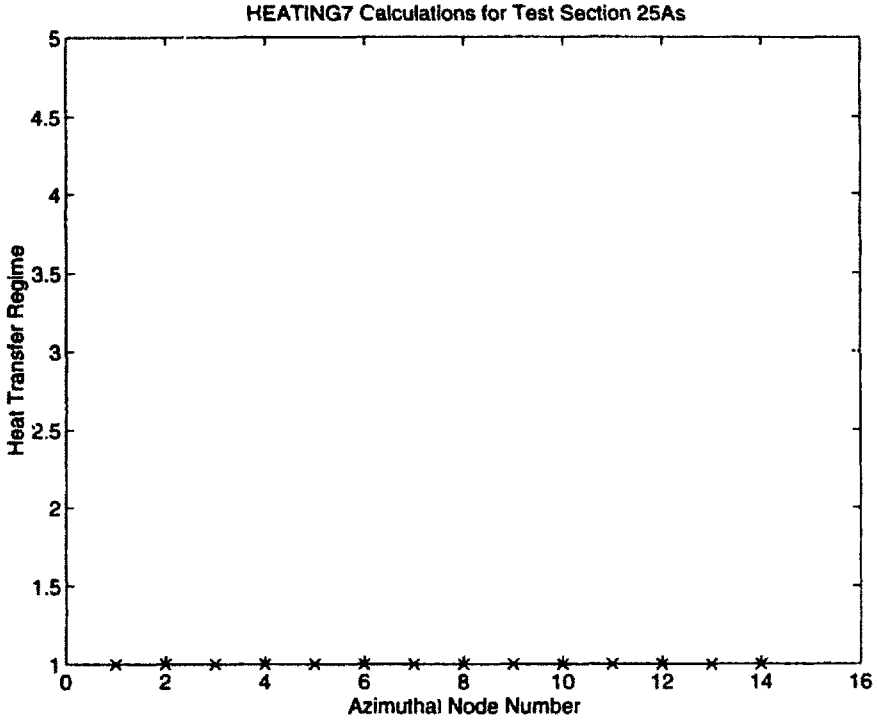

Figure F-47: Test Section 25A Azimuthal Thermal Region Profile
1: Single Phase Liquid; 2: Boiling; 3: T $\geq$ T (homogeneous nucl.); 4: T $\geq$ T (crit)

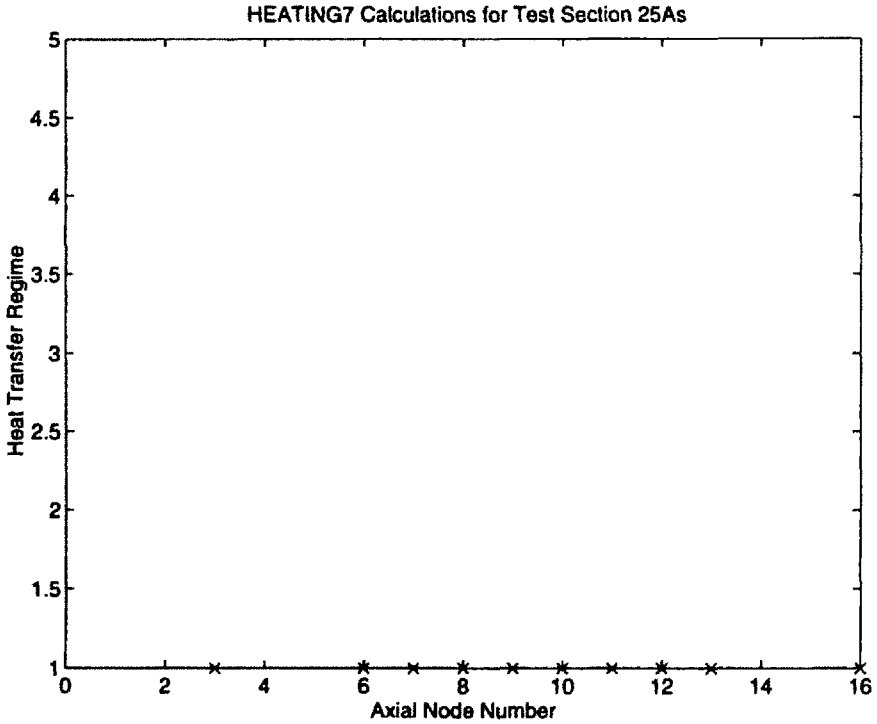

Figure F-48: Test Section 25A Axial Thermal Region Profile
1: Single Phase Liquid; 2: Boiling; 3: T $\geq$ T (homogeneous nucl.); 4: T $\geq$ T (crit)

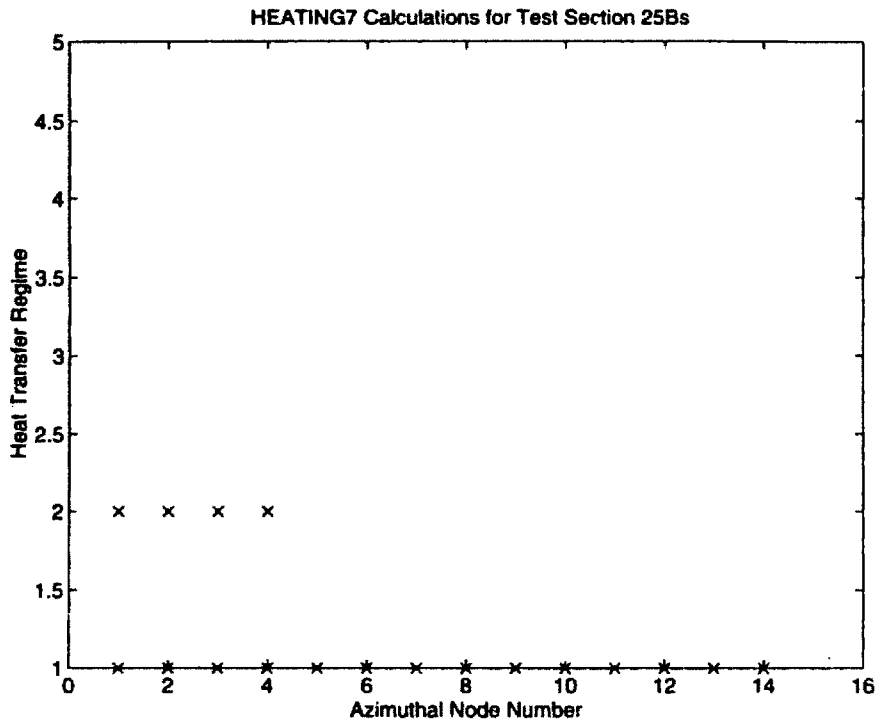

Figure F-49: Test Section 25B Azimuthal Thermal Region Profile
1: Single Phase Liquid; 2: Boiling; 3: T $\geq$ T (homogeneous nucl.); 4: T $\geq$ T (crit)

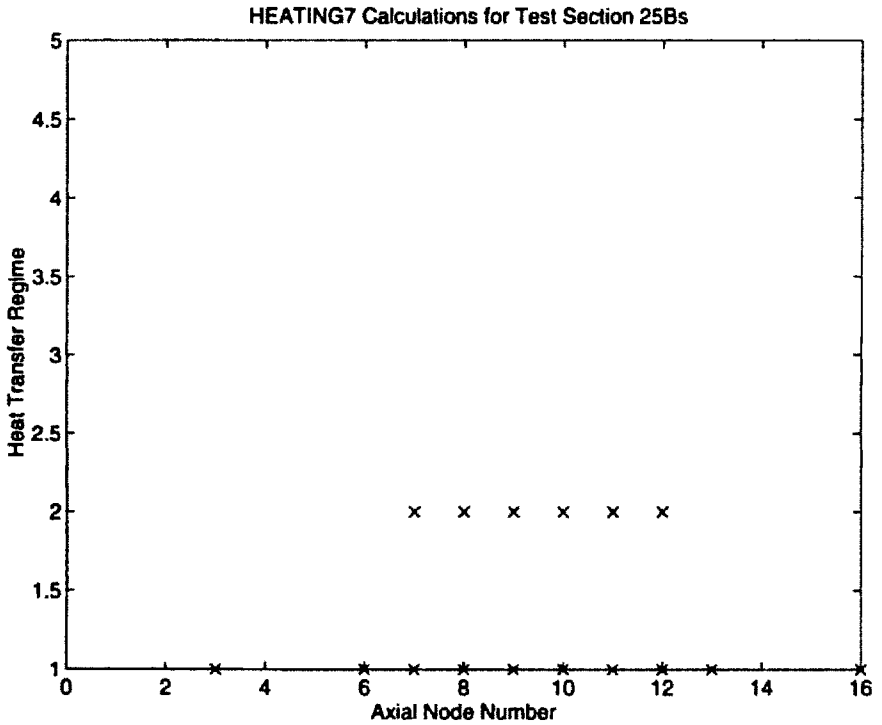

Figure F-50: Test Section 25B Axial Thermal Region Profile
1: Single Phase Liquid; 2: Boiling; 3: T $\geq$ T (homogeneous nucl.); 4: T $\geq$ T (crit)

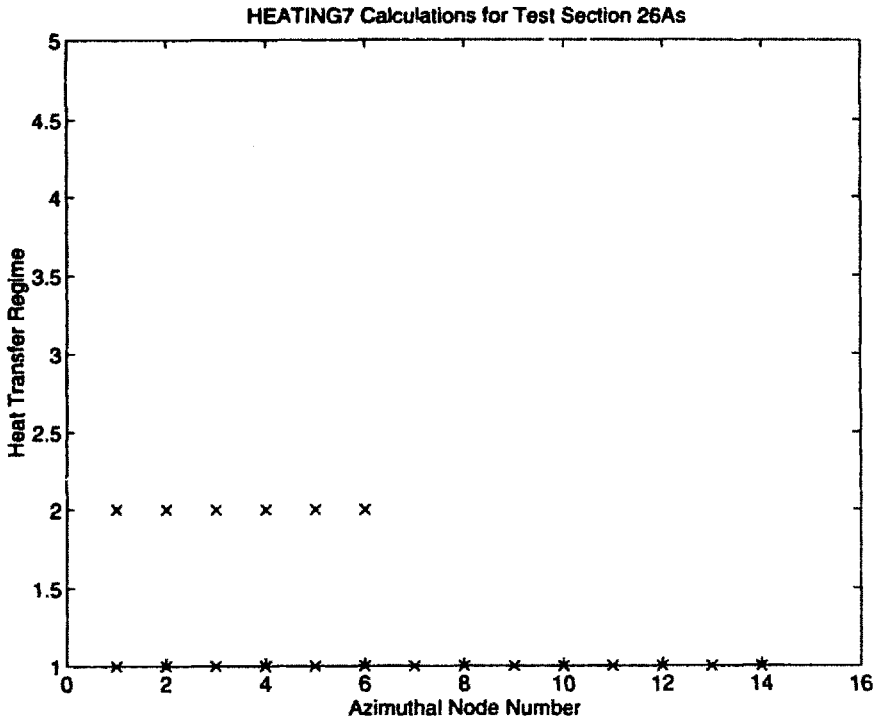

Figure F-51: Test Section 26A Azimuthal Thermal Region Profile
1: Single Phase Liquid; 2: Boiling; 3: T $\geq$ T (homogeneous nucl.); 4: T $\geq$ T (crit)

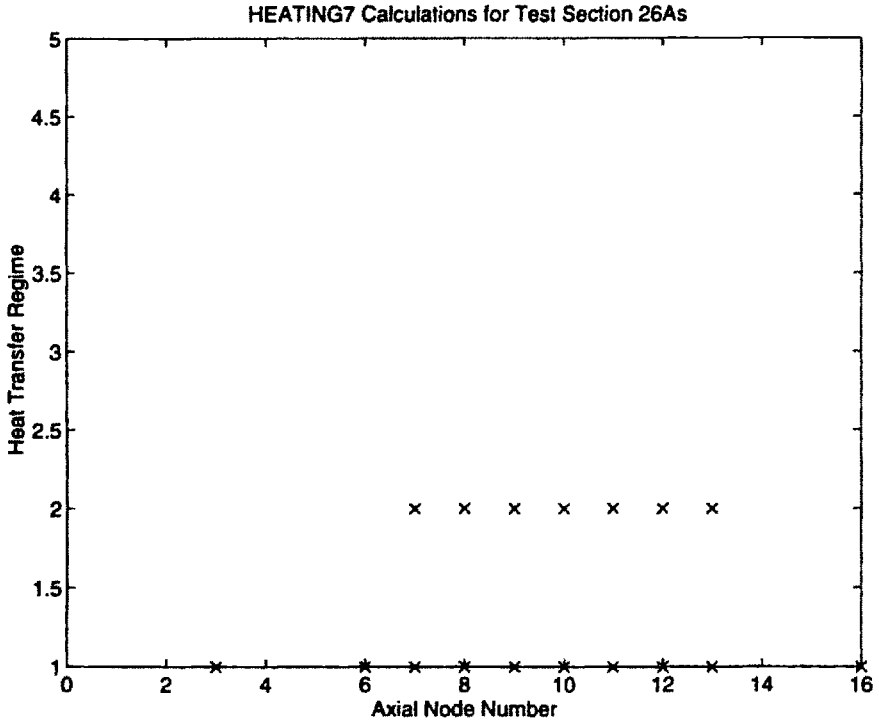

Figure F-52: Test Section 26A Axial Thermal Region Profile
1: Single Phase Liquid; 2: Boiling; 3: T $\geq$ T (homogeneous nucl.); 4: T $\geq$ T (crit)

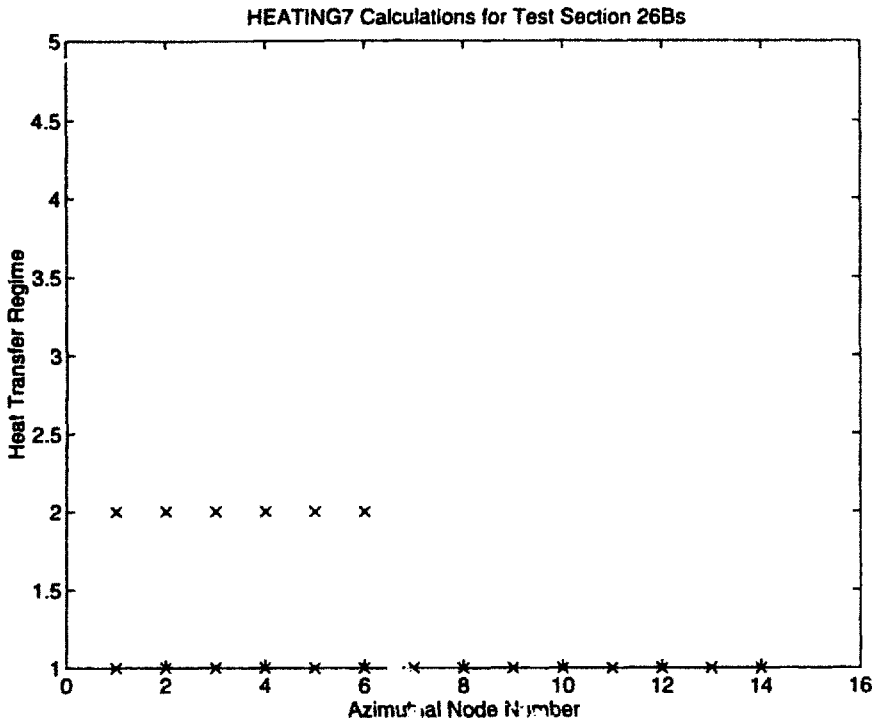

Figure F-53: Test Section 26B Azimuthal Thermal Region Profile
1: Single Phase Liquid; 2: Boiling; 3: T $\geq$ T (homogeneous nucl.); 4: T $\geq$ T (crit)

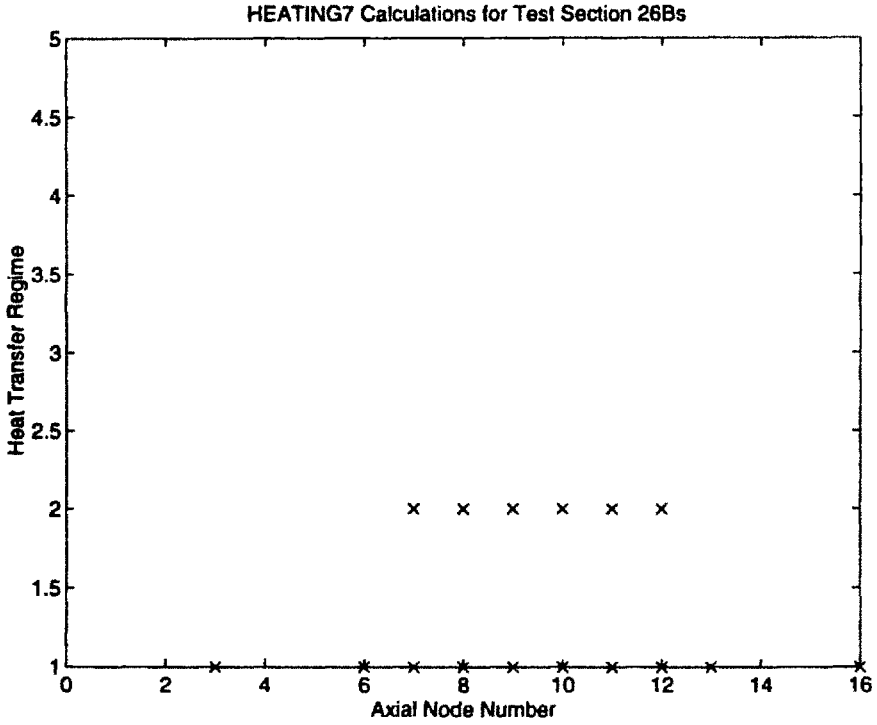

Figure F-54: Test Section 26B Axial Thermal Region Profile
1: Single Phase Liquid; 2: Boiling; 3: T $\geq$ T (homogeneous nucl.); 4: T $\geq$ T (crit)

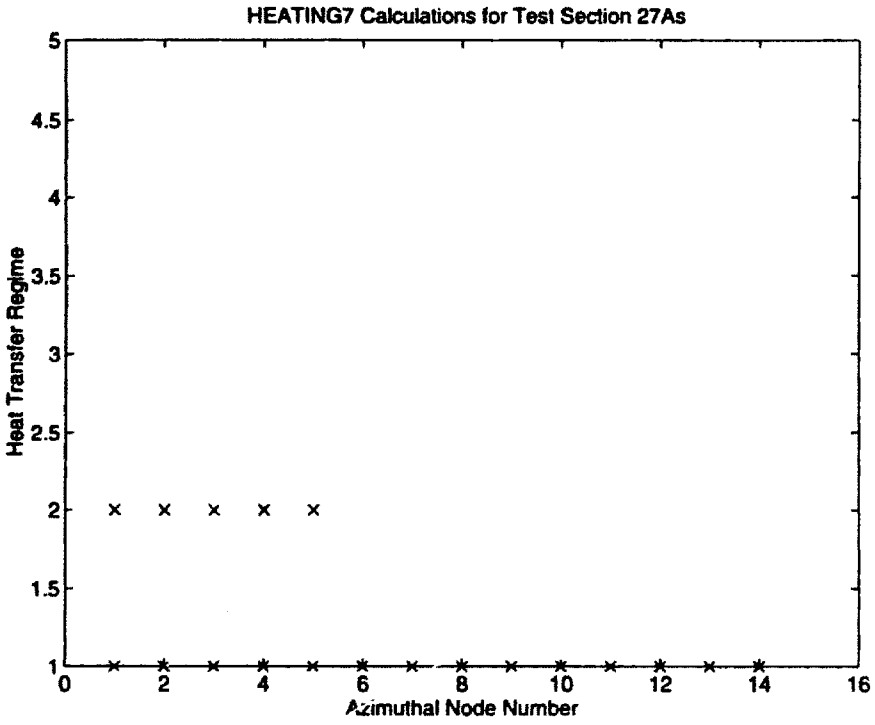

Figure F-55: Test Section 27A Azimuthal Thermal Region Profile
1: Single Phase Liquid; 2: Boiling; 3: T $\geq$ T (homogeneous nucl.); 4: T $\geq$ T (crit)

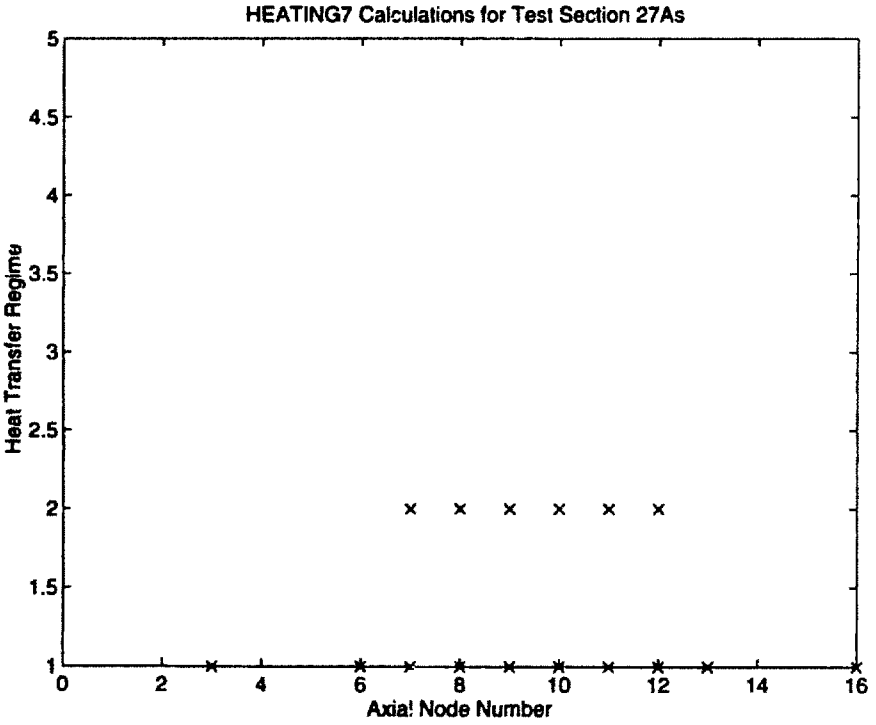

Figure F-56: Test Section 27A Axial Thermal Region Profile
1: Single Phase Liquid; 2: Boiling; 3: T $\geq$ T (homogeneous nucl.); 4: T $\geq$ T (crit)

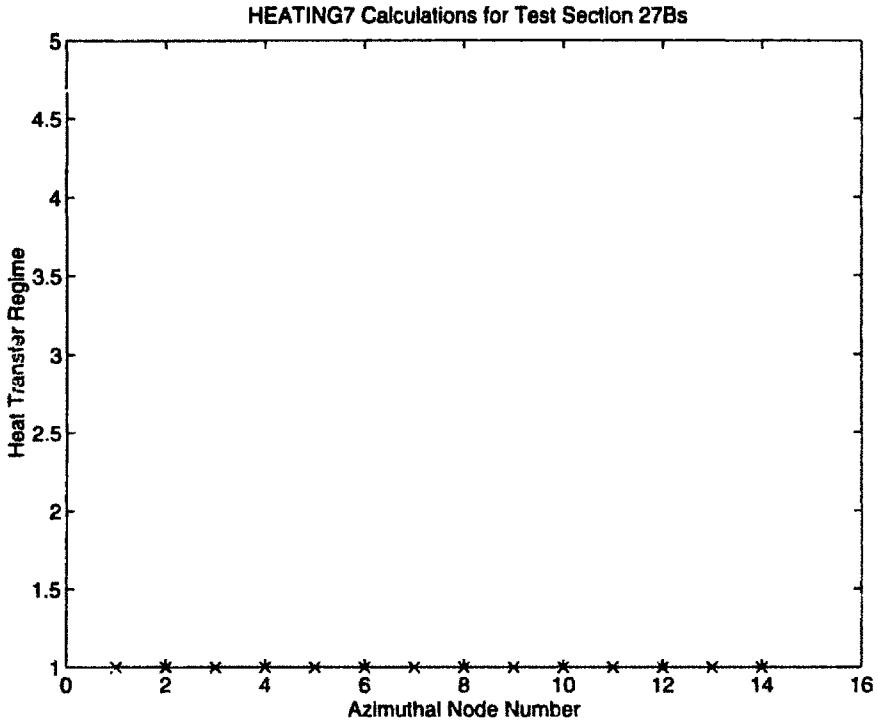

Figure F-57: Test Section 27B Azimuthal Thermal Region Profile
1: Single Phase Liquid; 2: Boiling; 3: T $\geq$ T (homogeneous nucl.); 4: T $\geq$ T (crit)

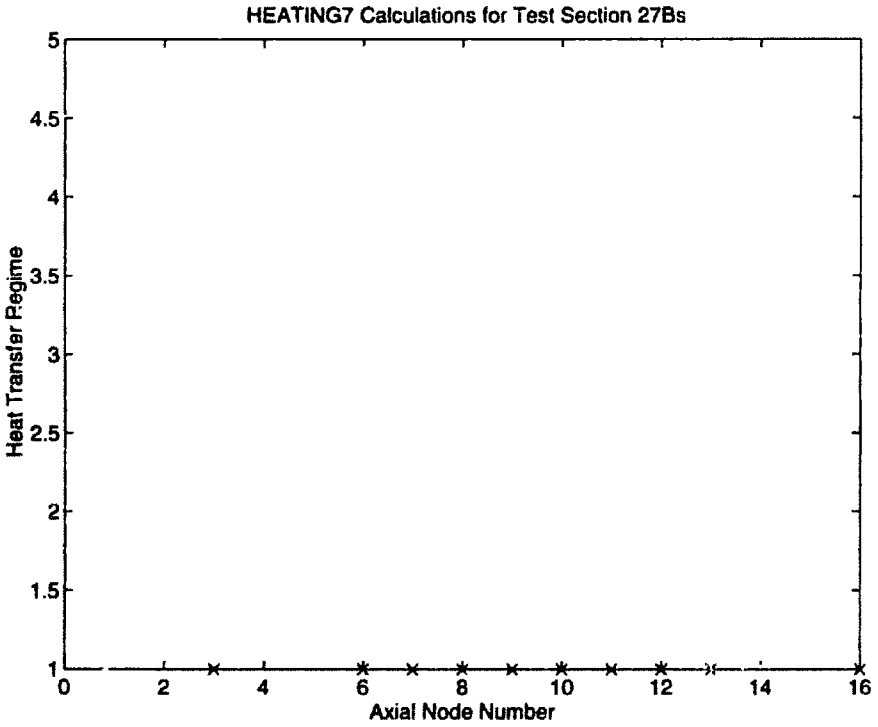

Figure F-58: Test Section 27B Axial Thermal Region Profile
1: Single Phase Liquid; 2: Boiling; 3: T $\geq$ T (homogeneous nucl.); 4: T $\geq$ T (crit)

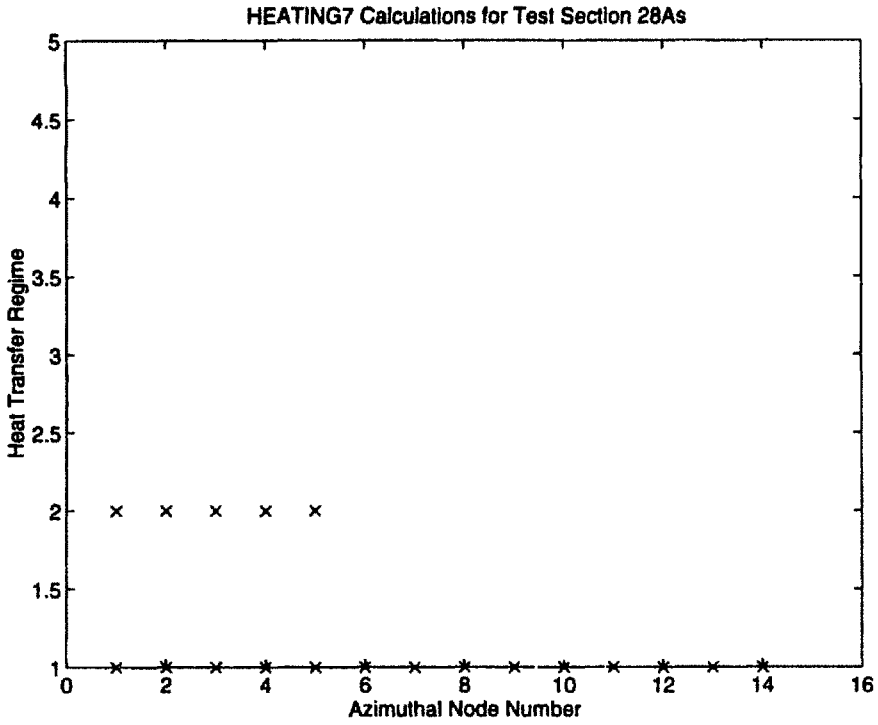

Figure F-59: Test Section 28A Azimuthal Thermal Region Profile
1: Single Phase Liquid; 2: Boiling; 3: T $\geq$ T (homogeneous nucl.); 4: T $\geq$ T (crit)

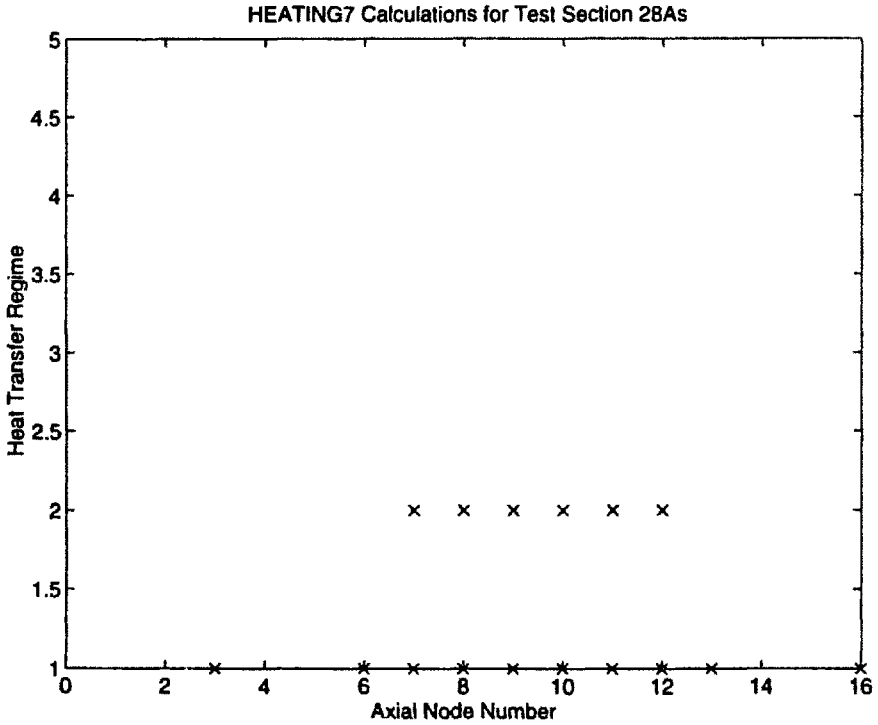

Figure F-60: Test Section 28A Axial Thermal Region Profile
1: Single Phase Liquid; 2: Boiling; 3: T $\geq$ T (homogeneous nucl.); 4: T $\geq$ T (crit)

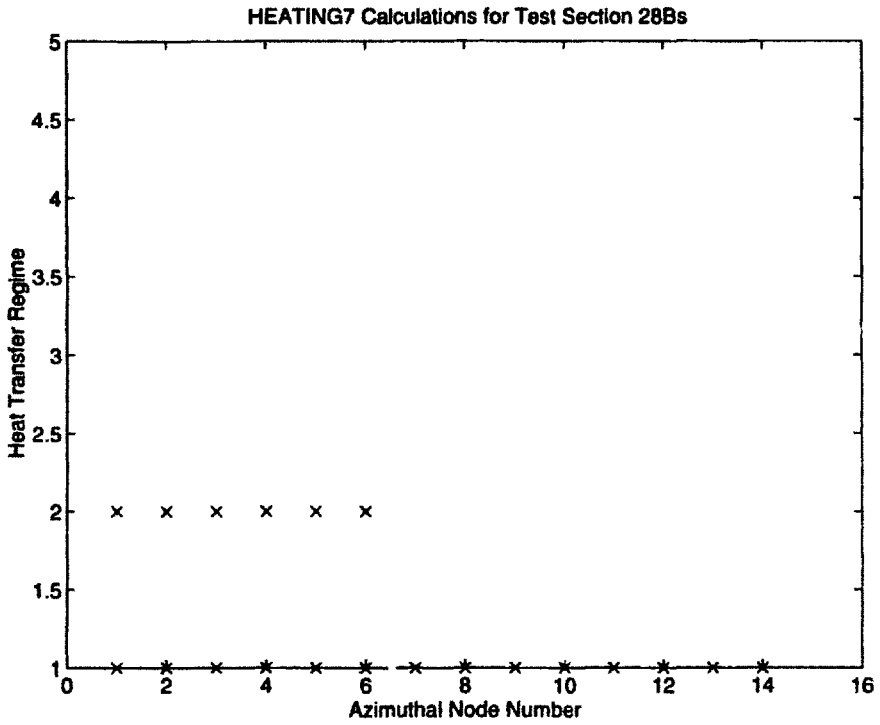

Figure F-61: Test Section 28B Azimuthal Thermal Region Profile
1: Single Phase Liquid; 2: Boiling; 3: T $\geq$ T (homogeneous nucl.); 4: T $\geq$ T (crit)

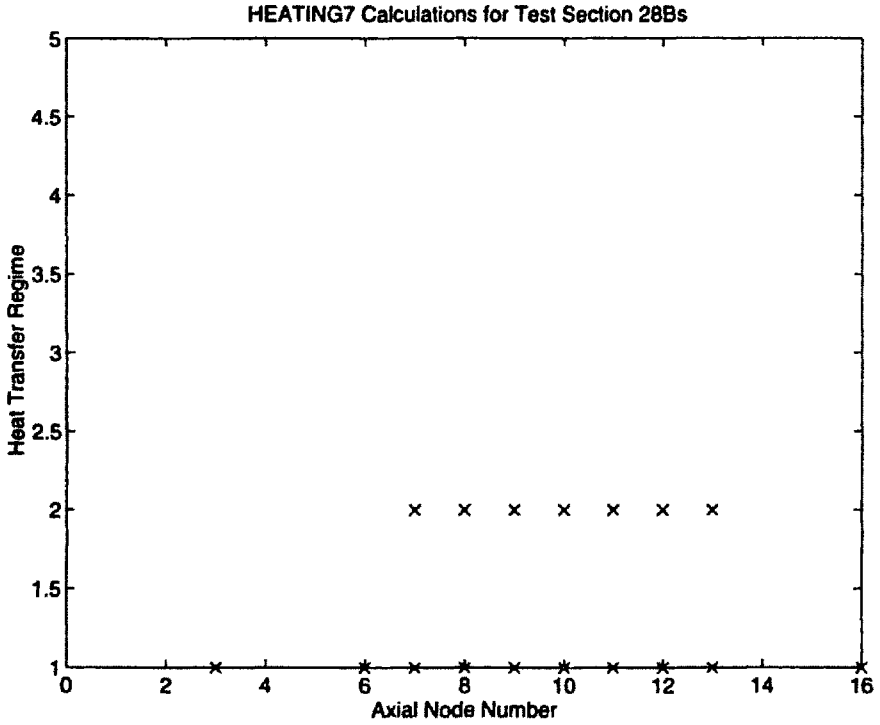

Figure F-62: Test Section 28B Axial Thermal Region Profile
1: Single Phase Liquid; 2: Boiling; 3: T $\geq$ T (homogeneous nucl.); 4: T $\geq$ T (crit)

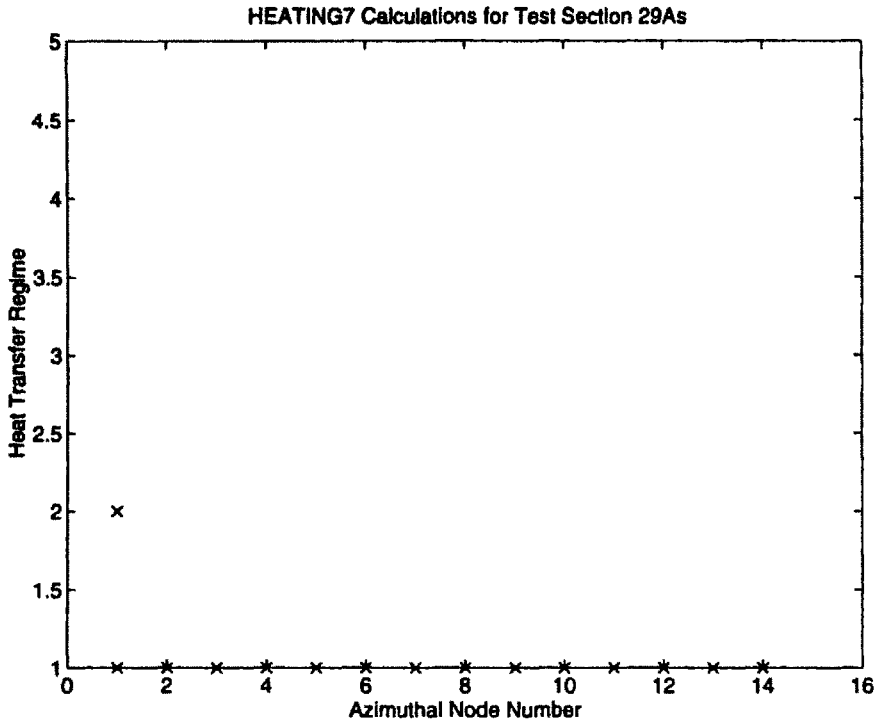

Figure F-63: Test Section 29A Azimuthal Thermal Region Profile
1: Single Phase Liquid; 2: Boiling; 3: T $\geq$ T (homogeneous nucl.); 4: T $\geq$ T (crit)

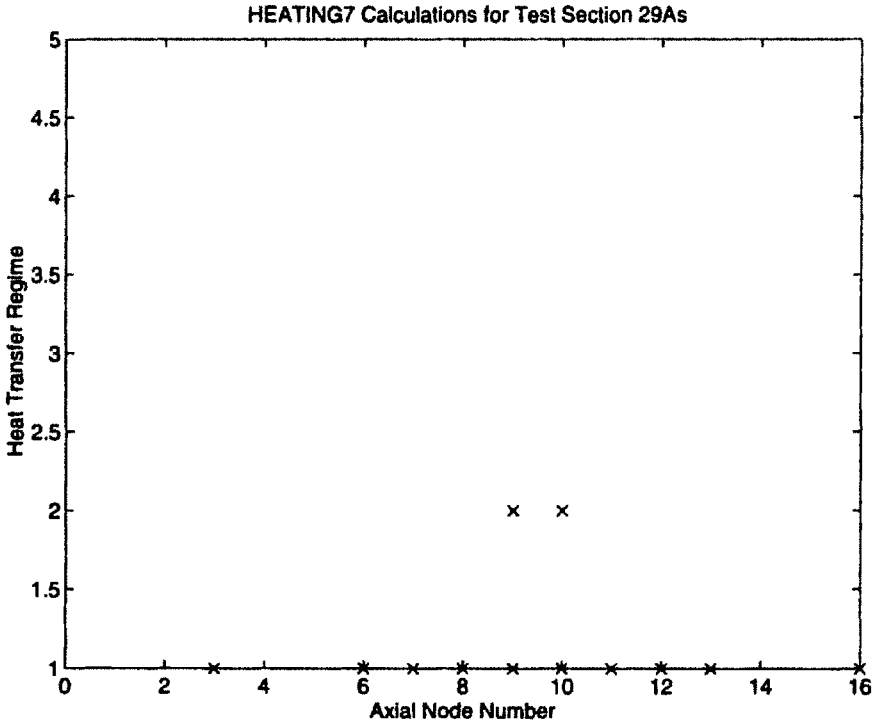

Figure F-64: Test Section 29A Axial Thermal Region Profile
1: Single Phase Liquid; 2: Boiling; 3: T $\geq$ T (homogeneous nucl.); 4: T $\geq$ T (crit)

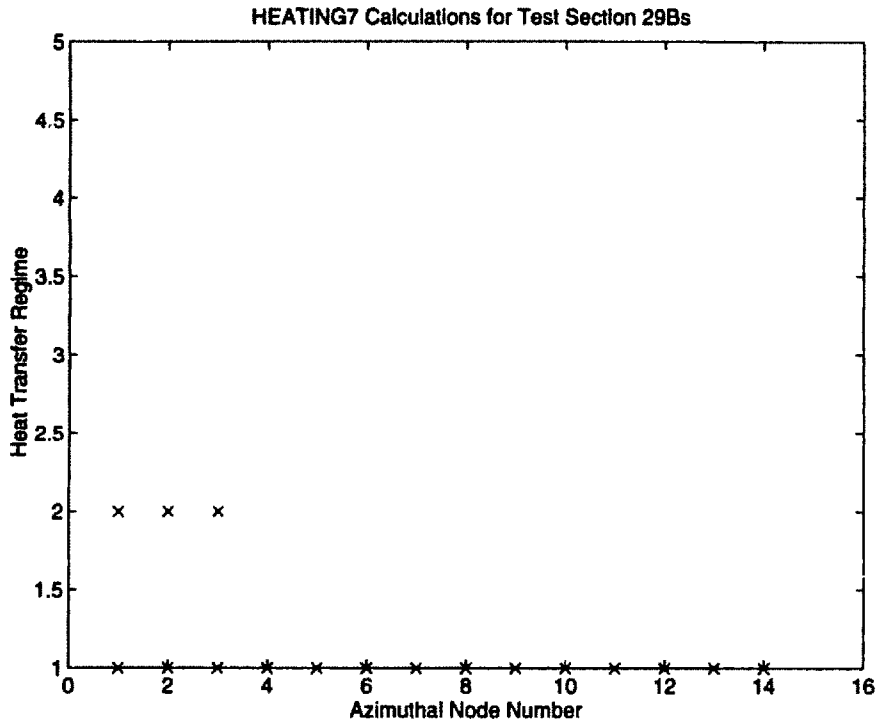

Figure F-65: Test Section 29B Azimuthal Thermal Region Profile
1: Single Phase Liquid; 2: Boiling; 3: T $\geq$ T (homogeneous nucl.); 4: T $\geq$ T (crit)

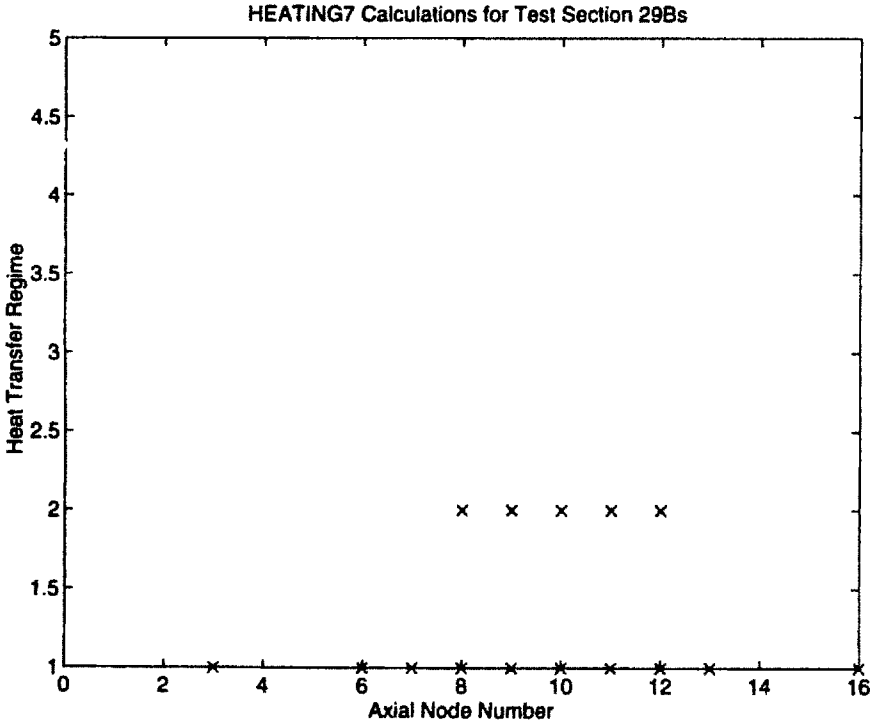

Figure F-66: Test Section 29B Axial Thermal Region Profile
1: Single Phase Liquid; 2: Boiling; 3: T $\geq$ T (homogeneous nucl.); 4: T $\geq$ T (crit)

Appendix G

Data Reduction Results:

Concentration Factor Profiles

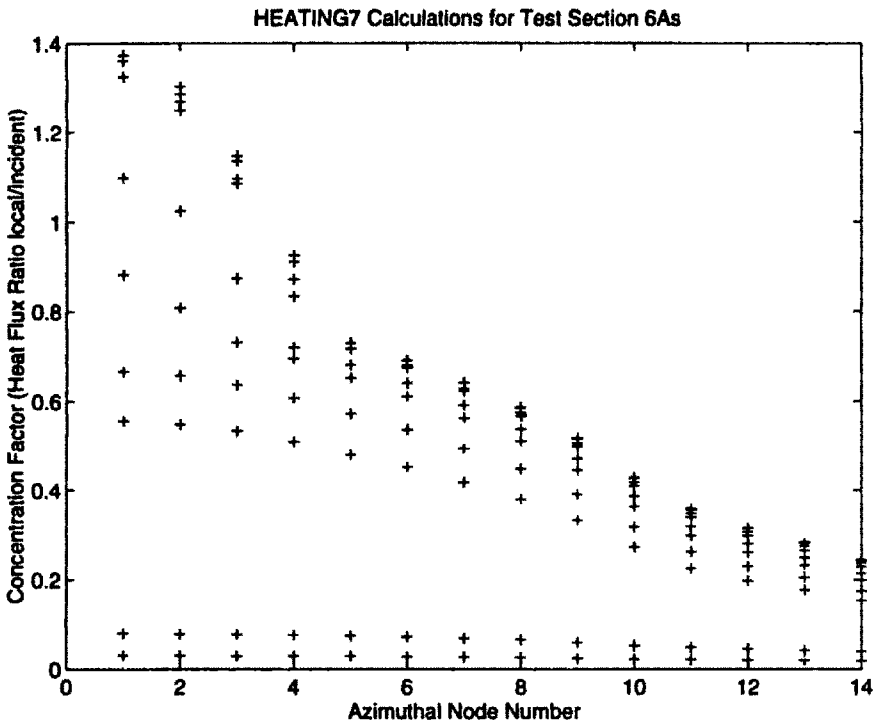

Figure G-1: Test Section 6A Azimuthal Concentration Factor Profile

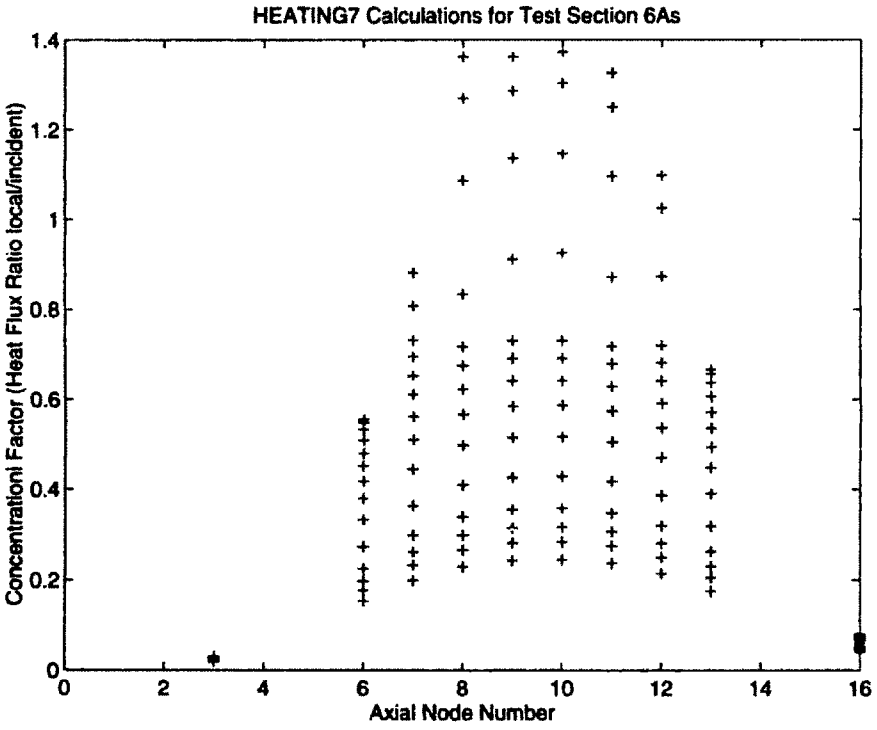

Figure G-2: Test Section 6A Axial Concentration Factor Profile

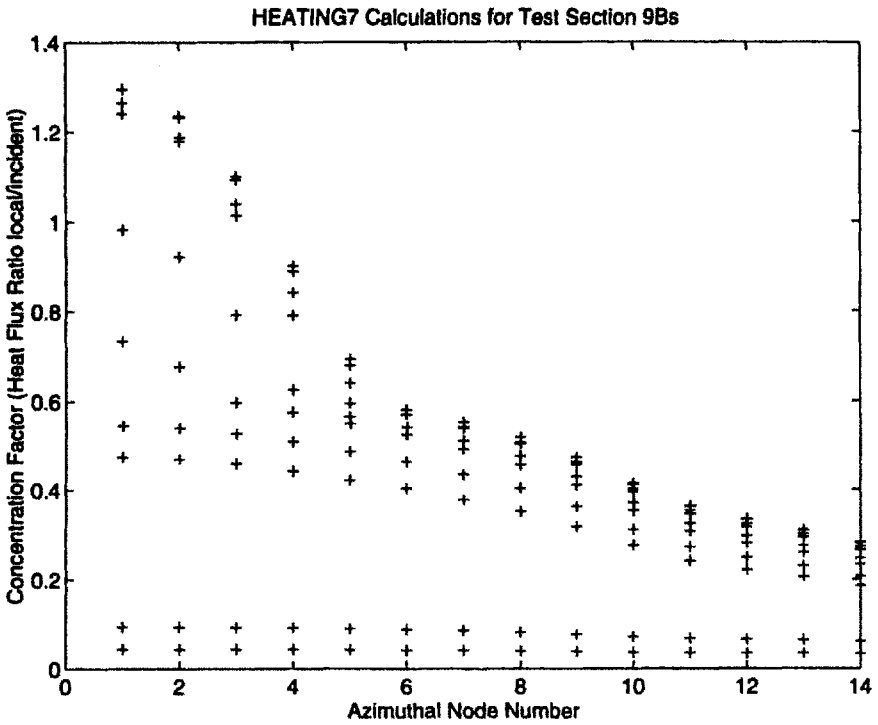

Figure G-3: Test Section 9B Azimuthal Concentration Factor Profile

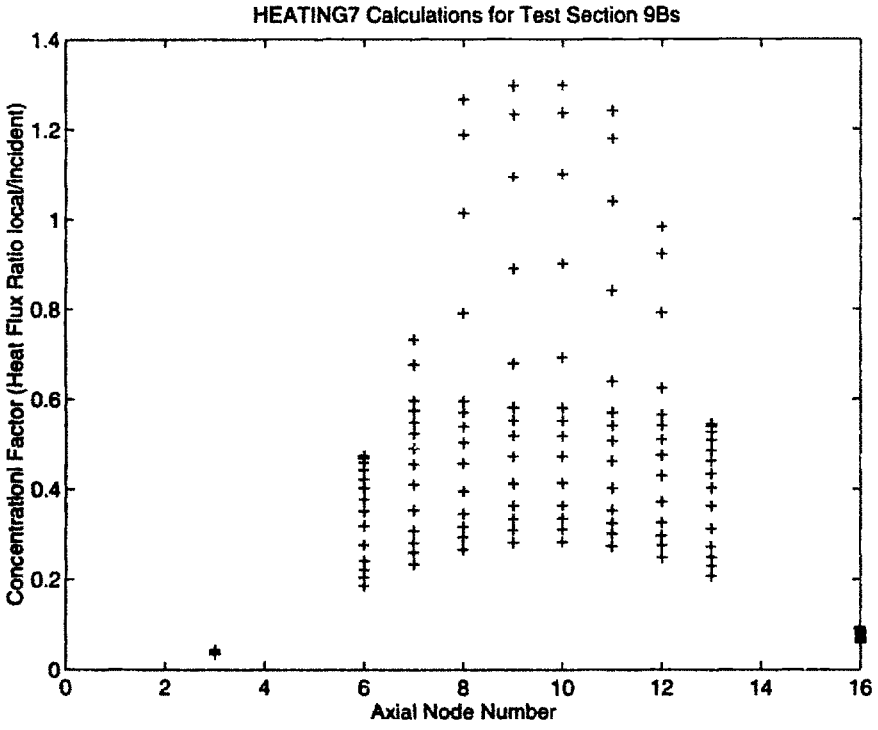

Figure G-4: Test Section 9B Axial Concentration Factor Profile

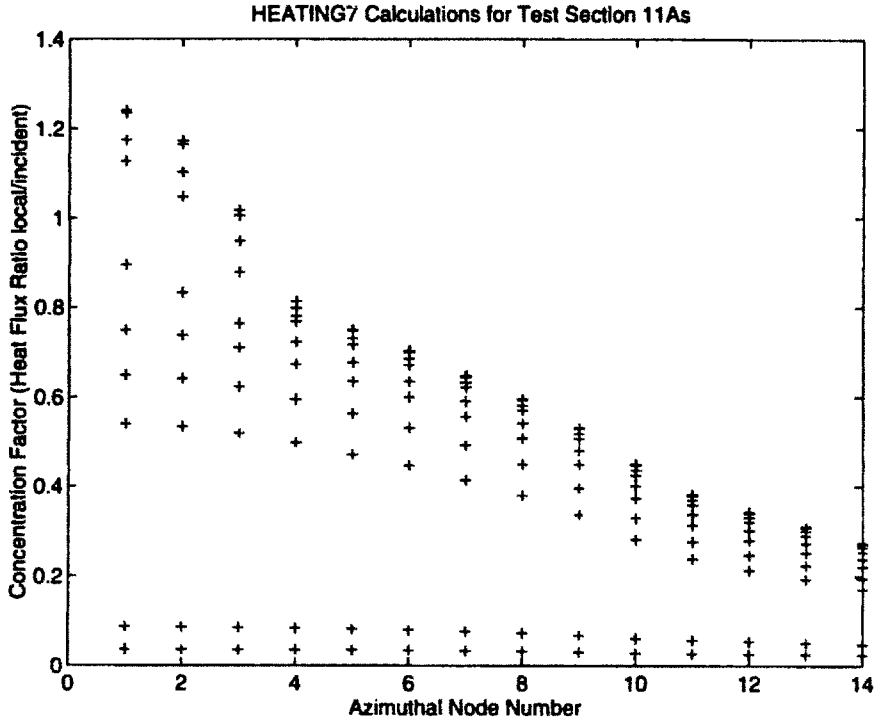

Figure G-5: Test Section 11A Azimuthal Concentration Factor Profile

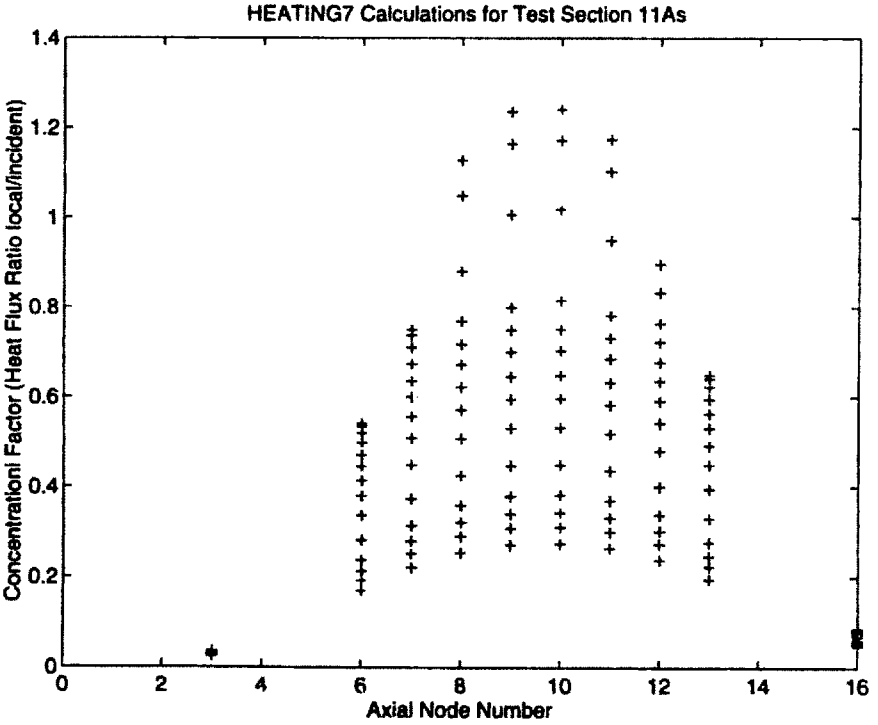

Figure G-6: Test Section 11A Axial Concentration Factor Profile

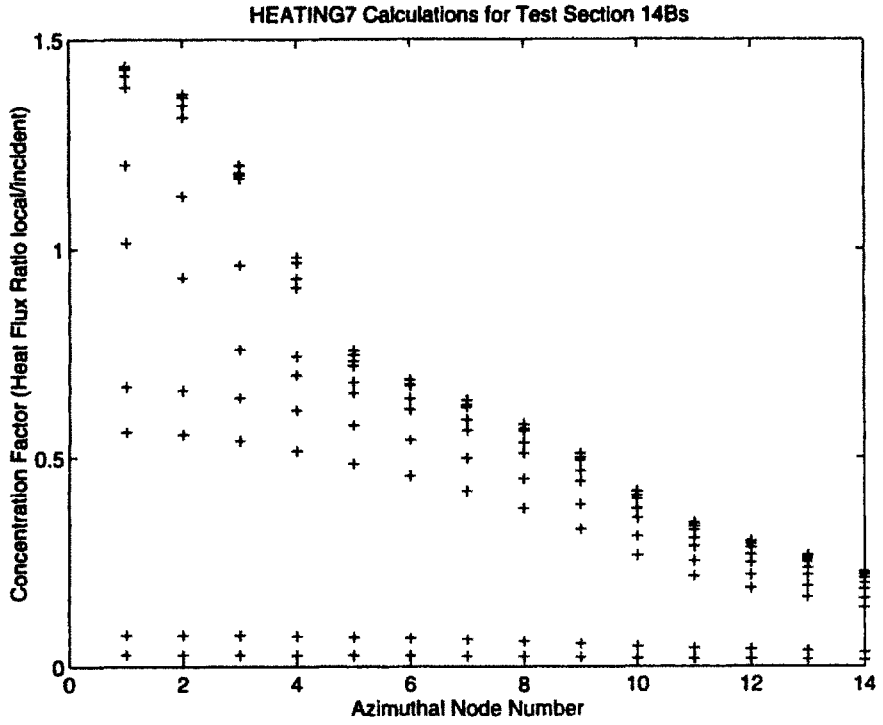

Figure G-7: Test Section 14B Azimuthal Concentration Factor Profile

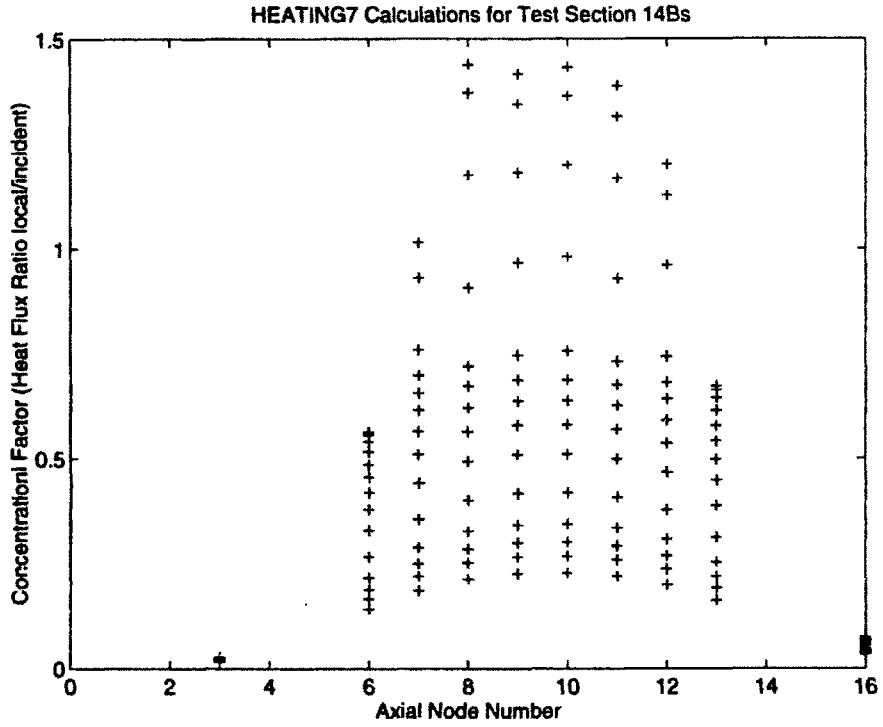

Figure G-8: Test Section 14B Axial Concentration Factor Profile

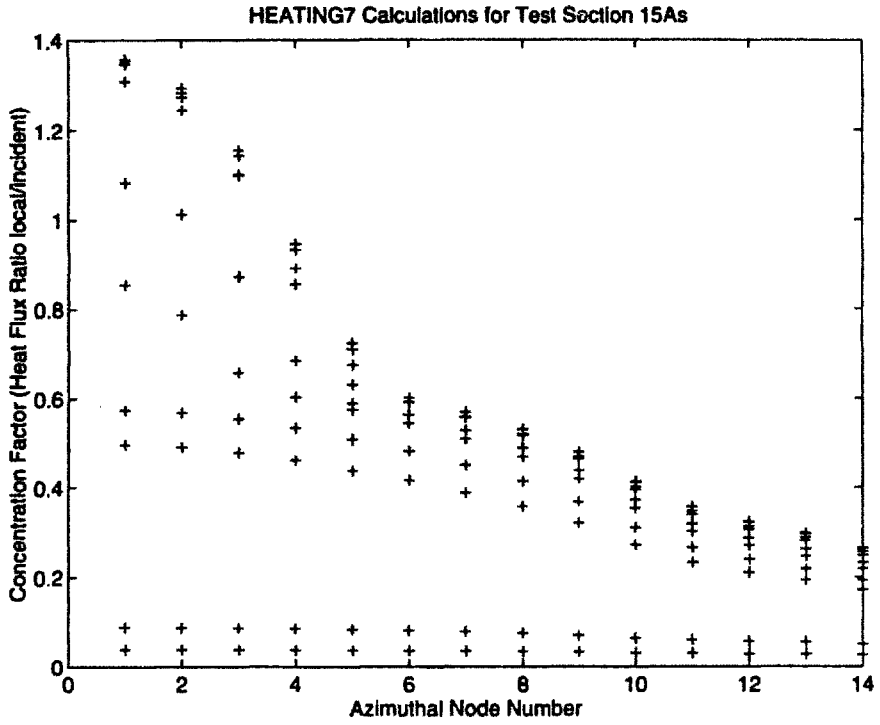

Figure G-9: Test Section 15A Azimuthal Concentration Factor Profile

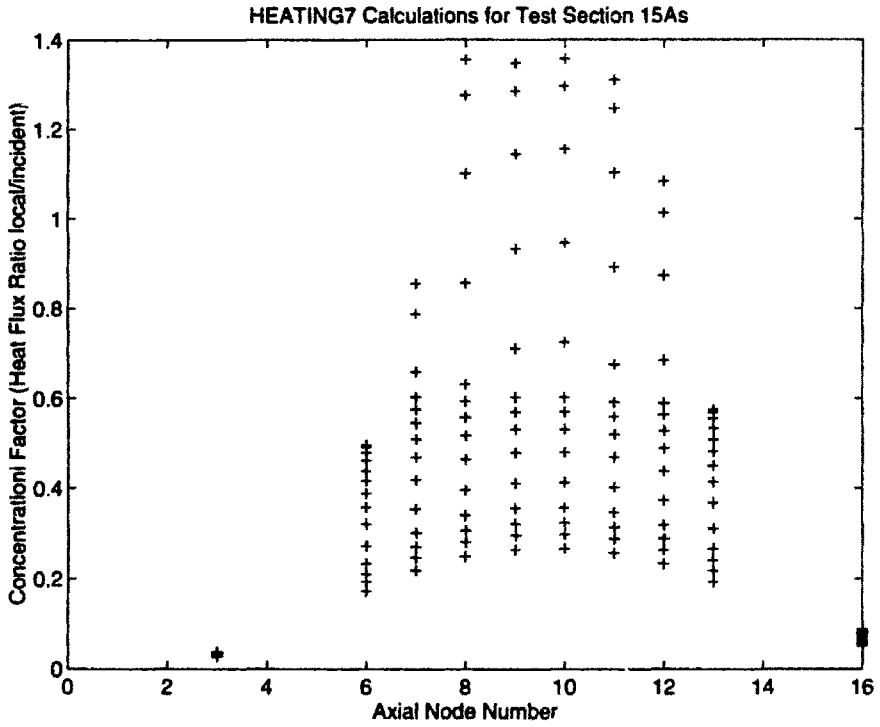

Figure G-10: Test Section 15A Axial Concentration Factor Profile

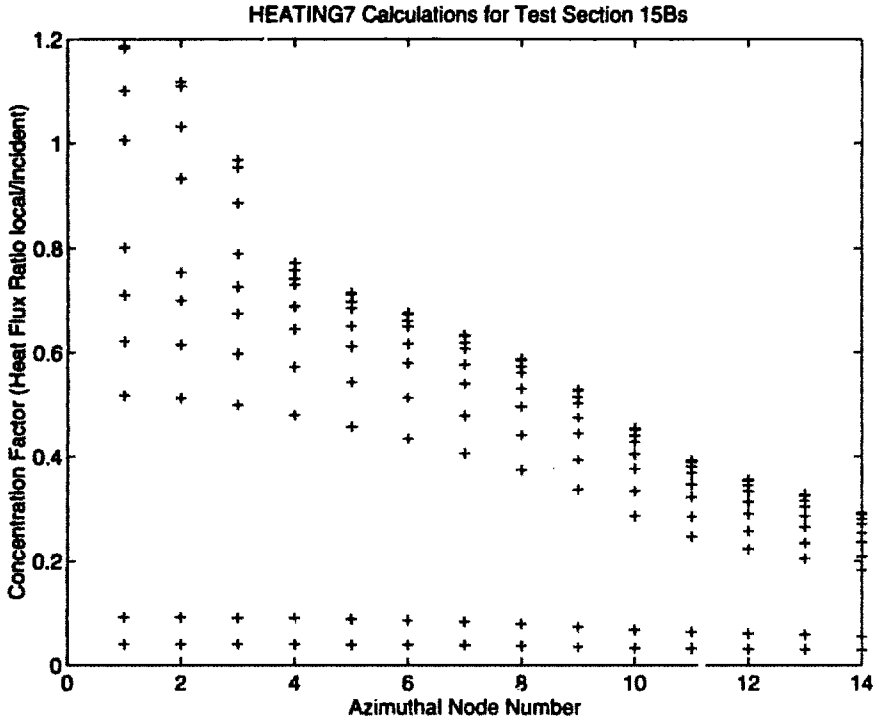

Figure G-11: Test Section 15B Azimuthal Concentration Factor Profile

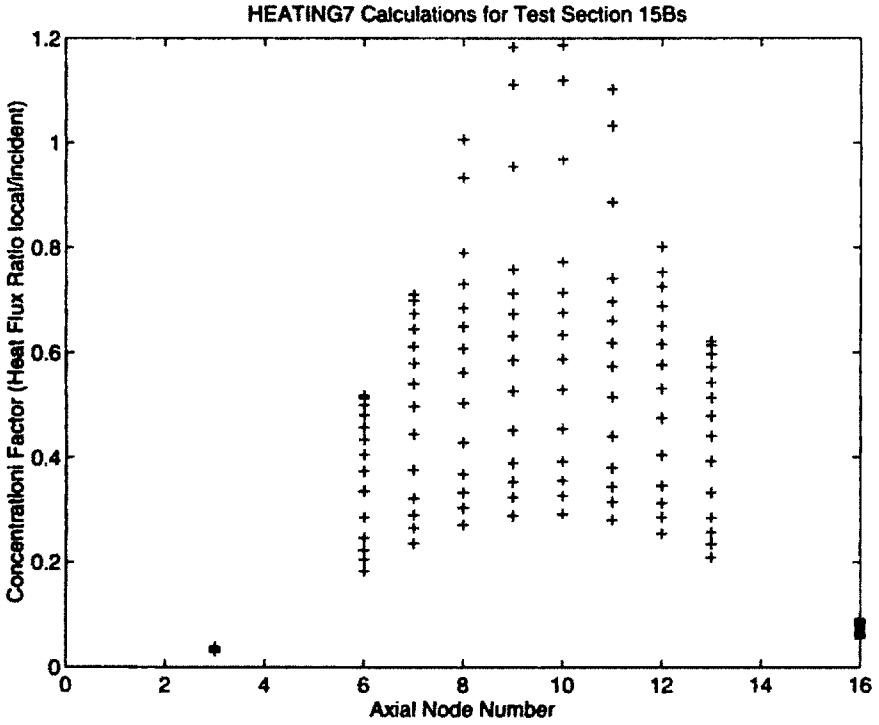

Figure G-12: Test Section 15B Axial Concentration Factor Profile

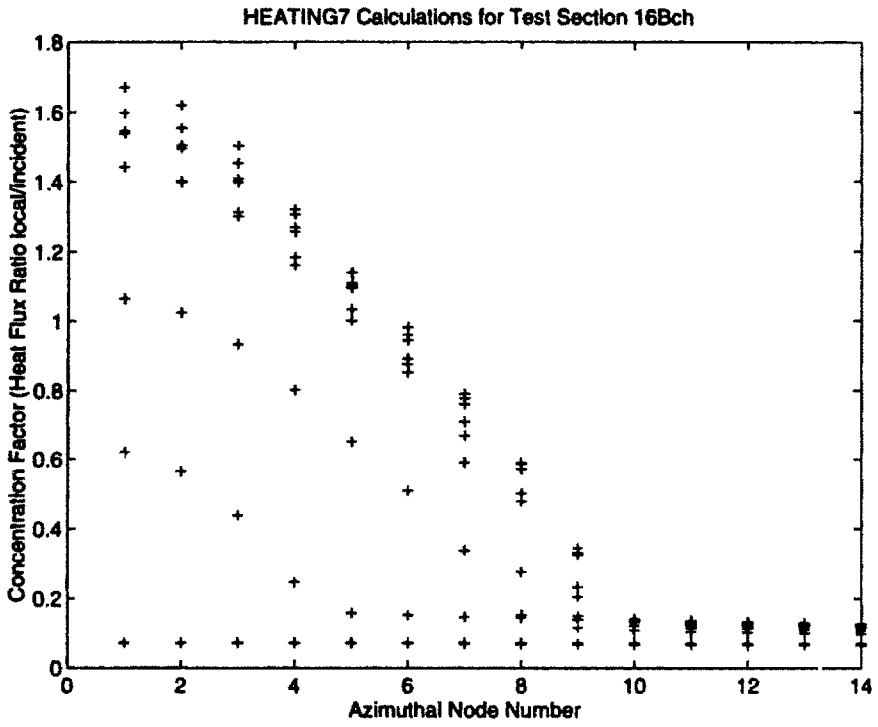

Figure G-13: Test Section 16B^{ch} Azimuthal Concentration Factor Profile

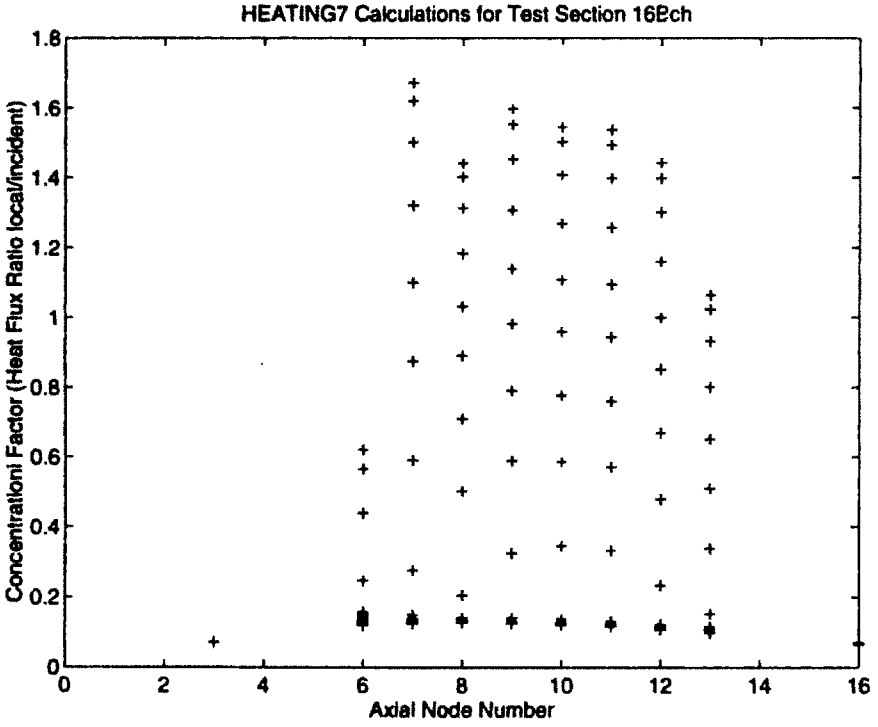

Figure G-14: Test Section 16B^{ch} Axial Concentration Factor Profile

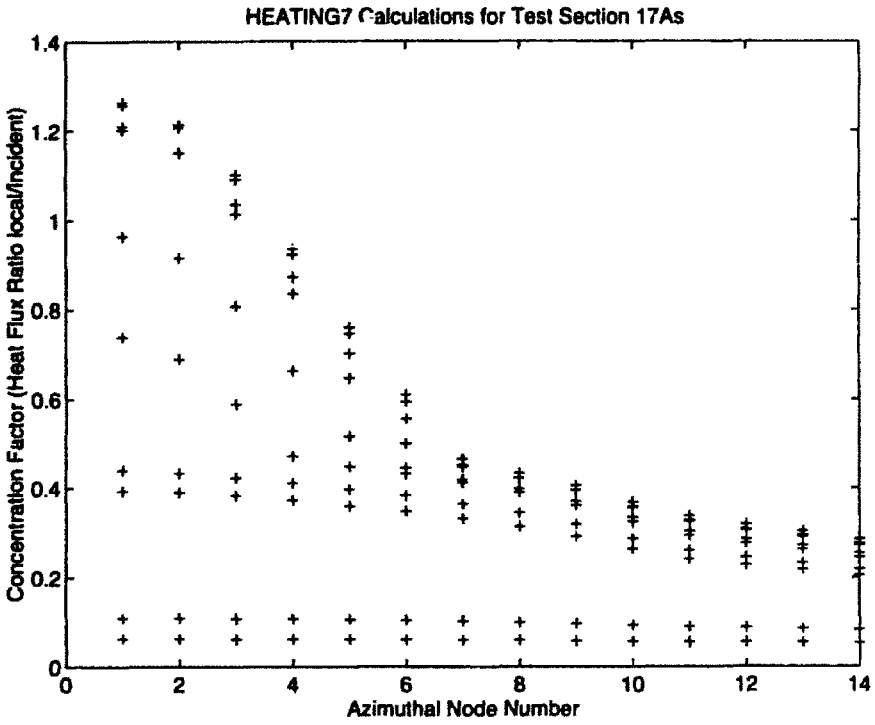

Figure G-15: Test Section 17A Azimuthal Concentration Factor Profile

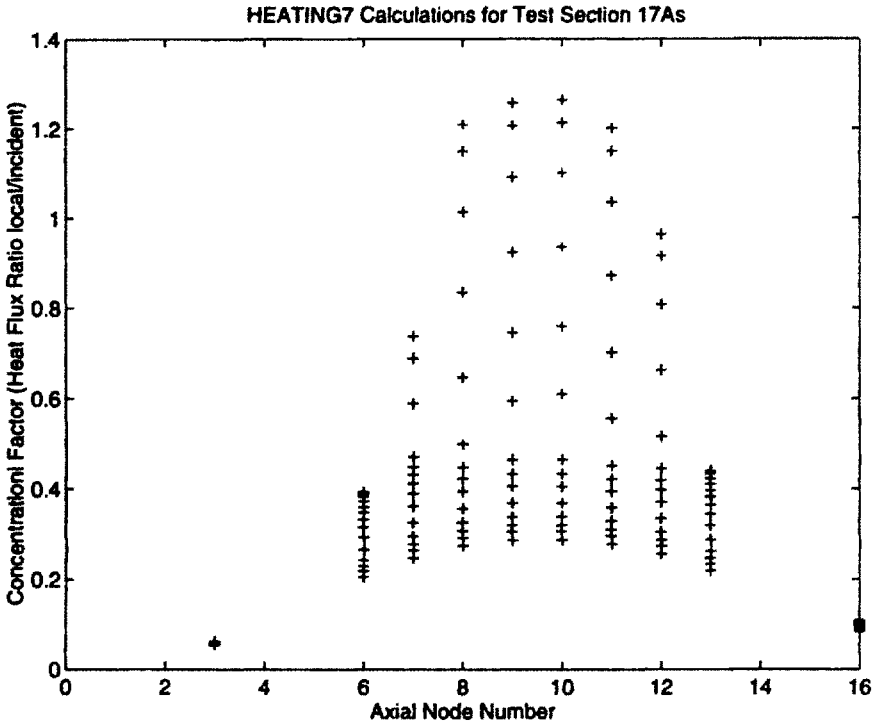

Figure G-16: Test Section 17A Axial Concentration Factor Profile

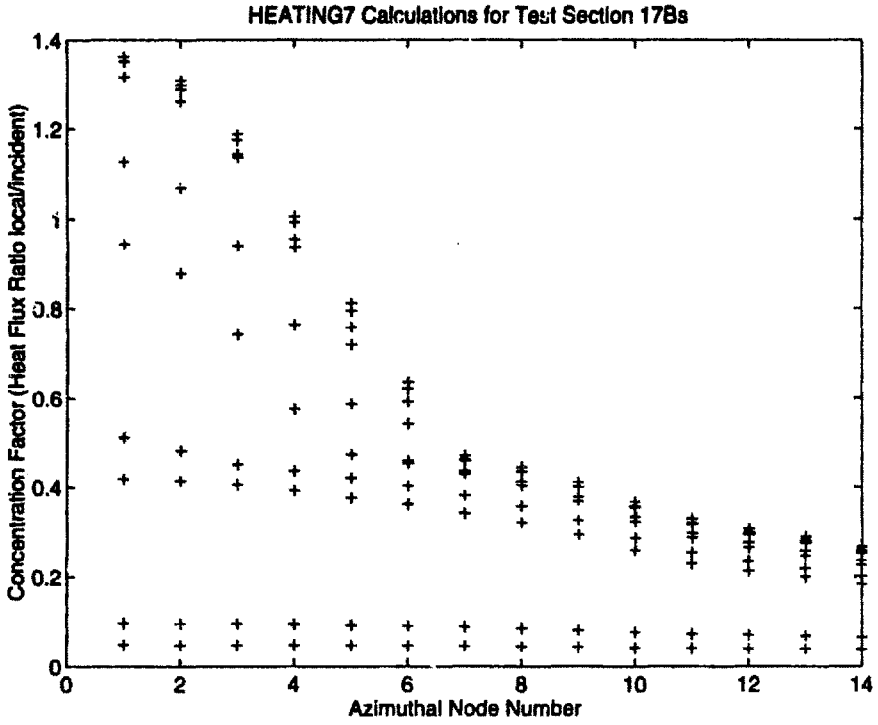

Figure G-17: Test Section 17B Azimuthal Concentration Factor Profile

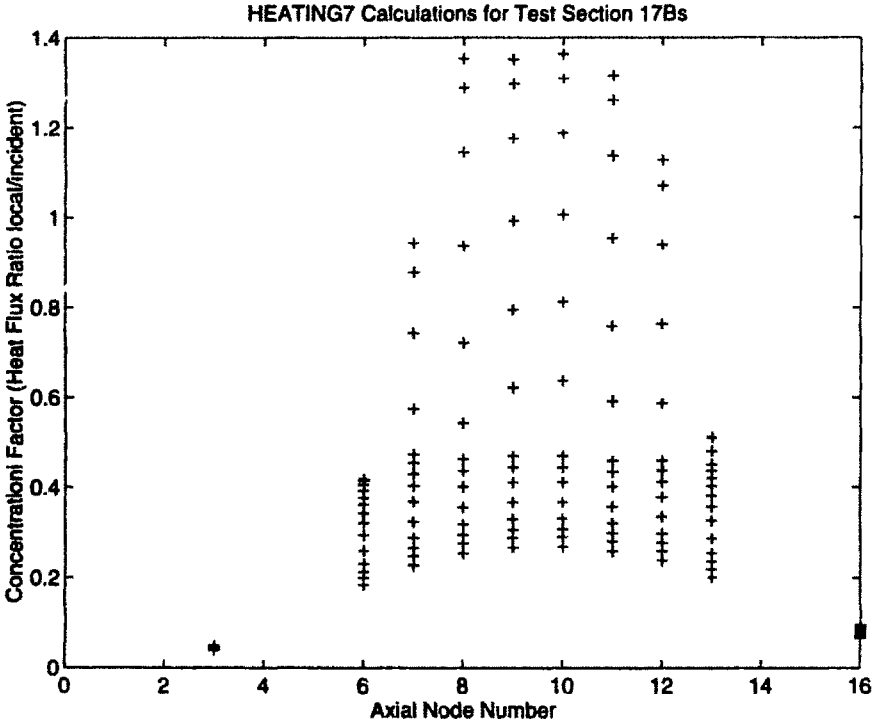

Figure G-18: Test Section 17B Axial Concentration Factor Profile

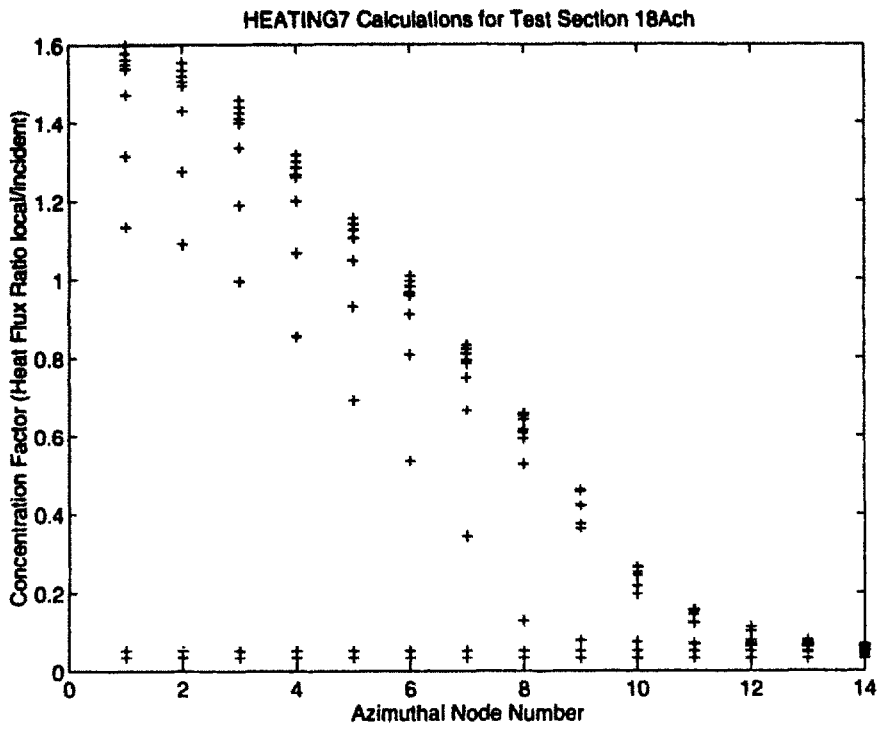

Figure G-19: Test Section 18A^{ch} Azimuthal Concentration Factor Profile

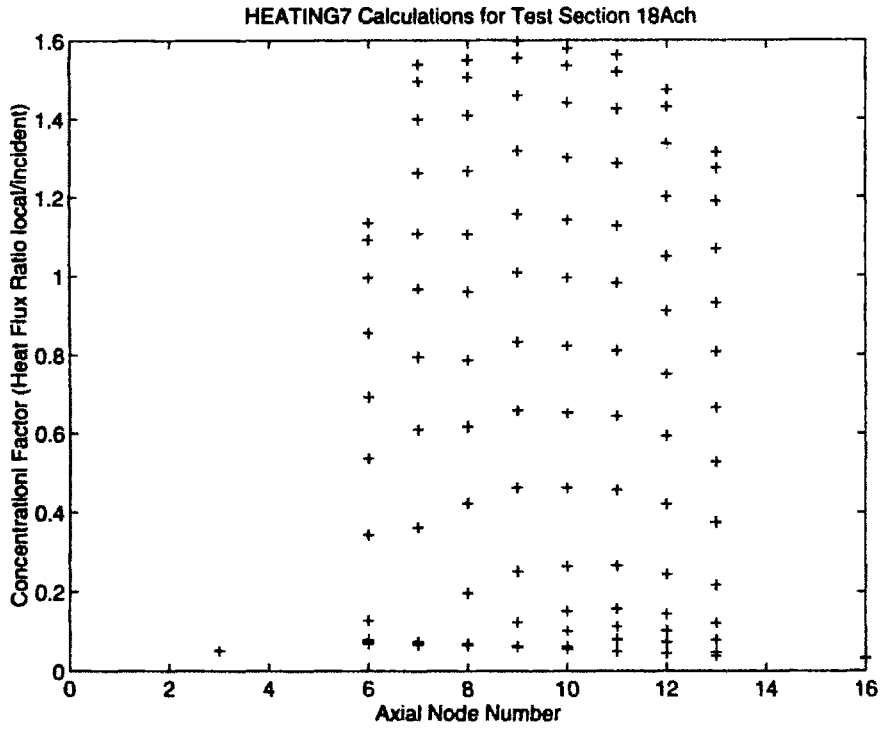

Figure G-20: Test Section 18A^{ch} Axial Concentration Factor Profile

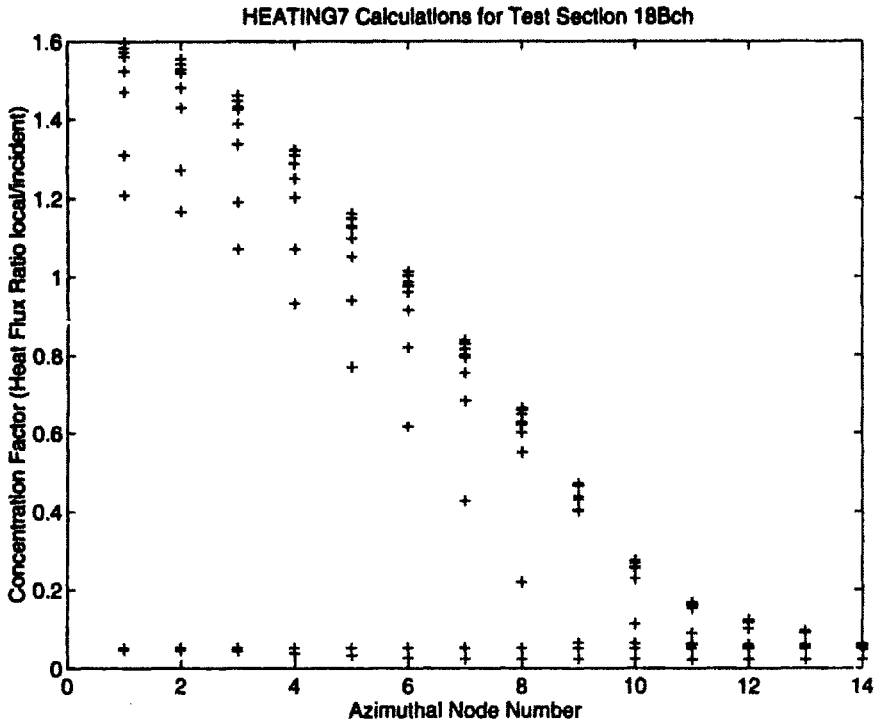

Figure G-21: Test Section 18B^{ch} Azimuthal Concentration Factor Profile

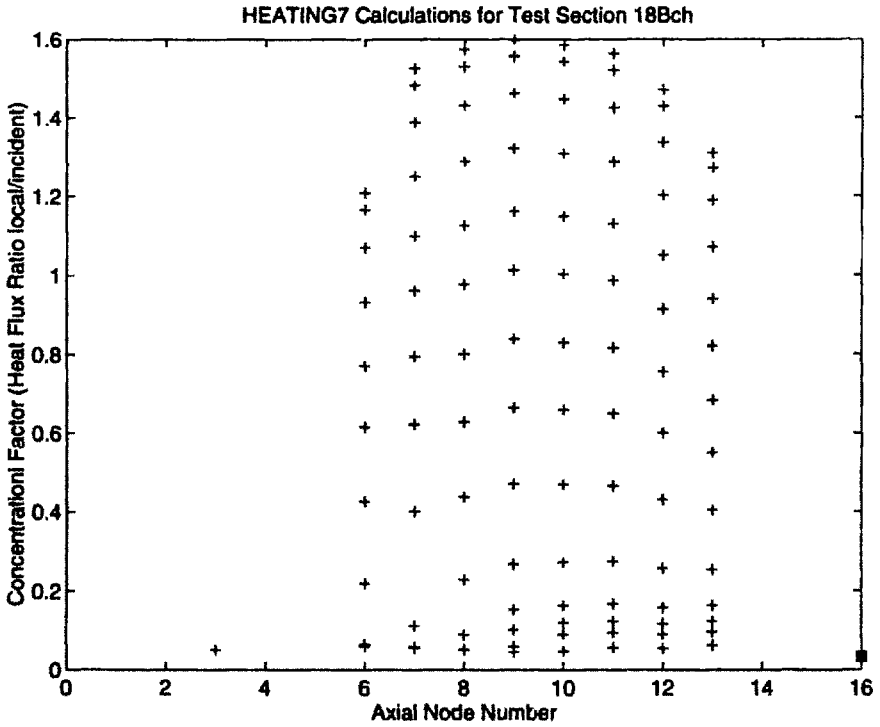

Figure G-22: Test Section 18B^{ch} Axial Concentration Factor Profile

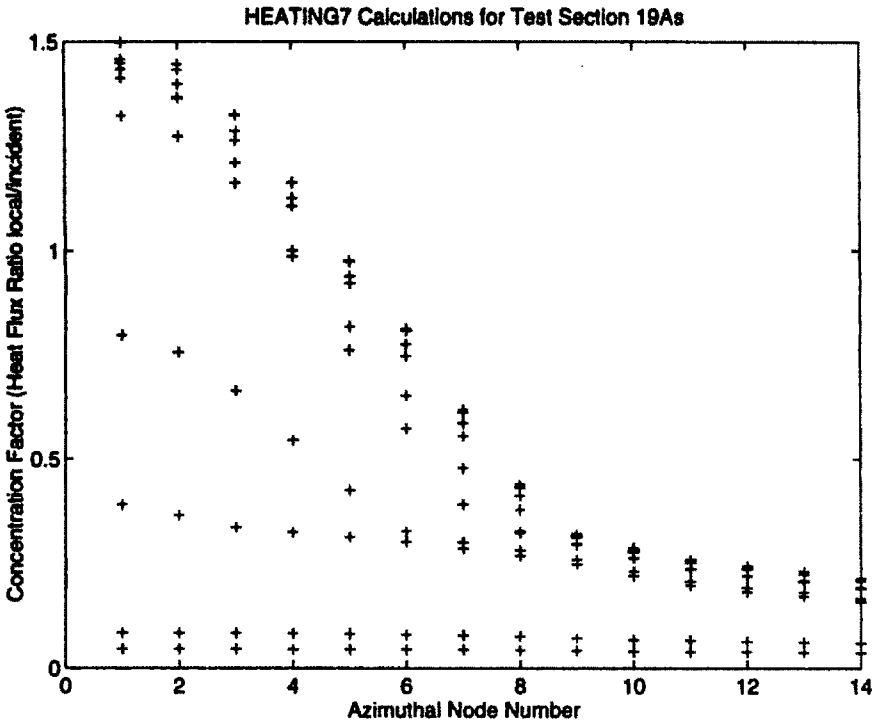

Figure G-23: Test Section 19A Azimuthal Concentration Factor Profile

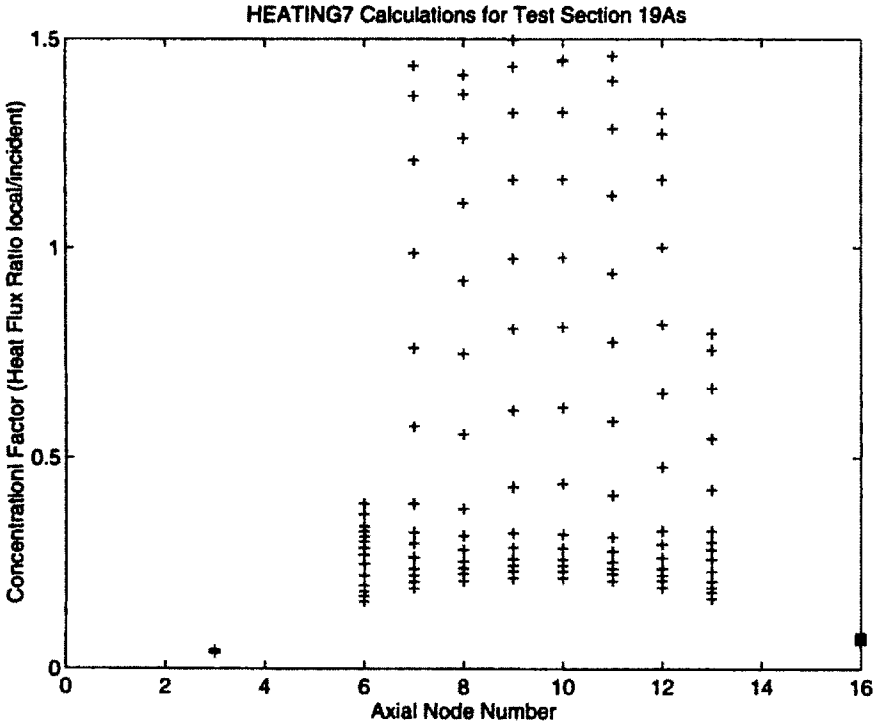

Figure G-24: Test Section 19A Axial Concentration Factor Profile

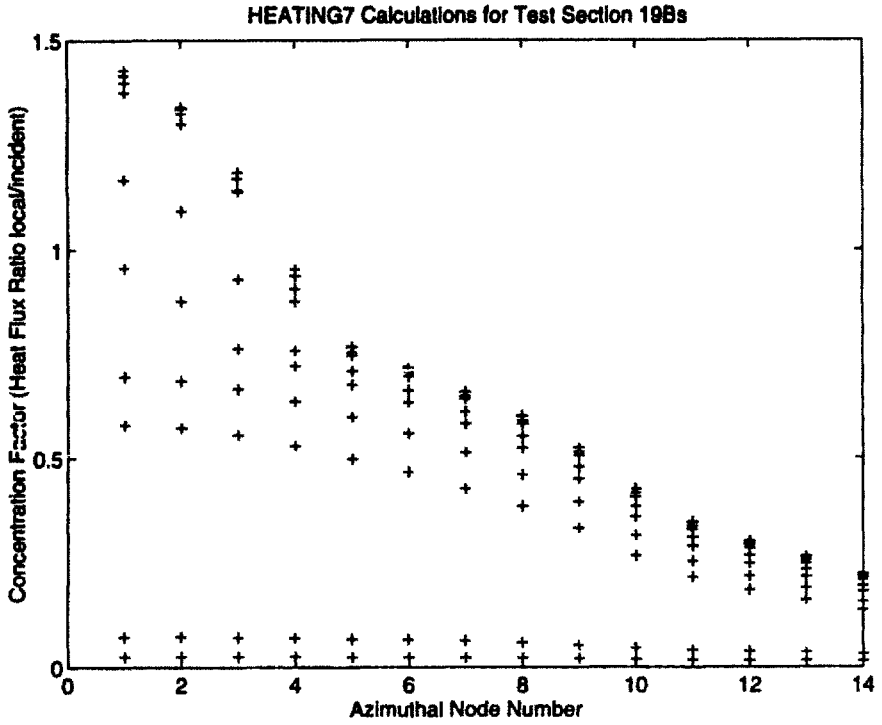

Figure G-25: Test Section 19B Azimuthal Concentration Factor Profile

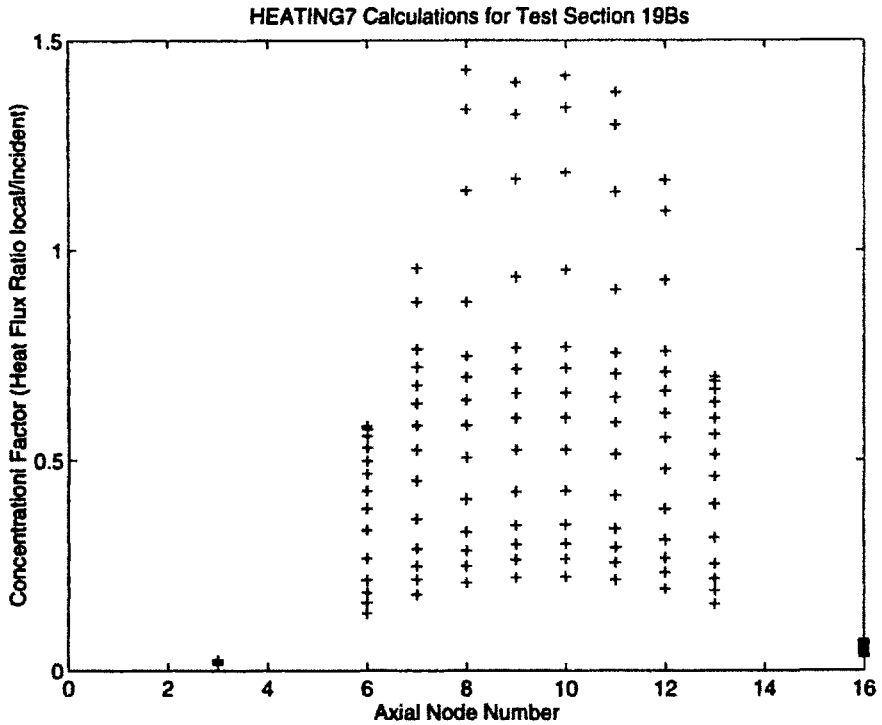

Figure G-26: Test Section 19B Axial Concentration Factor Profile

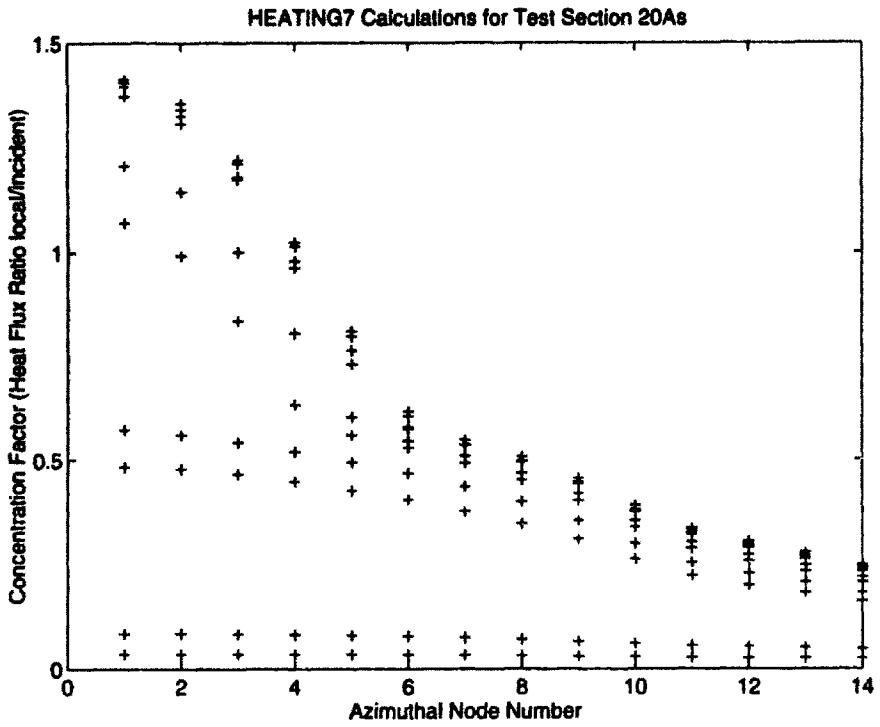

Figure G-27: Test Section 20A Azimuthal Concentration Factor Profile

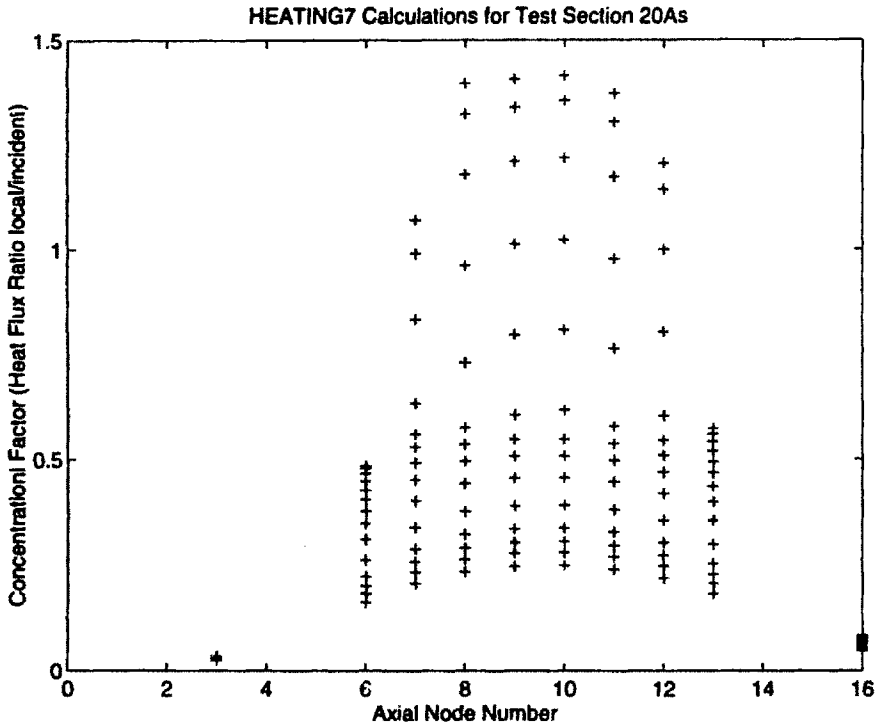

Figure G-28: Test Section 20A Axial Concentration Factor Profile

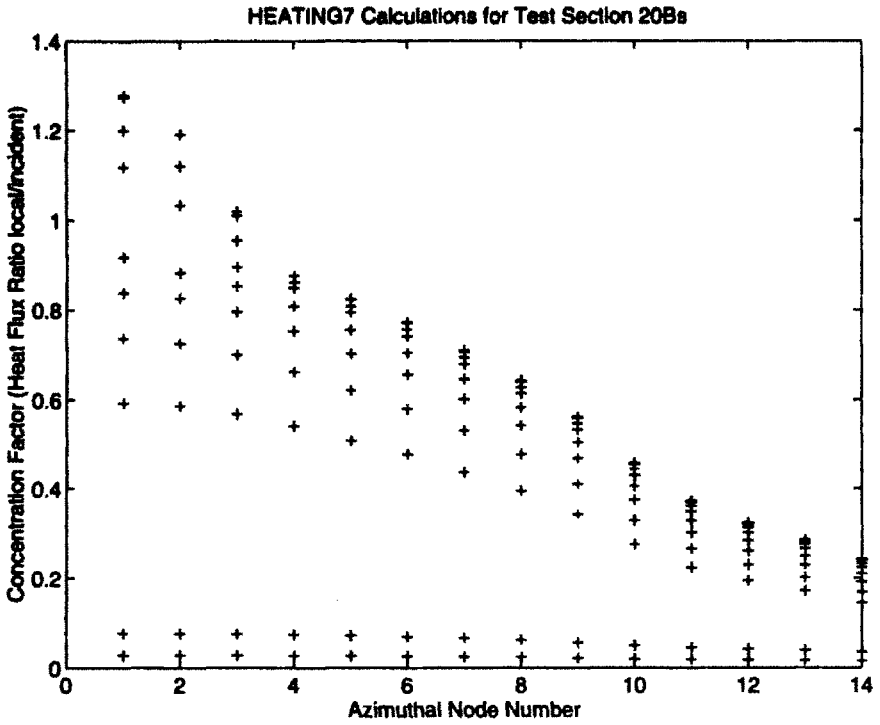

Figure G-29: Test Section 20B Azimuthal Concentration Factor Profile

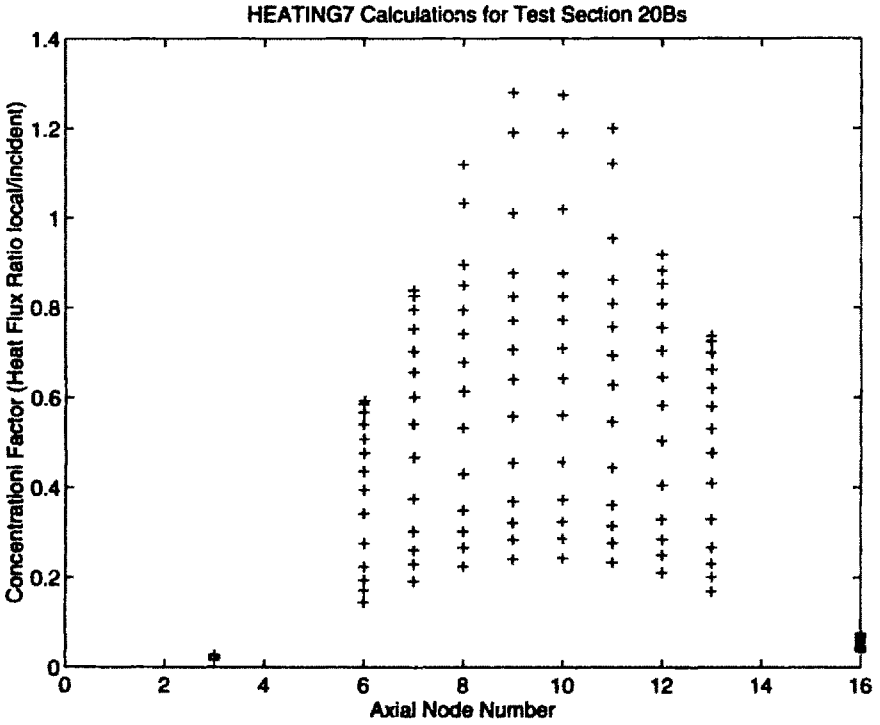

Figure G-30: Test Section 20B Axial Concentration Factor Profile

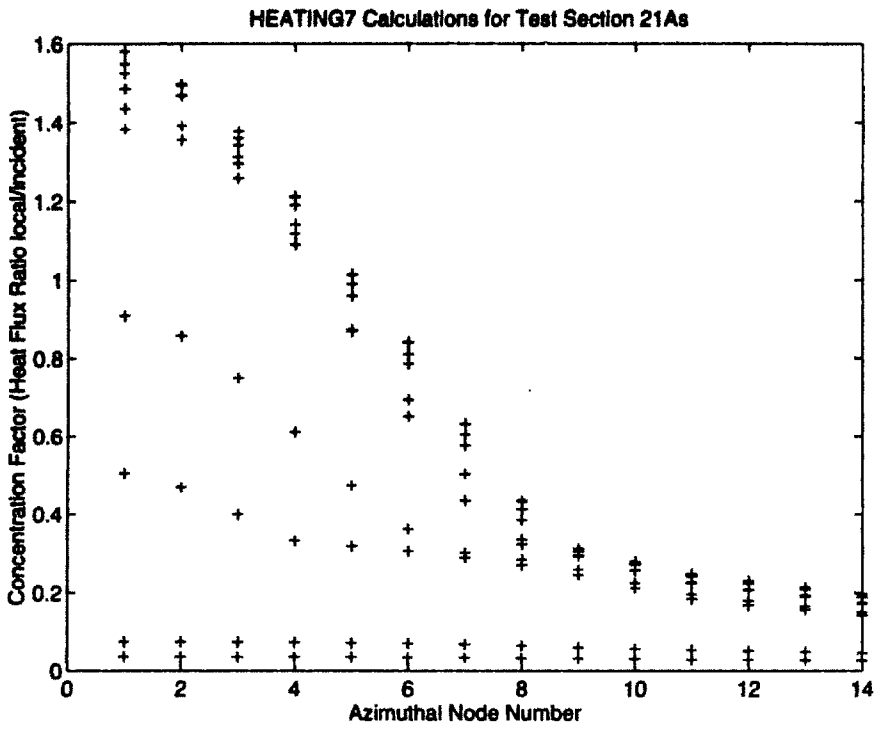

Figure G-31: Test Section 21A Azimuthal Concentration Factor Profile

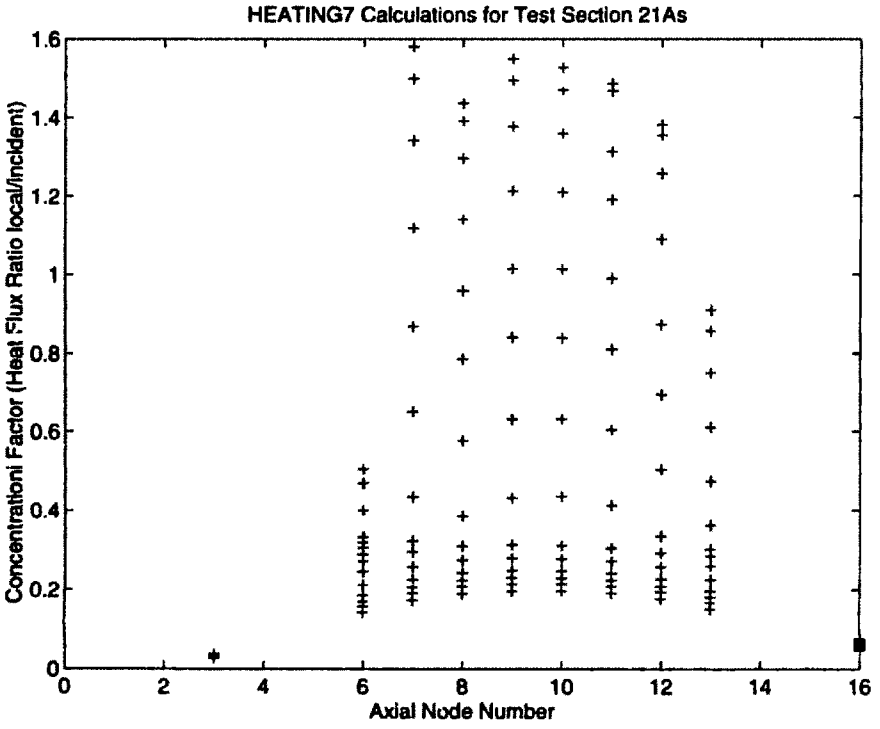

Figure G-32: Test Section 21A Axial Concentration Factor Profile

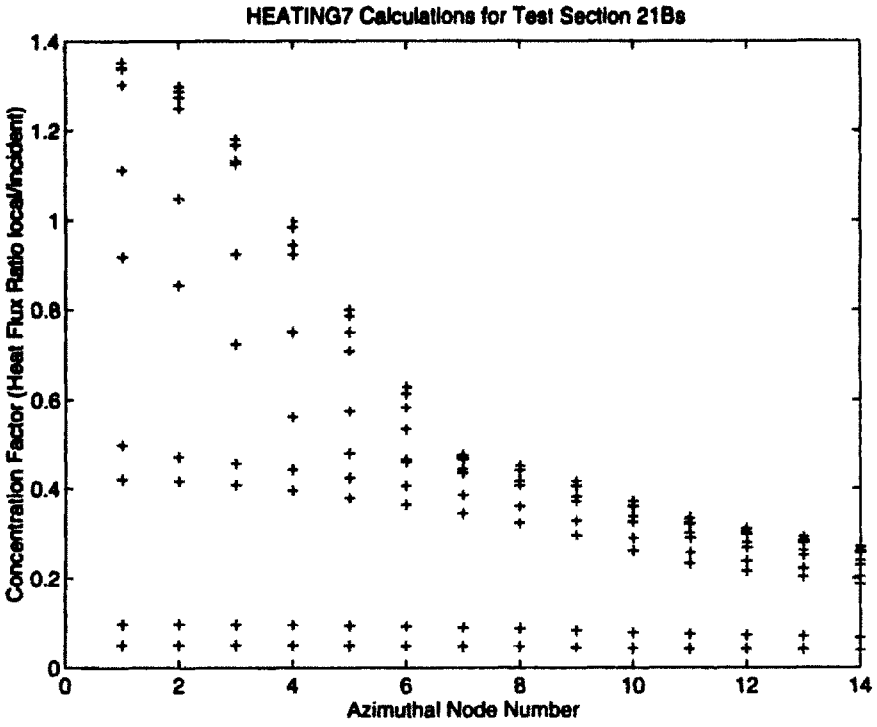

Figure G-33: Test Section 21B Azimuthal Concentration Factor Profile

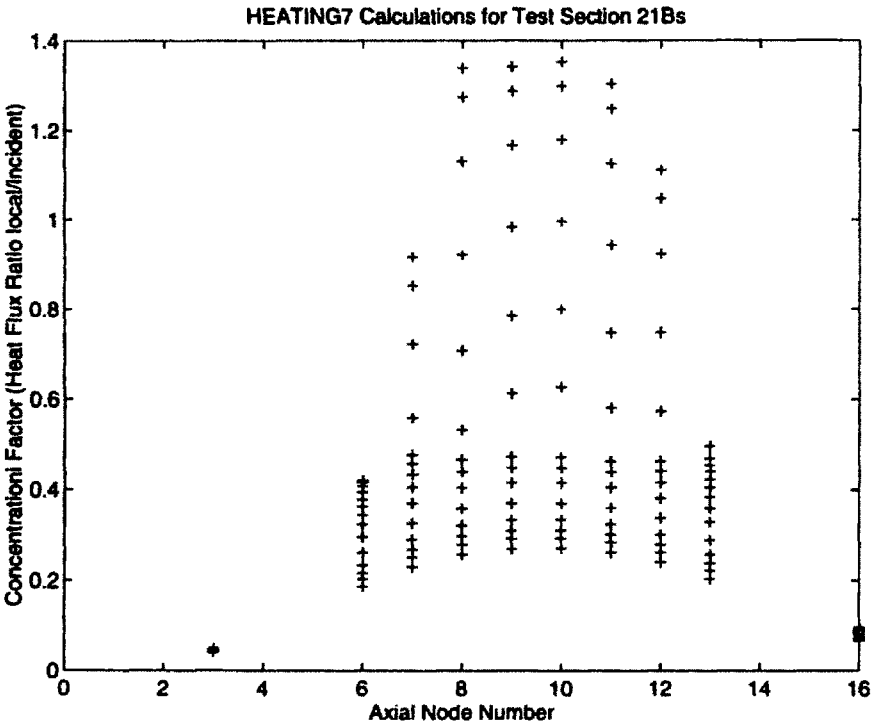

Figure G-34: Test Section 21B Axial Concentration Factor Profile

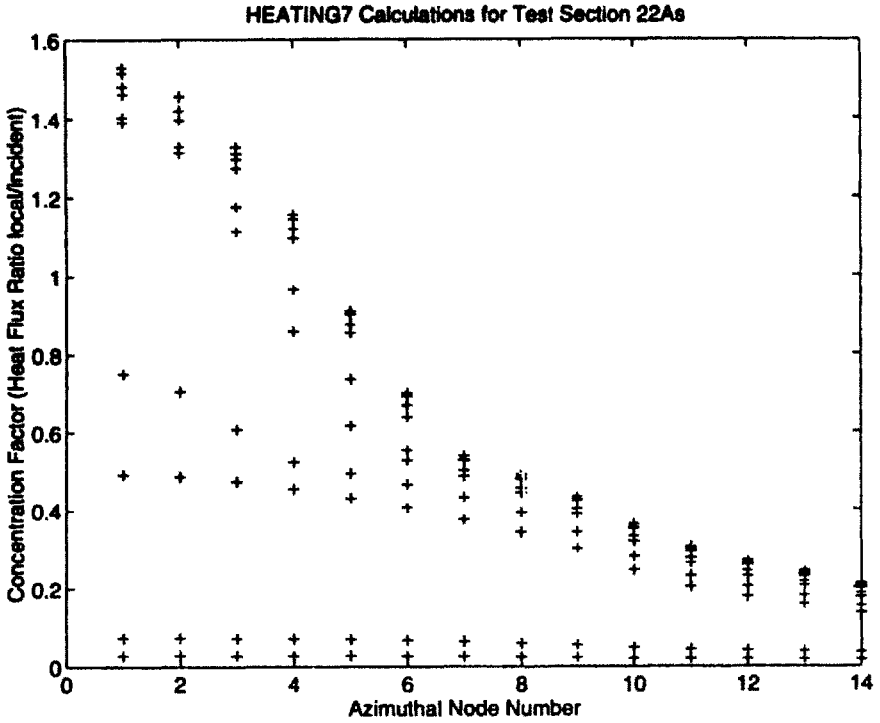

Figure G-35: Test Section 22A Azimuthal Concentration Factor Profile

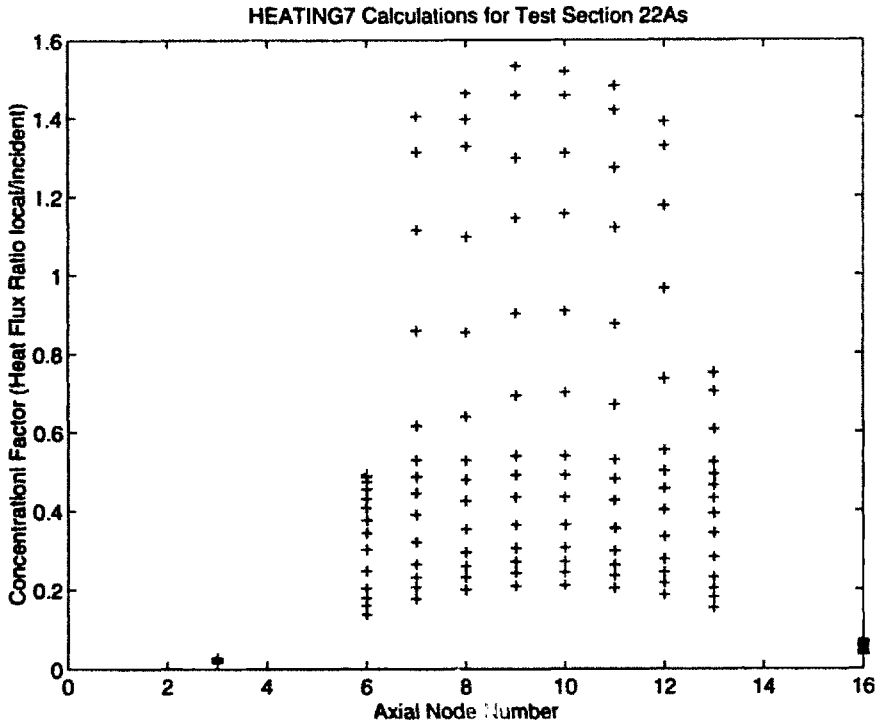

Figure G-36: Test Section 22A Axial Concentration Factor Profile

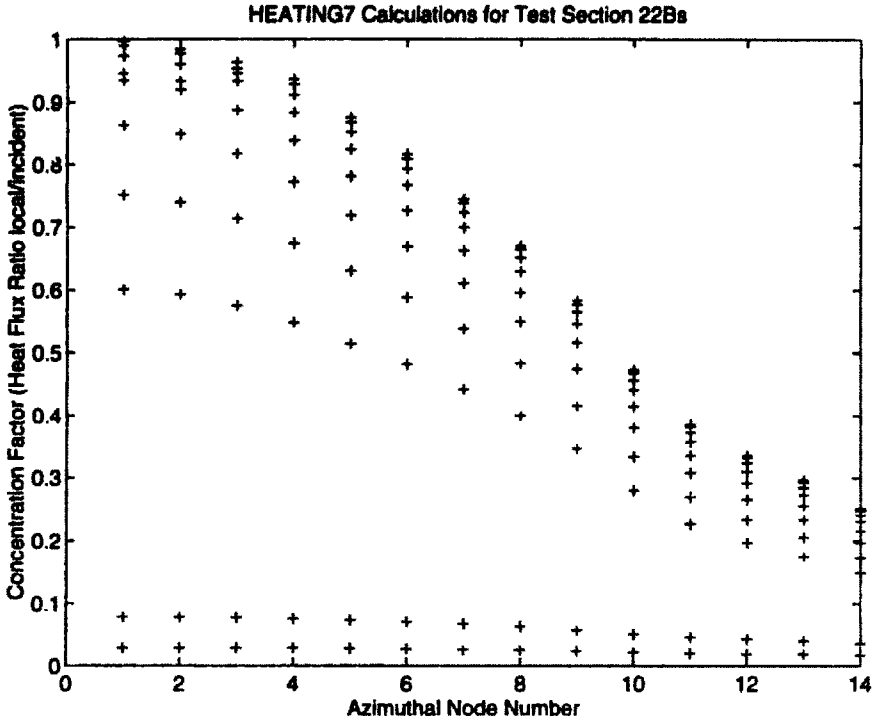

Figure G-37: Test Section 22B Azimuthal Concentration Factor Profile

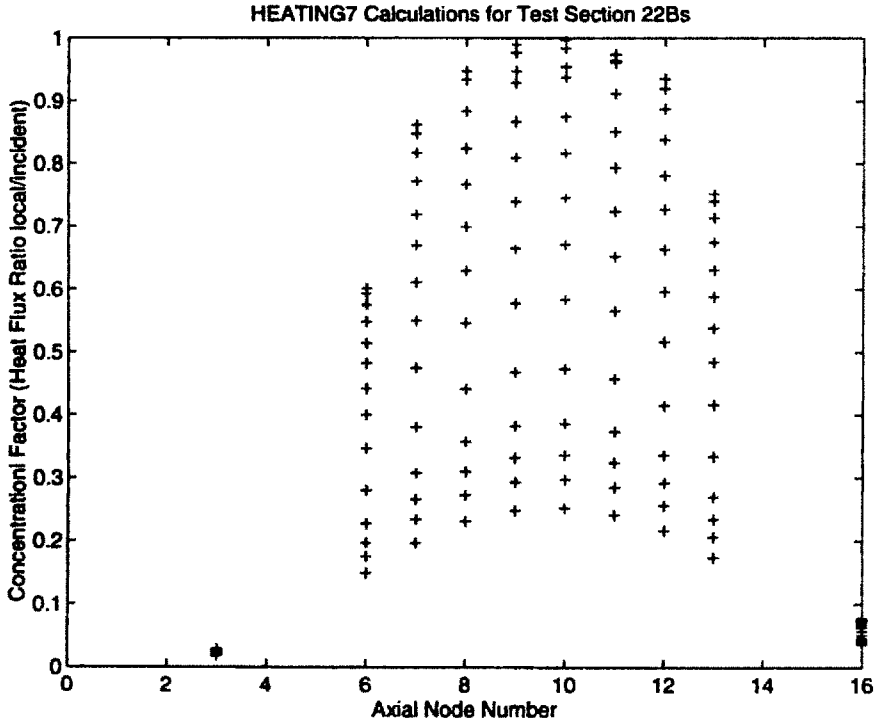

Figure G-38: Test Section 22B Axial Concentration Factor Profile

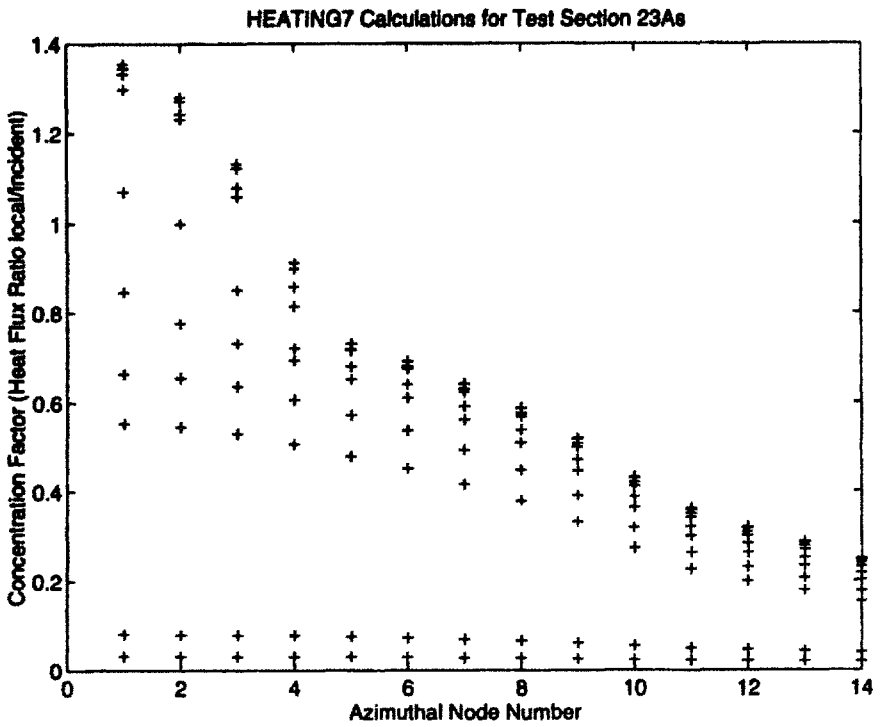

Figure G-39: Test Section 23A Azimuthal Concentration Factor Profile

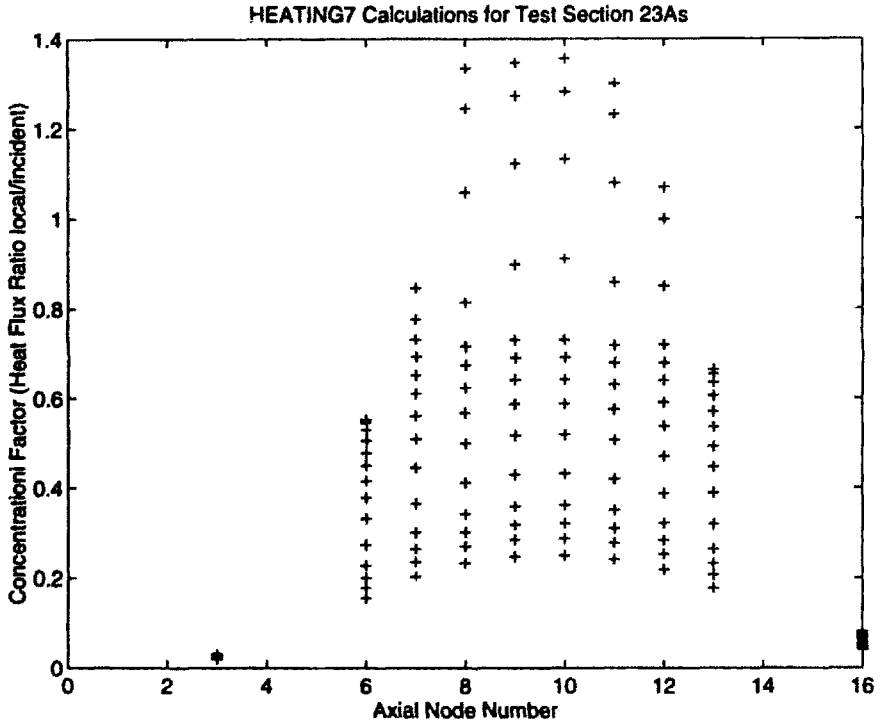

Figure G-40: Test Section 23A Axial Concentration Factor Profile

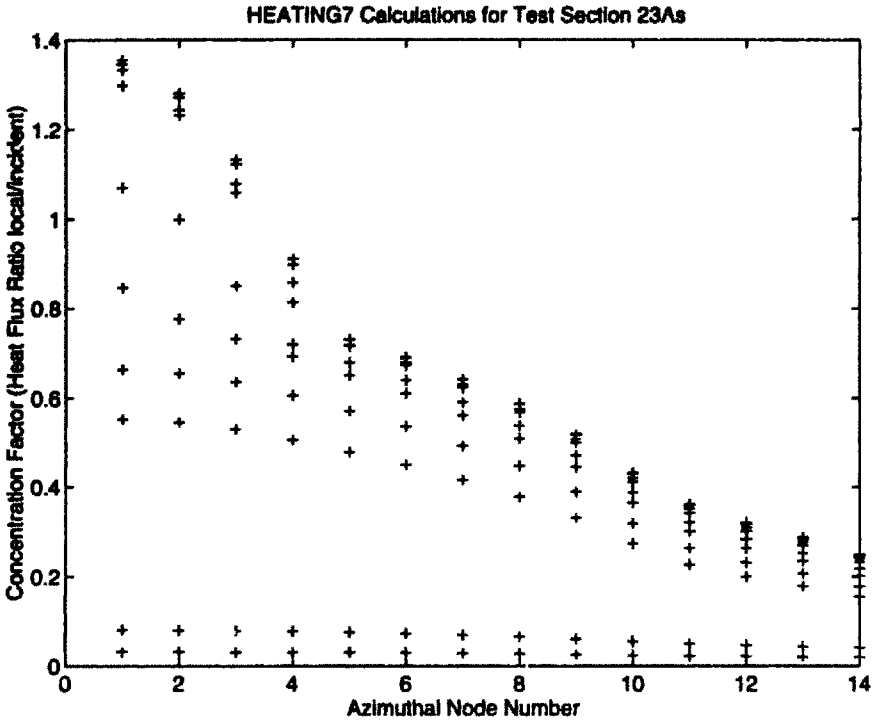

Figure G-41: Test Section 23B Azimuthal Concentration Factor Profile

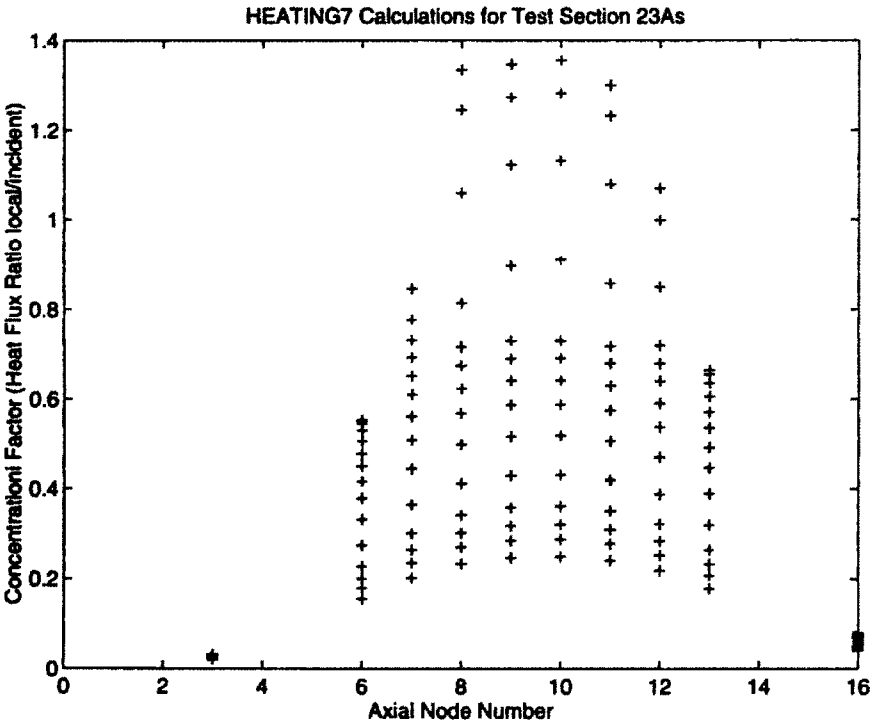

Figure G-42: Test Section 23B Axial Concentration Factor Profile

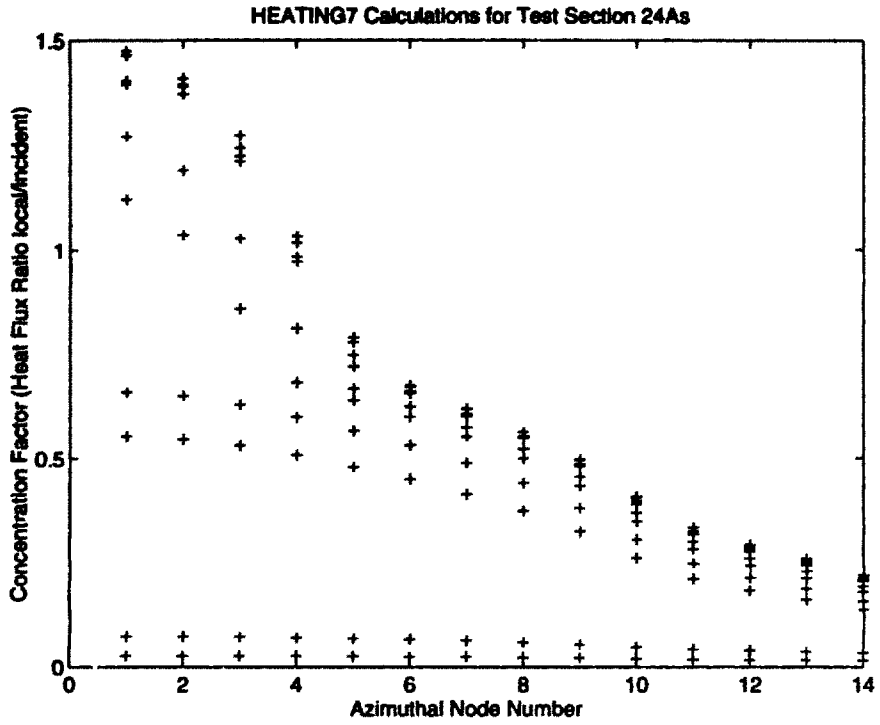

Figure G-43: Test Section 24A Azimuthal Concentration Factor Profile

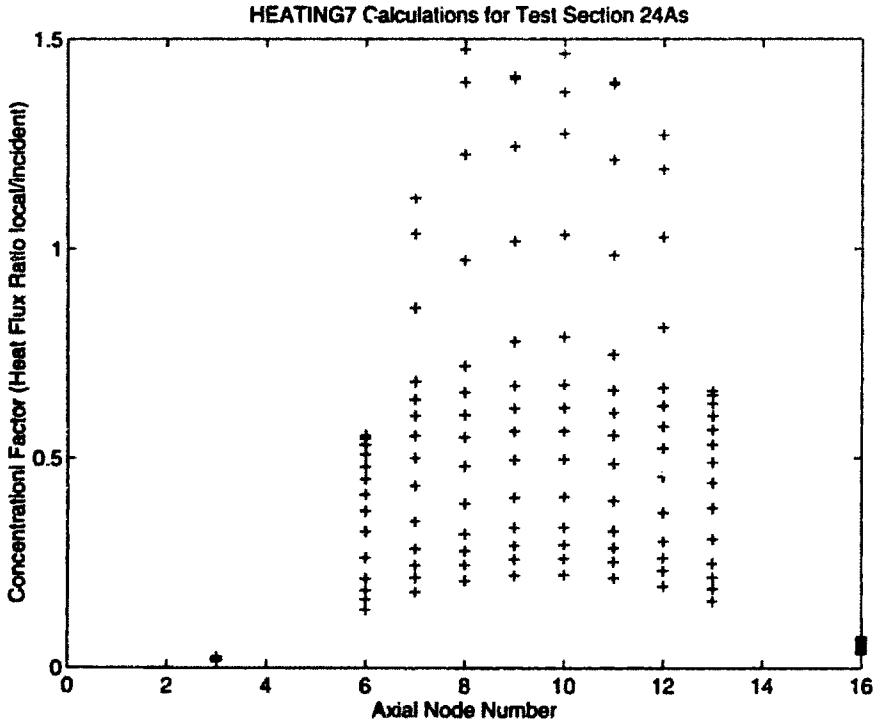

Figure G-44: Test Section 24A Axial Concentration Factor Profile

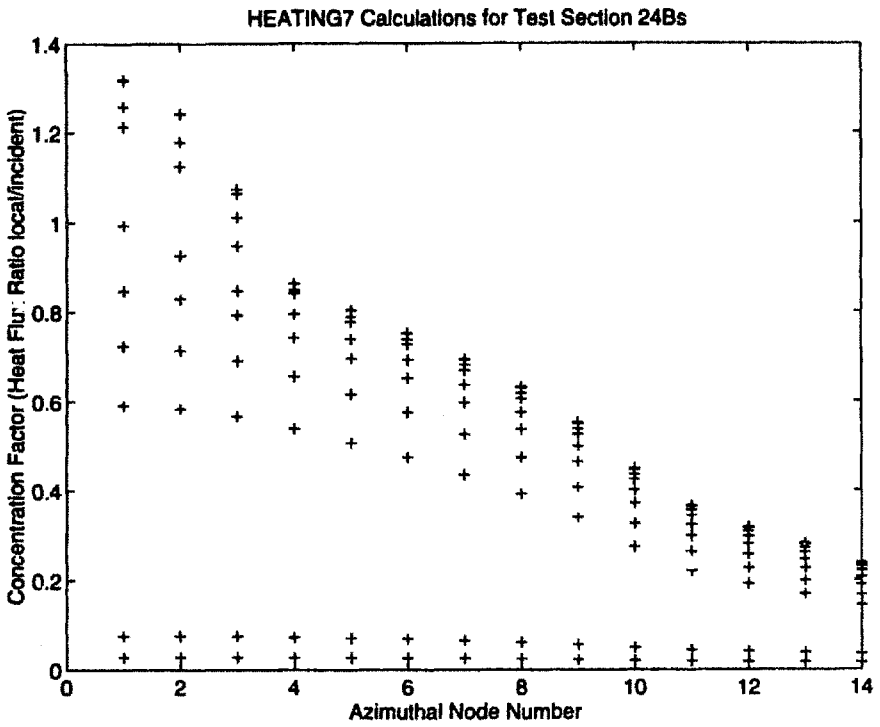

Figure G-45: Test Section 24B Azimuthal Concentration Factor Profile

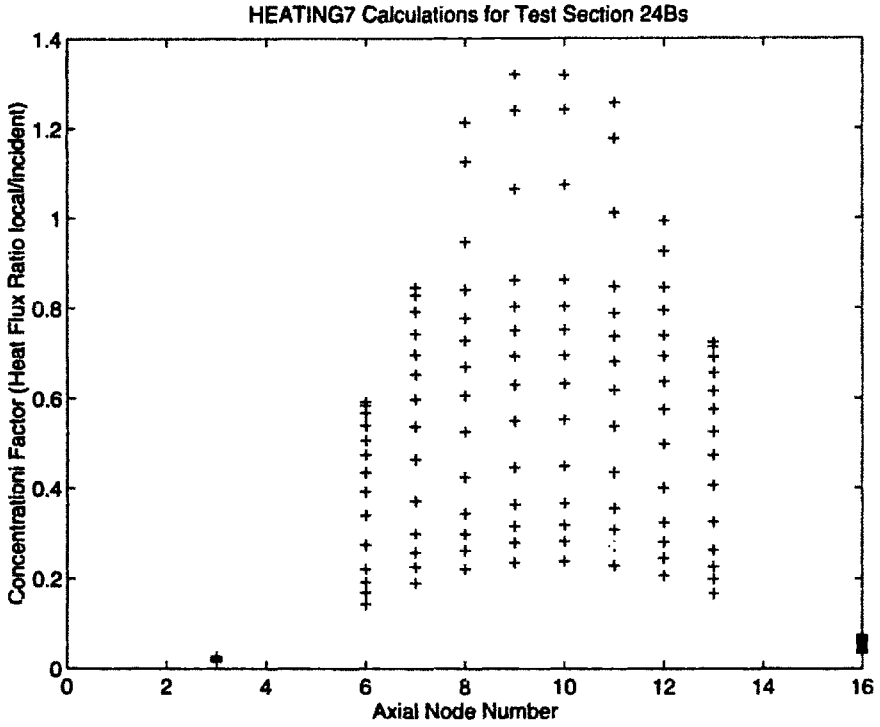

Figure G-46: Test Section 24B Axial Concentration Factor Profile

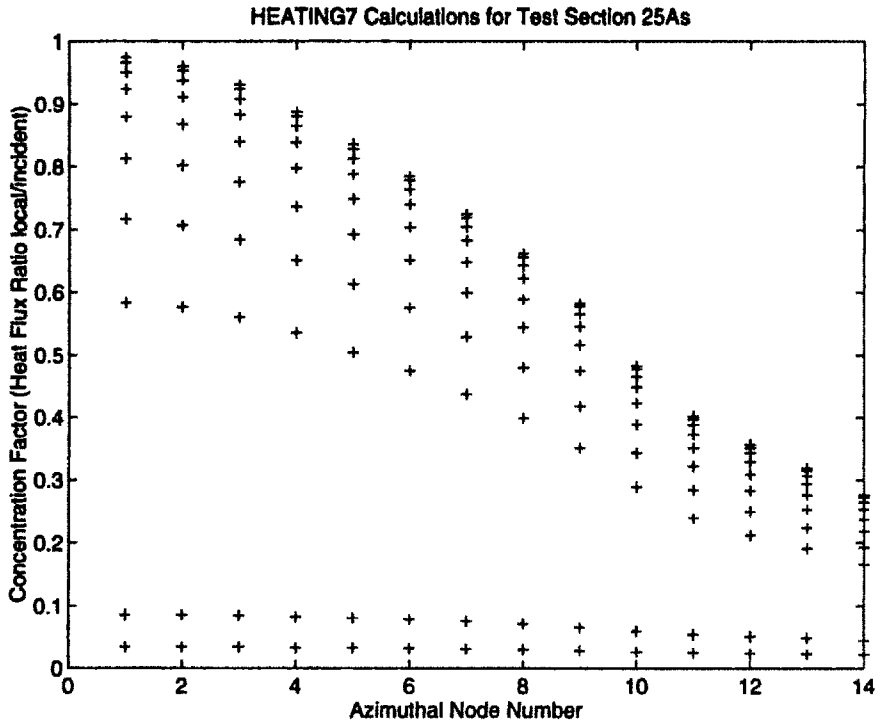

Figure G-47: Test Section 25A Azimuthal Concentration Factor Profile

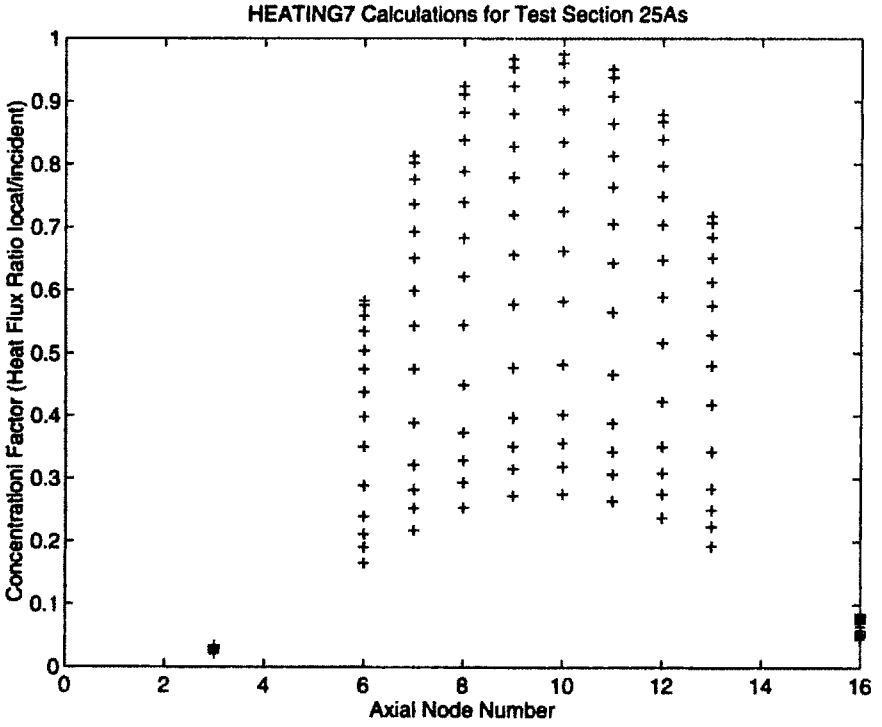

Figure G-48: Test Section 25A Axial Concentration Factor Profile

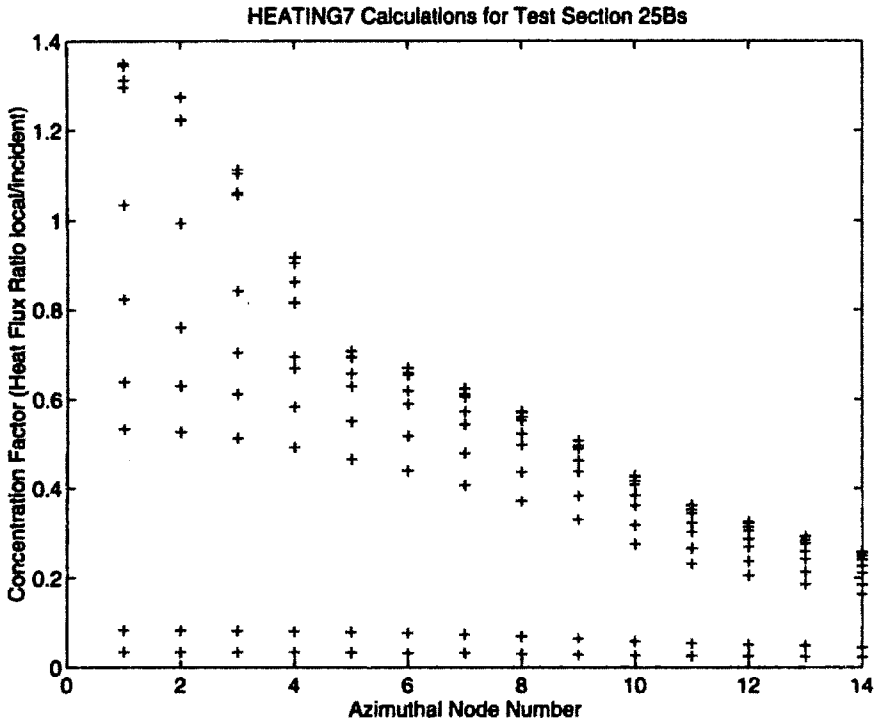

Figure G-49: Test Section 25B Azimuthal Concentration Factor Profile

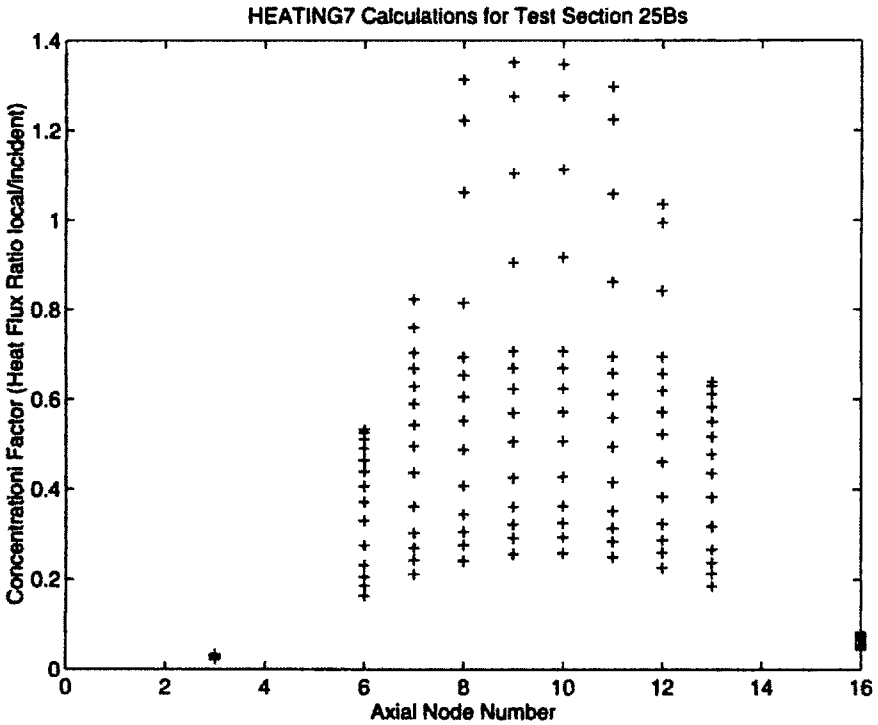

Figure G-50: Test Section 25B Axial Concentration Factor Profile

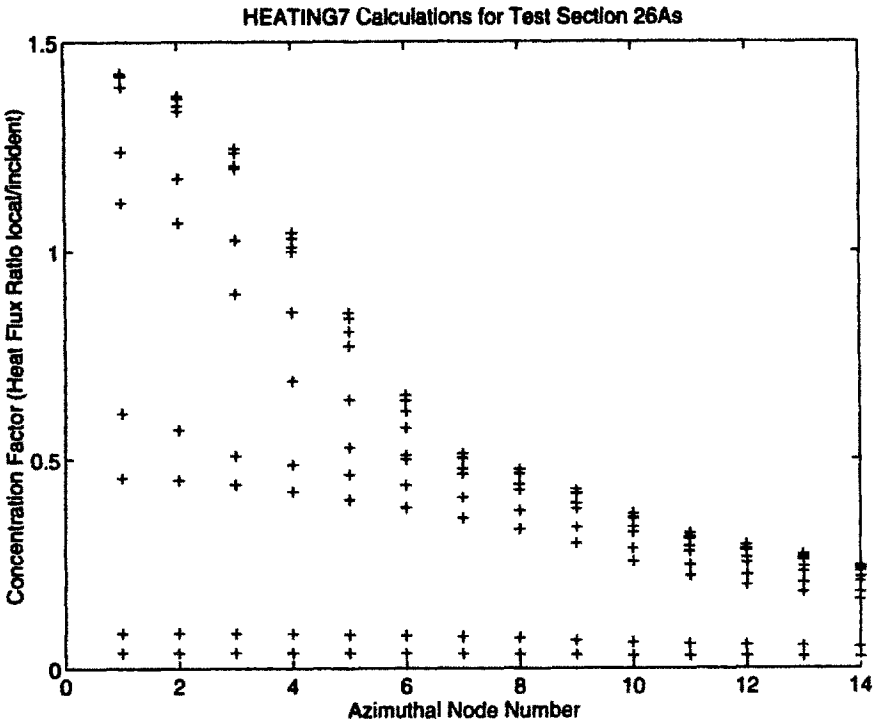

Figure G-51: Test Section 26A Azimuthal Concentration Factor Profile

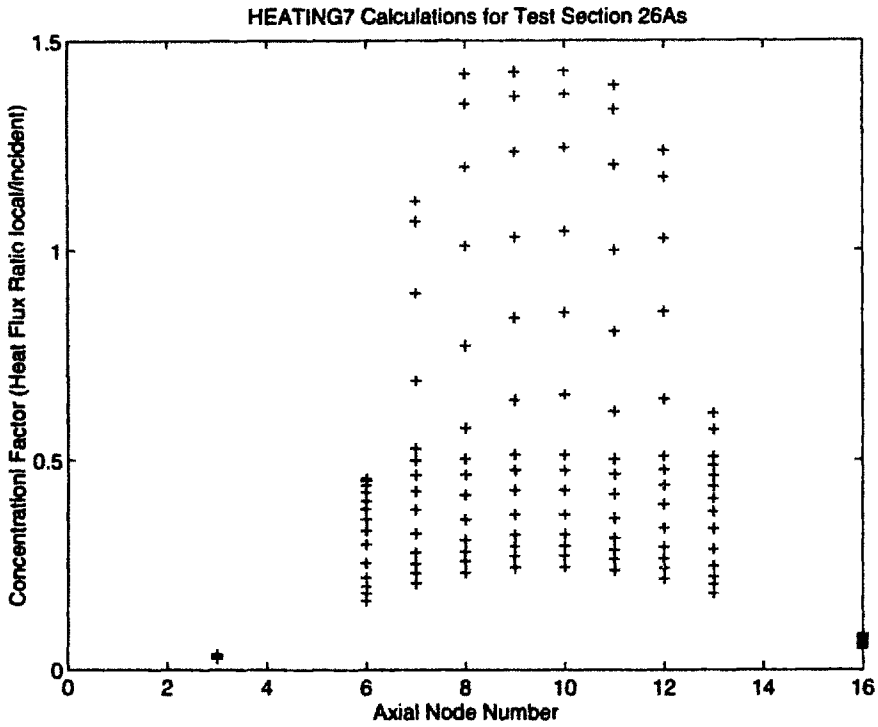

Figure G-52: Test Section 26A Axial Concentration Factor Profile

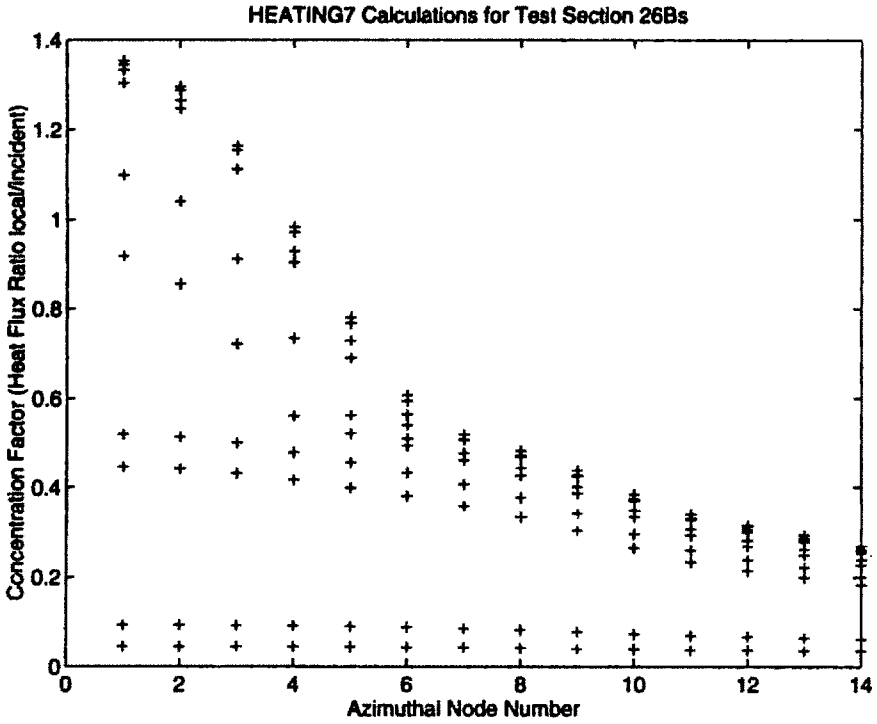

Figure G-53: Test Section 26B Azimuthal Concentration Factor Profile

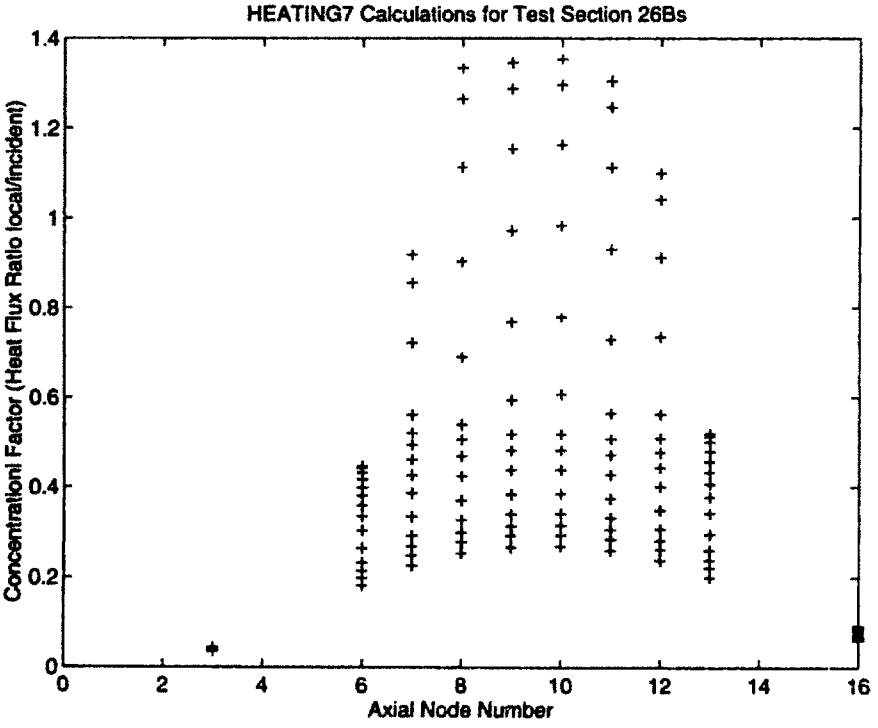

Figure G-54: Test Section 26B Axial Concentration Factor Profile

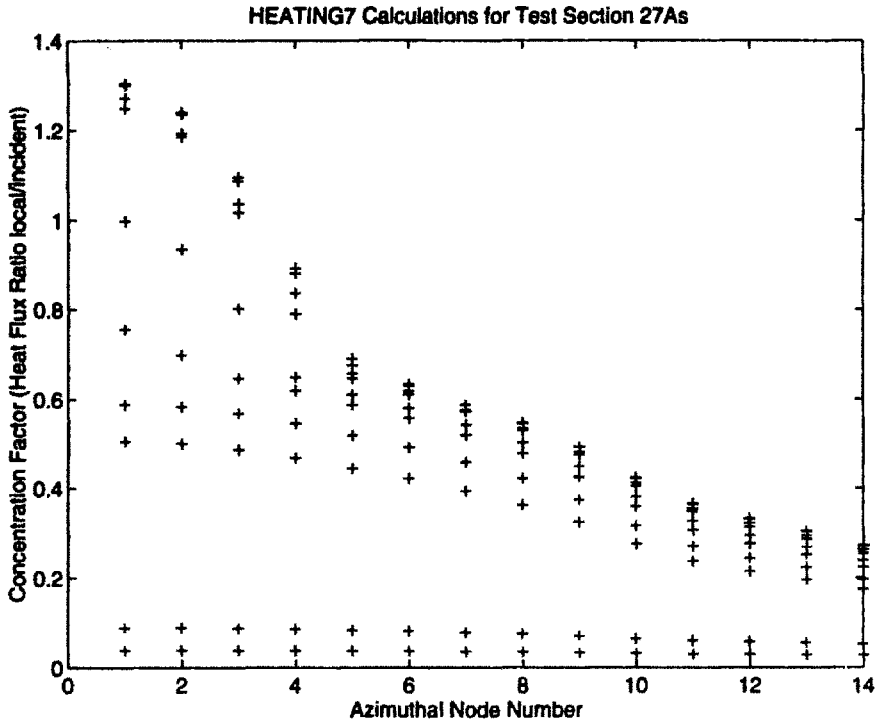

Figure G-55: Test Section 27A Azimuthal Concentration Factor Profile

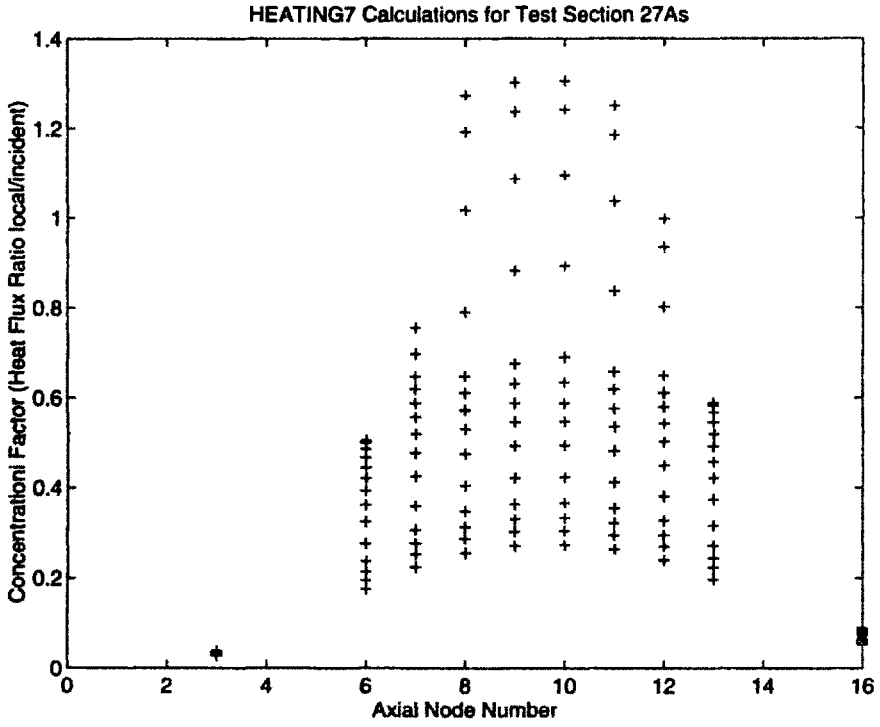

Figure G-56: Test Section 27A Axial Concentration Factor Profile

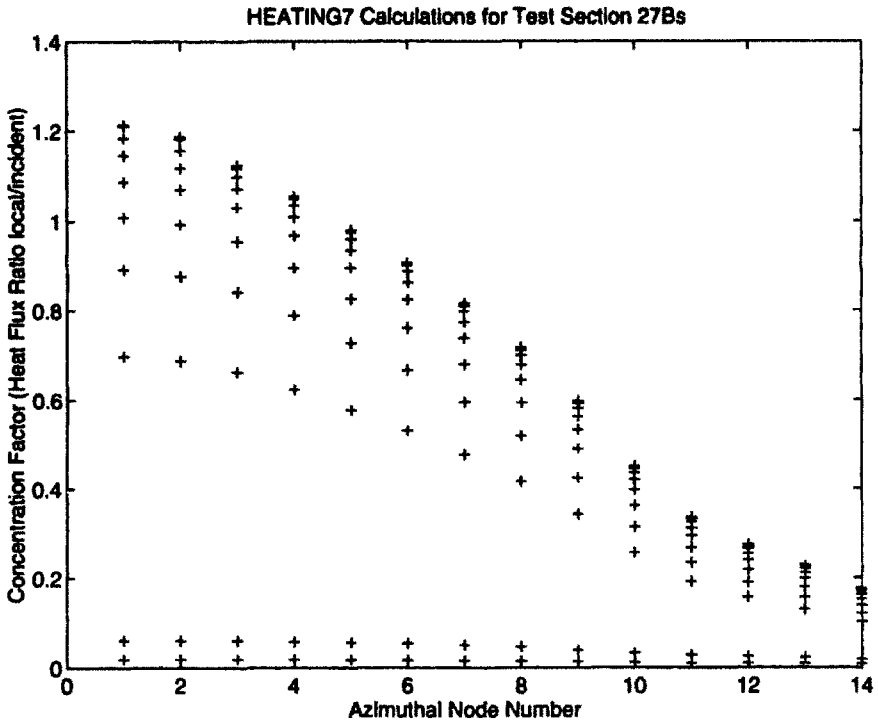

Figure G-57: Test Section 27B Azimuthal Concentration Factor Profile

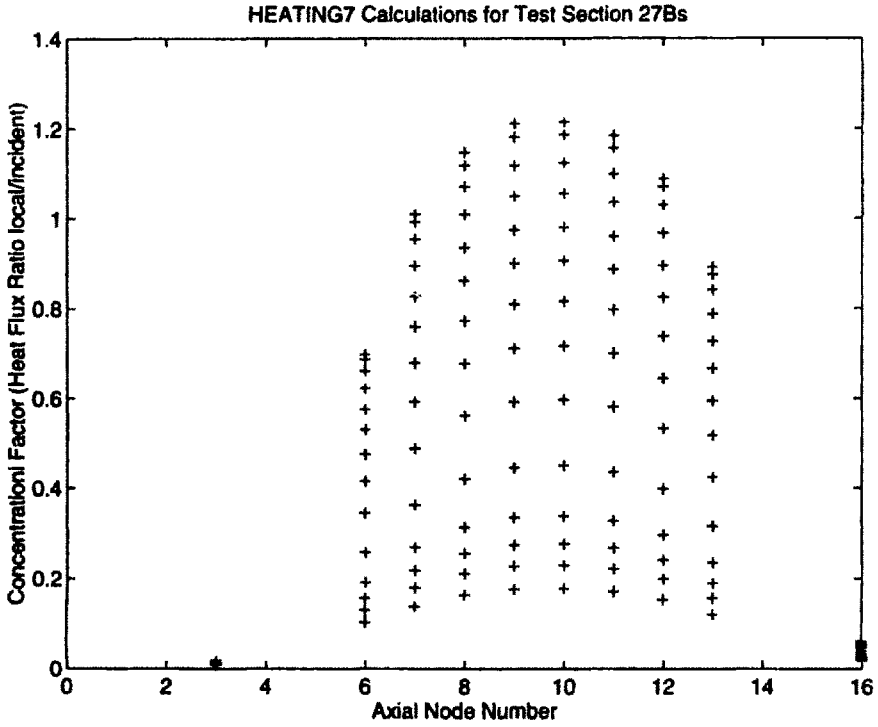

Figure G-58: Test Section 27B Axial Concentration Factor Profile

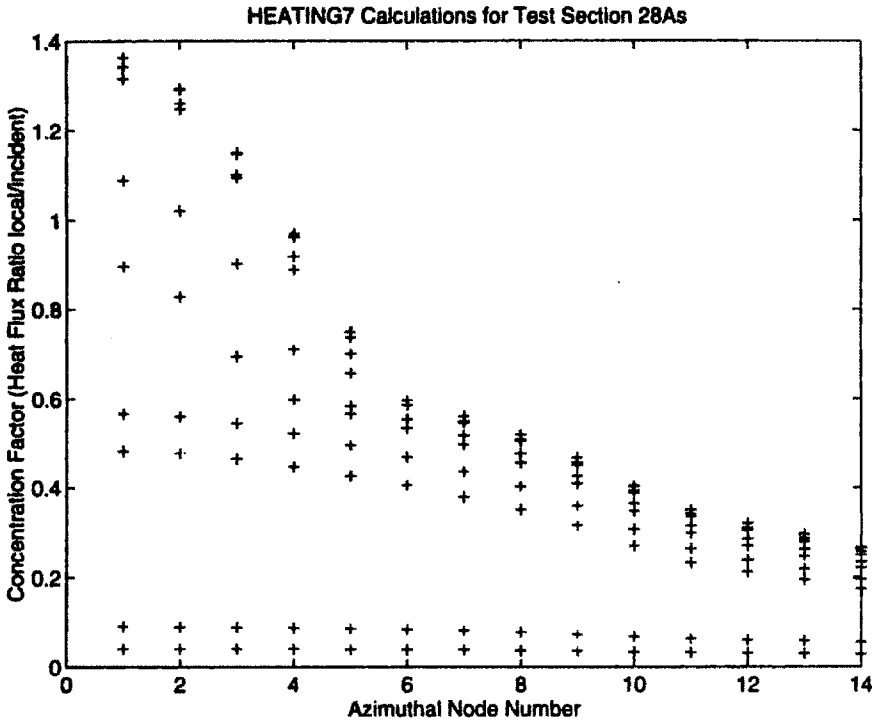

Figure G-59: Test Section 28A Azimuthal Concentration Factor Profile

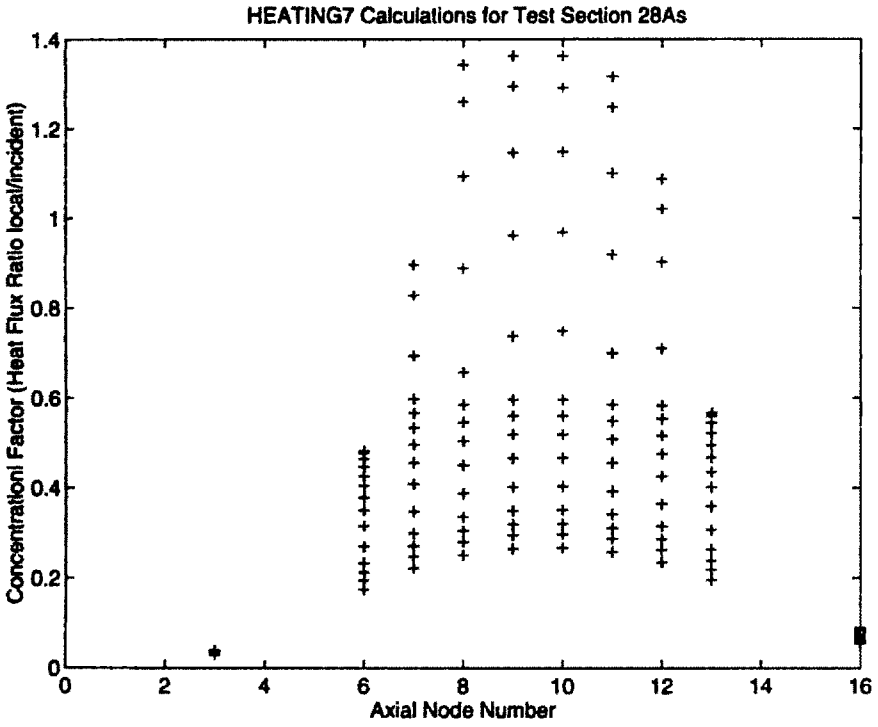

Figure G-60: Test Section 28A Axial Concentration Factor Profile

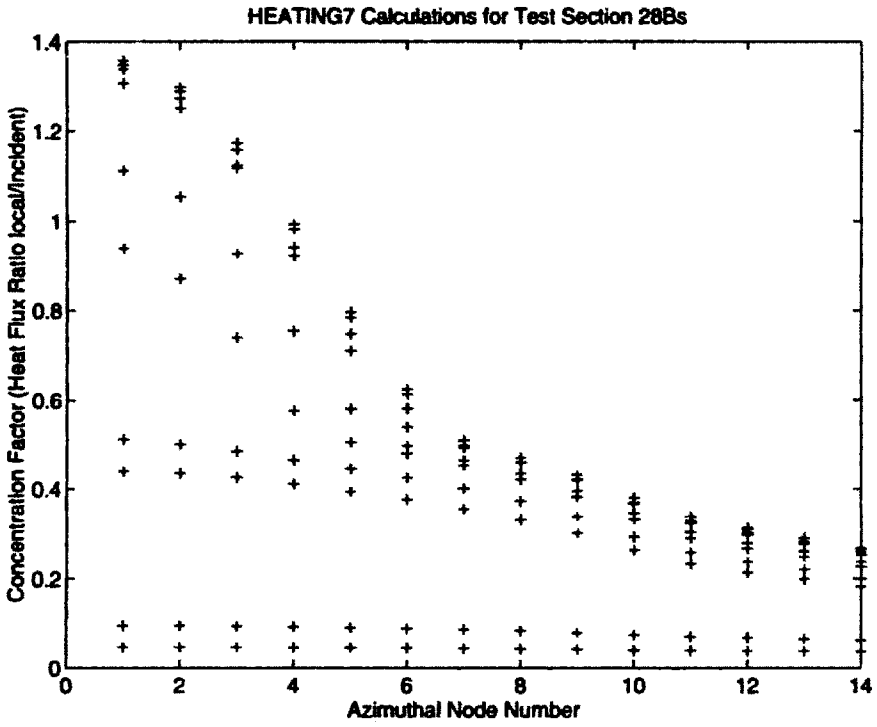

Figure G-61: Test Section 28B Azimuthal Concentration Factor Profile

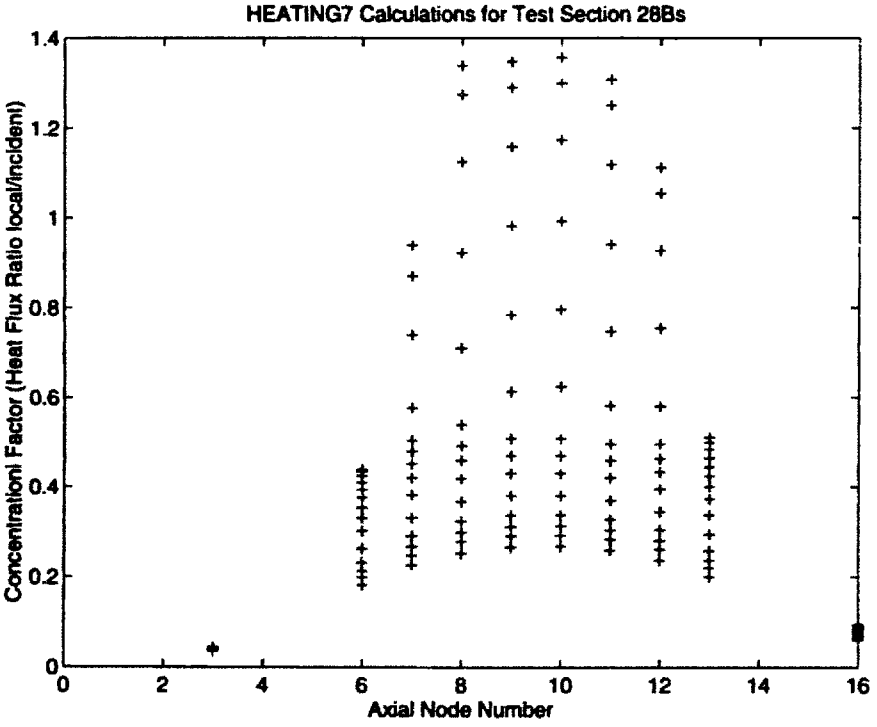

Figure G-62: Test Section 28B Axial Concentration Factor Profile

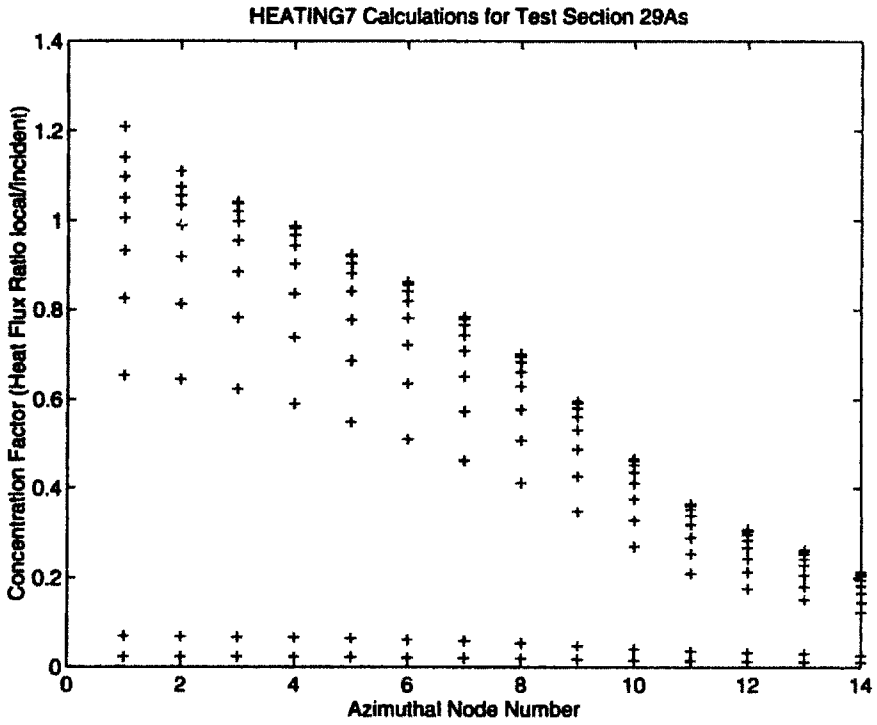

Figure G-63: Test Section 29A Azimuthal Concentration Factor Profile

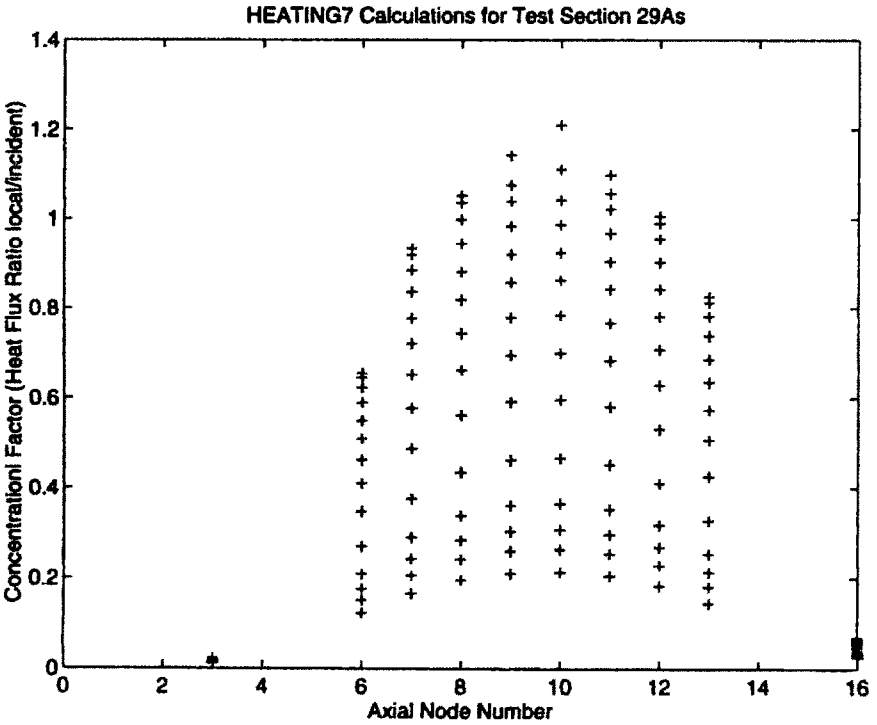

Figure G-64: Test Section 29A Axial Concentration Factor Profile

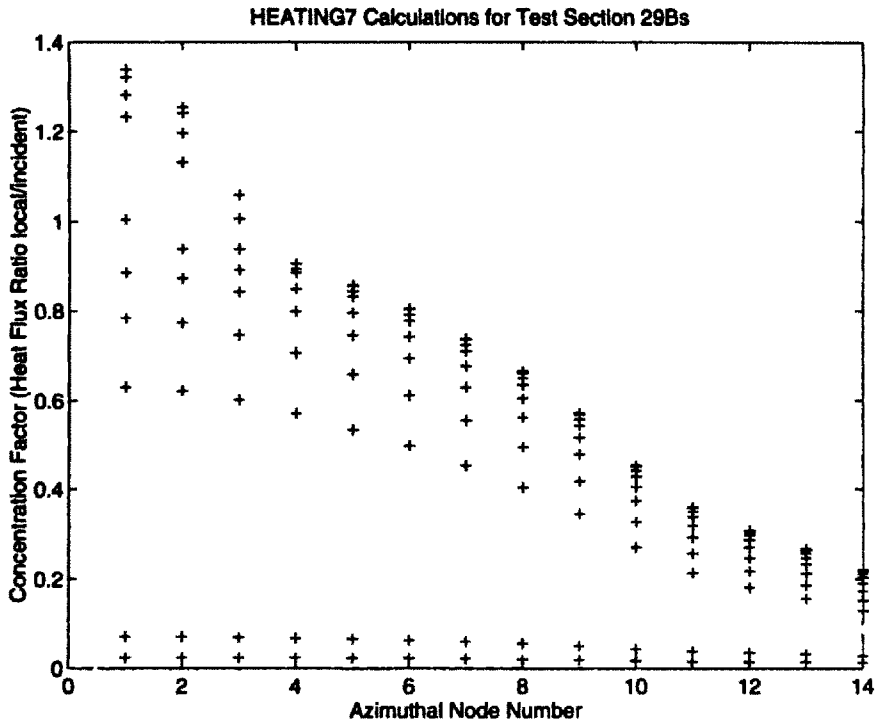

Figure G-65: Test Section 29B Azimuthal Concentration Factor Profile

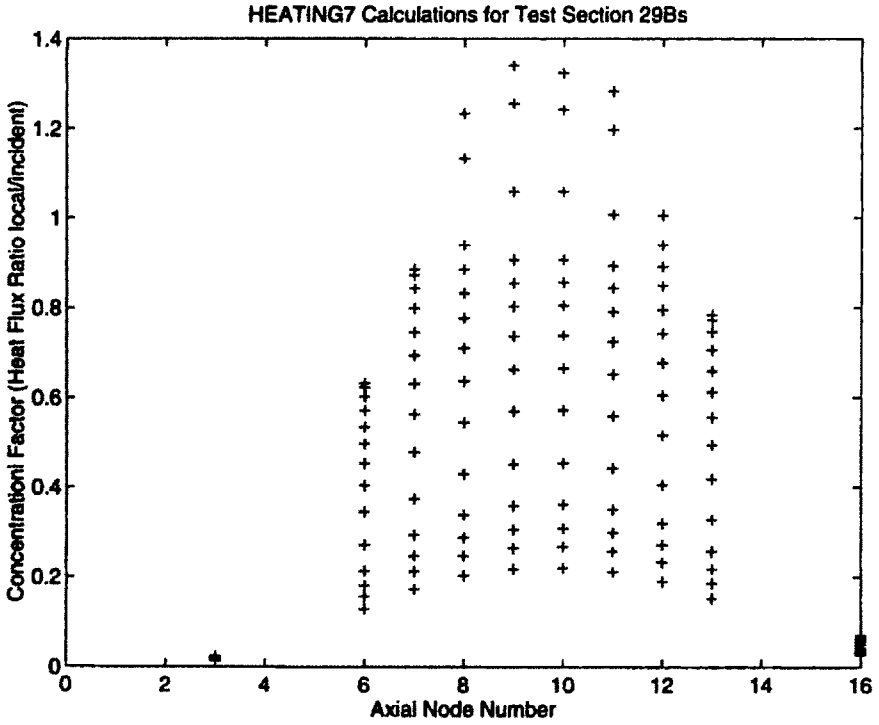

Figure G-66: Test Section 29B Axial Concentration Factor Profile

Appendix H

Data Reduction Results: Measured and Calculated Temperatures

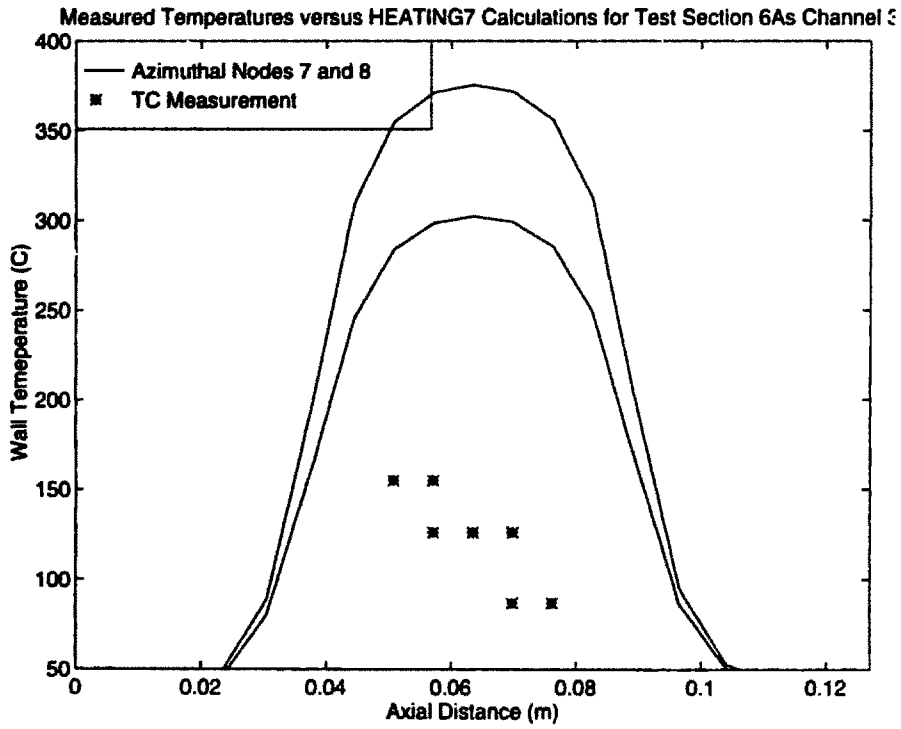

Figure H-1: Test Section 6As Channel 3 Comparison of Measured to Calculated Temperatures (Axial Direction)

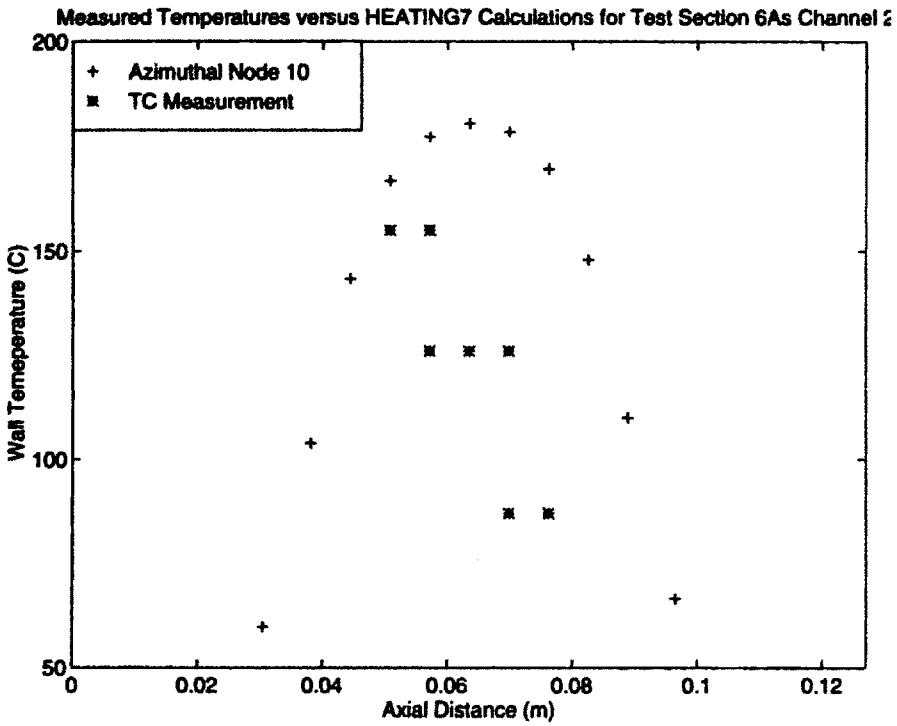

Figure H-2: Test Section 6As Channel 2 Comparison of Measured to Calculated Temperatures (Axial Direction)

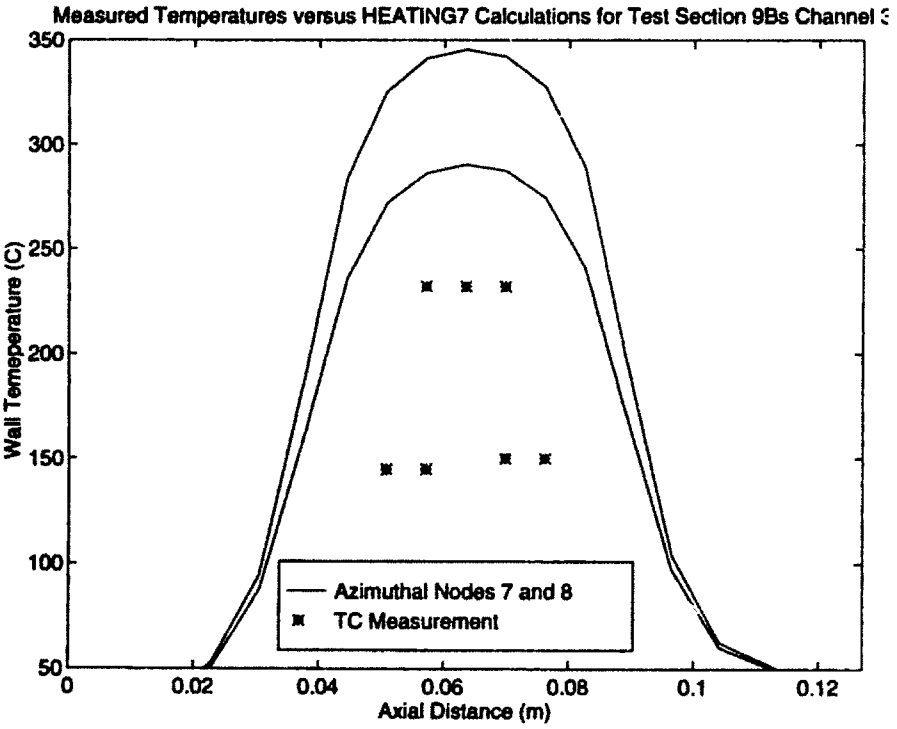

Figure H-3: Test Section 9Bs Channel 3 Comparison of Measured to Calculated Temperatures (Axial Direction)

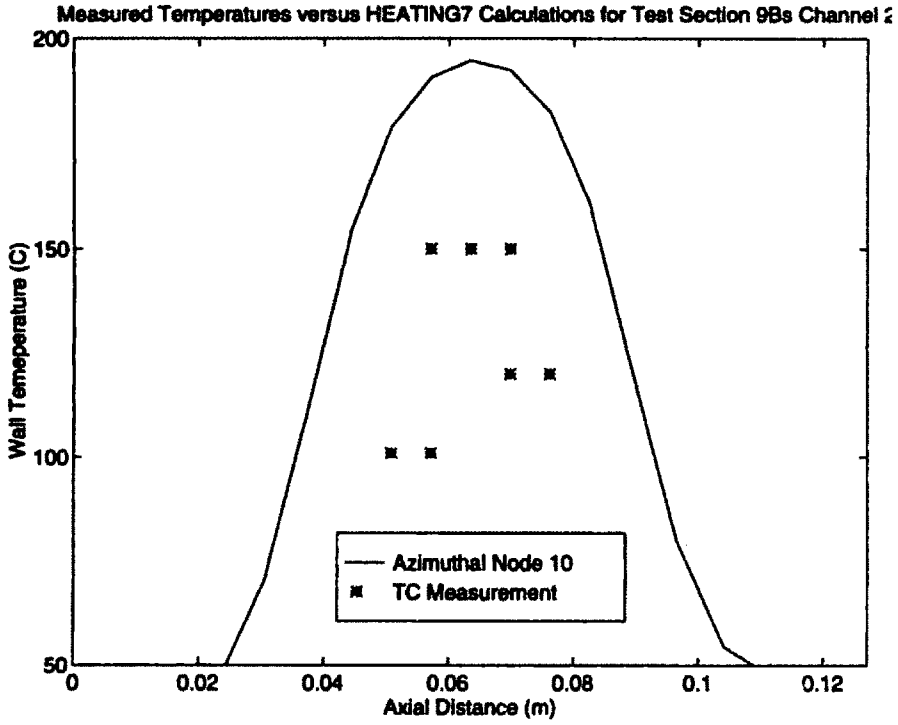

Figure H-4: Test Section 9Bs Channel 2 Comparison of Measured to Calculated Temperatures (Axial Direction)

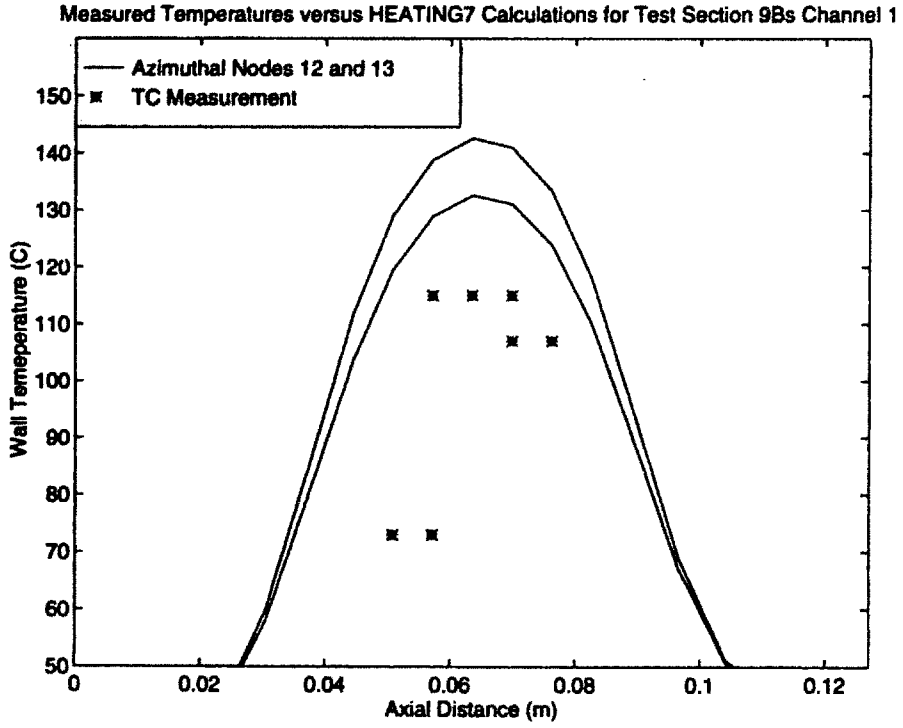

Figure H-5: Test Section 9Bs Channel 1 Comparison of Measured to Calculated Temperatures (Axial Direction)

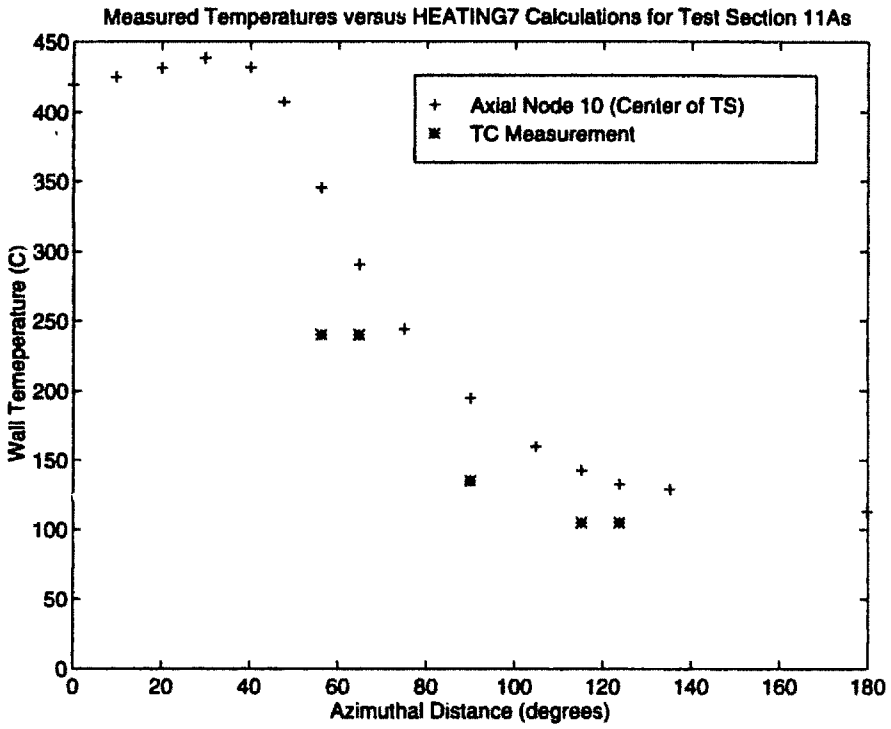

Figure H-6: Test Section 11As Comparison of Measured to Calculated Temperatures (Azimuthal Direction)

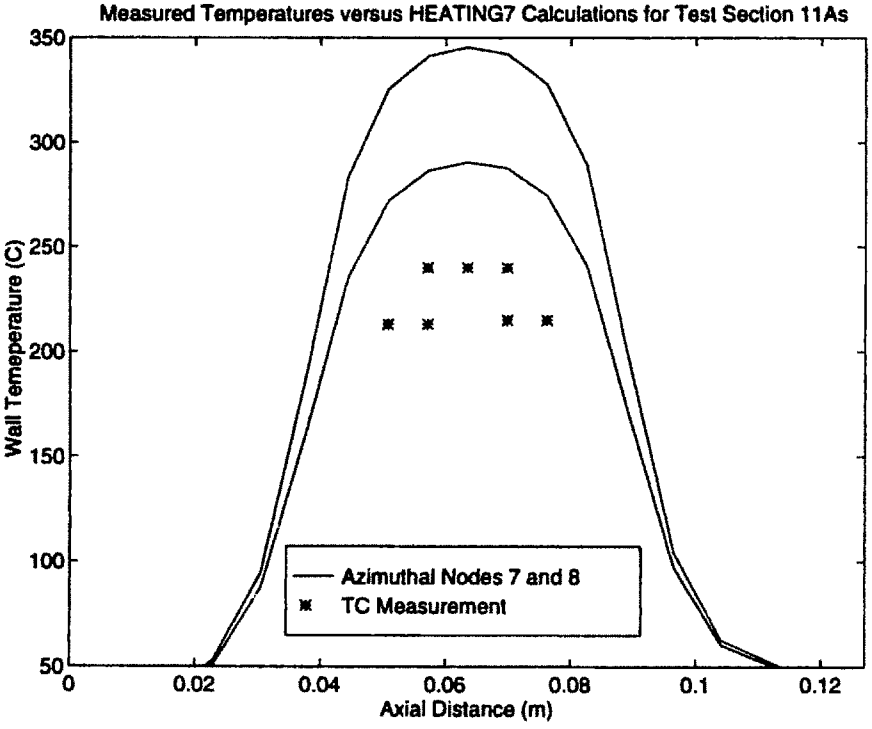

Figure H-7: Test Section 11As Comparison of Measured to Calculated Temperatures (Axial Direction)

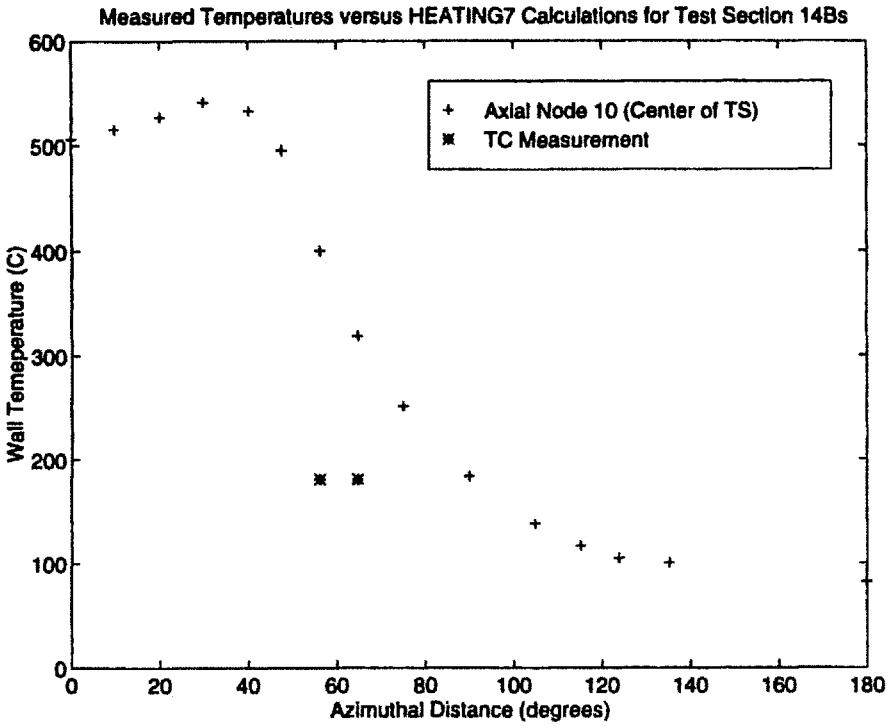

Figure H-8: Test Section 14B Comparison of Measured to Calculated Temperatures (Azimuthal Direction)

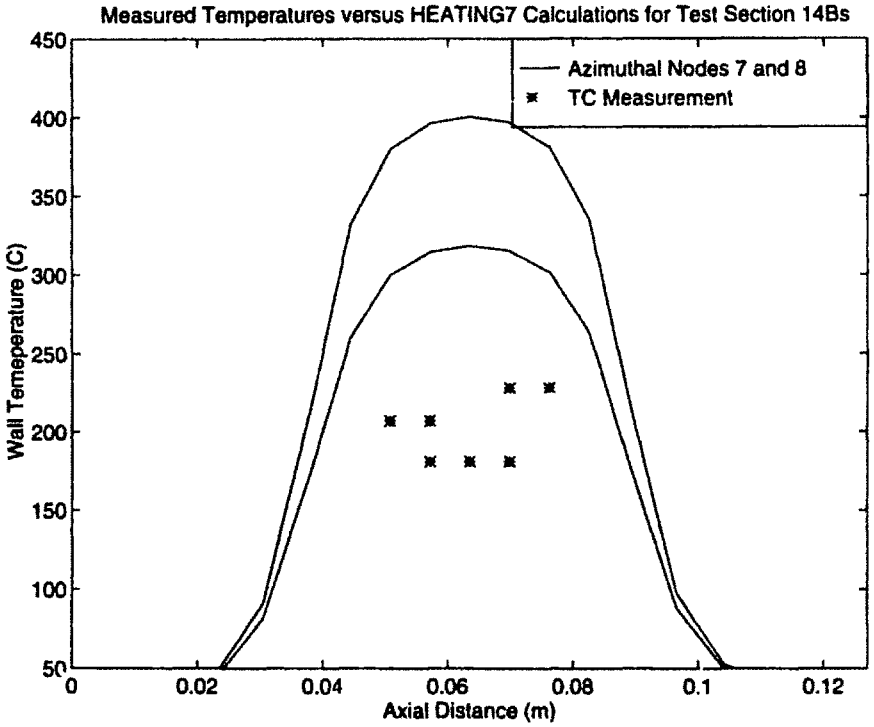

Figure H-9: Test Section 14B Comparison of Measured to Calculated Temperatures (Axial Direction)

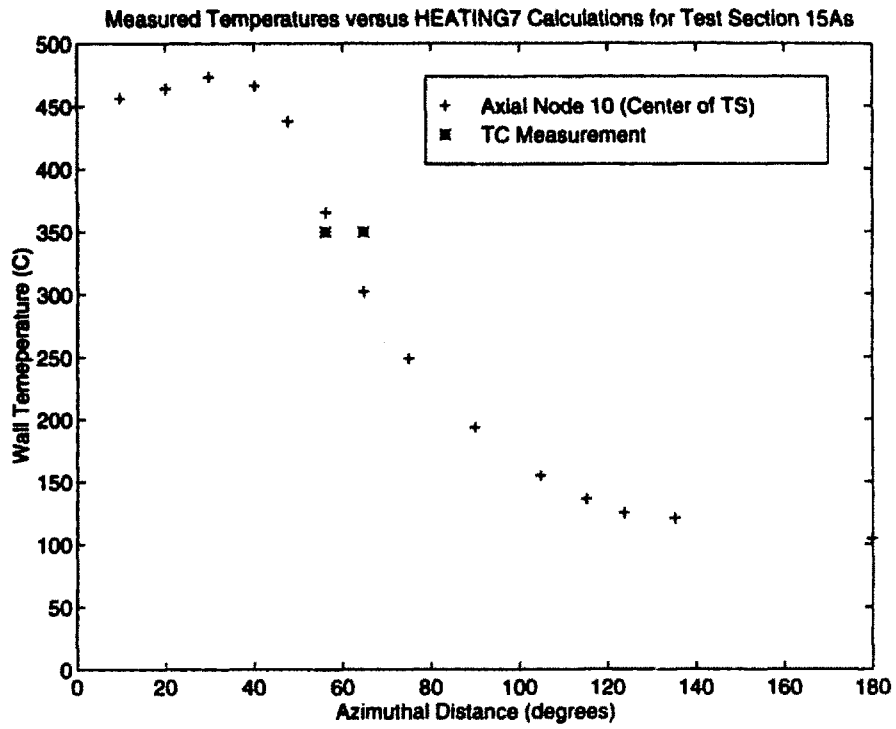

Figure H-10: Test Section 15A Comparison of Measured to Calculated Temperatures (Azimuthal Direction)

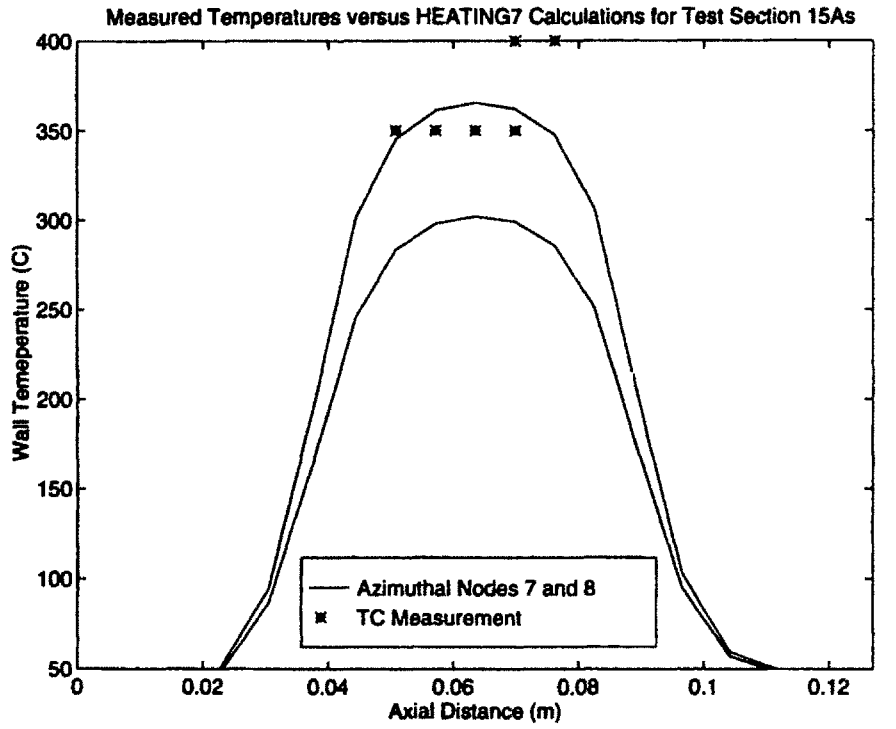

Figure H-11: Test Section 15A Comparison of Measured to Calculated Temperatures (Axial Direction)

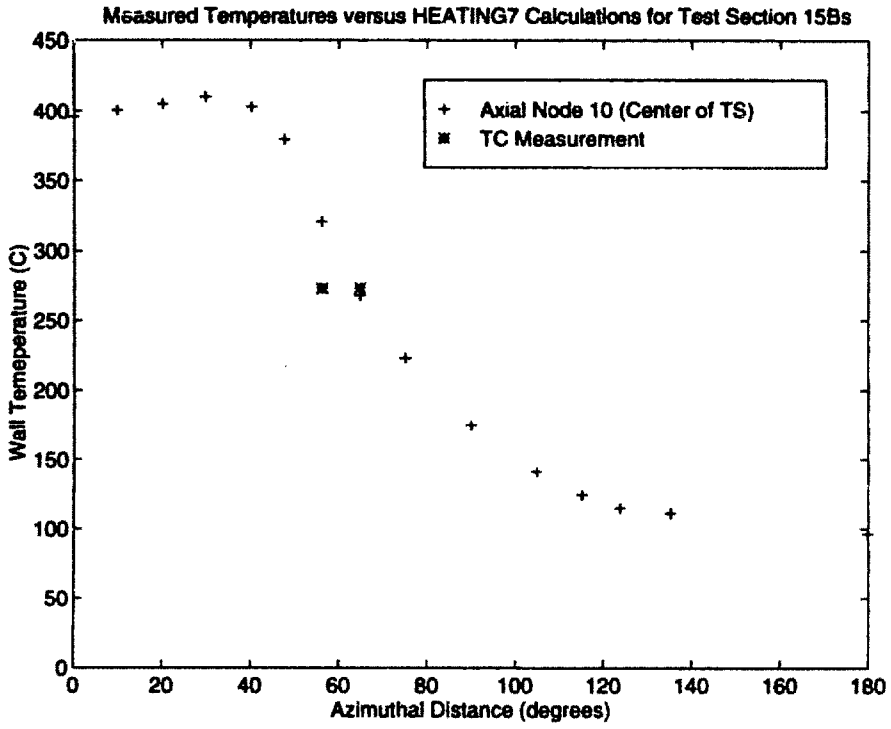

Figure H-12: Test Section 15B Comparison of Measured to Calculated Temperatures (Azimuthal Direction)

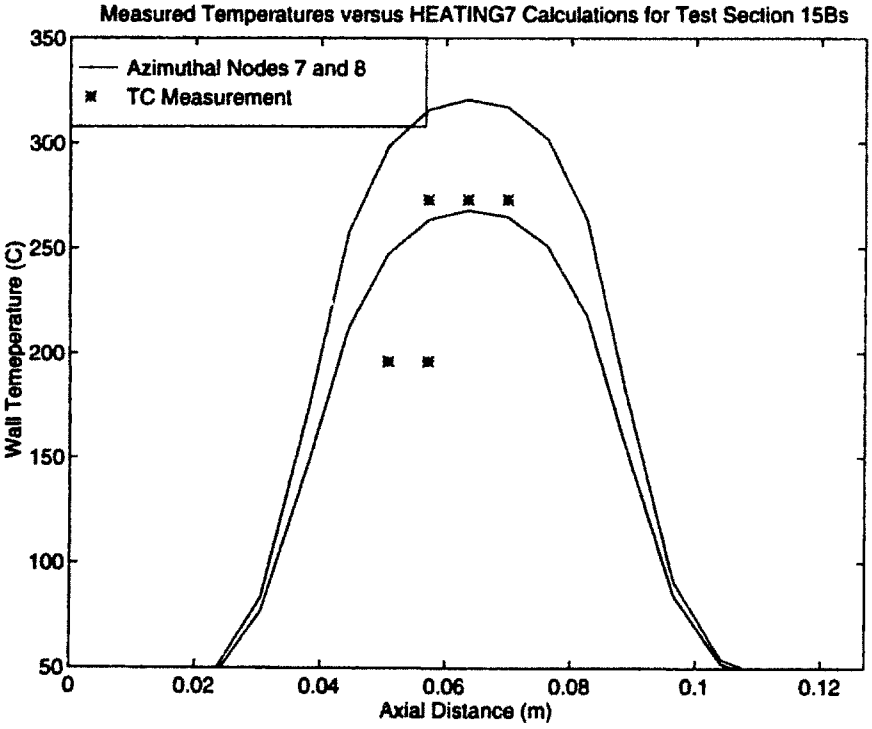

Figure H-13: Test Section 15B Comparison of Measured to Calculated Temperatures (Axial Direction)

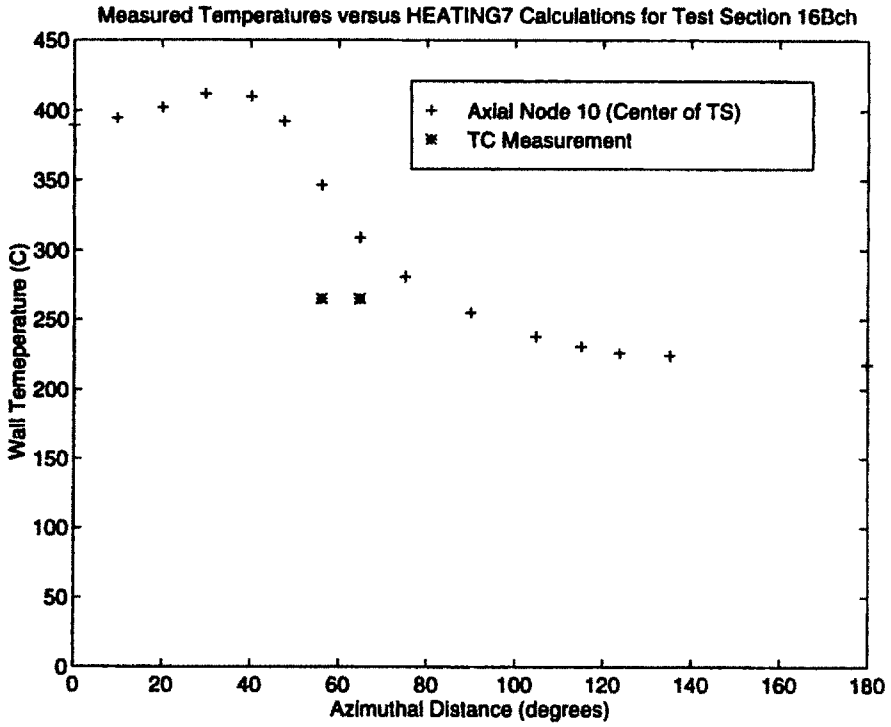

Figure H-14: Test Section 16B^{ch} Comparison of Measured to Calculated Temperatures (Azimuthal Direction)

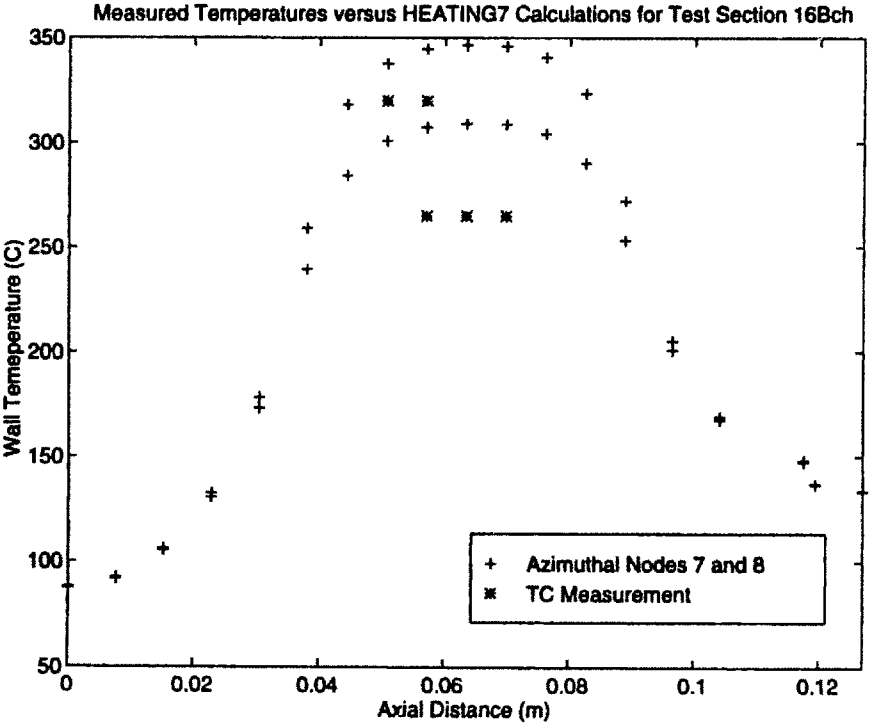

Figure H-15: Test Section 16B^{ch} Comparison of Measured to Calculated Temperatures (Axial Direction)

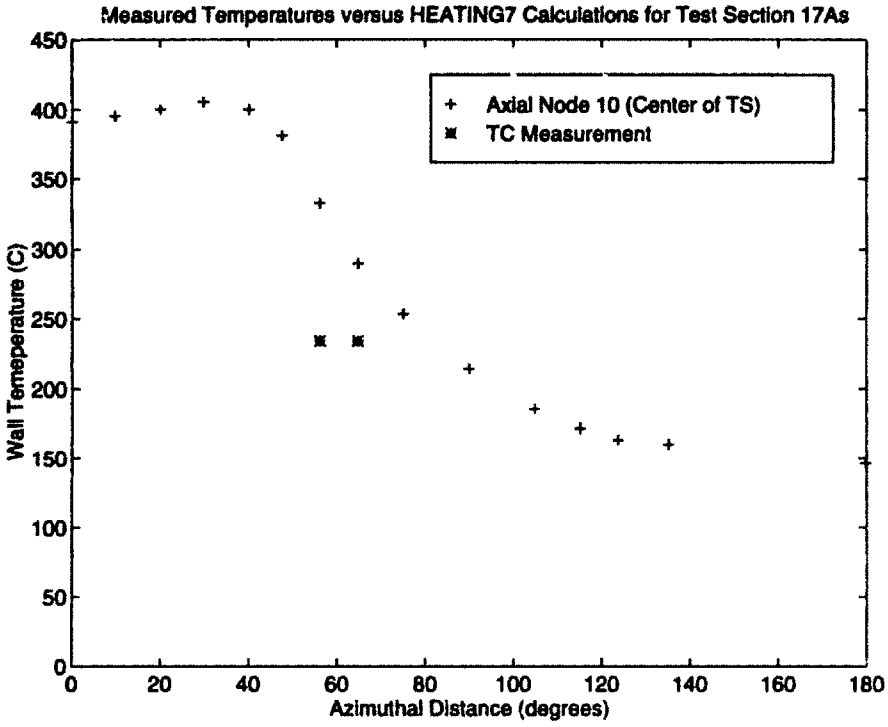

Figure H-16: Test Section 17A Comparison of Measured to Calculated Temperatures (Azimuthal Direction)

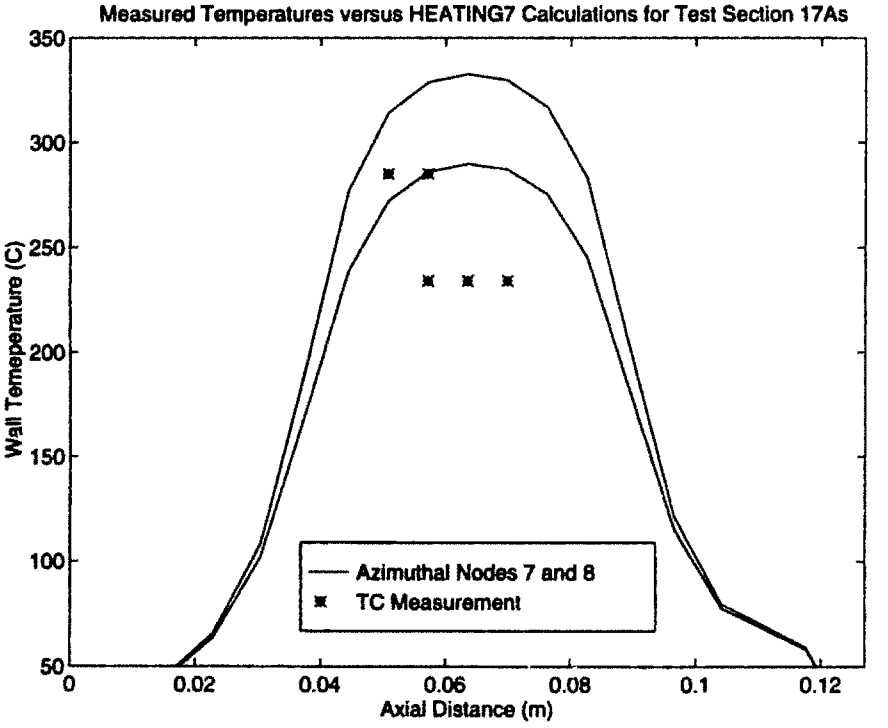

Figure H-17: Test Section 17A Comparison of Measured to Calculated Temperatures (Axial Direction)

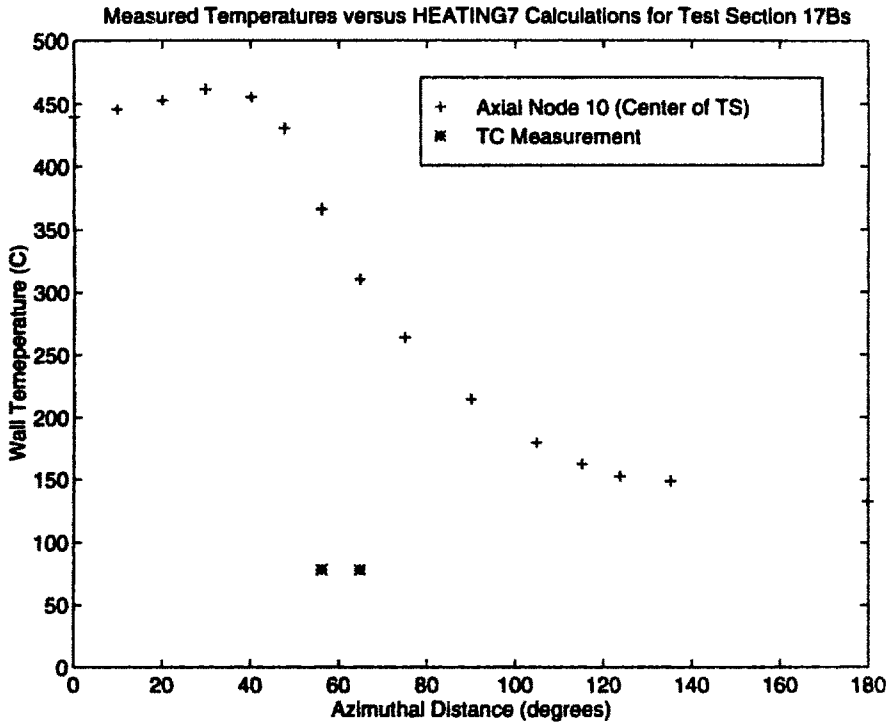

Figure H-18: Test Section 17B Comparison of Measured to Calculated Temperatures (Azimuthal Direction)

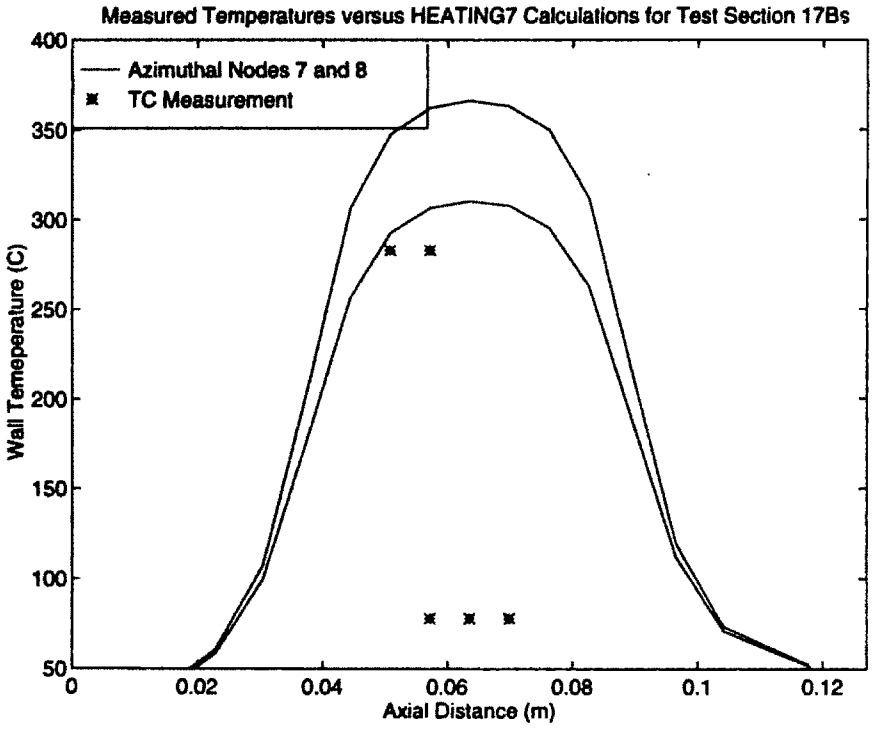

Figure H-19: Test Section 17B Comparison of Measured to Calculated Temperatures (Axial Direction)

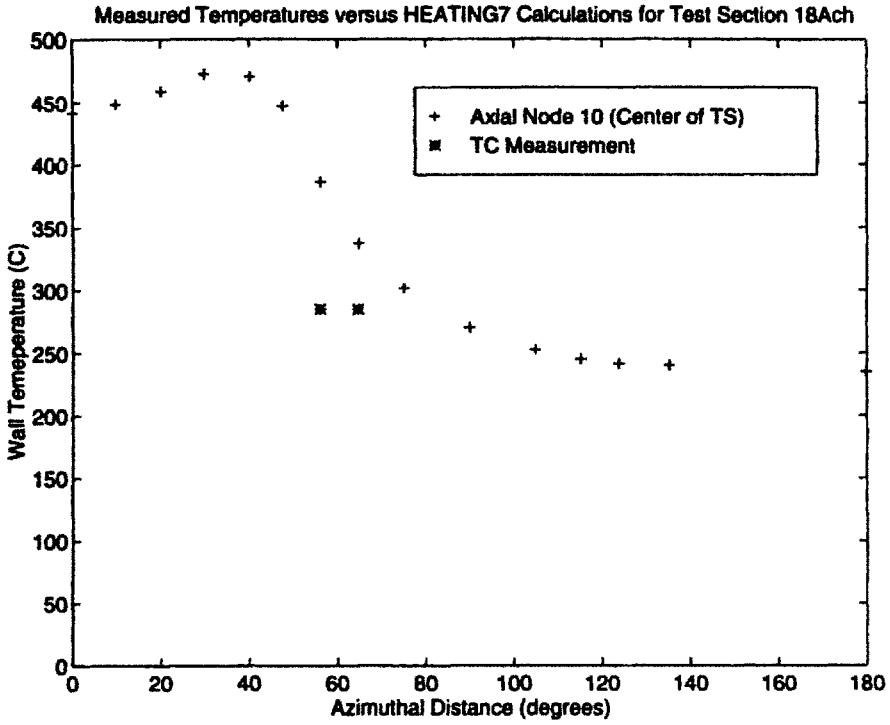

Figure H-20: Test Section 18A^{ch} Comparison of Measured to Calculated Temperatures (Azimuthal Direction)

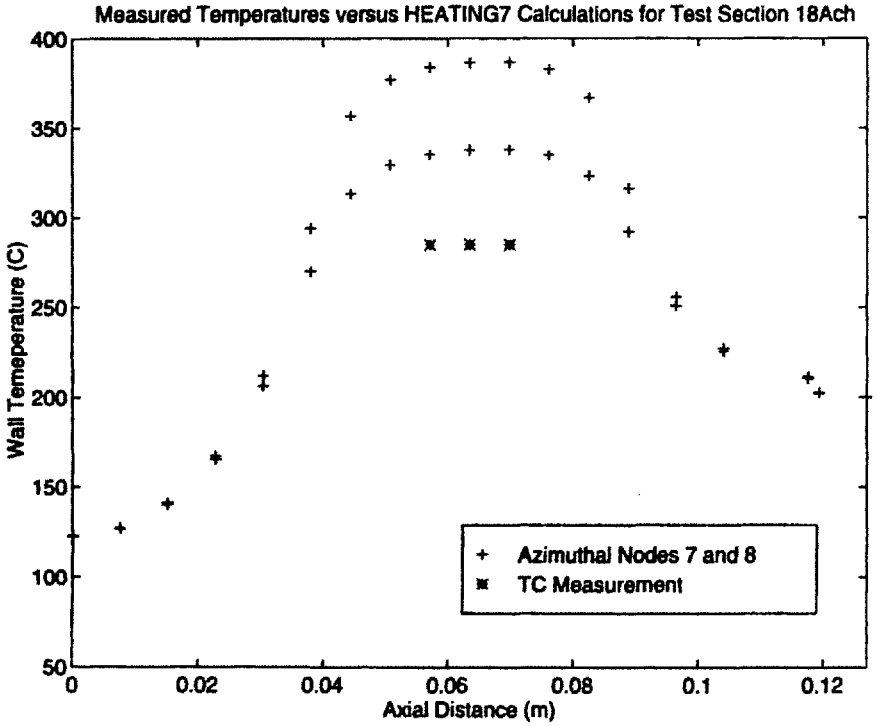

Figure H-21: Test Section 18A^{ch} Comparison of Measured to Calculated Temperatures (Axial Direction)

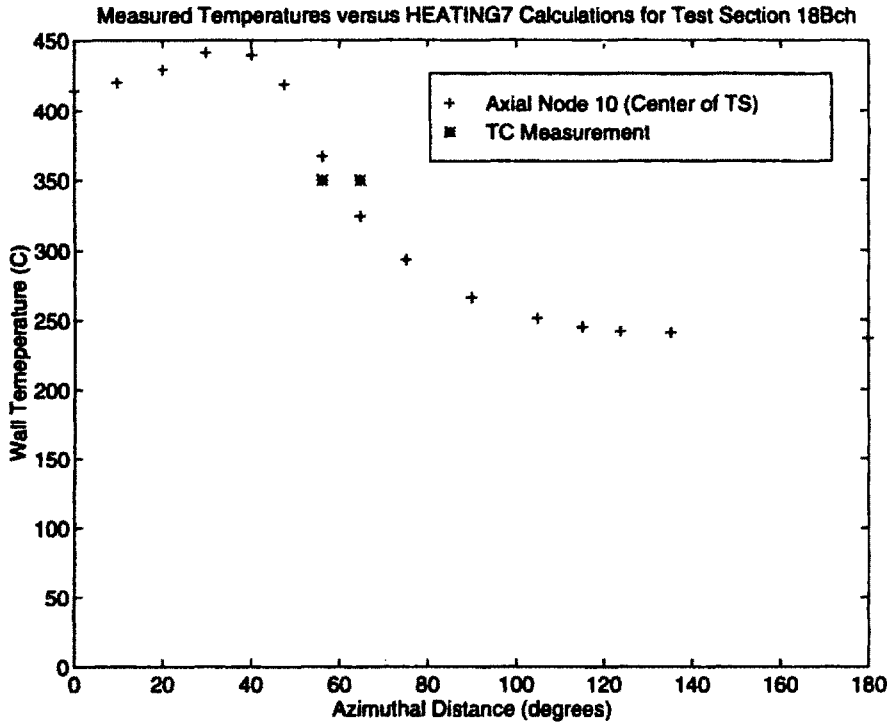

Figure H-22: Test Section 18B^{ch} Comparison of Measured to Calculated Temperatures (Azimuthal Direction)

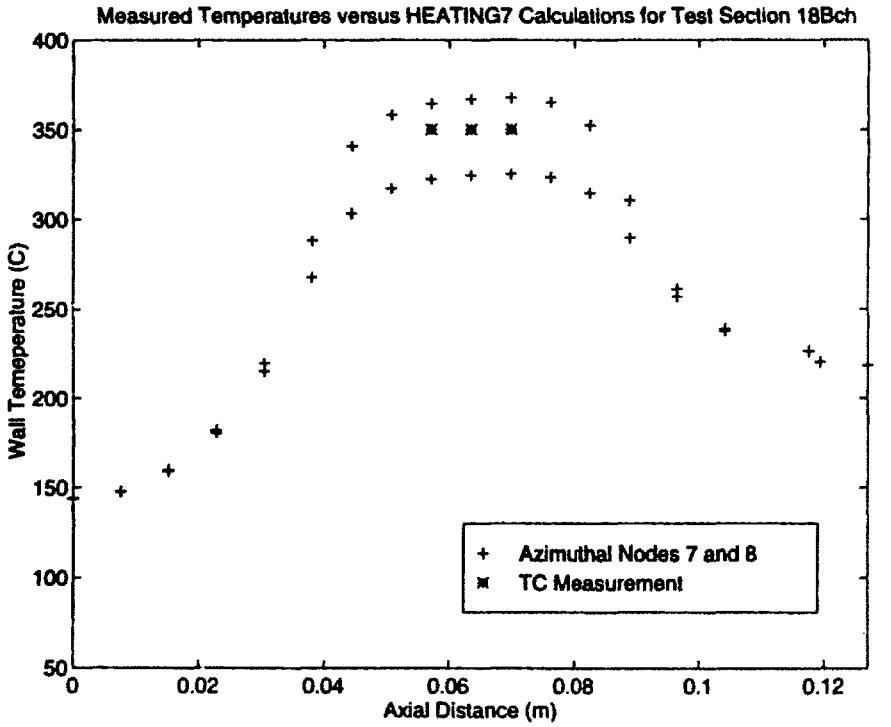

Figure H-23: Test Section 18B^{ch} Comparison of Measured to Calculated Temperatures (Axial Direction)

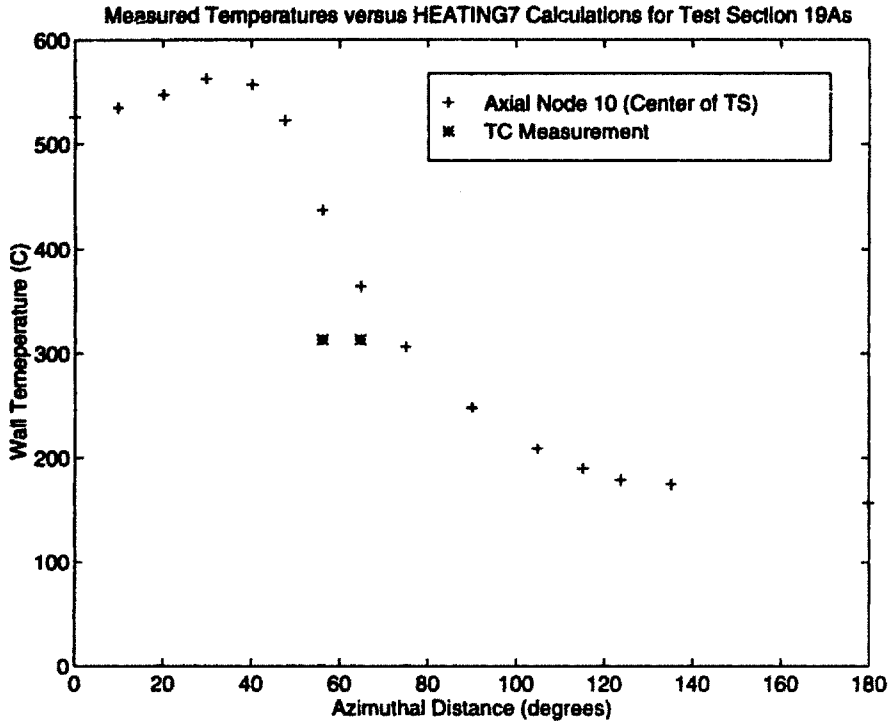

Figure H-24: Test Section 19A Comparison of Measured to Calculated Temperatures (Azimuthal Direction)

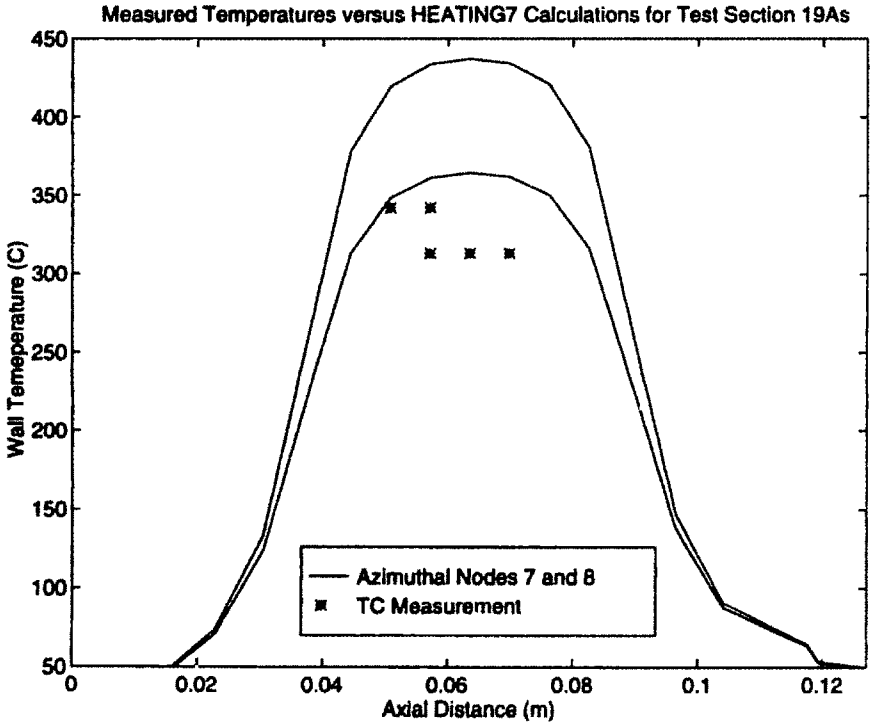

Figure H-25: Test Section 19A Comparison of Measured to Calculated Temperatures (Axial Direction)

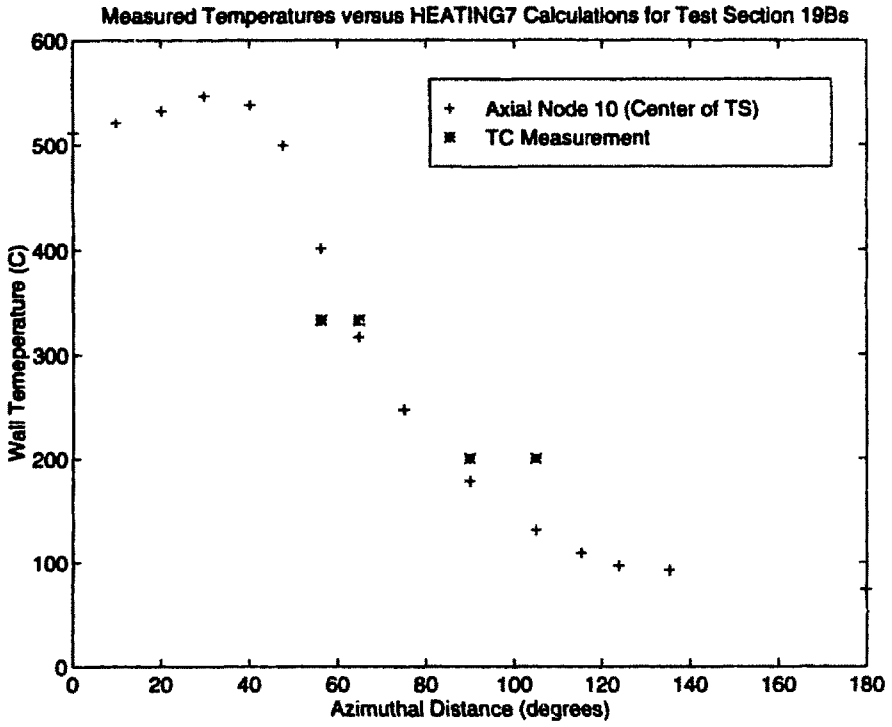

Figure H-26: Test Section 19B Comparison of Measured to Calculated Temperatures (Azimuthal Direction)

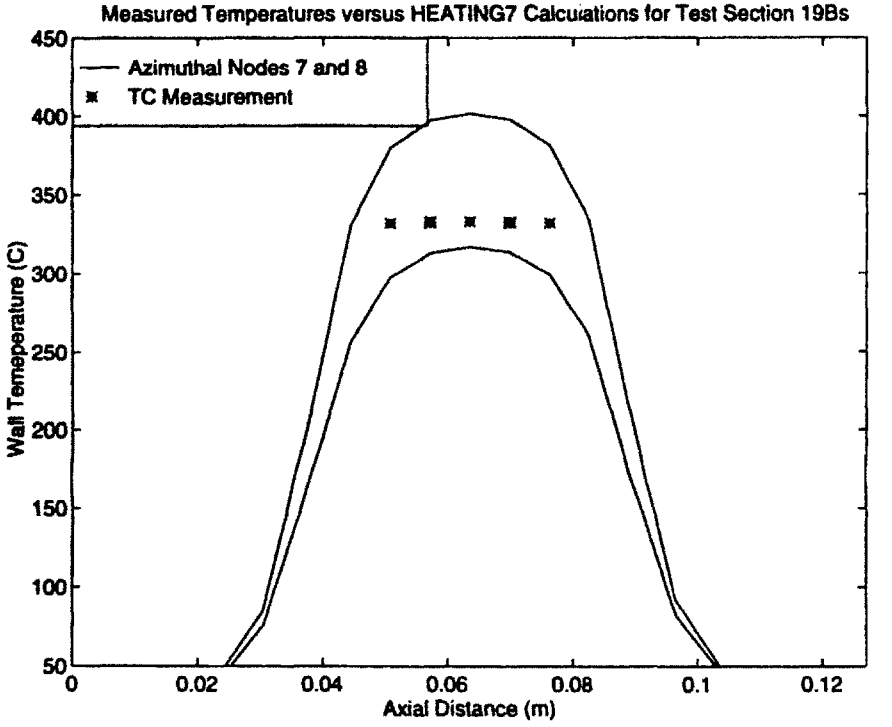

Figure H-27: Test Section 19B Comparison of Measured to Calculated Temperatures (Axial Direction)

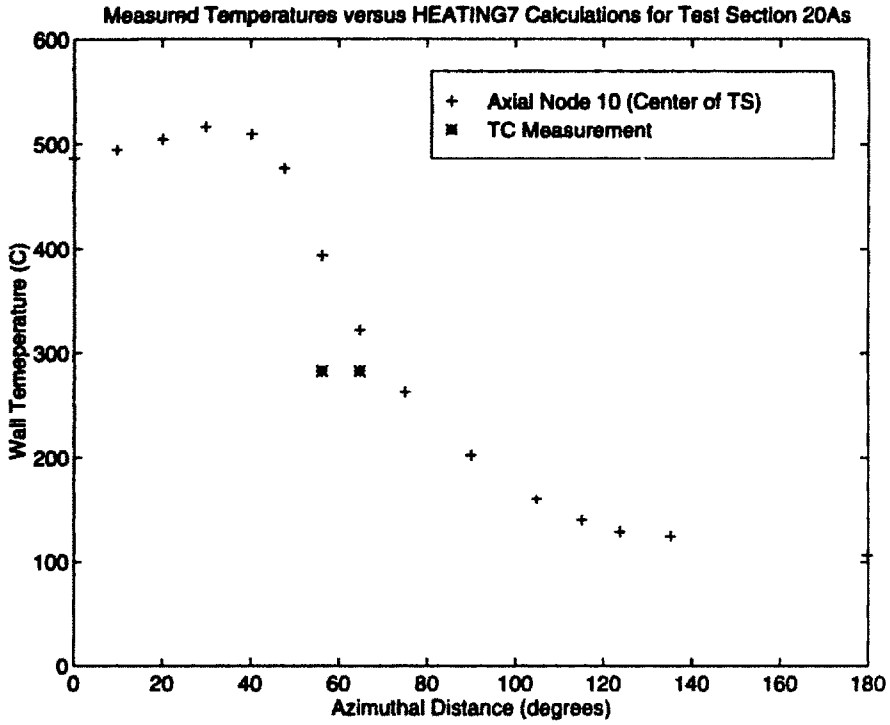

Figure H-28: Test Section 20A Comparison of Measured to Calculated Temperatures (Azimuthal Direction)

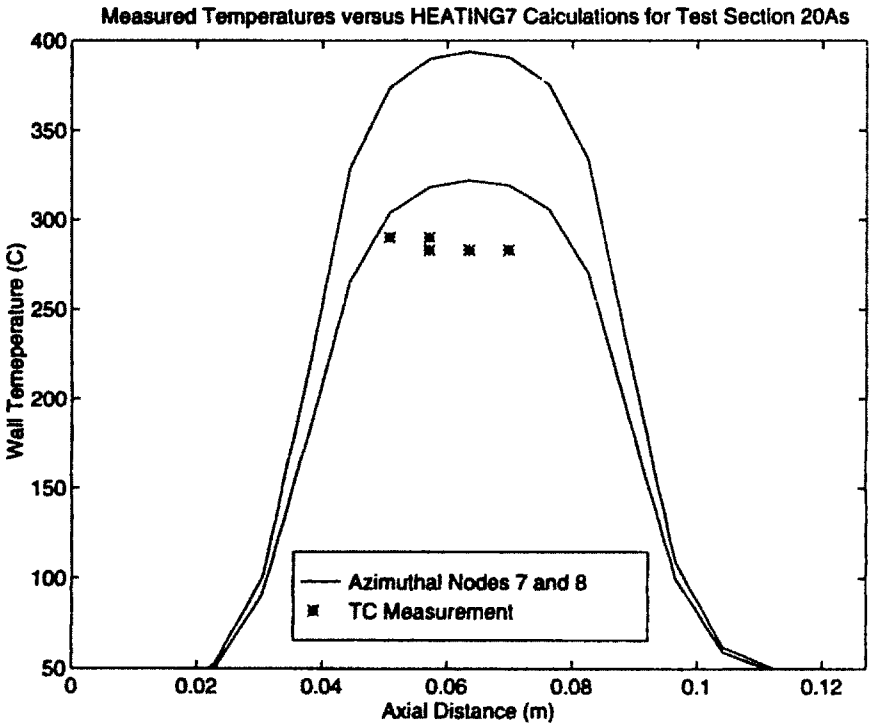

Figure H-29: Test Section 20A Comparison of Measured to Calculated Temperatures (Axial Direction)

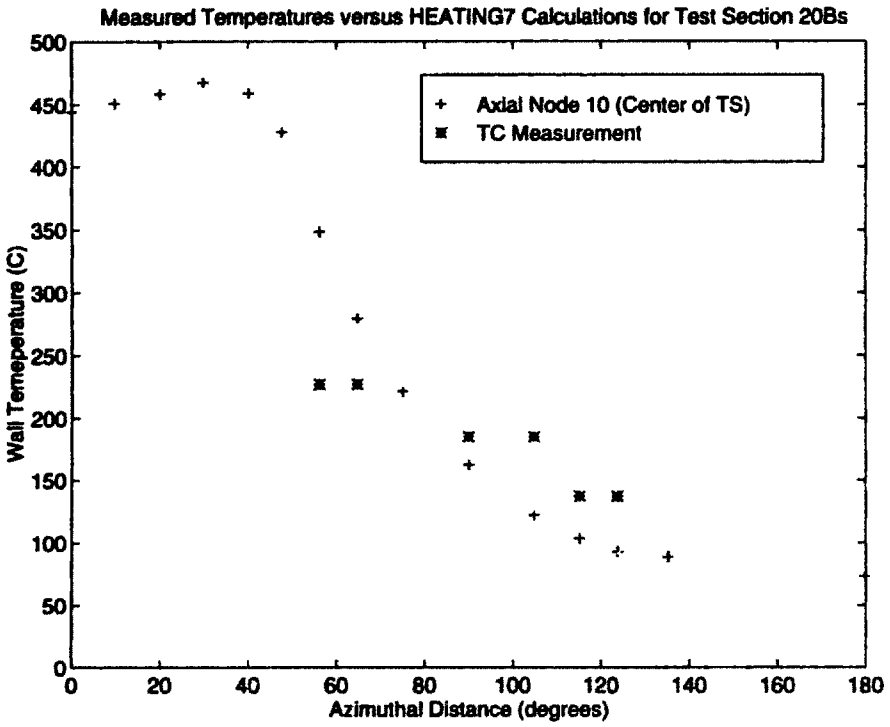

Figure H-30: Test Section 20B Comparison of Measured to Calculated Temperatures (Azimuthal Direction)

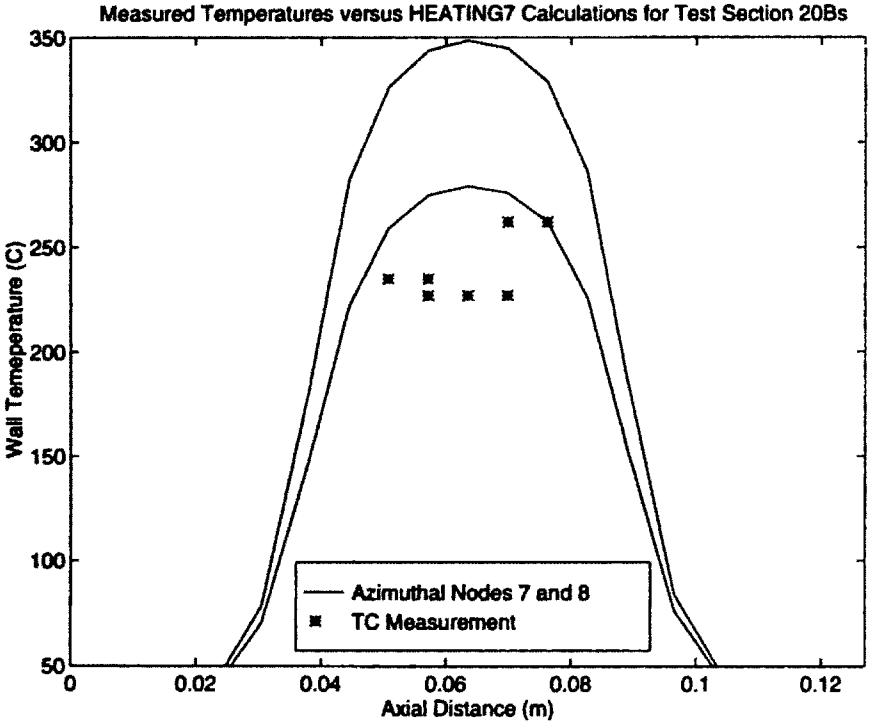

Figure H-31: Test Section 20B Comparison of Measured to Calculated Temperatures (Axial Direction)

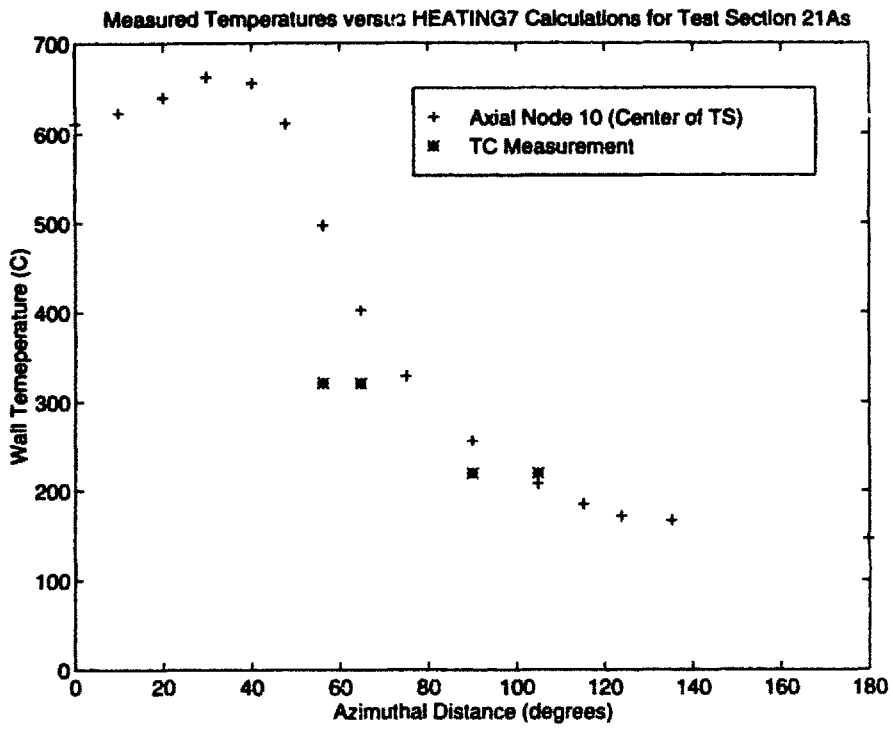

Figure H-32: Test Section 21A Comparison of Measured to Calculated Temperatures (Azimuthal Direction)

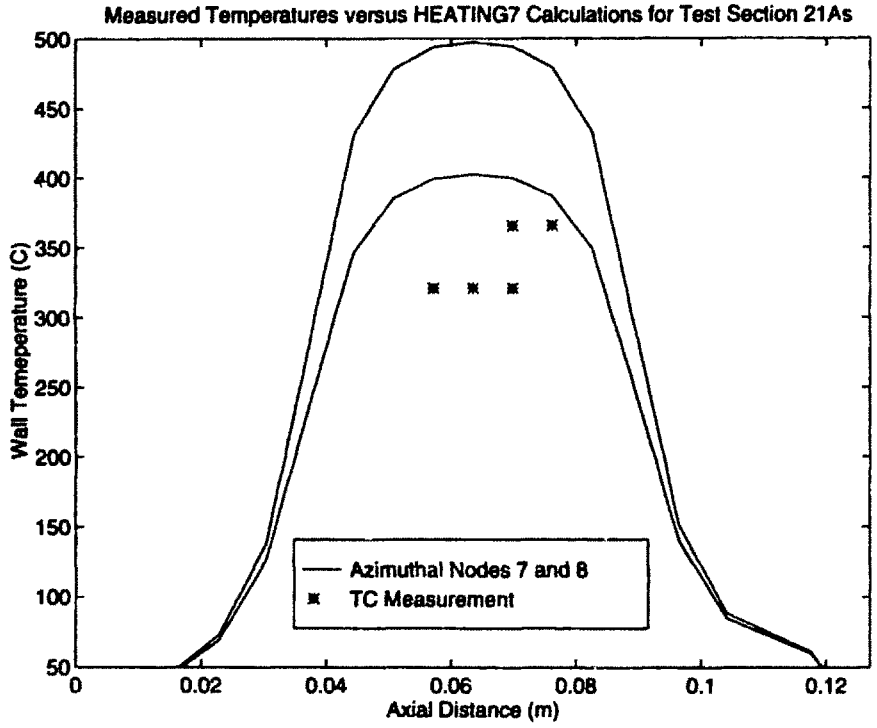

Figure H-33: Test Section 21A Comparison of Measured to Calculated Temperatures (Axial Direction)

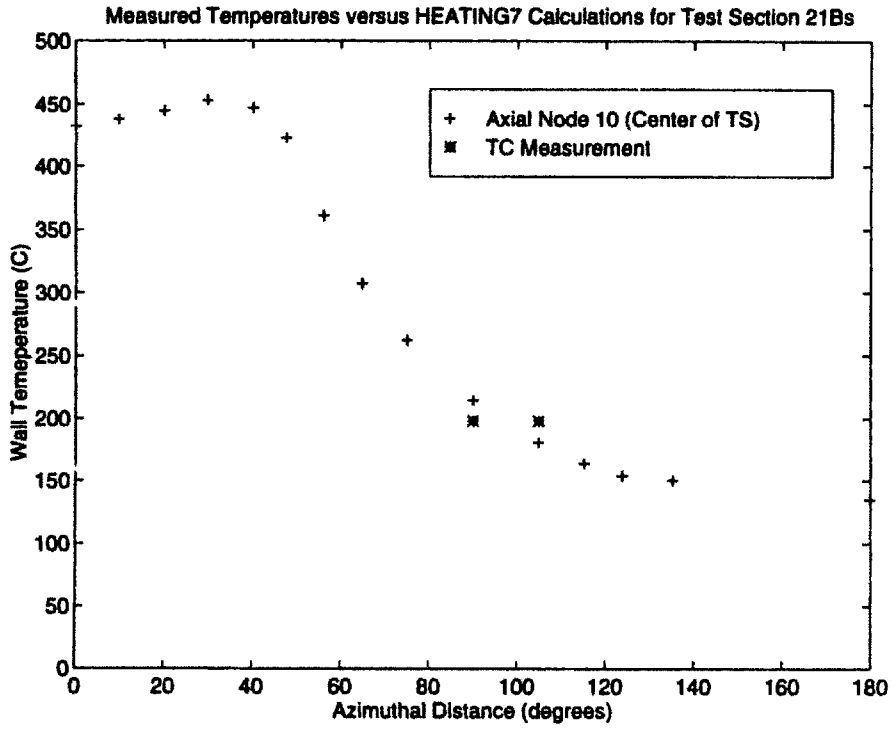

Figure H-34: Test Section 21B Comparison of Measured to Calculated Temperatures (Azimuthal Direction)

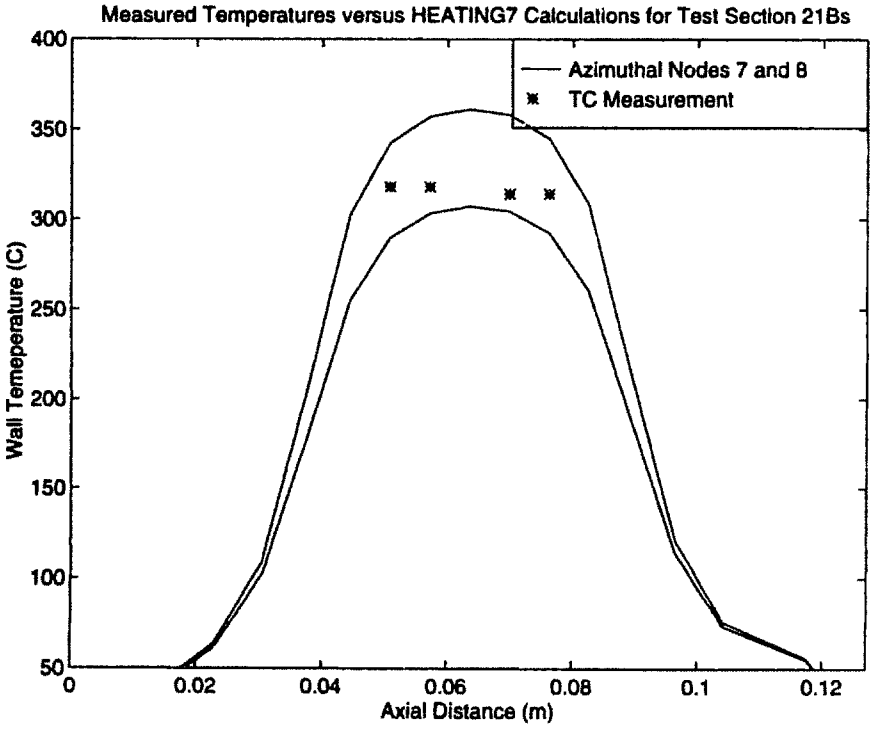

Figure H-35: Test Section 21B Comparison of Measured to Calculated Temperatures (Axial Direction)

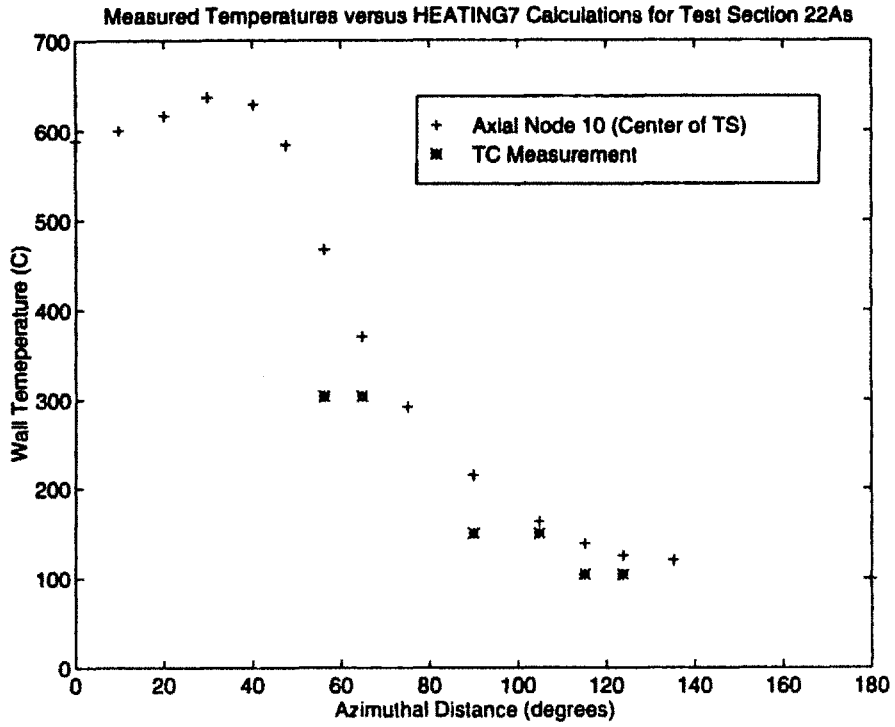

Figure H-36: Test Section 22A Comparison of Measured to Calculated Temperatures (Azimuthal Direction)

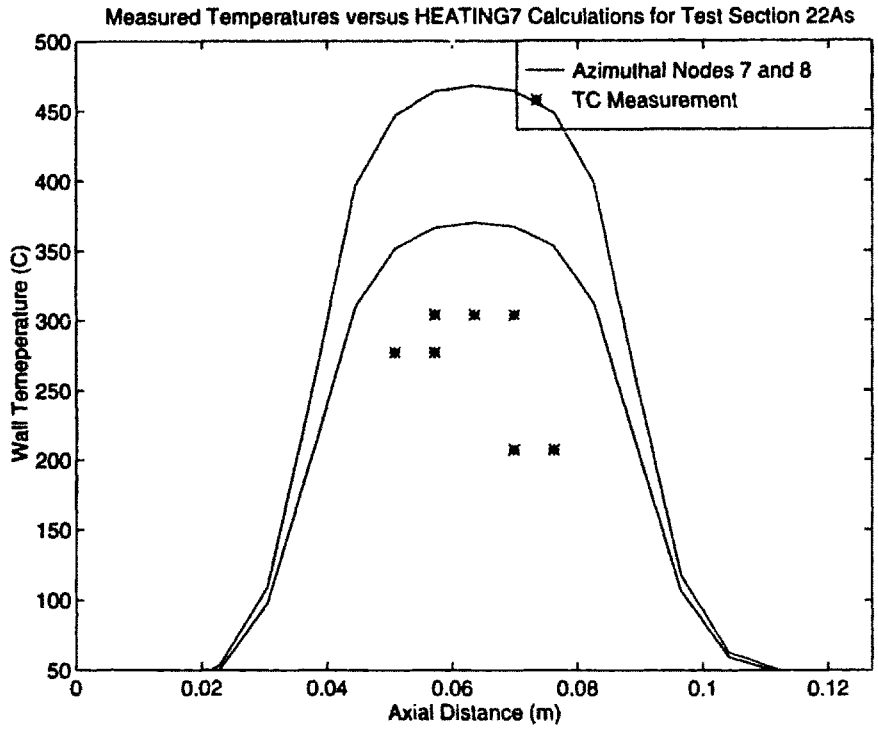

Figure H-37: Test Section 22A Comparison of Measured to Calculated Temperatures (Axial Direction)

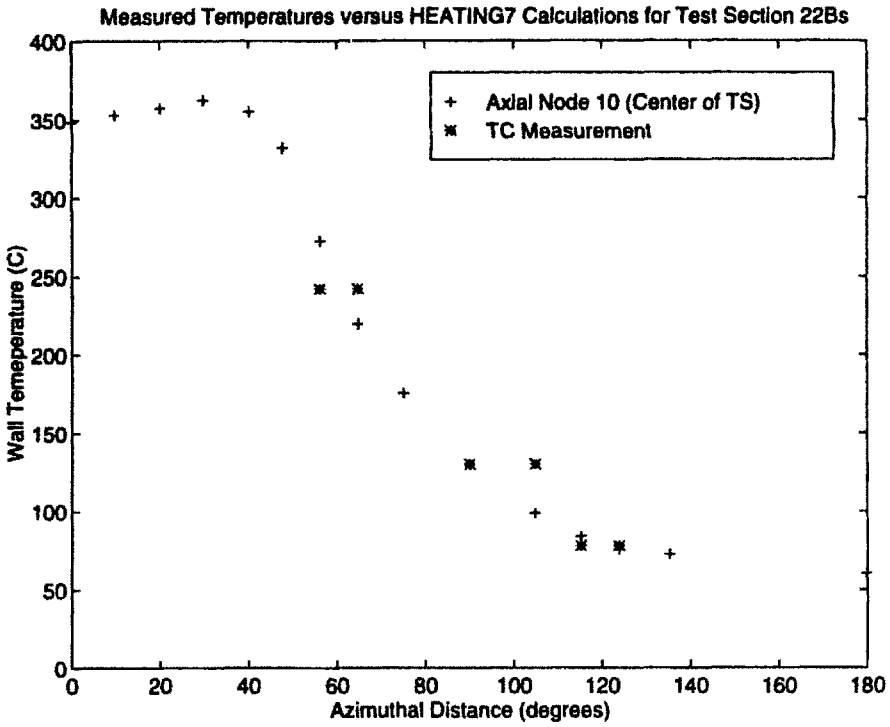

Figure H-38: Test Section 22B Comparison of Measured to Calculated Temperatures (Azimuthal Direction)

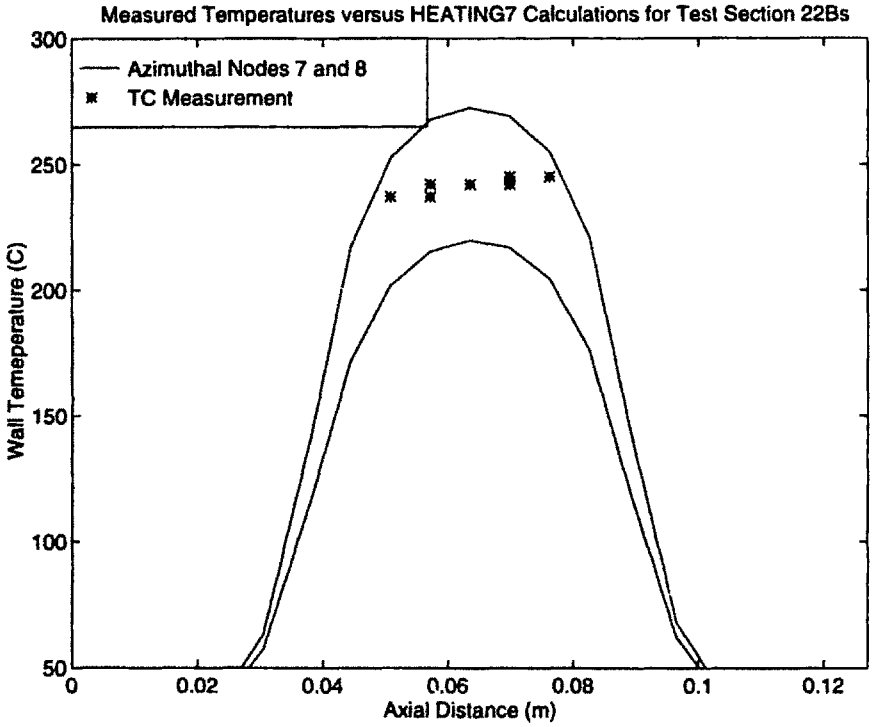

Figure H-39: Test Section 22B Comparison of Measured to Calculated Temperatures (Axial Direction)

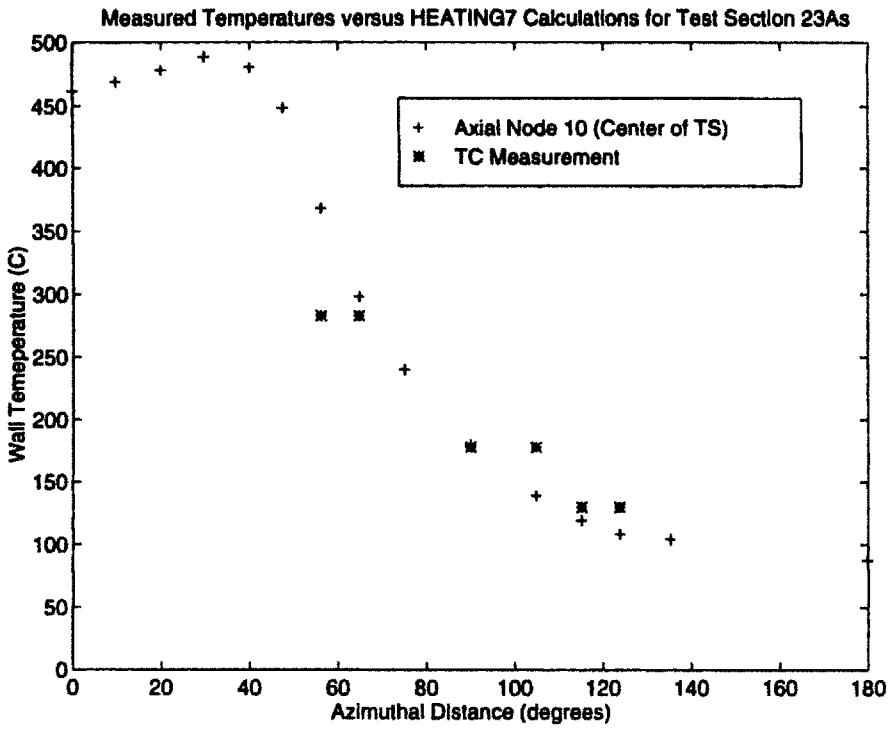

Figure H-40: Test Section 23A Comparison of Measured to Calculated Temperatures (Azimuthal Direction)

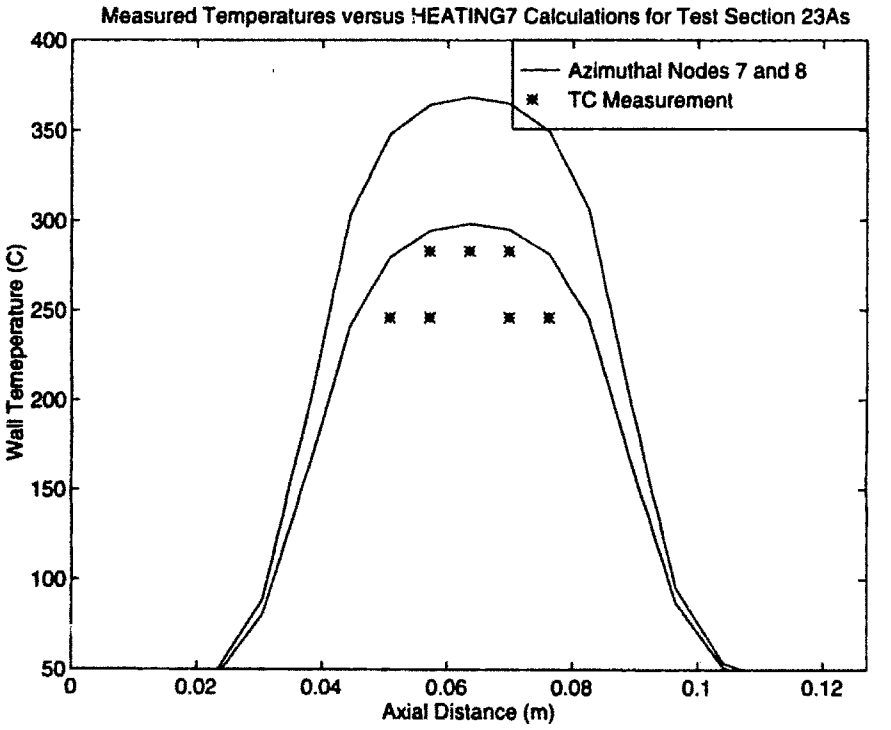

Figure H-41: Test Section 23A Comparison of Measured to Calculated Temperatures (Axial Direction)

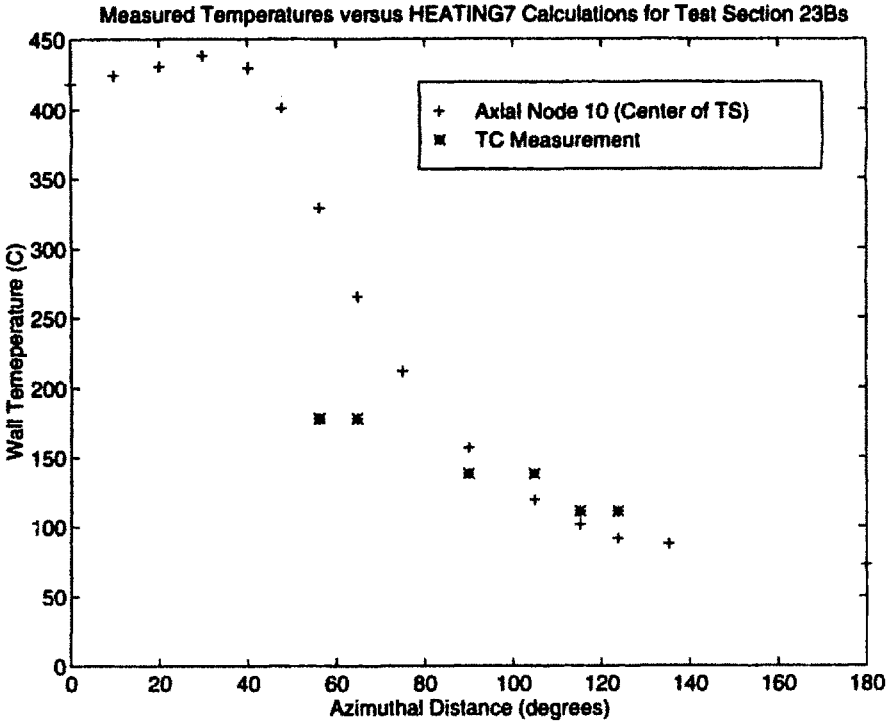

Figure H-42: Test Section 23B Comparison of Measured to Calculated Temperatures (Azimuthal Direction)

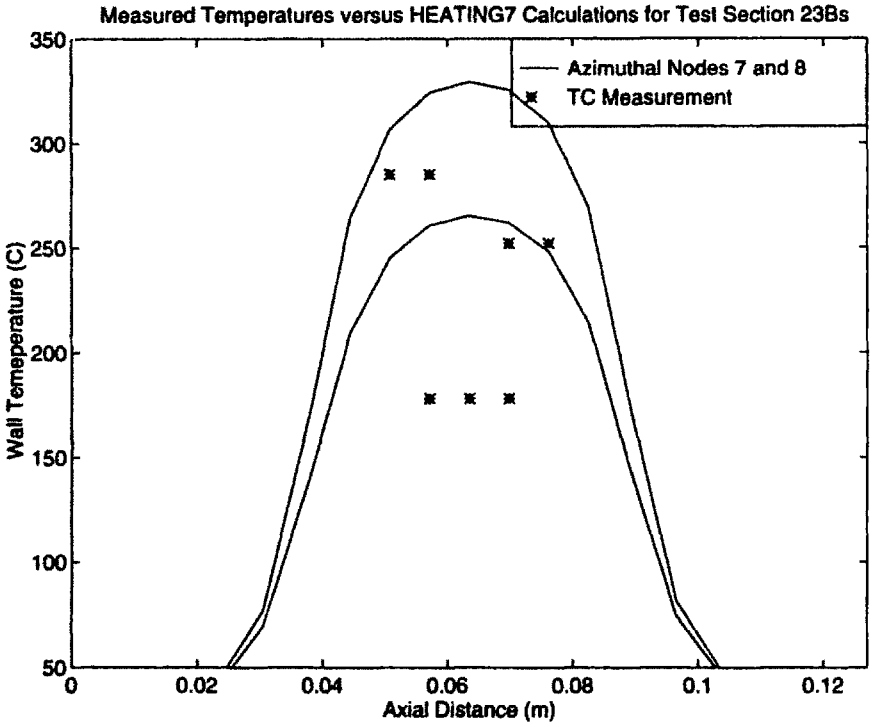

Figure H-43: Test Section 23B Comparison of Measured to Calculated Temperatures (Axial Direction)

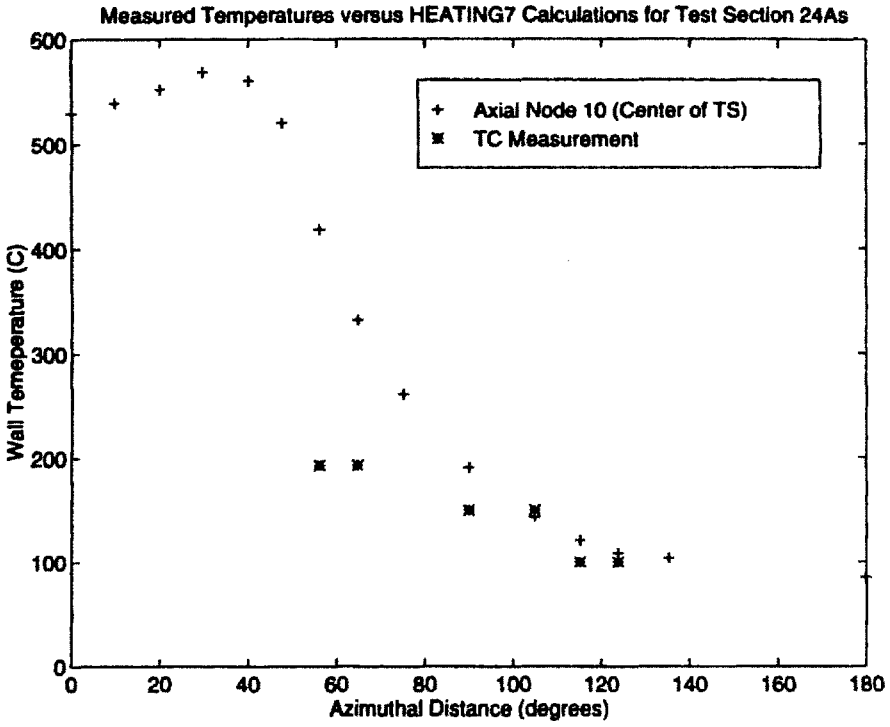

Figure H-44: Test Section 24A Comparison of Measured to Calculated Temperatures (Azimuthal Direction)

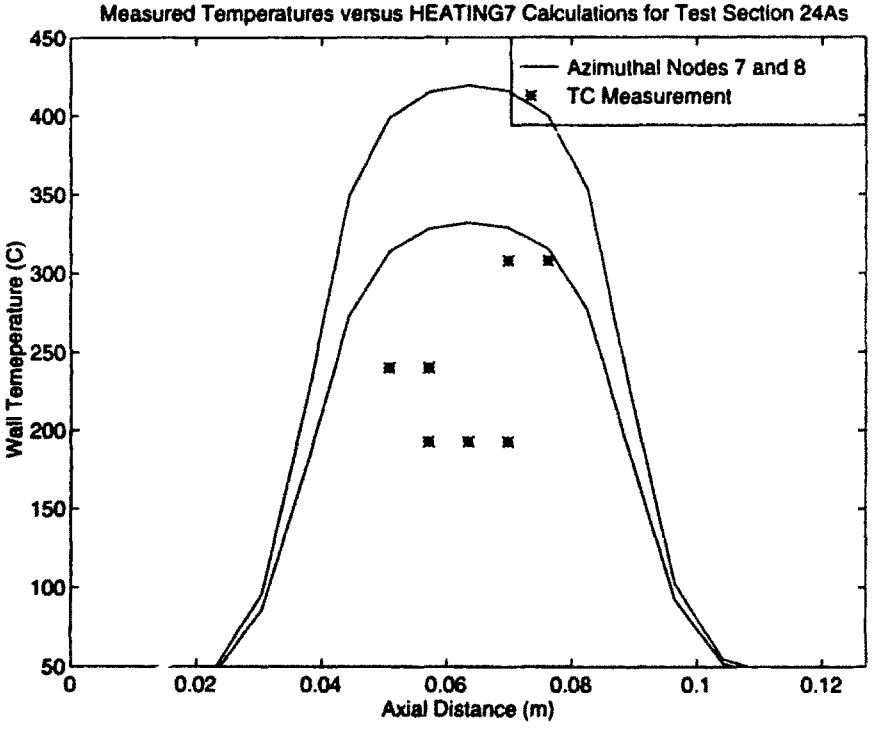

Figure H-45: Test Section 24A Comparison of Measured to Calculated Temperatures (Axial Direction)

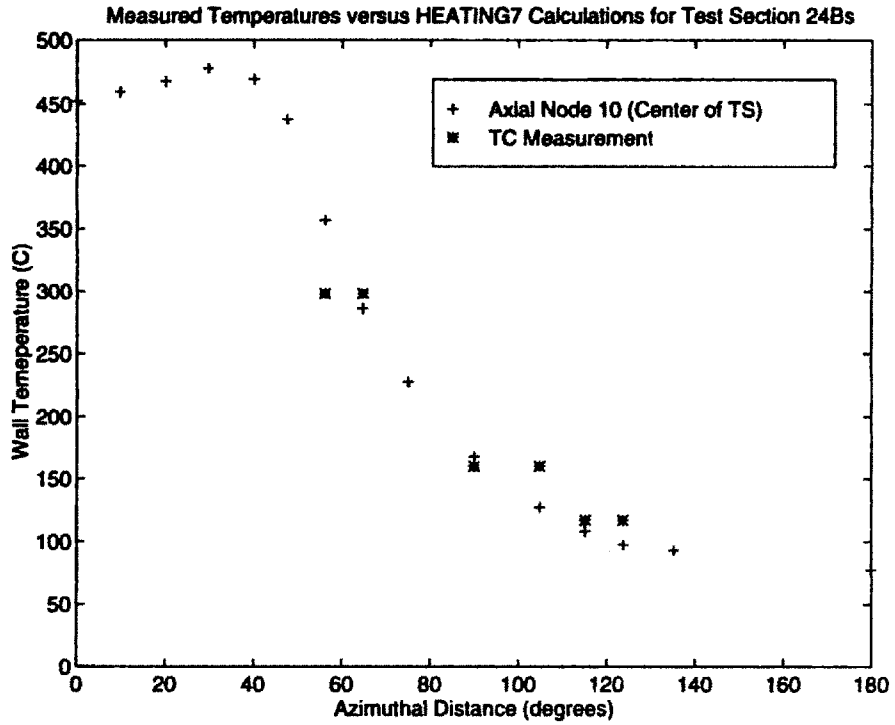

Figure H-46: Test Section 24B Comparison of Measured to Calculated Temperatures (Azimuthal Direction)

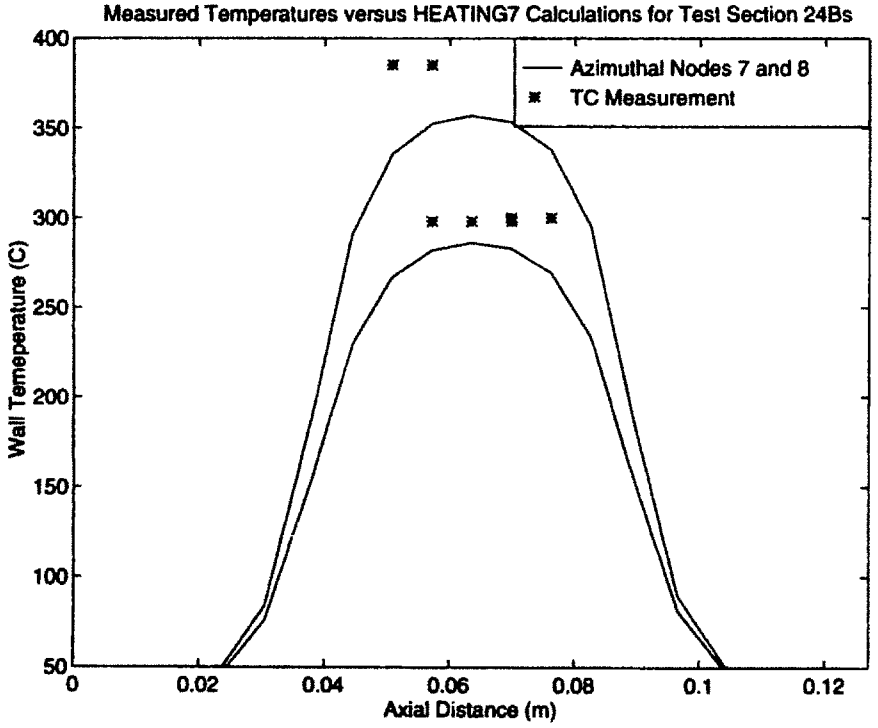

Figure H-47: Test Section 24B Comparison of Measured to Calculated Temperatures (Axial Direction)

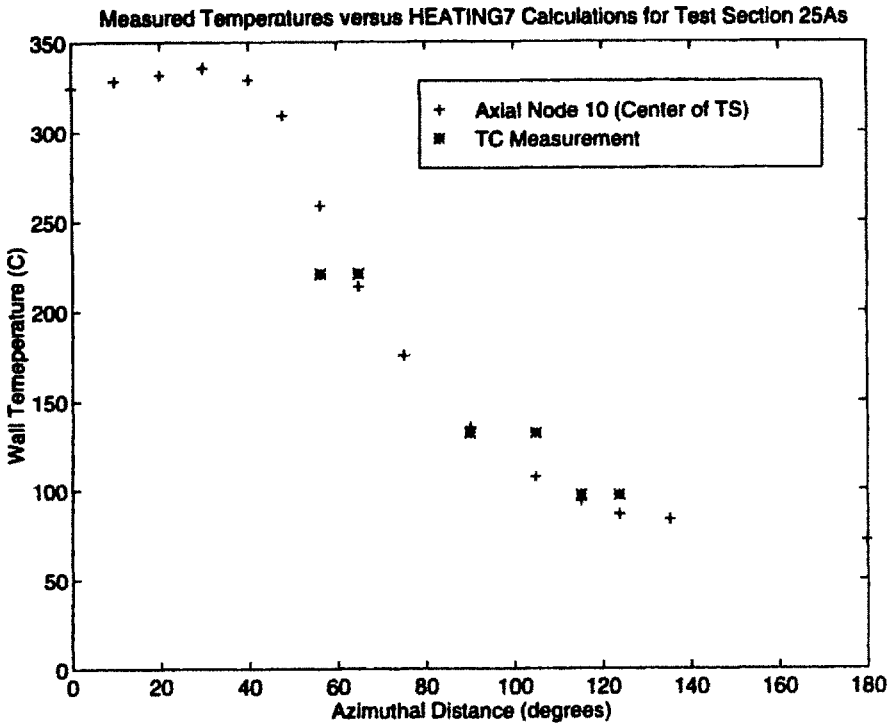

Figure H-48: Test Section 25A Comparison of Measured to Calculated Temperatures (Azimuthal Direction)

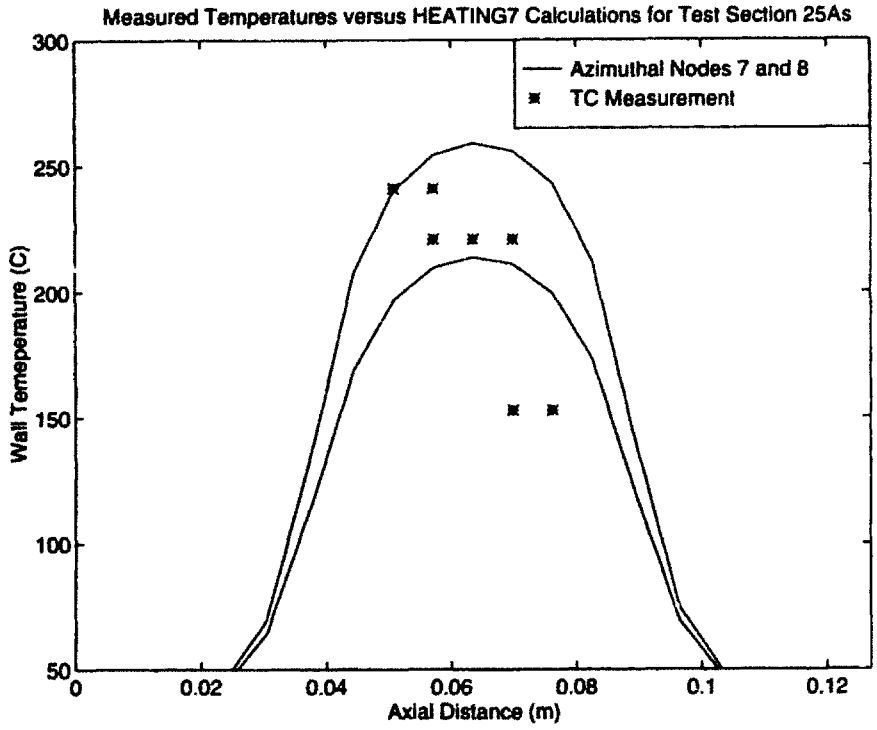

Figure H-49: Test Section 25A Comparison of Measured to Calculated Temperatures (Axial Direction)

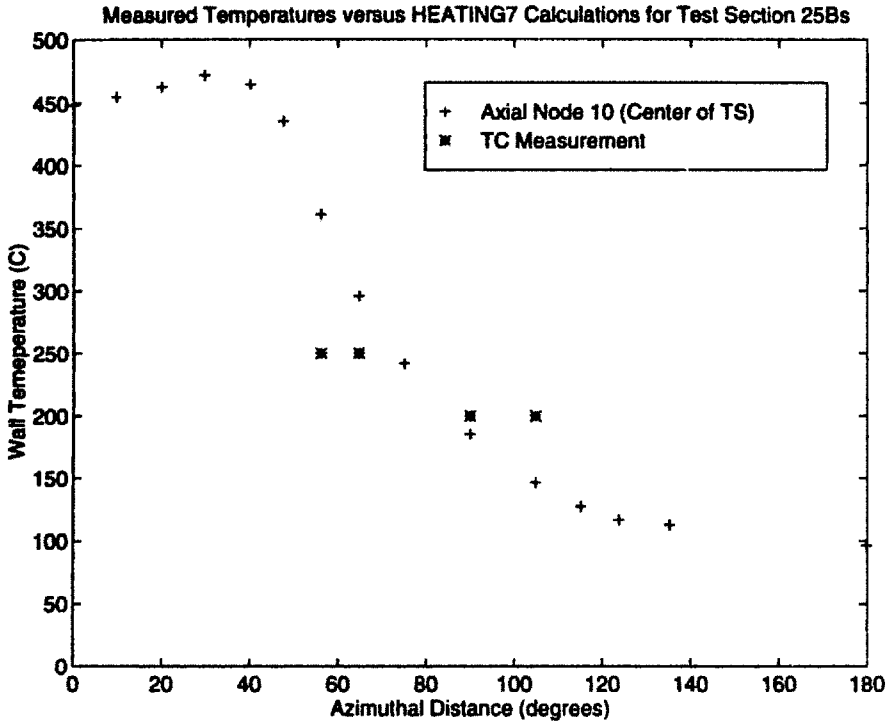

Figure H-50: Test Section 25B Comparison of Measured to Calculated Temperatures (Azimuthal Direction)

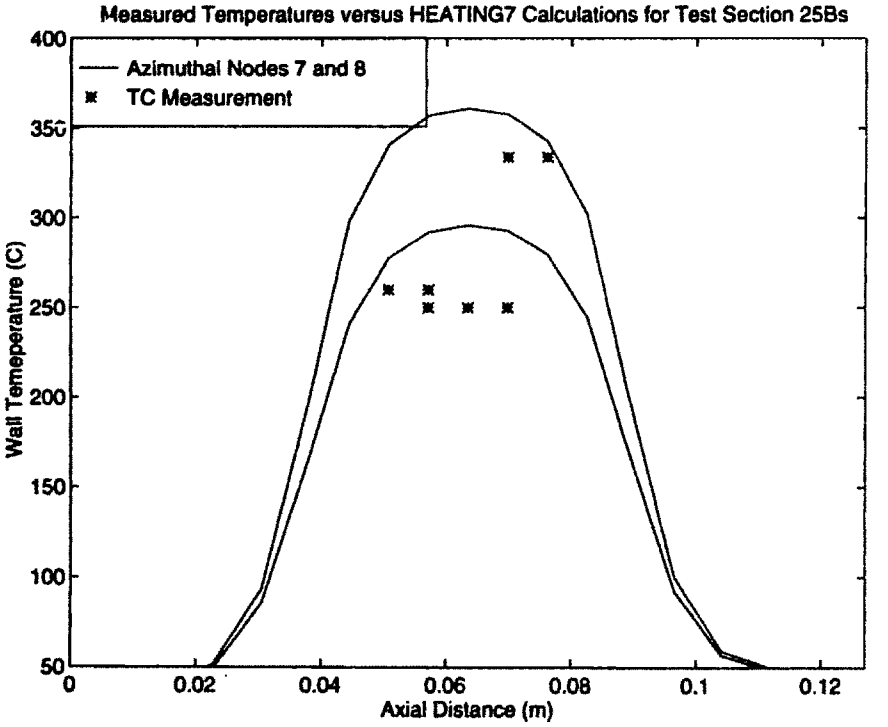

Figure H-51: Test Section 25B Comparison of Measured to Calculated Temperatures (Axial Direction)

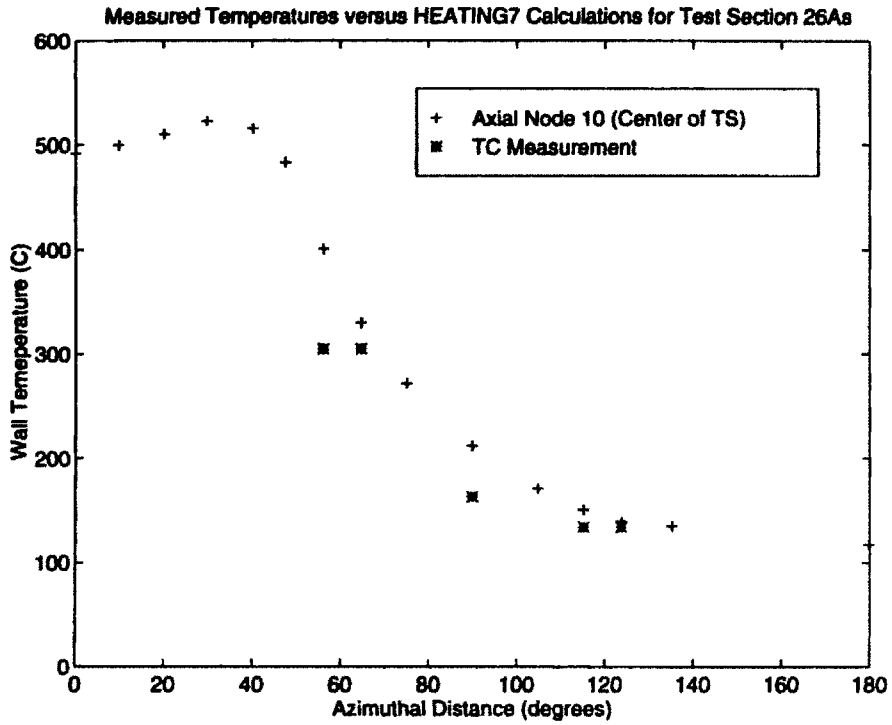

Figure H-52: Test Section 26A Comparison of Measured to Calculated Temperatures (Azimuthal Direction)

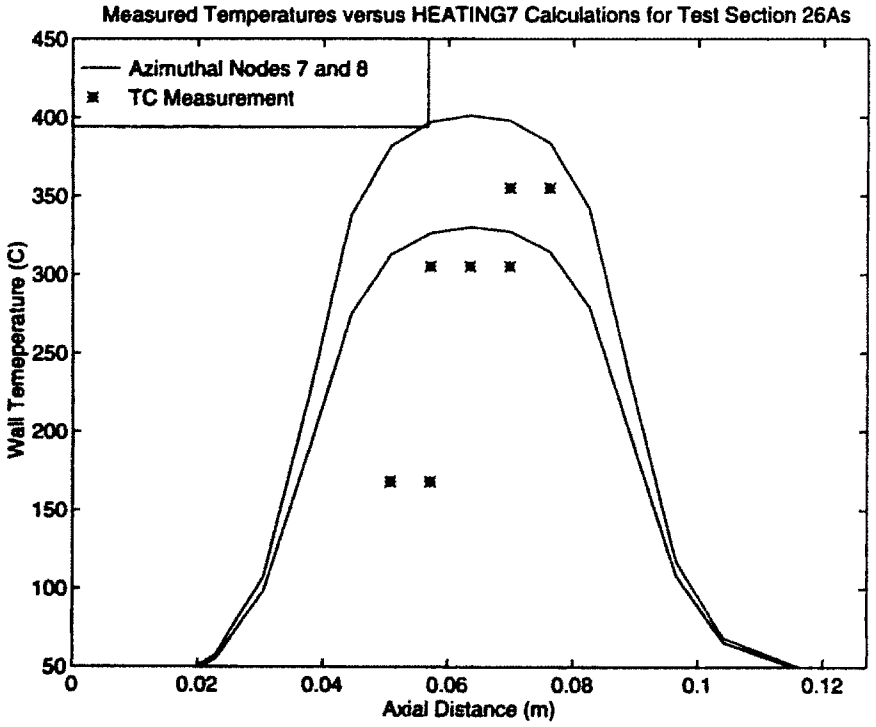

Figure H-53: Test Section 26A Comparison of Measured to Calculated Temperatures (Axial Direction)

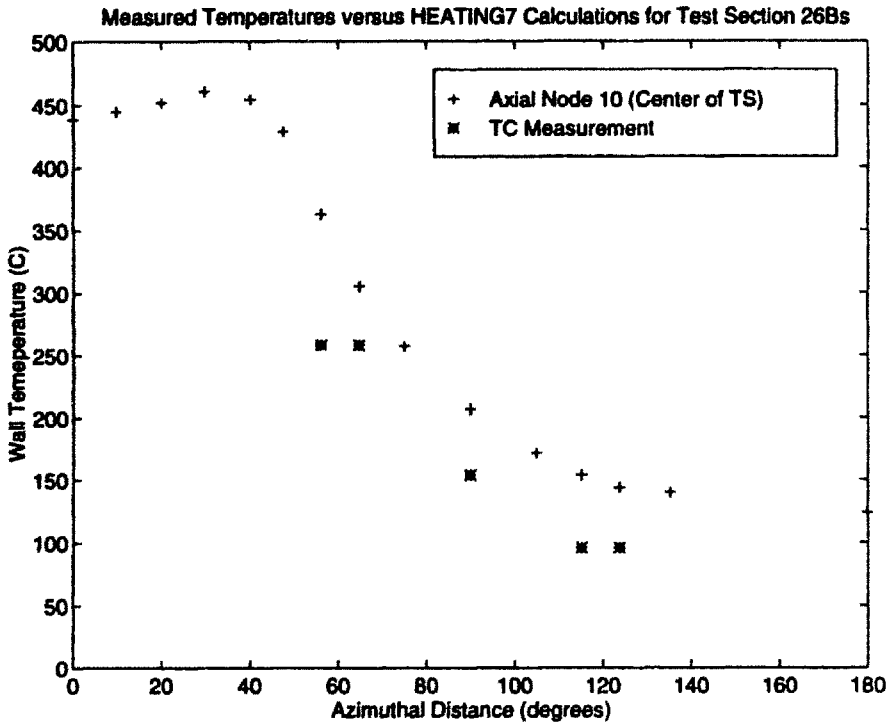

Figure H-54: Test Section 26B Comparison of Measured to Calculated Temperatures (Azimuthal Direction)

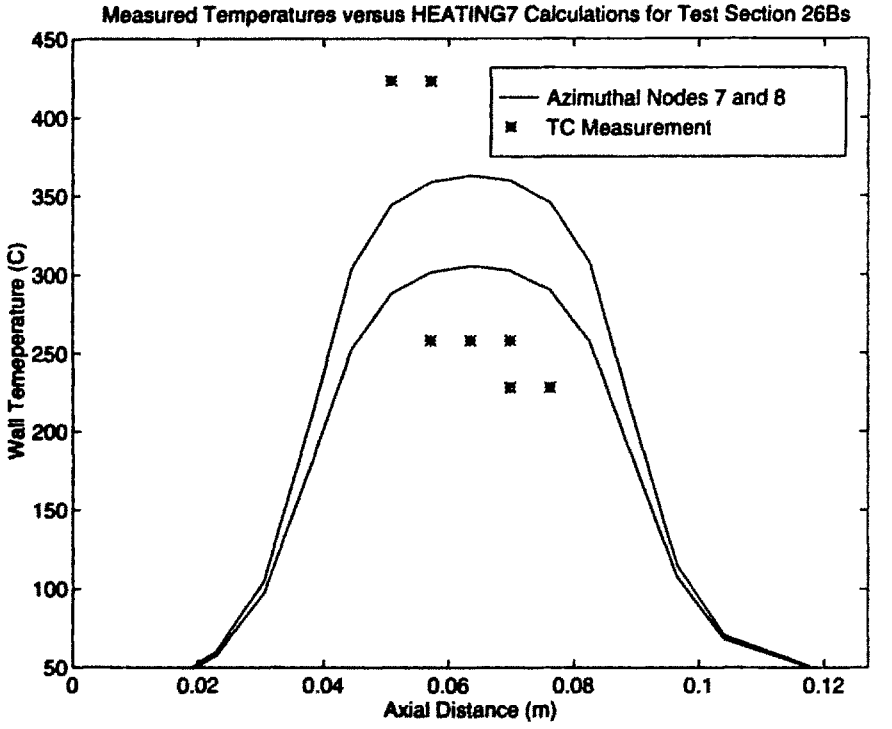

Figure H-55: Test Section 26B Comparison of Measured to Calculated Temperatures (Axial Direction)

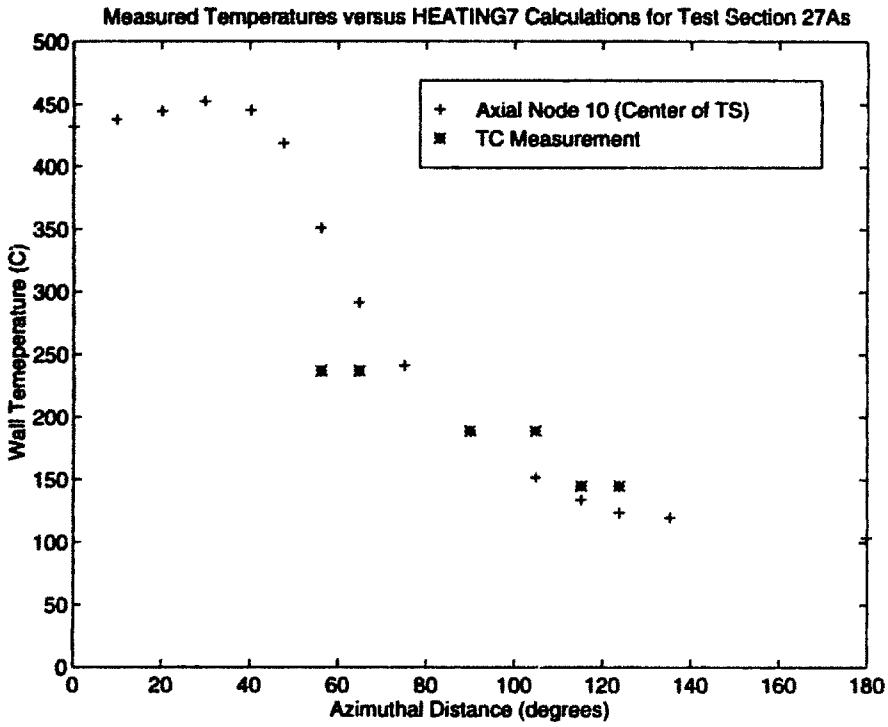

Figure H-56: Test Section 27A Comparison of Measured to Calculated Temperatures (Azimuthal Direction)

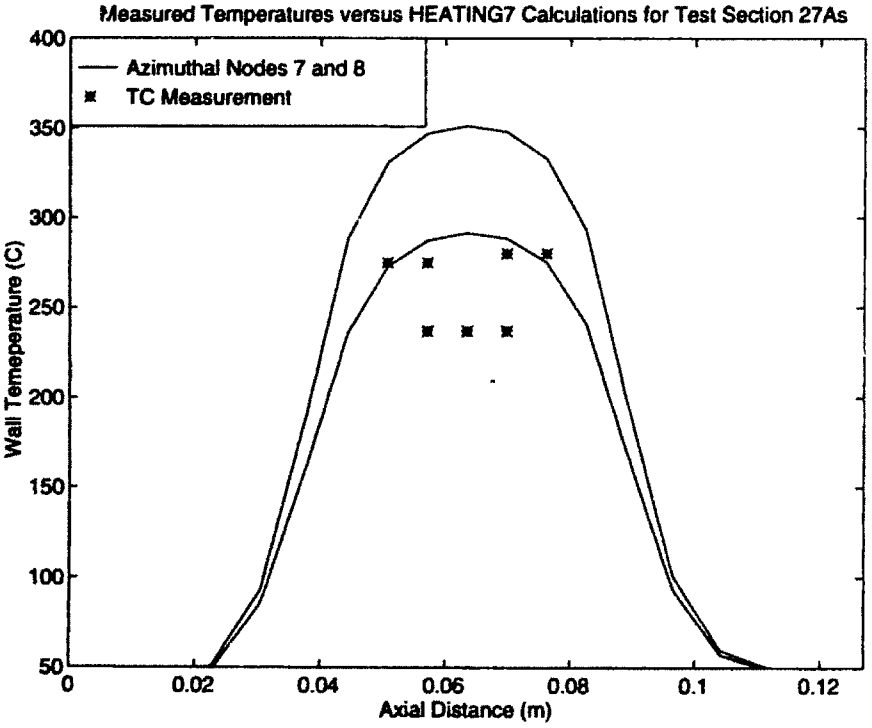

Figure H-57: Test Section 27A Comparison of Measured to Calculated Temperatures (Axial Direction)

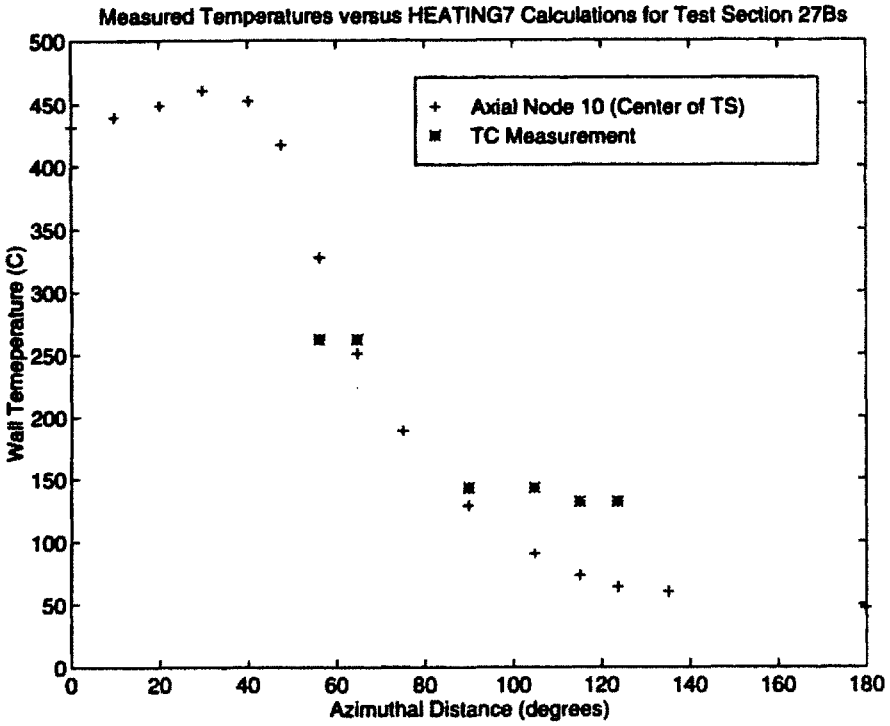

Figure H-58: Test Section 27B Comparison of Measured to Calculated Temperatures (Azimuthal Direction)

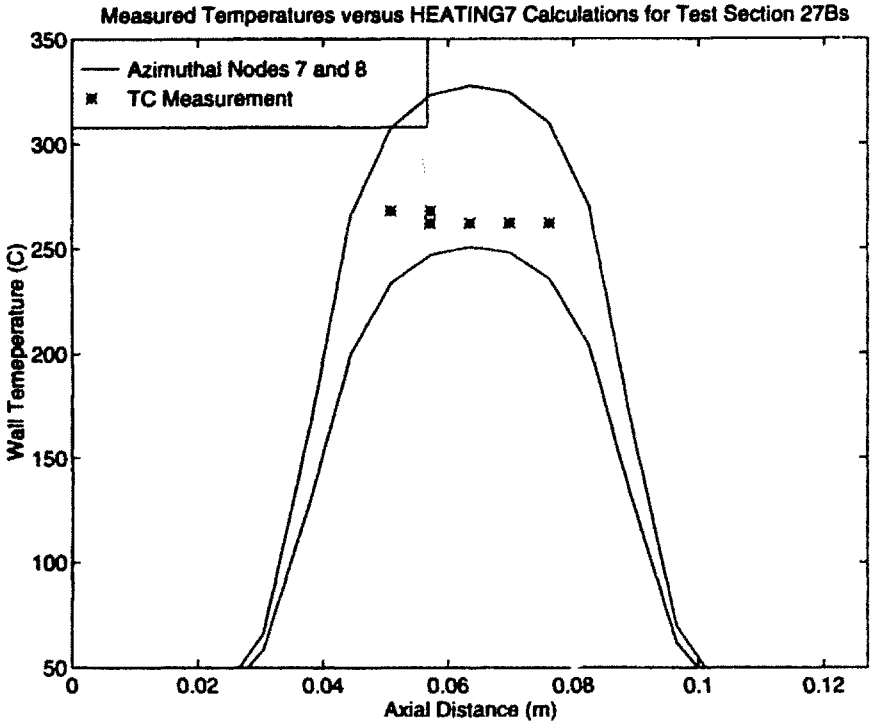

Figure H-59: Test Section 27B Comparison of Measured to Calculated Temperatures (Axial Direction)

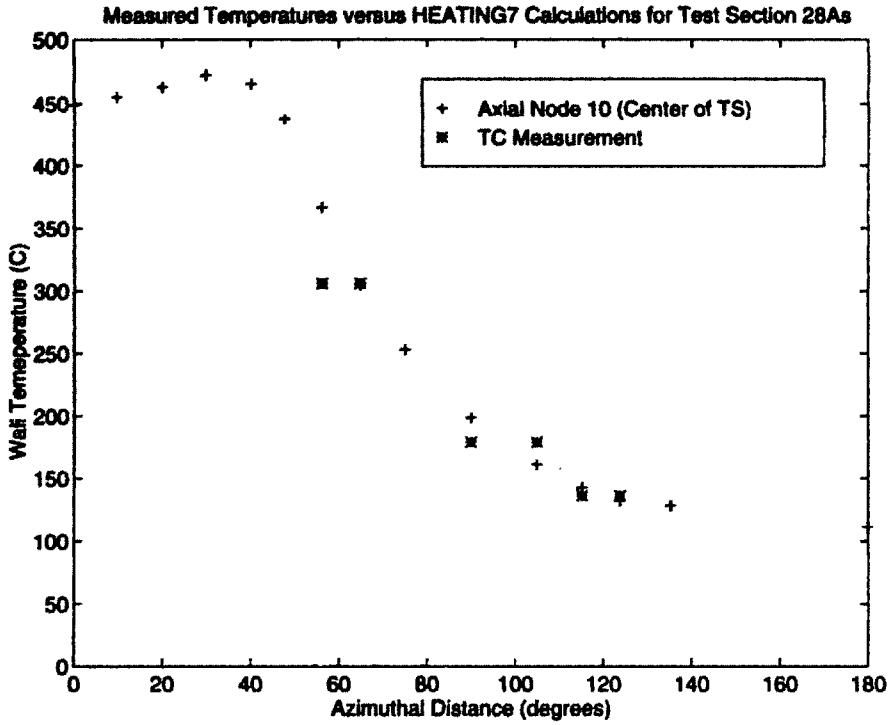

Figure H-60: Test Section 28A Comparison of Measured to Calculated Temperatures (Azimuthal Direction)

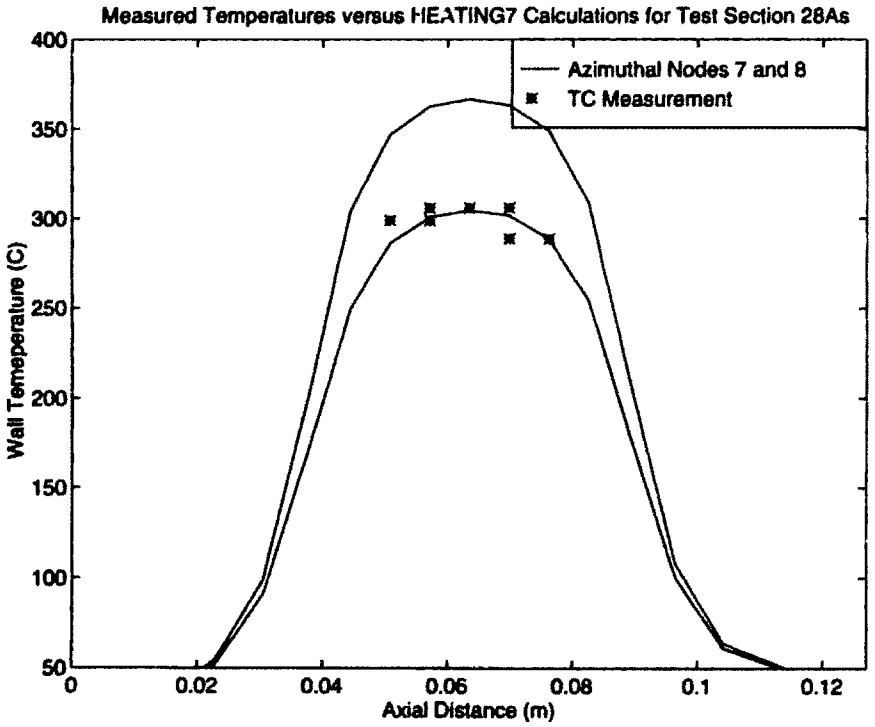

Figure H-61: Test Section 28A Comparison of Measured to Calculated Temperatures (Axial Direction)

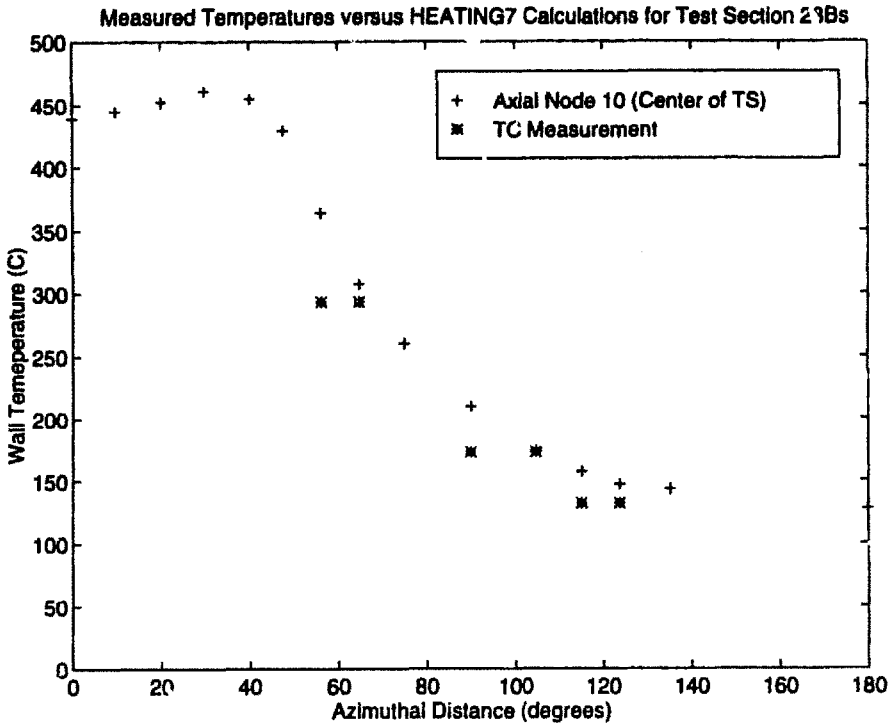

Figure H-62: Test Section 28B Comparison of Measured to Calculated Temperatures (Azimuthal Direction)

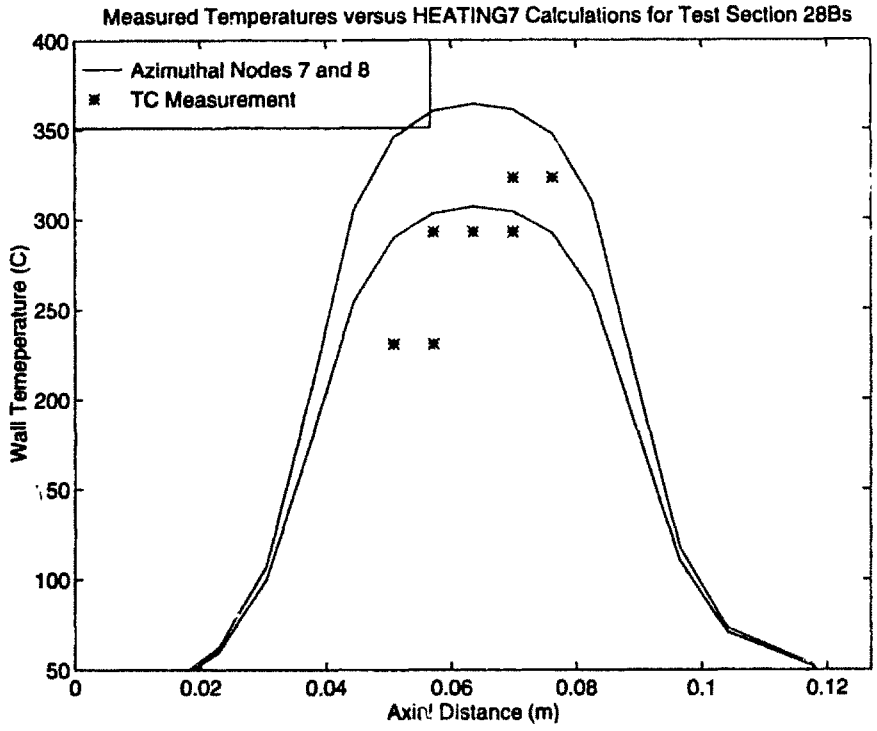

Figure H-63: Test Section 28B Comparison of Measured to Calculated Temperatures (Axial Direction)

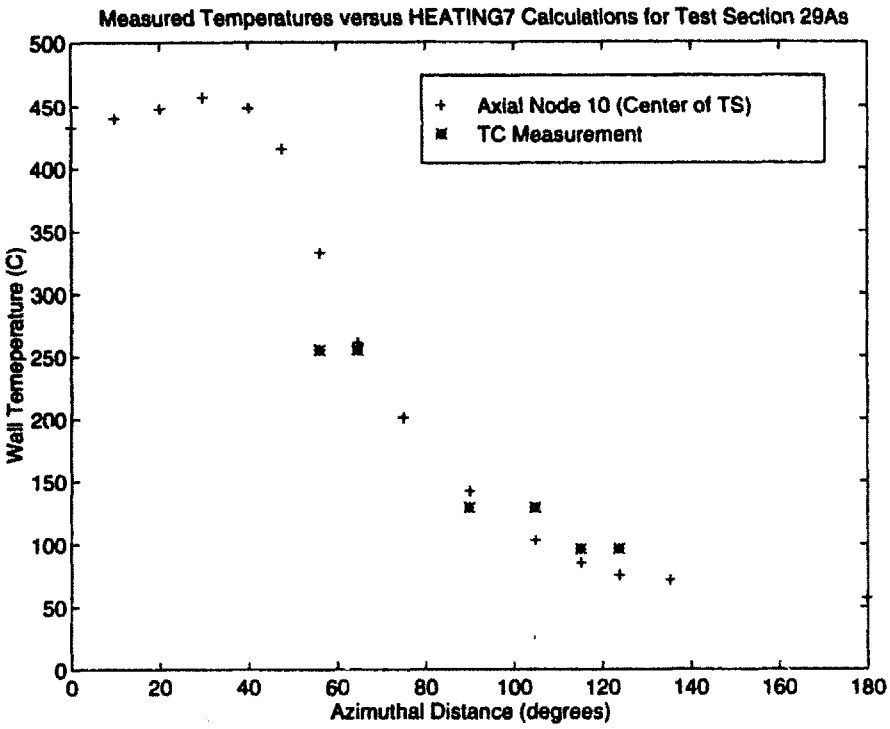

Figure H-64: Test Section 29A Comparison of Measured to Calculated Temperatures (Azimuthal Direction)

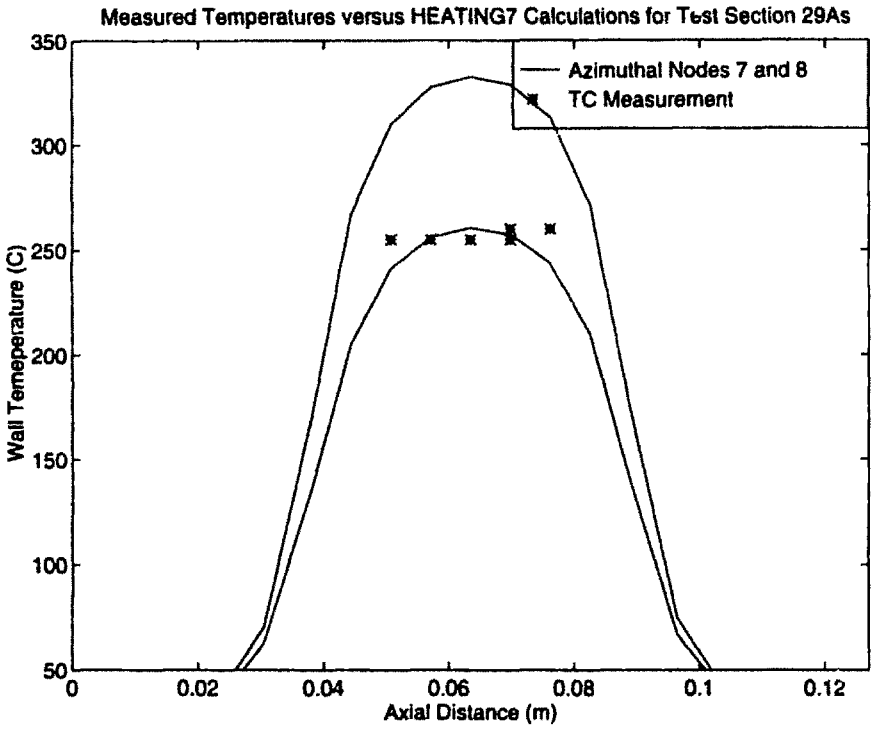

Figure H-65: Test Section 29A Comparison of Measured to Calculated Temperatures (Axial Direction)

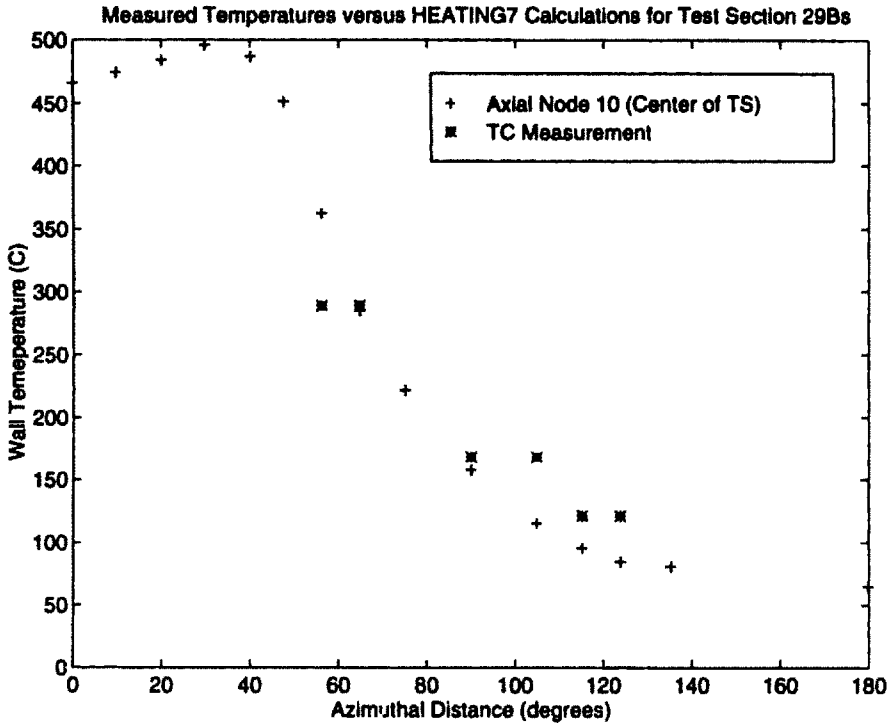

Figure H-66: Test Section 29B Comparison of Measured to Calculated Temperatures (Azimuthal Direction)

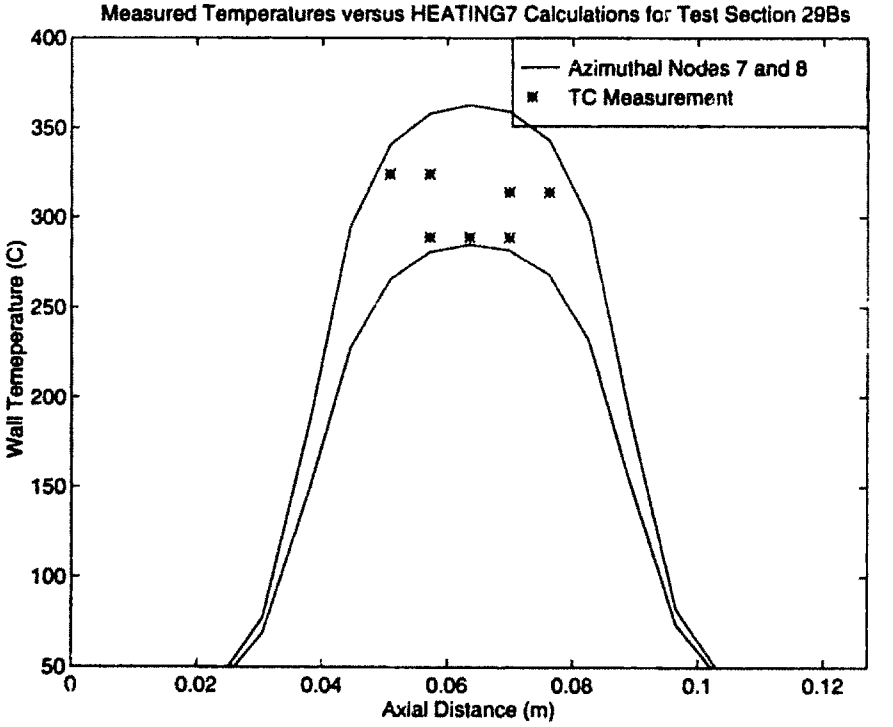

Figure H-67: Test Section 29B Comparison of Measured to Calculated Temperatures (Axial Direction)